Cloud Publications
International Journal of Advanced Remote Sensing and GIS
2017, Volume 6, Issue 1, pp. 2006-2022
ISSN 2320 – 0243, doi:10.23953/cloud.ijarsg.31

Research Article | Open Access

Land Use Classification and Analysis Using Radar Data Mining in Ethiopia

Haile K. Tadesse[1,4], John J. Qu[2,4], Alonso A. Aguirre[1], Maction Komba[2], and Viviana Maggioni[3]

[1]Environmental Science and Public Policy, George Mason University, 4400 University Drive, Fairfax, VA, USA
[2]Geography and Geoinformation Science, George Mason University, 4400 University Drive, Fairfax, VA, USA
[3]Civil, Environmental & Infrastructure Eng., George Mason University, 4400 University Drive, Fairfax, VA, USA
[4]Global Environment and Resources Institute (GENRI), 4400 University Drive, Fairfax, VA, USA

Publication Date: 1 March 2017

DOI: https://doi.org/10.23953/cloud.ijarsg.31

Abstract Land use classification in tropical areas, is hindered by frequent cloud cover which limits the availability of optical satellite data. Satellite-borne radar is a possible alternative to optical data for land use classification in tropical areas. However, radar data is affected by noise (i.e., speckle) that must be minimized before its use in land classification. Median, Lee-Sigma, and Gamma-MAP de-speckling techniques were applied to Fine Beam, Dual polarization (FBD) PALSAR radar data acquired over central Ethiopia. Each of the de-speckled images were then subjected to supervised classification using Maximum Likelihood, C4.5, Multilayer Perceptron and Stacking techniques. Validation results indicated that de-speckling techniques improved classification accuracy by up to 25%, 20% and 16% using Gamma-MAP, Median and Lee-Sigma respectively. Gamma-MAP de-speckling in combination with the Multilayer perceptron classifier achieved the best overall classification accuracy at 91.2%. This study proved the importance of radar data as an alternative source of information for land use classification in the tropics. Further research should focus on the application of radar data for forest fire detection and crop classification. The use of fully polarized radar data has the potential to further improve the proposed land use classification in tropical countries.
Keywords *PALSAR; Speckle; C4.5; Multilayer Perceptron; Maximum Likelihood; Algorithms*

1. Introduction

Land use changes such as deforestation are recognized as a key component of global change (Patz et al., 2004; Soria-Ruiz et al., 2010). The major driving factors for deforestation are agricultural expansion and urbanization (DeFries et al., 2010). “The global rate of tropical deforestation continues at staggering levels, with nearly 2–3% of forests lost globally each year” (Patz et al., 2004). As a consequence, land use change, land degradation, and poverty are increasingly impacting many countries in Africa. Therefore, it is crucial to accurately assess land use and deforestation. Remote sensing plays a fundamental role in determining land coverage changes in areas where direct in-situ observations are sparse or not available at all. This research focuses on land use classification and

analysis using radar data, and different techniques of classification and data processing techniques in Ethiopia.

Radar is an active sensor which sends energy to illuminate the earth surface and to detect the portion of back scattered energy. Radar sensors receive scattered energy from the surface feature and the amount and direction of scattering is affected by the type of material, moisture content, angle of illumination and angle of backscatter retrieval, surface roughness and surface geometry. The presence of noise or speckle in radar images is a source of uncertainty in the retrieved data. Radar sensors produce microwaves and these waves may create dark or light pixels when the wave comes in contact with the target (Noreiga and Fabian, 2000). This is due to the coherent nature of the radar wave (Jenson, 2005), which may create an artificial heterogeneity for a homogeneous region. Speckle affects image classification and interpretation (Nyoungui et al., 2002). Therefore, it is crucial to reduce speckle noise before radar data is used in classification studies (Maghsoudi et al., 2012). Different speckle reduction techniques such as median can be used to preserve image sharpness and detail. De-speckling techniques use a moving window with a size defined by the user. The mean filter is the least effective method of speckle reduction; it is useful only for applications where loss of spatial resolution is not a problem (ERDAS, 1999). The Sigma and Lee filters utilize the statistical distribution of the digital numbers (DN) values within the moving window. According to a study by Capstick and Harries (2001), Lee-Sigma, and Gamma-MAP produced the best results for identifying agricultural crops. Median filter produced the best result in speckle reduction and in detail preservation (Qiu et al., 2004). The three de-speckling techniques evaluated for land use classification in Ethiopia were median, Lee-Sigma, and Gamma-MAP.

After pre-processing, image classification algorithms are commonly applied to compile land cover maps. The most widely adopted parametric classification method is the maximum likelihood algorithm. Supervised maximum likelihood classification (MLC) is the most popular statistical classification algorithm (Emrahoglu et al., 2003) and is usually preferred unless there are particular reasons for believing that data do not follow a Gaussian distribution (Pal and Mather, 2003). Most applications of MLC method assume that each class has an equal probability of occurring in the study area and has a multivariate normal distribution. However, this assumption may not be true for remote sensing images. Therefore, C4.5, Multilayer Perceptron and Stacking classification methods were also included in this study.

C4.5 is a non-parametric classification method. It is an extension of the Iterative Dichotomiser 3 (ID3) algorithm (Chandra and Paul, 2007). C4.5 is a decision tree approach used for classification in which the classification procedure recursively partitions a data set into smaller subdivisions on the basis of a set of tests defined at each branch or node (Friedl and Brodley, 1997). In a decision tree, the hypothesis, rules, and conditions may be considered as the trunk, a limb, and a leaf of a tree, respectively (Jensen, 2005). It is possible to see the stages of classification at each branch. Decision trees yield a set of rules which are easy to interpret and suitable for deriving a physical understanding of the classification process (DeFries and Chan, 2000). In decision tree, a minimum error or entropy is used as a threshold to select each class (Kumar et al., 2010).

Multilayer Perceptron (MLP) is an Artificial Neural Networks (ANN) which can be used for land use classification. The input layer may include images of reflectance, texture, slope, etc. Neural networks use less statistical assumptions than maximum likelihood algorithms and makes no prior assumptions of normal distribution A research study by Yuan et al. (2009), recommends that in complex land use mapping applications, supervised MLP networks may be used to derive detailed and more accurate image classification. The difficulties in conventional classification can be improved using Neural Network (NN) (Kumar et al., 2010). According to Idol et al. (2015), classification algorithms such as NN are important for radar data classification. Therefore, in this study in Ethiopia, MLP was applied to classify land use and compare its classification accuracy results to that of MLC and C4.5 decision tree

classifiers. Besides this, MLP and C4.5 were combined using Stacking method to classify the images. Stacking is a method of combining multiple classifiers. The objective of the study is to produce land cover maps using different techniques of image enhancement and classification techniques in central Ethiopia.

2. Study Area and Data Sources

2.1. Study Area

Ethiopia has a total area of 1,127,127 km^2, and it is the third largest country in Africa. Agriculture is the main economic sector and the majority of the population lives in rural areas. Extensive dependence on traditional agriculture has resulted in over-exploitation and natural resources degradation for centuries (Getu and Hurni 2001; Bewket, 2002; Darbyshire et al., 2003). Unsustainable agricultural practices have exposed the country to rapid deforestion, soil erosion, and biodiversity loss, among other issues. A study by Dessie and Kleman (2007) shows that during the past half-century, the total forest cover has decreased from 16% in 1972 to 2.8% in 2000 in the south central rift valley region of Ethiopia. Badege (2001) showed rapid decline of forest cover in the country over the last 100 years, which is due to many factors. A recent study in northern Ethiopia has shown that forest disturbance and excessive utilization of forest products for fuel wood had a significant effects on tree species composition and diversity (Berhane et al., 2015). Inappropriate land management policies, based on poor land use information enhance desertification and loss of agrobiodiversity (Taddese, 2001).

The study area is located in Kombolcha, central Ethiopia. The study area was selected based on the history of land use changes in the region and availability of radar data. The study area has experienced substantial land cover changes since early last century (Tekle and Hedlund, 2000).The agro-ecology of the research area in Amhara regions is "*Weyna Dega*" (midlands) and the temperature ranges from 15^{o}C to 25^{o}C depending on topographic elevation. Weyna Dega is one of the traditional agro-climatic zone in Ethiopia. The main rainy season is from July to September and the average annual rainfall is 866.25 mm (*Desse* station). The major cities in the research study are Kombolcha (11^o 4'N and 39 ^{o} 44'E) and Haik. Kombolcha has an estimated total population of 68,766 (CSA, 2005). The administrative *weredas* included in this site are Bati, Desie Zure, Werebabu, Tehuledere, and Kombolcha. The main economic sectors in Kombolcha study area are agriculture, livestock, and industry.

2.2. Data Sources

This study investigated the possibility of retrieving information on land use and land cover from satellite-based radar data. Specifically, this study used data collected by Phased Array type L-band Synthetic Aperture Radar (PALSAR) board of the Advanced Land Observation Satellite (ALOS). ALOS was launched on January 24, 2006 by Japan Aerospace Exploration Agency. PALSAR is an L-band (wavelength of 23.62 cm) active microwave sensor for day and night data collection with spatial resolution of 12.5 m at ground. Fine Beam Dual Polarization (FBD) with HH and HV bands was used. HH is Horizontal, Horizontal Polarization, whereas, HV is Horizontal, Vertical Polarization. The radar image used for this study is PALSAR from 02/06/2008. Figure 1 shows the PALSAR radar image and study area location in Ethiopia.

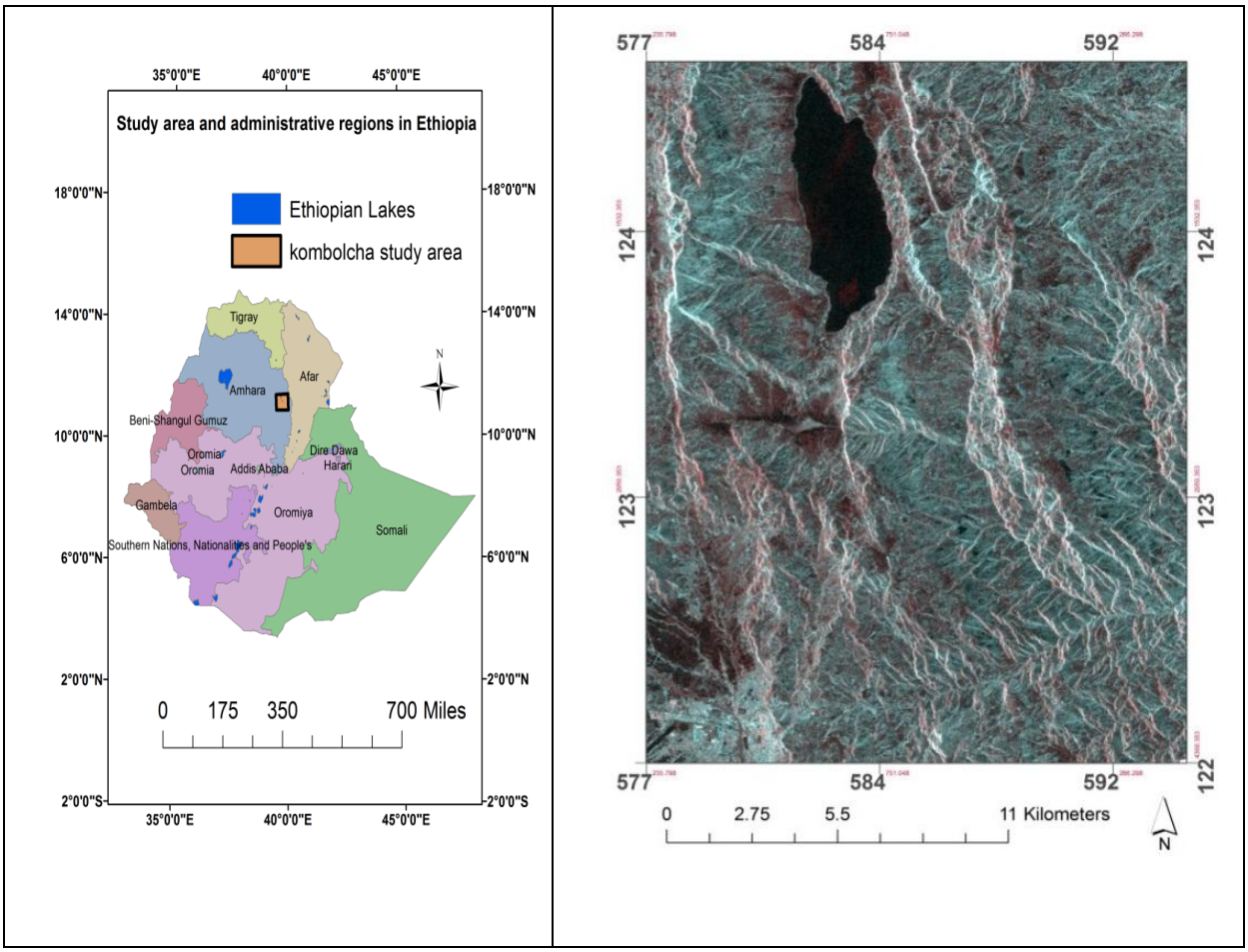

Figure 1: *Study area in central Ethiopia and PALSAR data from June 02, 2008 (HH and HV)*

3. Methodology

The objective of this study was to analyze the impact of different de-speckling and classification techniques on land use classification. The specific objectives are the following:

A) To determine which de-speckling approach produces the best input radar images for land use classification, and
B) To analyze which combination of de-speckling and supervised classification approaches produces an accurate land cover classification.

The steps of this study include: i) remote sensing image collection, ii) data collection, iii) image enhancement, iv) land use classification, and v) accuracy assessment and analysis.

3.1. Data Processing and Analysis

The original radar data were converted to GeoTIFF data format using Mapready software (2.3) from the Alaska Satellite facility. The data was projected to universal transverse marcetor projection. Then, image enhancement methods were applied in order to observe the impacts of these techniques on land use classification accuracy. All image enhancement techniques were applied using a moving window of different sizes. The window size ranged from 7 ×7 to 27 × 27. Window size determines the number of pixels to be included in each statistical analysis. The image enhancement methods adopted

in this study were Median, Lee-Sigma and Gamma-MAP de-speckling filters. Median filter replaces the pixel of interest by the median digital value (DN) with in the window. Lee-Sigma assumes normal distribution and both mean and variance are used to estimate the value of the particular pixel. The formula used to calculate the DN value for the Lee filter is shown in the following set of equations (ERDAS, 1999):-

$$DN_{out} = [Mean] + K[DN_{in} - Mean] \quad (1)$$

where Mean is the average of the pixels in a moving window. K is defined by the following equation:

$$K = \frac{Var(x)}{[Mean]^2 \sigma^2 + Var(x)} \quad (2)$$

where the variance of x [Var (x)] is defined as:

$$Var(x) = \left\{\frac{[Variance\ within\ window] + [Mean\ within\ window]^2}{sigma^2 + 1}\right\} - [Mean\ within\ window]^2 \quad (3)$$

The Maximum A Posteriori (MAP) filter assumes non-Gaussian distribution and it considers statistical and geometrical characteristics of the pixels. Gamma-MAP filter estimates the original pixel DN and maximums the posterior density function (ERDAS, 1999).

$$I\hat{}^3 - I\ I\hat{}^2 - \sigma\ (I\hat{} + - DN) = 0 \quad (4)$$

where II^ is sought value, I is mean value, DN is input value, and σ is original image variance

Figure 2 shows unfiltered and de-speckled radar data images from the Kombolcha study area using those de-speckling techniques. Applying these filters increases the visual separation of the land cover units. Increasing window size increases the separability of land cover units after Median; Lee-Sigma and Gamma-MAP filters are applied.

3.2. Land use classification and accuracy assessment

3.2.1. Land use classification

Supervised image classification was used for this study. This classification method requires prior knowledge of the available land covers. Therefore, all primary and secondary data were collected for calibration and validation purposes. The land covers considered were forest, agriculture, water and urban. A representative signature or area of interest identification (AOI) was used to train and calibrate the classification algorithm. The statistical values of these training samples were evaluated using transformed divergence. Four classification algorithms were applied after pre-processing:- Maximum Likelihood (MLC), C4.5 (decision tree), Multilayer Perceptron (MLP) and a combination of classifiers or Stacking. The open source software, WEKA was used for Multilayer Perceptron (MLP), C4.5 decision tree and stacking classification. All training and validation pixels were exported from ERDAS to WEKA for C4.5, Multilayer Perceptron and Stacking classification methods.

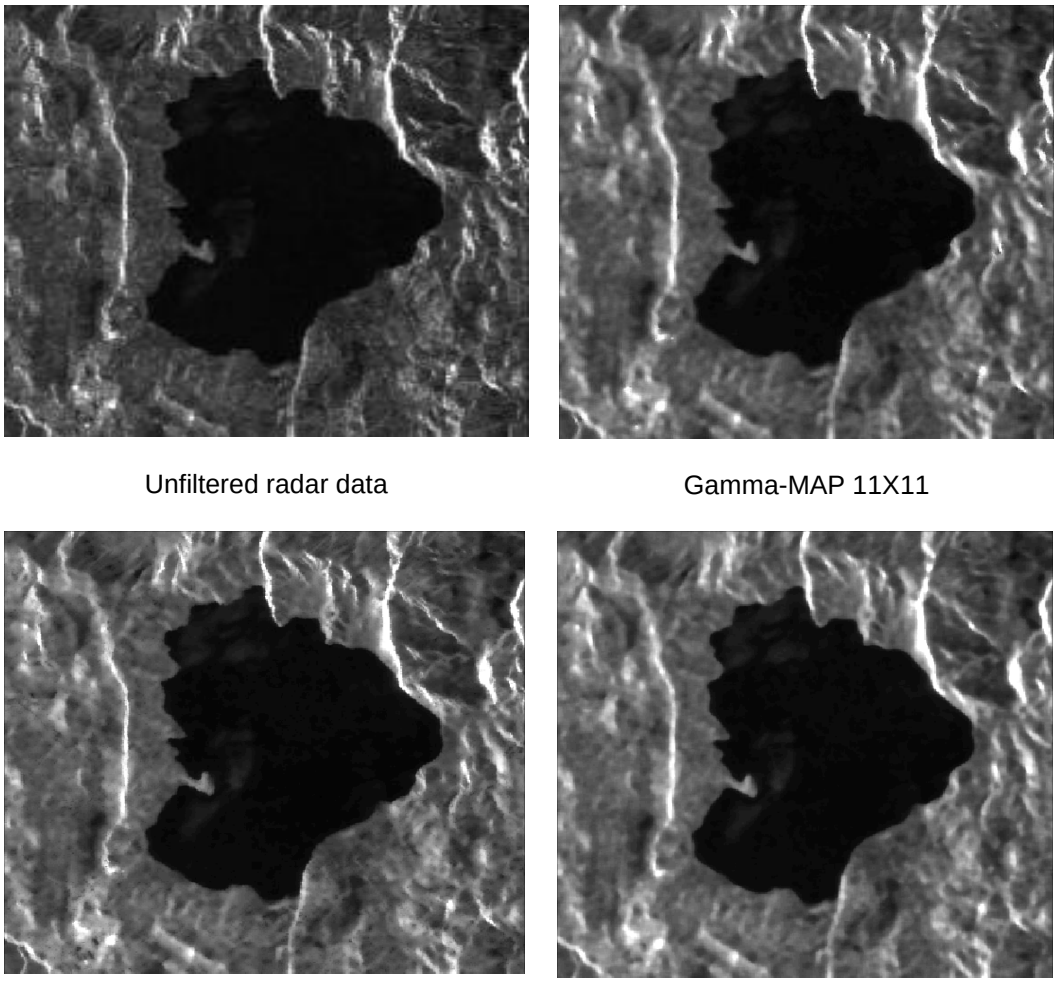

Figure 2: *Unfiltered and de-speckled radar images using Gamma, Lee-sigma and Median at 11×11 windows*

The Maximum likelihood classification considers both mean and variability of brightness values in each class and estimates the probability of each pixel to be assigned to the individual class (Campbell, 2002). It is a parametric classifier and that assumes normally distributed data. The equation for the maximum likelihood classifier is as follows:

$$D = \ln(ac) - [0.5 \ln(|Covc|)] - [0.5 (X-Mc)T (Covc-1) (X-Mc)] \quad (5)$$

where *D* is weighted distance (likelihood), *c* is a particular class, *X* is the measurement vector of the candidate pixel, *Mc* is the mean vector of the sample of class *c*, *ac* is percent probability that any candidate pixel is a member of class *c* (defaults to 1.0, or is entered from *a priori* knowledge), *Covc* is the covariance matrix of the pixels in the sample of class *c, |Covc|* is the determinant of *Covc*, *Covc-1* is the inverse of *Covc*, ln is natural logarithm function, and *T* is transposition function (ERDAS, 1999).

C4.5 is one of the ways to represent decision tree classification. It divides the data step by step using the available bands or criteria to assign to each node (Figure 3). C4.5 removes unnecessary nodes using pruning. Decision tree computes threshold value using nearest neighbor algorithm to assign to each arc (Pinho et al., 2008). C4.5 algorithm uses gain ratio to select the splitting attribute (Chandra and Paul, 2007).

$$Gain\ Ratio\ (S,A) = \frac{Gain\ (S,A)}{SplitInfo\ (S,A)} \quad (6)$$

where SplitInfo (S, A) is the information due to the split of S on the bases of values attribute of A. Gain (S, A) is the information of example set of S on attribute A (Chandra and Paul, 2007). Figure 3 shows how a land cover such as water, urban class is classified at each node or tree.

Multilayer Perceptron is based on Artificial Neural Networks (ANN) and it contains an input layer, one or more hidden layers, and an output layer (Jensen, 2005). The input layer receives such data as image pixels, DEM, and others. The hidden layer or "brain" of the multilayer perceptron calculates and produces an output. The MLP output is analyzed with the known classes provided during training. Multilayer Perceptron makes no prior assumptions of normal distribution. The MLP equation for forward computation is the following.

$$Vj^{(l)} = \sum_{i=0}^{p} Wji^{(l)}(n) Yi^{(l-1)}(n) \quad (7)$$

where $Yi^{(l-1)}(n)$ is the function signal for neutron i in the previous layer and $Wji^{(l-1)}(n)$ is the weight of neutron j in the layer l (Kumar et al., 2010)

```
B2 <= 38
|  B1 <= 10: W (2118.0/13.0)
|  B1 > 10
|  |  B2 <= 27
|  |  |  B1 <= 11
|  |  |  |  B2 <= 16: A (160.0/5.0)
|  |  |  |  B2 > 16
|  |  |  |  |  B2 <= 17: A (60.0/19.0)
|  |  |  |  |  B2 > 17
|  |  |  |  |  |  B2 <= 18: W (24.0/5.0)
|  |  |  |  |  |  B2 > 18: A (21.0/5.0)
|  |  |  B1 > 11
|  |  |  |  B1 <= 17: A (6308.0/36.0)
|  |  |  |  B1 > 17
|  |  |  |  |  B1 <= 20: A (406.0/31.0)
|  |  |  |  |  B1 > 20: U (6.0)
|  |  B2 > 27
|  |  |  B1 <= 17
|  |  |  |  B2 <= 29
|  |  |  |  |  B1 <= 13: F (32.0)
|  |  |  |  |  B1 > 13: A (67.0/1.0)
|  |  |  |  B2 > 29: F (1462.0)
```

Figure 3: *Structure of C4.5 decision tree*

Stacking combines multiple classification algorithms using a single data set. According to Breiman (1996), stacked regressions is a method for forming linear combinations of different classifiers. The classifiers are divided into base-level and meta-level classifiers (Chen et al., 2009). After each base-level classifier predicts a probability distribution over the possible class value, meta-level classifier combines the obtained predictions (Todorovsci et al., 2003).

$$Pc(x) = ((Pc(c_1|x), Pc(c_2|x), \ldots Pc(c_k|x)) \quad (8)$$

where (c_1, c_2… c_k) is a set of possible class values, and $Pc(c_1|x)$ is the probability that x belongs to class c_j.

According to Steele (2000), combining substantially different classifiers are most useful for classification. For this research in Ethiopia, MLP and C4.5 are relatively different and were combined using stacking regression. The impact of such classifier combination was evaluated.

3.2.2. Accuracy assessment

Land use classification errors may result from image processing errors, registration errors and from spectral inseparability between classes. Classification error is the assignment of a pixel belonging to one category to another category during the classification process (Campbell, 2002). A map requires unbiased representation of the land cover in order to be considered as accurate (Foody, 2002). Accuracy assessment plays a fundamental role in making effective decisions based on maps generated from remote sensing data (Plourde and Congalton, 2003). Therefore, ground truth data collected from field using GPS, satellite images and other sources such as land use map were used to analyze the accuracy of each classification. For this study, two polygon validation sites for each land cover were used. A contingency table was used to analyze producer, user and overall accuracy of the digital classification applied. Besides, a Kappa analysis was also included. Kappa analysis is a measure of the difference between the observed agreement between two maps and the agreement that might be attained solely by chance matching of the two maps (Campbell, 2002). Therefore, this research analyzed kappa coefficient of agreement, overall accuracy, producer, and consumer accuracy. According to Congalton (1991), the equation for KHAT statistic which is an estimate of Kappa analysis can be calculated as:

$$\mathrm{KHAT} = \frac{\sum_{i=0}^{r} \mathrm{Xii} - \sum_{i=0}^{r} (\mathrm{Xia} * \mathrm{Xib})}{N^2 - \sum_{i=0}^{r} (\mathrm{Xia} * \mathrm{Xib})} \quad (9)$$

where r is the number of rows in the matrix; Xii is the number of observation in row i and column I; Xia and Xib are the marginal total of row i and column i, respectively; and N is the total number of observation.

4. Results

In total, 12,229 pixels were used to validate the land cover classification accuracy. These pixels include a sample for water (3,316), urban (2,293), forest (3,183) and agriculture (3,437). The following section presents the classification results for Maximum Likelihood, C4.5, Multilayer Perceptron and Stacking (C4.5 and MLP). The results of each classification algorithms were compared to the original radar data. In addition, classification accuracies were compared among the classification algorithms applied.

4.1. Maximum Likelihood Classifier (MLC)

The original radar image without any enhancement methods produced 66% overall classification accuracy using MLC. The maximum overall accuracy achieved using Median de-speckling and Maximum Likelihood classifier is 86.4% (Table 1). In all de-speckling methods, there is no difference in water classification accuracy because the digital value of water is very different compared to the other land covers. Lee-sigma, Gamma-MAP and Median de-speckling techniques improved the overall classification accuracy by about 15%, 18% and 20% respectively using window size 27×27. This shows overall accuracy improvement to more than 80% by using de-speckling. Increasing window size beyond 27×27 did not increase the overall accuracy result. Lee-sigma produced the lowest percentage increase in overall classification accuracy compared to Median and Gamma-MAP. This may be related to the normal distribution assumption in Lee-sigma. The overall kappa statistic for Median de-speckling at 27×27 window size is 0.82. This is almost 30% increase compared to the unfiltered radar (Figure 5). Overall, these de-speckling techniques have improved the separability of these land cover units.

Urban producer accuracy improved by 58% using Median de-speckling at 27 × 27 window size. Gamma-MAP and Lee-sigma at 27 kernel size also improved urban producer accuracy by 53% and 33% respectively. Similarly, Median, Gamma-MAP and Lee-Sigma at 27 × 27 windows improved the producer accuracy for forest by 38%, 36% and 33% respectively. Agriculture's producer accuracy improved by 5% using Lee-Sigma at this window size. Increasing window size beyond 19*19 decreased the accuracy of agriculture when other filters were used. Median de-speckling produced the best urban producer accuracy in all the window sizes used. Lee-sigma produced the lowest urban producer accuracy (49%). However, Lee-sigma achieved the best agriculture producer accuracy in all window sizes. Besides this, Lee-sigma is the best filter to identify the tree cover within urban land use (Figure 4).

These results indicate that classification accuracy is dependent on the de-speckling technique. Median de-speckling produced 100% urban user accuracy beyond 19 × 19 window size.

Overall, all de-speckling techniques improved urban user accuracy to more than 90%. User classification accuracy for agriculture and forest improved by 45% and 17%, respectively when Median filtering was applied. Only forest user accuracy was below 90% when Median de-speckling at a 27 × 27 window size was applied. Such classification accuracy improvement shows the importance of radar data de-speckling techniques for land use mapping. All de-speckling techniques in this study improved both the overall classification and individual land cover accuracies. Smaller window sizes were best for identifying forest patches within the cities (Figure 4). Increasing window size reduced the forest cover within the city.

Table 1: *Land use classification accuracy matrix using Median de-speckled data at 27 × 27 window size*

	Reference data					
	Water	Urban	Forest	Agriculture	Total	User A. (%)
Water	**3316**	0	0	0	3316	100.0
Urban	0	**1728**	0	0	1728	100.0
Forest	0	565	**2893**	808	4266	67.8
Agriculture	0	0	290	**2629**	2919	90.1
Total	3316	2293	3183	3437	12229	
Producer A. (%)	100.0	75.4	90.9	76.5		
					Overall Accuracy	**86.4%**
					Overall Kappa Statistics	**0.8**

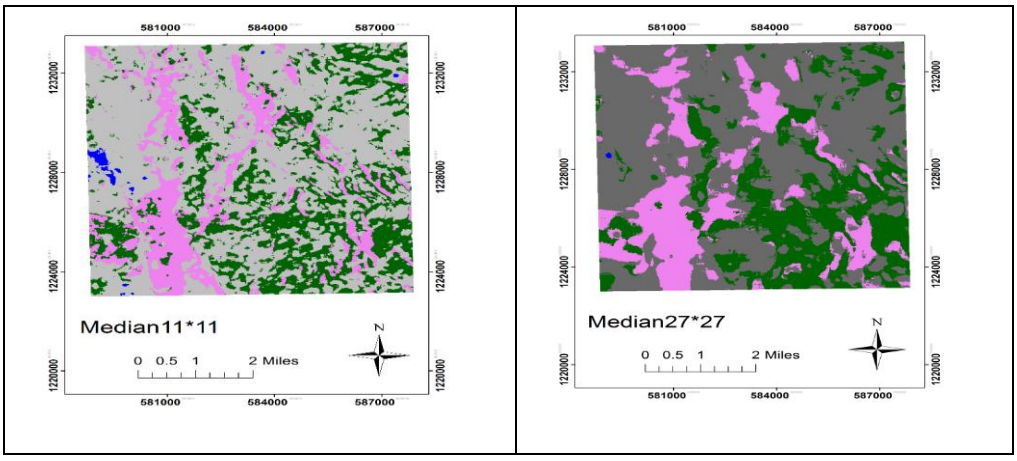

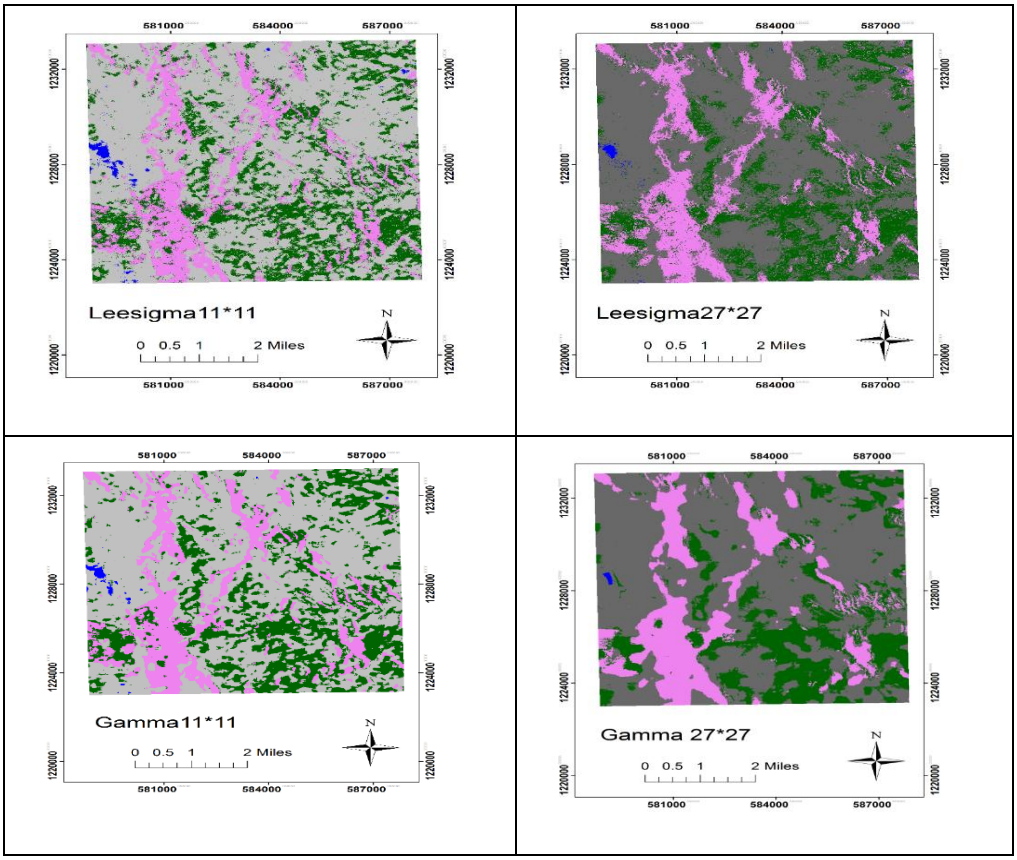

Figure 4: *Land use map using Gamma-MAP, Lee-sigma and Median de-speckling (Urban, pink; Forest, green; Agriculture, grey, and Water, blue)*

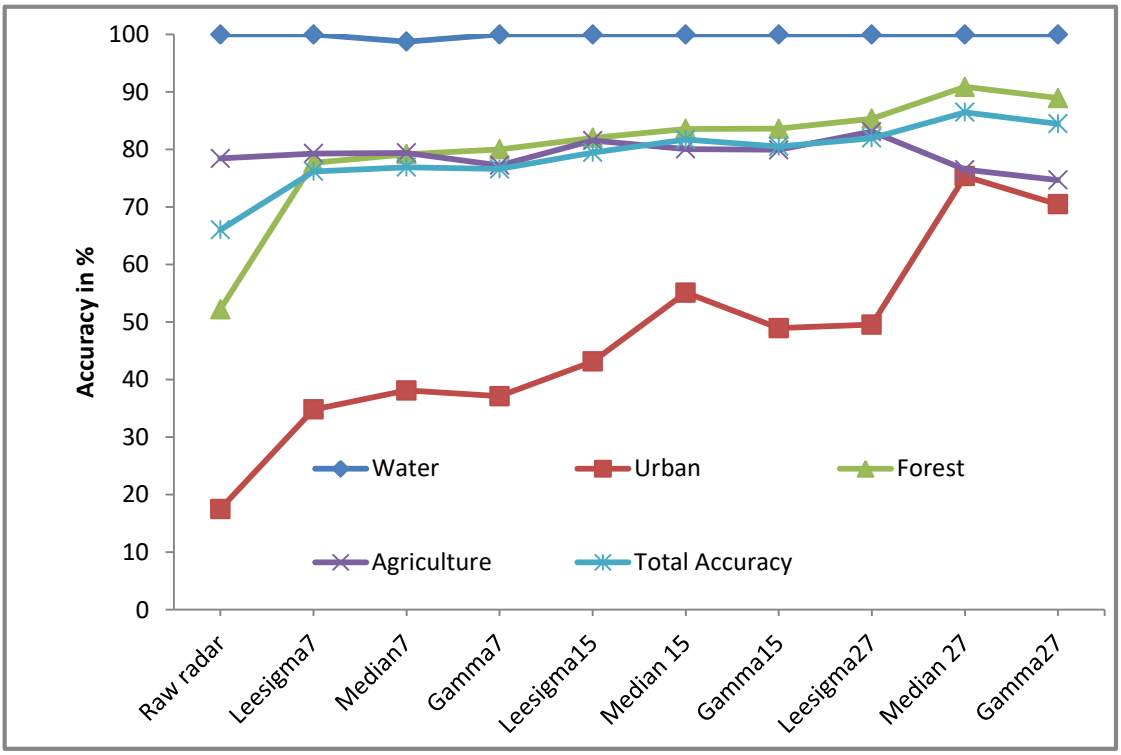

Figure 5: *Original radar and de-speckled image classification accuracy*

4.2. C4.5- Decision tree classifier

The maximum overall land cover classification accuracy achieved using C4.5 classifier and Median de-speckling is 83.3% at a 27 × 27 window size (Table 2). This is 3% lower than the classification accuracy produced by the MLC classifier. The maximum overall classification accuracy at 27 × 27 window size using Lee-Sigma and Gamma-MAP is 82.6% and 83.1% respectively. All the de-speckling techniques used in this study produced more or less the same overall accuracy assessments. However, these speckling suppression methods have different user and producer classification accuracy results. Such variability in classification accuracy indicates the importance of trying different classification algorithm.

Gamma-MAP achieved 94.2% urban producer accuracy using decision tree. This was 30% and 20% higher classification accuracy than the accuracy achieved by Lee-Sigma and Median de-speckling respectively. In all window sizes, Lee-sigma achieved the lowest urban producer accuracy. However, the maximum forest producer accuracy (75%) achieved by the C4.5 classifier was accomplished using Lee-Sigma. Median achieved 90.4% agriculture producer classification accuracy. This agriculture's producer accuracy was 7% greater than Lee-sigma and Gamma-MAP's agriculture producer accuracy. Both classification algorithms (C4.5 and MLC) produced similar urban producer accuracy. However, agriculture producer accuracy improved by 14% when C4.5 was applied. On the other hand, forest producer accuracy is 25% lower than the producer accuracy achieved by MLC classifier (Figure 6). In the C4.5 decision tree classifier, more forest pixels were classified as urban and agriculture compared to the MLC classifier.

Median de-speckling at 27 × 27 window size produced 81.8% urban user accuracy. It was about 11% and 18% higher than the user accuracy result of Lee-Sigma and Gamma-MAP respectively. At this window size, forest has more or less similar user accuracy by all the de-speckling techniques. However, Gamma-MAP produced the highest agriculture user accuracy; and it was 15% and 10% higher than the user accuracies obtained by Median and Lee-Sigma respectively. The maximum urban user accuracy achieved in C4.5 is 18% lower than the accuracy produced by MLC. Forest user accuracy is similar in both classifiers. However, agriculture user accuracy is 10% more in MLC compared to the user accuracy achieved by decision tree. Water user and producer accuracy is the same (100%) in both classifiers at this window size. The maximum kappa coefficient achieved by C4.5 and MLC is 0.78 and 0.82, respectively, when Median at window 27 × 27 was applied.

4.3. Multilayer Perceptron classifier (MLP)

Multilayer Perceptron produced the highest overall classification accuracy (91.2%) using Gamma-MAP in this study site. In all de-speckled radar data, MLP classifier achieved the best overall classification accuracy. The overall classification accuracy using Median and Lee-sigma was 87.3% and 83.5%, respectively (Table 2). This overall accuracy is greater than the classification accuracy produced by both MLC and C4.5 (Figure 5). MLP also achieved the highest overall classification accuracy at all window sizes. MLP achieved the highest forest producer accuracy (91.9%) using Gamma-MAP (Table 2). Agriculture had the highest producer accuracy in MLP classifier using Lee-sigma filtering. Urban producer accuracy improved by 21% when MLP was applied compared to MLC. However, Multilayer perceptron's urban producer accuracy is 2% lower than C4.5 urban producer accuracy. The overall kappa statistic achieved by MLP is 0.88. This is 5% and 10% improvement compared to MLC and C4.5 classifiers, respectively. Table 2 presents the land use confusion matrices for the best overall classification accuracy achieved using C4.5, MLP and Stacking algorithms.

Table 2: *Classification matrices for de-speckled radar data using C4.5, MLP, and Stacking at 27 × 27 window size*

Methods	Classified Image					Producer A. (%)
	Water	Urban	Forest	Agri	Total	
C4.5 & Median						
Water	**3316**	0	0	0	3316	100.0
Urban	0	**1677**	616	0	2293	73.1
Forest	0	322	**2092**	769	3183	65.7
Agri	0	52	279	**3106**	3437	90.4
Total	3316	2051	2987	3875	12229	
User A.	100	81.8	70.0	80.2		
	Overall accuracy and Kappa statistics, 83.3%, 0.78					
MLP & Gamma						
Water	**3316**	0	0	0	3316	100
Urban	0	**2110**	183	0	2293	92
Forest	0	94	**2926**	163	3183	91.9
Agri	0	0	631	**2806**	3437	81.6
Total	3316	2204	3740	2969	12229	
User A.	100	95.7	78.2	94.5		
	Overall accuracy and Kappa statistics, 91.20%, 0.88					
Stacking &Gamma						
Water	**3316**	0	0	0	3316	100
Urban	0	**2098**	195	0	2293	91.5
Forest	0	192	**2784**	207	3183	87.5
Agri	0	0	546	**2891**	3437	84.1
Total	3316	2290	3525	3098	12229	
User A.	100	91.6	79	93.3		
	Overall accuracy and Kappa statistics, 90.70%, 0.87					

4.4. Stacking (C4.5 and MLP)

Stacking C4.5 and MLP classifiers improved the overall classification accuracy by 2% using Gamma-MAP at 7 × 7 window size. The other combinations did not improve the overall classification in this study site. Combining C4.5 and MLP produced 90.7% overall classification accuracy using Gamma-MAP filtering and this is lower than the overall accuracy achieved using MLP alone. Using this de-speckling and combining the two classifiers, only agriculture's producer accuracy improved, and only by 1%. However, both urban and forest producer accuracies decreased, and this affected the overall classification accuracy. The overall kappa statistic is 0.87 in stacking, which is 1% lower than MLP kappa statistic. The maximum classification accuracies achieved using Median and Lee-sigma are 85.1% and 84.1%, respectively, in Stacking method of classification (Figure 6).

5. Conclusion and Discussion

The main aim of this research was to evaluate and compare the performance of classification and radar data filtering techniques. The original radar data without any filtering process produced less valid overall classification accuracy. Therefore, applying enhancement and filtering processes to remove speckle or noise is essential. All image enhancement techniques used in this study produced some significant classification accuracy improvements compared to the original radar data. However, classification accuracy improvements of these image enhancement techniques depend on the type of classification algorithms applied. In this study, the overall and individual land cover classification has improved by applying different filtering techniques.

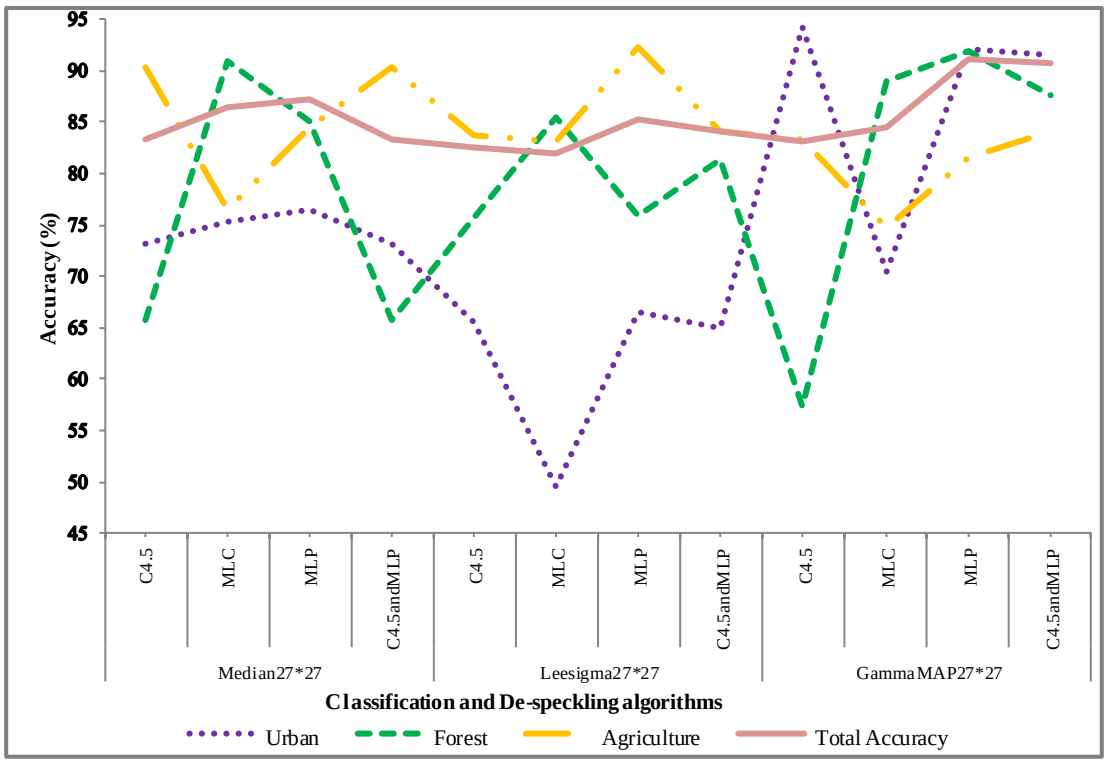

Figure 6: Land use classification accuracy using different speckle filtering and classification algorithms (MLC, C4.5, MLP and stacking)

The highest and the lowest overall classification accuracies in this study were 91.2% and 82.1%, respectively. The highest urban producer accuracy (94%) achieved in Kombolcha was obtained using C4.5 classifier and Gamma-Map de-speckling (Figure 6). However, MLC and Lee-sigma produced the lowest urban producer accuracy (49%) at the 27 × 27 window size. MLP achieved the maximum forest (91%) and agriculture (92%) producer accuracy using Gamma-MAP and Lee-sigma de-speckling respectively. C4.5 and MLC achieved the lowest forest and agriculture producer accuracies, respectively. Overall, the results were dependent on each combination of classifier and filtering techniques applied. The best result in this study was achieved using Gamma-MAP de-speckling and Multilayer perceptron classifier. However, Qiu et al. (2004) found Median filter the best result in speckle reduction.

Enhancement techniques, data source, and classification algorithms have important impacts on the reliability of a given land cover classification map. Therefore, it is very important to apply different combinations of image enhancement techniques and classification algorithms to achieve the best results. Overall, this research study demonstrated that the importance of radar data as an alternative source of remote sensing data for land cover classification and carbon sequestration quantification in Ethiopia and other tropical areas. Past studies have also demonstrated the importance of satellites radars for monitoring and estimating forest change, as well as for flooding detection and quantification and land cover classification (Kuntz and Siegert, 1999; Saatchi et al., 2000; Gaveau et al., 2003). Ethiopia, with inadequately studied physical features, can greatly benefit from the use of radar-based data analysis for its development, land use and environmental plans. The remote sensing data gaps caused by cloud cover and other factors can be filled by radar data in different parts of the world. Further research on the application of radar data for crop classification and forest fire detection may be useful. Besides this, additional research on polarization, post classification filtering, texture, data fusing and other data mining techniques may be important to further analyze radar data applications.

5.1. Comparison among different de-speckling techniques

All the de-speckling techniques used in this research study improved the classification accuracy. Speckle algorithms can produce satisfactory results when used properly (Nyoungui et al., 2002).The overall classification accuracy improvement using Gamma-MAP 27 × 27 was 25% higher compared to unfiltered radar data (Table 2). The other filtering techniques, Median and Lee-sigma also improved the overall classification by 20% and 17% respectively. In this study area, Lee-sigma de-speckling achieved the lowest overall classification accuracy. Lee-Sigma assumes normal distribution among the land cover units and this may lead to the lower overall classification compared to the other speckle filtering techniques. Overall, increasing window size from 7 × 7 to 27 × 27 increased the overall classification accuracy. However, increasing window size beyond 27 did not improve the overall accuracy. This may be due to the fact that de-speckling may also degrade the digital number of each pixel which has an impact on land use classification when increased beyond an ideal size.

The impacts of these speckling techniques on producer and user accuracy of each land cover units were different. The significant effect of de-speckling techniques was on urban producer and use accuracy. The validation results emphasized the importance of image enhancement methods on radar data for better land use classification. Without these image noise filtering techniques, the classification results achieved by the original PALSAR radar data would be less useful for policy decisions. Besides this, the classification accuracy result of each data sources was also dependent on type of filtering applied. Such improvements in the overall classification accuracy showed that PALSAR radar data can provide an enormous potential to study land cover, deforestation, and crop classification in tropical areas where optical data collection is restricted due to cloud cover.

5.2. Comparison among different classification algorithms

This study also analyzed the effectiveness of factoring in the different classification algorithms. The highest classification accuracy achieved by MLC, C4.5, MLP and Stacking were 86.4%, 83.3%, 91.2% and 90.7%, respectively (Table 1 and 2). Such overall classification is good and very important for tropical areas. Where cloud cover limits the availability of optical data, 78% overall accuracy using radar data is very useful (Idol et al., 2015). This study by fur demonstrated above 85% overall classification accuracy. The stacking method also improved the overall classification accuracy by 2% using a smaller window size (7 × 7). Overall, different machine learning techniques have contributed to varied but improved classification accuracy. The results achieved using different classifiers were, however, comparable. This indicated that other data mining techniques can be effectively used for land use classification in addition to the Maximum Likelihood classifier. Yuan et al. (2009) also recommends supervised MLP. However, Multilayer Perceptron, C4.5 and Stacking methods require more time to prepare and classify the data than Maximum Likelihood classifier (MLC). This study has indicated that the classification accuracy improvements may be dependent on the type of classification and filtering algorithms applied. Overall, Multilayer perceptron achieved the best classification in this study and further research should apply in to other study areas. In conclusion, landscapes are not homogenous, and different combinations of classifiers and pre-processing techniques will achieve the best results.

Acknowledgments

The authors would like to thank NASA and Alaska Satellite facility for providing and funding the radar images.

References

Badege, B. Deforestation and land degradation on the Ethiopian highlands: A strategy for physical recovery. *Northeastern African studies*. 2001. 8 (1) 7-26.

Berhane, A., Totland, Ø., Haile, M., and Moe, S.R. Intense use of woody plants in semiarid environment of Northern Ethiopia: Effects on species composition, richness and diversity. *Journal of Arid Environments*.2015. 114; 14-21.

Bewket, W. Land Cover Dynamics since the 1950s in Chemoga Watershed, Blue Nile Basin, Ethiopia. *Mountain Research and Development.* 2002. 22; 263-269.

Breiman, L. Stacked regressions. *Machine Learning*. 1996. 24; 49-64.

Capstick, D., and Harris, R. The effects of speckle reduction on classification of ERS SAR data. *International Journal of remote sensing*. 2001. 22 (18) 3627-3641.

Campbell, J.B., 2002: Introduction to remote sensing, third edition. The Guilford Press, New York.

Chandra, B., and Paul, P. Prediction of forest cover using Decision tree. *Ind. Soc. Agri. statistics*, 2007. 61 (2) 192-198.

Chen, J., Wang, C., and Wang, R. Using Stacked Generalization to Combine SVMs in Magnitude and Shape Feature Spaces for Classification of Hyperspectral Data. *IEEE, Transactions on Geoscience and remote sensing*. 2009. 47 (7) 2193-2205.

Congalton, R.G. A review of Assessing the Accuracy of Classifications of Remotely Sensed Data. *Remote Sens. Environ*, 1991. 37; 35-49.

Darbyshire, I., Lamb, H., and Umer, M. Forest clearance and regrowth in northern Ethiopia during the last 3000 years. *The Holocene*. 2003. 13; 537-546.

DeFries, R.S., Rudel, T., Uriarte, M., and Hansen, M. Deforestation derive by Urban population growth and agricultural trade in the twenty first-century. *Nature Geoscience.* 2010. 3; 178-181.

DeFries, R.S., and Chan, J.C. Multiple Criteria for Evaluating Machine Learning Algorithms for Land Cover Classification from Satellite Data. Remote Sens. Environ. 2000. 74; 503-515.

Dessie, G., and Kleman, J. Pattern and Magnitude of Deforestation in the South Central Rift Valley Region of Ethiopia. *Mountain Research and Development*. 2007. 27 (2) 162-168.

ERDAS, 1999: ERDAS Imagine field guide fifth edition, revised and expanded. Atlanta, Georgia.

Emrahoglu, N., Yegingil, I., Pestemalci, V., Senkal, O., and Kandirmaz, H.M. Comparison of a new algorithm with the supervised classification. *International Journal of Remote Sensing*. 2003. 24 (4) 649-655.

Foody, G.M. Status of land cover classification accuracy assessment. *Remote Sensing of Environment.* 2002. 80; 185-201.

Friedl, M.A., and Brodley, C.E. Decision Tree Classification of Land Cover from Remotely Sensed Data. *Remote Sensing of Environment*. 1997. 61; 399-409.

Gaveau, D.L.A., Balzter, H., and Plummer, S. Forest woody biomass classification with satellite based radar coherence over 900 000 km^2 in Central Siberia. *Forest Ecology and Management*. 2003. 174; 65-75.

Getu, Z., and Hurni, H. Implications of Land Use and Land Cover dynamics for mountain resource degradation in the northwestern Ethiopian highlands. *Mountain Research and Development*. 2001. 21; 184-191.

Jenson, J.R., 2005: Introductory Digital Image Processing: A Remote sensing Perspective. Third edition. Pearson Prentice Hall. Upper Saddle River, NJ, USA.

Idol, T., Haack, B., and Mahabir, R. Comparison and integration of space borne optical and radar data for mapping in Sudan. *International Journal of Remote Sensing*. 2015. 36 (6) 1551-1569.

Kumar, U., Kerle, N., and Punia, M. Mining Land Cover Information Using Multilayer Perceptron and Decision Tree from MODIS Data. *J Indian Soc. Remote Sens*. 2010. 38 (4) 592-603.

Kuntz, S., and Siegert, F. Monitoring deforestation and land use in Indonesia with multitemporal ERS data. *International Journal of Remote Sensing*. 1999. 20; 2835-2853.

Maghsoudi, Y., Collins, M.J., and Lecki, D. Speckle reduction for the forest mapping analysis of multi-temporal Radarsat-1 images. *International Journal of Remote Sensing*. 2012. 33 (5) 1349-1359.

Nyoungui, A., Tonye, E., and Akono, A. Evaluation of speckle filtering and texture analysis methods for land cover classification from SAR images. *International Journal of remote sensing*. 2002. 23 (9) 1895-1925.

Noriega, J.R.R., and Fabian, D.L. Spatial Filtering of Radar Data (RADARSAT) for Wetland (Brackish Marshes) Classification. *Remote Sensing of Environment*. 2000. 73; 143-151.

Pal, M., and Mather, P.M. An assessment of the effectiveness of decision tree methods for land cover classification. *Remote Sensing of Environment*. 2003. 86; 554-565.

Patz, J.A, Daszak, P, Tabor, G.M, Aguirre, A.A, Pearl, M, Epstein, J, Wolf, N.D, Kilpatrick, A.M, Foufopoulos, J., Molyneux, D., and Bradley, D.J. Unhealthy Landscapes: Policy Recommendations on Land Use Change and Infectious Disease Emergence. *Environment Health Perspectives*. 2004. 112 (10) 1092-1098.

Pinho, C.M.D., Silva, F.C., Fonseca, M.C, and Monteiro, A.M.V. 2008. Intra-urban Land Cover Classification from high resolution images using C4.5 Algorithm. *The International Archives of the Photogrammetry, Remote Sensing and Spatial Information Sciences.2008.* 37(B7) 695-699.

Plourde, L., and Congalton, R.G. Sampling Method and Sample Placement: How Do They Affect the Accuracy of Remotely Sensed Maps? *Photogrammetric Engineering & Remote Sensing*. 2003. 69 (3) 289-297.

Qiu, F., Berglund, J., Jensen, J.R., Thakkar, P., and Ren, D. Speckle noise reduction in SAR imagery using adaptive median filter. *GIScience and Remote Sensing*. 2004. 41 (3) 244-266.

Saatchi, S.S., Nelson, B., Podest, E. and Holt, J. Mapping land cover types in the Amazon Basin using 1 km JERS-1 mosaic. *International Journal of Remote Sensing.* 2000. 21; 201-1234.

Souza, Jr. C., Firestone, L., Silva, L.M., and Roberts, D. Mapping forest degradation in the Eastern Amazon from SPOT 4 through spectral mixture models. *Remote Sensing of Environment*. 2003. 87; 494-506.

Soria-Ruiz, J., Fernandez-Ordonez, Y., and Woodhouse, I.H. Land-cover classification using radar and optical images: a case study in Central Mexico. *International Journal of Remote Sensing*. 2010. 30 (12) 3291-3305.

Steele, B.M. Combining Multiple Classifier: An application using Spatial and Remotely Sensed Information for land Mapping. *Remote Sensing of Environment*. 2000. 74; 545-556.

Taddese, G. Land Degradation: A Challenge to Ethiopia. *Environmental Management*. 2001. 27 (6) 815-824.

Tekle, K., and Hedlund, L. Land cover changes between 1958 and 1986 in Kalu District, southern Wello, Ethiopia. Mountain Research and Development. 2000. 20 (1) 42-51.

Todorovsci, L., and Dzerosci, S. Combining Classifiers with Meta Decision trees. Machine learning. 2003. 50; 223-249.

Yuan, H., Van Der Wiele, C.F., and Khorram, S. An Automated Artificial Neural Network System for Land Use/Land Cover Classification from Landsat TM Imagery. *Remote Sensing*. 2009. 1; 243-265.

Cloud Publications
International Journal of Advanced Remote Sensing and GIS
2017, Volume 6, Issue 1, pp. 1988-1993
ISSN 2320 – 0243, doi:10.23953/cloud.ijarsg.29

Research Article | Open Access

Image Compression Based on Multilevel Adaptive Thresholding using Meta-Data Heuristics

Gowri Sankar Reddy D[1] and Veera V.C. Reddy[2]

[1]ECE Department, S V University College of Engineering, Tirupati, Andhra Pradesh, India
[2]EEE Department, S V University College of Engineering, Tirupati, Andhra Pradesh, India

Publication Date: 5 January 2017

DOI: https://doi.org/10.23953/cloud.ijarsg.29

Abstract Satellite image processing involves very often the need of compression. The compression of satellite images will reduce storage requirements and conserves transmission bandwidth. In this paper, a lossy image compression method is proposed based on multilevel adaptive thresholding using Meta-Data heuristics to compress the Landsat-8 satellite images. In the proposed method the number of thresholds is fixed in accordance with the bitrate required and the Peak Signal to Noise Ratio (PSNR) is improved by entropy based adaptive thresholding. Test image of Landsat-8, Band 3, 5 is used for performing the compression and the performance metric PSNR is measured for uniform thresholding and the proposed method. The proposed method gives improvement in the PSNR and the method is computationally simulated using Fixed Point Binary scaling.
Keywords *PSNR; BPP; DN (digital numbers); Threshold*

1. Introduction

Satellite image data is very memory thirsty, a typical Lansat-8 image with 11 bands, requires memory in the order of 2.4GB. This drives a search for better image compression algorithms. Wallace (1992) explained JPEG compression standard which ruled the technology for years for performing compression. JPEG standard is based on DCT (Discrete Cosine Transform) and is having advantages of real transform. The JPEG methods have limitations like blocking artifact at low bitrates, Huffman table requirement for low bitrates. The JPEG 2000 (ISO, 2000) method is based on wavelet; this method offers better resolution scalability, better PSNR at low bit rates. This method has limitations like ringing effect.it was explained that the histogram influences threshold selection and the better thresholds will reduce intra and inter class variances (Otsu, 1979). Sahoo (1988) explored different thresholding methods. Sujoys (2014) approach of image compression based on multilevel thresholding and the entropy was maximized using differential evolution. Kapur (1985) worked on gray-level picture thresholding using the entropy of the histogram. Borodkin et al. (2006) explained that Lloyd-Max quantization gives better results in non-uniform quantizers. In the course of time several evolutionary algorithms have originated based on thresholding of images. Landsat images are of sizes 7811 x 7641, 16 bit length with the intensity variation of 0-65535 (Wuldaer, 2014).

In our method we proposed a method to compress Landsat-8 images based on non-uniform thresholding.

2. Uniform Thresholding Method

The Thresholding technique basically makes an approximation of the image histogram by properly choosing the set of thresholds, when the image is thresholded into n+1 levels only; log2(n+1) bits are required to represent the image. In our work we used Band 3 & Band 5 for compression. The thresholds are stored in an array, and used as metadata for decoding. The variable bit rate is obtained by varying the number of bits n.

Geo Tiff Information of Band 5

File Mod Date: '08-Mar-2014 13:42:26'
File Size: 119430538, Format: 'tif',
Height: 7811, Width: 7641, Bit Depth: 16,
Color Type: 'grayscale'
PCS: 'WGS 84 / UTM zone 44N'
Projection: 'UTM zone 44N'
Map Sys: 'UTM_NORTH'
Zone: 44, CT Projection: 'CT_Transverse Mercator'
GCS: 'WGS 84', Datum: 'World Geodetic System 1984'
Ellipsoid: 'WGS 84', Semi Major: 6378137,
SemiMinor: 6.3568e+06, PM: Greenwich', PM Long to Greenwich: 0
UOM Length: 'meter', UOM Length in Meters: 1,
UOM Angle: 'degree'
UOM Angle in Degrees: 1

In Figure 1 the typical histogram of the image Band 5 is shown and Digital Numbers (pixel values) frequency is plotted.

The simple method of uniform thresholding is obtained on the histogram and the image gray value is rounded to the nearest threshold.

Step size = (r-p)/2^n (1)

where p=minimum intensity level, r=maximum intensity level, n=number of bits to address the thresholds.

3. Proposed Method

The typical histogram of band-5 is shown in the Figure 1. The Figure reveals the pixel variation is from p=5744 to r=55417. The probability density plot of Band 5 is shown in the Figure 2. Mostly the Probability density function plot of Landsat 8 images appears to be Laplacian distribution. The distribution is broadly classified in to two categories. The first one which covers the area of probability density functions from μ- σ to μ+ σ. Most of the slope of the curve is obtained in this region. The second region is rest of the region of probability density function.

The threshold assignment of first category is chosen such that the number of step levels n_1 is nearly double to that of uniform step size. This increases the entropy in the granular region. The rest of the thresholds are fixed according to the slopes of the curve of the Probability density function. The

thresholds n_2, n_3 are obtained based on equation 4 and the thresholds are fixed with weighted average method as show in equation 5 for obtaining entropy maximization.

The proposed method is simulated in Matlab 2013a, Intel® core™ (i5-4460) using fixed point Binary scaling. The results are shown in the Table 1. The PSNR is calculated from the equation 6. It is seen from the results nearly 3db gain is obtained when compared with the uniform quantizer. The original image of band 5 at 16 bits per pixel is shown in the Figure 4 and the reconstructed image of band 5 at 8 bits per pixel is shown in Figure 5. The average encoding time is nearly 350 seconds and average decoding time requires decoding time is nearly 5 seconds.

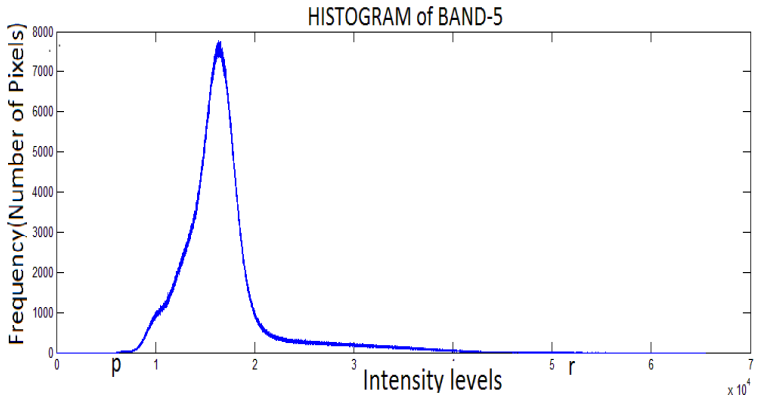

Figure 1: *Histogram of Band-5*

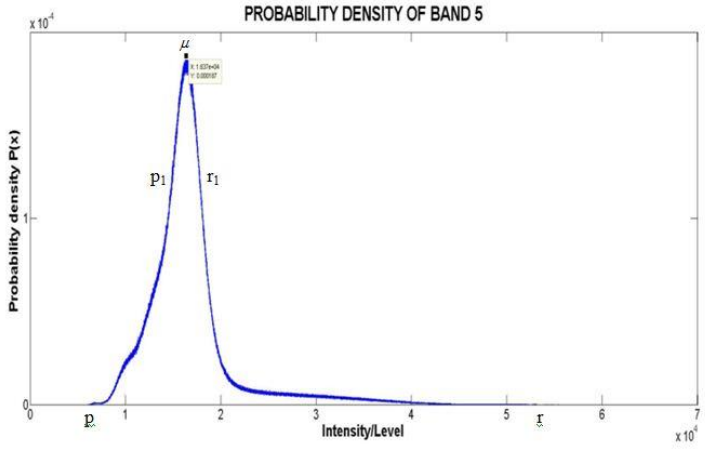

Figure 2: *Probability Density of Band 5*

Laplacian Distribution Equation

$$P(x)=\frac{1}{2b}e^{-|x-\mu|/b} \qquad (2)$$

μ =mean, σ=standard deviation =sqrt(2) * b.

$$p1 = \mu - \sigma,\ r1 = \mu + \sigma. \qquad (3)$$

$$\frac{n_2}{n_3} = \frac{\sum_{p}^{p_1} p(x)}{\sum_{r_1}^{r} p(x)} \qquad (4)$$

Where n_2 = number of levels from p to p_1.
n_3 = number of levels from r_1 to r.
n_1 = numbers of thresholds in the first region form p_1 to r_1.
nt = total number of thresholds.
Total levels=n_1 +n_2+n_3.

A typical values for n_t =255, n_3=131, n_1=76, n_2=48

$$T = (\sum p(x)*x)/ \sum p(x) \qquad (5)$$

$$PSNR = 10\log10(R^2/MSE) \qquad (6)$$

$$MSE = \frac{\sum_{MN}[I(m,n) - C(m,n)]^2}{(M*N)}$$

where M=number of rows, N= number of columns
I= original image, C= reconstructed image
R= 65535.

Table 1: *Calculated PSNR*

Band 3				Band 5			
Uniform method		Proposed method		Uniform method		Proposed method	
Bits per pixel	PSNR In db	Bits per pixel	PSNR In db	Bits per pixel	PSNR In db	Bits per pixel	PSNR In db
4	40.1	4	45.5	4	37.8	4	41
5	46.2	5	51.7	5	44.3	5	47.1
6	52.1	6	56.8	6	50.6	6	53.2
7	58.1	7	62.8	7	56.7	7	59.3
8	64.1	8	68.6	8	62.8	8	66.23

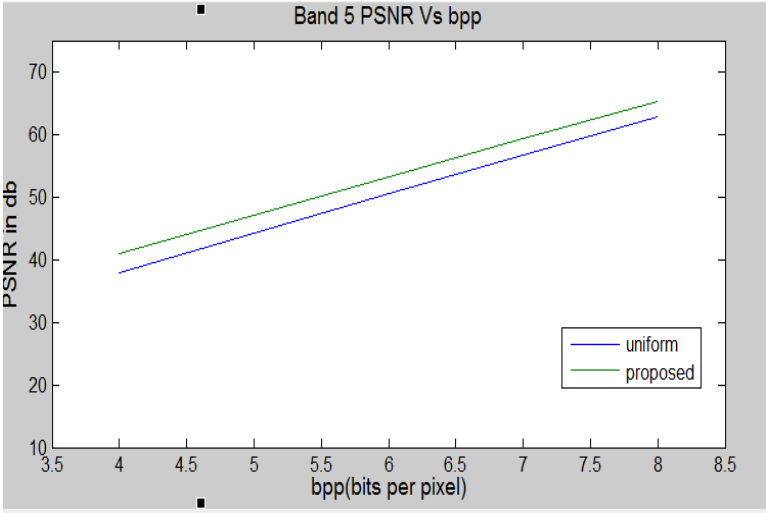

Figure 3: *Band 5 PSNR Vs bpp*

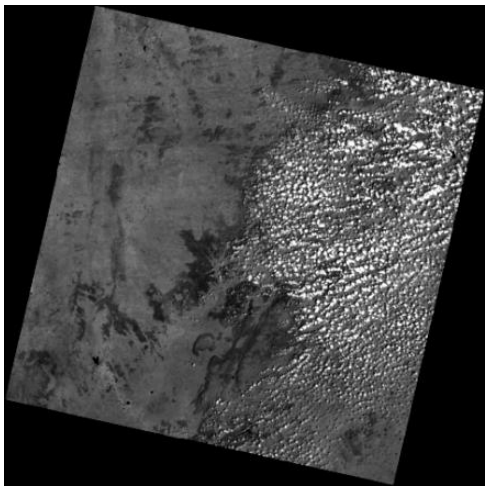

Figure 4: *Original image of band 5 at 16 bits per pixel*

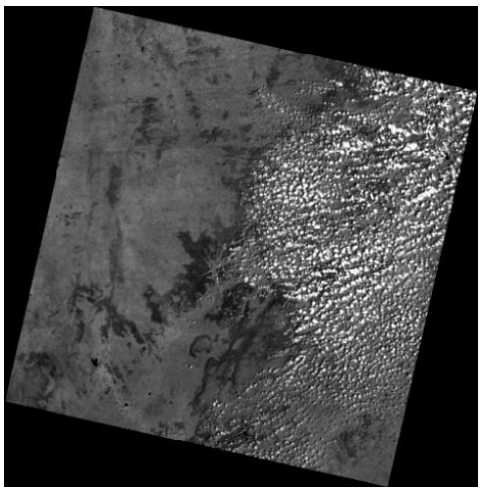

Figure 5: *Reconstructed image of band 5 at 8 bits per pixel*

Discussion

Since satellite images conserves bandwidth and are memory thirsty, the image compression plays a vital role in satellite image processing several things like memory requirements, computational complexity and retrieval time are to be considered for designing of satellite image compression algorithms. In our work we proposed method based on adaptive thresholding method and the method appeals in terms of variable bitrate and less retrieval time.

Conclusion

The proposed method gives better PSNR than the uniform quantization. Hence for Landsat images the proposed method can be applied to improve the PSNR for different bitrates. The proposed method for a compression rate of 8 bits per pixel has advantages like less retrieval time, non-requirement of an exclusive compiler and the PSNR is merely lossless.

References

Wallace, G.K. *The JPEG Still Picture Compression Standard.* IEEE Transactions on Consumer Electronics. 1992. 38 (1) xviii-xxxiv.

ISO, 2000. *Information Technology-JPEG 2000 Image Coding System-Part 1: Core Coding System*. ISO/IEC 15444-1:2000(E).

Otsu, N. *A Threshold Selection Method from Gray Level Histograms*. IEEE Transactions on System, Man and Cybernetics. 1979. 9; 62-66.

Sahoo, P.K., Soltani, S., Wong, A.K.C., and Chen, Y. *A Survey of Thresholding Techniques.* Computer Vision Graphics Image Processing. 1988. 41; 233-260.

Sujoy Paul and Bitan Bandyopadhyay, 2014: *A Novel Approach for Image Compression Based on Multi-Level Image Thresholding using Shannon Entropy and Differential Evolution.* Proceeding of the 2014 IEEE Students Technology Symposium, Kharagpur. 28, February - 2, March. 56-61.

Kapur, J.N., Sahoo, P.K., and Wong, A.K.C. *A New Method for Gray-Level Picture Thresholding using The Entropy of the Histogram*. Computer Vision Graphics Image Processing. 1985. 29; 273-285.

Borodkin, S.M., Borodkin, A.M., and Muchnik, I.B. *Optimal Requantization of Deep Grayscale Images and Lloyd-Max Quantization.* IEEE Transactions on Image Processing. 2006. 15 (2) 445-448.

Roy, D.P., et al. *Landsat-8: Science and Product Vision for Terrestrial Global Change Research.* Remote Sensing of Environmental. 2014. 145 (5) 154-172.

Cloud Publications
International Journal of Advanced Remote Sensing and GIS
2017, Volume 6, Issue 1, pp. 2001-2005
ISSN 2320 – 0243, Crossref: 10.23953/cloud.ijarsg.34

Review Article | Open Access

Urban Ecological Balance and Planning by Applying the Methods of Bioregionalism

Jenitha Jerome

Department of Environmental Sciences, All Saints' College, Thiruvananthapuram

Publication Date: 5 January 2017

DOI: https://doi.org/10.23953/cloud.ijarsg.34

Abstract Bioregionalism is an interdisciplinary that examines interconnections and framework, determined to form a whole or complete picture of a geographically specific region. Natural balance, government, humanity, society, terrain, economics and history are all the fundamental aspects of place and integral to bioregional analysis. Bioregionalism recognizes the human place within, not outside the environment. This kind of understanding of place is essential for creating sustainable urban areas (Kate Matysek, 2004). India is an economically developing country, the phases of our country is also changing in many ways. As it grows the Carbon emission - Green House Gas is being increased which is due to urbanization and expansion of Industries which automatically reduces and pollutes the precious resources such as Water, Air, Land and Biomass. The reduction of biomass automatically is a key reason for Climate Change. Though these changes are happening worldwide, India has its vital role in this by ranking 4th in the world by emitting approximately 2,00,08,333 Kgs/Year. The associations between sustainability of the environment and new urban design are concentrated and the Urban Bioregionalism is proposed through this paper. The concept bioregionalisation is to design or to develop the city as the green city with reducing greenhouse gas. In this concept we propose three different policies which are i) Government Policy, which discusses about the part of government works and rules to develop for expanding cities. ii) Public Orientation, this explains how a group of people such as activity clubs to co-operate each other and work on Environment Sustainability. iii) Individual Activities, is to discuss how each individual have to work on waste management and reducing the greenhouse gas emission (Luccarelli, M., 1995). As we know Sustainable development over the Environment which is defined as development that meets the needs of the existing without destroying the ability of forthcoming generations to encounter their own needs. Hence, urban bioregionalisation helps to balance the ecosystem in future.
Keywords *Ecosystem; Climate Change; Sustainability; Bioregionalism; Urbanization; Biomass; Policies*

1. Introduction

Human activities take place in the circumstance of certain types of associations between the social order and the bio-physical world and there is a great implication in understanding the ethical values of different groups around the world. These flairs perceive "different evidence, imperatives, and

problems, and prescribe different solutions, strategies, technologies, roles for economic sectors, culture, governments, and ethics. Today, whether in growth or decline, cities are faced with regulatory requirements and disintegrating infrastructure. Incremental urban restructuring of localities through planning and designing to the specifics of local ecology has the potential to restore a balance between urban areas and natural systems. Such planning and design would reconsider current patterns of locality development and the public's relationship to urban greenspace that perpetuate the separation of human and natural systems.

Urban inhabitants in the developed countries is detached from the environment and its natural, to a certain extent as a effect of issues of urban form and standard of living choice. This substantial separation of human and natural systems has exposed urban residents from the consequences of their performance for the environment, with a subsequent lack of general environmental acquaintance and perceptive of Earth's life-sustaining processes. This extrication has been recommended to provide communal attitudes that have led to over utilization of natural resources and deprivation of the Earth. Urban development is enhanced in infrastructures of concrete and pavement. In these environments, little contemplation is waged to minor level amalgamation of nature and nature activities at the neighbourhood and community level that might allow for recurrent contact among humans and other group of living beings, and consequent environmental knowledge and community building (Brulle, R., 2000 et al.). Integrating nature and natural systems into the built environment while simultaneously nurturing active civilian involvement in those and other natural systems has the impending to bring about environmental responsiveness and community identity. This in turn might bestow to an overall environmental ethic, whereby people would comprehend local conservationism and perform in ways that do not contribute to environmental decrepitude. Such an ethic might eventually lead to sustainable and durable patterns of urban living. A numeral hypothetical idea provides frameworks for refining the environmental ethic, including environmental education, experiences in nature active community commitment, ecological urban design and bioregional values.

2. Aims and Objectives of the Study

1) Ecological Sustainability
2) Controlling the emission of green gas
3) Green City Management towards 22nd Century
4) Biomass balance and Lost rate
5) Policies to develop green City

3. Methodology

Urban Bioregionalism is a representation of arising changes toward sustainable urban expansion and retrofit proposed to commence fundamentals of bioregionalism into existing cities. This review intends an iterative method for incremental changes towards an altered association between humans and nature through new ways of living and involving with nature (Steiner, F.). Through neighbourhood stewardship and the social activities the changes to the sustainable environmental and through the participation of the individuals that place in the substantial realm. Urban bioregionalism implements and broach bioregional principles of sagacity of consign and community, ecological responsiveness, dynamic contribution, stewardship, perceptible natural systems, and green cities.

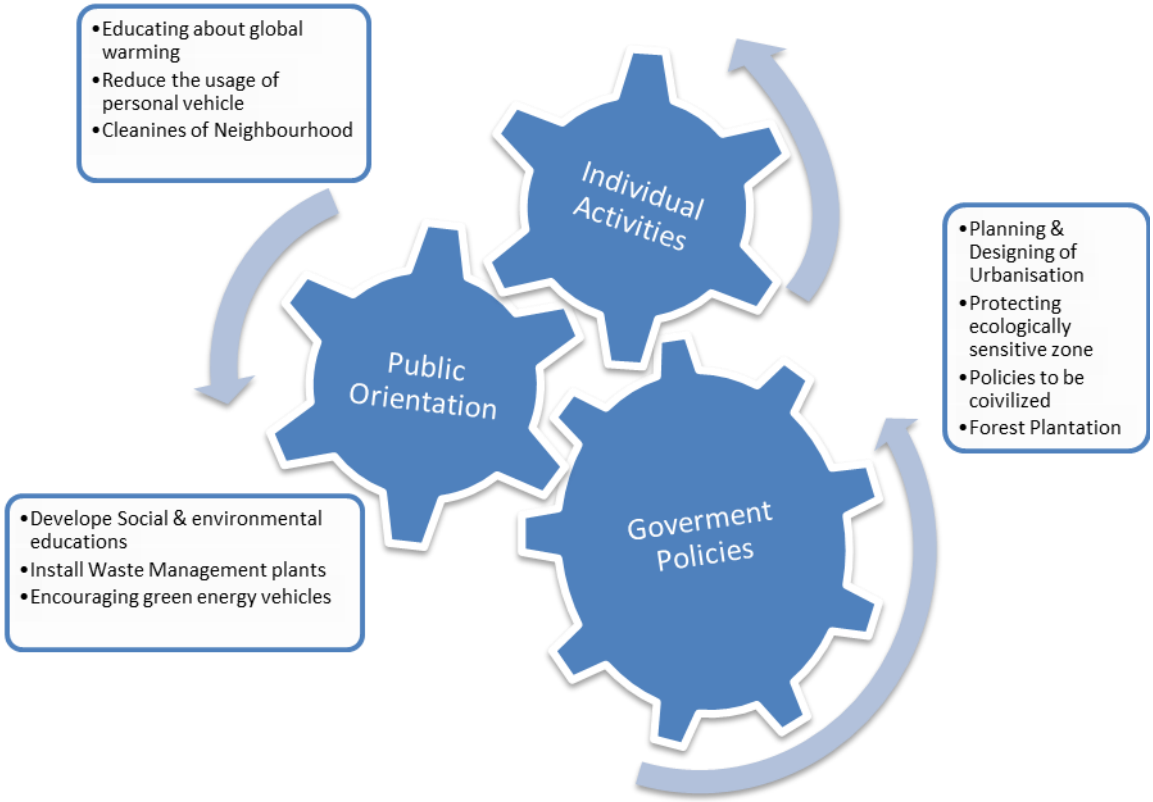

4. Government Policies

By considering the environmental changes instead of planning the disaster & drought management it is always better to prevent those disasters. The government should develop the policies and programs to apply in the principles of Urban Bioregionalism and also ensure the provision of resources for further planning of environmental sustainability. There are many policies developed by the scientist who have done many research over the sustainability of the environment. In such way HLWG report by Dr. Kasthuriranagan and many scientists had developed few policies to protect the biological substantial of the Western Ghats. In such way few more policies can be developed by the scientific advisor or by the suggestion of environmentalist. The policies and rules should be developed as it shapes the incremental changes over the ecological sustainability. These policies should reflect opportunities for nature actions through the support or execution of public programs such as community parks, forest plantation, ongoing nature maintenance, Waste management, Waste water treatment plants, and other environmental; restoration projects (Beatley, T., 2011). There should be rules made to real estate and construction business as their project should not disturb the ecological system or at least consideration of balancing the ecological system. The government should make the policies as such the wetlands and the natural reservoirs should be protected. By implementing specific bioregional projects such as water shed management, waste management while approving urban expansion. Decisions should be made as the Urban sprawl should not defect the ecological conservations.

5. Public Orientation

As there are many environmental activists and servicing clubs are available, they could take chances to enhance the urban sprawl and bio-regionalization of urban. The importance of daily activities in shaping people's experiences requires that urban bioregionalism be focused on the local scale of the neighbourhood, the community. The physical realm of the neighbouring environment is the background for living experiences. The orientation and the stewardship could be like the followings

- Restoration of neighbouring parks

- Installing new parks in the neighbourhood
- Team should be formed to collect the house hold wastes and to clean the surrounding
- Educating about personal Organic Farming

Through these experiences, Installing and maintaining the parks will help to reduce the carbon gas which is around or the in the neighborhood (Andersson, E. et al.). The waste collectors are should be the organization which converts or recycle the collected waste such as bio waste can converted as natural fertilizers and the plastics can be recycled. Hence it will not affect the neighbourhood in forthcoming days. The organic farming and the plantations, as it will provide the food for the personal consumption. The identity of the place is the identity of the community, the identity of the community is how they behave the neighbours and the cause of the neighbourhood. The clubs in the surrounding location are the responsible for the cause and loss of the sustainable environment. This should be fostered and educated to the upcoming generation, it is also where social and environmental learning occurs Barlett, P. (Ed.) (2005).

6. Individual Actions

Individual actions should be reflecting in the transformation and as the learning actions of implementing the bio-regionalization. Every person should have three essential policies to sustain the environment of their own surroundings. The policies are explained as they follow:

a) Resistance
b) Renewal
c) Restoration

If these are followed by every person in urban life style the future will not be counting the green city in fingers. Resistance: it is to resist yourself from continues demolishing of the natural system and the brutal consistent of general ethnicity; as explained in "*Living by Life: Some Bioregional Theory and Practice", Jim Dodge.* Renewal: Implementing the activities and developing the knowledge to achieve the recovery of the ecological system. This can be done by extra efforts of every individual such as i) installing rain water collector method, ii) building the house with proper drain system, as it should not affect other water bodies in your surroundings, iv) organic farming for your own consumption, v) tree plantation in your surrounding and maintaining it. By doing this it will automatically develop the connection between you and the natural system, this tends to protect the environment. Restoration: It is the process where you restore the past destructed natural activities; this can be done by installing bird breeding nest and the facilities for them. Convert your backyard as a sanctuary gets connected with nature helps you to bond with neighbors and wildlife (Church, S.P., 2013). Individual actions can be subjective through brooding and renovate learning processes during or following neighbourhood-oriented stewardship activities, or by public discourse. The bioregional urbanism representation includes a mutual arrow to illustrate an association between neighbourhood-oriented stewardship and individual actions. Such actions contribute to the environmental learning of others while influencing personal behaviours within their own daily lives (Newman, L. et al., 2009).

7. Conclusion

As much as engorgement of urban is increasing, the other natural resources are automatically in state of decrease. This leads to economy crisis of the country. When the ecological balance cannot be protected or maintained it obviously end at economical disaster. As we have to import most of the raw materials from other countries. To avoid the crisis of our ecology and the economy I suggested the government or the planners and each and every civilians to follow the management plans as I proposed above. It encourages the accessibility of the natural system and the life style, further more it increases the implementation of bioregionalization ideals in higher dwellers. Although the management plans may seem simplistic in terms, it can provide the platform for Urban planner. As those policies

discussed where to recreate a connection between the natural system and Urban dwellers. There might be the difficulties to follow these plans as per the reality. But the small-scale of planning to sustain the environment can be achievable. Besides the development of the balance between the Urban life style and the Environmental sustainability the future generations have to be educated to protect the natural attributes and to develop the Urban forest. It might create the pride of ownership by understanding the ecological system.

References

Andersson, E. et al. Reconnecting cities to the biosphere: stewardship of green infrastructure and urban ecosystem services. *Ambio.* 2014. 43 (4) 445-453.

Barlett, P. (Ed.) (2005). Urban Place. Cambridge, MA: MIT Press.

Beatley, T., 2011: Biophilic Cities: Integrating Nature into Urban Design and Planning. Washington, DC: Island Press.

Brulle, R., 2000: Agency, Democracy, and Nature: the U.S. Environmental Movement from a Critical Theory Perspective. Cambridge, MA: The MIT Press.

Carr, M., 2004: Bioregionalism and Civil Society, Democratic Challenges to Corporate Globalism. Vancouver: UBC Press.

Jim Dodge: Living by Life: Some Bioregional Theory and Practice.

Kate Matysek, 2004: Theory and planning for urban biosphere reserves: an Australian example.

Lehmann, S. Green urbanism: formulating a series of holistic principles. Surveys and Perspectives Integrating Environment and Society. 2010. 3 (2) 1-10.

Luccarelli, M., 1995: Lewis Mumford and the Ecological Region: The Politics of Planning. New York, NY: Guilford Press.

Newman, L., and Dale, A. In praise of mundane nature: the unsung nature in alleyways and backyards plays an important – and undervalued – role in urban lives. *Alternatives Journal*. 2009. 35 (2) 32-35.

Steiner, F. Landscape ecological urbanism: origins and trajectories. *Landscape and Urban Planning*. 2011. 100 (4) 333-337.

Cloud Publications
International Journal of Advanced Remote Sensing and GIS
2017, Volume 6, Issue 3, pp. 2080-2087
ISSN 2320 - 0243 doi: 10.23953/cloud.ijarsg.70

Research Article | Open Access

Potential Groundwater Accumulations Assessment in Drought Prone Area using Remote Sensing and GIS Technology

Jothibasu, A.[1], Venkatesan, A.[2], Gunasekaran, S.[1]

[1]Centre for Geoinformatics and Planetary Studies, Department of Geology, Periyar University, Salem
[2]Department of Geology, Periyar University College of Arts and Sciences, Mettur Dam, Salem

Publication Date: 25 March 2017

DOI: https://doi.org/10.23953/cloud.ijarsg.70

Abstract Water plays a crucial role in the socio-economic development of India. Safe drinking water is required for the very large and growing population. Water has also become a major factor for the growth of the agricultural and industrial sectors. In the present study, the application of remote sensing and GIS techniques is applied for delineation of potential groundwater zone. The failure of monsoon and extensive groundwater usage lead to frequently drought condition. This has been visually observed during the field visit most of the dry wells extended to the depth of more than 50 m depth which is in unusual conditions in hard rock terrain. Similarly bore wells are using for extraction of groundwater with an average depth of 150 m (bgl). The study area annual average rainfall is 628 mm. In the present study the potential groundwater zones were demarcated through analysis of hydrogeology, geomorphology and lineaments with the help of IRS P6 LISS III satellite data and field investigation. The thematic maps like geology, geomorphology, lineament density, drainage density, land use and land cover and soil were reclassified and integrated for generation of groundwater potential map through GIS technique. Reclassification of thematic maps, ranking and weights assignment and were done through subjective and field experience. The final result is obtained through GIS overlay analysis. The groundwater condition in the major formations such as hornblende biotite gneiss, charnockite in the study area is controlled by secondary porosities like joints and fractures. The lineaments and associated fractures and buried pediments are important zones for potential groundwater accumulations and suitable for groundwater development for agriculture.
Keywords *Groundwater; Potential Zones; GIS; Remote Sensing; Index Overlay Method*

1. Introduction

Groundwater is one of the most valuable natural resources, immensely important and dependable source of water supply in all climatic region of all over the world (Todds and Mays, 2005). Although it is more dynamic renewable natural resource yet availability with good quality and quantity in appropriate time and space is more important (Chaudhary et al., 1996). The GIS technique is not only useful in mapping groundwater potential zones through spatial integration but also provides the controlling terrain parameter. GIS and remote sensing tools are widely used for the management of various natural resources (Krishna Kumar et al., 2011; Magesh et al., 2011). Remote sensing has become a

vital tool for groundwater targeting, because the topographic expression and terrain characteristics have a direct relation to the characteristics of rocks and subsurface geological conditions. Integration of remote sensing data in the GIS environment is very useful in delineating various groundwater potential zones in a meaningful way (Agarwal et al., 2004).

The number of studies had attempted to clarify spatial variability of groundwater potential in different terrain conditions using technologies like aerial photography and GIS. Remote sensing from satellite has recently become a valuable tool that provide quick and baseline information on sub-surface water conditions. With this information, one can find out the factors controlling the occurrence potential and movement of groundwater such as geological structures, geomorphology, soil, land use land cover and other related characteristics of the area (Anbazhagan, 2002). This data can be spatially integrated by means of geographic information system and finally groundwater potential zones can be delineated. In this field attempts have already been made in different parts of the country by various authors like, Chaudhary et al. (1996), Krishnamurthy et al. (1996), Das et al. (1997), Goyal et al. (1999), Pratap et al. (2000), Nag (2005), Vijith et al. (2007), Suja Rose et al. (2009), Kumar Pradeep (2010) etc. Vagaries of monsoon and semi-arid to hot climate further aggravate the situation. Due to limited number of rainy days, natural depressions the study area also remains dry during most of the time of year. In the present study, an attempt has been made to assess the potential groundwater accumulation zones by an integrated approach of remote sensing and GIS technology.

2. Study Area

The Uppar Odai sub-basin is located in the Amaravati River basin in the state of Tamil Nadu, India, and falls between 77°6′36″E–77°32′24″E longitude and 10°26′40″N–10°55′48″N latitude. The aerial coverage of the Uppar Odai sub-basin is 1280 km2. It covers the major part of Tiruppur district and a small area of Coimbatore district (Figure 1). The annual average rainfall in the sub-basin is 625 mm, which is much lower than the state average rainfall (970 mm). A subtropical climate prevails throughout the region. The maximum temperature ranges from 27 to 35°C and minimum temperature varies from 17 to 23°C. There are four distinct seasons, namely southwest monsoon, northeast monsoon, winter season and hot weather period, prevailing in the study area. The rainfall pattern, as recorded at the rainfall stations, indicates that the precipitation is mostly uncertain, uneven or unequally distributed. It is slightly higher in the central and western parts and decreases in the northern and eastern parts of the sub-basin. The highest average annual rainfall of 738 mm is observed in the central part and the lowest amount of rainfall is 573 mm received in the northern part of the sub-basin.

3. Materials and Methods

The IRS P6 LISS III satellite data are visually interpreted for the preparation of lineament density, geomorphology and land use/land cover. The thematic layers and their corresponding categories are assigned a knowledge base ranking from 1 to 5 depending on their suitability to hold groundwater. The maximum value is given to the feature with highest groundwater potentiality and minimum being to the lowest potential feature. Based on these ranks their weightage are calculated and added to each layer (Sitender & Rajeshwari, 2011).

From the various methods available for determining interclass dependency, a probability weighted approach has been adopted that allow a linear combination of probability weights of each thematic map and different categories of derived thematic maps by assessing their importance in groundwater occurrence (Sitender & Rajeshwari, 2011). This process involves raster overlay analysis which is called multi-criteria evaluation techniques (MCE). The ‘Raster Calculator’ option of spatial analyst extension in Arc GIS 9.3 is used to prepare the integrated final groundwater potential map of the study area. This map indicates the potentiality of groundwater occurrence in the study area which is then

classified into three categories based on the mean and standard deviation values namely high, moderate and low.

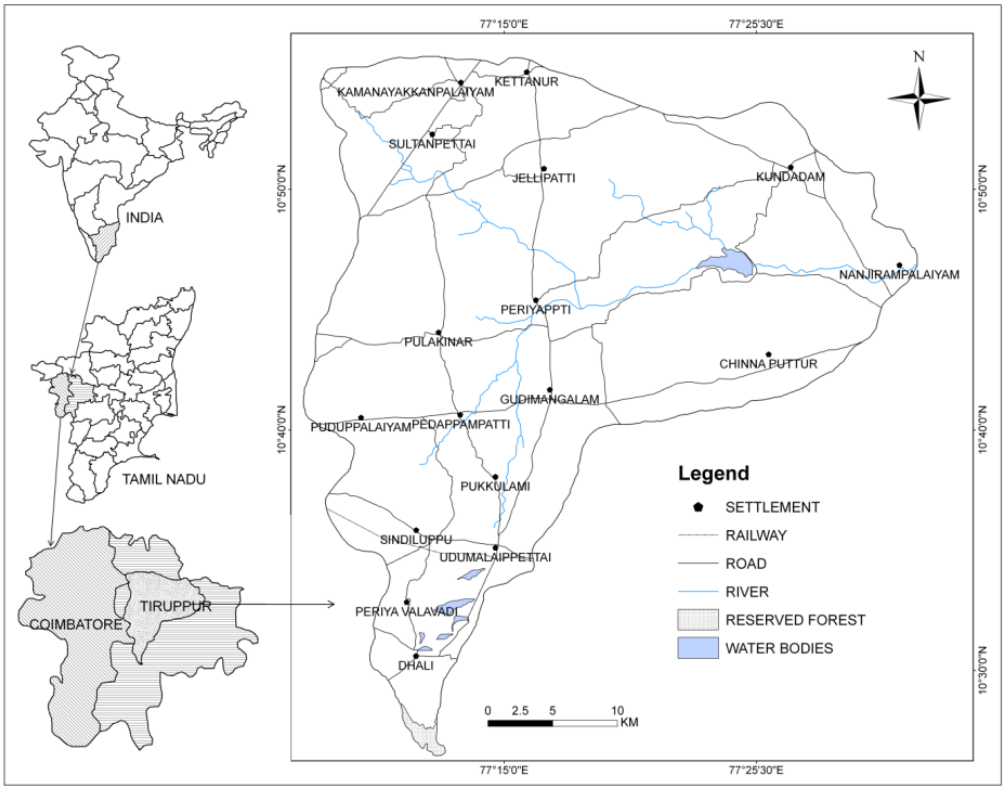

Figure 1: *Location map of the study area*

3.1. Geology Map

The study area is covered by the Precambrian age of crystalline rocks. The recent formation is marked by river alluvium and soil. Geological map of the study area was generated from Geology map of Tamil Nadu published by GSI (1969). The study area is characterized by outcrops of hornblende biotite gneiss, limestone and calcareous sandstone, charnockite, pink migmatite gneiss, felsic porphyry, pyroxene granulites and ultra-basic complex. Overall classified the geology ranked to seven, all the classes were merged together to form single class to weightage given by based on knowledge to one to five.

3.2. Drainage Density

In order to generate drainage density for the study area, the entire basin was divided into square grids of equal area of 1 km x 1 km. In each square grid the total length of streams of all order is measured. This was done for all grids and then points of equal drainage density were contoured. The drainage density for the study area is found to from zero to 4500 m per square kilometer. On the basis of drainage density the entire basin was divided into three zones like High, Medium and Low then rank and weightage given based on knowledge.

3.3. Lineaments Density

Lineament is defined as mappable, simple or composite linear feature on the surface whose parts is aligned in a rectilinear or slightly curvilinear relationship and differs distinctly from adjacent feature due to its distinct trend. Lineaments were delineated from FCC and PCA. Lineaments are of great

importance in groundwater studies as they are considered to zones of maximum infiltration. They are considered to be surface manifestations of joints, fractures, faults and dykes. Dykes act as except for the central and S-E zone where land form is almost a plain. Major lineaments and intersection were delineated separately as it is an important factor in finding potential zones groundwater (Sitender and Rajeshwari, 2011). High lineament density is considered to be highly favourable location for potential groundwater zones.

3.4. Geomorphology

The regional geomorphological units were delineated based on the IRS P6 LISS III image characteristics like tone, texture, shape, colour, associations, background and also with considerations from the unsupervised classification, geology map and toposheets and visual interpretation was carried out. The units identified are linear, narrow and generally barren (Sitender and Rajeshwari, 2011). Structurally may be strike controlled feature and is of structural origin. Groundwater prospect is poor in this region. Structural Hills are mostly linear to arcuate hills showing definite trends associated with folding and faulting. Hills other than that of structural control are formed due to differential weathering and erosion.

Normally barren lands with sparse vegetation and poor groundwater potential. Valleys that are mostly fracture controlled and are of fluvial origin. Narrow valleys filled with unconsolidated sediments which are deposited by streams and rivers. Depending on to thickness of the fill, the groundwater prospects vary from very good to good.

3.5. Land Use /Land Cover

Land use/land cover plays important role in the occurrence and development of groundwater. Agricultural land, forest cover and settlement are the prominent land use types in the study area. The main land use/land cover units in the study area are agriculture land, settlement or built up areas. Water bodies, scrub land, outcrop area, forest, mudflat and salt affected areas. Of these various units, agricultural land and forest cover occupies maximum aerial extent.

3.6. Soil

Development planning of problematic lands particularly on watershed basis requires through knowledge of soil resources. The soil resource inventory provides information of various attributes e.g. texture, depth, slope, erosion, extent of salinity, water logging etc. Major portion of the study area is covered by Mixed Red and Black soil and also it covers maximum area in this region and small southern part of the study is covered by red sandy soil. These two soil types were classified fourth ranking and weightage given based on knowledge. All six thematic maps are shown in Figure 2.

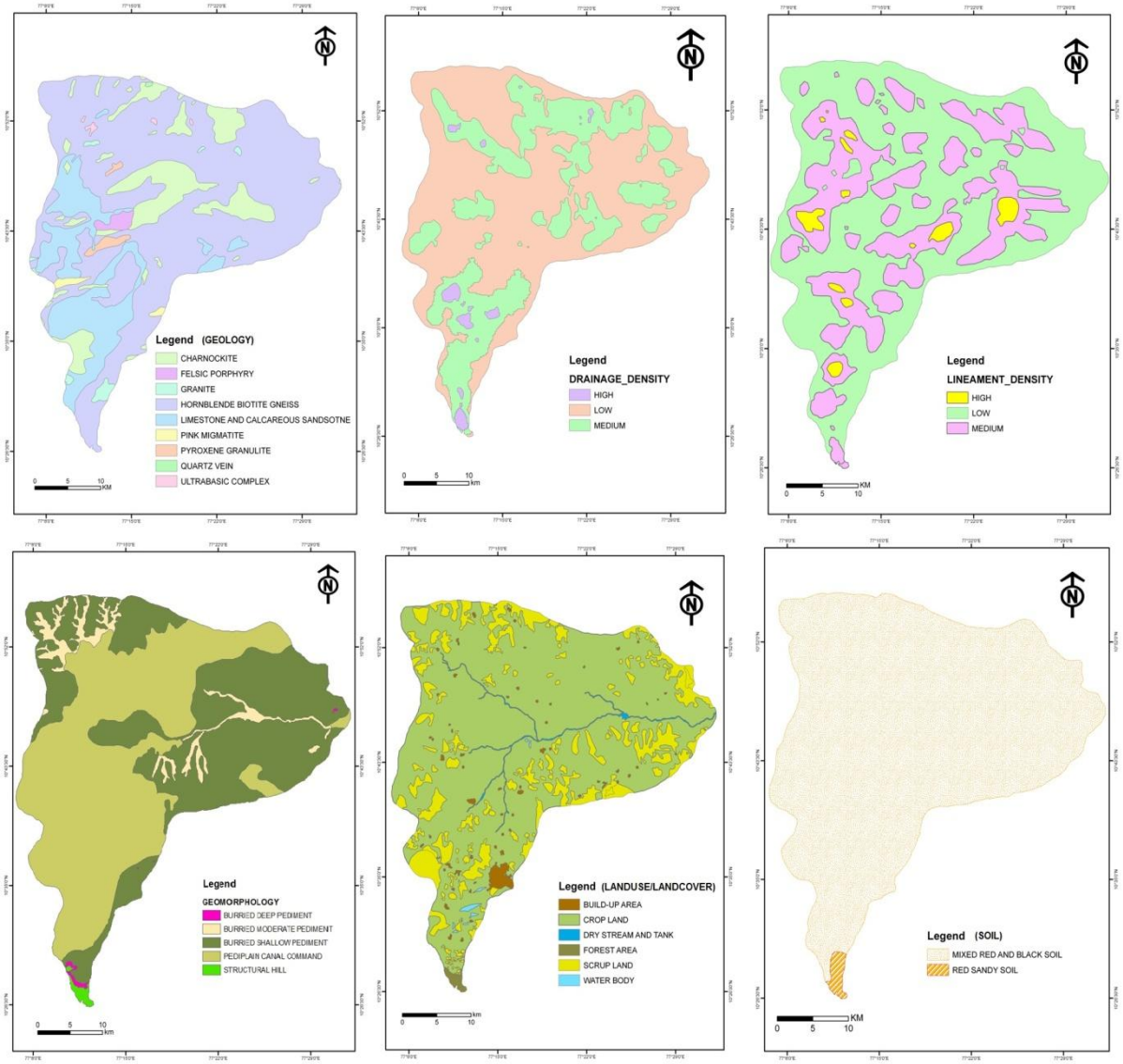

Figure 2: *Different parameters selected for groundwater accumulation in the study area*

4. Results and Discussion

The normalized weights of different features of the six themes were obtained in the similar manner as presented in Table 1. After deriving the normal weights of all the thematic layers and each feature under individual themes, all the thematic layers were integrated with one another using MapInfo GIS software in order to demarcate groundwater potential zones in the study area. In the first step, the geomorphology layer was integrated with the geology layer. The weight of each polygon of the integrated layer was derived by adding the weights of polygons of the original two layers and the process was continued for the remaining five themes to obtain a final integrated layer. The final weights of each polygon in the final integrated layer were derived by summing up the weights of polygons from individual layers and the highest derived sum of the weights in the final integrated layer was divided into three equal classes, i.e. 'high', 'moderate' and 'low', in order to delineate groundwater potential zones (Figure 3). The delineation of groundwater potential zones was done by grouping the polygons in the final integrated layer having weights of any of the three classes.

Groundwater potential map clearly indicate that alluvial plain which is composed of sand, silt and clay with nearly level slope and very low drainage density has excellent potentiality. Piedmont plain with

gentle slope and low drainage density poses good to very good potential while plain with coarse to fine sand has good to moderate potential due to less water holding capacity. Structural hills and linear ridges with steep slope and high drainage density but due to presence of high lineament density offer poor to moderate potential. Structural hills with low lineament density, very steep slope and very high drainage density lie in very poor potential zones (Sitender and Rajeshwari, 2011). Thus the generated groundwater potential map serves as a base line for future exploration.

Table 1: *Thematic features, ranking and weights*

Thematic Maps	Classes Within Each Maps	Overall Ranking	Weights	Total Weights
Lineament Density	High	10	2	20
	Medium		4	40
	Low		2	20
Drainage Density	High	9	1	9
	Medium		4	36
	Low		5	45
Geology Map	Charnockite	7	2	14
	Felsic porphyry		3	21
	Granite		4	28
	Limestone and Sandstone		4	28
	Pink Migmatite		3	21
	Pyroxene Granulite		2	14
	Quartz vein		2	14
	Ultrabasic complex		2	14
	Hornblende Biotite Gneiss		4	28
Land use/Land cover	Build-up land	6	3	18
	Crop land		5	30
	River		1	6
	Reserved Forest		2	12
	Scrub land		4	24
	Tank		2	12
Geomorphology	Buried shallow pediment	5	2	10
	Buried deep pediment		4	20
	Pediplain canal command		1	5
	Structural Hill		5	25
	Buried Moderate pediment		3	15
Soil Map	Mixed Red and Black soil	4	3	20
	Red sandy soil		5	8

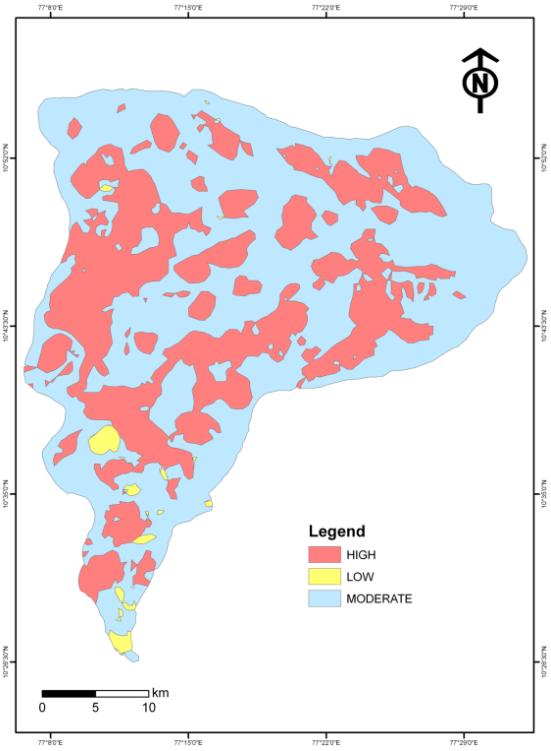

Figure 3: *Potential groundwater accumulations of the study area*

5. Conclusion

In the present study, multi-criteria evaluation technique using raster based GIS analysis is attempted to delineate the groundwater potential zones. Remote sensing and GIS have proved as vital tools in delineating groundwater potential zones based on the integration of various thematic maps. Occurrence of groundwater has a direct relationship with the geomorphology and slope of the area. In hard rock area potentiality for groundwater occurrence is influenced by the presence of lineaments. The groundwater condition in the major rocks such as Hornblende Biotite Gneiss, Charnockite in the study area is controlled by secondary porosities like joints and fractures. The lineaments and associated fractures and buried pediments are important zones which have potential groundwater and suitable for groundwater development for agriculture.

References

Anbazhagan, S. (2002). Remote Sensing and GIS Based Hydrological Studies in Kinzig Basin, Germany. Geomatics 2002, Conference on IT Enabled Spatial Data Services September 18-20, Centre for Remote sensing, Bharathidasan University Tiruchirappalli. 218-222.

Chaudhary, B.S., Manoj Kumar, Roy, A.K., & Ruhal, D.S. (1996). Application of Remote Sensing and Geographic Information Systems in Groundwater Investigations in Sohna Block, Gurgaon District, Haryana (INDIA). *International Archives of Photogrammetry and Remote Sensing, XXXI*(Part B6), 18-23.

Das, S., Behra, S.C., Kar, A., Narendra, P., & Guha, N.S. (1997). Hydrogeomorphological Mapping in Groundwater Exploration using Remotely Sensed Data – Case Study in Keonjhar District in Orissa. *Journal of Indian Society of Remote Sensing, 25*(4), 247-259.

Goyal, S., Bhardwaj, R.S., & Jugran, D.K. (1999). *Multi-criteria Analysis using GIS for Groundwater Resource Evaluation in Rawasen and Pilli Watershed, Uttar Pradesh.* Retrieved from http://www.gisdevelopment.net.

Krishnamurthy, J., Kumar, N.V., Jayaraman, V., & Manivel, M. (1996). An Approach to Demarcate Groundwater Potential Zones through Remote Sensing and Geographical Information System. *International Journal of Remote Sensing, 17*(10), 1867-1884.

Nag, S.K. (2005). Application of Lineament Density and Hydrogeomorphology to Delineate Groundwater Potential Zones of Bagmundi Block in Purulia District, West Bengal. *Journal of the Indian Society of Remote Sensing, 33*(4), 521-529.

Pratap, K., Ravindran, K.V., & Prabakaran, B. (2000). Groundwater Prospects Zoning using Remote Sensing and Geographical Information System: A Case Study in Dala-Renukoot Area, Sonbhadra District, Uttar Pradesh. *Journal of the Indian Society of Remote Sensing, 28*(4), 249-263.

Sitender & Rajeshwari. (2011). Delineation of groundwater potential zones in Mewat District, Haryana, India. *International Journal of Geomatics and Geosciences, 2*(1), 270-281.

Suja Rose, R.S., & Krishnan, N. (2009). Spatial Analysis of Groundwater Potential using Remote Sensing and GIS in the Kanyakumari and Nambiyar Basins, India. *Journal of the Indian Society of Remote Sensing*, 37(4), 681-692.

Todd, D.K. (1980). *Groundwater Hydrology*. Second Edition. New York: John Wiley and Sons Inc. 556.

Vijith, H. (2007). Groundwater Potential in the Hard Rock Terrain of Western Ghats: A Case Study from Kottayam District, Kerala using Resourcesat (IRS-P6) data and GIS Techniques. *Journal of the Indian Society of Remote Sensing, 35*(2), 163-171.

Cloud Publications
International Journal of Advanced Remote Sensing and GIS
2017, Volume 6, Issue 1, pp. 1994-2000
ISSN 2320 - 0243, doi:10.23953/cloud.ijarsg.30

Research Article | Open Access

Estimation and Assessment of Spatial Variations in Water Availability in West Flowing River Basin of Kutch, Saurashtra and Marwar (WFR-KSM basin) using Geospatial Technology

Ila Agnihotri[1], Punia M.P.[2], and Sharma J.R.[3]

[1]Regional Remote Sensing Centre-West (RRSC-W/NRSC), Indian Space Research Organization, Jodhpur, Rajasthan, India
[2]Birla Institute of Technology, Jaipur, Rajasthan, India
[3]National Remote Sensing Centre (NRSC), Indian Space Research Organization, Jodhpur, Rajasthan, India

Publication Date: 5 January 2017

DOI: https://doi.org/10.23953/cloud.ijarsg.30

Abstract The availability and distribution of water varies nationally and regionally. The availability of fresh water is stressed due to growing population coupled with sustainable developmental efforts, the uneven distribution of water resources over time & space, their modification through human use & abuse and many others. The study area is WFR-KSM basin which lies between 67°52' to 75°19' E longitudes and 20°53' to 26°57' N latitudes, covering areas in Rajasthan, Gujarat and whole of Diu. Hydrologically, it is divided into six sub basins and 268 watersheds (India-WRIS). The annual and monsoon season water availability in the basin, its sub basins and watersheds for water year 2013-14 was calculated by SCS curve number method using IMD 0.25 degree rainfall, NRSC NR Census LULC, NBSS & LUP soil data and MODIS evapotranspiration data. The water availability in the basin was estimated to be 34.67 BCM annually and 47.4 BCM in monsoon season ranging from 0 to 505 MCM annually and from 0 to 647.23 MCM in monsoon season in the watersheds of the basin. The spatial interpretation of water availability in watersheds indicated more water availability in the southern part of the basin and less water availability in the watersheds lying in northern part of the basin.

Keywords *Basin; GIS; Remote Sensing; Kutch; Marwar; Rainfall; Runoff; Saurashtra; SCS; Water*

1. Introduction

Water is an essential natural resource for sustaining life on earth. The availability and distribution of water varies spatially. India is endowed with rich water resources but the potable water is limited and varies spatially throughout the country. The availability of fresh water is further stressed due to growing population, developmental efforts, uneven distribution of water resources over time & space, their modification through human use & abuse and many others. All these result in intensifying the pressure on water resources leading to conflict among users and eventually lead to excessive pressure on the environment. These situations demand for proper management of water resources. This, in turn, calls for a reliable and adequate statistics on available water resources and related aspects.

The assessment of water availability means different things to different communities. Many envisions have proposed the concept of national assessment of water availability based on the indicators of the status and trends in storage volumes, flow rates, and uses of water nationwide. There are several spatial scales at which the indicators of water availability could be reported. The assessment would use basic hydrological data collected from different sources by the responsible agencies to create the indicator variables. This process of computing indicators from the basic data would help to elucidate uncertainties in our knowledge of the Nation's hydrological conditions.

In India, the gauge data is not homogenously available for all the catchments. The hydrological modeling approach was followed for the estimation of runoff in the catchments. This paper presents the estimation of water availability in the WFR-KSM basin, its sub basins and watersheds and their spatial interpretation. Here yield is calculated as indicator of water availability in the hydrological units.

2. Literature Review

Barlow (2002) presented the concepts of nationwide assessment of water availability in United States and the variables used to represent the same at several temporal and spatial scales. The lack of runoff information in India is mentioned by Ningaraju, Ganesh Kumar and Surendra (2016). They used SCS-CN method and GIS for the estimation of runoff in ungauged Kharadya milli watershed in Karnataka, India.

SCS-CN method is used globally for the calculation of runoff. Rao et al. (2014) used Land use/land cover (LULC) maps (1:250k scale) prepared using AWiFS sensor data of IRS-P6 satellite generated under Natural Resources Census (NR census) project by Indian Space Research Organization (ISRO) and Soil maps (1:250k scale) of the National Bureau of Soil Survey and Land Use Planning (NBSS & LUP) in the calculation of runoff. Gangodagamage and Aggarwal (2012) presented the use of LISS-3 data, derived land use and SCS curve number method for the generation of hydrological model for the Bata River basin which is a tributary of the Yamuna River, India. Ahmad and Verma (2016) used SCS-CN method for estimation of runoff depth in Kharun River basin in Chhattisgarh state of India. Choi, Kim and Lim (2016) used SCS runoff curve number for the estimation of approximate amount of runoff in several forested watersheds of Korea. Al-Jabari, Sharkh and Al-Mimi (2016) used SCS method in GIS domain for the assessment of runoff from Wadi Su'd watershed in southern Palestine. Chavda, Makwana, Parmar, Kunapara and Prajapati (2016) used SCS-curve number method in GIS domain for the estimation of surface runoff and water availability in semi-arid Ozat catchment in Gujarat, India. Khatun (2016) used SCS-curve number method in GIS domain for the estimation of surface runoff in Kushkarni River Basin of West Bengal, India. N. Kamuju (2016) used SCS-curve number method using NR census land use land cover as input in GIS domain for the calculation of temporal runoff in Karha river basin in Maharashtra State, India. Haidu and Ivan (2015) used Simplified SCS-CN mode number method for the estimation of volume of water draining from urban rooftops in a municipality of Romania.

3. Study Area

The study area is located in western India which is defined by the rivers flowing westwards towards the Arabian Sea with their respective drainage areas. The basin enclosing this area is West Flowing River Basin of Kutch, Saurashtra and Marwar (WFR-KSM basin). The basin boundary is represented by basin delineated on west flowing rivers of Kutch and Saurashtra including Luni in India-WRIS project (Water Resources Information System) project and having area 1, 84,865.96 Sq. Km (GIS). The basin is spread over western India in the states of Rajasthan (13 Districts), Gujarat (13 Districts), and Daman & Diu (1 District). The area represents wide diversity of relief features and variability in terms of topography. In the west lie shallow wetlands of Rann of Kutch; eastern area is bounded by river Banas and hilly terrain of Aravalli chain; northern part is represented by Luni River which is an active tectonic

sedimentary basin and southern part is covered by other important smaller rivers such as Shetrunji, Machhu, Rupen and Bhader.

Hydrologically, the WFR-KSM Basin is divided into six sub-basins and 268 watersheds. The sub basins are named according to main river system in them, Luni Upper Sub-basin (38.03%), Luni Lower sub-basin (15.81), Saraswati sub-basin (14.77%), Drainage of Rann sub-basin (11.50%), Bhadar and other WFR sub-basin (10.02%), and Shetrunji and other EFR sub-basin (9.87%).

4. Goal and Objectives

The goal of this research was to estimate the water availability in WFR-KSM basin, its sub basins and watersheds along with their spatial assessment using geospatial techniques. The objectives to attain this goal were (1) To calculate water availability using hydrological modeling, and (2) To analyze the spatial variations in water availability. The water availability was calculated for the annual and monsoon season of the water year 2013-14 i.e. from June 2013 to May 2014.

5. Software and Data Used

The softwares used were Arc map 10, Geospatial Modeling Environment (GME), MS excel and ASAP utilities (excel add in) tool. The data used were IMD Precipitation grid (0.25° x 0.25°) of year 2013-14; NR census LULC (1: 250k) by NRSC/ISRO for the year 2013-14; Soil texture layer at 1:50k scale from NBSS & LUP; and MODIS 0.05 degree evapotranspiration (ET) data which is 1 square km monthly gridded dataset for the year 2013-14.

6. Analytical Methods Used

The water availability was calculated for each hydrological unit using SCS Curve Number Method in Arc Map environment. The SCS curve number method also known as the hydrologic soil cover complex method was developed by Soil Conservation Service (SCS) of United States Department of Agriculture (USDA) is a simple method used to calculate direct runoff based on rainfall by using antecedent soil moisture conditions, soil, land cover and the curve number (CN) which characterizes the runoff potential of the soil land cover complex (SCS). The method is well established and widely used.

The basis of SCS curve number equation is water balance equation that can be expressed as

$$P = I_a + F + Q \qquad \text{..... (1)}$$

Where P is total precipitation, I_a is initial abstraction, Q is direct runoff and F is cumulative infiltration excluding I_a and Q. There are two assumptions along with the water balance equation: First concept states that the ratio of actual amount of direct runoff (Q) to maximum potential runoff (= P - I_a) is equal to the ratio of actual infiltration (F) to the potential maximum retention, S. The equation is:

$$\frac{Q}{P - I_a} = \frac{F}{S} \qquad \text{..... (2)}$$

The second concept is that the amount of initial abstraction (Ia) is some fraction, represented by λ, of the potential maximum retention (S), given by

$$I_a = \lambda S \qquad \text{..... (3)}$$

Combining the equations (1), (2) and (3), For P>λS; and Q=0 for P≤λS

$$Q = \frac{(P - I_a)^2}{P - I_a + S} = \frac{(P - \lambda S)^2}{P + (1 - \lambda)S}$$

The curve number represents a dimensionless number which is a representation of potential maximum retention (S) of the catchment. The S as well as CN depends on soil-vegetation-land use complex of the catchment along with antecedent runoff conditions prior to the rainfall. The S and CN are defined as

$$S = \frac{25400}{CN} - 254; \text{ and } CN = \frac{25400}{S + 254}$$

The CN is a dimensionless parameter ranging from 0 for infinitely abstracting catchment indicating zero potential retention (S = ∞) to 100 for impervious catchment. The CN depends on soil type, antecedent runoff conditions and land use land cover.

7. Methodology

Annual and monsoon season (June to September) water availability were calculated for the basin, six sub basins and 268 watersheds (hydrologic units), using the subsequent steps. IMD rainfall data was converted in 0.25 degree grid. MODIS evapotranspiration (ET) data was downloaded and converted in 0.05 degree grid layer. The rainfall and ET values were assigned to basin, sub basins and watersheds in Geospatial Modelling Environment. The LULC and Soil layers were prepared for hydrological modeling. The runoff was calculated for each hydrological unit using SCS Curve number method in Arc Map environment. The calculated values were converted in volume terms, were spatially mapped and interpreted using Arc Map.

8. Results

Annual and monsoon season water availability was calculated for WFR basin, its sub basins and watersheds in water year 2013-14. The water availability is represented by the surface runoff which was calculated using SCS curve number method in average antecedent runoff conditions.

The annual water availability in the basin was estimated to be 34.67 BCM. The sub-basin wise water availability ranges from 1.21 BCM in Luni lower sub basin to 9.59 BCM in Luni upper sub basin. The watershed wise average water availability ranges from 0 in the watersheds of Kutch district to 505 MCM in the southern coastal part of the basin in the border of Junagadh and Porbandar districts. The minimum value was 0 and maximum value varies from 458.57 to 545.51 MCM. The annual water availability in the watersheds of WFR-KSM basin for the water year 2013-14 is depicted in Map 1.

The monsoon season water availability in the basin was 47.4 BCM. The sub-basin wise water availability ranges from 2.31 BCM in Luni lower sub basin to 11.48 BCM in Luni upper sub basin. The watershed wise average water availability ranges from 0 in the watersheds of Kutch district to 647.23 MCM in the southern coastal part of the basin in Junagadh district. The minimum value was 0 and maximum value varies from 561.71 to 695.53 MCM. The monsoon season water availability in the watersheds of WFR-KSM basin for water year 2013-14 is depicted in Map 2.

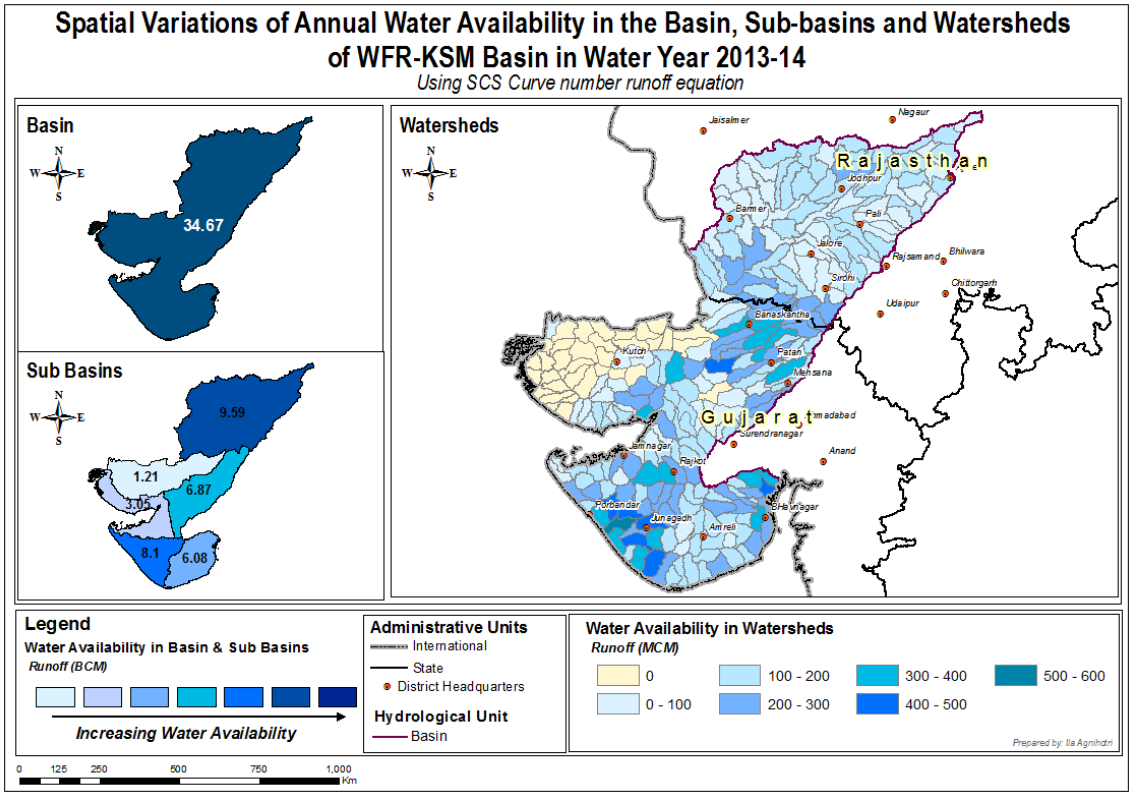

Map 1: *Annual Water Availability in WFR-KSM Basin, its Sub-basins and Watersheds*

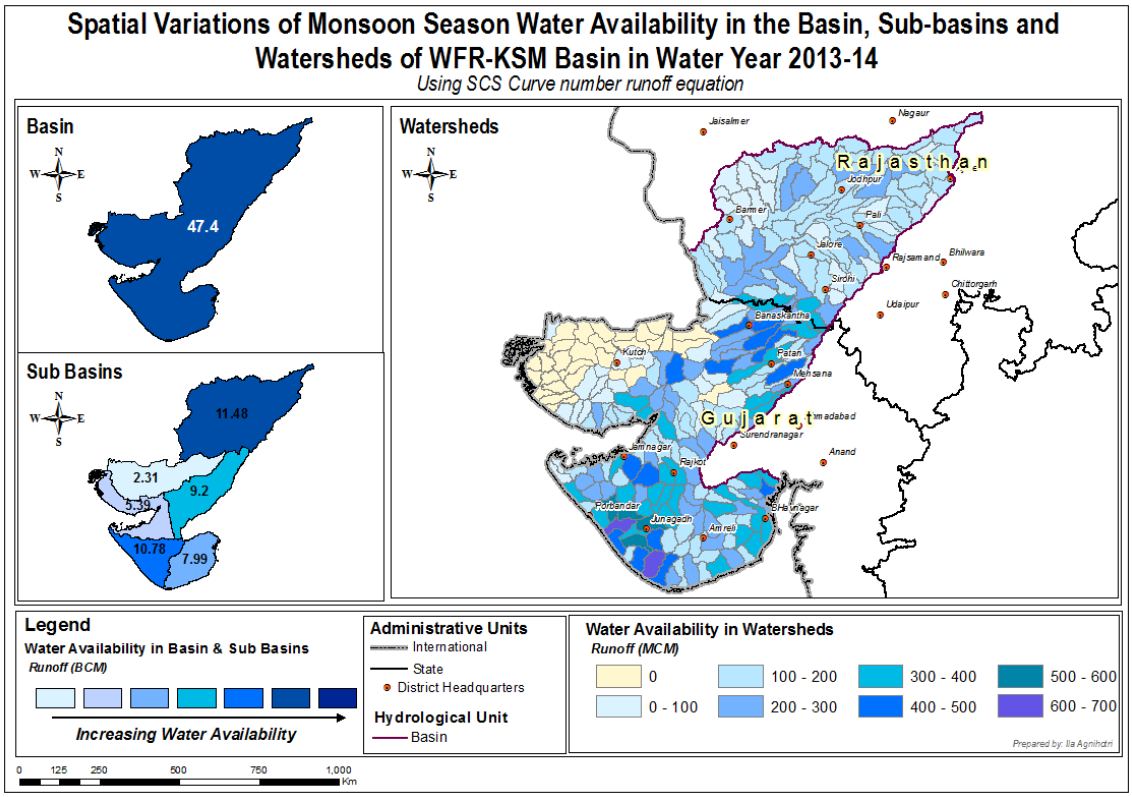

Map 2: *Monsoon Season Water Availability in WFR-KSM Basin, its Sub-basins and Watersheds*

The spatial variations of water availability were assessed in terms of pattern of water availability in watersheds. Water availability in the watersheds varies spatially. The watersheds in Gujarat were exhibiting more water availability as compared to those in Rajasthan (<300 MCM). More water availability was observed in monsoon season in the watersheds facilitating the differentiation in water availability disparities in the watersheds of Rajasthan and Gujarat. The watersheds with high runoff were clustered in the southern part of the basin near Junagadh district. A cluster of watersheds in Kutch district were exhibiting no water availability as most of this region is characterized by saline marsh and runoff in saline marsh does not contribute to fresh water availability.

9. Conclusion

The annual water availability in the basin was estimated to be 34.67 BCM ranging from 1.21 BCM to 9.59 BCM in sub-basins and from 0 to 505 MCM in the watersheds. The monsoon season water availability in the basin was estimated to be 47.4 BCM ranging from 2.31 BCM to 11.48 BCM in sub-basins and from 0 to 647.23 MCM in watersheds.

The spatial variations in terms of pattern of water availability in the watersheds indicated that the water availability increases from northern to southern part of the basin with more runoff clustering in southern watersheds lying in Gujarat and a cluster of watersheds with no freshwater runoff in Kutch district. More water availability was observed in monsoon season in the watersheds facilitating the differentiation in water availability disparities in the watersheds of Rajasthan and Gujarat.

References

Gangodagamage, C., and Aggarwal, S.P. Integrating Satellite based Remote Sensing Observations with SCS Curve Number Method for Simplified Hydrologic Modeling in Ungauged Basins. *Asian Journal of Geoinformatics.* 2012. 12 (3) 29-39.

CWC, 2010: CWC Water Year Book of Mahi, Sabarmati and other west flowing rivers 2009-10. CWC, New Delhi.

Chavda, D.B., Makwana, J.J., Parmar, H.V., Kunapara, A.N., and Prajapati, G.V. Estimation of Runoff for Ozat Catchment using RS and GIS Based SCS-CN Method. *Current World Environment*. 2016. 11 (1) 212-217.

Ningaraju, H.J., Ganesh Kumar, S.B., and Surendra, H.J. Estimation of Runoff Using SCS-CN and GIS method in ungauged watershed: A case study of Kharadya mill watershed, India. *International Journal of Advanced Engineering Research and Science*. 2016. 3 (5).

Choi, H.T., Kim, J., and Lim, H. Estimating the SCS runoff curve number in forest catchments of Korea. *Geophysical Research Abstracts*. 2016. 18 EGU2016-7210-1.

Ahmad, I., and Verma, M.K. Surface Runoff Estimation using Remote Sensing & GIS based Curve Number Method. *International Journal of Advanced Engineering Research and Science*. 2016. 3 (2).

Haidu, I., and Ivan, K. Rainwater Management aiming to improve the Quality of Urban Surface Runoff. *Studia Geographia*. 2015. 2; 35-44.

Durga Rao, K.H.V., Rao, V.V., Dadhwal, V.K., Sharma J.R., and Jyothsna, R. Transforming to hydrological modelling approach for long-term water resources assessment under climate change scenario–a case study of the Godavari Basin, India. *Current Science*. 2014. 106 (2) 293-299.

Kamuju, N. An Innovative Approach for Estimation and Evaluation of Spatially Distributed Hydrological Parameters with Temporal Resolution of Land Use-Land Cover Classes Using Remote Sensing and GIS based RINSPE Model. *International Journal of Research & Development Organization*. 2016. 2 (3) 17-37.

Barlow, P.M. Concepts for national assessment of water availability and use: report to congress. U.S. Geological Survey Circular 1223. 2002. U.S. Department of the Interior, U.S. Geological Survey, Virginia.

Al-Jabari, S., Sharkh, M.A., and Al-Mimi, Z. Assessment of Runoff Potential for a small Watershed in Southern Palestine. *International Water Technology Journal*. 2016. 6 (1).

Khatun, S. Estimation of Runoff for Ozat Catchment using RS and GIS based SCS-CN method. *International Research Journal of Earth Sciences*. 2016. 4 (5) 1-10.

USDA, 1999: Module 205-SCS Runoff Equation. USDA, Washington. [Online]. Available: http://www.wcc.nrcs.usda.gov/ftpref/wntsc/H&H/training/SCS-runoff-equation.pdf

USDA: National Engineering Handbook Hydrology-NEH Part 630. [Online]. Available: http://www.nrcs.usda.gov/wps/portal/nrcs/detailfull/national/water/?cid=stelprdb1043063

USDA, 1986: Urban Hydrology for Small Watersheds-TR-55. USDA, Technical Release 55. Natural Resources Conservation Service, USDA. [Online].
Available: http://www.nrcs.usda.gov/Internet/FSE_DOCUMENTS/stelprdb1044171.pdf

Mockus, V., 1964: National Engineering Handbook, Section 4-Hydrology, USDA-SCS, Washington, D.C. [Online]. Available:
http://www.nrcs.usda.gov/wps/portal/nrcs/detailfull/national/water/?cid=stelprdb1043063

Cloud Publications
International Journal of Advanced Remote Sensing and GIS
2017, Volume 6, Issue 1, pp. 2124-2134
ISSN 2320 – 0243, Crossref: 10.23953/cloud.ijarsg.257

Research Article | Open Access

Comparative Morphometric Analysis of Three Watersheds of the Jhabua Region, M.P., using Remote Sensing and GIS Techniques

Anjali Gupta, Punwatkar, V.L.

Dept. of Geology, Govt. M.V.M., Bhopal, M.P., India

Publication Date: 29 April 2017

DOI: https://doi.org/10.23953/cloud.ijarsg.257

Abstract In the present study, Morphometric analysis has been conducted using Geographical Information System (GIS) techniques to assess the geo-hydrological characteristics of watersheds (Mod nadi, Sapan nadi, and Negri nadi) of Mahi river basin (Jhabua region). The basin is characterized by dendritic drainage pattern. The region is semi-arid (Agro-ecological zone of India), which belong to highly drought prone zone and degraded lands. Morphometric analysis of drainage system is an important factor of characterization of watershed. It furnishes the advantageous parameters for the ground water potential zone assessment, identification of places for water harvesting structure, water resource management and geological nature of the river system. GIS techniques has been used for assessing various morphometric characteristics of the drainage basin, as they proved to be very efficient and a powerful tool for the manipulation and analysis of spatial information mainly for the feature identification and extraction of information for better understanding. Using DEM data and GIS & Remote sensing techniques, morphometric analysis is carried out through mathematical analysis of drainage system of watersheds, which involves measurement of linear, Arial and relief aspects of the river basin.

Keywords *Morphometric Analysis; Mahi Basin; GIS; Remote Sensing*

1. Introduction

Remote sensing, Geographical information system (GIS) coupled with ASTER (DEM) has proved to be an efficient tool in delineation of drainage pattern and water resources management and its planning. GIS and image processing techniques was used for the assessment of morphological features and analysing their properties.

The Mahi river basin extends over states of Madhya Pradesh, Rajasthan and Gujrat having total area of 34,842 sq.km with maximum length of 330 K.m. and width of about 250 km. It lies between $72^0$21'to $75^0$19' East longitudes and $21^0$46' to $24^0$30' North latitudes. Anas, the main tributary of Mahi, originates in south eastern part of Jhabua tahsil and flows in Northwest direction, It then runs through Meghnagar and Thandla tahsil along the western boundary of the Jhabua district with Dahod of Gujrat. The average rainfall in the Mahi basin is 785 mm. The South - West monsoon sets in by the middle of June and withdraws by the first week of October. About 90 percent of total rainfall is received during the

monsoon months of which 50 percent is received during July and August. The rainfall is mainly influenced by the southwest monsoon.

Morphometric analysis of a watershed gives a quantitative description of the drainage system, which is an important feature of the characterization of watersheds (Strahler, 1964). The Morphometric analysis of the drainage basin and channel network play an significant role in understanding the geo-hydrological behavior of drainage basin and expresses the existing geology, geomorphology, structural, climate background of the catchment area. Morphometry is the measurement and mathematical analysis of the formation of the earth's surface, shape and dimension of its landforms. This analysis can be carry out through measurement of Linear, Arial and Relief aspects of the basin and slope contribution (Nag and Chakraborty, 2003). Morphometric parameters requires preparation of drainage map, ordering of various streams, measurement of the perimeter, catchment area, channel length, drainage density and the other parameters, which help in recognize the nature of the drainage basins. Integrated use of remote sensing and GIS techniques can be used for complete morphometric analysis and watershed prioritization studies. Remote sensing and Geographical Information System (GIS) techniques are being extensively used since quite some time in watershed related studies as very effective tools in determination of the basin geometry i.e., Morphometric analysis or quantitative description of watershed morphologic characteristics.

2. Study Area

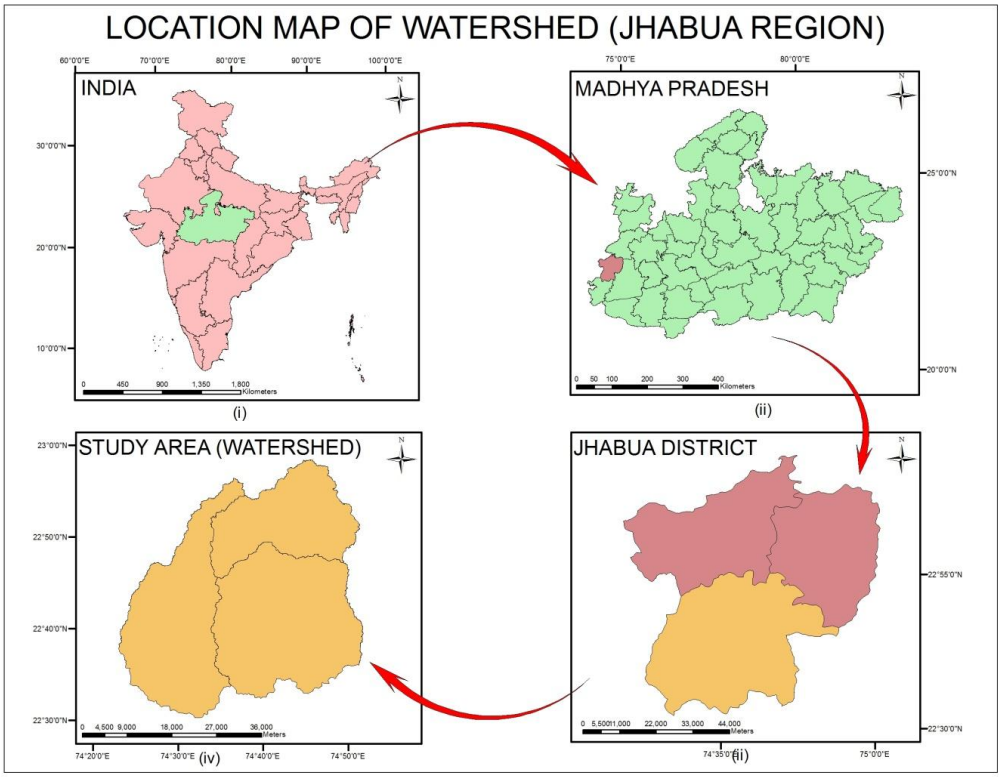

Figure 1: *Location map of study area*

The study area (watershed) is situated in Jhabua region located between latitude 22°30'31" N to 22°56'55" N and longitude 74°22'42" E to 74°37'4" E on SOI Toposheet nos. 46J/5, 46J/6 46J/9, and 46J/10. Watershed -1 falling in Mod nadi, watershed- 2 sapan nadi and watershed -3 negri nadi, all rivers are tributary of Mahi river basin in Jhabua region, western part of Madhya Pradesh, covers an area of 1643.79 sq.km (Figure 1). Physiographical the area is characterized by undulating topography. Jhabua in surrounded by one of the dense forest areas of Madhya Pradesh. Over the last four to five decades, more than 80 per cent of its forests were extremely degraded. The causes included intensive

cultivation on uplands and clearing of forests by wood contractors. Loss of forests led to loss of land productivity, diminishing employment opportunities, and outward migration of local people. The impact was felt more deeply by the tribal's who constitute 83 per cent of the district's population, and whose survival is closely linked to forests. Over this period, Jhabua witnessed some severe droughts and famines. The processes of deforestation and land degradation have caused extensive disorganization of water management systems. Migration in search of employment and sustenance swelled, during the 1990s, almost 65 percent of the local population was migrated out.

3. Data Evaluation and Methodology

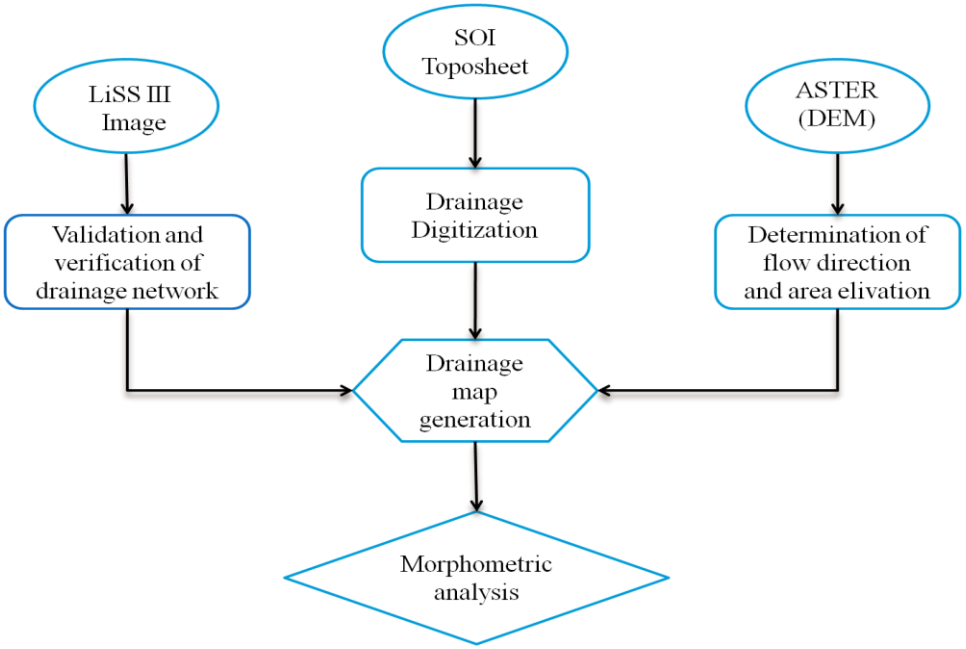

Flow Chart 1: *Showing drainage map preparation using different data sets*

Survey of India (SOI) toposheets no. 46j/5, 46j/6, 46j/9, and 46j/10 on 1:50,000 scale and Indian Remote Sensing Satellite (IRS-1) of LISS-III with 23.5 m spatial resolution in digital arrangement were used for drainage map preparation and quantitative analysis has been done (Figure 2, 4 & 6). The SOI toposheets and satellite data were geometrically rectified and georeferenced to world space coordinate system with digital image processing software (ERDAS IMAGINE 2011), and Digitization work by (ArcGIS 10). The order was given to each stream by subsequent stream ordering technique (Strahler, 1964). The attribute were assigned to create the digital data base for drainage layer of the watershed.

Various morphometric parameters of the basin were computed. Parallel channels flowing away from a central high point (Jensen, 2006). Properties of the stream networks are very important to study the landform making process (Strahler, 2002).

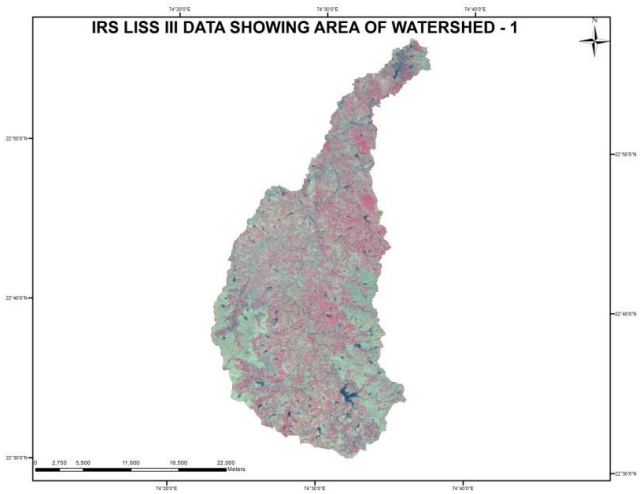

Figure 2: *LISS III Image of watershed 1 (Jhabua region*)

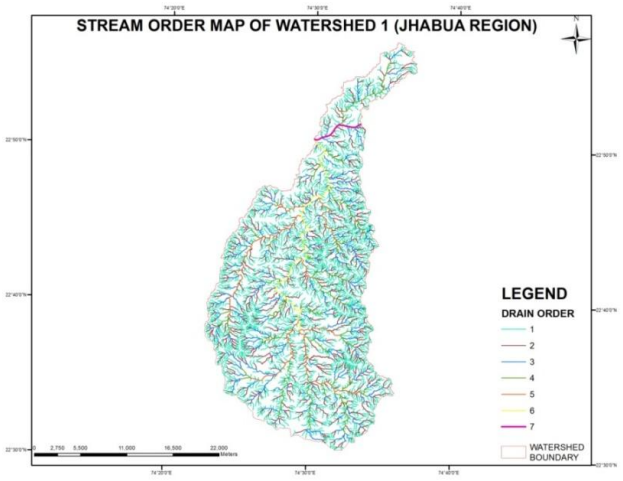

Figure 3: *Drainage network map of watershed 1 (Jhabua region)*

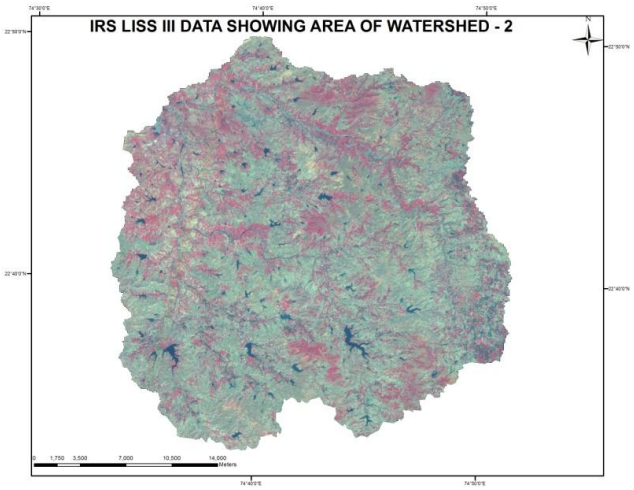

Figure 4: *LISS III Image of watershed 2 (Jhabua region)*

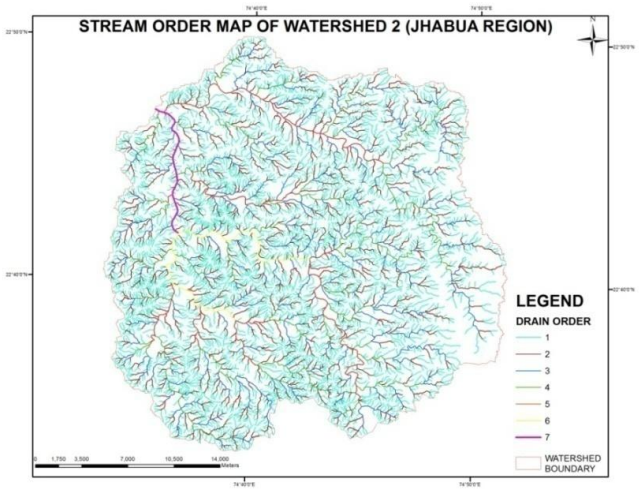

Figure 5: *Drainage network map of watershed 2 (Jhabua region)*

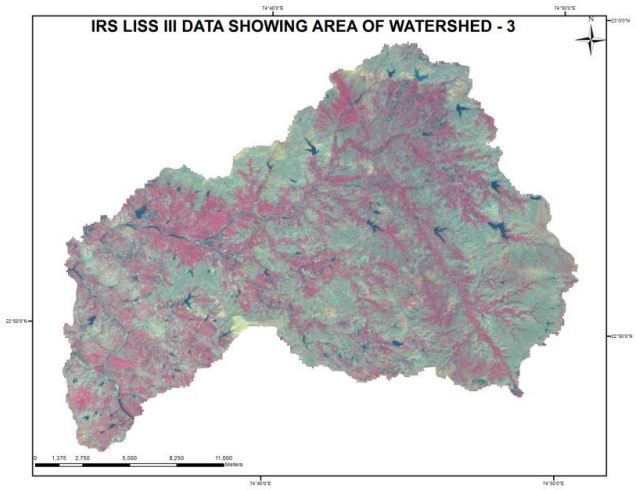

Figure 6: *LISSIII Image of watershed 3 (Jhabua* region)

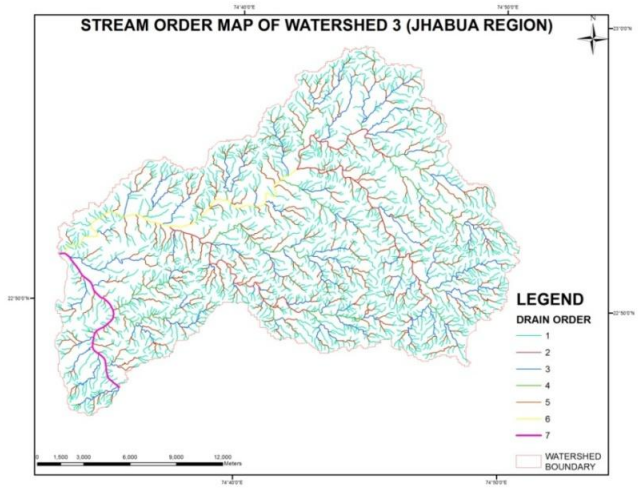

Figure 7: *Drainage network map of watershed 3 (Jhabua region)*

Morphometric parameters: The morphometric parameters were analysed in three categories:

1) **Linear aspect,** includes Number of Stream (Nu), Stream Length (Lu), Mean Stream Length (Lsm), Stream Length Ratio (Rl), Bifurcation Ratio (Rb) and Mean Bifurcation Ratio (Rbm),

2) **Arial aspect,** includes Drainage density (Dd), Drainage texture (T), Stream Frequency (Fs), Elongation ratio (Re), Circularity ratio (Rc), Form factor (Rf), Texture Ratio (T), Shape index (Sw), Drainage intensity (Di), Constant Channel maintenance (C),

3) **Relief aspect,** includes relative relief (R), Relief Ratio (Rh), and Ruggedness Number (Rn) Based on the drainage orders, the watershed has been classified as 7 order to analyse linear, arial and relief morphometric parameters as shown in Table 1,

***Table 1**: Methodology adopted for computation of morphometric parameters*

	Morphometric parameters	**Methods**	
LINEAR	Stream Order(U)	Hierarchical order	
	Stream Length(Lu)	Length of the stream	
	Mean Stream Length (Lsm)	Lsm=Lu/Nu	Where: Lu= Length of Stream in order(u)
			Nu= No. of Stream in order (u)
	Stream Length Ratio (R_L)	R_L=Lu/L(u-1)	Where: Lu= Length of Stream in order(u)
			Lu-1= the total stream length of its next lower order
	Bifurcation Ratio (Rb)	Rb=Nu/(Nu+1)	Where: Nu=Total no of stream segments of order
			Nu+1=Number of segments of the next higher order
	Mean Bifurcation Ratio(Rbm)	Rbm= Average of bifurcation ration of all order	
ARIAL	Stream frequency (Fs)	Fs= Nu/A	Where: Nu= Total no of streams of all order
			A= Area of the basin
	Drainage texture (Rt)	Rt=Nu/P	Where: Nu= Total no of streams of all order
			P= Perimeter
	Form factor (Rf)	Rf=A/Lb^2	Where: A= Area of the basin
			Lb2 = Square of basin length
	Circularity ratio (Rc)	Rc = 4pi*A/P^2	Where: Pi = 'Pi' value i.e., 3.14 or 22/7
			A= Area of the basin
			P= Perimeter
	Elongation ratio (Re)	Re = 2/Lb*sqrt(A)/Pi	Where: A= Area of the basin
			Pi = 'Pi' value i.e., 3.14 or 22/7
			Lb = Basin length
	Drainage density (Dd)	Dd = Lu/A	where: Lu = Total stream length of all order
			A = area of the basin
	Length of overland Flow (Lg)	Lg = 1/Dd*2	Where: Dd= Drainage density
	Constant Channel maintenance(C)	C=1/Dd	Where: Dd= Drainage density
	Texture Ratio (T)	T= N1/P^2	Where: N1 = No. of drainage in order one
			P = Perimeter

	Shape index (Sw)	$Sw = Lb^2/A$	Where: Lb = Basin length A = Area
	Drainage intensity (Di)	Di = Fs/Dd	Where: Fs = stream frequency Dd = drainage density
RELIEF	Relative Relief (R)	R=H-h	Where: H= maximum height of the basin h= minimum height of the basin
	Relief Ratio (Rh)	Rh=R/L	Where: R= total relief of the basin L = Basin length
	Ruggedness number (Rn)	Rn = R*Dd/1000	Where: R= total relief of the basin Dd = drainage density

4. Results and Discussion

Table 2: *Results showing comparative Morphometric analysis of Watershed (Jhabua region)*

Stream Order (U)	WS-1			WS-2			WS-3		
	No of Stream (Nu)	Stream Length (Lu) in (m)	Mean Stream Length (Lsm) in (m)	No of Stream (Nu)	Stream Length (Lu) in (m)	Mean Stream Length (Lsm) in (m)	No of Stream (Nu)	Stream Length (Lu) in (m)	Mean Stream Length (Lsm) in (m)
1	3100	1314.92	0.42	4346	1738.64	0.4	1706	821.76	0.48
2	715	467.34	0.65	963	568.35	0.59	374	287.8	0.76
3	175	249.32	1.43	218	308.09	1.41	84	167.55	1.99
4	38	123.38	3.24	46	169.42	3.68	18	55.16	3.06
5	8	68.43	8.55	9	71.75	7.97	4	41.41	10.35
6	1	31.5	31.5	2	24.52	12.26	1	20.58	20.58
7	1	6.37	61.37	1	11.18	11.18	1	11.59	11.59

Stream Order (U)	WS-1		WS-2		WS-3	
	Stream Length Ratio (R_L)	Bifurcation Ratio (Rb)	Stream Length Ratio (R_L)	Bifurcation Ratio (Rb)	Stream Length Ratio (R_L)	Bifurcation Ratio (Rb)
1&2	0.36	4.33	0.32	4.51	0.35	4.56
2&3	0.53	4.08	0.54	4.41	0.58	4.45
3&4	0.49	4.6	0.54	4.73	0.32	4.66
4&5	0.55	4.75	0.42	5.11	0.75	4.5
5&6	0.46	8	0.34	4.5	0.49	4
6&7	0.2	1	0.45	2	0.56	1

Water shed	Basin area	Perimeter	Length	Elongation ratio (Re)	Form factor (Rf)	Circularity ratio (Rc)
WS-1	574.78 Sq.Km.	169.69 Km.	43.87 Km.	0.61	0.3	0.062
WS-2	682.32 Sq.Km.	146.08 Km.	33.84 Km.	0.87	0.59	0.1
WS-3	390.02 Sq.Km.	131.02 Km.	30.02 Km.	0.74	0.42	0.07
Water shed	**Drainage density (Dd)**	**Stream frequency**	**Drainage texture (Rt)**	**Mean Bifurcation**	**Drainage intensity (Di)**	**Constant channel**

		(Fs)		Ratio(Rbm)		maintenance(C)
WS-1	3.98	7.03	29.8	4.46	1.76	0.25
WS-2	4.26	8.18	38.23	4.21	1.92	0.23
WS-3	3.65	5.6	16.7	3.86	1.53	0.27

Water shed	Length of overland Flow (Lg)	Texture Ratio (T)	Shape index (Sw)	Relative Relief (R)	Relief Ratio (Rh)	Ruggedness number (Rn)
WS-1	0.13	18.26	3.34	331	0.007	1.32
WS-2	0.11	29.75	1.67	342	0.01	1.46
WS-3	0.13	13.01	2.31	286	0.009	1.04

4.1. Linear Aspects

Stream order (u): Stream order is the first step for analyse Morphometry of a watershed. It is defined as a measure of the position of a stream in the hierarchy of tributaries. Stream ordering based on the method proposed by Strahler (1964) as smallest fingertip stream are designated as order 1. Where two first stream orders join, a stream segment formed of order 2; Where two of order 2 joins, a stream segment of order 3 is formed; and so 4th. In our study area Dendritic drainage pattern is seen in the plateau and hilly parts of the drainage basin indicating the homogeneity in texture and lack of structural control. The study area watershed delineate 7th order drainage segment (Figures 3, 5 & 7).

Stream number (Nu): The count of stream segment in a given order is known as stream number. According to Horton's standard the number of streams is adversely correlated with the order, i.e. stream number decreases with increase in stream order.

Stream length (Lu): Stream length is one of the most important hydrological features of the basin indicate the variation of surface run-off behaviours. It is the total length of streams in a particular order. Variation from its general behaviour designate that the land is characterised by high relief and/or moderately steep slopes, underlain by varying lithology and feasible uplift across the basin (Singh and Singh, 1997). The observation demonstrates that the area depends only on the drainage characteristics for movement of water.

Mean Stream Length (Lsm): The mean stream length of a channel is a dimensional property and reveals the characteristic size of drainage network components and its contributing basin surfaces (Strahler, 1964). The observation demonstrates that the area depends only on the drainage features for flow of water. The mean stream length (Lsm) has been calculated by dividing the total stream length of order by the number of streams.

Stream length Ratio (R_L): Stream length ratio (R_L) defined as the ratio of the mean length of an order to the next lower order of stream segment. Stream lengths refers that the mean stream lengths of stream segments of each of the successive orders of a watershed tend to estimate through geometric sequence in which the first term (stream length) is the average length of segments of the first order (Horton, 1945).

Bifurcation ratio (Rb): This is dimensionless parameters that express the ratio of the number of streams of any given order (Nu) to the number in the next lower order. If bifurcation ratio is not same from one order to its next order, then these irregularities are credited to geological and lithological development of a drainage basin. Bifurcation ratio is an important parameter that expresses the degree of consequence of drainage network (Strahlar). Bifurcation ratios range from 1 to 4.7 in all three watershed (Table 2).

Mean Bifurcation Ratio (Rbm): To arrive at a more representative bifurcation number Strahler (1953) used a weighted mean bifurcation ratio obtained by multiplying the bifurcation ratio for each successive pair of orders by the total numbers of streams involved in the ratio and taking the mean of the sum of these values. The average bifurcation ratio in the three watersheds is 3.86 to 4.46, because of possibility of variations in geometry and lithology. The highest Rb in ws-1 (4.7), ws -2 (5.11) is found between 4th & 5th order whereas in ws-3 (4.6) is found between 3rd & 4th order, indicates higher runoff and discharge and less permeable rock hills connected with steep slopes. In addition, the irregularity in peak flows depends on the lithological and geological development of drainage basin.

4.2. Arial aspects

Stream frequency (Fs): Stream frequency (Fs) is the ratio of total number of stream segments of all orders to the basin area. According to Reddy Found that lowers Fs values indicate permeable sub-surface material and low relief, whereas higher values are the characteristic of resistant sub-surface material, high relief and light vegetation. The stream frequency of our ws-1 is 7.03, in ws-2 8.18 and ws-3 5.6.

Drainage texture (Rt): Strahler, Defined drainage texture as the total number of stream segments of all orders divided by the perimeter of the watershed. Drainage texture indicates comparative spacing of drainage lines, which are more important in impermeable material, compared to the permeable material.

Smith, classified drainage density into five classes of drainage texture, *i.e.* less than 2, indicates very coarse, between 2 to 4 is coarse, between 4 to 6 is moderate, between 6 to 8 is fine and greater than 8 is very fine drainage texture. The Jhabua tehsil has a value of drainage texture is 16.7 to 38.23 which falls under very fine drainage texture.

Form factor (Rf): According to Horton (1932) form factor defined as the ratio of basin area to square of the basin length. Small value of form factor shows the basin will be more elongated. Rf values of the study area vary from 0.3 to 0.59 indicate that they are to be elongated circular shape and signifying flatter peak flow for longer duration.

Circularity ratio (Rc): Circularity ratio (Rc), as the ratio of the area of the basin (A) to the area of a circle having the same circumference as the perimeter (P) of the basin. Circularity ratio (Rc) is influenced by the length and frequency of streams, land use/land cover, geological structures, climate, relief and slope of the basin. In the study area, the Rc value is 0.062 to 0.1, indicating that the area is characterized by high relief, resulting high discharge of runoff and low permeability of sub soil conditions.

Elongation ratio (Re): It is the ratio between the diameter of the circle of the same area as the drainage basin and the maximum length of the basin. A circular basin is more capable in run-off discharge than an elongated basin (Singh and Singh, 1997). The value of Re in the study area was found to be 0.61 to 0.87 associated with high relief and steep ground slope (Strahler, 1964).

Drainage density (Dd): Horton (1932) defined the drainage density (Dd) is an important indicator of the linear scale of landform elements in stream eroded topography. It is the ratio of total channel segment lengths cumulated for all orders within a basin to the basin area, which is expressed in terms of km/sq.km. Density is associated to climate, lithology, relief, in- filtration capacity, vegetative cover, surface roughness and run-off index. Out of which only surface roughness has no significant correlation with drainage density (Syed Ahmad Ali, Nazia Khan). According to (Nag, 2002) drainage density values between 0.55 and 2.09 km/km^2 correspond to humid regions. Found that low drainage density generally results in areas of highly resistant rocks or permeable subsurface material, low relief and dense vegetation. High drainage density results due to weak or impermeable subsurface material,

thin vegetation and high relief. Low drainage density leads to coarse drainage texture whereas high drainage density leads to fine drainage texture. In our study area have high drainage density i.e. 3.65 to 4.26 km/km^2 which are indicative of less permeable subsurface material, thin vegetative cover and moderate to high relief (Table 2).

Length of overland Flow (Lg): It is the extent of water over the ground before it gets concentrated into definite stream channels, (Horton, 1945). Length of overland flow relates inversely to the average slope of the channel and is quite synonymous with the length of sheet flow to a large degree. The average length of overland flow is approximately half the average distance between stream channels and is consequently around equals to half of equal of drainage density. The value of Length of Overland Flow of the watersheds is 0.13, 0.11, & 0.13 (Table 2). The value is equals to the half of the constant channel maintenance.

Constant channel maintenance (C): Schumm (1956) defined as the inverse of drainage density or the constant of channel maintenance as a property of landforms. The constant of channel maintenance indicate the relative size of landform units in a drainage basin and has a specific genetic association (Strahler, 1957). The Constant of Channel Maintenance of the ws-1 is 0.25, ws-2 0.23, and ws-3 0.27 (Table 2). This low value indicates high structural disturbances, low permeability, steep to very steep slopes and high surface run off.

Texture Ratio (T): Texture ratio (T) is depending on the underlying lithology, infiltration capacity and relief aspect of the land. In the present study the texture ratio of the WS -1 18.26 & WS-2 29.75 indicating ultra-fine texture whereas the value of WS -3 is 13.01 indicating fine texture. The texture ratio is defined as the ratio between the first order streams and perimeter of the basin (Rt = Nl / P). Based on ratios texture (Rt) values, Smith et.al, proposed classification of drainage texture. For Rt value of 4.0 and below, the texture is coarse; value between 4.0 to 10.0, has intermediate texture; value above 10.0, has fine texture and for Rt value above 15.0, the texture is ultra fine (bad land topography).

Shape index (Sw): Speed of water and sediment yield along the length and relief of the drainage basin is largely affected by the shape. The shape index values for watersheds of the study area range from 3.34, 2.31 in WS1 & 3, to 1.67 in WS 2 as shown in (Table 2). In terms of, WS 1 and 3 will have the shorter basin lag time, while WS 2 will have the longer basin lag time.

Drainage intensity (Di): According to Faniran (1968) the drainage intensity is the ratio of the stream frequency to the drainage density. This study shows a low drainage intensity of 1.76, 1.92, 1.53 for the watershed 1, 2 and 3 (Table 2). These low values of drainage intensity indicate that drainage density and stream frequency have little effect on the extent to which the surface has been lowered by agents of denudation. These low values of drainage density, stream frequency and drainage intensity, surface runoff are not speedily removed from the watershed, making it highly susceptible to flooding, gully erosion and landslides.

4.3. Relief aspects

Relative Relief (R): Relative relief termed as ‘amplitude of available relief or local relief’ is defined as the difference in height between the highest and the lowest points in a unit area. It is an important morphometric variable used for the overall evaluation of morphological characteristics of terrain. Melton (1958) suggested to calculate relative relief by dividing the difference of height between the highest and lowest points in the basin (H) with basin perimeter (P), thus relative relief = H/P. Relative relief is calculated on the basis of highest and lowest elevations and the data of relative relief so derived are classified into three categories viz. (i) low relative relief = 0m – 100m, (ii) moderately relative relief 100m – 300 m and (iii) high relative relief = above 300m. In our study area the value of

relative relief are in ws -1 331, ws-2 342, ws-3 286 indicating relative relief for ws- 1 & 2 is comparatively high then ws-2.

Relief Ratio (Rh): The relief ratio is the ratio of the maximum relief to the horizontal distance along the longest dimension of the basin equivalent to the principal drainage line (Schumm, 1956). It is a measure of the overall steepness of a drainage basin and is an indicator of the strength of the erosion processes operating in the basin. Its value normally increases with decreasing drainage size and area of a given drainage basin (Gottschalk, 1964). In the present study Rh ranges from a minimum of 0.007, 0.009 in WS 1 & 3 to a maximum of 0.01 in WS 2 lower values of Rh indicate that low erosion processes are taking place.

Ruggedness number (Rn): According to Farrukh et al., ruggedness number indicates the structural complexity of the terrain in association with the drainage density and relief aspects. It also indicates that the area is susceptible to soil erosion. Calculated comparatively Rn of ws -1 is 1.32, ws-2 is 1.46, and ws-3 is 1.04. The value shows of ws 1 and 2 are high ruggedness number then ws-3.

5. Conclusions

Remote sensing and GIS techniques are convenient tools for morphometric analysis. The present study demonstrates the value of remote sensing and GIS techniques in prioritizing watersheds based on morphometric analysis. The morphometric analysis has been carried out during measurement of linear, areal and relief aspects of basins. It has been found that the area is 7th order drainage in all watershed of Jhabua Region. On the basis of the morphometric studies, it is concluded that the hydrologic response of the all watershed in Jhabua tehsil represents dendritic to sub-dendritic drainage pattern. The large number of first order streams indicates uniform lithology and gentle slope gradient. All three watersheds show fine to very fine drainage texture. The bifurcation ratio and constant channel maintenance value indicates steep to very steep slopes and higher surface run off discharge and less permeable rock hills. The high drainage density indicates the basin is low permeable subsoil, thin vegetation cover, high relief and fine drainage texture. The value of constant channel maintenance varies from 0.23 to 0.27 indicating steep to very steep slopes and high surface run off. The watersheds are in active stage of degradation and show that are possibly having high erosion. Hence, suitable soil erosion control measures are required in these watersheds to preserve the land from further erosion for development of the area to maintain the ecological environment.

References

Altaf, F., Meraj, G., & Shakil, A. Romshoo, Morphometric Analysis to Infer Hydrological Behaviour of Lidder Watershed, Western Himalaya, India. *Hindawi Publishing Corporation Geography Journal*. 2013, 14.

Abdel Ghaffar, M.K., Abdellatif, A.D., Azzam, M.A., & Riad, M.H. Watershed Characteristic and Potentiality of Wadi El-Arish, Sinai, Egypt. *International Journal of Advanced Remote Sensing and GIS.* 2015. 4; 1070-1091.

Ali, S.A., & Khan, N. Evaluation of Morphometric Parameters-A Remote Sensing and GIS Based Approach. *Open Journal of Modern Hydrology*. 2013. 3; 20-27.

Gottschalk, L.C., 1964: *Reservoir sedimentation. In Handbook of Applied Hydrology*. V.T. Chow (Ed.), section 7-1, New York, USA: McGraw-Hill.

Hardely, R.F., & Schumm, S.A. Sediment sources and drainage basin characteristics in upper Cheyenne River basin United States. *Geological survey water-supply paper*. 1961. 1531-B. 10-19.

Horton, R.E. Erosional Development of streams and their drainage basins, Hydro physical approach to quantitative morphology. *Geological Society of American Bulletin*. 1945. 56; 275-370.

Horton, R.E. Drainage Basin Characteristics. *Transactions of American Geophysics Union*. 1932. 13; 350-361.

Horton, R.E. Erosional Development of Streams and their Drainage Basins: A Hydrophysical Approach to Quantitative Morphology.

Jensen, J.R., 2006: *Remote Sensing of the Environment*. 1 st edition, New Delhi: Dorling Kindersley (India) Pvt. Ltd.

Obi Reddy, G.P., Mji, A.K., Chary, G.R., Srinivas, C.V., Tiwary, P., & Gajbhiye**,** K.S. GIS and Remote Sensing Applications in Prioritization of River Sub Basins Using Morphometric and USLE Parameters-A Case Study. *Asian Journal of Geoinformatics*. 2004a. 4 (4) 35-48.

Melton, M.A. Geometric properties of mature drainage basin systems and their representation in their E4 phase space. *Journal of Geology.* 1958. 66; 35-56.

Mostafa Kamel Abdel Ghany. Quantitative Morphometric Analysis of Drainage Basins between Qusseir and Abu Dabbab Area, Red Sea Coast, Egypt using GIS and Remote Sensing Techniques. *International Journal of Advanced Remote Sensing and GIS*. 2015. 4; 1295-1322.

Nag, S.K. Morphometric Analysis Using Remote Sensing Techniques in the Chaka Sub Basin, Purulia District, West Bengal. *Journal of the Indian Society of Remote Sensing*. 1998. 26 (1-2) 69-76.

Strahler, A.N. Hypsometric Analysis of Erosional Topography. *Bulletin of the Geological Society of America*. 1952. 63 (11) 1117-1142.

Smith, K.G. Standards for Grading Texture of Erosional Topography. *American Journal of Science*, 1954. 248; 655-668.

Schumm, S.A. Sinuosity of Alluvial Rivers on the Great Plains. *Bulletin of the Geological Society of America.* 1963. 74; 1089-1100.

Schumm, S.A. Evolution of Drainage systems and Slopes in Badlands at Perth Amboy, New Jersey. *Geological Society of America Bulletin*. 1956. 67; 597-646.

Singh, S., & Singh, M.C. Morphometric analysis of Kanhar river basin. *National Geographical J. of India*. 1997. 43 (1) 31-43.

Smith, K.G. Standards for grading textures of erosional topography. *Am. Jour. Sci*. 2002. 248; 655-668.

Strahler, A.N., 1964: *Quantitative geomorphology of drainage basins and channel networks*. Handbook of Applied Hydrology. New York: McGraw Hill Book Company. 411.

Strahler, A.N., 1964: *Quantitative Geomorphology of Drainage Basins and Channel Networks*. In: V.T. Chow (Ed.), Handbook of Applied Hydrology. New York: McGraw Hill Book Company. Section 4-11.

Strahler, A.N., & Strahler, A.H. *A Text Book of Physical Geography*. New York: John Wiley & Sons.

Tribhuvan, P.R., & Sonar, M.A. Morphometric Analysis of a Phulambri River Drainage Basin (Gp8 Watershed), Aurangabad District (Maharashtra) using Geographical Information System. *International Journal of Advanced Remote Sensing and GIS*. 2016. 5; 1813-1828.

Cloud Publications
International Journal of Advanced Remote Sensing and GIS
2017, Volume 6, Issue 1, pp. 2023-2032
ISSN 2320 – 0243, Crossref: 10.23953/cloud.ijarsg.32

Research Article | Open Access

Morphometric Analysis of Singki River Catchment using Remote Sensing & GIS: Papumpare, Arunachal Pradesh

Mahendra S. Lodhi and Masoom Reza

GB Pant National Institute of Himalayan Environment and Sustainable Development, NE-Unit, Itanagar, India

Publication Date: 5 January 2017

DOI: https://doi.org/10.23953/cloud.ijarsg.32

Abstract River is playing an important role in landform development, its shapes the structure of area. River process is a natural phenomenon supported by many agents such as precipitation. It has participated role in changing river behaviour, rainfall contributes in the volume of water and work as an agent in erosional process. Carrying scientific study to understand the characteristics of the area, river is one of the assets which describe the aspects and phenomenon related to Landforms. With the help of remote sensing & GIS, we can extract all the physical information of river, called morphometric parameters. The Singki river catchment accumulated an area of 79.8 Km^2 and has elevation 2353 metre; the rugged and irregular terrain surface shapes Dendritic drainage pattern.
Keywords *Geology; Morphometry; River Catchment; Remote Sensing & GIS*

1. Introduction

Himalaya known as water tower of Asia because all the major rivers of India originate from Himalayan regions and all are perennial, the huge amount of Area is under Cryosphere. Arunachal Pradesh has five major rivers and its tributary including nine all are originates from Himalaya such as Siang is known as Yarlung-Tsangpo in Tibet originates from Angsi Glacier in Tibet and also known as Brahmaputra in Assam, Siang is the main tributary of River Brahmaputra, there are many small tributary joins Siang is Siyum, Yamne, Yameng etc. The River Subansiri is largest tributary of River Brahmaputra joins in the North Lakhimpur district of Assam, the river originates from China and has total length of 442 km. River Kameng is originated from Glacial Lake situated in Gori Chen Mountain district Tawang and also known as Jia-Bharali in Assam and a Tributary of Brahmaputra. From Eastern part of state a river flow towards South direction and later joined Brahmaputra called Dibang; it originates from Keya Pass on the Indo-China border. Before joining Brahmaputra River Lohit discharge water to River Dibang.

Singki River flows in the foothills of Himalayan state, Arunachal Pradesh. The state is situated in the far-eastern region of India and also receives first dawn of Sunlight. The Singki River has 5^{th}order of streams and has characteristics of dendritic pattern (Figure 1). The river has a minimum discharge of 8857 MLD which is sufficient for Itanagar Town and it is controlled & managed by PHED department (Paron Omem et al., 2014). Singki is a perennial river flows with high velocity all year round and

transported high boulders. River channel erosion is common in Singki basin because of deforestation near the banks of river and high velocity streams supported by many non-perennial streams helps in increase in the volume of the river which is also an important factor contributing in erosional and carrying process. On the other hand, the micro-climate playing its role literally, it influences on both the discharge of water and sediment to and along the channel and the channel boundary characteristics.

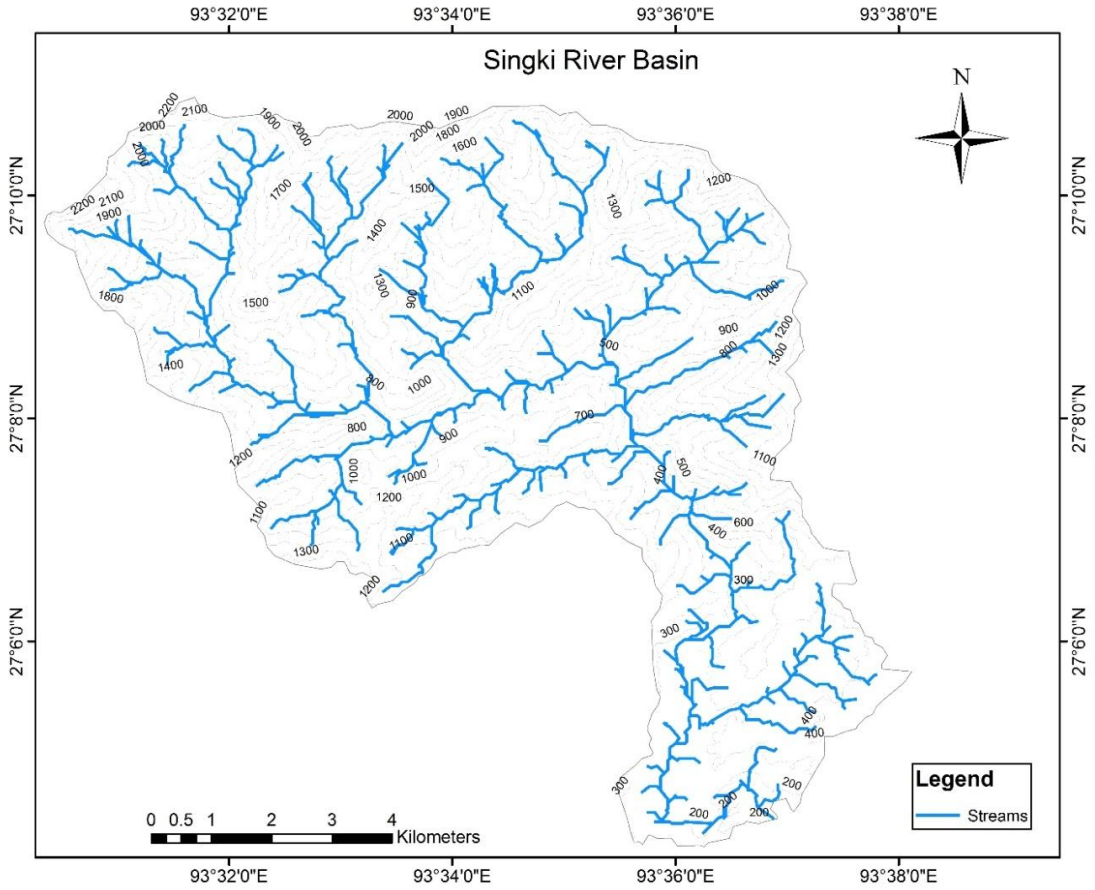

Figure 1: *Showing the Drainage Pattern of Singki River Basin with Elevation in metre*

2. Study Area

Singki River basin falls in Papumpare district of Arunachal Pradesh (Figure 2). The total area of the Singki river basin is 79.8 Sq.km. The study area is located lies between longitude 93°30'- 93°38"E and latitude 27°4'- 27°12'N. The study area falls under tropical climate. It has moderate temperatures in summer and is very cold in winters. The warmest month of the year is August, with an average temperature of 27.5 °C. January has the lowest average temperature of the year. It is 15.2 °C. Itanagar features an oceanic climate (Köppen climate classification Cwa), with dry, mild (however, cold by Indian standards) winters and cool, wet summers (en.climate-data.org).

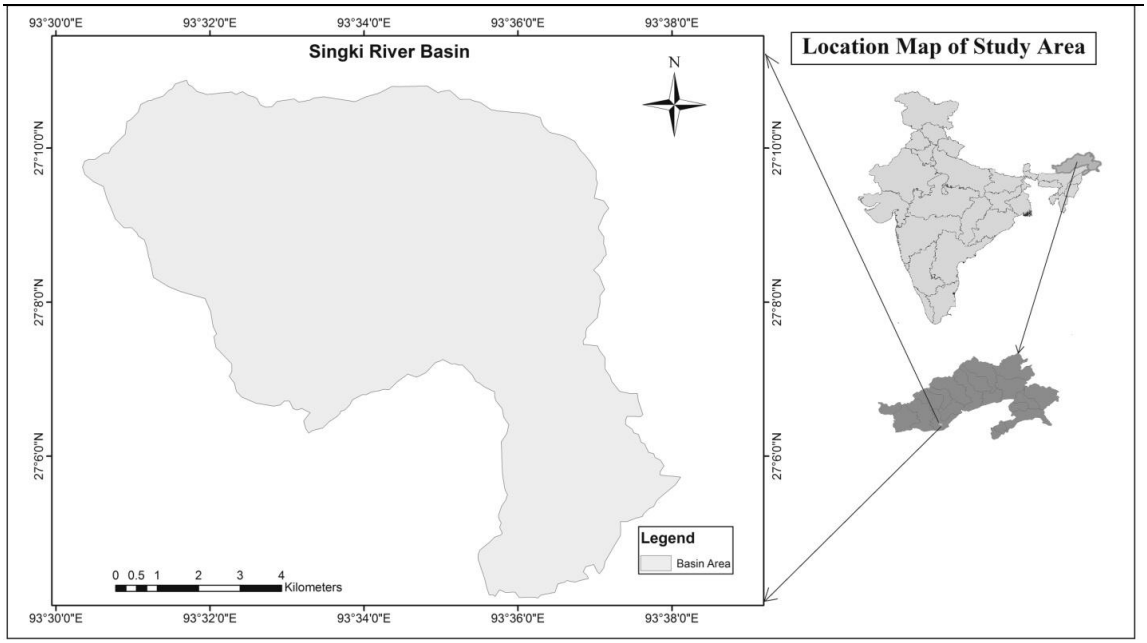

Figure 2: *Location Map of the Study Area*

2.1. Geology

The lithosphere of Singki river catchment has characterized by numbers of formations consist of four types such as a) Lower Permian-lower Gondwana group-Bichom formation: constituted of dark grey Quartzite rocks, Shale/slate, sandstone and siltstone with coaly material and is thrusted over Siwaliks group and lie under Bomdila group. b) Lower Miocene-lower Pleistocene-Siwalik group-Dafla formation: consist of indurated sandstone and shale at bottommost, massive sandstone along with siltstone, clay and gravel. C) Paleoproterozoic-Biotite Granite Gneiss-Tourmaline. d) Paleoproterozoic-Bomdila Group-Tenga Formation consists of Gneissic rock types belong to Precambrian age, shale and Intrusive Granite etc. (Chakrabarti, 2016)

2.2. Climate

The climate is warm and temperate in Itanagar. In winter, there is much less rainfall in Itanagar than in summer. The climate here is classified as Cwa by the Köppen-Geiger system. The average temperature is 27.5 °C. The average annual rainfall is 2694 mm. The driest month is December, with 13 mm of rainfall. With an average of 489 mm, the most precipitation falls in July. The warmest month of the year is August, with an average temperature of 27.5 °C. January has the lowest average temperature of the year. It is 15.2 °C. The difference in precipitation between the driest month and the wettest month is 476 mm. During the year, the average temperatures vary by 12.3 °C (en.climate-data.org).

3. Methodology

3.1. GIS Based Data Collection

In the present study, extracting physical information of Singki River and prioritization of streams has been done using Remote Sensing and GIS techniques. Survey of India toposheets were also referred for the delineation of watershed boundary and draining network. The study was carried out on watershed level using Digital Elevation Model and using GIS software ArcGIS 9.3 for digitization and Arc Hydro tools using Aster Digital Elevation Model for delineating streams and watershed boundary. The following data/Software was used for the study:

- Aster - DEM data (30×30m)
- ArcGIS 9.3
- Erdas 9.1

3.2. Morphometric Analysis

The basin morphometry includes the analysis of the characteristics of linear, areal and relief aspects of drainage basins. It is a method of extracting physical information of the river and its basin. The formulas adopted for computation of morphometric analysis are given by many geomorphologist and experts (Table 1).

Table 1: *Formula used to quantify the Morphometric parameters*

Sl. No.	Morphometric Parameters	Formula	Reference
1.	Stream order	Hierarchical Rank	Strahler (1964)
2.	Stream Length	Lsm	Horton (1945)
3.	Mean stream length	Lū= Lu/Nu	Strahler(1964)
4.	Stream length ratio	Rl=Lu/Lu^{-1}	Horton (1945)
5.	Bifurcation Ratio	Rb= Nu/Nu^{+1}	Schumn(1956)
6.	Mean Bifurcation Ratio	Rbm	Strahler (1957)
7.	Relief Ratio	Rh=H/lb	Strahler (1957)
8.	Drainage Density	D=∑Lu/A	Horton(1932)
9.	Stream Frequency	Fs=∑Nu/A	Horton (1932)
10.	Drainage Texture	Rt=∑Nu/P	Horton(1945)
11.	Form Factor	Rf=A/Lb^2	Horton (1932)
12.	Circulatory Ratio	RC=4π ×A/P^2	Miller (1954)
13.	Elongation Ratio	$Rc = \frac{2\sqrt{A}}{\pi} / Lb$	Schuman(1956)
14.	Length of overland flow	Lg=1/D ×2	Horton (1945)

4. Results

1) Linear Aspect It is related to the channel patterns of the stream network and the topological characteristics of the stream segment (Savindra Singh, 2011).

a) Stream Order: The method of stream ordering proposed by Strahler in 1952. Stream order only increases when streams of the same order intersect. Therefore, the intersection of a first order and second order link will remain a second order link, rather than create a third order link. Singki river basin has 5^{th} order of stream (Figure 3) and has total length of all order of streams is 166.2 Km.

b) Stream Number (Nu): The total number of streams of all orders is 446. In 1^{st} order has 253, 2^{nd} order has 96, 3^{rd} order has 69, 4^{th} order has 27 and 5^{th} order has 1 streams (Table 3).

c) Stream Length (Lu): The length of the stream of all order calculated through GIS software, the total length is 166.2 Km. The order wise length is 1^{st} order has 83.1 km, 2^{nd} order has 35.2, 3^{rd} has 21 km, 4^{th} has 9.8 km and 5^{th} order has 17 Km (Table 2).

d) Bifurcation Ratio (Rb): The ratio between the two orders of stream segments; lower to the next higher order, called Bifurcation ratio. If the bifurcation ratio of any drainage is low, chances of flooding increases, the flow of water will accumulate in particular streams rather than spreading. Comparatively by analysing the bifurcation ratio of sub basins we can easily analyse which portion of drainage basin is having higher risk of flooding (Waugh, 2002).

e) Stream Length Ratio (Rl): The ratio between the number of stream length of particular stream order and the lower order (Table 3).

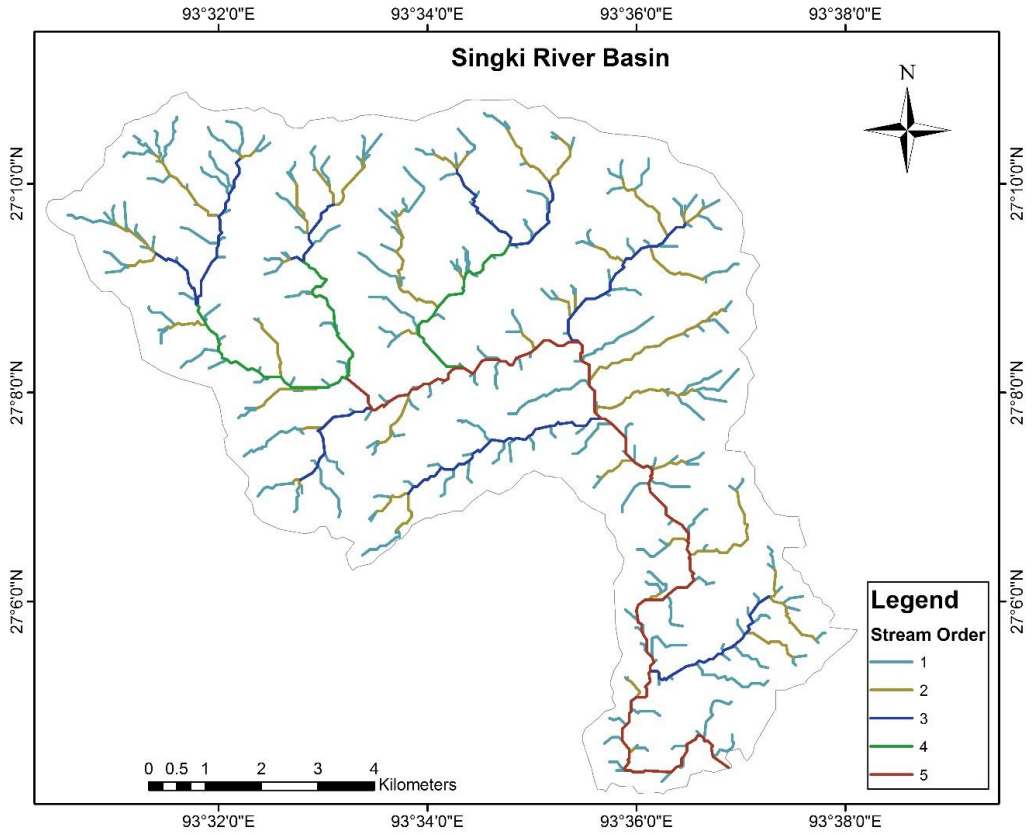

Figure 3: *Showing the Stream Ordering of Singki River*

Table 2: *Showing the distribution of Length (in km) Order Wise*

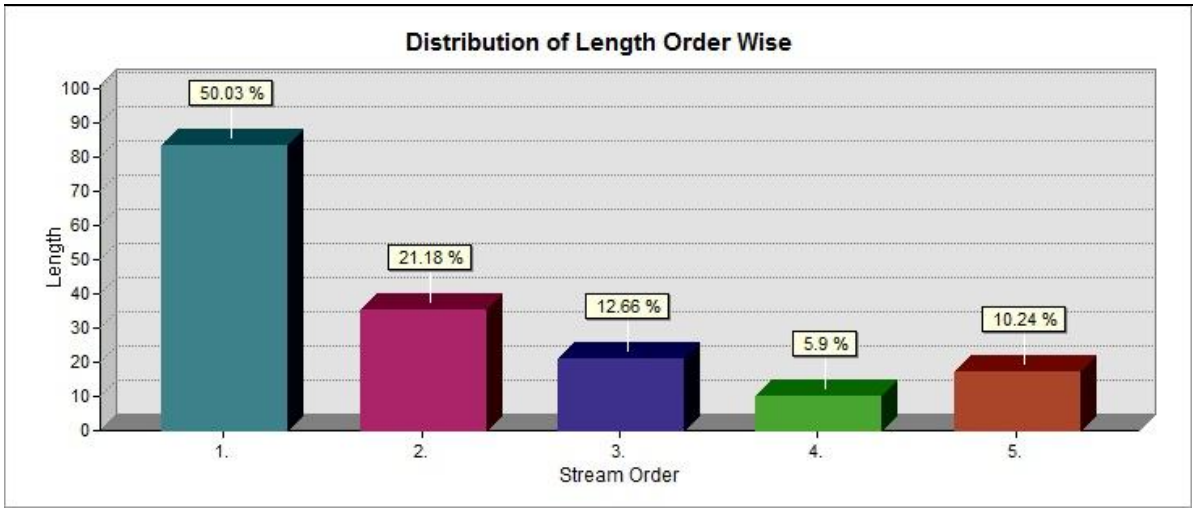

2) Areal Aspect

a) Basin Area: The basin boundary demarcated from Digital Elevation Model with the help of ArcGIS software. The area of Singki Basin is 79.8 Km^2. The area has undulating terrain surface and forms dendritic drainage pattern (Figure 1). Because of Altitude ranges from 167m to 2353 m the river velocity is high and terrain is sloppy too (Table 3).

b) Stream Frequency: Stream frequency is the measure of segments of streams per unit area of a basin. The stream frequency of Singki river is 5.6 Km (Table 3).
c) Drainage Density: It is the ratio of total stream length of the basin to basin area. The drainage density of Singki is 2.08 Km^2. higher drainage density reflects the weak subsurface materials, scattered vegetation and mountain relief (ZavoianuI, 1985).
d) Drainage Texture: It defines the total number of streams in the basin of all orders over length of the Perimeter. The drainage texture of Singki basin is 2.08 km^2 (Table 3).The low density with highly spaced channels forms in hard and erosion resistant layer and high drainage density with low spaced channels appears on erosion landforms.
e) Form Factor: It is defined as the ratio of the basin area to the square of the basin length. This factor indicates the flow intensity of a basin of a defined area (Horton, 1945). The form factor is should always less than 0.13 it indicates the basin has elongated and lower peak flows of longer duration.
f) Elongation Ratio (Re): is defined by Schumm (1956) as the ratio of the diameter of a circle with the same area as that of the basin to the maximum basin length. Strahler states that this ratio runs between 0.6 and 1.0 over a wide variety of climatic and geologic types. The varying slopes of watershed can be classified with the help of the index of elongation ratio, i.e. circular (0.9-0.10), oval (0.8-0.9), less elongated (0.7-0.8), elongated (0.5-0.7), and more elongated (less than 0.5).The elongation ratio of Singki River is 0.23 (Table 3).
g) Circularity Ratio: Miller (1953) Introduced basin circulatory ratio and defined it as the ratio the basin area to the area of a circle having a circumference equal to the perimeter of the basin. The circulatory ratio of study area is 0.4 (Table 3). He described the basin's circulatory ratio ranges from 0.4-0.5 indicates strongly elongated and highly permeable homogeneous layers.
h) Length of Overland Flow: It is all about the soil infiltration capacity when it's exhausted due to heavy precipitation, the excess water flow towards channel and steep slope. It is important parameters to analyse runoff and flood process. According to Horton (1945), this parameter is in most cases half the average distance between the stream channels and hence it approximately equals to half the reciprocal of drainage density. The length of overland flow of Singki basin is 0.24 (Table 3).

3) Relief Aspect

a) Basin Relief: It is the vertical distance between the highest elevation point and lowest point of the basin. Basin relief of Singki is 2186m (Figure 4).
b) Relief Ratio: It is the ratio between the basin relief and basin length. It analyse the terrain steepness of a drainage basin and it also indicates the intensity of erosional processes operating on slopes. Possibility of a close correlation between relief ratio and hydrology characteristics of a basin is suggested by Schumm (1956), who found that sediment loss per unit area is closely correlated with relief ratio. The relief ratio is 89.6 m/km (Table 3).

Table 3: *Results*

Sl. No.	Morphometric Parameters	Formula	Result	Reference
1.	Stream order	Hierarchical Rank(u)	1^{st}, 2^{nd}, 3^{rd} ,4^{th},& 5^{th} (orders)	Strahler (1964)
2.	Stream Length	Lsm	Total stream length=166.2 km	Horton (1945)
3.	Mean stream length	Lsm=Lu/Nu	Orders 1^{st} =0.32km 2^{nd} =0.36km 3^{rd}=0.30km 4^{th} = 0.36km 5^{th} = 17 km	Strahler(1964)
4.	Stream length ratio	$Rl=Lu/Lu^{-1}$	$2^{nd}/1^{st}$ =0.42	Horton (1945)

			$3^{rd}/2^{nd}$ =0.6 $4^{th}/3^{rd}$=0.46 $5^{th}/4^{th}$ =1.7	
5.	Bifurcation Ratio	Rb= Nu/Nu^{+1}	$1^{st}/2^{nd}$ =2.63 $2^{nd}/3^{rd}$ =1.39 $3^{rd}/4^{th}$ = 2.55 $4^{th}/5^{th}$ = 27	Schumn(1956)
6.	Mean Bifurcation Ratio	Rbm	Rb= 8.39	Strahler (1957)
7.	Relief Ratio	Rh=H/lb	89.62 m/km	Strahler (1957)
8.	Drainage Density	D=∑Lu/A	2.08 km^2	Horton(1932)
9.	Stream Frequency	Fs=∑Nu/A	5.6 km	Horton (1932)
10.	Drainage Texture	Rt=∑Nu/P	9	Horton(1945)
11.	Form Factor	$Rf=A/Lb^2$	0.13	Horton (1932)
12.	Circulatory Ratio	$RC=4\pi \times A/P^2$	0.4	Miller (1953)
13.	Elongation Ratio	$R_c = \frac{2\sqrt{A}}{\pi} / Lb$	0.23	Schuman(1956)
14.	Length of overland flow	Lg=1/D ×2	0.24	Horton (1945)

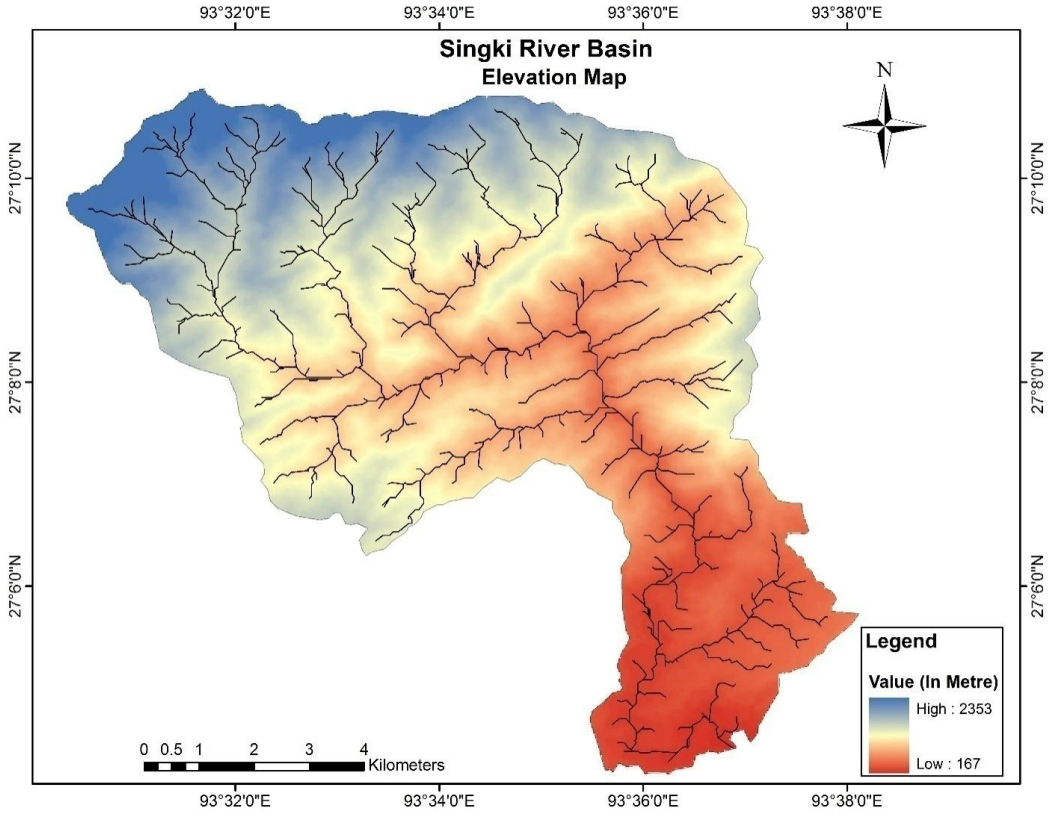

Figure 4: *Showing the Basin Relief Using ASTER Digital Elevation Model (30×30) m*

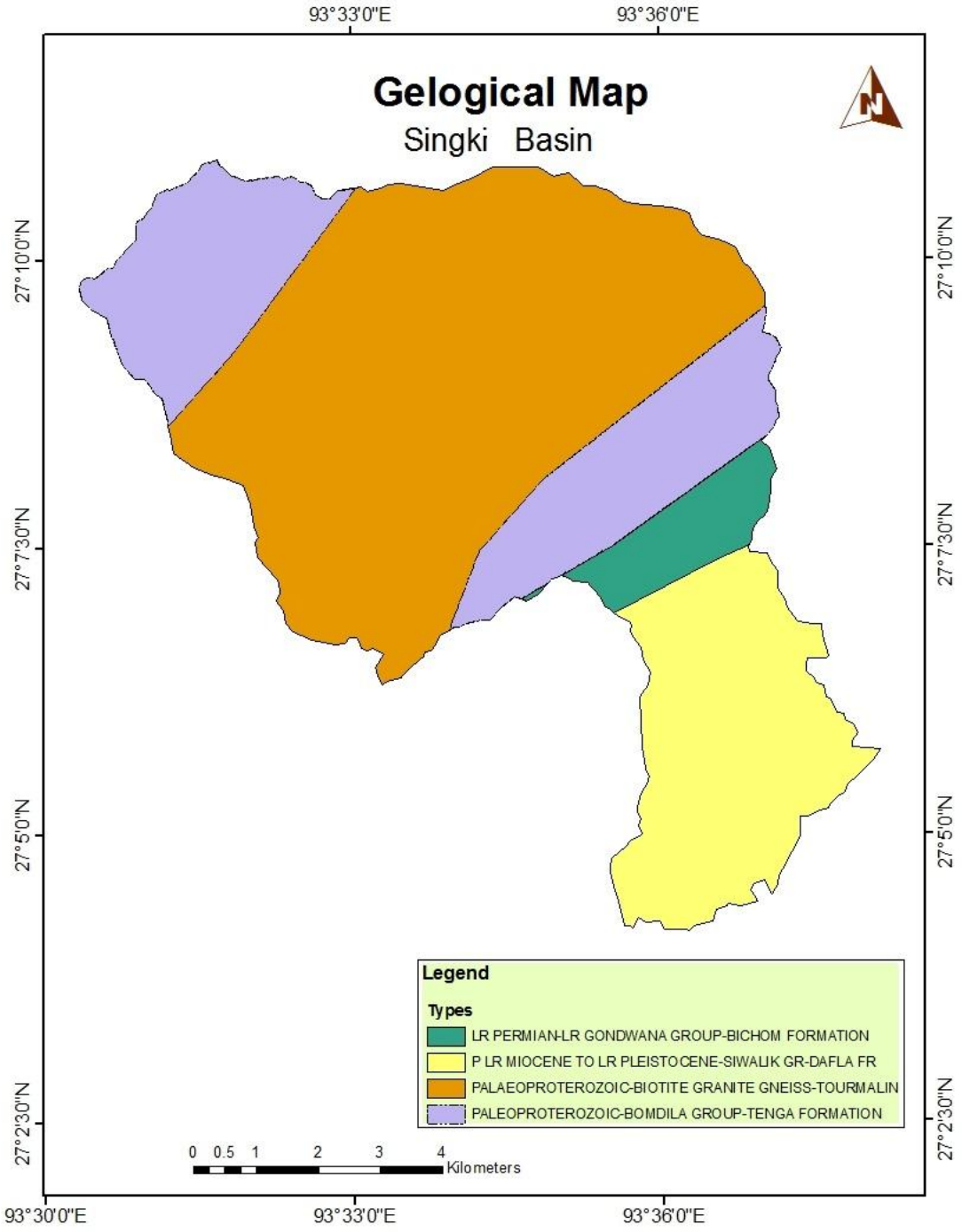

Figure 5: *Geological Map of Singki Basin*

4. Discussion

Singki River is the lifeline of Itanagar, and it plays very important role in the fulfillment of drinking water supply in the capital city of Arunachal Pradesh. The river is very important because it is the only source of pure water in Itanagar area and has minimum discharge of 8857 MLD which is sufficient for Itanagar Town. Hence the government built many small reservoirs near river to maintain the stability of drinking water supply.

The Singki River has dendritic drainage pattern which reveals the surface characteristics, the area has very irregular and hard rock surface. Generally this type of area has horizontal sedimentary or intrusive igneous rock where reasonably the rock mass is homogeneous (Press, F., and Sevier, R., 1982).

The remote sensing and GIS is advanced technology to study earth surface with high accuracy, in this study Aster DEM has been used to extract the information of the Singki River with the help of GIS software. The hydrology toolset of GIS is very flexible to use and helps to accumulate all the physical information. The use of digital elevation model (DEM) make so easy to delineate watershed and sub-watershed boundary and also helps in carrying out sub-watershed study separately. With the use of GIS software we can calculate all the geometrical information quickly using UTM projection in an accurate manner and it is time saving process.

Acknowledgement

The non-imagery satellite data (Digital Elevation Model) has been downloaded from the USGS website. And it is freely available, which helps to undertake this research. I acknowledge the USGS to provide useful data.

References

Paron Omem et al. Probability of Aluminium Toxicity in Water Treatment Plant Itanagar: A Case Study. *International Journal of Innovative Research in Science, Engineering and Technology*. 2014. 3 (Special Issue 4) 139-143.

Singh, Savindra, 1998: *Geomorphology.* Edition 2011. Prayag Pustak Bhavan, UP, India. 358.

Strahler, A.N. Dynamic Basic of Geomorphology. *Bulletin of the Geological Society of America*. 1952. 63; 923-28.

Zavoianul, 1985: *Morphometry of drainage basins development in Water Science.* Vol 20. Elsevier, Oxford, Amsterdam, New York. 133.

Strahler, A.N., 1964: *Quantitative geomorphology of drainage basins and channel networks.* In Handbook of Applied Hydrology. McGraw-Hill, New York. 4.39-4.76.

Waugh, David, 2002: *Geography: An Integrated Approach*. 3rd ed. Nelson Thornes Limited.

Schumm, S.A. Evolution of drainage systems and slopes in badlands at Perth Amboy, New Jersey. *Geological Society of American Bulletin*. 1956. 67; 597-646.

Miller, V.C., 1953: A quantitative geomorphic study of drainage basin characteristics in the Clinch Mountain area Virginia and Tennessee. Technical Report 3, Dept. of Geology, Columbia Univ., New York. 1-30.

Horton, R.E. Erosional Development of streams and their drainage density: hydro physical approach to quantitative geomorphology. *Bulletin of the Geological Society of America*. 1945. 56; 275-370.

Press, F., and Raymond Sevier, 1982: *Earth*, Second Edition, W.H. Freeman & Co Ltd, San Francisco. 613.

Strahler, A.N. Quantitative analysis of watershed geometry. *Trans. American Geophysical Union*. 1957. 38; 913-920.

Horton, R.E. Drainage Basin Characteristics. *Trans. American Geophysical Union.* 1932. 14; 275-370.

Chakrabarti, B.K., 2016: Geology of the Himalayan Belt: Deformation, Metamorphism, Stratigraphy, First Edition, Elsevier, Netherland. 145-152.

Climate Data, 2016: *Climate: Itanagar*. http://en.climate-data.org/location/24706/#climate-graph.

Cloud Publications
International Journal of Advanced Remote Sensing and GIS
2017, Volume 6, Issue 3, pp. 2050-2067
ISSN 2320 – 0243, Crossref: 10.23953/cloud.ijarsg.36

Case Study | Open Access

Coupling Universal Soil Loss Equation and GIS Techniques for Estimation of Soil Loss and Sediment Yield in Algash Basin

Issamaldin Mohammed[1,2], Hatim Nuh[1], Ahmed Abdalla[2]

[1]Department of Remote Sensing, Dams Implementation Unit, Khartoum, Sudan
[2]Department of Surveying Engineering, Faculty of Engineering, University of Khartoum, Khartoum, Sudan

Publication Date: 21 March 2017

DOI: https://doi.org/10.23953/cloud.ijarsg.36

Abstract Soil erosion is a global problem which has social, environmental and economical adverse effects. Soil erosion reduces soil productivity and water quality, therefore this study was conducted as an effort to estimate the average and total soil loss and moreover the total sediment yield in Algash water basin which extends from Eritrea to the downstream in east of Sudan. The study utilized from GIS and remote sensing to analyze the soil loss, based on Universal Soil Loss Equation (USLE), this model is one of the most widespread models are used for soil loss estimation. Soil erosion was determined as function of five parameters using USLE, the rainfall erosivity factor (R) was estimated from annual mean rainfall for last 8 years, the soil erodiblity factor (K) was determined based on soil characteristics, topographic factor (LS) was estimated using SRTM, the forth factor is crop management factor (C) and it was estimated using Normalized Difference Vegetation Index (NDVI) and the support practice factor (P) was estimated using derived slope data and a produced land cover map. Based on the above analysis the annual average soil loss ranged from zero to 118.86 ton/ha.year per pixel and the total soil loss from the whole study area was found to be 32,916,840.87 ton/ha.year.
Keywords *Algash Basin; GIS, Remote Sensing; soil erosion; sedimentation; soil loss; USLE*

1. Introduction

Soil erosion is currently considered as one of the most significant concerns; it has negative impacts in soil, water quality and aquatic life. Accordingly, soil erosion represents a serious threat of food security, environment and life quality due to the soil deterioration (Graaff, 1996; Eswaran et al., 2001). It is one of the slowest and slight detectable processes, it mostly happens due to man-made interventions rather than a product of climatic inputs and natural hazards such as volcanoes, cyclones and natural fires. This regard is due to the sustainable passive human contribution on the Earth's surface which significantly affects the permanent vegetation cover. Furthermore, soil erosion such as coastal inundation which on hand is caused by coastal land floods due to e.g. huge tidal waves and storms, or sand swept away. On the other hand, the global warming also has considerable effects such as the growing melting ice caps based on thermal expansion which leads to sea level rise and setting new elevated costal water and losing sediments from land. Based on aforementioned facts,

Favis-Mortlock and Guerra (2000) emphasized that the impact of natural processes is negligible with respect to human activities.

Soil erosion is problematic because it leads to the permanent soil degradation where recovery by natural restoration processes may not achieved over decades. Moreover, other off-site damages arise from eroded chemical-sediments caused by deposited materials in the nearby sites which may also affect surface water system. The difficulties in monitoring the erosion processes are due to the limitation of the direct measurements of soil loss over small areas where hydraulic conditions have to be taken into account. The negative impacts of land cover type in watershed ecosystems have been a common concern worldwide. For example agriculture clearing or any objects can intercept water flow which increases the amount of surface runoff and sediments that carried by it. However, when the natural vegetation is permanently converted to agriculture, the frequency and magnitude of floods will change and the sedimentation will occur (Knox, 1977; Jacobson and Primm, 1997; Boix-Fayos et al., 2008).

The Universal Soil Loss Equation (USLE) is a conservation planning and empirical tool that is used to estimate erosion in different land-use patterns. The estimation of the soil loss is based on physical modeling and information that are jointly combined with further in-situ datasets to assist in effective conservation planning. To successfully preserve water and soil resources, the knowledge of the effective key factors and appropriate methodologies is necessary (see e.g. Wischmeier and Smith, 1965, 1978; Wischmeier et al., 1971; Renard et al., 2011). In other words, USLE is an empirical based model which used to quantify the average annual soil loss at the basin scale and simulation of soil erosion. Since the spatial distribution of soil erosion must be considered, remote sensing and geographical information system (GIS) are heavily used in interaction with USLE model due to the amount of data that are needed and the ability of these techniques to handle these types of data (Bayramin et al., 2003).

The joint combination of USLE and GIS is extensively used in different studies for estimation the soil erosion hazard in the past decades by a large group of scientists who utilized USLE-GIS for understanding and analyzing the impacts of the soil erosion. Mati et al. (2000) used USLE and GIS for assessing the soil erosion risk in Ng'iro North Basin of Kenya, Meusburger et al. (2010) assessed the advantages of the vegetation parameters of QuickBird imagery in soil erosion model by considering a supervised classification, Prasannakumar et al. (2012) used the revised form of USLE beside GIS for a quantitative evaluation of the annual soil loss over the mountainous Pampa sub-watershed in India. Ali and Hagos (2016) compiled thematic layers from different data sources and methodologies in the context of USLE to estimate soil erosion in Awassa catchment in Ethiopian Rift Valley due to the loss of the vegetation cover due to the population increase. In this paper, the USLE coupled with the Geographic Information System (GIS) techniques are utilized to estimate soil erosion hazard in Algash Basin of Sudan using data from erosion plots and reconnaissance surveys (cf. Mohammed, 2016). Through years Al-gash River bed rises up mainly due to sedimentation process. Furthermore, Algash Delta agricultural project irrigation system suffers from the same problem, thus, the current study attempts to investigate the risk of sediments carried by Algash River to Sudan in order to assist the concerned authorities toward better environmental management strategies and land use planning. The primary aim of this study is to estimate the aver-age soil loss for year 2015 using rainfall, digital elevation model (DEM), land cover data and soil data, thus the underlying objectives to achieve that aim are firstly producing a land cover map, secondly identifying potential high risk areas of soil erosion and finally, estimating the total annual loss and calculation of the sediment yield.

The organization of this paper comes as follows, the geographic setting of the study area is presented in Section 2, USLE with its necessary factors and GIS techniques are explained in Section 3, the results and analysis are addressed and analyzed in Section 4 and finally the concluding remarks are

drawn in Section 5.

2. Study Area

The study area is located between 14°5'9.5" – 15°27'58.5" N and 36°30'7.45" – 39°26'7.5" E in the overlapping area between three East-African neighboring countries which are Eritrea, Ethiopia and Sudan, but the large part of the study area is located in Eritrea (see Figure 1). The drainage area is about 2,203,183.76 ha. The climate is semi-arid over the study area where little rainfalls from June to September due to the Ethiopian summer monsoon. An average of 260 mm of rainfall per year, is concentrating from June to September. Precipitation is lowest in January, with an average of 0 mm. The greatest amount of precipitation occurs in August, with an average of 114 mm at an average temperature of 32.5 (see Merkel, 2009). In Algash Watershed there are six soil types, the classification is according to the existing editions of the FAO World Reference Base for Soil Resources. The most dominant type is Leptosols which is very shallow soils over hard rock or in unconsolidated very gravelly material; it occupies 54.64% of the total study area. The second most dominant type is Cambisols with 21.81% (FAO, 2003).

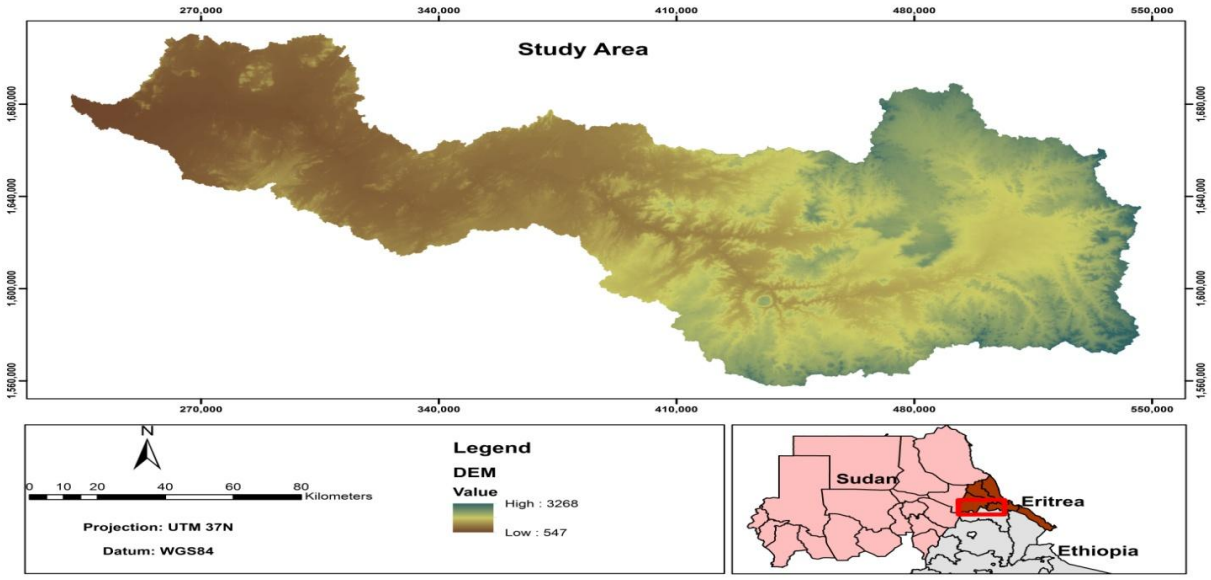

Figure 1: *study area location*

3. Methods and Materials

The USLE and its revised version RUSLE are commonly used to quantify the soil loss in the tropical areas (Khosrowpanah et al., 2001). The USLE model is suitable only for estimating erosion caused by water. It was adopted by the Soil Conservation Service in U.S, the model was developed by (Wischmeier and Smith, 1965) using data for more than 10,000 test plots in U.S. for 20 years (Wischmeier and Smith, 1965). It integrates a number of factors where many methodologies are used to estimate these factors. One of the factors is the rain and runoff-factor (R-factor), also called the soil erosivity factor. This factor determines the erosive effect of precipitation on soil loss. Another factor is the erodibility or K-factor, this determines the influence of soil properties on soil loss during rainfall events (Renard et al., 2011; The, 2011). The USLE soil loss equation is given as follows:

$$A=R\times K\times L\times S\times C\times P \qquad (1)$$

where A is the soil loss in ton/acre or in ton/ha; R, the rainfall and runoff factor, is the number of rainfall erosion index units, plus a factor for runoff from snowmelt or applied water where such runoff is significant, thus the R factor increases with the increase in storm intensity; K, the soil erodibility factor, is the soil loss rate per rainfall erosion index unit for the specified soil under Unit Plot conditions, the K-factor reflects the ability of the soil to be eroded; L and S are the slope length and steepness factors in relation to the conditions on a unit plot; C, the cover and management factor, is the ratio of soil loss from an area with specified cover and management to that from an identical area under the tilled continuous fallow Unit Plot conditions, thus C-factor indicates the crop practices which contribute in soil conservation (C thus ranges from a value of zero for completely non-erodible conditions, to a value of 1.0 for the worst-case Unit Plot conditions); and P, the support practice factor, This factor is similar to the C-factor because it indicates the practices which help in soil conservation but through reducing the runoff amount, P factor is the ratio of soil loss with a support practice such as contouring, strip cropping, or terracing to that with straight-row farming up and down slope (Renard et al., 2011).

Table 1 shows the data used in the current study. Utilizing the GIS techniques, the framework included preprocessing of the DEM which is used to delineate the watershed and generating the slope.

Table 1: *Input datasets*

Dataset	Year	Format	Source
DEM	2015	Digital Raster	USGS
Landsat 8	2015	Digital Raster	USGS
Rainfall	1983-2015	Digital Raster	TAMSAT
Soil	1995	Digital Shapefile	FAO

Furthermore, a landsat 8 image was used to generate the land cover map and cover management factor, raw data of the rainfall are provided by a research group in University of Reading (known as TAMSAT) that cover all Africa by (0.0375 spatial resolution and monthly temporal resolution based on the estimation from the satellite imagery was used in generating the rainfall erosivity factor. Also a soil map of scale (1:5,000,000) was used in this study from world soil map of FAO of the United Nations in order to estimate the soil erodibility K-factor (see Figure 2).

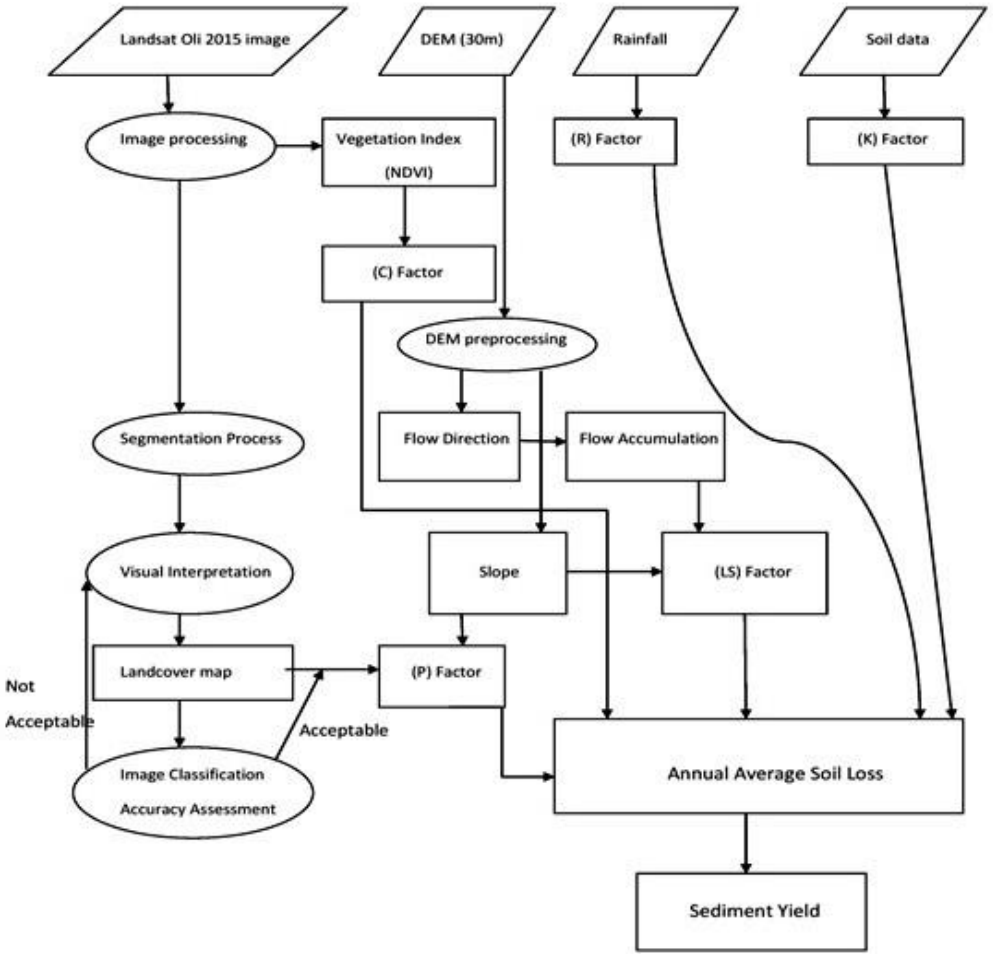

Figure 2: *the frame work*

3.1. Rainfall erosivity factor

Rainfall erosivity factor (R) represents a relation between kinetic energy of the storm and the maximum intensity in thirty minutes, therefore this factor is directly related to the detachment of soil by raindrop. The model that was used to estimate the rainfall erosivity factor is suggested by Eltaif et al. (2010) and it is expressed by formula:

$$R = 23.61 \times e^{0.0048P} \qquad (2)$$

where R is the rainfall erosivity factor in MJ.mm/ (ha.hr.year) and P is Annual average rainfall in mm/year.

3.2. Soil erodibility factor

Erodibility of soil refers to how easy that soil could be eroded. Soil erodibility factor depends on the properties (texture, organic content, gravel content and permeability) and the profile of the soil, thus it reflect the effect of the soil type (Renard et al., 1997). The K-factor indicates the ability of soil to be eroded. The K-factor in this study was calculated using the Kuery tool (Borselli et al., 2012), the Kuery tool is available and free over the internet, the tool requires to calculate the climate and gravel content, if the gravel content is more than 10% then the percentage of gravel must be input to the tool in

addition to the both sand and clay content, otherwise the organic matter should be input into the tool; therefore a relation between organic matter and organic carbon content was used (see Pribyl, 2010):

$$SOM = 2 \times SOC \quad (3)$$

where SOM is the soil organic matter (%) and SOC is the soil organic carbon (%).

3.3. Topographic factor

Topographic factor (LS) reflects the topography effect on sheet and rill erosion in respect to USLE model (Wischmeier and Smith, 1965). It consists of two factors: slope length (L) and slope gradient (S). These two factors are usually considered together to make the calculation easy. Slope length increasing causes a rise in runoff amount due to the accumulation of the runoff from unit area to another in downslope direction and the velocity of runoff rises when the slope steepness increases, these two factors contribute together in increasing the soil erosion when their values are high (Kim, 2006). The (LS) factor is calculated based on the DEM and the relevant estimated accuracy depends on the resolution of the DEM. In this study SRTM (30m) was used to calculate the (LS) factor. The raster calculator in ArcMap was used to do this task using the following expression (Mitas and Mitasova, 1999):

LS = Power((“Flow Accumulation” * Cell Size/22.13),0.6) * Power(Sin(“Slope” * 0.01745)/0.0896,1.3)

where the slope is in degrees.

Since USLE model is only suitable for sheet and rill erosion, an upper boundary should be set for the boundary length, this will maximize the flow accumulation to the upper value. In other words, the 6 value in flow accumulation means that the maximum flow length is 180 m results from the flow accumulation cannot exceed 6 pixels multiply by the cell size which is 30 m as shown in Jabbar (2003); Parveen and Kumar (2012).

3.4. Cover management factor

The cover management or C-factor is related to land cover type, it represents a management to reduce the soil erosion amount. Basically this factor represents the relation between erosion in bare lands and erosion under a cropping system. The C-Factor depends on the vegetation type, stage of growth and cover percentage (Parveen and Kumar, 2012). One of remotely sensed based methods to calculate the C-Factor depends on normalized difference vegetation index (NDVI) which indicates the existence of vegetation cover (Van Leeuwen and Sammons, 2004). The C-Factor basically is the percentage of vegetation (Parveen and Kumar, 2012). Since the study area is located in a tropical climate, the following formula is used to determine the dimensionless C-factor (Durigon et al., 2014):

$$C = \frac{1 - NDVI}{2} \quad (4)$$

3.5. Support practice factor

The support practice factor or P-factor reflects the effect of practices which reduce the water runoff and then reduce the soil erosion. Kim (2006) defined the P-factor as the ratio of the soil loss with a specific

support practice to the corresponding soil loss with straight row upslope and downslope tillage and it depends on the slope. It varies from zero to one, where zero represents very good practices that reduce soil erosion and one represents no practices, thus any land cover except the agricultural land has one value unless there are some management practices such as terracing. The land cover map of the study area was produced using the eCognition software and visual interpretation of the Landsat scene where P-factor values were assigned. The collection of the ground truth points for the accuracy assessment of the image classification is not always achievable, instead, higher resolution images could be used to extract test points (Mather, 2005). In this study 140 reference points based on Google Earth images were used and randomly distributed. Then kappa coefficient method was applied to assess the accuracy in addition to the overall accuracy. Kappa coefficient was calculated using an extension script imported to ArcGIS software environment. The support practice factor was determined according to the criteria of the developers of USLE model (Wischmeier and Smith, 1965) as shown in Table 2.

Table 2: *P-factor values*

Land use type	Slope (%)	P-factor
Agricultural land	0 - 5	0.1
	5 - 10	0.12
	10 - 20	0.14
	20 - 30	0.19
	30 - 50	0.25
	50 - 100	0.33
Other land	All	1

3.6. Sediment yield and sediment delivery ratio

Sediment yield is defined as the sediment amount which actually discharged from the catchment area (Vanoni, 1975). Erosion process consists of three processes: detachment, transport and sedimentation. The runoff takes the eroded soil particles in downslope direction and some of these particles are considered as suspended sediments during the transportation process until the runoff reaches the outlet of the basin. In the outlet point (the lowest point within the catchment area) the sediment is measured and it is called the sediment yield. The sediment yield has an inverse relationship with the drainage area (Walling, 1983) and many factors are controlling sediment yield (such as the soil erosion rate, stream capacity and annual precipitation), thus there are many formulas that link up the sediment yield to the soil erosion. The most common formula that defines the sediment delivery ratio as a ratio of sediment yield to total annual soil loss of the basin is found in (Brune, 1953; Williams, 1977):

$$SDR = \frac{SY}{SL} \qquad (5)$$

where SDR defines sediment delivery ratio which is varying from 0 to 1, SY is the sediment yield and SL is the soil loss per unit area above the measuring point.

The above equation is reasonable to model the relationship between sediment yield and soil loss since the amount of sediment as a function of land cover, soil type and conservation practice which are incorporated factors in USLE model for determine soil loss (Robinson, 1977). Many recent researches have attempts to model this relationship, with different included factors (e.g. sediment yield and

drainage density) whereas other studies consider landuse as most influence factor in sediment yield (Syvitski, 2003), or topography, while the climate is considered as a dominant factor (Walling, 1996). Many researchers build a model to determine the sediment delivery ratio (Williams, 1977; Renfro, 1975; Williams and Berndt, 1972). Usually these models are not applicable except where they were developed (Becvar, 2005), the most generalized model is that which was globally tested on a number of 300 watersheds around the world. It inversely relates the sediment delivery ratio to the drainage area using a power function Vanoni (1975) as follows:

$$SDR = 0.42 \times A^{-0.125} \quad (6)$$

where SDR is sediment delivery ratio and A is the basin area (in squared miles).

4. Results and Discussion

4.1. Rainfall erosivity factor

The R-factor is highly affected by the density and duration of the rain storm. It has a great influence on the soil erosion, particularly, at the first two phases of erosion soil process (detachment and transportation), the higher value of rainfall erosivity factor, the higher risk of soil erosion (Kefi et al., 2009).

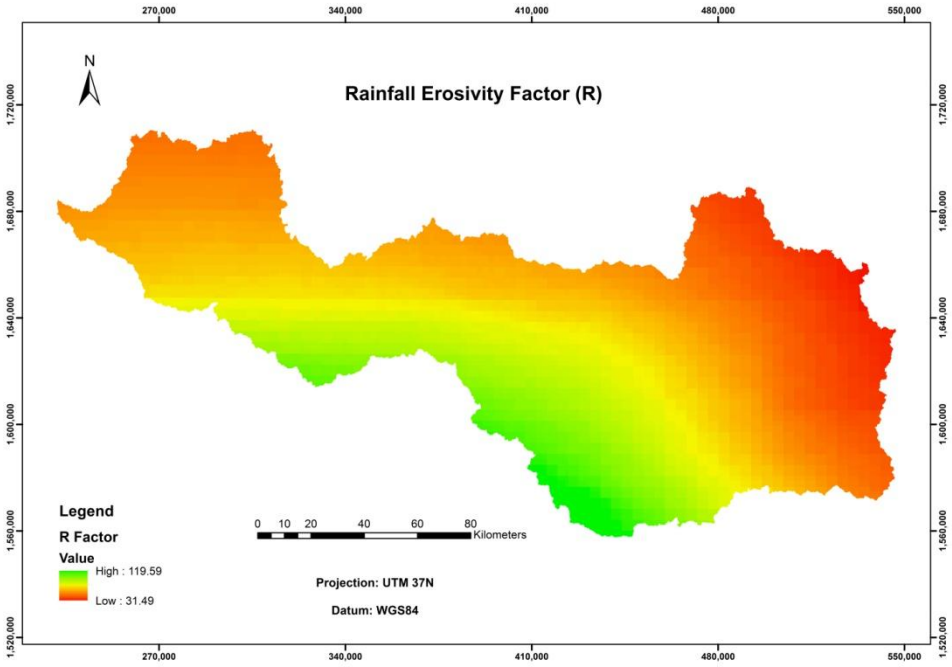

Figure 3: *Rainfall erosivity factor*

The result of erosivity calculation showed that the rainfall erosivity is bounded by 31.9 and 119.59 MJ mm/ha year with a mean value of 61.95 MJ mm/ha year. Figure 3 shows that the high values of erosivity were concentrated in the southern part of the study area (green). Whereas the low values were concentrated in north-east part (red). This pattern is following the natural distribution of the rainfall over the area.

4.2. Soil erodibility factor

This factor indicates the ability of soil to be eroded; the soil erodibility factor depends on the soil structure, permeability, organic matter content and particle size, as well as on chemical and physical properties of the soil. The Leptosols type was the dominant type with 54.64% of the study area, followed by Cambisols with 21.81%. Leptosols is the only type which contains more than 10% gravel contents, generally, the sandy soils has low K values because of low runoff and due to the high infiltration rate, The Leptosols case in Table 3 shows that the soil types are easily detached. The Vertisols have lower value than Nitisols due to higher clay content.

Table 3: *Percentages of soil texture (sand, silt and clay), organic content (SOC and SOM)*

Soil type	Sand	Silt	Clay	SOC	SOM	Gravel	K
Leptosols	50	30	20	0.72	1.44	31	0.00898
Fluvisols	44	33	23	0.73	1.46	1	0.02254
Cambisols	45	31	24	0.87	1.74	1	0.02249
Lixisols	63	15	22	0.6	1.2	1	0.0244
Vertisols	21	25	54	1.07	2.14	1	0.01587
Nitisols	24	27	49	2.45	4.9	1	0.0189

As seen in Figure 4 below, the dominant erodibility factor was 0.00898 which associated with Leptosols soil type (green color) and followed by (K factor) value 0.02249 which associated with Cambisols soil type (orange color).

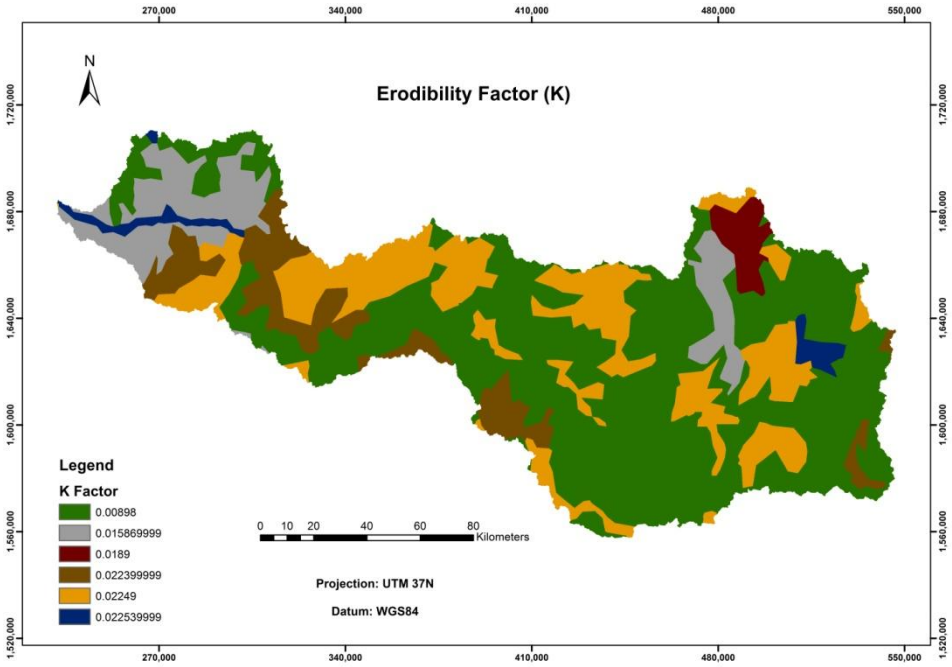

Figure 4: *Soil erodibility factor*

4.3. Topographic factor

The topographic factor (LS) reflects the effect of the slope length and slope gradient in the soil erosion. The higher the slope length and slope gradient, the greater erosion will occur. Topographic factor along with rainfall erosivity are the key factors in USLE that means if these two factors are high, the sediment generation will also be high as mentioned before (Kefi et al., 2009). The LS-factor varies

from 0 to 77.08 with a mean value of 4.21, the increase in LS-factor increases the erosion because the runoff will be faster and then its energy will increase. From Figure 5 vast areas have high LS values between 40 and 77.

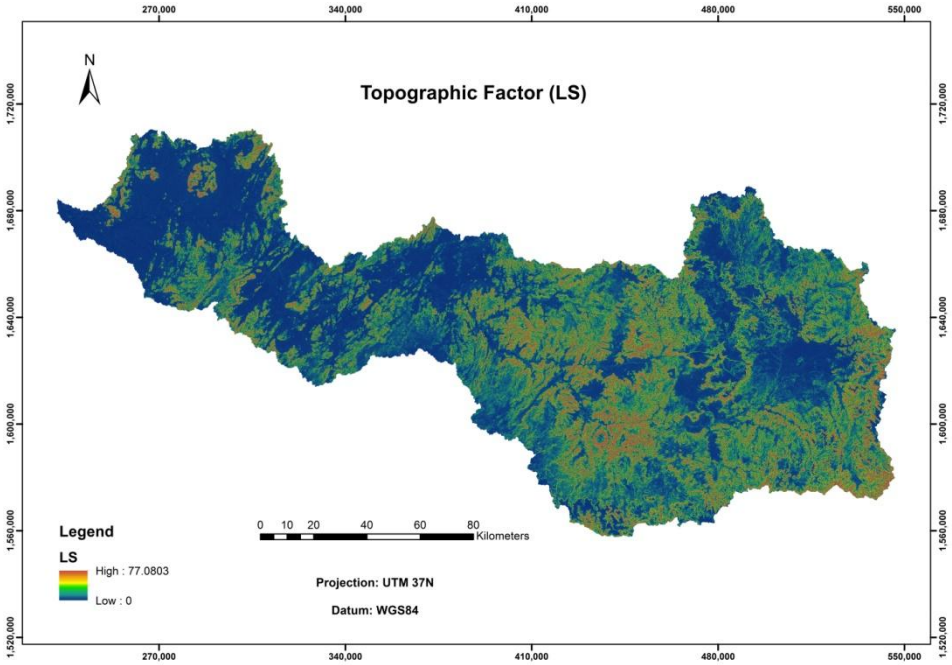

Figure 5: *Topographic factor*

4.4. Cover management factor

The crop management factor basically related to the vegetation percentage. The soil erosion is sensitive to vegetation cover (Renard and Ferreira, 1993; Benkobi et al., 1994; Biesemans et al., 2000), thus the NDVI can be calculated and then the C-factor will be determined, C and NDVI are inversely proportional. C-factor varies from 0.181641 to 1 as shown in Figure 6. When the C-factor is lower, this means that the ability of the area to be eroded is less. The highest values were found in urban and bare areas due to lack of vegetation (dark green), while the lowest values were found in the sides of the main channel (bright green), also in south area there is some vegetation which results in brighter area.

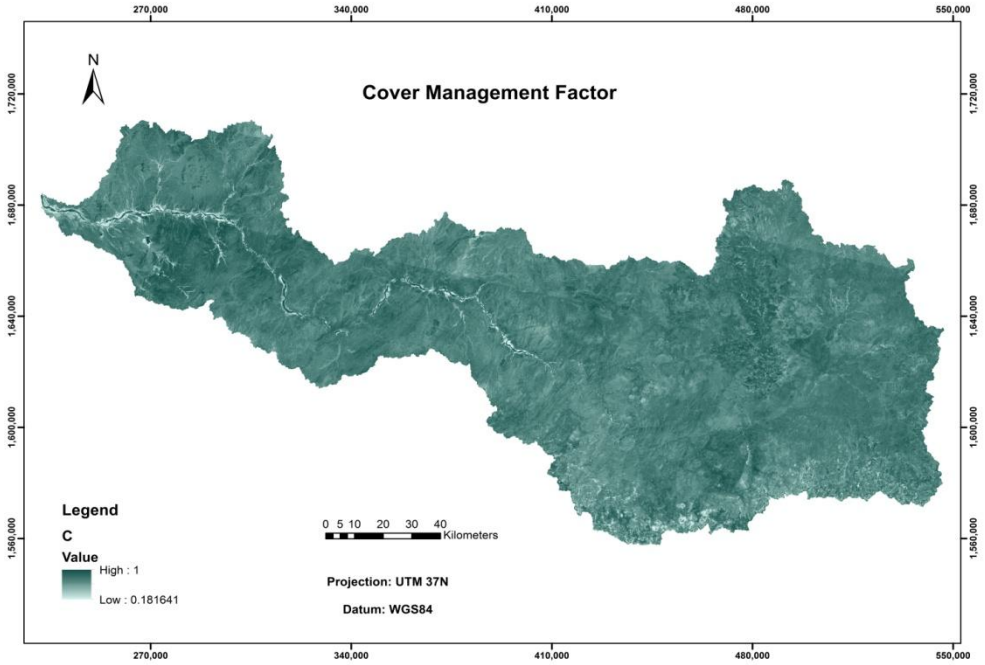

Figure 6: *Cover management factor*

4.5. Support practice factor

In order to obtain the P-factor, the land cover map was produced. It consists of five classes (water, bare land, natural vegetation, urban area and agriculture) and no more detailed classes due to spatial resolution (15m) of Landsat images (more detailed classes require higher resolution images). The most important advantage of using satellite images in land-cover mapping is their large coverage. There was no need to apply the geometrical correction since the images were geometrically corrected. With an overall accuracy of 80% and Kappa coefficient 71.41%, the land cover classes in the study area are produced as shown in Figure 7. It can be clearly seen that the urban areas are isolated among the study area and the water bodies represent small portions of the area. The agricultural areas are found on the valley strip due to abundance of water in rainy seasons, except a few discrete farms in the north of the study area and several ones in south west area.

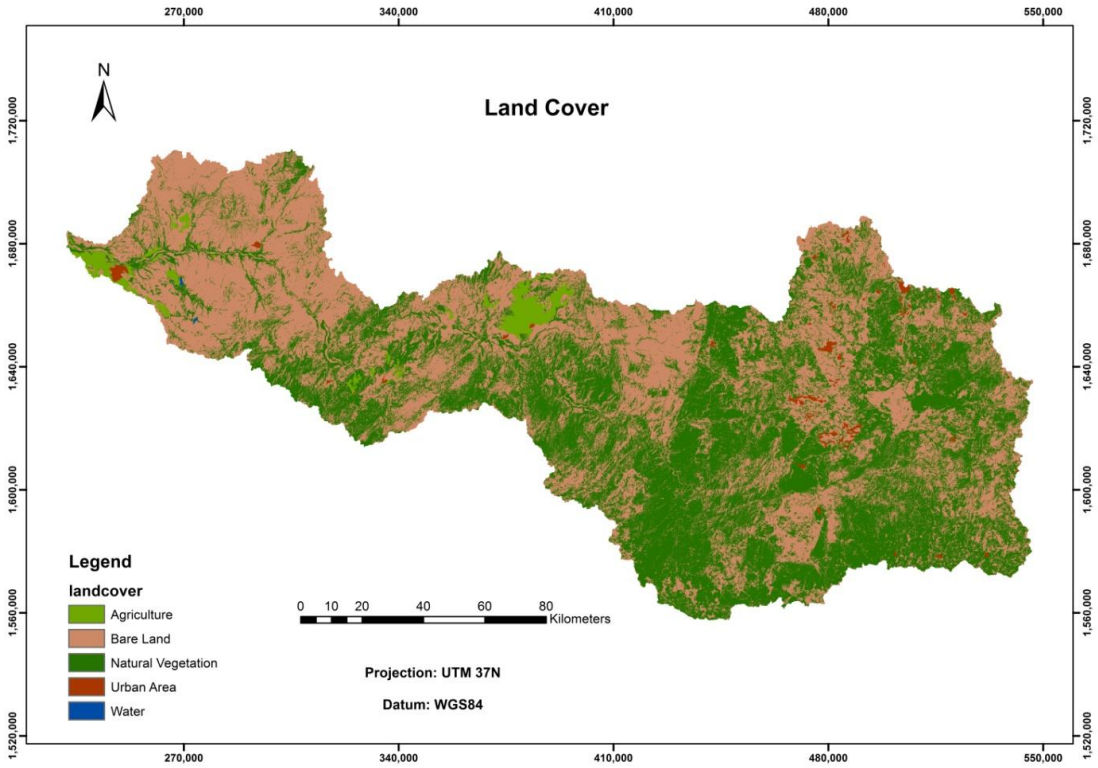

Figure 7: *Land cover map*

Since there is no support practice in the study area, each land cover type has a value of one except the agricultural areas (see Figure 8) as the support factor depends on the slope Wischmeier and Smith (1965).

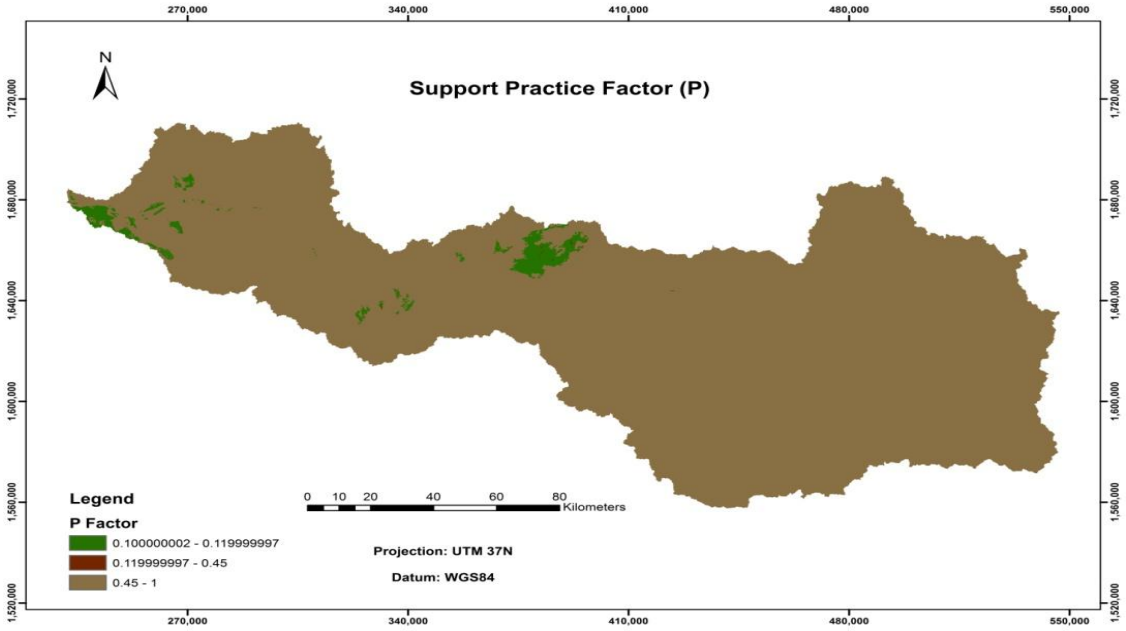

Figure 8: *P-value map*

4.6. Soil loss

The USLE parameters were calculated as shown above to quantify the soil loss amount by applying equation 1. The average annual soil loss on pixel scale varies from zero to 118.86 (ton/ha/year). The average soil loss for the whole study area was estimated as 1.4 ton/ha/year. These amounts are considered as on-site effect which reduce the soil productivity in the study area. Figure 9 shows the spatial distribution of soil erosion amounts.

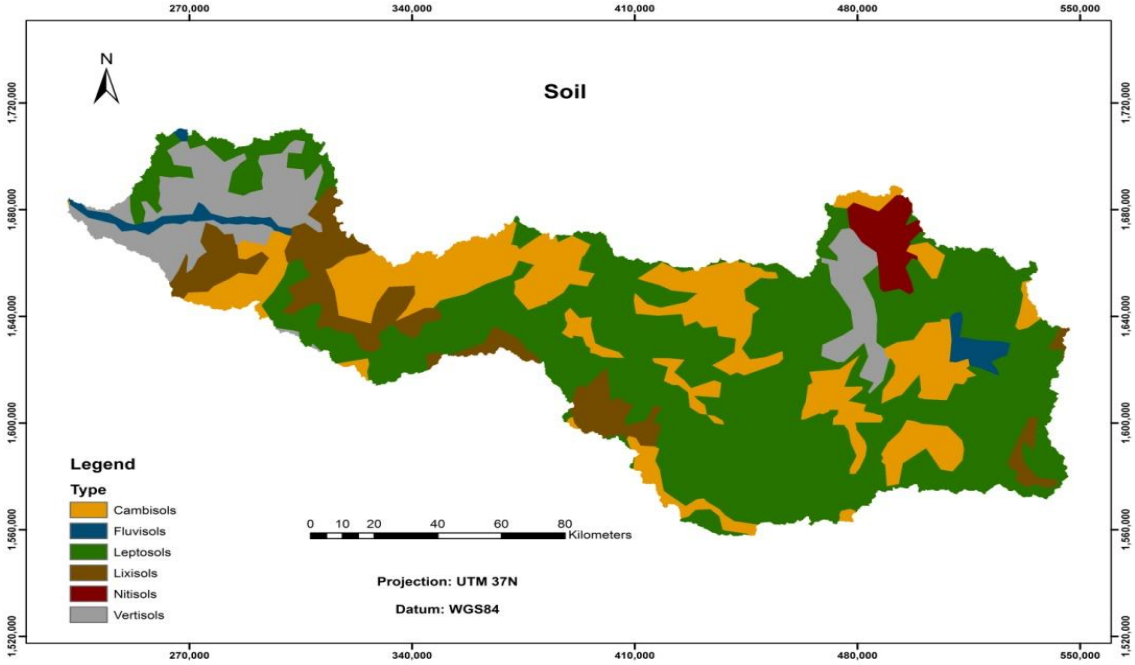

Figure 9: *Soil loss amount*

It can be seen from Figure 9 that there is a spatial variation in average soil loss amount. That is due to the variability in the factors (rainfall, topography, vegetation, soil types and their characteristics, and the human practices effect in agricultural and urban areas) which influence the soil erosion rates. Based on Morgan (2005), the soil erosion results were classified into seven zones as illustrated in Figure 10.

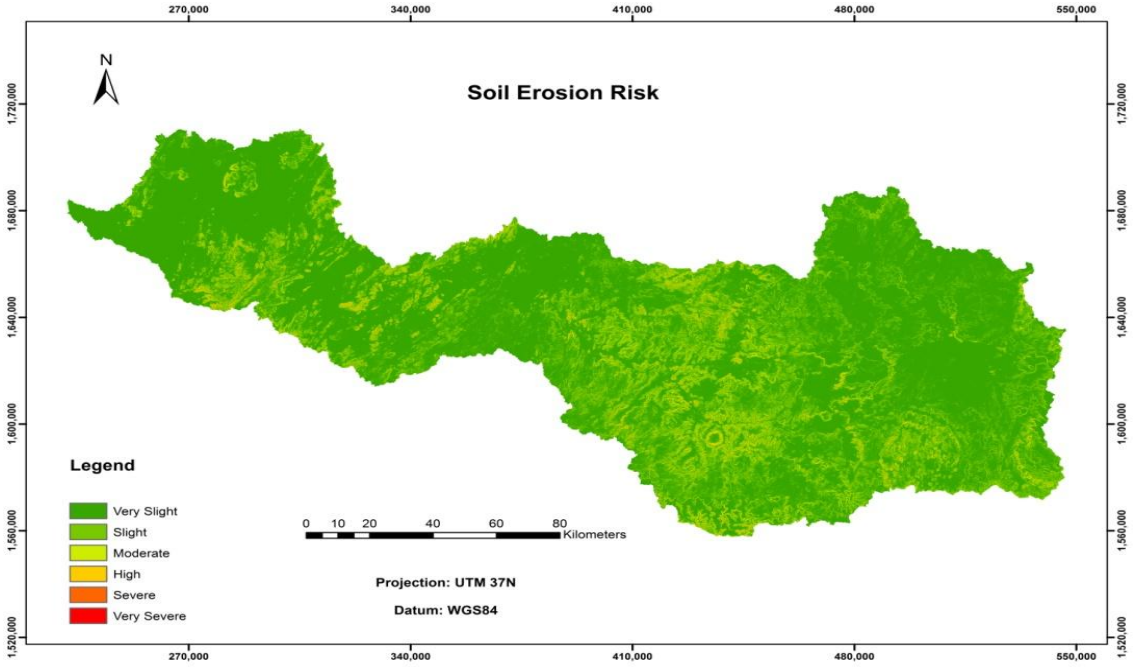

Figure 10: *Soil erosion risk map*

From Table 4, it can be clearly seen that the very slight zone (0 – 2 ton/ha.year) was occupied by the most of the study area (77.27%), followed by slight and moderate zones which are 15.16% and 6.05% respectively. Only 0.0002796% and 0.0000042% were classified as severe and very severe potential risk respectively.

Table 4: *Soil erosion zones*

Soil type	Sand	Silt	Clay	SOC	SOM	Gravel	K
Leptosols	50	30	20	0.72	1.44	31	0.00898
Fluvisols	44	33	23	0.73	1.46	1	0.02254
Cambisols	45	31	24	0.87	1.74	1	0.02249
Lixisols	63	15	22	0.6	1.2	1	0.0244
Vertisols	21	25	54	1.07	2.14	1	0.01587
Nitisols	24	27	49	2.45	4.9	1	0.0189

Figure 11 below proves that the mean annual soil loss is proportional to the slope due to the effect of topographic factor as mentioned by Zhang et al. (2015). When the slope is more than 140% the mean annual soil loss will reach the maximum mean annual soil loss (7.76 ton/ha.year), in contrast when the slope is very low (0-2%), the mean annual soil loss will be very low (0.08 ton/ha.year).

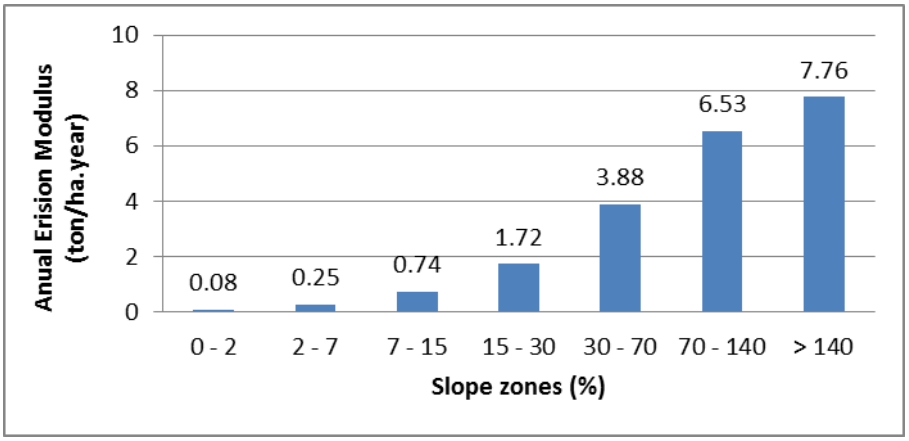

Figure 11: *Slope zone and equivalent average annual erosion*

4.7. Sediment delivery ratio and sediment yield

The total annual soil loss in the study area is estimated to be 32,916,840.87 ton/ha.year which is a significant amount of soil erosion but it is reasonable with respect to some previous studies (Bizuwerk et al., 2003; Ouyang et al., 2005), this amount is directly related to the on-site effect of soil erosion, the off-site effect was on Algash Delta (Sudan). Large amount of eroded soil will be available as suspended matter during the transportation process, therefore the sediment delivery ratio after applying equation 6 was 0.0337836 and the sediment yield normally enters Sudan was 1,112,048.778 ton/ha.year and that result was found using equation 5.

5. Conclusion

The Universal Soil Loss Equation model and GIS techniques were combined to analyze the soil erosion rate and to identify high risk areas in the study area located in the overlapping area between Eritrea, Sudan and Ethiopia. Furthermore, the off-site effect of eroded soil was quantified and the sediment yield was estimated after calculating the sediment delivery ratio. The mean annual soil loss was 1.4 ton/ha.year per pixel and bounded by 0 and 118.86 ton/ha.year. The analysis showed that the slope has a significant effect on soil erosion rate, higher value of slope, higher rate of soil erosion. The maximum value of the soil erosion modulus which was 7.6 ton/ha.year in areas where slope was more than 140% and by 6.53 ton/ha.year for 70 - 140% slope zones as shown in Figure 11. The results showed that 77.27% of study area within the very slight soil loss zone and 15.16% in the slight zone, whereas only 0.000284% of the study area was falls in the severe and very severe zone. The off-site effect was represented by soil yield value and sediment delivery ratio was 0.0337836. Therefore, the sediment yield entered into East of Sudan is estimated as 1,112,048.778 ton/ha.year.

References

Ali, S. A., & Hagos, H. (2016). Estimation of soil erosion using USLE and GIS in Awassa Catchment, Rift Valley, Central Ethiopia. Geoderma Regional.

Bayramin, I., Dengiz, O., Baskan, O., & Parlak, M. (2003). Soil erosion risk assessment with icona model; case study: Beypazarı area. *Turkish Journal of Agriculture and Forestry*, *27,* 105-116.

Becvar, M. (2005). Estimating typical sediment concentration probability density functions for European rivers.

Benkobi, L., Trlica, M., & Smith, J. L. (1994). Evaluation of a refined surface cover subfactor for use in rusle. *Journal of Range Management*, 74-78.

Biesemans, J., Van Meirvenne, M., & Gabriels, D. (2000). Extending the rusle with the Monte Carlo error propagation technique to predict long-term average off-site sediment accumulation. *Journal of Soil and Water Conservation*, *55,* 35-42.

Bizuwerk, A., Taddese, G., & Getahun, Y. (2003). Application of GIS for modeling soil loss rate in awash river basin, Ethiopia.

Boix-Fayos, C., de Vente, J., Mart´ınez-Mena, M., Barber´a, G.G., & Castillo, V. (2008). The impact of land use change and check-dams on catchment sediment yield. *Hydrological Processes, 22,* 4922-4935.

Borselli, L., Torri, D., Poesen, J., & Iaquinta, P. (2012). A robust algorithm for estimating soil erodibility in different climates. Catena*, 97*, 85-94.

Brune, G. M. (1953). Trap efficiency of reservoirs. *Eos, Transactions American Geophysical Union, 34,* 407-418.

Durigon, V., Carvalho, D., Antunes, M., Oliveira, P., & Fernandes, M. (2014). Ndvi time series for monitoring rusle cover management factor in a tropical watershed. *International Journal of Remote Sensing, 35,* 441-453.

Eltaif, N., Gharaibeh, M., Al-zaitawi, F., & Alhamad, M.N. (2010). Approximation of rainfall erosivity factors in north Jordan. *Pedosphere, 20,* 711-717.

Eswaran, H., Lal, R., & Reich, P. (2001). Land degradation: an overview in responses to land degradation. In E.M. Bridges, I.D. Hannam, L.R. Oldeman, F.W.T. Pening de vries, S.J. Scherr, S. Sompatpanit (Eds.), In: Proceedings of 2nd International Conference on Land Degradation and Desertification, Khon Kaen, Thailand. Oxford Press, New Delhi, India.

FAO (2003). Harmonized world soil database. Retrieved Feb. 2, 2016, from http://www.fao.org/soils-portal/soilsurvey/soil-maps-and-databases/harmonized-world-soil-database-v12/en/.

Favis-Mortlock, D. T., & Guerra, A. J. T. (2000). *Soil Erosion: Application of Physically Based Models*. 1 Edition, Environmental Science, Berlin Heidelberg: Springer-Verlag.

Graaff, J. D. (1996). The price of soil erosion: an economic evaluation of soil conservation and watershed development. Landbouwuniversiteit Wageningen (Wageningen Agricultural University), Wageningen, Netherlands.

Jabbar, M. T. (2003). Application of GIS to estimate soil erosion using rusle. *Geospatial Information Science, 6,* 34-37.

Jacobson, R. B., & Primm, A. T. (1997). Historical land-use changes and potential effects on stream disturbance in the Ozark plateaus, Missouri. US Geological Survey water-supply paper, 1-85.

Kefi, M., Yoshino, K., Zayani, K., Isoda, H. (2009). Estimation of soil loss by using combination of erosion model and GIS: case of study watersheds in Tunisia. *J Arid Land Stud, 19,* 287-290.

Khosrowpanah, S., Heitz, L., Water of the Western Pacific., E.R.I. (2001). Rainfall erosivity factors (R-factors) for selected islands in the Federated States of Micronesia (FSM)/ by Shahram Khosrowpanah, Leroy Heitz. Water and Environmental Research Institute of the Western Pacific, University of Guam Mangilao, Guam.

Kim, H. S. (2006). Soil erosion modeling using RUSLE and GIS on the Imha watershed, South Korea. Ph.D. thesis. Colorado State University.

Knox, J. C. (1977). Human impacts on Wisconsin stream channels. *Annals of the Association of American Geographers, 67,* 323-342. http://dx.doi.org/10.1111/j.1467-8306.1977.tb01145.x

Mather, P. (2005). *Computer Processing of Remotely-Sensed Images: An Introduction*. Wiley.

Mati, B. M., Morgan, R. P., Gichuki, F. N., Quinton, J. N., Brewer, T. R., Liniger, H. P. (2000). Assessment of erosion hazard with the USLE and GIS: A case study of the Upper Ewaso Ng'iro North basin of Kenya. *International Journal of Applied Earth Observation and Geoinformation, 2,* 78-86.

Merkel, A., 2009. *Climate-data*. Retrieved from http://en.climate-data.org/country/144 on February 1, 2016.

Meusburger, K., Konz, N., Schaub, M., & Alewell, C. (2010). Soil erosion modelled with usle and pesera using quickbird derived vegetation parameters in an alpine catchment. *International Journal of Applied Earth Observation and Geoinformation, 12.*

Mitas, L., & Mitasova, H. (1999). Spatial interpolation. In: P. Longley, M.F. Goodchild, D.J. Maguire, & D.W. Rhind, (Eds.), *Geographical Information Systems: Principles, Techniques, Management and Applications (*pp.481-492) 2nd ed. Wiley.

Mohammed, I. (2016). Estimating soil erosion using universal soil loss equation and GIS in Algash Basin. MSc Thesis. Department of GIS and Cartography, Faculty of Geo-graphical and Environmental Sciences, University of Khartoum.

Morgan, R. (2005). *Soil Erosion and Conservation* (3rd ed). Oxford, England: Wiley-Blackwell.

Ouyang, D., Bartholic, J., & Selegean, J. (2005). Assessing sediment loading from agricultural croplands in the great lakes basin. *Journal of American Science, 1,* 14-21.

Parveen, R., & Kumar, U. (2012). Integrated approach of universal soil loss equation (USLE) and geographical information system (GIS) for soil loss risk assessment in upper south koel basin, Jharkhand.

Prasannakumar, V., Vijith, H., Abinod, S., & Geetha, N. (2012). Estimation of soil erosion risk within a small mountainous sub-watershed in Kerala, India, using revised universal soil loss equation (rusle) and geo-information technology. *Geoscience Frontiers, 3.*

Pribyl, D. W. (2010). A critical review of the conventional soc to som conversion factor. *Geoderma, 156,* 75-83.

Renard, K., & Ferreira, V. (1993). Rusle model description and database sensitivity. *Journal of environmental quality, 22,* 458-466.

Renard, K., Yoder, D., Lightle, D., & Dabney, S. (2011). Universal soil loss equation and revised universal soil loss equation. *Handbook of Erosion Modelling*, 135-167.

Renard, K. G., Foster, G. R., Weesies, G. A., McCool, D. K., & Yoder, D. C. (1997). Predicting soil erosion by water: a guide to conservation planning with the Revised Universal Soil Loss Equation (RUSLE). No. 703, US Government Printing Office, Washington, USA.

Renfro, G. (1975). Use of erosion equations and sediment delivery ratios for predicting sediment yield. *Present and Prospective Technology for predicting sediment yields and sources*, 33-45.

Robinson, A. (1977). Relationship between soil erosion and sediment delivery. International Association of Hydrological Sciences, 159-167.

Syvitski, J. P. (2003). Supply and flux of sediment along hydrological pathways: research for the 21st century. *Global and Planetary Change, 39,* 1-11.

The, S.H. (2011). Soil erosion modeling using RUSLE and GIS on Cameron highlands, Malaysia for hydropower development. Ph.D. thesis. University of Iceland and University of Akureyri.

Van Leeuwen, W. J., & Sammons, G. (2004). Vegetation dynamics and erosion modeling using remotely sensed data (modis) and GIS, In: Tenth biennial USDA forest service remote sensing applications conference, pp. 5-9.

Vanoni, V. A. (1975). Sedimentation engineering: American society of civil engineers. manuals and reports on engineering practice. No. 54. p. 745.

Walling, D. (1983). The sediment delivery problem. *Journal of Hydrology, 65,* 209-237.

Walling, D.E. (1996). Erosion and Sediment Yield: Global and Regional Perspectives: Proceedings of an International Symposium Held at Exeter, UK, from 15 to 19 July 1996. 236, IAHS.

Williams, J. (1977). Sediment delivery ratios determined with sediment and runoff models. *IAHS Publ 122,* 168-179.

Williams, J. R., & Berndt, H. D. (1972). Sediment yield computed with universal equation. *Journal of the Hydraulics Division, 98*.

Wischmeier, W. H., Johnson, C. B., & Cross, B. V. (1971). A soil erodibility nomograph for farmland and construction sites. *Journal of soil and water conservation, 26,* 189-193.

Wischmeier, W. H., & Smith, D. (1978). Predicting Rainfall Erosion Losses: A Guide to Conservation Planning. Agriculture handbook, Science and Education Administration, U.S. Department of Agriculture.

Wischmeier, W. H., & Smith, D. D. (1965). Predicting Rainfall-erosion Losses from Cropland East of the Rocky Mountains: Guide for Selection of Practices for Soil and Water Conservation. Agriculture handbook, Agricultural Research Service, U.S. Department of Agriculture.

Zhang, Z., Sheng, L., Yang, J., Chen, X. A., Kong, L., & Wagan, B. (2015). Effects of land use and slope gradient on soil erosion in a red soil hilly watershed of southern china. *Sustainability, 7,* 14309-14325.

Cloud Publications
International Journal of Advanced Remote Sensing and GIS
2017, Volume 6, Issue 3, pp. 2068-2079
ISSN 2320 – 0243, Crossref: 10.23953/cloud.ijarsg.33

Research Article | Open Access

Delineation of Groundwater Potential Zone in Baliguda Block of Kandhamal District, Odisha using Geospatial Technology Approach

Kamal Ku. Barik[1], Dalai P.C.[1], Goudo S.P.[1], Panda S.R.[1], Nandi D.[2]

[1]Dept. of Earth Sciences, Sambalpur University, Jyoti Vihar, Burla, Odisha, India
[2]Dept. of RS & GIS, North Orissa University, Takatpur, Mayurbhanj, Odisha, India

Publication Date: 21 March 2017

DOI: https://doi.org/10.23953/cloud.ijarsg.33

Abstract Assessment of groundwater potential zones is extremely important for protection of water quality and management of groundwater systems. Groundwater Potential Zones (GPZ) are demarcated with the help of geospatial techniques. The parameters, considered for identifying the GPZ such as geology, geomorphology, slope, drainage density, lineament density, rainfall, soil and landuse and land cover (LULC) are generated using satellite data and toposheet. Later, they are integrated with each other applying weighted overlay in ArcGIS. Suitable ranks are assigned for each category of these parameters. For various geomorphic units, weight factors are decided based on their capability to store groundwater. This procedure is repeated for all other layers and resultant layers are reclassified. The groundwater potential zones are classified into three categories like Poor, Good and Excellent. The use of aforesaid methodology is demonstrated in a selected study area in Baliguda block of Kandhamal district in Odisha.
Keywords *Groundwater Potential Zone; GIS; Lineament; rainfall*

1. Introduction

Groundwater is one of the most valuable natural resources, which supports human health, economic development and ecological diversity. Because of several inherent qualities, it has become an immensely important and dependable source of water supplies in all climatic regions including both urban and rural areas of developed and developing countries. The groundwater occurrence in a geological formation primarily depends on the formation of porosity. High relief and steep slopes impart higher runoff, while topographical depressions increase infiltration. An area of high drainage density also increases surface runoff compared to low drainage density area. Surface water bodies like rivers, ponds, etc., can act as recharge zones [1]. The remote sensing (RS) and Geographic information system (GIS) tools can open new paths in water resource studies. Analysis of remote sensing data supported by the survey of India (SOI) topographical sheets and collateral information with necessary ground truth verifications help in generating the baseline information for groundwater targeting [2]. The different hydrogeological themes can be used to identify the groundwater potential zones of the present area. Identification of groundwater occurrences using remote sensing data is based on indirect analysis of directly observable terrain features like geological structures,

geomorphology, landuse and Landcover, drainage density, rainfall data and their hydrologic characteristics. Also lineaments play significant roles in groundwater exploration in all type of terrains. Application of RS and GIS can be utilized in as multi criteria analysis of resources evaluation and ground water Potential zone study. Integration of RS and GIS has proved to be an effective tool in determination of groundwater potential and other studied in various parts of the world [3; 4, 5; 6; 7; 8; 9; 10; 11]. Several studies have been made to delineate groundwater Potential zones using geospatial techniques. These methods utilize cost effective tools in producing valuable data on geological, hydrogeological and geomorphological parameters that help in delineating groundwater potential zones. The main goal of this study is to map groundwater potential zone based on terrain, hydrological and geological parameters employing multi criteria approach. These parameters are very closely associated with groundwater accumulation.

2. Study Area

The study area is a part of Kandhamal district lying between 19^0 34' to 20^0 36' north latitude and 83^0 34' to 84^0 34' east longitude. Kandhamal district is bound by Boudh district in the north, Rayagada district in south, Ganjam and Nayagada district in the east and Kalahandi district in the west. Kandhamal district is divided into 12 blocks and Baliguda block is one of them. The study area comprises an area of 812 km^2. Physiographically, the entire district is located on a high altitude zone with hill ranges and narrow valley tracks which ultimately guide the socioeconomic condition of the people. Almost 66 % of the land area is covered with dense forest. The maximum temperature recorded in this area is 45.5^0C and minimum temperature 2^0C. The annual average rainfall is 1163mm.

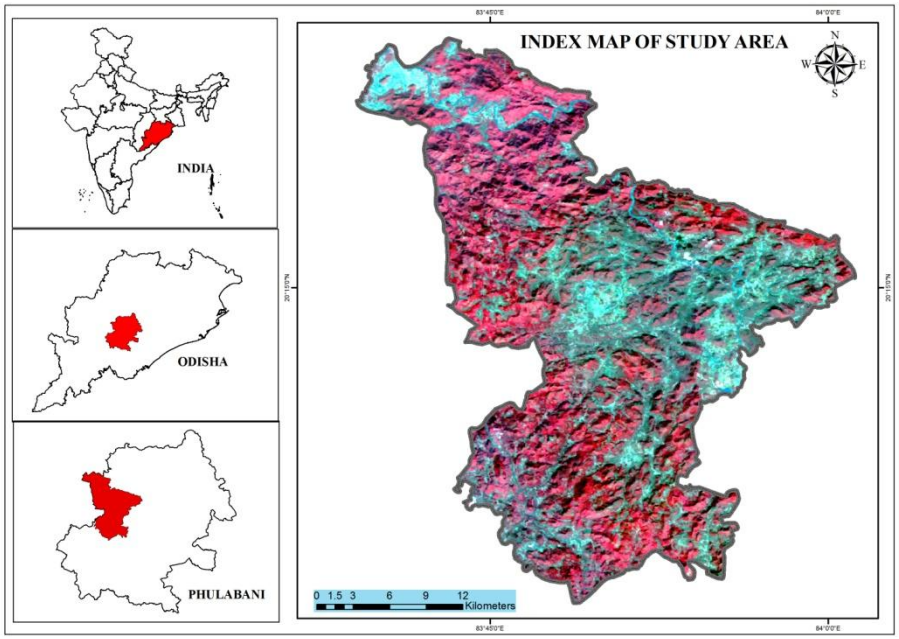

Figure 1: *Location map predicted the study area*

3. Materials and Methodology

For carrying out the present piece of work the open source Landsat data were collected from http//www.earthexplorer.usgs.gov site and has been analyzed to fulfill the objectives. Landsat 8 OLI data and SRTM DEM have been used for this study proposed. SOI toposheet number at 1:50,000 have also been used. The lithology map was collected from Geological Survey of India (GSI),

Bhubaneswar and was later scanned, rectified and digitized on Arc GIS to prepare the of lithology thematic layer of the study area. The rainfall data was collected from regional office of Indian Meteorological Department, Bhubaneswar. The slope map was generated from SRTM DEM. The digital (FCC_S) of Landsat OLI were visually interpreted for preparing different thematic layers like Geomorphological map, Landuse and Landcover and lineament density map of Baliguda block. The drainage map was prepared from SOI toposheet and the drainage density map was prepared from Arc GIS software. In order to access groundwater Potential zones, different thematic layers Viz. Geomorphology, LULC, Drainage density, Lineament density, Slope, Soil and rainfall were generated from satellite imagery and the conventional data were in corporated with the help of Arc GIS 9.3 software. The methodology adopted flowchart for the present study is shown in Figure 2.

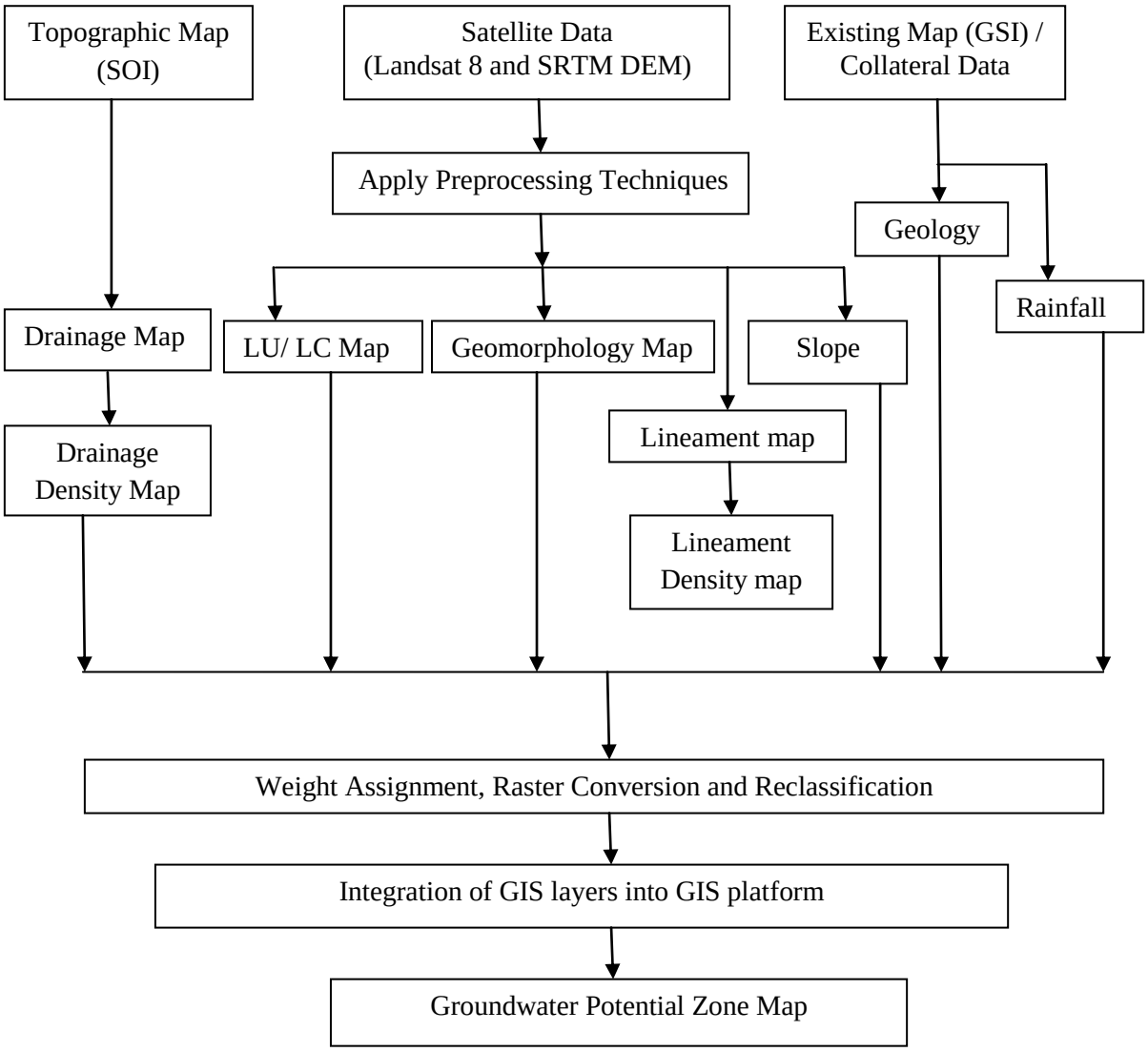

Figure 2: *Flow chart of the methodology of assigning the groundwater Potential of the study area*

GIS packages are used creation for digital data base, data integration and analysis. All thematic maps are digitized in continuous manner in vector format and the digitized values were then assigned. Different polygons in the thematic maps were labeled separately. Initially each one of the polygons in the final thematic layers was qualitatively visualized into one of the category Viz. (i) Excellent, (ii) good, (iii) moderate and (iv) Poor, in terms of their importance and occurrence of groundwater. Then suitable

weights were assigned to each thematic feature after considering their characteristics. Knowledge based weight assignment was carried out for each feature and they were integrated and analyzed using the weighted aggregation method [12, 13]. In this method, the total weights of the final integrated polygon were derived as sum or product of the weights assigned to different layers according to their suitability. Finally the groundwater prospect or Potential zone map was generated.

3.1. Categorization of thematic layers

To assess the groundwater prospect of an area, it is necessary to understand different types of landforms, geology, soil characteristics, slope and recent land utilization of that area. The information in groundwater characteristic of the various parameters is initially generated in descriptive forms, which revels the parameters support the occurrences of groundwater. The criteria adopted for different thematic layers are given bellow.

3.2. Delineation of groundwater Potential zone

Considering all the themes and features in an integrated layer, the groundwater potential index (GWPI) is calculated as.

$$GWPI = GwGr + LwLr + DwDr + LIwLIr + RwRr + SwSr + GMwGMr$$

Where Gw represents weight of geology and Gr represents rank on the theme;
Lw represent weight of LULC and Lr represents rank on the theme;
Dw represent weight of drainage density and Dr represents rank on the theme;
LIw represent weight of lineament density and LIr represents rank on the theme;
Rw represent weight of rainfall and Rr represents rank on the theme;
Sw represent weight of soil and Sr represents rank on the theme;
GMw represent weight of geomorphology and GMr represents rank on the theme;

4. Results and Discussion

The occurrence of groundwater in an area is governed by several factors, such as topography, geology, geomorphology, landuse, soil, rainfall, drainage density, and lineament density for which thematic layers are prepared for their input into a GIS.

4.1. Geology

Lithology is a very important factor in predicting groundwater Potential zones. Three types of lithological units namely charnockite, sand and silt and sandstone are found in the study area shown in Figure 3. As sand and silt are under alluvium group, it has been given higher weightage as compared to sedementary rock like sandstone. Charnockite has lesser amount of porosity for percolation of groundwater in contrast to alluvium and sedimentary rock, so it has been given as less weightage. The weights assigned to different thematic layers and the derivation of weights for indivisual themes are shown in Table 1.

4.2. Geomorphology

The hydrogeomorphology in hard rock terrain is highly influenced by the lithology and structure of the underlying formation and is considered as one of the most important features in evaluating the groundwater Potential and prospect [14]. Formations associated with river/water bodies and flood plains have higher water retention capability and therefore constitute the best landforms for higher

groundwater Potential. The geomorphology of the study area is shown in Figure 4. The flood plain region of the study area, shown in green color receives good recharge and has excellent prospects. The pediplain region covers a majority of the study area and the groundwater reserve in these regions is very limited due to less recharge. The river channels and water bodies, characterized by highly porous and permeable materials perform as good groundwater prospects. The structural hills and denudational hills in the study area, shown in blue and yellow color comprise the runoff zones and are not suitable for groundwater.

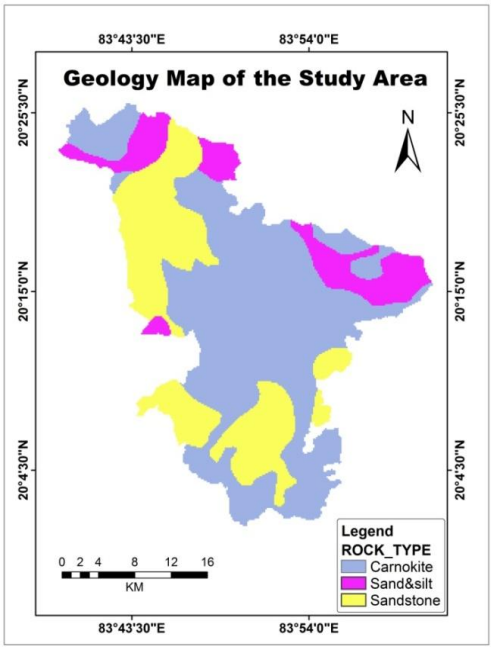

Figure 3: *Geology Map of the study area*

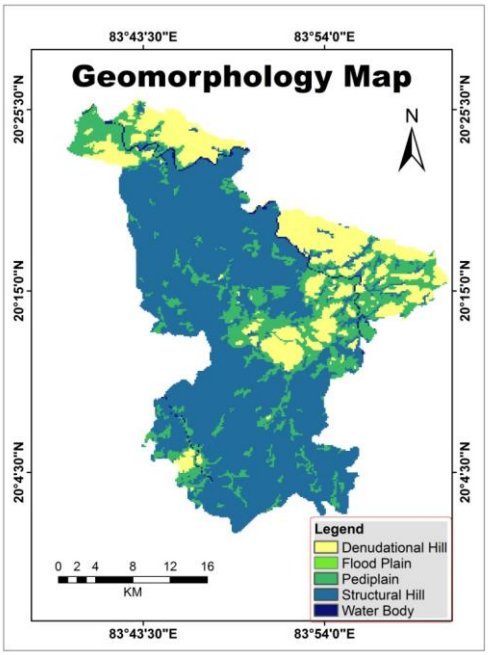

Figure 4: *Geomorphology Map depict the study area*

4.3. Soil

The soil of the study area are divided in to four main categories namely clay, sand, sandy loam and sandy clay loam are shown in Figure 5. Rank and weights have been assigned on the basis of infiltration or porosity rate of the soil. Sand and sandy clay loam have high infiltration rate and have been given high rank whereas most of the areas have been cover with sandy loam. It has been marked with low rank because sandy loam has low infiltration capacity. The last categories of soils are clay and it has also low infiltration capacity as compared to sandy clay loam.

4.4. Drainage density

Drainage density is an important parameter for evaluating groundwater prospects. The drainage map of the study area, shown in Figure 6 is used for the preparation of drainage density (Figure 7). High drainage density values are favourable for runoff low groundwater Potential zone. High ranks are assigned to low drainage density area and vice versa. Based on the drainage density value, the area was classified into seven group's viz. 0 - 59.86, 59.86 – 119.73, 119.73 – 179.60, 179.60 – 239.47, 239.47 – 299.34, 299. 34 – 359.21, 359.21 – 419.08 m/ Sq.km. Low drainage density causes more infiltration and the result is good water Potential as compared to high drainage density regions. Higher ranking were given to lower drainage density regions and vice versa.

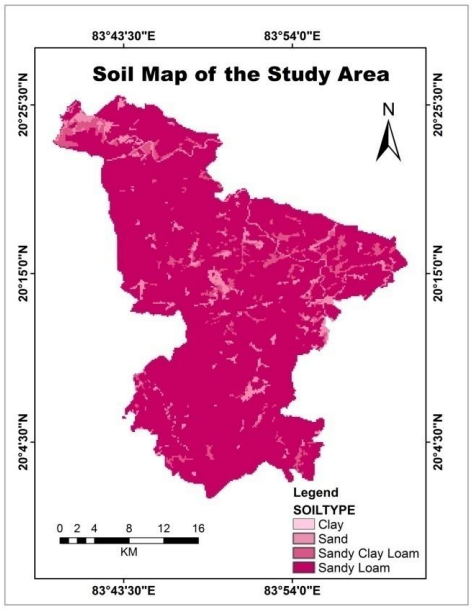

Figure 5: *Soil Map of the study area*

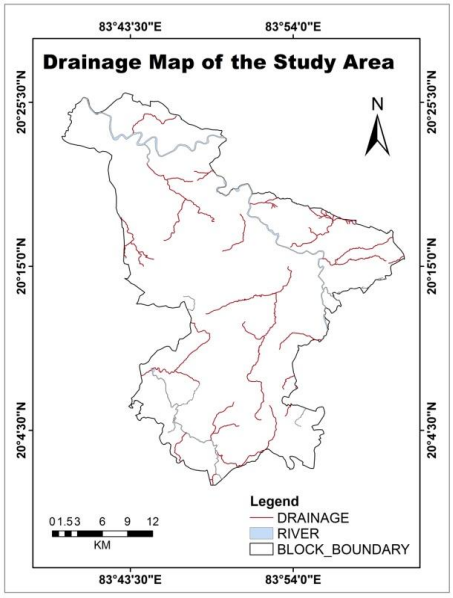

Figure 6: *Drainage map of the study area*

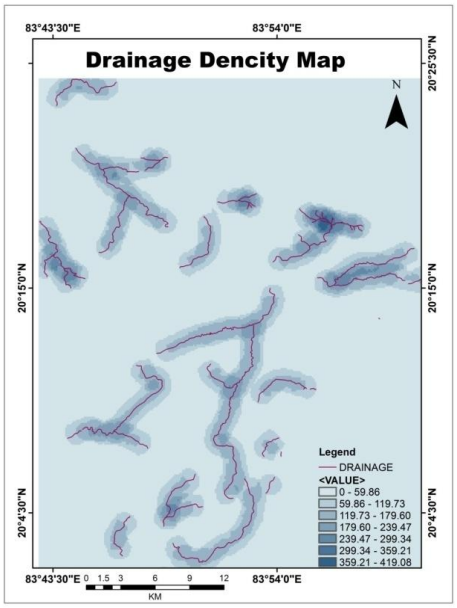

Figure 7: *Drainage density map of the study*

4.5. Lineament Density

The lineament is the result of faulting and fracturing and hence is the indicator of porosity and permeability of hard rock areas and it may be of significance in groundwater study. The geological linear features are assumed to be zones of fracture in bed rocks where prospects of more groundwater may be expected [15, 16]. Lineaments are normally shown in tonal, texture, relief drainage, vegetation linearity and curvilinearity in satellite data [17]. Accordingly, the lineament density map was prepared from the lineament map (Figure 8). The lineament density map shows (Figure 9) low density as compared to other parts of the study area. The minimum linear density was found in 0-42.06 and the

highest density was 126.18 – 168.24 m/ km^2. Higher values of lineament density will have more recharge and hence better prospects for groundwater.

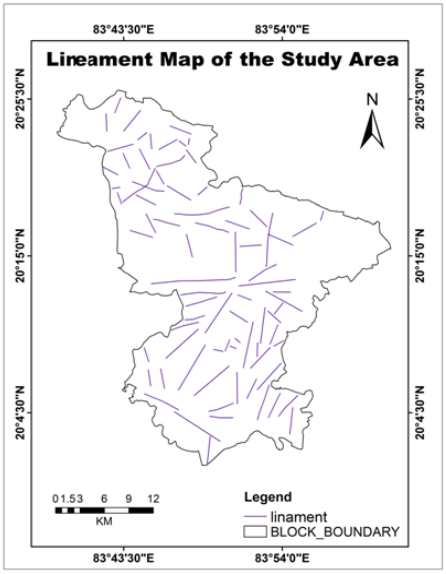

Figure 8: *Lineament map of the study area*

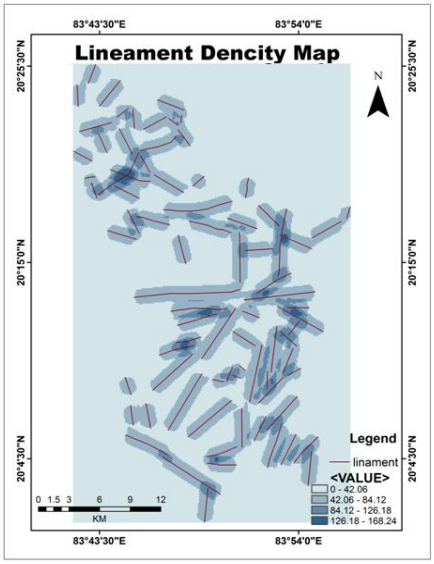

Figure 9: *Lineament density map of the study*

4.6. Landuse / Landcover

The study area consists of agricultural lands, built up land, scrub, forest, wasteland and water bodies are shown in (Figure 10). From the landuse point of view agricultural lands are Moderate sites for groundwater exploration. The areas occupied by water bodies are coming under Very High categories and the Reserve Forests are coming under Moderate categories. Lands which are not used for any purpose are treated or classified as wasteland and hence it is categorized as Poor for groundwater prospects. Lands with scrub are categorized as Low Moderate categories.

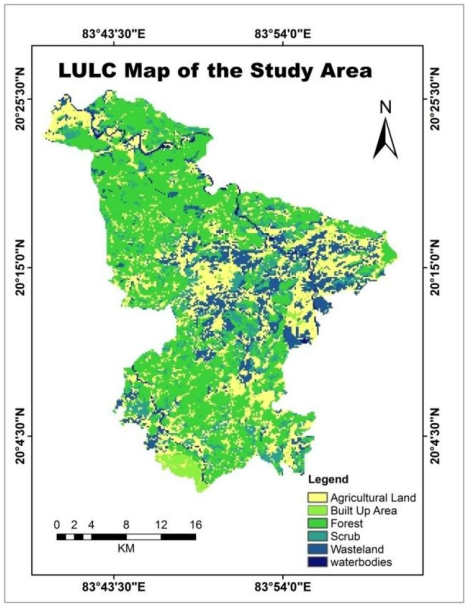

Figure 10: *LULC map of the study area*

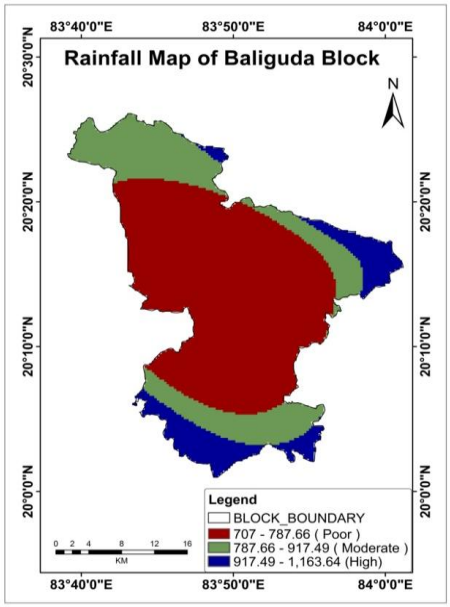

Figure 11: *Rainfall map of the study area*

4.7 Rainfall

Rainfall is the main source of groundwater recharge. In the present study, the thematic layer of rainfall has been developed on the basis of 12 points data by the use of Inverse Distance Weighted (IDW) method in Arc GIS platform. Figure 11 illustrates the rainfall map of the study area. The total area is depicted as coming under three rainfall zones. The area 707-787.66 mm rainfall falls into Poor for groundwater storage categories. The areas with 787.66 – 917.49 mm rainfall are considered as Highly Moderate categories. The area having a rainfall of 917.49 – 1163.64 mm are slotted under relatively High category for groundwater recharge

4.8 Slope

Slope is one of the most significant parameters for groundwater exploration. Slope of any area affects the runoff and recharge of surface water. In terms of groundwater recharge, an area with flat terrain topography falls into Very Good category and has relatively more infiltration rate. Figure 12 illustrate the slope map of the study area. Topographically, the area is categorized into plain to steeply sloping hills. The slope varies from 00 to 9.260. On the basis of degree of slope, the study area has been classified into four slope classes. The area having 0 0 – 1.16 0 falls into High for groundwater storage categories because of the nearly flat terrain and relatively high infiltration rate. The areas with 1.160 – 2.430 slopes are considered as Good due to slightly undulating topography. The area having a slope of 2.430- 3.810 cause relatively high runoff and low infiltration and hence categorized as Poor and the area having 3.810 – 9.26 0 are considered as very poor due to high slope and runoff.

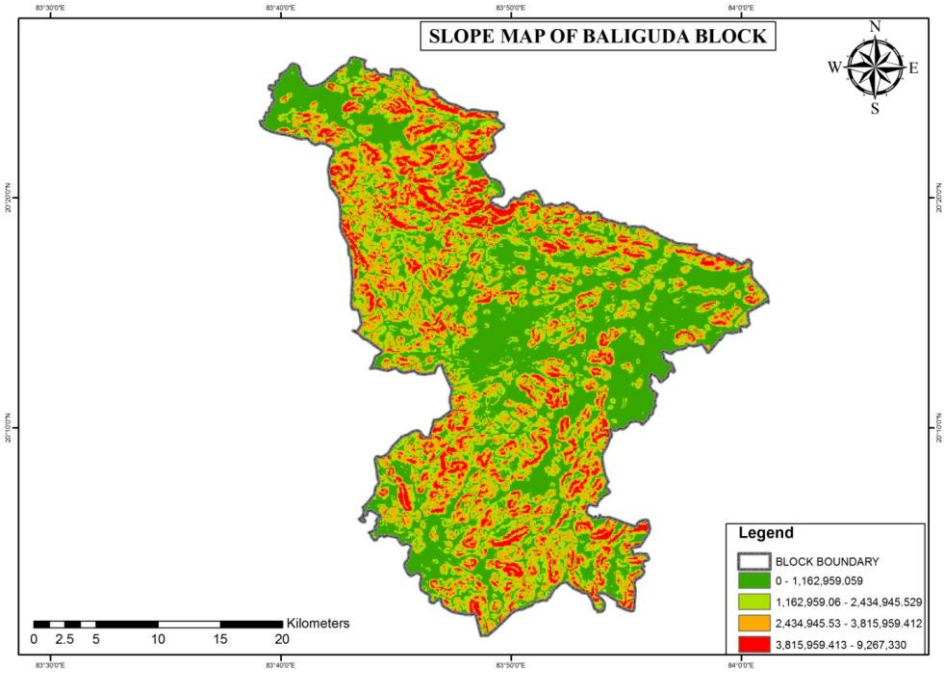

Figure 12: *Slope map of the study area*

4.9. Integration of thematic layers using weightage overlay analysis Model

Depending on the groundwater potentiality, each class of the main eight thematic layers (Geomorphology, Geology, LULC, Soil, Drainage Density, Lineament Density, slope and rainfall) are qualitatively placed in one of the categories viz. Very High, High, Highly Moderate, Moderate, Poor and Very Poor. The weights and ranks have been chosen basing on the judgment of works carried out by

researchers or knowledge of expert gained through similar work on groundwater potentiality mapping [18; 19; 20; 21]. All the thematic maps are converted into raster format and superimposed by weighted overlay method (rank and weight wise thematic maps and integrated with one another through in GIS software). For assigning the weight, the geomorphology and geology were assigned higher weight whereas the drainage density and lineaments were assigned lower weights. After assigning weights to different parameters, individual ranks were given for sub variable. The maximum value is given to the feature indicating highest groundwater potentiality and the minimum given to the lowest groundwater potentiality. In LULC, the highest rank values are given to water body and low rank values are assigned to build up area. Similarly in geology, highest values are assigned to charnockites and lowest values to sand and silt. Among the various lineament density classes, the very high lineament density categories are assigned higher rank values as this category has greater chances of groundwater infiltration. In landforms, water body has highest rank 9 and structural hill has lowest rank 1. The overlay analysis is tabulated in Table 1. All the thematic maps have been integrated using Groundwater Potential Index (GWPI) formula in GIS. A final groundwater Potential map (Figure 13) is prepared based on the above technique. In the present study, the groundwater Potential zones have been categorized into three type's viz. Excellent, Good and Poor. Table 2 gives the upper and lower limits of weights considered for demarcating these three types of groundwater prospective areas.

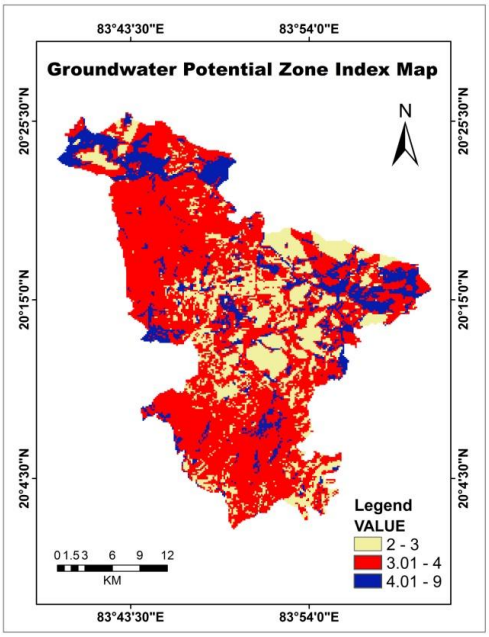

Figure 13: *Groundwater Potential Index map of the study area*

Table 1: *Thematic Map Weight and Feature Ranking*

Theme	Sub-Classes	Category	Rank	Influence (weight) %
Geomorphology	Water body	Very High	**9**	**25**
	Structural hill	Very poor	**1**	
	Denudational hill	Poor	**2**	
	Pediment	Moderate	**4**	
	Flood plain	High	**8**	
Geology	Sand and silt	High	**8**	**18**
	Sand stone and conglomerate	Highly Moderate	**6**	
	Charnockite	Poor	**3**	

LAND USE/ LAND COVER	Agricultural land	High	**8**	**8**
	Built Up land	Very Poor	**2**	
	Forest	Highly Moderate	**6**	
	Scrub	Low Moderate	**5**	
	Wasteland	Poor	**3**	
	Water Body	Very High	**9**	
Soil	Sandy loam	Poor	**3**	**15**
	Sandy clay loam	High	**8**	
	Clay	Highly Moderate	**6**	
	Sand	Very High	**9**	
Drainage Density	0-59.86	Poor	**3**	**6**
	59.86-119.73	Highly Moderate	**6**	
	119.73-179.60	High	**8**	
	179.60-419.08	Very High	**9**	
Lineament Density	0 - 42.06	Poor	**3**	**7**
	42.06 - 84.12	Highly Moderate	**6**	
	84.12 - 126.18	High	**8**	
	126.18 - 168.24	Very High	**9**	
Slope	0^0 - 1.16^0	High	**8**	**12**
	1.16^0- 2.43^0	Highly Moderate	**6**	
	2.43^0-3.81^0	Poor	**3**	
	3.81^0- 9.26^0	Very poor	**1**	
Rainfall	707 – 787.66	Poor	**3**	**9**
	787.66 - 917.49	Highly Moderate	**6**	
	917.49 -1163.64	High	**8**	

Table 2: *Weightage Range of Groundwater Potential Zone*

Groundwater Category	Weightage Table
Excellent	>4.01
Good	3.01- 4.0
Poor	<3.01

5. Conclusion

In this study it has been established that geospatial technology can provide appropriate platform for convergent analysis of large volumes of multidisciplinary data and decision making for groundwater studies. These techniques have been successfully used and demonstrated for evaluation of groundwater potential. The weightage Index overlay model has been found very useful in the mapping of groundwater prospective zones. This groundwater Potential information will be useful for identification of suitable location for extraction of water. From this study it is observed that remote sensing and GIS technique can be used effectively to delineate groundwater recharge potential zones map, which can be used for improvement in the groundwater recharge and holding for the study area and later on may be for various purposes like identification of location of structures for artificial recharge, locations of new tube wells and efficient groundwater management for betterment of the society.

Acknowledgement

Author would like to thanks Director of CGWB, Regional Centre Bhubaneswar and Dr. S. Nanda, Assistant Professor, SRM University for providing for their keen interest encouragement for this work. The authors are thankful to all the anonymous reviewers for giving valuable suggestions which improve the quality of the manuscript.

References

[1] Murugesan, B., Thirunavukkarasu, R., Senapathi, V., Balasubramanian, G.: Application of remote sensing and GIS analysis for groundwater potential zone in kodaikanal Taluka, South India. Earth Sci. 7, 65-75 (2012)

[2] Waikar, M.L., Nilawar, A.P.: Identification of Groundwater Potential Zone using Remote Sensing and GIS Technique. International Journal of Innovative Research in Science, Engineering and Technology, 3, 12163-12174 (2014)

[3] Chaturvedi, R.S., Bhattacharya, D.C., Kamal, P., Krishnamurthy, J., Sunder Raman, N.: Integrating remote sensing techniques in groundwater exploration – a typical case study from Bundelkhand region in Uttar Pradesh. In Proceedings, National Symposium on Remote Sensing in Development and Management of Water Resources, Ahmadabad. 267-276 (1983)

[4] Raj, S., Sinha, A.K.: An integral approach for the delineation of potential groundwater zones using satellite data: case study, Udaipur district, Rajasthan. Journal of Asia-Pacific Remote Sensing, 2, 61-64 (1989)

[5] Baldev, S., Bhattacharya, A., Hegde, V.S.: IRS-1A application for groundwater targeting. Current Science, 61, 172-179 (1991)

[6] Gustafsson, P.: High-resolution satellite data and GIS as a tool for assessment of groundwater potential of a semi-arid area. In IXth Thematic Conference on Geologic Remote Sensing, Pasadena, California, 8-11 (1993).

[7] Krishnamurthy, J., Srinivas, G.: Role of geological and geomorphological factors in groundwater exploration: a study using IRS LISS data. International Journal of Remote Sensing, 16, 2595-2618 (1995)

[8] Shahid, S., Nath, S.K., Roy, J.: Groundwater potential modeling in a soft rock area using a GIS. International Journal of Remote Sensing, 21, 1919-1924 (2000)

[9] Jasrotia, A.S., Kumar, R., Saraf, A.K.: Delineation of groundwater recharge sites using integrated remote sensing and GIS in Jammu district, India. International Journal of Remote Sensing, 28, 22, 5019-5036 (2007a).

[10] Jasrotia, A.S., Bhagat, B.D., Kumar, A.: Remote Sensing and GIS Approach for Delineation of Groundwater Potential and Groundwater Quality Zones of Western Doon Valley, Uttarakhand, India. (2012b). doi:10.1007/s12524-012-0220-9

[11] Taylor, P., Saraf, A.K., Choudhury, P.R., Roy, B., Sarma, B., Vijay, S.: GIS based surface hydrological modeling in identification of groundwater recharge zones. International Journal of Remote, 37-41 (2013)

[12] ESRI (Environmental System Research Institute): User Guide ARC/INFO, the Geographic Information System Software (Redlands, CA USA: ESRI. Inc) (1988)

[13] ESRI (Environmental System Research Institute): User Guide ARC/INFO, Training Course Class Materials, Vol. 1. (Redlands, CA USA: ESRI. Inc) (1989)

[14] Kumar, M.G., Agarwal, A.K., Bali, R.: Delineation of potential sites for water harvesting structures using remote sensing and GIS. J Indian Soc Remote Sens., 36, 323-334 (2008).

[15] Das, D. Enhancement analysis of geological linear features for groundwater information extraction. Abs Vol Int Conference on Management of Drinking Water 1. Chennai: CLRI (1997)

[16] Rao, N.S., Chakradhar, G.K.J., Srinivas, V.: Identification of groundwater potential zones using remote sensing techniques in and around Guntur Town, Andhra Pradesh. India. J Indian Soc Remote Sens., 29; 69-78 (2001)

[17] Sukumar, M., Venkatesan, N, Nelson, K.B.C.: A Review of Various Lineament Detection Techniques for high resolution Satellite Images. International Journal of Advanced Research in Computer Science and Software Engineering, 4, 72-78 (2014)

[18] Krishnamurthy, J., Venkatesa Kumar, N., Jayaraman, V., Manivel, M.: An approach to demarcate groundwater potential zones through remote sensing and GIS. Int. J. Remote Sensing, 17, 1867-1884 (1996)

[19] Saraf, A.K., Choudary, P.R.: Integrated remote sensing and GIS for groundwater exploration and identification of artificial recharge sites. Int. J. Remote Sensing, 19, 1825-1841 (1998)

[20] Elewa, H.H., Qaddah A.A. Groundwater potentiality mapping in the Sinai Peninsula, Egypt, using remote sensing and GIS-watershed-based modeling. Hydrogeol. Journal, 19, 613-628 (2010).

[21] Samy, I.E., Mohamed, M.M. Natural hazards susceptibility mapping in the Kuala Lumpur, Malaysia: An assessment using remote sensing and geographic information system (GIS). Geomatics Nat. Hazards and Risk J., 4, 1-21 (2013)

Cloud Publications
International Journal of Advanced Remote Sensing and GIS
2017, Volume 6, Issue 2, pp. 2033-2049
ISSN 2320 – 0243, Crossref: 10.23953/cloud.ijarsg.35

Case Study | Open Access

Horticultural Fruit Crop Plantations Mapping using Geo-informatics Technology in Gujarat State, India

Vijay Singh[1], Ajay N. Patel[1], Apurva Dalwadi[1], Jaydipsinh Kathota[1], Jignesh Suthar[2] and Manik H. Kalubarme[1]

[1]Bhaskarcharya Institute for Space Applications and Geo-informatics (BISAG), Department of Science & Technology, Government of Gujarat, Gandhinagar - 382007
[2]Department of Horticulture, Government of Gujarat, Gandhinagar

Publication Date: 18 February 2017

DOI: https://doi.org/10.23953/cloud.ijarsg.35

Abstract The cultivation and production of horticultural crops is known as "Golden Revolution" and India has emerged as the second largest producer of fruits and vegetables in the world. The Central Government of India has started National Horticulture Mission (NHM) for overall development of Horticulture and Gujarat Government has also started Gujarat State Horticulture Mission (GSHM). This mission being implemented in 16-potential districts and covers major fruit crops in the state like mango, sapota, Aonla, banana, coconut etc. Under the GSHM, mapping of fruit crop plantations using Indian Remote Sensing Satellite (IRS) data in Gujarat State was carried out jointly by the Directorate of Agriculture, Govt of Gujarat and Bhaskaracharya Institute for Space Applications and Geo-informatics (BISAG), Govt of Gujarat. The major objective of this project was mapping of fruit crop plantations at village-level and preparation of village-level Horticultural Atlas of Gujarat State. High spatial resolution digital data from IRS LISS-IV and CARTOSAT-1 with spatial resolutions of 5.8m and 2.5m respectively, covering major fruit growing districts in Gujarat state was analysed for identification and delineations of fruit crop plantations in each survey number on cadastral map. The cadastral maps of each village were geo-referenced with satellite data and survey number boundaries were superimposed on the satellite data. Fruit crop plantations were located during field visits and their GPS locations were transferred to the satellite images with cadastral maps for unique identification and accurate mapping. The fruit crops in different districts of Gujarat State were identified on the high resolution satellite data based on the planting pattern and tree-crown density. The survey numbers having fruit crop plantations were delineated on the CARTOSAT-1 data. The fruit crop plantation maps of each village were prepared and complied at village and taluka level using open-source Quantum GIS software for preparation of village-level horticultural atlas of Gujarat State. The area under fruit crop plantations was also estimated. The results of this alternate method of mapping fruit crop plantations using high resolution, single-band CARTOSAT-1 panchromatic data on cadastral maps with survey numbers gave very good results for preparation village-level horticultural atlas of Gujarat State. Field survey in different villages was also carried out for accuracy assessment of survey numbers mapped as horticultural plantations.

Keywords *CARTOSAT-1; Gujarat State Horticultural Mission (GSHM); High spatial resolution; Indian Remote Sensing Satellite (IRS); Cadastral maps*

1. Introduction

The term “Horticulture” which is a part of agriculture is concerned with the raising of so called garden crops. At present, fruits, vegetables, flowers etc. are grown not only within the backyards, but also in large areas in open fields on a commercial scale. Traditionally garden crops include fruits, vegetables and flowers. But today‘s horticulture deals not only the fruits, vegetables and flowers but also other important crops like spices, condiments, plantation crops, medicinal and aromatic plants etc. Besides cultivation of these crops, present day horticulture deals with the utilization and improvement of these crops. Horticultural crops play a unique role in India’s economy by improving the income of rural people. The cultivation and production of horticultural crops is known as **"Golden Revolution**” and India has emerged as the second largest producer of fruits and vegetables in the world. Horticulture crops have inherent advantage of providing higher productivity per unit of land compared to other crops, resulting in higher income and higher employment generation in rural Areas. Fruit trees have been cultivated since time immemorial in India. Today, India is the second largest producer of fruits in the world after China and almost all kind of fruit crops can be favourably grown in India due to its diverse agro-climatic zones. The area under fruit crops in 2011-12 was 6.58 million ha with a production of 77.52 million tonnes, which contributes to a 32 percent share in total horticultural production (Anon, 2012). Among the major fruit producing countries, India ranks number two after China (Hand Book on Horticulture Statistics, 2014) (Figure 1).

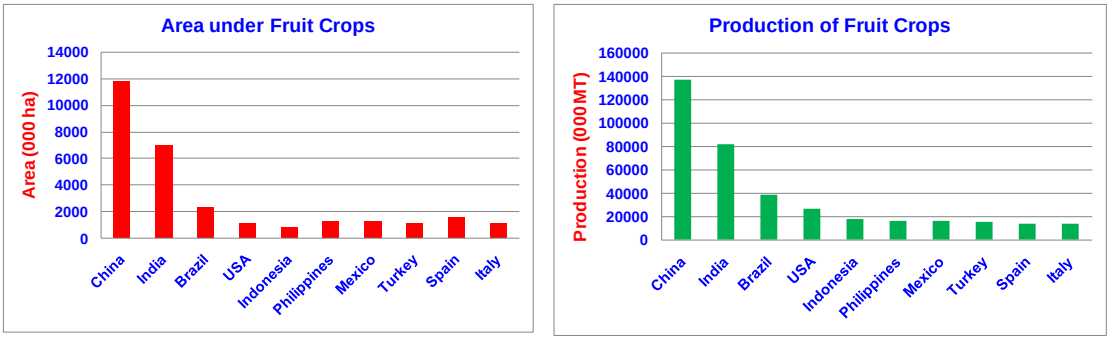

Figure 1: *Area and production of fruit crops in major fruit producing countries in the world (2012-13)*

India is one of the leading producers of horticultural crops in the Globe. Horticultural crops cover 13.08 % of the total area under agriculture and contribute to about 28 % of the GDP. These crops accounts for 37 % of the total exports of agricultural commodities. Due to planned emphasis laid on horticulture, India is accredited as the second largest producer of fruits and vegetables. India is the largest producer and consumer of cashew nut, tea and spices and it is third largest producer of coconut. India exports fruits, vegetables, processed products, flowers, seeds and planting materials, spices, cashew nut, tea, coffee etc. India is the largest producer of mango, banana, grape and litchi. However, the bulk of the production is consumed domestically. Of the total global exports for fruits, India’s share is only 0.3%. Fruits accounts for about 11% of total horticultural export from country. Grape and mango together constitute 60% of India‘s exports of fresh fruits. Citrus, banana, apple and papaya are other important fruits for export.

1.1. Horticulture in India

Over the years, horticulture has emerged as one of the potential agricultural enterprise in accelerating the growth of economy. Its role in the country's nutritional security, poverty alleviation and employment

generation programmes are becoming increasingly important. It offers not only a wide range of options to the farmers for crop diversification, but also provides ample scope for sustaining large number of Agro-industries which generate huge employment opportunities. On account of significant increase in production in horticultural crops across the country, a Golden Revolution is in the offing and India has emerged as a leading player in the global scenario. It has now emerged as the world's the largest producer of and exporter of Tea, Coffee, Cashew nut, Spices Exports of fresh and processed fruits, vegetables, cut flowers, dried flowers have also been picking up. As a result of a number of thoughtful research, technological and policy initiatives and inputs, horticulture in India, today, has become a sustainable and viable venture for the small, marginal & big farmers. It is a matter of satisfaction that their food consumption levels and household income have increased.

Presently our country is next to China in area and production of fruits and vegetable crops and has been contributing 10% of fruits and 14% of vegetable of the total world production. India leads the world in the production of mango, banana, sapota, acid lime and cauliflower while the highest productivity of grape is also recorded here. India occupies second position in production of onion and third in cabbage production globally. Fruits such as mango, banana, citrus, guava and apple account for 75 per cent of the total fruit production in the country. The horticulture sector constituted nearly 20 per cent of agricultural GDP and contributes 4 per cent in the national economy (Netherlands Enterprise Agency, 2015).

1.1.1. *Area and Production of Horticulture Crops in India during last two Decades*

The area under horticulture crops which was 12.77 million hectares during 1991-1992 has increased to 23.69 million hectares during 2012-13. The total production during this period has increased from 95.56 million tons during 1991-1992 has increased to 268.85 million tons during 2012-13 (Figure 2). The production share of various horticultural crops in India is given in (Figure 3). The share of vegetables and fruits production is around 61 % and 30 %, respectively. A large variety of fruit crops are grown in India. Of these, mango, banana, citrus, papaya, guava, pineapple, sapota, jackfruit, litchi, grapes, apple, pear, peach, plum, walnut etc. are the important ones. India accounts for 10 per cent of the total world production of fruits. It leads the world in the production of mango, banana, sapota and acid lime besides recording highest productivity in grape. The leading fruit growing states in India are Maharashtra, Karnataka, Andhra Pradesh, Bihar and Uttar Pradesh (Naik and Thippesh, 2014). The area and production of major fruit crops in leading fruit producing states in India are given in Figure 4. Among the major fruit producing states in India, Gujarat State ranks number three in terms of both area and production of fruit crops after Andhra Pradesh and Maharashtra States (Hand Book on Horticulture Statistics, 2014).

1.2. Horticulture in Gujarat

Horticulture is a priority sector in agriculture by virtue of its vast potential in improving the socio economic condition of the farmers in Gujarat State. Gujarat has tropical & sub-tropical climate, with temperature ranging from a minimum of 13^{o}C to 27^{o}C in January and a maximum of 45^{o}C in May-June. The normal annual rainfall of Gujarat state is 852 mm and has about 1600 Km long coastal area. However, there is a wide annual variation in rainfall, affecting the productivity of the crops. The climate favours for development of fresh fruits like; Kesar-Alphanso Mangoes, Sapota, Banana, Aonla and Dates. The vegetables like; Okra, Beans, Cucurbits, Onion Potato, the spices like, Cumin, Fennel, Chilly, Coriander, Garlic and the flowers like, Rose, Lily, Marigold, Jasmine and Tuberose. Grapes, Cashew nut Medical and Aromatic crops like Aloevera, Palmarosa are emerging as potential new crops in suitable areas of the state. Investment in protected cultivation of floriculture and medical plant projects, tissue culture units, fruit and vegetable processing units are initiated in the state which shows shining future of Horticulture in the Gujarat State.

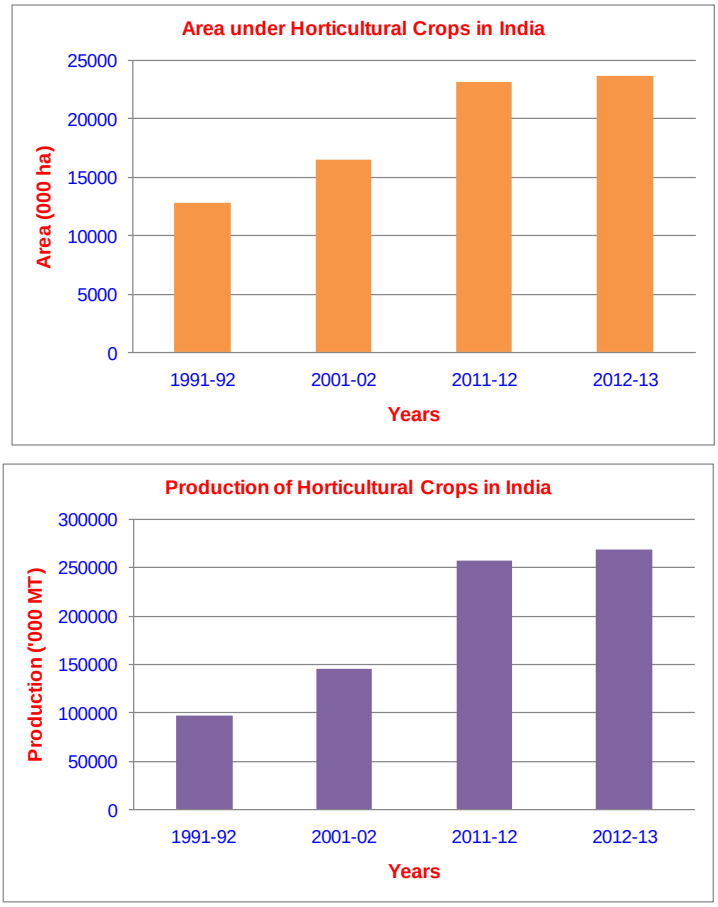

Figure 2: *Area and production of horticultural crops in India during last two decades*

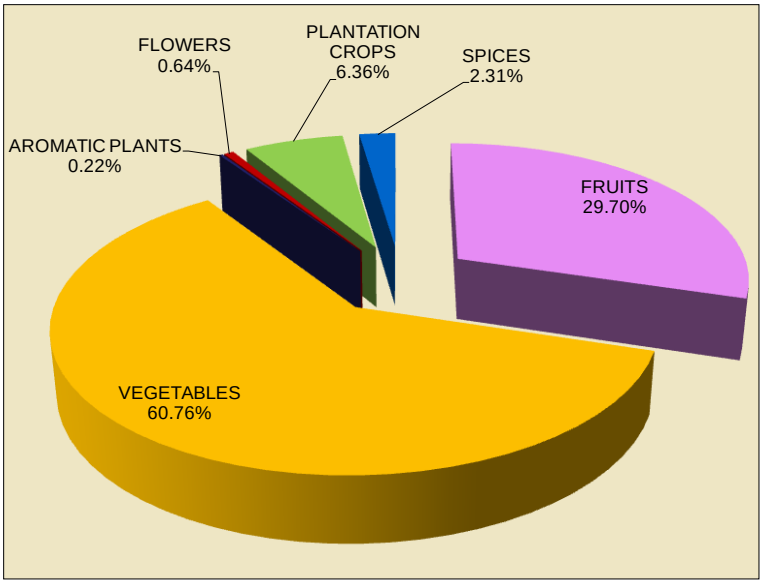

Figure 3: *Production share of various horticultural crops in India*

1.2.1. *Gujarat Horticulture Mission*

The Central Government has started National Horticulture Mission (NHM) from the year 2005-06 for overall development of Horticulture. The Gujarat Government has also registered "Gujarat Horticulture Mission" under the Chairmanship of Principal Secretary of Agriculture. At the district level district

mission committee has been formed under the Chairmanship of District Development Officer. The work of Horticulture Mission has been done in the State by this registered mission. Gujarat State Horticulture Mission (GSHM) a registered society has been formed for implementation of NHM in the state. The mission is being implemented in 16 potential districts and covers important horticultural crops of the state viz, Mango, Chiku, Aonla, Banana, Papaya, Lime, Cumin, Fennel, and Flowers, Medicinal and Aromatic crops, etc.

1.2.2. *Area & Production of Fruit Crops in Gujarat State*

The major crops covered under fruit crops are Mango, Chiku, Citrus, Ber, Banana etc in the Gujarat State. The estimated area under fruit crops has increased from 160.02 thousand ha during the year 1995-96 to 398.37 thousand ha during the year 2012-13. Similarly the estimated production of fruit crops has increased from 21.29 lakh M.T., during the period 1995-1996 to 85.31 lakh MT., during the year 2012-13. The area and production of major fruit crops in Gujarat State during the period of 1987-88 to 2012-13 are given in Figure 5.

(Horticulture in Gujarat 2011-12 & 2012-13)

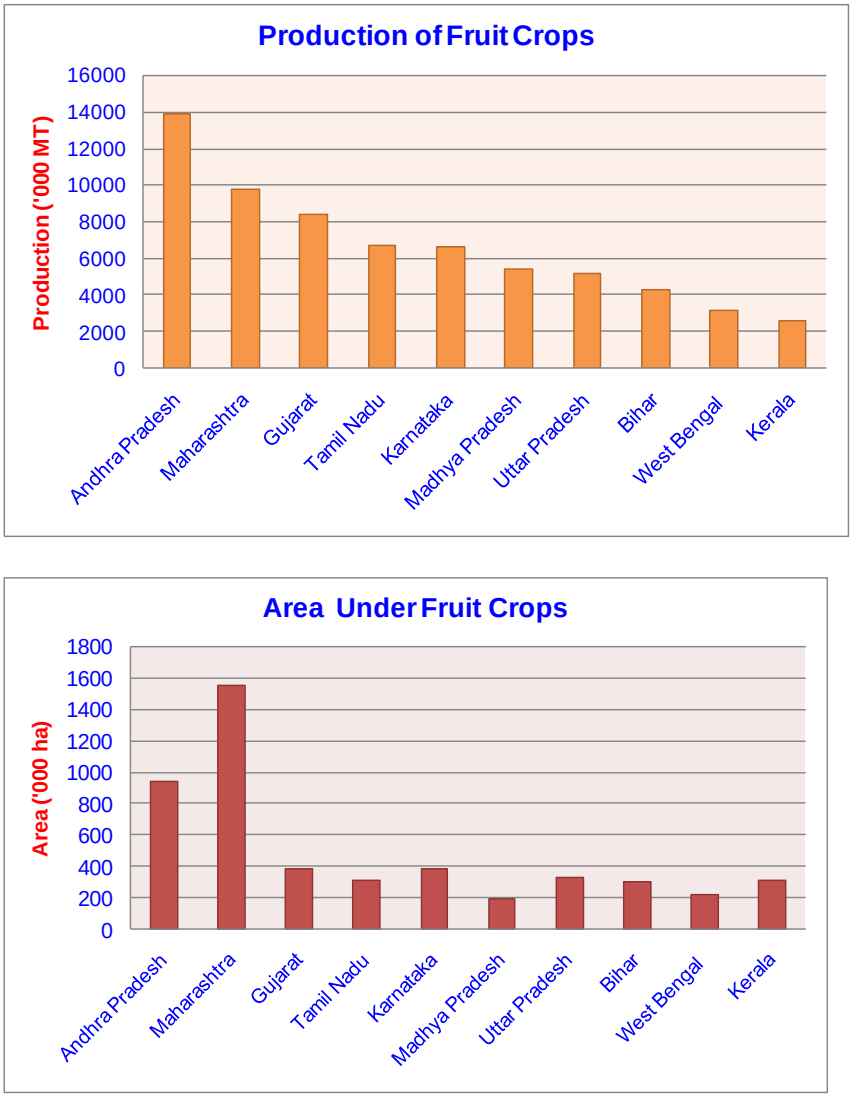

Figure 4: *Area and production of fruit crops in major states of India during 2012-13*

1.2.3. *Major Fruit Crops Producing Districts in Gujarat State*

The major crops covered under fruit crops are Mango, Chiku, Citrus, Ber, Banana etc. in the Gujarat State. The estimated area under fruit crops has increased from 160.02 thousand ha during the year 1995-96 to 398.37 thousand ha during the year 2012-13. Similarly the estimated production of fruit crops has increased from 21.29 lakh M.T., during the period 1995-1996 to 85.31 lakh MT., during the year 2012-13. The estimated area under fruit crops for mango, chiku, citrus and banana has increased in 2012-13 to 141.26 thousand ha., 28.81 thousand ha, 40.79 thousand ha, and 70.58 thousand ha as compared to 52.88 thousand ha., 13.73 thousand ha.,12.91 thousand ha., 24.09 thousand ha in the year 1996-97 respectively. The estimated production under fruit crops for mango, chiku, citrus, ber been, and banana has increased in 2012-13 to 1003.71 thousand M.T., 309.89 thousand M.T., 433.12 thousand M.T., 128.63 thousand M.T., 4523.49 thousand M.T., as compared to 288.93 thousand M.T., 120.76 thousand M.T., 68.70 thousand M.T., 115.74 thousand M.T., 903.66 thousand M.T., in the year 1996-97, respectively. In the case of fruits Crops, the percentage share to total fruits Crops for mango, Chiku, Citrus, and Banana, works out to percentage 11.77%, 3.63%, 5.08%, 53.02%, for the year 2012-13, respectively in the Gujarat State. The fruit crop-wise districts with share of production (%) in Gujarat state during 2012-13 for mango, chiku, citrus and banana crops is given in Figure 6.

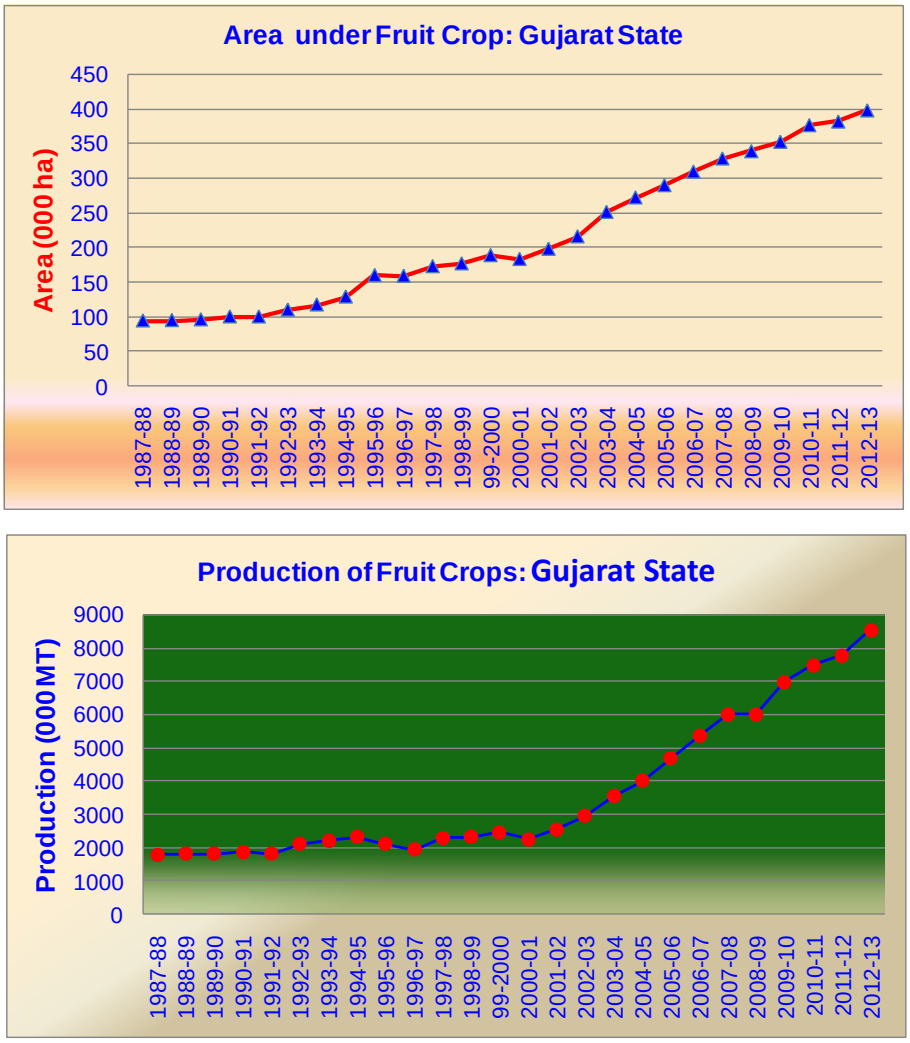

Figure 5: *Area and production of fruit crops in Gujarat state during last 25-years*

1.3. R S and GIS Studies for Horticultural Crops

The delineation of orchards and spatial analysis using geospatial technology can provide additional information for management decision making, such as the prediction of fruit yield, the quantification and scheduling of precise and proper fertilizer, irrigation needs, and the application of pesticides for pest and disease management. Therefore, today, the use of Remote Sensing (RS) has becoming importance for the general detection of the growth and health of orchards on a larger scale. Similarly, digital imaging technology is increasingly being used for intensive site-specific management of orchards (Panda et al., 2010). With an adequate database, GIS can serve as a powerful analytic and decision making tool for fruit culture development particularly in big country like India, where agro-ecological zones is so diverse. GIS is one of the most widely used techniques for mapping fruit trees. The determination of spatial distribution of slope exposure and slope inclination in fruit growing areas will help in determining the ecological suitability of an area for fruit growing and their influence to a large extent in both directions of fruit production and fruit quality.

The delineation of orchards and spatial analysis using geospatial technology can provide additional information for management decision making, such as the determination of fruit yield, the quantification and scheduling of precise and proper fertilizer, irrigation needs, and the application of pesticides for pest and disease management. Ultimately, it will improve profits for producers (Panda et al., 2009). Geospatial technology is a combination of four essential tools: remote sensing, geographic information systems (GIS), global positioning systems (GPS), and information technology or data management (Lobell et al., 2005).

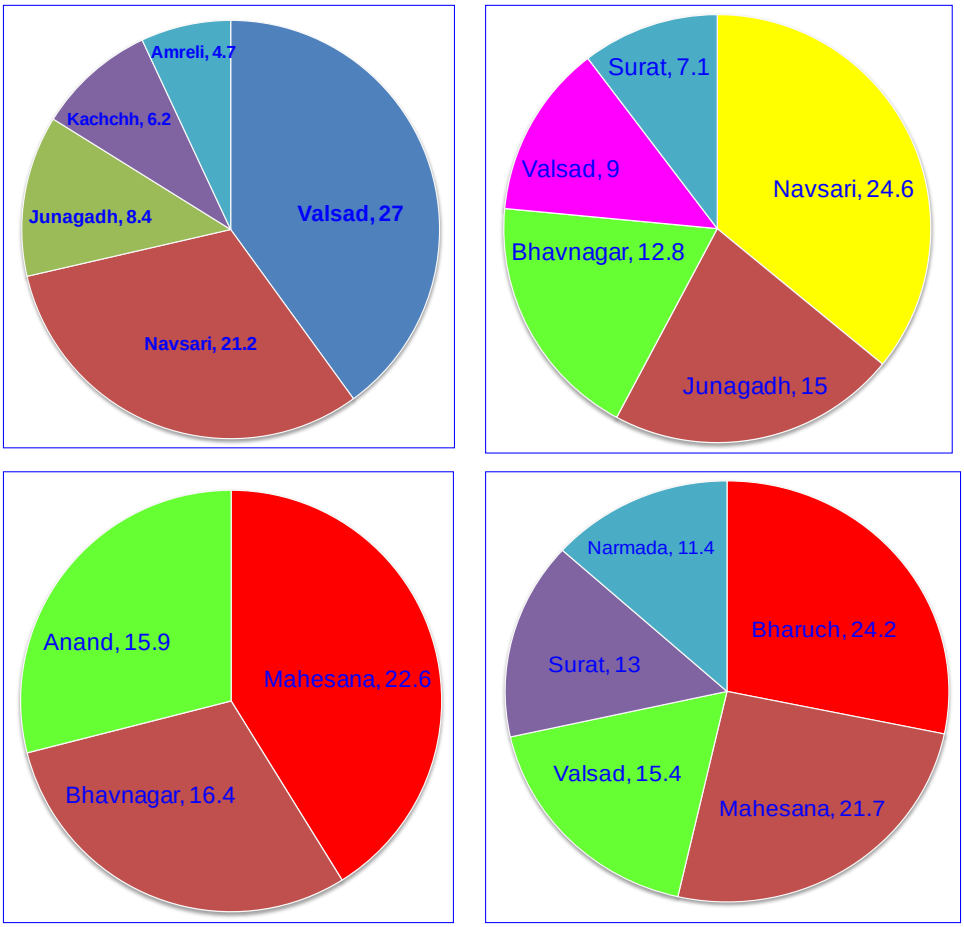

Figure 6: *Fruit crop-wise districts with major share of production (%) in Gujarat state (2012-13)*

A study for identification and mapping of apple and almond plantations was conducted in the Kumarsain tehsil of Shimla district using Indian remote sensing satellite (IRS-IB) LISS-II data. False Colour Composites (FCC) of October 27, March 30 and April 20, 1992 were visually analysed for mapping apple and almond plantations. The results indicated that IRS LISS-II data of month of April on 1:50,000 scale was found very useful for identification and mapping of apple and almond plantations in this region (Kimothi et al., 1997). Recognising importance of horticulture in promoting livelihood and employment opportunity and bringing prosperity to the state, the Govt. of India has extended National Horticulture Technology Mission Programme to Himachal Pradesh. The objective of Mission is to develop horticulture based farming system that is economically viable and ecologically sustainable using all the modern tools and techniques available. The space technology including remote sensing, Global Positioning System (GPS) and Geographical Information System (GIS) are the advanced tools that aid in gathering and updating information and develop scientific management plans. Updated and accurate database is pre-requisite for systematic planning of horticulture sector be it area expansion, increase in productivity or creating post-harvest handling facilities. With this aim, a study was carried out to generate block wise database on apple plantation in Shimla which is the largest apple growing district of Himachal Pradesh. Remote sensing data from the Indian Remote Sensing satellites like IRSP6 has been used along with other international sensors to generate apple orchard maps, orchard conditions in term of density, terrain parameters like elevation, slope, aspect etc. The GIS tools have been used to characterize the orchard distribution pattern in relation to terrain parameters (Sharma and Panigrahi, 2007).

The Haryana state has a rich diversity of horticultural crops due to the presence of diverse agro-climatic zones ranging from sub-tropical and semi-arid to sub-humid. A study was carried out in Adampur and Hisar-IInd development blocks of Hisar district using satellite data of World View-2 (March to Dec., 2011) and IRS-P6-LISS-III (Feb., 2011). The results of this study indicated that, total area under horticultural crops was 7, 865 hectares during 1966-67, which had increased to 45, 910 hectares by the end of 2010-11 of whole Haryana state. Citrus is the major crop of the study area followed by Guava, kinnu and anola. According to this investigation the total area under the horticulture fruit crops was 506.23 ha in Adampur block and 445.88 ha in Hisar-II block (Veena, 2014).

2. Objectives

The project on mapping of horticultural fruit crops in Gujarat State was carried out jointly by the Directorate of Agriculture, Govt of Gujarat and Bhaskaracharya Institute for Space Applications and Geo-informatics (BISAG), Govt of Gujarat. The major objectives of this were as follows:

i) Mapping of Horticultural fruit crops using high resolution Indian Remote Sensing Satellite (IRS) LISS-IV and CAROTSAT-1 digital data covering major fruit crops growing districts in Gujarat State;
ii) Mapping of fruit crops grown at plot-by-plot in each survey number on the cadastral maps;
iii) Preparation of village-level Horticultural Atlas of Gujarat State;
iv) District and Taluka-level area estimation under fruit crops.

3. Methodology

Remotely sensed images are a quick and inexpensive means to differentiate fruit trees or orchards from other land-uses. Geographic Information Systems (GIS) can also help in delineation of fruit crop orchard boundary, ground truth data collection, and preparation of other spatial data from the geo-referenced cadastral maps (Panda and Hoogenboom, 2009). Identification and discrimination of various vegetation types /land cover classes requires use of subtle differences in their spectral data and hence rely mostly on digital image processing techniques. As fruit crops have similar spectral characteristics to forested vegetation, supervised classification is not the best procedure to distinguish these crops even using high resolution Remote Sensing data. Therefore, in the present study geo-

referenced cadastral boundaries with survey numbers were superimposed on the high resolution IRS LISS-IV and CARTOSAT-1 digital data. The fruit crop plantations were delineated in each survey number based on planting pattern with canopy density observed on the CARTOSAT-1 digital data.

3.1. Horticultural Plantations Mapping Procedure

Mapping of horticultural plantations especially fruit crops in different districts using Indian Remote Sensing Satellite (IRS-P6) LISS-IV and CARTOSAT-1 digital data consisted of following procedural steps:

i) IRS LISS-IV and CARTOSAT data preparation and geo-referencing;
ii) Administrative (district/block/village) boundary superimposition;
iii) Geo-referencing of Cadastral maps with IRS LISS-IV and CARTOSAT-1 data;
iv) Superimposing GPS locations of various fruit crop sites collected during field visits on the geo-referenced Satellite and cadastral maps;
v) Identification & delineation of various fruit crops on the survey numbers of each cadastral map superimposed on CARTOSAT digital data;
vi) Generation of spatial information in GIS environment at the taluka and district-level;
vii) Generation of thematic maps showing fruit crops extent in each district;
viii) Quality checks and accuracy assessment based on Field data.

3.2. Study Area

The mapping of major fruit crops in Gujarat State was carried out in those districts where fruit crops are grown on large scale. The major fruit growing districts in Gujarat State consists of Junagadh, Amreli, Bhavanagar, Navsari, Valsad, Mehsana, Vadodara, Bharuch, Surat, Gandhinagar, Ahmedabad, Kheda, Anand district. Various fruit crops like Mango, Sapota (Chiku), Citrus, Banana, Ber, Coconut etc. are cultivated in these districts. The major fruit crop-wise districts and their contribution in total production of Gujarat state for some fruit crops is given in Figure 6.

3.3. Satellite Data Used

The high resolution data from Indian Remote Sensing Satellite (IRS-P6) LISS-IV and CARTOSAT-1 covering major districts in Gujarat State was acquired for mapping fruit crops. The details of IRS LISS-IV satellite data acquired for some of the districts are given in Table 1. The Cartosat-1 data with 2.5 m spatial resolution was also acquired for the all the fruit crops growing districts in Gujarat state.

***Table 1**: Indian Remote Sensing Satellite (IRS-P6) and CARTOSAT data used for village-level fruit crop plantations mapping in different Districts*

Sr. No.	District	Sensor	Path/Row	Date of Pass
1	Kachchh	LISS-IV	202/60	27-Apr-2009
2	Kachchh	LISS-IV	202/62	27-Apr-2009
3	Kachchh	LISS-IV	201/94	08-May-2007
4	Mahesana	LISS-IV	202/88	13-Apr-2009
5	Junagadh	LISS-IV	202/85	15-Mar-2009
6	Junagadh	LISS-IV	202/97	26-May-2009
7	Junagadh	LISS-IV	202/87	02-May-2009
8	Junagadh	LISS-IV	201/103	12-May-2008
9	Bhavnagar	LISS-IV	202/84	18-Apr-2009
10	Bhavnagar	LISS-IV	202/90	07-May-2009
11	Bhavnagar	LISS-IV	202/91	07-May-2009
12	Vadodara	LISS-IV	202/70	06-Mar-2008
13	Vadodara	LISS-IV	202/72	06-Mar-2008

14	Navsari	LISS-IV	202/67	23-Apr-2009
15	Navsari	LISS-IV	202/67	23-Apr-2009
16	Valsad	LISS-IV	202/67	23-Apr-2009
17	Valsad	LISS-IV	202/68	23-Apr-2009
18	Valsad	LISS-IV	202/69	23-Apr-2009

3.4. Collateral data

- Cadastral maps of major villages where fruit crops are grown on large scale were collected and digitized for superposing on the satellite digital data;
- Ground-Truth (GT) data of various fruit crops in selected villages was collected in each survey number where fruit crops are grown using the digitized village maps superposed on satellite digital data.

3.5. Geo-referencing and Transformation of Cadastral Map

Image rectification and geo-referencing involves the removal of random and systematic errors of image and transforming image to UTM coordinate system in WGS84 datum. IRS LISS-IV and CARTOSAT digital data was registered using Ground Control Points (GCPs) identified on image and Global Positioning System (GPS) measurements. For image rectification a large number of well distributed GCPs were identified in the image and their scan line – pixel coordinates were recorded. The GCPs identified on the image were accurately located on the ground and their Latitude-Longitude coordinates were recorded using the GPS. Using these GCPs and GPS measurements, second order polynomials with nearest neighbour (NN) resampling procedure, the georeferenced images were generated. Root Mean Square (RMS) errors of georeferencing were within ±0.5 to 0.75 pixels. The Cadastral maps of villages were superimposed over geo-referenced LISS-IV and CARTOSAT satellite images. The IRS LISS-IV geo-referenced images of two villages along with plot boundaries superposed from the cadastral maps are given in Figure 7 and CARTOSAT-1 image with plot boundaries superposed from the cadastral map is given in Figure 8.

Figure 7: *IRS LISS-IV image of Vanthali village with plot boundaries superimposed from cadastral maps*

3.6. Ground Truth (GT) data collection of fruit crop Plantations

Ground truth/field data collection is an important component in this project and an important source of information for verification and accuracy estimation / validation of thematic details mapped from satellite imagery. Initially a reconnaissance survey was carried out in each district where fruit crops are grown on large scale to identify fruit crops growing areas in each district and base maps were prepared for detailed ground truth data collection. The cadastral survey numbers were also superimposed on theses base maps for detailed and accurate identification of fruit crops. During detailed Ground truth data collection, hard copies of CARTOSAT-1 images with cadastral survey numbers along with Global Positioning System (GPS) were used for accurate marking of fruit crops on the high resolution CARTOSAT-1 data. This detailed Ground Truth (GT) information was used to prepare interpretation key for identification and delineation fruit crops in survey numbers of each village. The field photographs of various fruit crops grown in various villages along with GPS measurements were recorded to help in accurate mapping of fruit crops in various villages using CARTOSAT satellite images. Some of the field photographs of various fruit crops grown in different districts are given in Figure 9.

Figure 8: *CARTOSAT-1 image with plot boundaries superimposed from geo-referenced cadastral map*

4. Results and Discussion

4.1. Delineation and Mapping of Fruit Crop Plantations

In this study, the major trust was on identification and delineation of fruit crop plantations based visual interpretation rather than digital classification. The fruit crops in different districts of Gujarat State were identified on the high resolution IRS LISS-IV and CARTOSAT-1 data based on the planting pattern and tree-crown density. In this study an alternate method of mapping fruit crop plantations using high resolution, single-band CARTOSAT-1 panchromatic data on cadastral maps with survey numbers gave very good results for preparation village-level horticultural atlas of Gujarat State. Field survey in different villages was also carried out for accuracy assessment of survey numbers mapped as horticultural plantations. These fruit crop plantations were identified on CARTOSAT-1 data superimposed with cadastral map and survey numbers. The fruit crop plantations delineated using

CARTOSAT-1 data superimposed with cadastral map and survey numbers are given in Figures 10 and 11. These figures indicate those survey numbers only which have fruit crop plantations delineated on the CARTOSAT data along with cadastral boundaries.

Figure 9: *Field photos of major fruit crops: mango, banana papaya and coconut grown in different districts of Gujarat state*

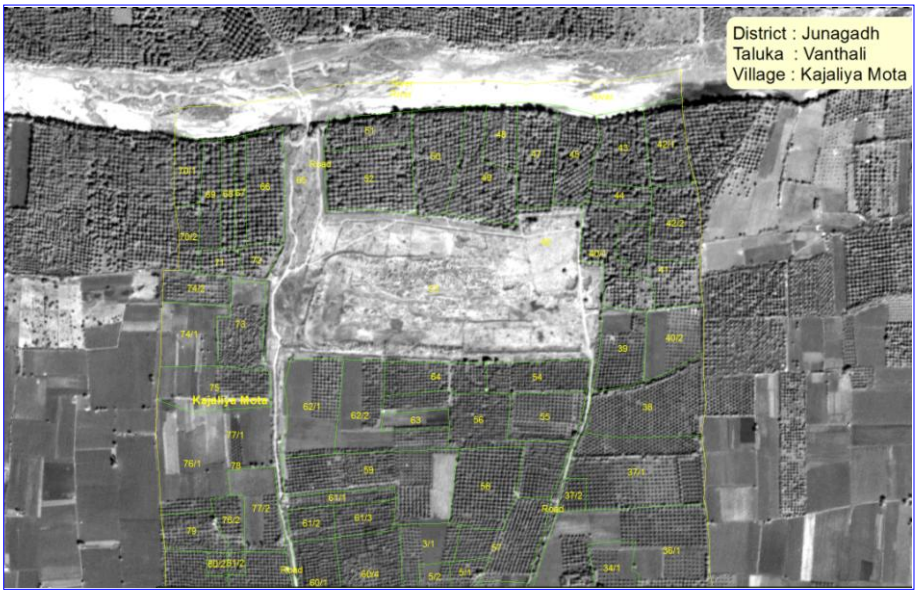

Figure 10: *CARTOSAT-1 image with survey numbers having fruit crop plantations in Vanthali Taluka*

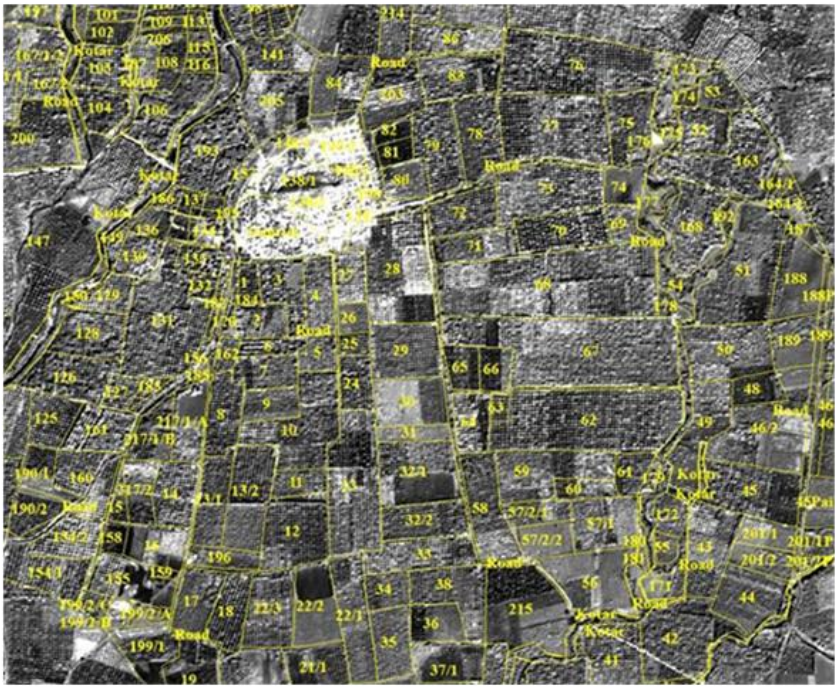

Figure 11: *CARTOSAT-1 image with survey numbers having fruit crop plantations in Talala Taluka*

4.2. Preparation of Taluka-level Horticultural Plantation Maps

The IRS-P6 LISS-IV and CARTSAT-1 satellite images covering different villages in each taluka having fruit crop plantations were analyzed for identification and delineation of fruit crop plantations. The cadastral maps were geo-referenced and superimposed on the satellite data along with survey numbers in each village. The survey numbers having fruit crop plantations were delineated on the CARTOSAT data. The fruit crop plantation maps of each village were complies at taluka level. The taluka-level fruit crop plantation maps showing the extent of fruit crop plantations along with village boundaries for Vanthali, Talala, Dhari and Pardi Talukas are given in Figures 12, 13, 14 and 15, respectively.

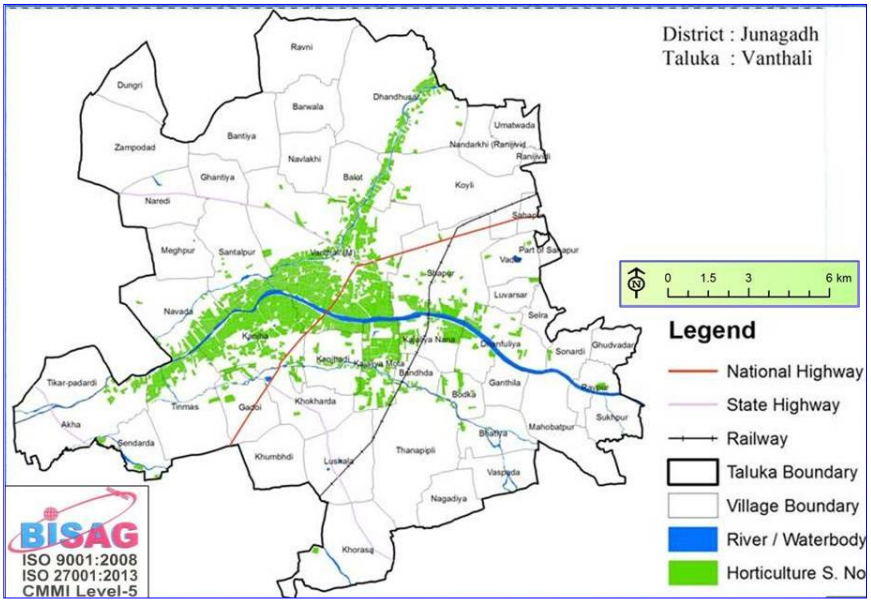

Figure 12: *Fruit crop plantations map of Vanthali Taluka, Junagadh district with village boundaries*

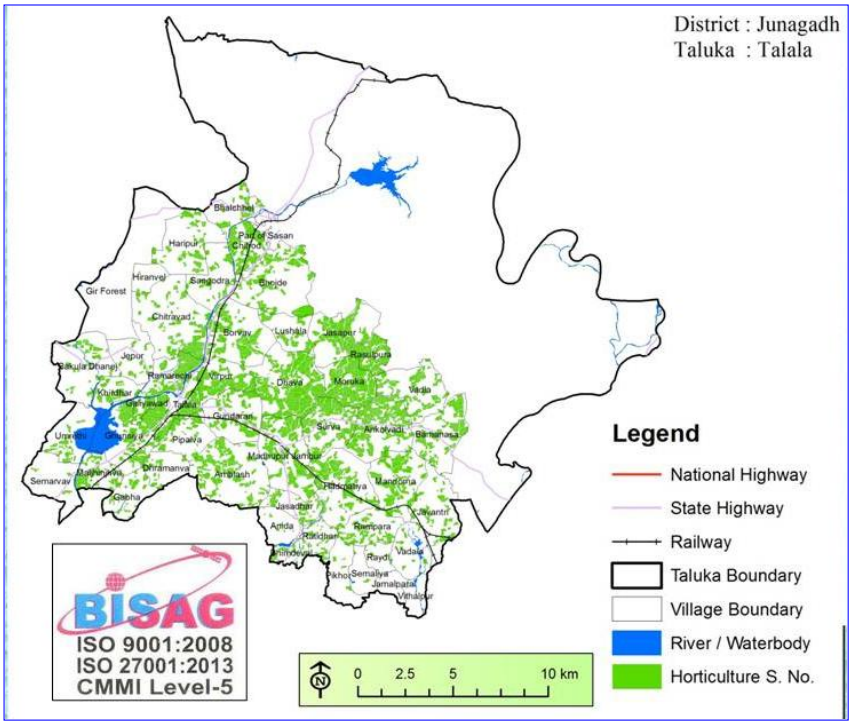

Figure 13: *Fruit crop plantations map of Talala Taluka, Junagadh district with village boundaries*

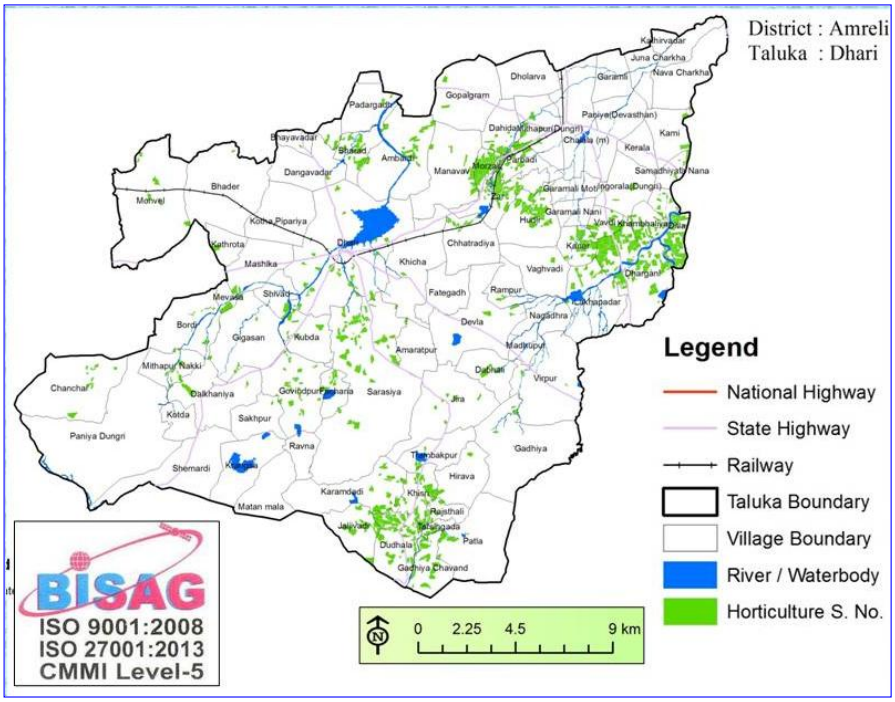

Figure 14: *Fruit crop plantations map of Dhari Taluka, Amreli district with village boundaries*

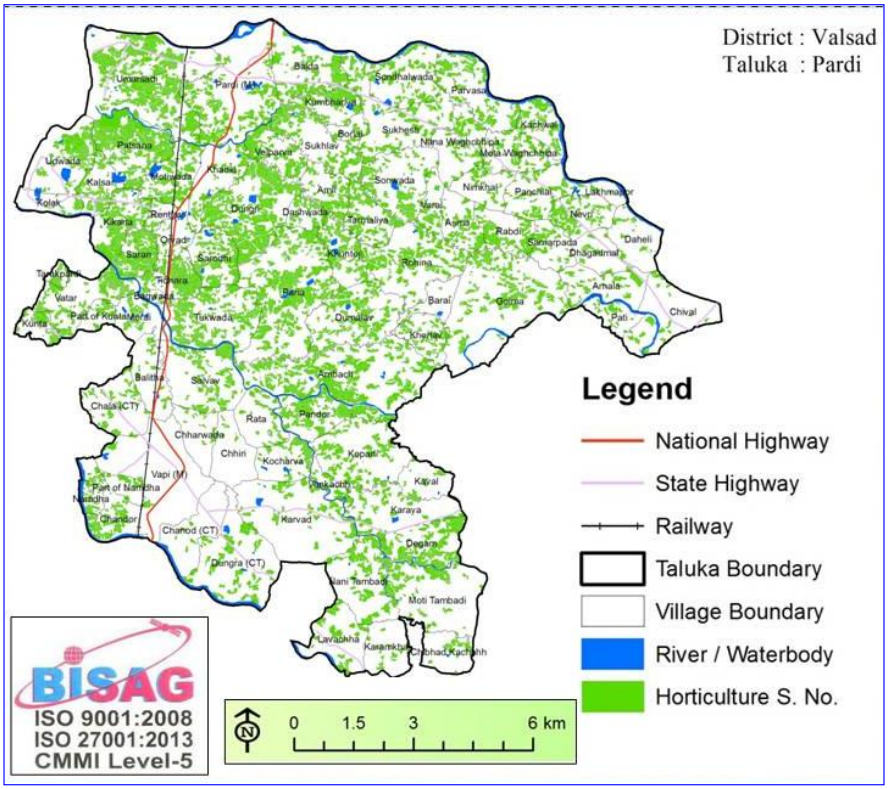

Figure 15: *Fruit crop plantations map of Pardi Taluka, Valsadi district with village boundaries*

4.3. Fruit Crops Plantations area compilation at taluka and district-level

The results of analysis of IRS-P6 LISS-IV and CARTSAT-1 satellite images covering different villages in each taluka having fruit crop plantations were compiled at village and taluka level. The results compiled at taluka-level were again compiled at district-level. The fruit crop plantations area estimates in Gujarat State are given in Table 2. This table indicates that, total area under fruit crops based on analysis of Indian Remote Sensing Satellite data is 177.74 thousand ha in Gujarat State. The major fruit crops growing top ten districts are: i) Valsad, ii) Junagadh, iii) Navasari, iv) Mahesana, v) Bhavnagar, vi) Amreli, vii) Kachchha, viii) Gandhinagar, ix) Vadodara and x) Anand (Figure 16).

4.3.1. *Preparation of Horticultural Atlas of Gujarat State*

The fruit crop plantations in different villages of each taluka were identified and delineated using IRS-P6 LISS-IV and CARTSAT satellite images. The cadastral maps were geo-referenced and superimposed on the satellite data along with survey numbers in each village. The survey numbers having fruit crop plantations were delineated on the CARTOSAT data. The fruit crop plantation maps of each village were compiled at taluka level. These village-level maps of each taluka were compiled in the form of Horticultural Atlas of Gujarat state.

Table 2: *District-wise Fruit Crops Area in Gujarat State based on satellite Data*

District-wise Fruit Crops Area: Gujarat State		
Sr.No.	District	Area (000' ha)
1	AHMEDABAD	2.851
2	AMRELI	8.179
3	ANAND	4.464
4	BANASKANTHA	1.461
5	BHARUCH	0.737
6	BHAVNAGAR	14.827
7	DOHAD	0.575
8	GANDHINAGAR	6.823
9	JAMNAGAR	0.496
10	JUNAGADH	35.118
11	KACHCHH	6.972
12	KHEDA	1.978
13	MAHESANA	18.726
14	NARMADA	0.250
15	NAVSARI	21.730
16	PANCHMAHA	0.730
17	PATAN	0.943
18	PORBANDAR	0.549
19	RAJKOT	0.908
20	SABARKANTHA	2.867
21	SABARKANTHA	2.643
22	SURENDRANAGAR	2.756
23	TAPI	0.553
24	VADODARA	5.016
25	VALSAD	35.592
	Total	177.743

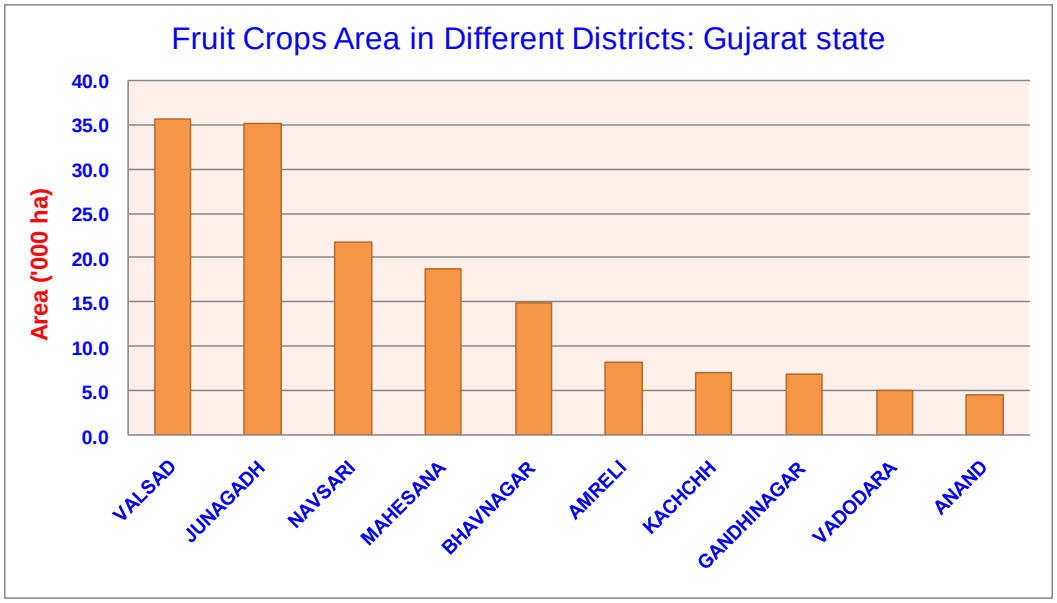

Figure 16: *District-wise fruit crop plantations area in Gujarat State based on IRS satellite data*

Acknowledgements

The authors like to express their sincere thanks to Shri T.P. Singh, Director, Bhaskarcharya Institute for Space Applications and Geo-informatics (BISAG), Department of Science & Technology, Government of Gujarat, Gandhinagar-382007, for fruitful discussions, suggestions and continuous guidance in carrying out this study. We are also thankful to the Department of Horticulture, Govt. of Gujarat for their kind cooperation.

References

Anonymous (2012). State of Indian Agriculture Statistic 2011, 2012. Ministry of Agriculture and Cooperation.

Hemla Naik, & Thippesh, D. (2014). Fundamentals of Horticulture and Production Technology of Fruit Crops. e-content, College of Agriculture, University of Agricultural and Horticultural Sciences, Shimoga.

Horticulture in Gujarat, 2011-12 & 2012-13, Directorate of Economics and Statistics, Government of Gujarat, Gandhinagar.

Hand Book on Horticulture Statistics 2014, Government of India, Ministry of Agriculture, Department of Agriculture and Cooperation, New Delhi.

Kimothi, M.M., Kalubarme, M.H., Dutta Sujay, Thapa Rajendra & Sood, R.K. (1997). Remote sensing of horticultural plantations in Kumarsain tehsil in Shimla district, Himachal Pradesh. *Journal of the Indian Society of Remote Sensing,* 25(1), 19-26.

Lobell, D.B., Ortiz-Monasterio, J.I., Asner, G.P., Naylor, R.L., & Falcon, W.P. (2005). Combining field surveys, remote sensing, and regression trees to understand yield variations in an irrigated wheat landscape. *Agron. J*., 97, 241-249.

Mamta Saxena. Indian Horticulture Database – 2014. Ministry of Agriculture, Government of India 85, Institutional Area, Sector-18, Gurgaon.

Netherlands Enterprise Agency, 2015. Horticulture Sector in Gujarat State – India. September 2015. 17.3.

Panda, S.S., Hoogenboom, G., & Paz, J. (2009). Distinguishing blueberry bushes from mixed vegetation land-use using high resolution satellite imagery and geospatial techniques. *Comput. Electron. Agr.*, 67, 51-59.

Parihar, J.S., Panigrahy, S., & Singh, Ashvir, (2002). Remote Sensing and GIS as a Tool for Precision. *Farming in Horticulture Sector in India*. 35-37.

Sharma, Alka & Panigrahi, S., (2007). Apple Orchard Characterization using Remote Sensing & GIS in Kullu District of Himachal Pradesh.
Retrieved from http://a-a-r-s.org/aars/proceeding/ACRS2007/Papers/TS23.6.pdf

Veena (2014). Horticulture Fruit Crops Mapping of Adampur and Hisar- IInd Blocks of Hisar District Using Geoinformatics Techniques. *International Journal of Science and Research*, 3(8), 1855-1859.

Cloud Publications
International Journal of Advanced Remote Sensing and GIS
2017, Volume 6, Issue 1, pp. 2097-2102
ISSN 2320 – 0243, Crossref: 10.23953/cloud.ijarsg.113

Research Article | Open Access

Urban Expansion and Loss of Agricultural Land: A Remote Sensing Based Study of Shirpur City, Maharashtra

Yogesh Mahajan[1], Shrikant Mahajan[2], Bharat Patil[3], Sanjay Kumar Patil[1]

[1]School of Environmental & Earth Sciences, North Maharashtra University, Jalgaon, Maharashtra, India
[2]Department of Geography, Shri D.H. Agrawal Arts, Commerce and College, Navapur, Maharashtra, India
[3]Department of Geography, R.C. Patel Arts, Commerce and College, Shirpur, Maharashtra, India

Publication Date: 8 April 2017

DOI: https://doi.org/10.23953/cloud.ijarsg.113

Abstract In present urban expansion is important field of geographic study. This is an attempt to study the urban expansion and land use pattern of Shirpur city of Dhule district (MS). For that purpose used land landsat images (1991, 2001 and 2011) of Shirpur city. These satellite images further processed and analyzed by GIS software. Shirpur city lies in Shirpur tehsil and administrative head quarter of tehsil. Total population of Shirpur city was 44246 in 1991 that increase up to 76905 in 2011. The total area of Shirpur city is 1113.36 hectares out of that 459.64 hectares area under built up in 1991 that increase 760.16 hectares in 2011. This expansion of city area responsible for loss of agricultural land there were 540.33 hectares in 1991 that has been decline 298.72 hectares in 2011. Finely it is concluded that the growing population and its increasing demands of land for non-agricultural activities responsible for turn agricultural land for built up area, industrial plants, roads and plotting for future growth of city.
Keywords *urban expansion; landsat images; population growth; agriculture*

1. Introduction

Today expansion of urban centers and their impacts are important study matter of urban geography. This is an attempt to study the urban expansion and changes in land use pattern of Shirpur city and their fringe area in Dhule district (MS). Over the world, the cities cover only about one percent of the earth's surface, but most of the issues happening in the cities greatly impact on the environment and global change [5]. Urbanization leads to urban spatial expansion due to the demand for development and housing growth, as well as facilities areas to serve human life of increasing population [8]. Land transformation is one of the most important fields of human geography. Increasing population size of urban centres demands land for non-agricultural activities like built up area, roads, market, shopping malls and industries etc. hence agricultural land decrease surround to the cities [2 and 4]. Bayo [3] illustrated the relationship between urban expansion and transportation cost, traffic, and the populations and their food requirements.

2. Study Area

Shirpur town is administrative headquarter of Shirpur tehsil (Dhule district, Maharashtra). It is situated at $21^0$21' 02'' North latitude and $74^0$53' 07'' East longitude (Toposheet No. 46 K/15) with an altitude of 159 meters from mean sea level. Shirpur is located on right bank of the Arunavati River (Figure 1) and Bombay-Agra highway.

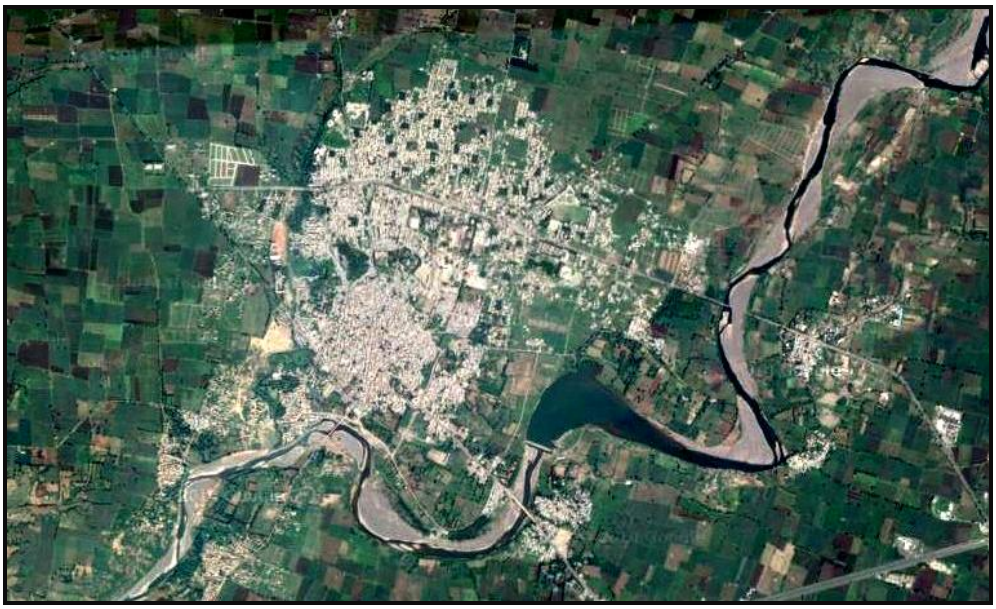

Figure 1: *Shirpur Town in Shirpur Tehsil*
(Source: Google map)

It is single urban centre of Shirpur tehsil hence the population of surrounding villages also depends on it for goods and administrative services. Hence surrounding population migrates towards Shirpur town for the purpose of better life style, medical facilities, education facilities, pleasure etc. That immigrants population and natural growth population has been of responsible for expansion of city. Shirpur is agriculturally well developed hence several agro based industries are setup at Shirpur like Textile mills and Oil refinery. Gold refinery and Steel Factory also help in economic growth of Shirpur town.

3. Database and Methodology

The present study is based on secondary source of data. The secondary data is the available from municipal corporation Shirpur, district statistics office Dhule, Census hand book, agricultural census etc. The methods applied includes bar diagram, pie chart, Graphs, Maps, Statistical analysis etc. Urban expansion of Shirpur town studied with help of decadal land sat images. These land sat images of 1991, 2001 and 2011 processed with the help of ERDAS Imagine software and GIS software.

3.1. Data Collection

Land satellite data of three dates of august month used for the study of general land use pattern in 1991, 2001 and 2011. Because in month of august land use and land cover is nearly everyone clear and proper. Land sat data of the past three decades has been downloaded from USGS Earth Explorer website. All the data are pre-processed and projected to the Universal Transverse Mercator (UTM) projection system. The details of collected satellite data are shown in the Table 1.

Table 1: *Details of Landsat Data Collected from USGS*

Sr. No	Landsat Image		Landsat Band			Date of Image
	Path	Row				
1	147	45	4	3	2	16th August 1991
2	147	46	4	3	2	16th August 1991
3	147	45	4	3	2	8th August 2001
4	147	46	4	3	2	8th August 2001
5	147	45	4	3	2	24th August 2011
6	147	46	4	3	2	24th August 2011

Source: USGS Earth Explorer website

The present study involves the collection of Toposheets from Survey of India and Shirpur city map from relevant authorities. Processing the imagery and image interpretation for development of Land use and Land cover maps is to be done in ERDAS Imagine software. The obtained maps are studied and analysed to detect the change in general land use pattern.

3.2. Data Processing and Classification

All the downloaded images contain different types of bands and stacking get the composite image create mosaic of landsat images using ERDAS image software. Selects Mosaic Landsat digital image data for classify each land cover class in the digital image. Generate sample land cover classes are called “training sites”. The ERDAS image classification software uses the training sites to identify the land cover classes in the entire image.

The classification of land cover is based on the spectral signature defined in the training set. The ERDAS digital image classification software determines each class on what it resembles most in the training set. In this study use supervised classification algorithms are maximum likelihood and minimum-distance classification [1]. The landsat images are classified by supervised classification through the steps select training areas generate signature file and classify. The classification finally gives the land use/cover image of the area on which analysis. Five land cover classes namely cultivable area, forest area, water bodies, built up area and barren land.

3.3. Population Changes and Urban Expansion

Explosion of population and immigrants in urban centers is mainly responsible for Urbanization or urban expansion. The term urbanization as traditionally measured by demographers is urban population divided by total population of a region [7]. The total population of Shirpur was 44246 in 1991 that increased 76905 in 2011. There are 40235 Males and 36670 females in Shirpur. There were 7532 houses in Shirpur town in 1991; these are increased up to 15187 in 2011. It means number of houses becomes double in last two decades (1991 to 2011). House hold size is decreased by 0.81 from 5.87 in 1991 to 5.06 in 2011. The population density of this town is 6910 persons per sq.km. in 2011 that was 3975 in 1991. The population density of Shirpur town is too much high than average density of Shirpur tehsil (179) and Dhule District (254).

Table 2: *Shirpur Town: Population Changes (1991-2011)*

Sr. No.	Particulars	Year			Changes in (1991-2011)
		1991	2001	2011	
1	Total Population	44246	61994	76905	32659
2	Total Houses	7532	11003	15187	7655
3	Household Size	5.87	5.63	5.06	-0.81
4	Population Density	3975	5570	6910	2935
5	Population Growth Rate	21.64	40.11	24.05	3.59
6	Literacy Rate	58.09	68.78	74.9	16.81
7	Sex Ratio	933	920	911	-22

Source: Census of India-2011 and compiled by the Researcher

According to Table 2 population growth rate has been continuously increased in Shirpur town due to immigrants from surrounding villages and natural growth of population. Growth in urban population goes with no equivalent growth in land supply [6]. 40.11% population growth rate noted in 1991 to 2001 but in last decade that observed 24.05%. The literacy rate also increase during last two decades from 58.09 to 74.90. The sex ratio of Shirpur town decreased from 933 in 1991 to 911 in 2011. Shirpur Town exerts very high population pressure on agriculture land that responsible for brought significant changes in agriculture.

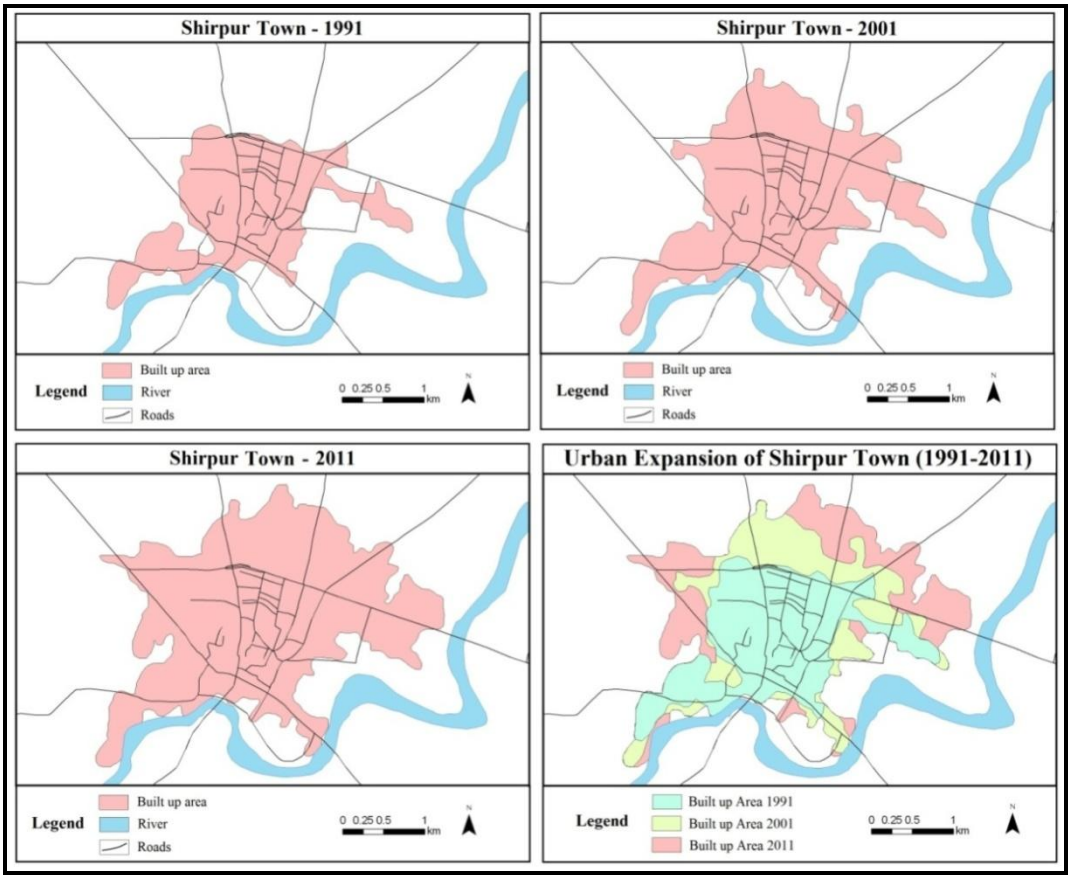

Figure 2: *Urban Expansion of Shirpur Town (1991-2011)*

(Source: Computed by the Researcher)

Table 3: *Land use Changes and Loss of Agricultural Land*

Sr. No.	Land Use		Year			Changes (1991-2011)
			1991	2001	2011	
1	Net Sown Area	in ha	531	465.22	291.84	-239.16
		in %	47.69	41.79	26.21	-21.48
2	Land not available for Cultivation	in ha	459.64	549.87	760.16	300.52
		in %	41.28	49.39	68.28	26.99
3	Other uncultivable land	in ha	91.25	68.77	32.34	-58.91
		in %	8.20	6.18	2.90	-5.30
4	Fallow land	in ha	9.33	7.36	6.88	-2.45
		in %	0.84	0.66	0.62	-0.22
5	Forest	in ha	22.14	22.14	22.14	0.00
		in %	1.99	1.99	1.99	0.00
6	Total Geographical Area	in ha	1113.36	1113.36	1113.36	0.00
		in %	100.00	100.00	100.00	0.00

Source: Revenue Record Office Shirpur and Computed by the Researcher

Shirpur city mostly expand towards North East and North West along with Shahada road (Figure 2) because of plane region, easily availability of water, being there all education institutes etc. Other hand towards south due to presence of Arunavati River, city has restrictions for expansion. Because of expansion of Shirpur city towards fringe area net shown area has been deduct by 21.48% from 531 hectare to 291.84 hectare. Now only 26.21% area under net shown (Table No. 3 and Figure No. 3).

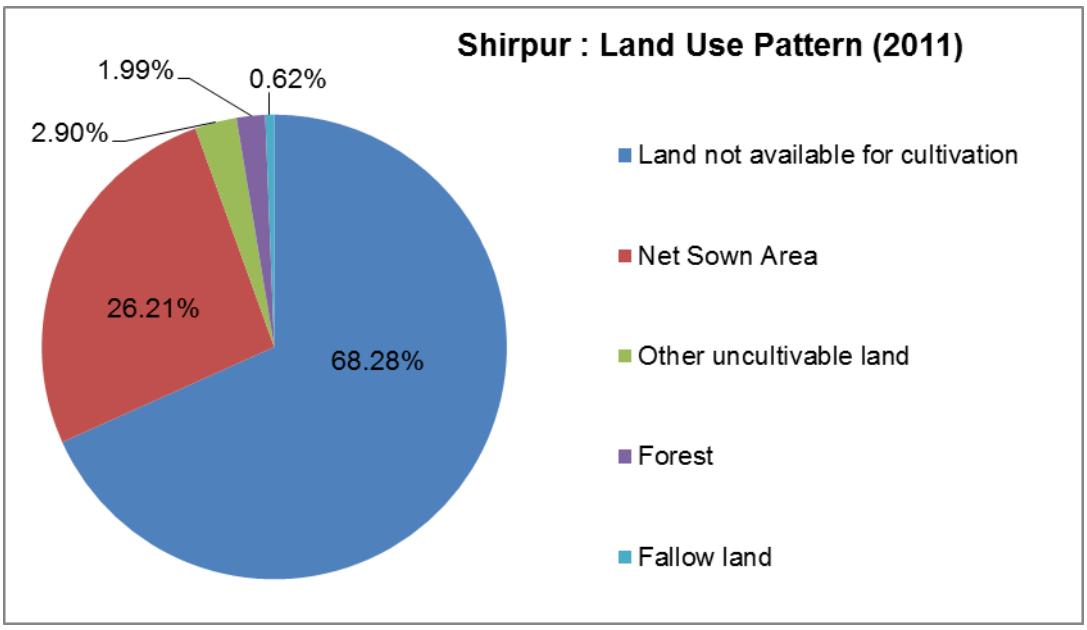

Figure 3: *Shirpur: Land Use Pattern (2011)*

(Source: Computed by the Researcher)

4. Conclusion

The research results showed that population explosion was the main cause of urban expansion. Shirpur City is the biggest industrial and commercial centre of Shirpur tehsil. The high economic growth, education facilities and employment opportunities caused influx of labour immigration.

According to demographic survey of 11 Oct. 2010, Shirpur City had 14 thousand immigrants in the population total of 76905. Local increase of population plus immigrants made the city become too stuffy. According to statistics, the urban population has increased 73.81% from 1991 to 2011.

The population density in 2011 reported 6910 people per square kilometres. In last two decades number of houses also became double in Shirpur town from 7532 in 1991 to 15182 in 2011. Due to housing demand and city development, agriculture land was transformed into land for houses, roads, industrial and commercial areas.

References

[1] Dam Trung Phuong: *Urban in Vietnam.* Construction Publishing House, Hanoi (in Vietnamese). (1995)

[2] Songsore, Jacob: Towards building a model of urban growth dynamics: the case of 'Large' Northern Ghanaian Towns. Universitas Legon. 6, 114-127 (1977)

[3] Bayo A.O.: City Planning, city growth and food security; the inevitable trinity in the Nigerian food equation. Agricultural Journal 1, 133-118 (2006)

[4] Mishra, V.: Population growth and intensification of land use in India. International Journal of Population Geography 8, 365-383 (2002)

[5] Vellinga, P., Herb, N.: Industrial transformation, science plan, IHDP. Report No. 12. Bonn, The international human dimensions program on global environmental change (1999)

[6] Olima Washington, H.A.: Urbanisation and housing challenges. Cities in Africa Conference. Rapporteur's Report (2003)

[7] Glenn, A.: Urbanization of the Non-Farm Population. A research note on the convergence of rich and poor nations. Koninkhjke Brill NV. Leiden (1984)

[8] Alkheder, S., Shan, J.: Urban growth simulation using remote sensing imagery and neural networks. In third international symposium remote sensing and data fusion over urban areas and the 5th international symposium on remote sensing of urban areas, March 14-16 (2005) Tempe, Arizona.

Cloud Publications
International Journal of Advanced Remote Sensing and GIS
2017, Volume 6, Issue 1, pp. 2088-2096
ISSN 2320 – 0243, Crossref: 10.23953/cloud.ijarsg.112

Research Article | Open Access

Estimation of the Relationship between Urban Vegetation and Land Surface Temperature of Calicut City and Suburbs, Kerala, India using GIS and Remote Sensing data

Chaithanya, V.V.[1], Binoy, B.V.[2], Vinod, T.R.[2]

[1]Department of Environmental Studies, Kannur University, Kannur, Kerala, India
[2]Center for Environment and Development, Thiruvananthapuram, Kerala, India

Publication Date: 8 April 2017

DOI: https://doi.org/10.23953/cloud.ijarsg.112

Abstract Land surface temperature was the most important determining factor for the analysis of urban heat island. The Vegetation content in urban areas has a great influence on the temperature variation of those areas. Satellite remote sensing is very much helpful in the analysis of urban heat islands by using Land Surface Temperature. By analyzing the Landuse, Temperature and NDVI from satellite images the temperature and the variations was studied. Landsat 7 images are used in the calculation of Temperature, NDVI and Landuse. Land surface temperature of Calicut Corporation was estimated by using Mono Window Algorithm from land sat 7 ETM images. Landsat images for the years 2003, 2008 and 2015 were down loaded from the USGS earth explorer web site. Temperature band or band 6 was used for the land surface temperature estimation. NDVI was derived from the band 3 and band 4 using the ERDAS imagine for the year 2003, 2008 and 2015. Supervised classification was done to classify the images in different land use categories like vegetation, built up and water bodies. From the temperature map a gradual increase in land surface temperature was noticed from 2003 to 2015. This is due to the decrease in urban vegetation as observed in the landuse. A negative correlation was obtained by correlating the NDVI with the temperature. The landuse changes between these three years are analyzed. The vegetated area was reduced in the year 2015 because of increasing the built up areas.
Keywords *NDVI; LST; LULC; Brightness Temperature; Thermal Band*

1. Introduction

Population growth, widespread industrialization and migration of rural population to urban areas lead to urban population growth, and expanding the urban sprawls. Urban growth and sprawl is a global phenomenon and have significant influence on the biophysical environment leading to severe ecological and environmental problems. Rapid and unplanned urbanization will change the land use/ land cover (LULC) of the area, especially reduction in vegetation cover which in turn increased the built-up areas. A major implication of urbanization is increase of land surface temperature (LST), mainly by heat discharge due to increased energy consumption, increased built-up surfaces having high heat capacities and conductivities, and decrease in vegetation cover. Vegetation cover usually

provide shade which helps lower surface temperature and also reduces air temperature through the process of evapotranspiration, in which plants release water to the surrounding air, dissipating ambient heat. The relationship between LST and urban vegetation cover has been extensively documented.

In the past, there were many studies focusing on the relationship between urban vegetation and LST (Weng et al., 2004). The advent of Geographical Information System (GIS) and satellite remote sensing technology has made it possible to study LST and urban vegetation remotely as well as in any scale from local to global. Satellite remote sensing provides an excellent cost-effective and time-saving methodology to analyze spatially and temporally distributed LST, since the coverage of satellite imagery extends over a large area (Senanayake et al., 2013). Several studies used the Landsat ETM+ imagery to develop LULC maps as well as for deriving the surface temperature. Numerous studies had been made to examine the effect of the vegetation on the LST, which showed that there was negative correlation between LST and urban vegetation abundance measured by Normal Difference Vegetation Index (NDVI) and the percent cover of urban vegetation (Weng et al., 2004; Chen et al., 2006; Mallik et al., 2008; Sundara Kumar et al., 2012).

However, in India studies focusing on the relationship between urban vegetation and LST using Landsat ETM+ imagery is rather limited. Hence through this study we examined the relationship between urban vegetation and LST of Calicut city, Kerala, India using Landsat ETM+ imagery. Specific objectives of this study were: i) to derive LST and to analyze their spatial variations using Landsat ETM+ thermal measurements; ii) to estimate urban vegetation abundance, Normalized Difference Vegetation Index (NDVI); and iii) to investigate the relationship between LST and NDVI.

2. Methodology

2.1. Study Area

The study was carried out in the Calicut city and suburbs (75°44’30”- 75°52’30” E, 11°12’- 11°19’ N), which is an important social-economic centre of Malabar region of Kerala, located in the coast of Southwest India. The climate of the city is humid tropical along with abundant rainfall, both from the south-west monsoon and north-east monsoon. Temperatures tend to remain constant with maximum values of between 30°C and 36°C, while the minimum between 22°C and 23°C. The average total annual rainfall was 3130 mm and the Relative humidity is around 79.3%. The extent of the study area is 207 km^2 (Figure 1) with a population of 4,32,097 people (Census, 2011) and the city is selected due to rapid urban development activities over the last two decades and heterogeneous LULC.

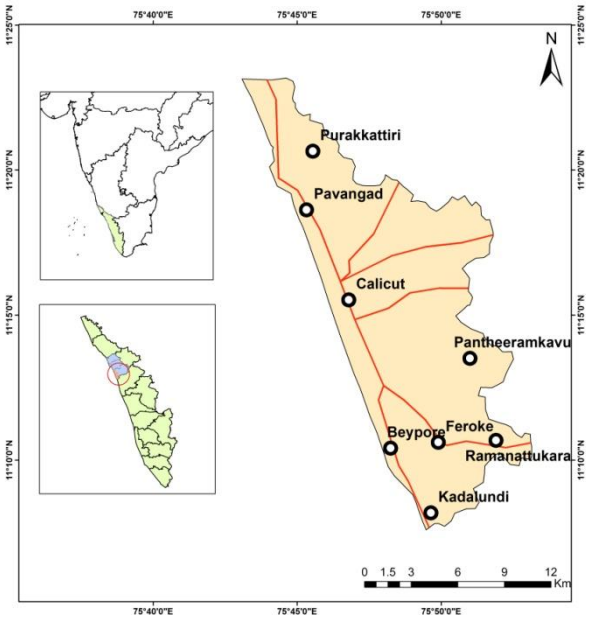

Figure 1: *A map of the study area*

2.2. Methods

Various stages involved in this study were i) satellite image acquisition and processing; ii) generation of land use/ land cover (LULC) map; iii) land surface temperature (LST) retrieval; iv) normalized difference vegetation index (NDVI) assessment; and vi) determination of the relationship between NDVI and LST. The conceptual flow of the applied methodology of this study is shown in Figure 2.

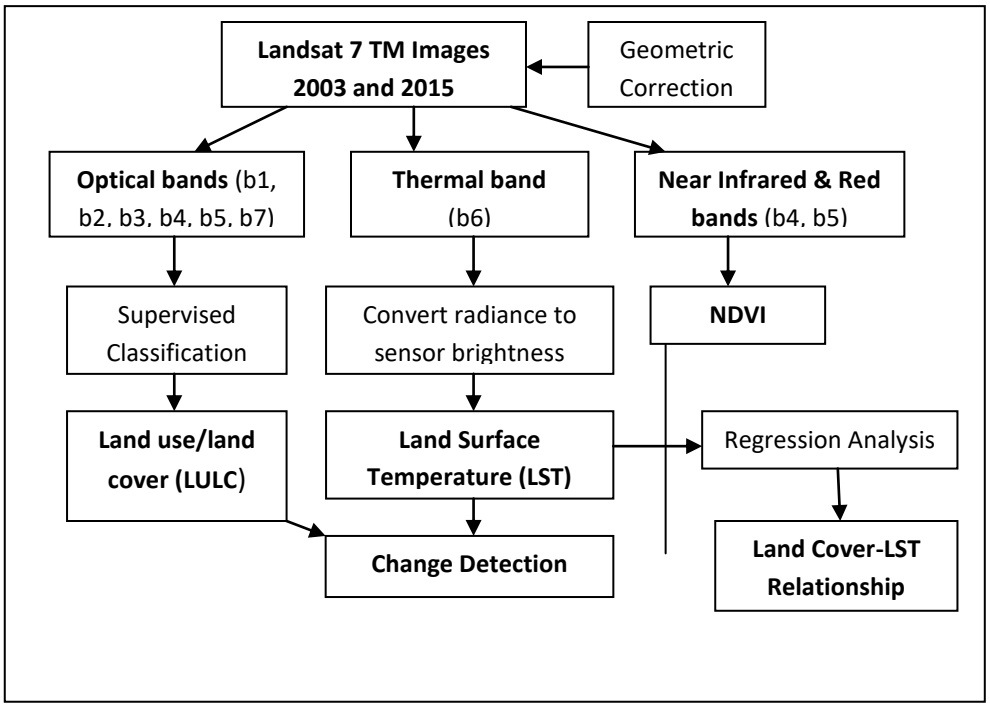

Figure 2: *Conceptual flow chart of the applied methodology*

2.2.1. *Satellite image acquisition and pre-processing*

Landsat 7 Enhanced Thematic Mapper Plus (ETM+) image (Row/Path: 145/52) of January 2003 and 2015 were used in this study (Table 1). These imageries were downloaded from USGS website. Using the ERDAS imagine digital image processing software, the multi-temporal images were co-registered to Universal Transverse Mercator Coordinate System (UTM 43 N / WGS84). Landsat 7 TM, ETM images bands 1-5 and 7 have a spatial resolution of 30 m, and the thermal infrared band (band 6) has a spatial resolution of 60 m. The images were further resampled using the nearest neighbor algorithm with a pixel size of 30 by 30 m for all bands including the thermal band. The resultant root mean square error (RMSE) was found to be less than 0.5 pixels. A subset function was used to limit the scene to the study area.

Table 1: *Details of Landsat data collected*

Date of image	Satellite/sensor	Reference system/ Path/ Row
11/01/2003	Landsat-7/ ETM+	WRS-II/145/52
15/01/2015	Landsat-7/ ETM+	WRS-II/145/52

2.2.2. *Generation of land use/land cover maps*

A supervised classification was carried out in ERDAS imagine 2013 using the maximum likelihood method; three land cover classes were identified including vegetation, water bodies and built up areas. The classified images were converted to shape files and imported to ESRI ArcGIS 10.2 feature class in a geographic database. The areas of the urban class were calculated from each feature class.

2.2.3. *Land surface temperature (LST) retrieval*

Land surface temperatures (LST) were derived from geometrically corrected Landsat ETM+ thermal infrared (TIR) band (band 6) images. The raw digital numbers (DNs) were converted to spectral radiances (L_λ) by using the following equation;

$$L_\lambda = L_{min} + (L_{max} - L_{min}) * DN/255$$

where, L_λ = Spectral radiance; $L_{min} = 3.200$ (spectral radiance of DN value 1); $L_{max} = 12.650$ (Spectral radiance of DN value 255); DN = Digital Number

The next step is to convert the spectral radiance to satellite brightness temperature (i.e., blackbody temperature, TB) under the assumption of uniform emissivity (Landsat Project Science Office, 2002). The conversion formula is;

$$T_B = \frac{K_2}{\ln\left(\frac{K_1}{L_\lambda} + 1\right)}$$

where T_B is effective at-satellite temperature in K, L_λ is spectral radiance in W/m^2 ster µm; and K_2 and K_1 are pre-launch calibration constants ($K_2 = 1282.71$ K, and $K_1 = 666.09$ mW $cm^{-2}sr^{-1}\mu m^{-11}$). The temperature is then converted from Kelvin to Celsius.

2.2.4. *Normalized difference vegetation index (NDVI) assessment*

Differentiation between vegetated and non-vegetated areas was made according to the normalized difference vegetation index (NDVI) values, which were computed from visible $(0.63 - 0.69)^{\mu m}$ and near-infrared $(0.76 - 0.90)^{\mu m}$ bands of the ETM+ images based on the following equation;

$$NDVI = \frac{R_{NIR} - R_{red}}{R_{NIR} + R_{red}}$$

where, R_{NIR} and R_{red} are the spectral reflectance in the TM and ETM+ red and near-infrared bands. The NDVI algorithm subtracts the red reflectance values from the near-infrared and divides it by the sum of near-infrared and red bands.

2.2.5. *Relationship between LST and NDVI*

To obtain the relationship between LST and NDVI, 49 sample points were measured within the study area. Regression analysis was carried out to determine the correlation between these two parameters. The regression equation models are retrieved by fitting the trend line using Microsoft Excel.

3. Results and Discussion

Results and analysis of this study is divided into four phases of outputs. The first output is the land use/land cover change for the year 2003 and 2015. The second output is a LST map of study area in 2003 and 2015. The third output is NDVI assessment for the year 2003 and 2015. The fourth output is correlation plotted onto vegetation indices with respect to LST.

3.1. Land use/ land cover changes

The Landsat TM image was classified into three classes using supervised classification in ERDAS Imagine 2013. As the aim of this study is to correlate the temperature distribution and vegetation cover, only three classes were derived: built-up areas, vegetation and water bodies. The land use/ land cover changes for the year 2003 and 2015 of the Calicut City and suburbs are significantly detected and presented in Figure 3a & b. The total acreage of the study area is 207 km^2. The detail acreage of the individual land cover of the study area is listed in Table 2. Over the period of 12 years, the total area for the vegetation category and water bodies decreased by 3.95% and 0.29% respectively and the built-up areas have expanded dramatically by 4.25%.

Table 2: *Land use / land cover changes as detected from LANDSAT multi-temporal images*

Land Use/ Land Cover Class	Area in km^2				
	2003	Percentage	2015	Percentage	Changes (%)
Vegetation	125.82	60.80	117.64	56.85	-3.95
Water body	10.31	4.98	9.70	4.69	-0.29
Built-up	70.82	34.22	79.61	38.47	+4.25
Total	206.95	100.00	206.95	100.00	

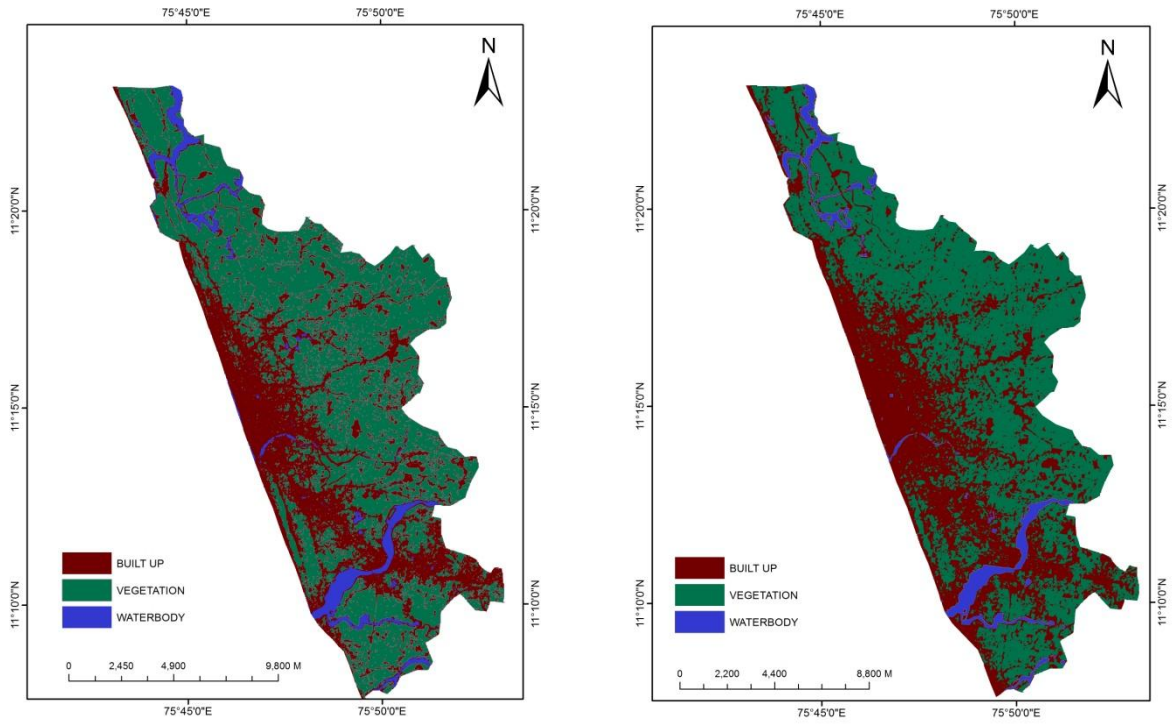

(a) (b)

Figure 3: *(a) Land use/ land cover map of 2003; (b) Land use/ land cover map of 2015*

3.2. Land surface temperature (LST)

From brightness temperature (TB) and Emissivity images the final Land Surface Temperature image was obtained by developing a temperature model in ArcGIS 10.2. The LST distributions of 2003 and 2015 are shown in the Figure 4a & b. The lowest and highest radiant temperature for 2003 were 18.2°C (in the high density vegetative area) and 30.7°C (in the built-up area) respectively. Meanwhile, for 2015 the radiant temperatures range between 24.9°C and 36.5°C. The highest temperatures were recorded within the built-up areas while the lowest was within vegetative areas. The implication of urban development especially in the coastal areas if Calicut city by replacing vegetative areas to built-up surfaces such as concrete, stone, metal and asphalt clearly increased the surface radiant temperature.

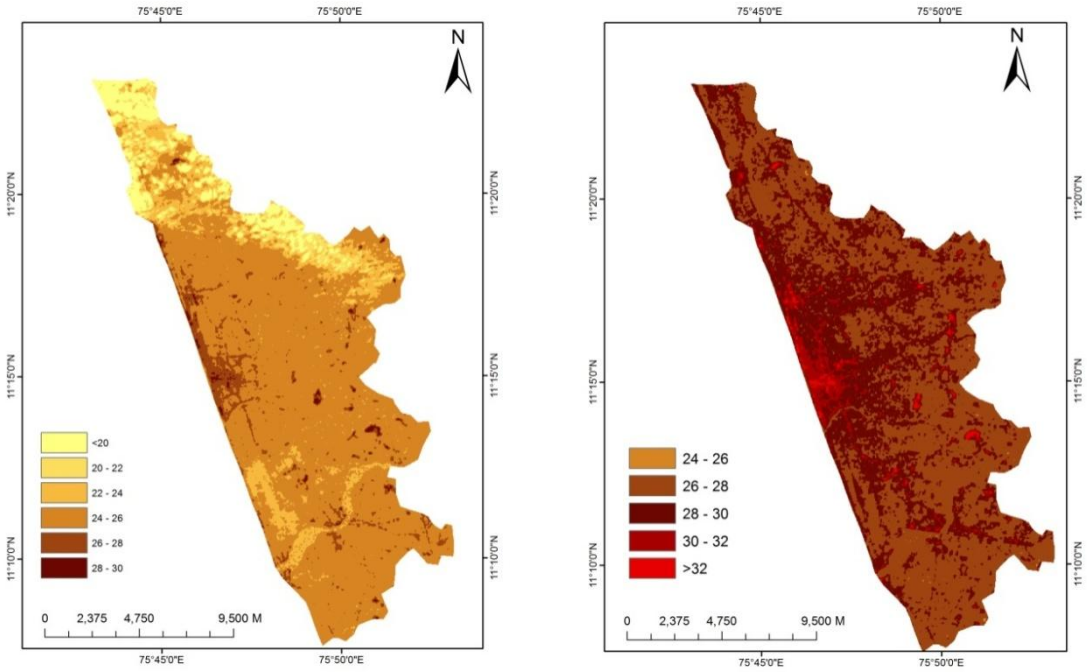

(a) (b)

Figure 4: *(a) LST (oC) for 2003; (b) LST (oC) for 2015*

3.3. Normalized difference vegetation index (NDVI)

Figure 5(a) & (b) show the NDVI maps generated from the Landsat 7 TM imagery for the year 2003 and 2015. The decrease in the vegetation growth coverage within the study area can clearly be seen. Lower NDVI values are clearly evident water bodies and built-up areas.

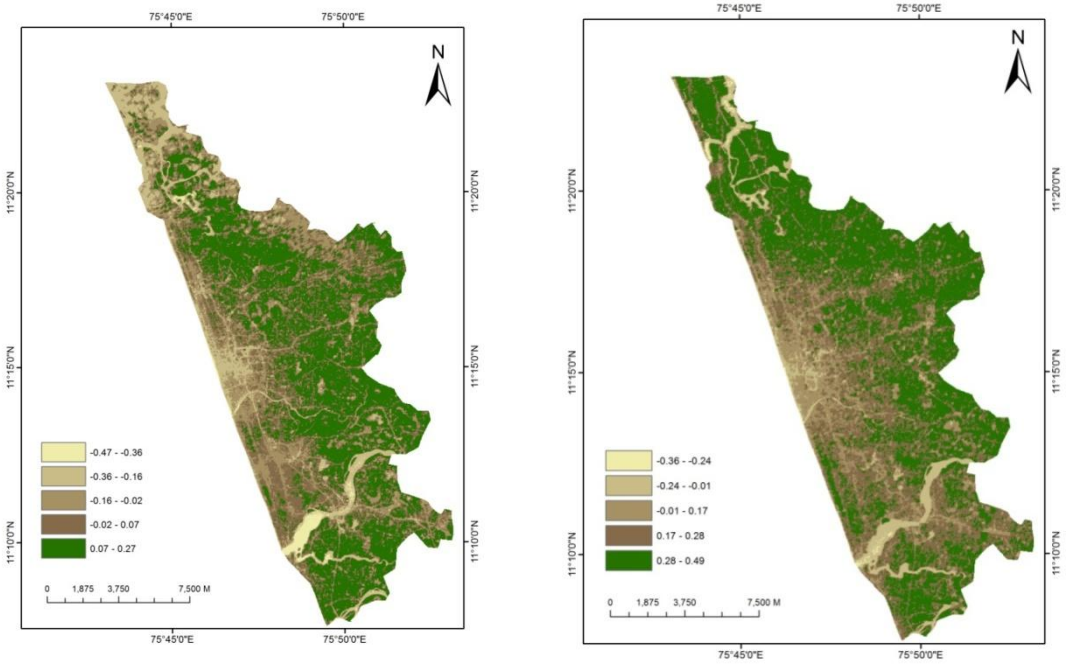

(a) (b)

Figure 5: *(a) NDVI image for 2003; (b) NDVI image for 2015*

3.4. Correlation between LST and NDVI

Land surface temperature (LST) is sensitive to vegetation cover. Figure 6(a) & (b) shows the correlation of LST and NDVI in the study area for the year 2003 and 2015 respectively. There is strong negative correlation between LST and NDVI values in Calicut city area. Thus, by greening landscaping in the urban area can help to reduce the radiant temperature of the built-up area. This study proves the positive impact of vegetation in built-up areas especially in urban centers and significantly important to help mitigate the phenomena of Urban heat island.

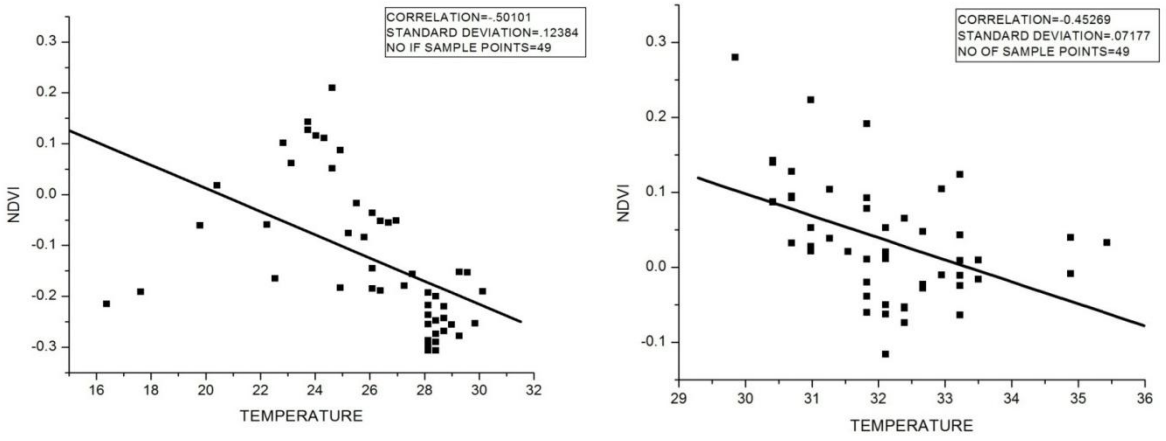

(a) (b)

Figure 6: *(a) Relationship of LST and NDVI in 2003; (b) Relationship of LST and NDVI in 2015*

4. Conclusion

Use of satellite remote sensing coupled with GIS provided a time and cost effective methodology for this analysis. Landsat 7 TM, ETM images were widely used to monitor the land cover changes and to analyse the spatial distribution of land surface temperature. The study is also based on the image analysis of Landsat 7 TM, ETM images to study the relationship between land surface temperature and the vegetation cover in Calicut city and suburbs, Kerala, India. The results revealed that the built-up areas in Calicut city and suburbs have expanded significantly on the expense of the vegetative areas. The total area captured in the image is equivalent to 207 km^2. In 2003, the built-up areas were 70.82 km^2 equivalents to 34.22 % of the total area and in 2015 reached an area of 79.61 km^2 equivalent to 34.47 % of the study area. Analysis the land surface temperature revealed slightly fluctuating values; the results show that LST and thermal signal of built-up and cleared land have distributed to rise average radiant temperature while vegetative areas and water bodies experiencing lower temperature.

Although this study is not conclusive, initial findings have shown that there are significant increases in the built-up areas in the Calicut city and suburbs over a period of 12 years which resulted in higher LST in built-up areas as compared to the vegetated areas. There is strong negative correlation between LST and NDVI, which indicates vegetation helps to reduce the LST of an area. Vegetation plays vital roles to alleviate the heat island effect by means of transpiration, shading and heat absorption to reduce the emissivity of the hard surface reflectivity by covering the built-up area by its shadow.

References

Chen, X.L., Zhao, H.M., Li, P.X., & Yin, Z.Y. (2006). Remote sensing image-based analysis of the relationship between urban heat island and land use/cover changes. *Remote Sensing of Environment, 104*(2), 133-146.

Mallik, J., Yogesh Kant, & Bharath, B.D. (2008). Estimation of land surface temperature over Delhi using landsat-7 ETM+. *J. Ind. Geophysics Union, 12*(3), 131-140.

Senanayake, I., Welivitiya, W., & Nadeeka, P. (2013). Remote sensing based analysis of urban heat islands with vegetation cover in Colombo city, Sri Lanka using Landsat-7 ETM+ data. *Urban Climate, 5*, 19-35.

Sundara Kumar, K., Udaya Bhaskar, P., & Padmakumari, K. (2012). Estimation of Land Surface Temperature to study Urban Heat Island effect using Landsat ETM+ Image. *International Journal of Engineering Science and Technology, 4*(2), 771-778.

Weng, Q., Lu, D., & Schubring, J. (2004). Estimation of land surface temperature-vegetation abundance relationship for urban heat island studies. *Remote Sensing of Environment, 89*, 467-483.

Cloud Publications
International Journal of Advanced Remote Sensing and GIS
2017, Volume 6, Issue 1, pp. 2114-2123
ISSN 2320 – 0243, Crossref: 10.23953/cloud.ijarsg.256

Case Study | Open Access

Land Use Land Cover of an Urban Area using Remote Sensing (Texture Analysis Applications) and GIS - A Case Study of Central Region of Almadinah Almunawarah, Saudi Arabia

Saleh Daqamseh

Department of Human Sciences & Technology, Geography, Taibah University, Medina, Kingdom of Saudi Arabia

Publication Date: 29 April 2017

DOI: https://doi.org/10.23953/cloud.ijarsg.256

Abstract In this study IKONOS images with high spatial resolution have been used for urban planning classification. This research explores approaches to improve urban planning and build up the data base for types of patterns area within the urban scheme in central of Almadinah Almunawarah using remote sensing based on Texture Analysis Applications and Geospatial Information System (GIS softwares). It has been compared with Traditional method (Field Survey) of urban planning classification in Almadinah Almunawarah. The activities of central Almadinah was divided into commercial area, investment area, industrial area, health services building, religious building, garden, infrastructure, government services building, and agricultural area. The results of this study showed the commercial and investments area was the largest area 6.5 km, and it is followed by religious services 3.2 km, while the third ring area the largest area was the agricultural housing area 16 km and then followed by commercial and investments area 5.3 km of the total area. This study recommends to use remote sensing data to classify the urban planning due to significantly improve land cover classification performance compare to traditional survey.
Keywords *classification; commercial area; IKONOS; image processing; geography; geospatial information; remote sensing; land cover*

1. Introduction

Recent advancements made in the development of satellite sensors, image processing techniques, urban classes' data collection techniques and GIS modeling have provided in combination a powerful tool for urban classification analysis and monitoring. A sensor orbiting the Earth on board the NASA's IKONOS satellites with high spatial resolution is now collecting the most detailed measurements ever made on the urban planning and classes. Like a sophisticated thermometer in space, the IKONOS can detect with high spatial resolution the details and changing of urban classes every 14 day over the entire globe through five spectral bands, or channels [4, 10, 22]. Urban area covers - Commercial area and investment area, industrial area, health services building, religious building, garden, infrastructure, government services building, agricultural area were extracted and monitoring from Almadinah Almunwarah, Saudi Arabia using high spatial IKONOS data sets, which have provided scientists with

improved measurement and monitoring capabilities over their predecessors. For instance, IKONOS can now better detect and mentoring the change of urban classes cover associated with signature value using information contained in the surface emissive and reflectance signatures. It also improves the accuracy in the measuring of classes' area.

In past the classification and planning organized in Almadinah city has been done based on traditional method of map digitizing of land cover classes and change detection were based in field survey [3, 6, 8]. This technique is useful for small area land cover classification but can't classify large area with many type of coverage classes and these methods are time consuming, it needs more effort and its low accuracy of land cover land use classification. Due to fast development and rapid urban expansion in Almadinah Almunwarah city and the need to update the map patterns of urban plans associated with data base build up to do proper urban planning and management of these areas a way that meets the growing work, housing, economic and investment activities need and distributed appropriately. It is appropriate considering the introduce of remote sensing (Texture analysis applications) and geographic information systems to monitoring this change with development of urban planning in the city of Medina and to update the databases of classes cover change. Due to previous studies related, many research done on land cover and land use classification using remote sensing data, urban planning and classification using pixel base classification [2, 23], land use land cover classification using land sat satellite image [5, 13, 16, 19], monitoring and change detecting of the urban scheme using quick bird satellite image [6, 21], IKNOS satellite data for urban planning [12, 15, 20]. Many works have been done on mapping and monitoring forest and vegetation, phytobiodiversity mapping using object oriented classification [18, 24]. However, mostly this work on pixel base classification without validation have been done between result extracted from satellite image and field work, also these work did not use the texture technique interpretation, which lead to low accuracy mapping land cover land use extraction.

In this research we have eliminated the Texture analysis applications technique and interpretation from IKONOS satellite image for more accurate land use land cover mapping and data base, which is a basic property, is an important technical to classify each feature and class cover. In other hand the research carry out with validation between result from satellite image and field work.

1.1. Study Area

The study area is Al-Madinah Almunawarah located at Eastern Part of Al Hijaz Region in the Kingdom of Saudi Arabia at latitude 24.28 06°E and longitude 39.36 6°N, as appeared in Figure 1. It is located in hot tropical region where it is subject to effect by the Mediterranean region in the north, and tropical season region in the south. Madinah is surrounded mostly by mountains, and it's height above sea level between (590-620 meters), where it's far from water bodies (240 km far from the Red Sea). Medina area is about 589 square kilometers and 99 square kilometers occupied by the urban area [14].

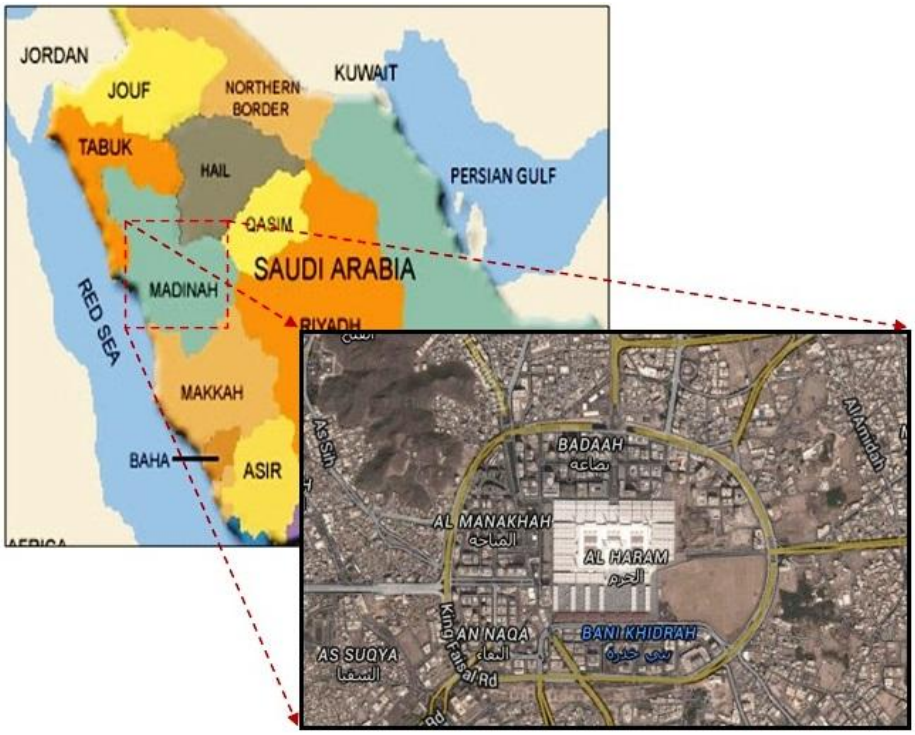

Figure 1: *Study area Al-Madinah Almunawarah, Saudi Arabia*

2. Data and Method

2.1. Data

The data have been used in this research acquired by Madinah development authority and downloading from the Global Land Cover Facility, www.landcover.org. The IKONOS datasets provide temporal and reliable information for extraction and monitoring of urban classes features. Obtaining the same information through traditional methods and field surveys would time consuming and use considerable human resources. Table 1 shows the details of IKONOS spectral band and spatial resolution.

Table 1: *Details of IKONOS spectral band and spatial resolution*

Satellite	Sensor	Band(s)	Spectral Range	Scene size	Pixel resolution
IKONOS-2	Multi-spectral	1 = Blue	455 - 520 µm	11× 11km	4 Meter
		2 = Green	510 - 600 µm		
		3 = Red	630 - 700 µm		
	panchromatic	4 = NIR	760 - 850 µm		
		Pan	760 - 850 µm		1 Meter

2.2. Image Registration

The IKONOS data sets were geo-referenced to the Universal Transverse Mercator (UTM) Projection using the “Georeference IKONOS” function in the ENVI software 4.2 version, which has provided automatic geometric correction of the IKONOS imageries including correction for orbit overlap and swath distortion (the bow-tie effect). This correction was done to enable checking the image coordinates with those of texture analysis class detection. The urban classes feature vector data was overlaid on the corrected images and an accuracy of < 0.6 pixel was obtained.

2.3. Texture analysis application

The Texture analysis applications is based on a methods that involve of six steps of processing: Magnetic resonance imaging (MRI) acquisition, region of interest (ROI) definition, region of interest ROI preprocessing, feature extraction and detections, feature selection process, and classification of each feature as shown the texture model and analysis in Figure 2. In texture analysis model none of these steps is working specific, and the process have to be done according to the methods and application. The texture analysis result can be more affected base on the process used throughout the methods. In this research, we provide description of each processing step of the texture analysis methods focusing on applications that explain many different methods.

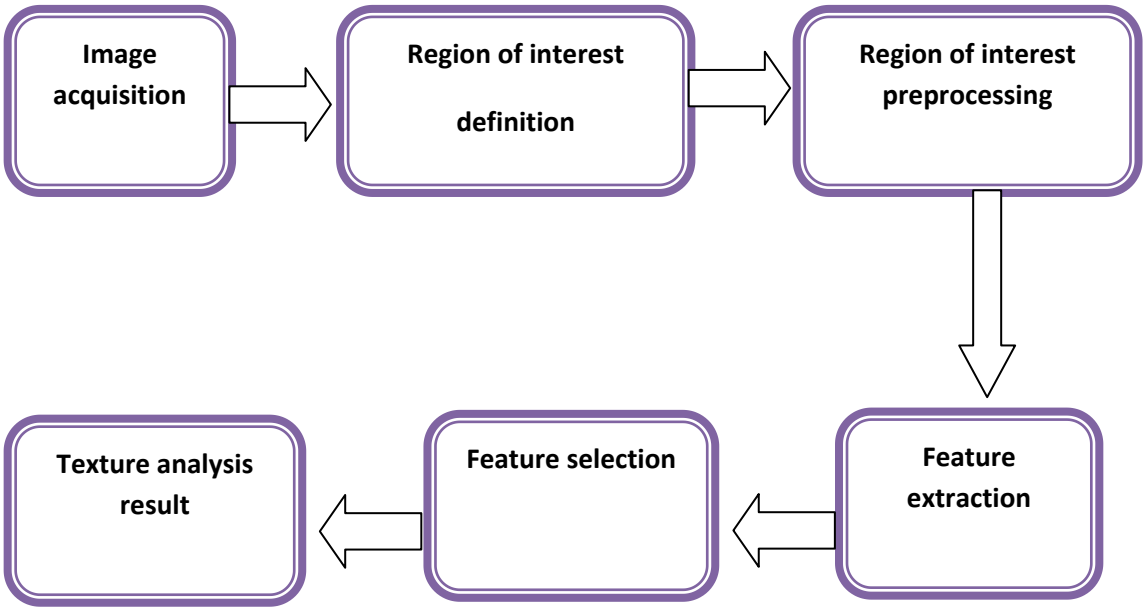

Figure 2: *Steps for MRI classification by means of texture analysis. ROI: region of interest. Resource (Larroza)*

The texture analysis and method were generally have distinction by high value accurate output for Built-up LULC specially when use for different features such as infrastructures, street grids, buildings and urban corridors, but it's have high commission error especially in low built-up in homogenous areas which have little to no textural variation, for this case we have used the modified texture analysis methods. In light of this reason, the processing of modified texture analysis which is used for correction based on textural analysis was only used for the low-built-up in homogenous areas to avoid increasing the omission error.

Because of this, in the high-built-up area the function of area of interest (AOI) was drawn around, and using the logic rule as shown in Figure 2. In other hand all Built-up pixels of MLC were retained as such used in the process of post-classification corrected (PCC) map. Then all the rest MLC Built-up patches of the research zone were process using modified texture role proposed by Feng [17]. Finally will reclassify the remainder of the MLC Built-up patches based on their NDVI threshold values. These threshold values were determined by detailed inspection of the textural images and NDVI images derived from the respective Landsat imageries corresponding to the LULC categories of interest which was guided with the use of orthorectified aerial photograph of the nearby period.

The texture analysis result can be more affected base on the process used throughout the methods. In this research, we provide description of each processing step of the texture analysis methods focusing on applications that explain many different methods. The texture analysis proposed by [7] ERDAS imagine software of the IKONOS spectral band was performed using a 5 × 3 moving window and the variance Equation (1):

$$V = \sum \frac{(X_{IJ} M)^2}{N-1} \qquad (1)$$

Where x_{ij} = DN pixel value (i, j), n =pixel number in the window and M definition is the mean of the moving window which is defined in drive Equation (2) [9]:

$$V = \sum \frac{X_{IJ}}{N} \qquad (2)$$

Satellite technology has been proven suitable for mapping environmental factors. In fact, the technology has been extensively used for large area vegetation monitoring. The spectral bands used for this purpose are visible and near infrared bands, as they provide useful information on chlorophyll absorption, which is also an indicator for healthy vegetation. Various mathematical combinations of these bands have been used for the computation of normalize different vegetation index (NDVI), which is an indicator of the presence and condition of green vegetation [9]. NDVI (Normalized Difference Vegetation Index) [11] which is the most widely used for vegetation index to interpretation and distinguish healthy vegetation from others classes feature in the satellite image or from non-vegetated areas. NDVI was derived using the expression given in Equation (3):

$$NDVI = \frac{(NIR - R)}{(NIR - R)} \qquad (3)$$

As shown in Table 1 the details of IKONOS spectral band and spatial resolution where NIR = Near Infra-Red (band 4 for IKONOS spectral band); R = Red (band 3 IKONOS spectral band).

3. Results and Discussion

The texture analysis methods have been applied into the extraction process in order to identify the feature and classes from the satellite image. Automatically apply the classification rules in the satellite image analysis and visualization software to determine land cover land use features. The image processing and enhancement for feature extraction was done using IKONOS imageries acquired 2012. The texture analysis algorithm was applied in this research. It is a part of the multi-process of six steps of processing. Individual features are perceived as the initial texture. These features are then sequentially merged pair-wise into larger ones with the purpose of minimizing the heterogeneity of the resulting features. The texture is based on various scales determined by properties of texture of each feature. The overall accuracies as well as Kappa index of agreement were computed for each class. Besides this, classification accuracy and stability within texture analysis methods were also assessed. The overall accuracies in texture analysis model and classification achieved were 88.023.

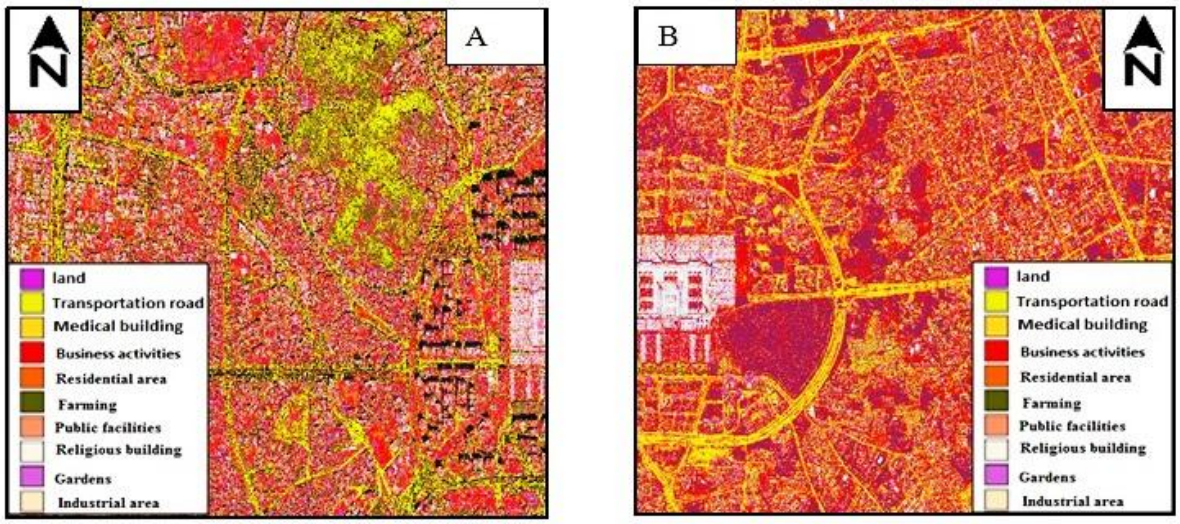

Figure 2: *(A and B) Feature and classes map of the central region Madinah Munanwarah in 2012*

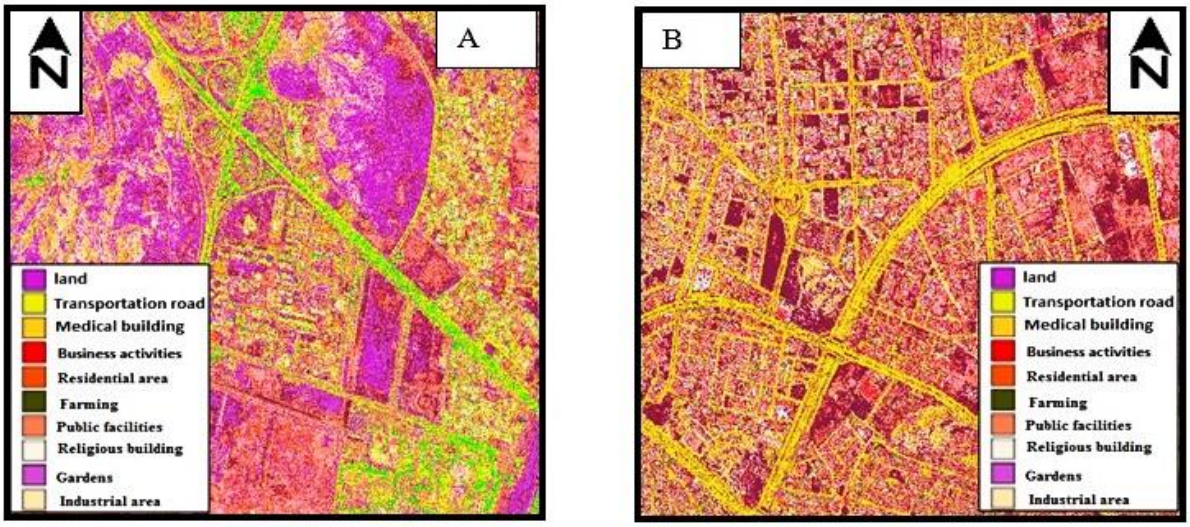

Figure 3: *(A and B) Feature and classes map of the third ring Madinah Munanwarah in 2012*

As shown in Figure 2 and 3, results of the texture analysis and process of Urban scheme from IKONOS 2012 satellite imagery the classification of percentage coverage within the urban area in the central region. It is cleared that the commercial activities occupies the highest percentage 4.5 km from the types of activities in the central area of the scheme while in the third ring area the residential and farming was the largest coverage 19 km from the total area.

The Central region of Almadinah Almunawarah were classified and divided using texture analysis and NDVI model into eight categories as show in Table 2. Business activities and investments, Industrial Area, Residential area and farming, Public facilities, Medical building, Religious building, Government building, Entertainment services and Gardens. In 2012 image classification, the Business activities and investments was found to have the largest coverage 4.5km in the total area of Central region - 58.43 %, and the second largest coverage into central region was found the religious building 4km; 28% of the total area in central region.

Table 2: *The investigated feature and classes extracted from IKONOS satellite image*

N	Urban planned patterns	N	Urban planned pattern
1	Business activities and investments	5	Medical building
2	Industrial Area	6	Religious building
3	Residential area and farming	7	Government building
4	Public facilities	8	Entertainment services and Gardens

As mention before the commercial activities occupies the highest percentage 6 km. It is attributed to that most population activities in central region of Almadinah Almunawarah and services are limited to the surrounding campus area in central region, and also because the Madinah city's considered as the second religious center for Muslims after Mecca. The increasing number of hotels requirement in the region because the number of visitors is estimated approximately 2 million visitors per year and all of them gather in the central area next to the Haram al-Sharif and in need of services. The facilities were so crowded in central area of commercial activities, but the third ring area increase the proportion of housing because the city's residents are turning to get away from traffic areas and population-enrollment.

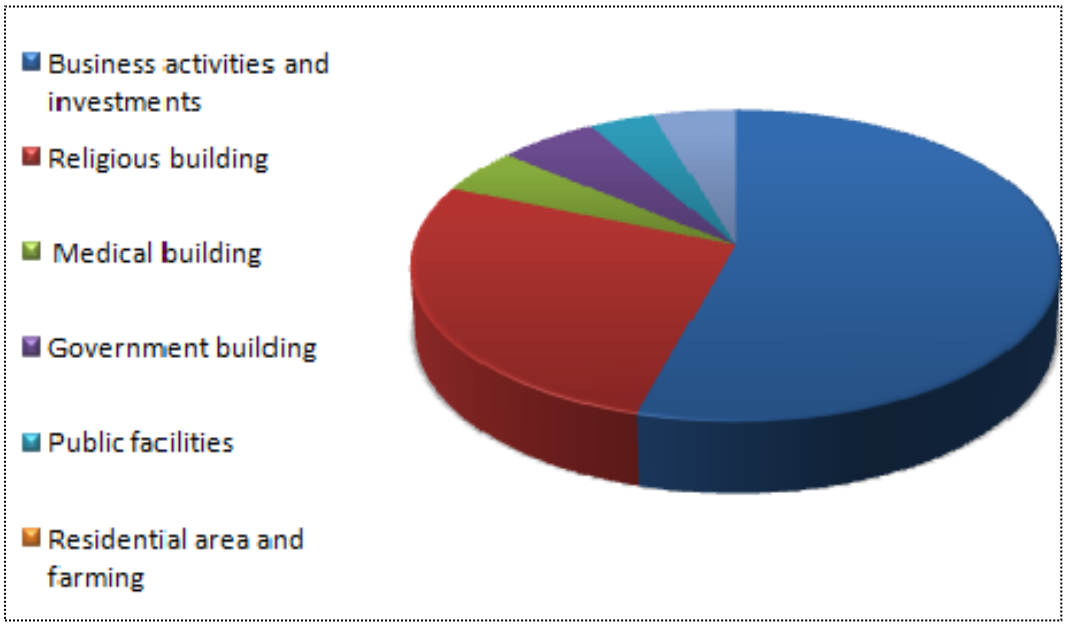

Figure 4: *Percentage of coverage area for each type activities in Al Madinah central region*

As shown in Figure 4 religious building come in second place of the activities in the central region Al Madinah Almunawarah. The coverage percentage almost 28% of the total area of central region, the government services and building was 6%, medical building 5%. The garden was 4%, while the public facilities coverage in central region 3%, residential area and farming was the smallest pattern within limited areas 0% from the total area of the central region due to the number of visitors which's more than 2 million and they are staying in central region near to Al-Ahram – Al-Sharief and they use the hotels in the central area.

In the third ring residential area and farming was dominate the rest of the patterns of the third ring with an total area 19 kilometers which is about 60% from the total area, and commercial activities coverage about 5.5 km 23%, and then comes government building 9%. The medical building was 6%, and the garden was 5%, while the industrial area in was the smallest area which cover less than 1% of the total area in the study area.

3.1. Validation & Comparison of Texture Analysis- Result and Field Survey Data (Field Work)

In order to checked the accuracy assessment of texture analysis result, the comparison has been done between field data and result detected by texture analysis from satellite image to check the validity of use the texture analysis. Table 3 show the result of texture analysis: percentage of coverage area for each class extracted from satellite image. Table 4 show the result of field survey data: percentage of coverage area for each class extracted from field work. The comparison has been done by applying linear regression coefficient and the ratio of validation in most classifications. The result of this comparison show high matching almost 89.5% between the two results in the central region.

Table 3: *Percentage of coverage area for each class extracted from satellite image*

Urban planned patterns	Area km^2	Urban planned patterns	Area km^2
Business activities and investments	5.8	Medical building	0.93
Industrial Area	0	Religious building	3.2
Residential area and farming	0	Government building	0.65
Public facilities	0.437	Entertainment services and Gardens	0.434

Table 4: *Percentage of coverage area for each class extracted from Field Survey*

Urban planned patterns	Area km^2	Urban planned patterns	Area km^2
Business activities and investments	6	Medical building	0.94
Industrial Area	0	Religious building	3
Residential area and farming	0	Government building	0.62
Public facilities	0.450	Entertainment services and Gardens	0.443

4. Conclusion

Remote sensing technology and GIS with texture analysis and methods have been tested and compared, the validation done with field survey. The accuracy assessment of texture analysis output was 92.7% for detection and identify of feature distribution coverage. IKONOS satellite image with high spatial resolution 1m significantly use and it is also enable the analysis to classifying central region of Almadinah Almunawarh. There are other factors contributed to the accuracy of classification in the central region and third ring in Almadinah Almunwarah, including radiometric correction and geometric correction as preprocessing of satellite image before start the process of classification. The matching between satellite image result and field survey data was almost 89.5%. Both results field survey and texture analysis results show the Business activities have the largest coverage area in central region. It is about 6km from the total coverage area, then the religious building with total area 3.2km, but the residential area and farming have the smallest coverage area 0% from the total area, while in the third ring the residential area have the largest coverage area with 19km. The research result shows that the distribution of feature and activities within the urban regions in the study area is affected tremendously by human activities. So the economic activities and investment in the central region constitute more than 60% of all other activities as a result of the large number of religious tourism in the Medina area.

References

[1] Comber, A.J.: The separations of land cover from land use using data primitives. Journal of Land Use Science 3, 215-229 (2008)

[2] Chen, B., Li, J., Ma, B., Wei, G.: Convolutional sparse coding classification model for image classification. IEEE International Conference on Image Processing (ICIP) (2016)

[3] Ferdaous, C.: Remote sensing image fusion for unsupervised land covers classification. Image Fusion 9, 132-148 (2011)

[4] Toscani, D., Archetti, F., Frigerio, M., Messina, E.: IKNOS: inference and knowledge in networks of sensors. International Journal of Sensor Networks, 8, 209-285 (2010)

[5] Büttner, G.C.B.: CORINE Land cover and land cover change products. In: Land Use and Land Cover Mapping in Europe. Remote Sensing and Digital Image Processing 12, 55-74 (2014)

[6] Bagan, H., Yamagata, Y.: Improved subspace classification method for multispectral remote sensing image classification. Photogrammetric Engineering & Remote Sensing, 76, 1239-1251 (2010)

[7] Feng, H., Jiang, Z., Han, X.: Texture segmentation for remote sensing image based on texture-topic model. IEEE International Geoscience and Remote Sensing Symposium (2011)

[8] Richards, J.A.: Supervised Classification Techniques. Remote Sensing Digital Image Analysis 8, 247-318 (2012)

[9] Kelsey, K., Neff, J.: Estimates of aboveground biomass from texture analysis of landsat imagery. Remote Sensing 6, 6407-6422 (2014)

[10] Wang, K., Feng, X., Xiao, P., Wu, G.: The research on recognition and extraction of river feature in IKNOS based on frequency domain. MIPPR 2009: Automatic Target Recognition and Image Analysis, 343-368 (2009)

[11] Liao, L., Song, J., Wang, J., Xiao, Z., Wang, J.: Bayesian method for building frequent landsat-like NDVI datasets by integrating MODIS and landsat NDVI. Remote Sensing 8, 452-489 (2016)

[12] Sun, L., Schulz, K.: The Improvement of land cover classification by thermal remote sensing. Remote Sensing 7, 8368-8390 (2015)

[13] Balakeristanan, M., Said, M.: Land use land cover change detection using remote sensing application for land sustainability 16, 767-789 (2012)

[14] Bob, M., Rahman, N., Elamin, A., Taher, S.: Rising groundwater levels problem in urban areas: a case study from the central area of Madinah City, Saudi Arabia. Arabian Journal for Science and Engineering 41, 1461-1472 (2015)

[15] Mölders, N.: Impact of land-cover and land-cover changes. In: Land-use and land-cover changes. Atmospheric and Oceanographic Sciences Library 5, 39-115 (2011)

[16] Verburg, P., Neumann, K., Nol, L.: Challenges in using land use and land cover data for global change studies. Global Change Biology 17, 974-989 (2011)

[17] Feng, Q., Liu, J., Gong, J.: UAV Remote sensing for urban vegetation mapping using random forest and texture analysis. Remote Sensing 7, 1074-1094 (2015)

[18] Beijma, S., Comber, A., Lamb, A.: Random forest classification of salt marsh vegetation habitats using quad-polarimetric airborne SAR, elevation and optical RS data. Remote Sensing of Environment 149, 118-129 (2014)

[19] Ganguly, S.: Long-term satellite data records for land-cover monitoring. Remote Sensing Applications Series Remote Sensing of Land Use and Land Cover 10, 91-112 (2012)

[20] Bachmann, T., Bettenhausen, M.: PURSUIT: an automatic classification tool for remote sensing data. IEEE International Geoscience and Remote Sensing Symposium (2014)

[21] Al-Fares, W.: Historical land use/land cover classification using remote sensing. Springer Briefs in Geography 5, 123-145 (2013)

[22] Gribb, W., Czerniak, R.: Land use/land cover classification systems and their relationship to land planning. In: Ahlqvist, O., Varanka, D., Fritz, S., Janowicz, K. (eds.) Land Use and Land Cover Semantics, pp.1-20. CRC Press (2015)

[23] Xu, X., Wu, X., Lin, F.: Defining Feature Space for Image Classification. Cellular Image Classification 19, 119-134 (2016)

[24] Lei, Z., Fang, T., Li, D. Land cover classification for remote sensing imagery using conditional texton forest with historical land cover map. IEEE Geoscience and Remote Sensing Letters 8, 720-724 (2011)

Cloud Publications
International Journal of Advanced Remote Sensing and GIS
2017, Volume 6, Issue 1, pp. 2204-2222
ISSN 2320 – 0243, Crossref: 10.23953/cloud.ijarsg.274

Research Article

Land Surface Temperature Extracts for Peri-Urban Heat and Rural Cool Troughs in Ghana

Divine Odame Appiah[1], Eric Kwabena Forkuo[2] and John Tiah Bugri[3]

[1]Department of Geography and Rural Development, Kwame Nkrumah University of Science and Technology, (KNUST) Kumasi, Ghana
[2]Department of Geomatic Engineering, Kwame Nkrumah University of Science and Technology, (KNUST) Kumasi, Ghana
[3]Department of Land Economy, Kwame Nkrumah University of Science and Technology, (KNUST) Kumasi, Ghana

Publication Date: 10 June 2017

DOI: https://doi.org/10.23953/cloud.ijarsg.274

Abstract The objective of this paper is to analyze the land surface temperatures (LST) derived from three satellite images as a proxy for urban heat island potential, through a peri-urban heat troughs (PuHT) to rural cool troughs (RuCT) continuum, concepts largely overlooked in the literature, in the Bosomtwe district of the Ashanti region of Ghana. Four Landsat satellite images from 2002, 2008 Enhanced Thematic Mapper+ (ETM+) and 2014 Landsat 8 Operational Land Imager and Thermal Infrared Sensor (OLI/TIRS) were geo-referenced and processed for classification using the maximum likelihood classifier algorithm in ERDAS Imagine 13. Land Use and Land Cover (LULC) transition analysis was performed in ArcMap for ArcGIS 10.2. Results indicate that, in order of importance, recent fallows and grasslands along with built up/bare land and concrete surfaces have been increasing in terms of coverage. A corresponding surface reflectance translated into LST values ranging between a minimum of 24ºC (297K) to a maximum of 53ºC (326K). Changing LULC types correlated with the land surface temperature fluxes, creating the RuCT and PuHT. This result explains the relatively substantial peri-urban land use dynamics in the district. Future studies should develop threshold values for RuCT and PuHT temperatures.
Keywords *Peri-urban heat trough (PuHT); Rural cool trough (RuCT); Land Surface Temperature (LST); Land Use Land Cover (LULC); Bosomtwe; Ghana*

1. Introduction

Land surface characteristics determine the amount of energy that is absorbed and emitted. The reflectance and emission properties of land surface features also determine the albedo that defines the percentage reflectance of solar energy from the earth surface (Ahrens, 2005). As a proxy for calculating the degree of hotness or coldness of the land surface, many researchers have used thermal infrared (TIR) satellite remote sensing to estimate land surface reflectance properties to extract surface temperature and moisture for climatic analysis (Rajeshwari et al., 2014; Liu and Zhang, 2011 and Srivastava et al., 2010). Land use and land cover (LULC) dynamics influence the ability of land surfaces to absorb or reflect solar radiation in varying proportions.

In furtherance of handling LULC dynamics, previous studies have indicated that depending on the type of LULC obtained, it could be possible to extract surface moisture and temperature characteristics from LULC maps generated from Advanced Space-borne Thermal Emission and Reflection Radiometer (ASTER), Landsat, MODIS and others (Ahrens, 2005; Liu and Zhang, 2011 and Srivastava et al., 2010). Accordingly, the energy emitted by the LULC mosaic as indicated by its surface energy fluxes and atmospheric conditions, aids in determining the varying energy fluxes of land surfaces (Vlassova et al., 2014).

In peri-urban landscapes, the complex mixture of settlement and vegetation exhibit different energy fluxes. This phenomenon determines the amount of surface temperature that can be sensed and recorded. In a study by Sobrino et al. (2004), the relationship between vegetation and land surface temperature was established by correlating normalized difference vegetation indices (NDVIs) with the temperature profiles of land use classes. Widyasamratri et al. (2013) found that there are limitations in accessing and using air temperature of an area to represent actual temperature characteristics in investigations of urban heat islands (UHIs) and similar phenomena. This limitation could be reduced through the use of NDVIs and correlated against estimated land surface temperature (LST) as proximate analysis for climate change analysis (Mbithi, nd; Weng, 2004; Weng, 2001).

As a result, the data obtained from NDVIs are typically used to determine the effectual land surface radiating temperature that affect surface energy and vapor fluxes interacting with the atmosphere (Yuan and Bauer, 2007). According to Vlassova et al. (2014), LULC dynamics reflects the surface temperature characteristics, which serve as surrogates for documenting climate change using proximate variables such as temperature and rainfall. This data reinforces the Intergovernmental Panel on Climate Change Fourth Assessment Report (IPCCAR4) and cited in (Meehl et al., 2007), that projected mean annual precipitation will demonstrate increasing and decreasing trends in high northern latitudes of the tropics and the subtropics, respectively.

LST estimates have been conducted by Widyasamratri et al. (2013) to measure the rate and intensity of urbanization in Jakarta, Indonesia. From that study a relationship between urbanization and UHI was established for the city. Modification of LULC types usually results in altered land surface temperatures (Asmat et al., 2016). The peri-urban mosaic consists of a complex mixture of rural and urban LULC classes, which clearly exhibits diverse surface reflectance and emissivity configurations (Rajeshwari and Mani, 2014). Using remote sensing and geographic information system (GIS) techniques; it is easier to estimate the surface temperature profiles of these peri-urban LULCs.

Research conducted by Voogt and Oke (2003), indicated that higher temperature values are associated with urban rock and built-up areas, while lower temperatures exemplify rural landscapes. These sharp temperature contrasts have aided in the measurement of environmental reflectance propensities of the various LULC types, which exhibit localized effects while contributing to regional and global heat budgets in the long term (Joshi and Bhatt, 2012).

Again, beyond the statistical assessment of land use and land cover changes (LULCCs) obtained from classified satellite images, LSTs correspond to certain land use classes that can be derived from the TIR band of the satellite image (Mbithi et al., nd; Urban et al., 2003). These results may portray the latent and sensible heat energy fluxes exhibited by the LULCC dynamics. From a temporal dimension, it is plausible to mimic the dynamics of particular climatic variables and to eventually, project some variability or even changes in local to regional climates (Blake et al., 2011; Iino and Hoyano, 1996 and Lipton and Ward, 2000). Satellite remote sensing with a GIS framework has been used to study UHI differentials (Quattrochi et al., 2000). These techniques were employed to juxtapose LULC variations with LST anomalies extracted from satellite images (Ambinakudige, 2011).

As an alternative to the analysis of LST as surrogate to climate change, the use of down-scaled Regional and Global Climate Models (RGCMs) has facilitated to an appreciable extent, the forecasting of future climate scenarios in many instances (Thomas, 2008). The RGCM data, with typically low spatial and temporal resolution of several degrees, usually have error-laden results to preclude their use in accurately simulating present-day climate (Bonan et al., 2002). In employing RCMs in regional climate simulations, higher spatial resolution data usually performs sufficiently for providing adequate scientific insights into regional climate change analysis (Khang et al., 2009). Some of these models, such as the CCSM3 2005 of the US National Center for atmospheric Research (NCAR) and the UKMO/HadGEM1 2004 of the United Kingdom, have high regional climate simulation capabilities (Khang et al., 2009).

In placing the current study in the context of conventional methods and procedures, the Bosomtwe district, with an area of 330km^2, is arguably too small to significantly influence local to regional climatic conditions in terms of rainfall and temperature variables if model downscaling methods are used. LULC dynamics extracted from satellite images prescribe different spatio-temporal changing dynamics of the LULC types, with their possible effects on land surface reflectance. This assumption underpins the use of LST extraction from satellite images and juxtaposing that data with the LULC types derived from the LULCC patterns observed in the Bosomtwe study area.

2. Theoretical Basis of Land Surface Temperature (LST) extraction Algorithms

In a study by Dousset and Gourmelon (Dousset, and Gourmelon, 2003) and cited by Chen et al. (2006), there is a methodological potential for establishing relationships between urban LST and LULC categories using satellite multi-sensor data. From this analysis Chen et al. (2006), a correlation between urban land uses, along with nighttime and daytime average LST profiles, was established.

According to Rajeshwari and Mani (2014), several algorithms have been developed and employed in the estimation of LST. Some of the frequently-used algorithms are Split-Window (SW), Sobrino, Mao, Dual-Angle, and Sob-Mao. Most studies focused on urban areas and arid and semi-arid regions. In many of these studies, a single thermal band was used. These approaches were used to extract the LSTs from ASTER and MODIS data (Sobrino et al., 2003). Again, Jiménez-Muñoz et al., (2006) and cited in Srivastava et al. (2010), used an NDVI-based approach to derive surface emissivity over agricultural areas using ASTER images. Further, Coll et al., (2005) had also compared LST estimates between ASTER and MODIS images in their study.

Inverting the radiative transfer equation (RTE) is the most appropriate process for retrieving LST from a single-channel identified in the TIR region, just like a Landsat image (Cristobal et al., 2009). This is expressed as per the wavelength of the spectrum sensed as follows:

$$L_{sensor,\lambda} = \left[\varepsilon_\lambda B_\lambda (T_s) + (1-\varepsilon_\lambda) L\downarrow_{atm,\lambda}\right]\tau_\lambda + L\uparrow_{atm,\lambda} \quad (1)$$

Where L_{sensor} is the top of atmospheric (TOA) radiance, $\boldsymbol{\varepsilon}$ represents the surface emissivity, B_λ (T_s) is the black body radiance derived by the Planck's law and T_s is the LST. $L\downarrow_{atm,\lambda}$ is the downwelling atmospheric radiance, $\boldsymbol{\tau}$ is the total atmospheric transmissivity between the surface and the sensor, and $L\uparrow_{atm,\lambda}$ is the upwelling atmospheric radiance. It should be noted that Eqn. (1) depends on the wavelength used and also on the observation orientation of sensor platform, although for Landsat, the nadir view offers better outcomes.

The atmospheric parameters τ, $L\downarrow_{atm,\lambda}$ and $L\uparrow_{atm,\lambda}$ are estimated from *in situ* radio-sounding operated on radiative transfer codes such as MODTRAN [31]. Therefore, from Eqn. (2), T_s is derived by using

the inversion of Planck's law. A further inversion of Eqn. (2) is used to correct atmospheric as well as emissivity effects on the measured data by the sensor. The crucial challenge of this method, however, is the need for radio-sounding to be simultaneously launched with the satellite tracking system (Cristobal et al., 2009).

Radiances are in W m^{-2} sr^{-1} μm^{-1} and wavelength in *μm*; the B term is Planck's law, expressed as follows:

$$B(\lambda, T_s) = \frac{c_1 \lambda^{-5}}{\exp\left(\frac{c_2}{\lambda T_s}\right) - 1} \qquad (2)$$

Where c_1 and c_2 are Planck's radiation constants, having values of 1.19104 x 10^8 Wμm^4 m^{-2} sr^{-1} and 1.43877 x 10^4 μm K, respectively, while T_s and λ are the surface temperature in K and thermal bands wavelength in *μm*. Accordingly, it is pertinent to note that the spectral magnitudes should be integrated over a band pass, in the case of Landsat sensors. This coheres with the work of Jiménez-Muñoz et al. (2013), which employed radiative transfer equation on a single-channel to extract LST.

2.1. The Concepts of Peri-Urban Heat Trough (PuHT) and Rural Cool Trough (RuCT)

Many studies have concentrated attention on the generation of temperature profiles to measure UHI fluxes (Liu et al., 2011; Srivastava et al., 2010; Mbithi et al., nd; Weng et al., 2004 and (Weng, 2001). UHI and its impact on rainfall may have been modified by local climate change; however, the quantitative dimensions are yet to be unraveled (Blake, 2011). Most of these studies have not considered explicitly the effects of PuHT systems becoming potential peri-urban heat islands in transition from the RuCT, into becoming ultimately, the so-called urban heat islands (UHIs) (Liu et al., 2011).

Both PuHT and RuCT concepts refer to the concentration of surface up-welling heat energy fluxes that can be sensed as evidence of changing land use patterns in peri-urban and rural landscapes, respectively. These sensible heat fluxes result from the modification and conversion of vegetative and rural LULC types to considerable built-up land use types (Carnahan and Larson, 1990; Baylis et al., 1999). These correlate with moderate to extreme LULC characteristics of the peri-urban and urban landscape, with varying LST configuration (Srivastava et al., 2010). PuHT could be described as the incipient stages of UHIs; the former, however, having a relatively wider geo-spatial dimension in comparison to the latter.

These surface temperature profiles occur due to the progressive increase in urbanization of the rural landscape. As a result, peri-urbanization processes ensue to alter the previously rural land surface characteristics into peri-urban and urban land surface configurations. The land surface characteristics, therefore, result in the RuCT, moderate PuHT and an ultimate UHI core in continuum. The resultant is a LST gradient that develops along the rural to urban lands surface continuum.

Previous studies on land surface heating fluxes have largely focused on core UHIs as surrogates of extraction urban climates (Srivastava et al., 2010). The literature, however, remains sparse on the potentially significant role of PUAs in fuelling the ultimate heat island system. This study proposes that, considering the relative rapidity with which rural landscapes are being converted into peri-urban land uses, with surface reflectance transforming into built-up and paved land uses, it is imperative to analyze the connections between RuCTs and the PuHT systems as potentially full-fledged heat island cell areas. The objective of this paper is to analyze the LST derived from three satellite images, as a

proxy for the creation of potential UHIs through PuHT and RuCT continuum, in the Bosomtwe district of the Ashanti region of Ghana. This paper discusses the omissions of LST transitions from the rural, with preponderance of vegetation, to the urban core with high built-up surfaces. It does so by relating the LULC dynamics of the Bosomtwe peri-urban district, to determine LST fluxes; typical of peri-urban areas. The introduction of the concepts of the RuCT and PuHT into the literature, give credence to the potential LST continuum profiles between the rural 'cool' and urban 'hot' areas, using the peri-urban areas as the transitional zones.

3. Materials and Methods

3.1. Profile of the study area

The study area lies within latitude 6º28'N—latitude 6º40'N and longitudes 1º20'W—longitude 1º37'W in the Ashanti region of Ghana. It has a land area of 330km^2, as seen in Figure 1. The largest Crater Lake in Ghana, Lake Bosomtwe, is located in the district. The area is characterized by a rolling topography which ranges between 500 and 1500m above sea level. The drainage patterns of rivers and streams of the district are dendritic and centripetal (Carnahan and Larson, 1990). Rivers that drain the basin include *oda, butu, siso, supan* and *adanbanwe*.

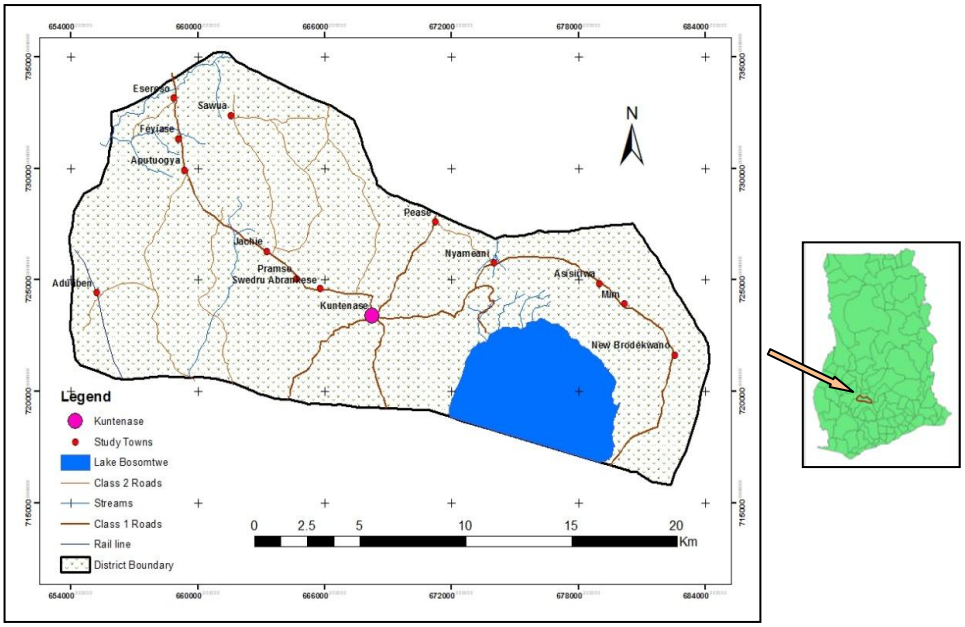

Figure 1: *Map of the Bosomtwe District showing the study communities in Ghana*

The district's rainfall regime is typical of the moist semi-deciduous forest zone of the country, showing two well-defined rainy seasons. The main rainy season occurs from March to July, while September to November constitutes the minor rainy season with an average annual rainfall of 1,400 mm. The mean monthly temperature is around 32°C with a relative humidity of up to 85%.

The district exhibits semi-deciduous forest vegetation characteristics, with different species of tropical trees with high economic value. The dominant tree species native to the district include: wawa *(Triplochiton scleroxylon),* mahogany *(Khaya ivorensis),* and onyina *(Ceiba pentandra)*. Through overharvesting, the original forest cover has been converted into secondary and grassland vegetation. Slash and burn agricultural methods as well as illegal gold mining activities are also responsible for the land and vegetation cover alterations.

The expansion of villages in the district is influenced by the proximity between the district and peripheral settlements of the greater Kumasi metropolitan area, the capital of the Ashanti region of Ghana. Increases in infrastructure, socioeconomic activities, and tourism have contributed to LULCCs in the district.

3.2 Data and Software

3.2.1 Sources of Data

Landsat 7 Enhanced Thematic Mapper (ETM), Landsat 7 Enhanced Thematic Mapper plus (ETM+), and Landsat 8 Operational Land Imager/Thermal Infrared sensor (OLI/TIRS) with a spatial resolution of 30m x 30m were used (see Table 1 and Figure 2(a-c)). The use of these images was informed by their availability and relative clarity in terms of cloud cover and other forms of instrument noise. The use of these three was based on their relative image quality which required minimal radiometric correction.

Table 1: *Satellite image characteristics*

Year	Satellite Sensor	Date acquired	Bands used
2002	Landsat 7 ETM	May 7	1,2,3,4,5,6
2008	Landsat 7 ETM+	February 16	1,2,3,4,5,6
2014	Landsat 8 OLI/TIS	January 8	2,3,4,5,10,11

Because of the coarser spatial resolution of Landsat TM/ETM/TIRS images at 30m x 30m, it was not methodologically expedient to downscale climatic variables from any regional climate model (RCM) for the analysis of climate change and variability to any appreciable extent in this study. It is therefore convenient to use another approach of extracting climate variability from the satellite image and comparing it with some air temperature point data (7), (11).

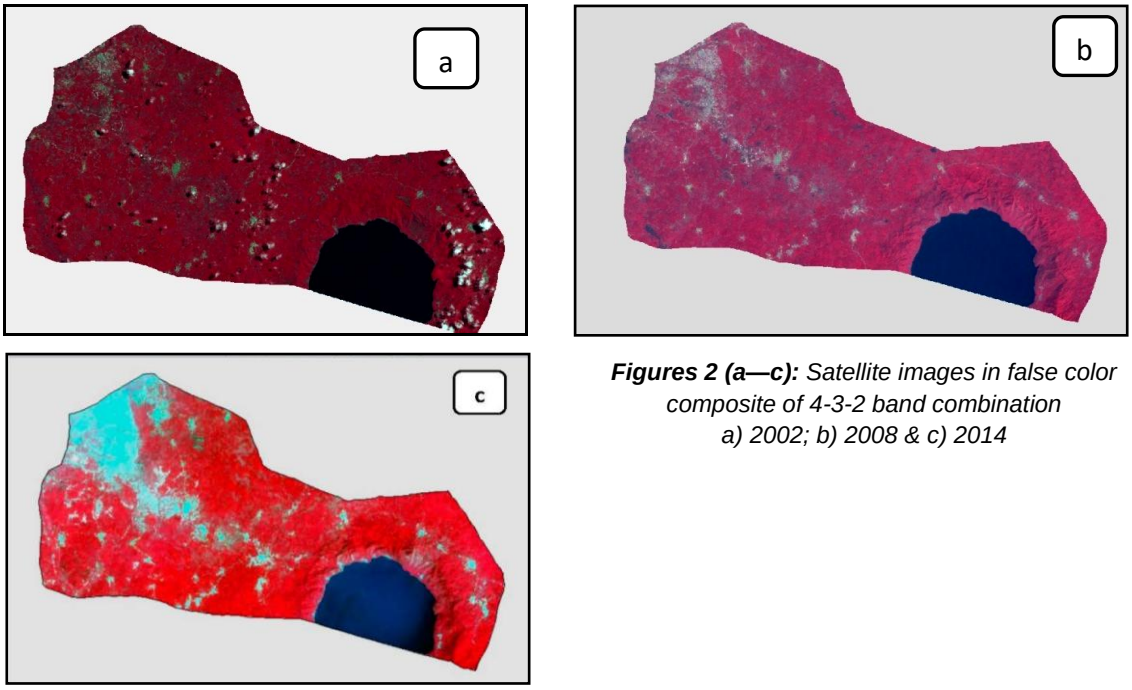

Figures 2 (a—c): *Satellite images in false color composite of 4-3-2 band combination*
a) 2002; b) 2008 & c) 2014

3.2.2 Software used

The Hexagon Geospatial ERDAS Imagine 13, ENVI 4.7, and ESRI's ArcGIS v.10.2 software were used for data analyses (Figure 3). The Garmin eTrex 20® Global Position System (GPS) receiver was used to randomly select 58 coordinates of selected LULC as ground control points (GCPs) during field work, at ±3m accuracy. These points were loaded and imputed into the remote sensing software to perform the accuracy checks on the image classification. The maximum likelihood classifier (MLC) algorithm was used, after satisfying the assumptions of image data normality.

The LULC classes were derived based on field experience and familiarity with the study area as well as their spectral characteristics. The LULC schema used was based on (Baylis et al., 1999) classes types identified as: dense forest (DF), low forest (LF), built-up/bare lands and concrete (BBC) surfaces, recent fallows and grassland (RFG) as well as water body (WB). Three criteria informed the selection of the images used: 1. The quality of the images with respect to the percentage of cloud cover and other image noise, 2. The years with considerable evidence of vegetation regeneration after the 1980s bush fires (due to prolonged drought conditions), and 3. The need to ascertain LULC trends over a 12-year period (which is considered long enough to detect and generate meaningful LULCCs).

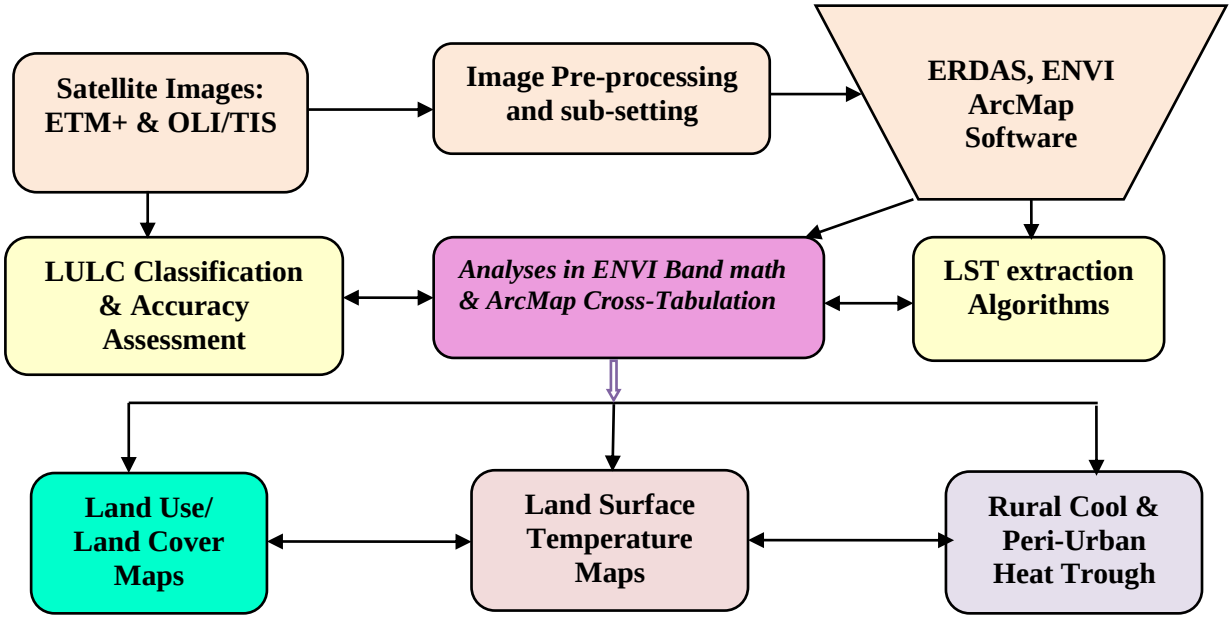

Figure 3: *Methodological flow chart of the LULC and LST extraction procedures*

3.2.3 Spectral Radiance Scaling Method

Conversion from digital numbers to top of atmosphere (TOA) radiance was performed using image meta data Kepner et al. (2000), in ENVI 4.7 software (Butt et al., 2015). In this regard, the formula to convert cell value as DN to cell value as radiance CV_{R1} for the three images, utilized the formula as follows:

$$CV_{RI} = \left(\frac{(L\max - L\min)}{QCALMax - QCAL\min} \right) X \left(QCAL - QCAL\min \right) + L\min \qquad (3)$$

Where CV_{RI} is cell value as radiance, QCAL is digital number, Lmin is spectral radiance scales to QCALmin, Lmax is spectral radiance scales to QCALmax, QCALmin is the minimum quantized calibrated pixel value (estimated as 1), and QCALmax is the maximum quantized calibrated pixel value (typically = 255) (Chander and Markham, 2003).

3.2.4. Apparent Brightness Temperature

The formula to convert radiance to temperature *without* atmospheric correction method was used in converting the radiance to temperature in Kelvin (Kepner et al., 2000). The apparent brightness temperature or at-sensor brightness temperature (T_b), was determined by applying blackbody principles, which is usually computed by means of Planck's law inversion using the Landsat image series USGS (2015), with the following simplified equation:

$$T_b = \frac{K_2}{\left(\frac{K_1 * \varepsilon}{CV_{R1}} + 1\right)} \tag{4}$$

Where, ε is the emissivity (*typically 0.95, and could as well be derived from NDVIs*). The K_1 and K_2 (K) (W m^{-2} sr^{-1} mm^{-1}), are calibration constants based on the Landsat thermal band configuration and CV_{R1} is the spectral radiance (W m^{-2} sr^{-1} mm^{-1}). In the case of Landsat 7, K_1 and K_2 are 666.09 and 1282.71, respectively. With Landsat 8, the K_1 and K_2 are 480.89 and 1201.14 (band 11), respectively.

Surface emissivity was considered in the estimation of T_s for the LULC targets (El-Magd et al., 2016). The LST (T_s) is estimated using the algorithm in equation 5.

$$T_S = \frac{T_b}{1 + \left(\lambda * \frac{T_b}{\rho}\right) \ln \varepsilon} \tag{5}$$

Where, T_b is the effective satellite temperature, T_s is the absolute LST in Kelvin, λ is the wavelength of the radiance emitted (λ = 11.5μm), ρ = (h × c) / σ = 1.438 ×10^{-2} (m K), h is Planck's constant (6.626 × 10^{-34} Js), c is the velocity of light (2.998 × 10^{8} m/s), σ is the Boltzmann constant (1.38 ×10^{-23} J/K), and ε is the composite emissivity. In this study, ε = 0.95 was used for the soil and vegetation (27). The operations were performed in ERDAS Imagine 13, ENVI Band Math and the ArcMap Raster calculator functions in ArcToolbox (Butt et al., 2015).

4. Results Discussions and Conclusion

4.1 Results of LULC Accuracy Assessment

The Kappa statistic is generally accepted as a measure of classification accuracy for both the model as well as user of the model of classification (35). Kappa values are characterized as <0 as indicative of no agreements and 0–0.2 as slight, 0.2–0.41 as fair, 0.41–0.60 as moderate, 0.60–0.80 as substantial and 0.81–1.0 as almost perfect agreement (Kepner et al., 2000; Chander and Markham, 2003). The overall classification accuracy of the images yielded substantial high *Kappa* statistics of 58%, 72.41% and 82.76% for the 2002, 2008 and the 2014 images, respectively. This is an indication of classification accuracy of moderately substantial to almost perfect agreement (Chander and Markham, 2003).

4.2. Results from 2002 LULC and LST analyses

The LULC class of 2002, as indicated by Figure 4, was an increase over the previous year (1986). In 1986, the LULC categories were 5834 ha, 9181 ha, 1201 ha, 12,722 ha, and 3494 ha for DF, LF, BBC, RFG and WB respectively. These served as the base year of analysis, in terms of vegetated land area coverage. In 2002, dense forest cover was 8760.9 ha of the land cover. A proportion of 30% of the land area was covered by low forest vegetation with 9329.8 ha. The built-up/bare land and concrete surfaces also covered an area of 5664.2 ha. The recent fallows and grassland were reduced to 4422.9 ha of the land area, while the lake covered an area of approximately 3434.9 ha of the total land area.

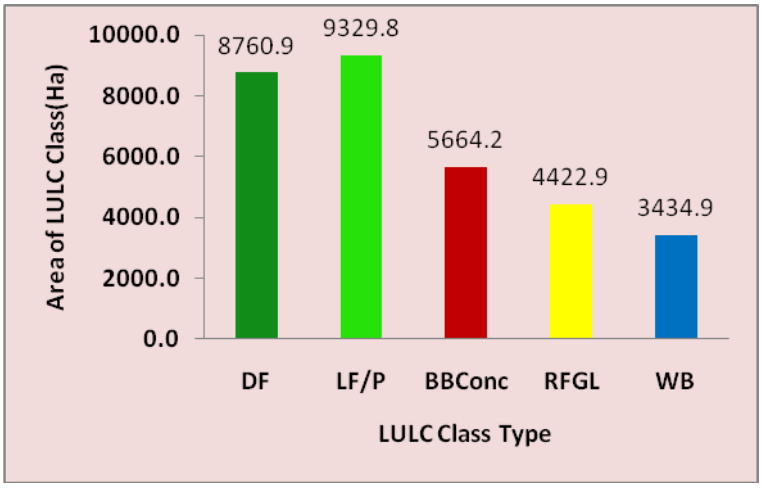

Figure 4: *The area of LULC (ha) for 2002*

The corresponding surface temperature ranged from a minimum of 24ºC (297K) to a maximum of 30ºC (303K), with the mean and standard deviation at 36ºC (308.5K) and 9K respectively. The surface temperature profile indicated an improved vegetated surface which had relatively reduced the surface heat fluxes, thereby, reducing the land surface temperature (Figure 5). This is *in tandem* with Coll et al. (2010)'s assertion that NDVI variables usually negatively correlate with the land surface temperature.

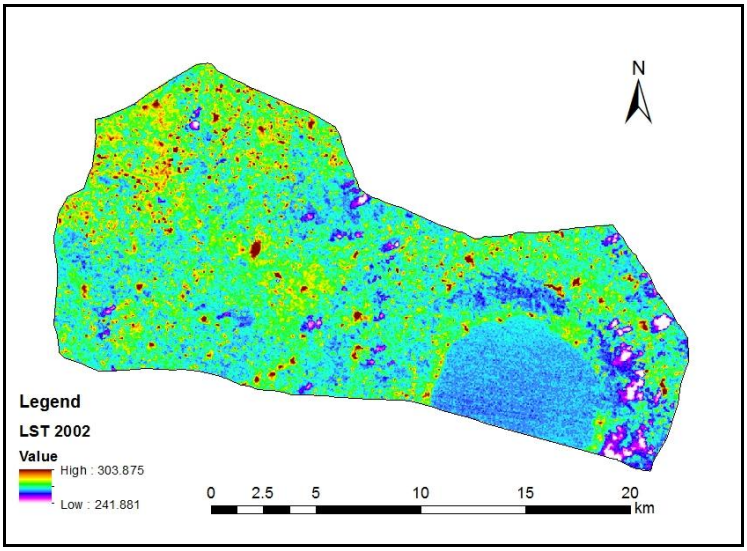

Figure 5: *The 2002 LST extracts showing the surface temperature fluxes*

4.3 Results from 2008 LULC and LST analyses

The land use classes for 2007 showed considerable increase in the DF cover constituting 10,299.9 ha of the total LULC classes in the area. The next cover in order of importance was RFG, which covered an area of 8434.9 ha. BBC surfaces ranked next in terms of coverage with 5451.2 ha. LF was next in terms of coverage importance with 5193.6 ha of the land area (Figure 6). An appreciable proportion of RFG was derived from the exposure of the land surfaces to agriculture and other modes of vegetation removal around the fringes of Lake Bosomtwe (Figure 7). A corresponding surface emission and reflectance translated into LST values ranging between 24ºC (297K) to 53ºC (326K). The mean temperature value was 38ºC (311.5K) and a standard deviation of 20.5K. This result explains; a relatively more rural than urban land use dynamics in the district. The rather high LST anomaly, however, was ostensibly due to the isolated patches of burnt-up surfaces emitting higher heat energy fluxes; in accordance of Stephan-Boltzmann law of surface emissivity (Irish et al., 2006). On the basis of this, the aggregate surface temperature values extracted from the 2008 satellite image gave credence to the rather higher aggregate surface maximum temperature values recorded than the aggregate maximum temperature recorded over the 2014 satellite image; even though, the latter year's built-up and paved surfaces were relatively higher than the former.

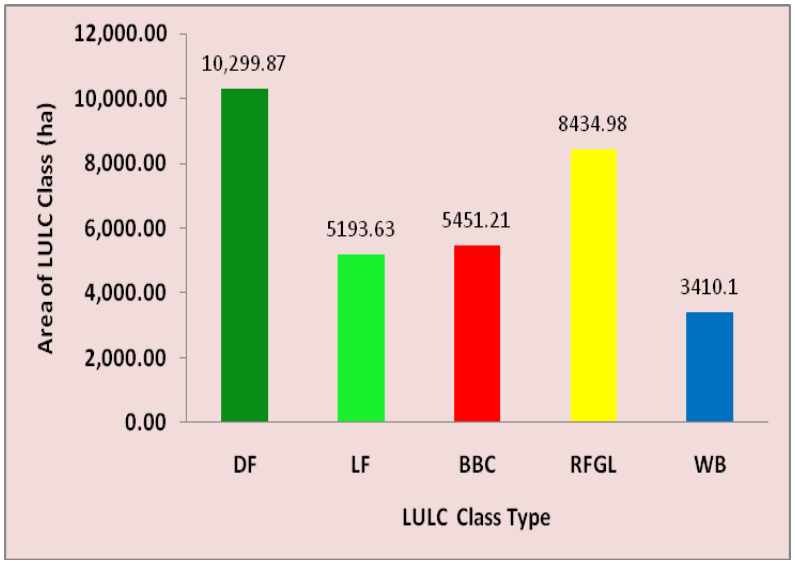

Figure 6: *The Area of LULC (ha) for 2008*

The temperature characteristics were in response to the surface vegetation removal. As human populations increase over time, the demand for land for residential and commercial uses other than forest and agriculture, dominates the landscape. Consequently, the surface becomes exposed to various degrees of heat energy fluxes from insolation with land surface features interactions (Jiménez-Muñoz, and Sobrino, 2013). The surface reflectance characteristics of the land use types, determine, to a greater extent the surface temperature profiles in accordance of the land surface emissivity and reflective capacities. This finding conforms to the result of Rozenstein et al. (2014), who studied global LST for the year for 2013, using at sensor brightness proxy, derived from Landsat with ASTER and AMSR-2 images.

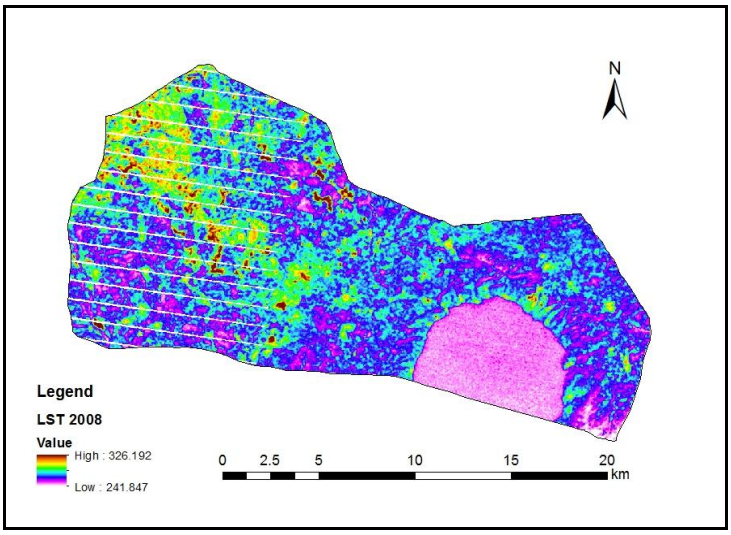

Figure 7: *2008 LST extracts showing the surface temperature fluxes*

4.4 Results from 2014 LULC and LST analyses

The 2014 image shows that the Bosomtwe district had experienced appreciable levels of land cover changes in terms of increasing BBC surfaces (Tursilowati et al., 2012). The LULC classes showed some startling revelation as far as the area coverage of the respective land uses was concerned (Baylis et al., 1999). Invariably, the BBC areas had increased with time up to the year 2014; this is evident by the many PuHT temperature profile, indicated by consistent peaking of the LST graphic for the 2014.

According to Appiah et al. (2015), in a similar work conducted in the study area, low forest cover maintained a high area of coverage with 10,947.83 ha of the total LULC. Recent fallows and grasslands were also next by area of coverage with 9366.75 ha. BBC surfaces, although showed an increase from observation, the statistics of 4596.93 ha by area coverage, indicated an apparent decrease in area from the 2010 image with 5454 ha; representing 14% of the total land area (Appiah et al. (2015). The area covered by the lake, WB, was 3424 ha of the total area (Figure 8).

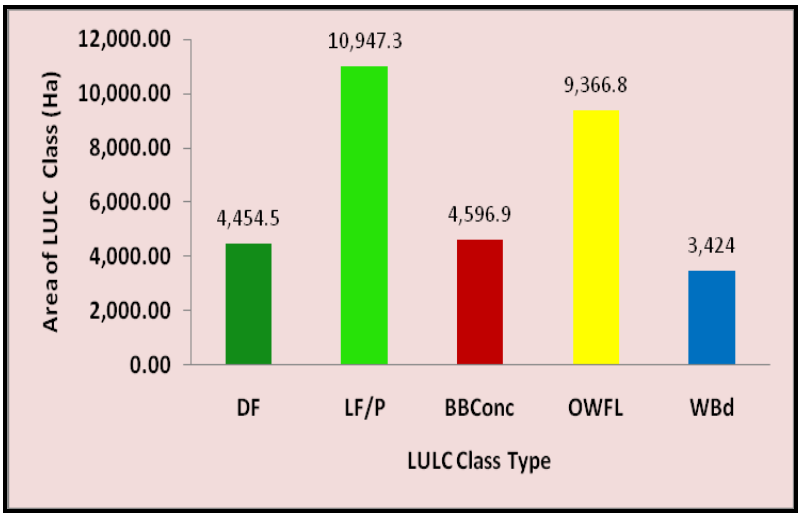

Figure 8: *The Area of LULC (ha) for 2014*

However, the classification scheme that included bare lands as part of the BBC areas resulted in a slower rate of increase in the BBC land uses, as certain parts of the bare lands were re-vegetated. In reality, therefore, the BBC land use type had been increasing with time. Field observations and other auxiliary statistical data, to support this claim for instance, showed increasing trends. Auxiliary data such as the number of houses recorded under the periods by the Ghana Statistical Services Population and Housing Census in 2010 has amply supported the fact that new residential houses increased from 12,399 to 15,525 between the years 2000 and 2010 (Tursilowati et al., 2012). This is indicative of increasing land surface temperature, associated, invariably, with increasing impervious surfaces (Yuan and Bauer, 2007). This was further evidenced by the relatively high LST of 37ºC (310 K) as compared to the minimum of 24 (297K).

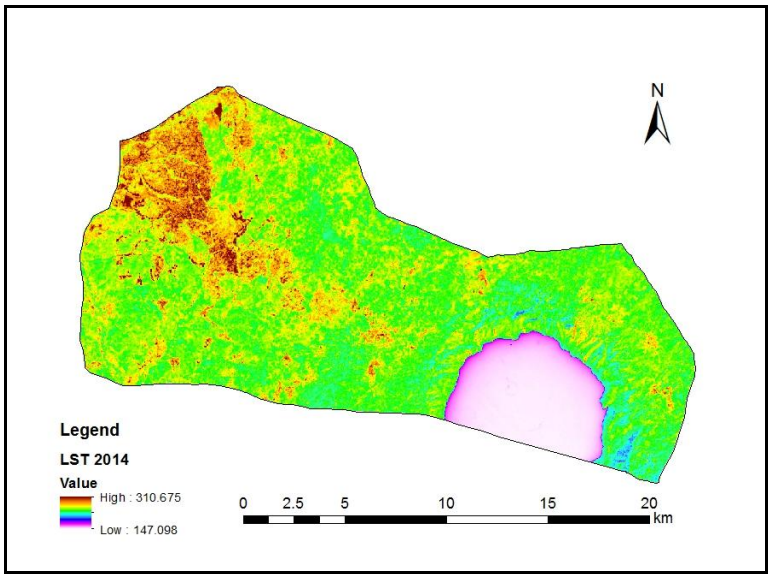

Figure 9: *2014 LST extracts showing the surface temperature fluxes*

The aggregated temperature values from the satellite image land surface temperature extractions are displayed in Figure 10 and Table 2. As indicated in the Figure 10, intermittent occurrences of peri-urban land uses create the heating troughs intervening the rural areas extending from east to west on the map area.

The changing LULC dynamics in the study area over the period under review indicated that there is a correlation between the land use conversion and modifications from one use type to another. As the LULC type changes, its corresponding surface energy emittance is reflected in the recording of the surface sensible heat. Certainly, the 2014 and the 2008 LST graphs depict the surface heat energy amplitude over the entire district, with the peaks indicating isolated pockets of PuHT, measured over the BBC areas. Usually, whenever the rural green and vegetated landscapes become converted into residential and other BBC uses, their surface energy fluxes are changed, and represented by the PuHT, which serves as the intervening energy flux between the RuCT and the ultimate fully-formed UHI; which is a future condition, using the business as usual LULC dynamics in the Bosomtwe district.

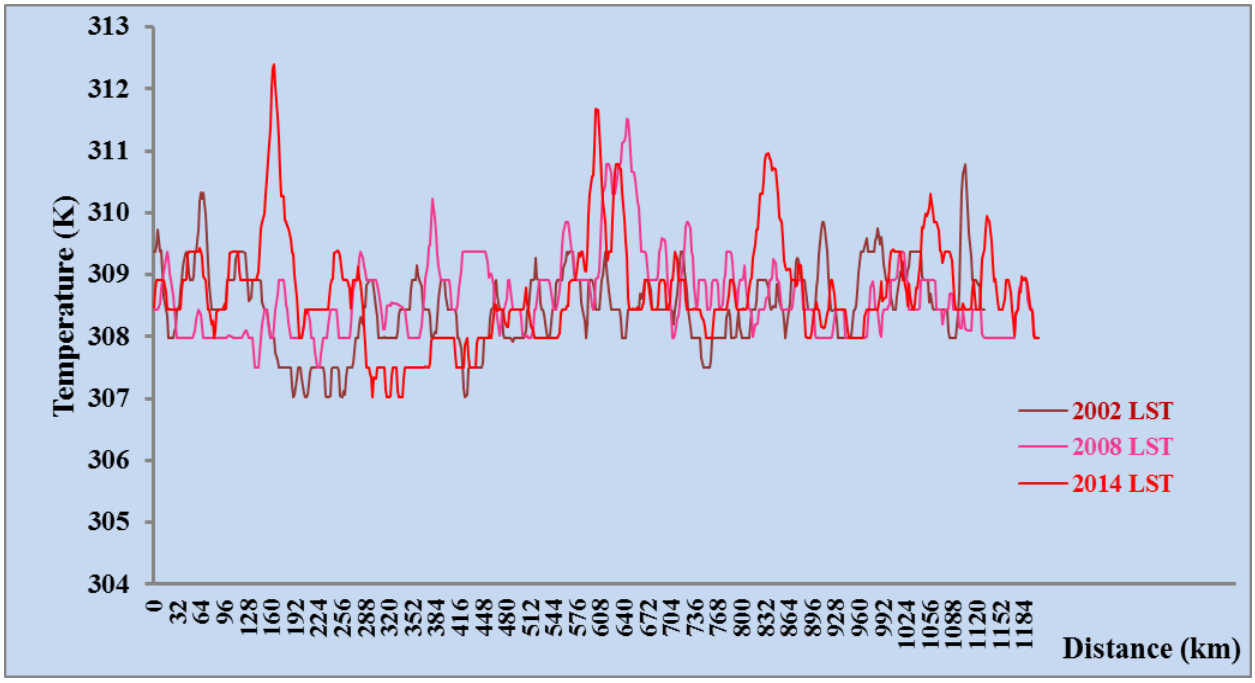

Figure 10: *The composite LST extracts for 2002, 2008 and 2014 showing the PuHT and RuCT areas*

Table 2: *Extracted Maximum, Minimum, Mean and Standard Deviation of Land Surface Temperature from Images*

Satellite Years	Max ºC (K)	Min ºC (K)	Mean ºC (K)
2002	30 (303)	24 (297)	27 (300)
2008	53 (326)	24 (297)	38 (312)
2014	37 (310)	24 (297)	31 (304)

The 12-year duration (2002-2014) also corresponded with an increase in the non-vegetative land uses; particularly, smallholding agriculture land for food crops production. The BBC as well as RFG, in comparison to the vegetated lands, such as the DF and LF covers, which also included some oil palm and citrus fruits plantations, actually increased. The composite statistics of LULC in terms of area in hectares is displayed in Figure 11.

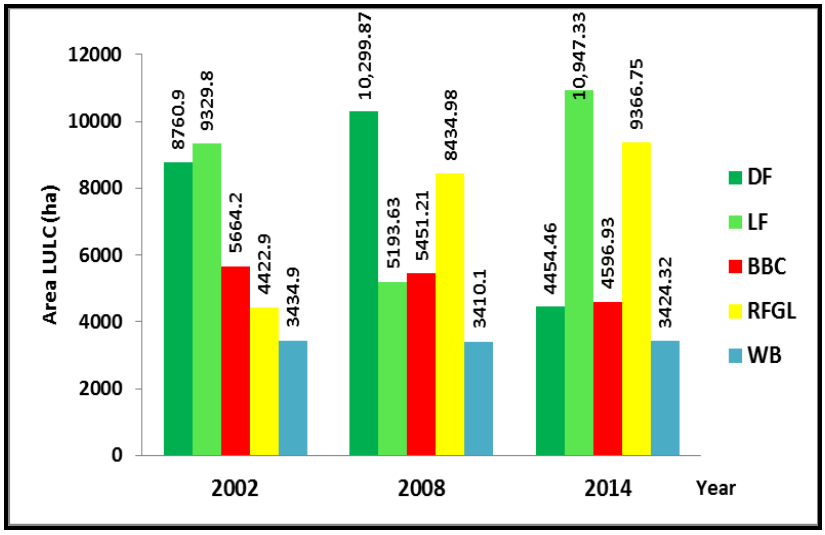

Figure 11: *Grouped bar graph of LULC area statistics in hectares*

4.5 Implications of LULC change on rural and peri-urban LST regimes

The LST regimes invariably corresponded with the LULC types, classified from the satellite images (2a—c). Areas with BBC land uses showed high emittance and reflectance for the records of high temperature profiles. These areas, according to Joshi and Bhatt (2011), are the causes of urban islands in highly dense built urban environments. In rural environments, however, the surface temperature characteristics were observed to be low in comparison to the urban areas. This observation was corroborated by (Ambinakudige, 2012) in a study of Bangalore, India, that anthropogenic activities alter the land cover and expose it to intense heating; thereby causing differential temperature regimes between the urban core and the rural outgrowth areas. The Bosomtwe district also demonstrates similar rural to urban temperature profile. By implication, as rural land uses are replaced by peri-urban BBC surfaces, they eventually become the potential driving forces of PuHT, with the tendencies to generate UHI conditions.

In this context, these PuHT conditions have higher likelihood of occurring in the fast-growing peri-urban towns in the district. Areas such as *Esereso, Jachie, Aputuogya, Kuntenase and Pramso* as shown in Figures 1 & 9, are likely to be influenced by their local micro-climates; and these are likely a function of the land use change dynamics. In the context of this study, an operational and postulated temperature threshold for the PuHT and RuCT in a tropical semi-deciduous climate zone, such as the Bosomtwe district was averaged at 31ºC (303K), which is 1ºC below the district's annual average.

The resultant effects of the changing temperature regime could be expressed in terms of reduced rainfall and increased temperature patterns for an area (Voogt and Oke, 2003). If this trend of LULC change continues into the future, a drastic near to full UHI is imminent in the rapidly urbanizing peri-urban fringes, considering business as usual scenarios. For replication, the temperature threshold values could be calibrated based on the type of climatic region under consideration. The associated land surface emissions from the various LULC types yielded corresponding LSTs, in consonance with a similar work by Kumar et al. (2016). This phenomenon, presents an opportunity for the formation of PuHT. When juxtaposed with the RuCT, there is the tendency for surface energy fluxes dissipation from the rural areas with high vegetation cover, to serve as carbon sinks that can regulate local surface warming effects (LSWE) (Maingi and Marsh, 2002; Boori et al., 2015).

The study has buttressed the fact that there exists a correlation between LULC emissivity and surface temperature profiles. These have tendencies to support the PuHT and RuCT concepts, proposed and espoused in this paper. The land surface configurations and their attendant variability in terms of temperature, suggest that the use of NDVI may not be an adequate measure of quantifying surface heat island (SUHI) systems; but with the addition of other approaches, this is reliable (Coll et al., 2010), (Ogashawara and Da Silva Brum Bastos, 2012), (Bhatt et al., 2013). To address this anomaly, Weng et al. (2004) postulated the use of vegetation fraction identified within a pixel. This is derived from a spectral combination of different LULC fragments, instead of solely relying on NDVI as a metric indicator. Their findings showed that vegetation fraction showed a moderate relationship with LST Appiah et al. (2015); Li et al. (2011) which coheres amply with the situation in the Bosomtwe district of Ghana.

4.6 Conclusion and Recommendation

This paper argued that, the transition from a rural to an urban area also exhibits a temperature profile that traverses through a RuCT through a PuHT, respectively, before achieving the ultimate UHI condition. The results obtained from the analyses of the LULC and the LST maps, have some land use and climate variability policy implications. The paper espouses that the land use pattern, in the Bosomtwe district's is changing from rural to peri-urban, through the replacement of the arable farm

lands and forest covers with built up concrete infrastructure. This observation, therefore, supports the PuHT and RuCT conditions that result from changing rural and peri-urban landscape configuration, as proposed by this study.

The land surface characteristics and their associated LST variability, suggest that the Bosomtwe district, a hitherto predominantly rural area is gradually becoming peri-urbanized. To address this anomaly, the implementation of the peri-urban land use policy framework of the Bosomtwe district assembly should be strictly enforced, where necessary. This would ensure that land uses that do not, as a matter of urgency require land use conversions from their original land use types such as forest covers and arable agricultural lands, would be preserved, to enhance surface cooling.

It is also proffered that in order to curtail the rapid development of PuHT systems, which are the fuelling cells of the UHIs; there is the need for the implementation of peri-urban greening and land use modification policy strategies. The implementation of these measures would serve as a mitigation measures that would preserve most of the rural landscape configuration, which would enhance more RuCT systems rather than the PuHTs that could adversely affect the local micro-climatic sub-system, with possible regional consequences on agriculture and other livelihood activities in the district.

A further investigation and the determination of an average temperature value as a threshold for the measurement of the RuCT and PuHT in tropical sub-humid climatic zones, where the study district is located is proffered, for further research.

Disclosures

All authors declare no conflict of interest in this paper.

Acknowledgement

The authors are grateful to the German Federal Ministry of Education (GMBF) through the West African Science and Service Centre of Climate Change and Adapted Land Use, for the financial support in the form of a scholarship for this study. We also thank the Department of Photogrammetry and Geoinformatics, Stuttgart University of Applied Sciences immensely, for the use of their Remote Sensing and GIS laboratory to get access to the current software for this study. We thank Ms Jemimah Abena Nyamekye and Patricia Aidoo for their proof-reading of the manuscript for the language and grammatical coherence. We finally thank the anonymous reviewers for their constructive critique of the paper.

References

Ahrens, C.D. 2005. *Essentials of Meteorology: An introduction to the Atmosphere*, 4th Edition, Belmont, USA: Thompson/Brooks/Cole, p.473.

Ambinakudige, S. 2011. Remote sensing of land cover's effect on surface temperatures: a case study of the urban heat island in Bangalore, India*. Applied Geographic Information System*, 7(1), pp.1-12.

Appiah, D.O., Adanu, S.K., Forkuo, E.K. and Bugri, J.T. 2015. Normalized Difference Vegetation Index Analysis of the Vegetation Cover in Bosomtwe Peri-Urban Settlement, Ghana*. Journal of Basic and Applied Research International*, 5(3), pp.146-156.

Appiah, D.O., Bugri, J.T. and Forkuo E.K. 2015. Modelling the Perspective of Agricultural Land Use Trajectories in a Peri-Urban District of Ghana. *Journal of Scientific Research & Reports*, 5(1), pp.16-31.

Appiah, D.O., Schroeder, D., Forkuo E.K. and Bugri, J.T. 2015. Application of Geo-Information Techniques in Land Use and Land Cover Change Analysis in a Peri-Urban District of Ghana. *International Journal of Geo-Information*, 4, pp.1265-1289.

Asmat, A., Mansor, S., Saadatkhah, N., Adnan, N.A. and Khuzaimah, Z. 2016. Land Use Change Effects on Extreme Flood in the Kelantan Basin Using Hydrological Model. Springer, ISFRAM, pp.221-236. DOI: 10.1007/978-981-10-0500-8_18.

Baylis, M., Meiswinkel, R. and Venter, G.J. 1999. A preliminary attempt to use climate data and satellite imagery to model the abundance and distribution of Culicoides imicola (Diptera: Ceratopogonidae) in Southern Africa. *Journal of the South African Veterinary Association*, 70(2), pp.80-89.

Bhatt, U.S., Walker, D.A., Raynolds, M.K., Bieniek, P.A., Epstein, H.E., Comiso, J.C., Pinzon, J.E., Tucker, C.J. and Polyakov, I.V. 2013. Recent Declines in Warming and Vegetation Greening Trends over Pan-Arctic Tundra. *Remote Sensing*, 5, pp.4229-4254.

Blake, R., Grimm, A., Ichinose, T., Horton, R., Gaffin, S., Jiong, S., Bader, D., and Cecil, L.D. nd. *Urban climate: Processes, trends, and projections. Climate Change and Cities: First Assessment Report of the Urban Climate Change Research Network*, In: C. Rosenzweig, W.D. Solecki, S.A. Hammer, S. Mehrotra (eds.), Cambridge, UK: Cambridge University Press, pp.43-81.

Bonan, G.B., Oleson, K.W. and Vertenstein, M. 2002. The land surface climatology of the community land model coupled to the NCAR community climate model. *Journal of Climatology*, 15, pp.3123-3149.

Boori, M.S., Balzter, H., Choudhary, K. Kovelskiy, V. and Vozenilek, V. 2015. *A Comparison of Land Surface Temperature, Derived from AMSR-2, Landsat and ASTER Satellite Data. Journal of Geography and Geology*, 7(3), 61-69.

Butt, A., Shabbir, R., Ahmad, S.S. and Aziz, N. 2015. Land use change mapping and analysis using Remote Sensing and GIS: A case study of Simly watershed, Islamabad, Pakistan. *The Egyptian Journal of Remote Sensing and Space Sciences*, 18, pp.251-259.

Carnahan, W.H. and Larson, R.C. 1990. An analysis of an urban heat sink. *Remote Sensing of Environment*, 33, pp.65-71.

Chander, G. and Markham, B. 2003. Revised Landsat-5 TM Radiometric Calibration Procedures and Post-calibration Dynamic Ranges. *IEEE Transactions on Geoscience and Remote Sensing*, 41(11), pp.2674-2677.

Chen, X-L., Zhao, H-M., Li, P-X. and Yin, Z-Y. 2006. Remote sensing image-based analysis of the relationship between urban heat island and land use/cover changes. *Remote Sensing of Environment*, 104, pp.133-146.

Coll, C. Galve, J.M., Sánchez, J.M. and Caselles, V. 2010. Validation of Landsat-7/ETM+ Thermal-Band Calibration and Atmospheric Correction with Ground-Based Measurements. *IEEE Transactions on Geoscience and Remote Sensing,* 48(1), pp.547-555.

Coll, C., Caselles, V. and Galve, J.M. 2005. Ground measurements for the validation of land surface temperatures derived from AATSR and MODIS data. *Remote Sensing of Environment*, 97, pp.288-300.

Cristobal, J., Jimenez-Munoz, J.C., Sobrino, J.A., Ninyerola, M. and Pons, X. 2009. Improvements in land surface temperature retrieval from the Landsat series thermal band using water vapor and air temperature. *Journal of Geophysical Research*, 114, pp.841-846, doi: 10.1029/2008JD010616.

Dousset, B. and Gourmelon, F. 2003. Satellite multi-sensor data analysis of urban surface temperatures and land cover. *Photogrammetry and Remote Sensing*, 58, pp.43-54.

ElMagd, I.A., Ismail, A. and Zanaty, N. 2016. Spatial Variability of Urban Heat Islands in Cairo City, Egypt using Time Series of Landsat Satellite Images. *International Journal of Advanced Remote Sensing and GIS*, 5, pp.1618-1638. doi:10.23953/cloud.ijarsg.48

Iino, A. and Hoyano, A. 1996. Development of a method to predict the heat island potential using remote sensing and GIS data. *Energy Building*, 23, pp.199-205.

Irish, R.R., Barker, J.L., Goward, S.N. and Arvidson, T. 2006. Characterization of the Landsat-7 ETM Automated Cloud-Cover Assessment (ACCA) Algorithm. *Photogrammetric Engineering and Remote Sensing*, 72(10), pp.1179-1188.

Jiménez-Muñoz, J.C, Sobrino, J.A., Gillespie, A., Sabol, D. and Gustafson, W.T. 2006. Improved land surface emissivities over agricultural areas using ASTER NDVI. *Remote Sensing of Environment*, 103, pp.474-487.

Jiménez-Muñoz, J.C. and Sobrino, J.A. 2013. A generalized single-channel method for retrieving land surface temperature from remote sensing data. *Journal of Geophysical Research*, 108(D22), pp.1-9.

Joshi, J.P. and Bhatt, B. 2012. Estimating temporal land surface temperature using remote sensing: a study of Vadodara urban area, Gujarat. *International Journal of Geology, Earth and Environmental Sciences,* 2(1), pp.123-130.

Kepner, W.G., Watts, C.J., Edmonds, C.M., Maingi, J.K., Marsh, S.E. and Luna, G. 2000. A Landscape Approach for Detecting and Evaluating Change in a Semi-arid Environment. *Environmental Monitoring and Assessment*, 64(1), pp.179-195.

Khang, Y., Khan, S. and Ma, X. 2009. Climate change impacts on crop yield, crop water productivity and food security– A review. *Progress in Natural Science*, 19(12), pp.1665-1674.

Kumar, S.K., Bhaskar, P.U. and Kumari, K.P. 2016. Emerging Urban Heat Islands in the New Capital Region of Andhra Pradesh, India - A Satellite based Evaluation. *International Journal of Advanced Remote Sensing and GIS*, 5, pp.1915-1929. doi:10.23953/cloud.ijarsg.69

Li, J., Song, C., Cao, L., Zhu, F., Meng, X. and Wu, J. 2011. Impacts of landscape structure on surface urban heat islands: A case study of Shanghai, China. *Remote Sensing of Environment*, 115, pp.3249-3263.

Lipton, A.E. and Ward, J.M. 1997. Satellite-view biases in retrieved surface temperatures in mountain areas. *Remote Sensing of Environment*, 60, pp.92-100.

Liu, L. and Zhang, Y. 2011. *Urban Heat Island Analysis Using the Landsat TM Data and ASTER Data: A Case Study in Hong Kong*. Remote Sensing, 3, 1535-1552.

Maingi, J.K. and Marsh, S.E. 2002. An Accuracy Assessment of 1992 Landsat-MSS Derived Land cover for the Upper San Pedro Watershed (U.S./Mexico); United States Environmental Protection Agency: Washington, DC, USA, 2002; 29p.

Mbithi, D.M., Demessie, E.T. and Kashiri, T. nd. The impact of Land Use Land Cover (LULC) changes on Land Surface Temperature (LST); a case study of Addis Ababa City, Ethiopia. Kenya Meteorological Services, Laikipia Airbase, Kenya, 8pp.

Meehl, G.A., Stocker, T.F. and Collins, W.D. 2007. Global climate projections. In: Solomon, S., Qin, D., Manning, M., et al., (eds.), *Climate change 2007: the physical science basis*. *Contribution of working group I to the fourth assessment report of the intergovernmental panel on climate change.* Cambridge: Cambridge University Press, p.749-844.

Mousivand, A., Verhoef, W., Menenti, M. and Gorte, B. 2015. Modelling top of atmosphere Radiance over Heterogeneous Non-Lambertian Rugged Terrain. *Remote Sensing*. 2015. 7, pp.8019-8044.

Ogashawara, I. and Da Silva Brum Bastos, V.A. 2012. Quantitative Approach for Analyzing the Relationship between Urban Heat Islands and Land Cover. *Remote Sensing*, 4, pp.3596-3618.

Quattrochi, D.A., Luvall, J.C., Rickman, D.L., Estes Jr., M.G., Laymon, C.A. and Howell, B.F. 2000. A decision support information system for urban landscape management using thermal infrared data. *Photogrammetric Engineering and Remote Sensing*, 66, pp.1195-1207.

Rajeshwari, A. and Mani, N.D. 2014. Estimation of land surface temperature of Dindigul District using Landsat 8 data. *International Journal of Research in Engineering and Technology*, 3(5), pp.122-126.

Rozenstein, O., Qin, Z., Derimian Y. and Karnieli, A. 2014. Derivation of Land Surface Temperature for Landsat-8 TIRS Using a Split Window Algorithm. *Sensors*, 14, pp.5768-5780.

Sobrino, J.A., El Kharraz, J. and Li, Z-L. 2003. Surface temperature and water vapour retrieval from MODIS data. *International Journal of Remote Sensing*, 24, pp.5161-5182.

Sobrino, J.A., Jiménez-Muñoz, J.C. and Paolini, L. 2004. Land surface temperature retrieval from LANDSAT TM 5. *Remote Sensing of Environment*, 90, pp.434-440.

Srivastava, P.K., Majumdar, T.J. and Bhattacharya, A.K. 2010. *Study of land surface temperature and spectral emissivity using multi-sensor satellite data*. *Journal of Earth System Sciences*, 119(1), pp.67-74.

Thomas, A. 2008. Agricultural irrigation demand under present and future climate scenarios in China. *Global Planetary Change*, 60, pp.306-326.

Tursilowati, L., Sri Sumantyo, J.T., Kuze, H. and Sri Adiningsih, E. 2012. Relationship between Urban Heat Island Phenomenon and Land Use/Land Cover Changes in Jakarta-Indonesia. *Journal of Emerging Trends in Engineering and Applied Sciences*, 3(4), pp.645-653.

Urban, A., Davídkovov, H. and Kysley, J. 2013. Heat- and cold-stress effects on cardiovascular mortality and morbidity among urban and rural populations in the Czech Republic. *International Journal of Biometeorology,* 58(6), pp.1057-1068.

USGS. 2015. Using the USGS Landsat 8 Product. Accessed on 28 January 2016 at http://landsat.usgs.gov/Landsat8_Using_Product.php

Vlassova, L., Pérez-Cabello, F., Mimbrero, M.R., Llovería, R.M. and García-Martín, A. 2014. Analysis of the Relationship between Land Surface Temperature and Wildfire Severity in a Series of Landsat Images. *Remote Sensing*, 6, pp.6136-6162.

Voogt, J.A. and Oke, T.R. 2003. Thermal remote sensing of urban climates. *Remote Sensing of Environment,* 86, pp.370-384.

Weng, Q. 2001. A remote sensing–GIS evaluation of urban expansion and its impact on surface temperature in the Zhujiang Delta, China. *International Journal of Remote Sensing*, 22(10), 1999-2014.

Weng, Q., Lu, D. and Schubring, J. 2004. Estimation of land surface temperature–vegetation abundance relationship for urban heat island studies. *Remote Sensing of Environment*, 89, pp.467-483.

Widyasamratri, H., Souma, K., Suetsugi T., Ishidaira H., Ichikawa Y., Kobayashi H. and Inagaki I. 2013. *Air Temperature Estimation from Satellite Remote Sensing to Detect the Effect of Urbanization in Jakarta, Indonesia*. *Journal of Emerging Trends in Engineering and Applied Sciences*, 4(6), pp.800-805.

Yuan, F. and Bauer, M.E. 2007. Comparison of impervious surface area and normalized difference vegetation index as indicators of surface urban heat island effects in Landsat imagery. *Remote Sensing of Environment,* 106, pp.375-386.

Cloud Publications
International Journal of Advanced Remote Sensing and GIS
2017, Volume 6, Issue 1, pp. 2156-2170
ISSN 2320 – 0243, Crossref: 10.23953/cloud.ijarsg.263

Case Study | Open Access

Innovative use of Geo-informatics Technology in e-Governance for District Urban Development Agency (DUDA), Narmada District, Gujarat State

Rakesh Shankar[2], Jinkal Prajapati[2], Ajay N. Patel[1], Krunal Patel[1], Manik H. Kalubarme[1]

[1]Bhaskaracharya Institute for Space Applications and Geo-informatics (BISAG), Department of Science & Technology, Government of Gujarat, Gandhinagar 382007, Gujrat, India
[2]Collector Office, Narmada district, Government of Gujarat, India

Publication Date: 30 May 2017

DOI: https://doi.org/10.23953/cloud.ijarsg.263

Abstract In order to make the process of monitoring government schemes and municipal activities more rational and transparent, geo-informatics based Municipality Decision Support System (DSS) has been developed by creating the database of all the municipal activities. The municipality DSS is a dynamic web-based system aimed at supporting decision makers take optimal decisions on various municipality activities such as resource prepositioning, gap analysis, prioritization, and resource optimization along with the day-to-day tasks to be accomplished by concerned officials. The main purpose of this software was to help the municipal authorities for various operations like: i) planning and development, ii) transparency of operations, iii) equal distribution of public funds, iv) implementation of various schemes under direct supervision of the municipal authorities. In the present study, Indian Remote Sensing Satellite (IRS) LISS-III (24 m resolution) and LISS-IV (5.8 m resolution) data covering the study area have been used for preparation of various thematic layers. Good governance is being recognized as an important goal by many countries across the world. Gujarat is a frontline State in the implementation of e-governance policies & projects and setting up of key infrastructure for e-Governance. The major vision of e-governance in Gujarat state is Minimum Government, Maximum Governance and institutionalizes 'Digital Gujarat' – towards the fulfillment of the larger vision of 'Digital India'. Every urban area needs GIS – a comprehensive map-based Geographical Information Systems (GIS) that powers urban planning and urban management. Therefore, the major vision of DUDA GIS was to develop a decentralized Ward Level e-Governance System and Web Based Monitoring System for the Municipality. For this purpose municipality needs a detailed and reliable digital database in Geographical Information System (GIS).

Keywords *e-Governance; Digital Gujarat; Decision Support System (DSS); dynamic web-based system; Indian Remote Sensing Satellite (IRS) LISS-IV (5.8 m resolution); sustainable development and inclusive growth of the State*

1. Introduction

In India during next decade, nearly fifty per cent of the population will be living in urban areas which will have a great challenge for urban development and management. This large scale urbanization will require to plan and develop urban areas in a systematic manner for improved quality of life in the urban areas. One of the major requirements for urban development is to have the accurate and timely information in geospatial forms that allows generation and use of different maps, GIS data and applications. Information of urban areas that characterizes the Social and Economic environment, Physical environment, services and amenities are critical in planning and development of urban areas. At the same time, the urban area also requires Urban Management as details of town planning or municipal functions – especially, regulation of land uses, building by-laws for management activities in urban planning, taxation and revenue, urban amenities planning, urban infrastructure management etc. Every urban area needs GIS – a comprehensive map-based Geographical Information Systems (GIS) that powers urban planning and urban management. The GIS must meet the needs of the city – at different levels of administration/planning/management, be based on modern data sources such as satellite and GIS databases, provide GIS-Decision Support System (DSS) for urban planning/management (www.mapmyindia.com). An overview of DSS in the area of solid waste management with specific reference to their development and applications in India has concisely been presented by Ohri and Singh, 2010.

1.1. Developments in the area of e-Governance in India

Among developing countries, India has been an early adopter of e-governance. The first wave can be considered to have evolved bottom-up. The Gyandoot project in Dhar district, which begun in 2000, and the successful effort during 2000-05 of e-governance in India, was Rural e-Seva in West Godavari district of Andhra Pradesh, were considered the forerunners in this direction. The second phase of e-governance in India started with inauguration of the National E-Governance Plan (NeGP) in 2006. Decentralization, right to information and community monitoring, as other three key areas of governance reform in India apart from e-governance, all aim at greater bottom-up participation, and accountability (Singh, 2012).

1.2. Citizen Centric e-Governance for India

Good governance is being recognized as an important goal by many countries across the world. These countries have taken up specific initiatives for open government. Freedom of information is being redefined and supported by detailed guidelines. The Internet revolution has proved to be a powerful tool for good governance initiatives. An important dimension of the Internet potential is the possibility of providing anytime-anywhere services. e-Governance has to be citizen friendly. Delivery of services to citizens is considered a primary function of the government (Abdul Kalam, 2014).

The ambitious Direct Benefit Transfer (DBT) system of the Government of India has been envisaged as a radical transformation in service delivery that bypasses the inefficiencies that traditional service delivery mechanisms have faced. Under the system, funds are transferred by banks directly to bank accounts of beneficiaries. These accounts are Aadhaar-enabled, in that they are linked to the beneficiary's Aadhaar number. Beneficiaries can link their existing bank accounts or open new accounts, even no-frill ones, using their Aadhaar number. The entire process of fund disbursal to beneficiary accounts is instantaneous (Abdul Muheet Chowdhary, 2014.)

1.3. e-Governance Activities in Gujarat State

Awarded for best e-Governance, Gujarat is a frontline State in the implementation of e-Governance policies & projects and setting up of key infrastructure for e-Governance. Gujarat Government focuses

on growth and development of new & emerging technology areas. It has been increasingly using the ICT (Information and Communication Technologies) to offer citizen based service as per convenient location with an initiative to improve the reach, make services more transparent and reduce response time with reducing costs. The Government is also proactive in its Initiatives and ranks first state in the country to have made e-Governance functional in all its Municipalities and Municipal Corporations (www.gujaratindia.com/).

The major vision of e-governance in Gujarat state is Minimum Government, Maximum Governance and institutionalizes 'Digital Gujarat' – towards the fulfillment of the larger vision of 'Digital India'. It also aims at ICT-enabled all-round sustainable development and inclusive growth of the State; to provide transparent, affordable and efficient public service delivery closer to the doorstep of citizens; and to ensure the socio-economic empowerment of all through Digital Inclusion (www.vibrantgujarat.com/).

On June 23, the Chief Minister's Office (CMO), Gujarat, won the prestigious 2010 United Nations Public Service Award (UNPSA) for innovative use of information technology to address public grievances. Major eGovernance and reach of initiatives include: i) Implementation of IT strategies to accomplish effective eGovernance, ii) Integrated Workflow and Document Management System (IWDMS) is implemented across the Government Secretariat, which increases Accountability, Transparency and Effectiveness in Government administration, iii) State Wide Attention on Public Grievances by Application of Technology (SWAGAT), etc. (www.csinihilent-egovernanceawards.org/publications/SectionIII.pdf).

1.4. Concept of District Urban Development Agency (DUDA) GIS for Rajpipla

For effective implementation of a considerable number of infrastructure and social sector programs by the Urban Local Bodies, it has become essential to develop a proper mechanism at the district level to oversee and monitor the implementation of the programs by the Urban Local Bodies. Therefore, the major vision of DUDA GIS was to develop a decentralized Ward Level e-Governance System and Web Based Monitoring System for the Municipality. For this purpose municipality needs a detailed and reliable digital database in Geographical Information System (GIS). This will help the municipality to identify deficiencies both quantitatively and geographically in the field of physical infrastructure, health, education, shelter and economy, enabling the municipality to plan in a holistic manner. For proper planning and monitoring the Municipality activities the DUDA GIS System (DGS) was inaugurated by Chief Minister of Gujarat State. The main purpose of this software was to help the municipal authorities for various operations like: i) planning and development, ii) transparency of operations, iii) equal distribution of public funds, iv) and v) implementation of various schemes under direct supervision of the municipal authorities.

1.5. Key Functions of DUDA GIS

Rapid urbanization has led to basic infrastructural issues in urban areas. To mitigate these problems and facilitate urban populace with the superior quality of Infrastructure as well as to materialize the Dream of "Clean Gujarat - Nirmal Gujarat" - the Integration & coordination of various urban development polices and schemes was quite essential. Municipal GIS for DUDA provides information to about the wards and facilities available, various schemes executed by the government, grievances redressal system besides facilitating administrators/planners to have a one stop online planning tools towards better governance.

For effective implementation of a considerable number of infrastructure and social sector programmes by the Urban Local Bodies, it has become essential to develop a proper mechanism at the district level to oversee and monitor the implementation of the programmes by the Urban Local Bodies. Accordingly, DUDA GIS was conceptualized by the Narmada Collector through technical support from

the Bhaskaracharya Institute of Space Applications and Geo-Informatics (BISAG), Department of Science & Technology, Govt. of Gujarat, Gandhinagar. The key functions of DUDA GIS are as follows:

- To allocate grants to Municipality of the district under various urban development schemes.
- Ensure quality standards of development and infrastructural works in municipal areas.
- Regular reviews and evaluation of various urban development schemes and works at district-level.
- To follow orders and instructions from State-level Nodal Agency for Urban development.
- To check progress of the infrastructural works at regular interval.
- To coordinate and correspond with banks for speedy sanctioning of loans/subsidies to urban poor.
- To ensure effective and efficient utilization of allocated grants and resources in achieving desired outcome with respect to various urban development schemes.

1.6. Location of the Narmada District

Narmada district is situated in the south of Gujarat State and surrounded by Vadodara, Bharuch and Surat districts. The district is spread over 2775 sq.km, having four talukas with 552 villages, two town and 221 panchayats. The four talukas are Sagabara, Dediapada, Nandod and Tilakwada. All four taluka predominantly tribal areas and overall tribal population of the district is 78%. Nearly 90 percent population resides in villages. Nandod (Rajpipla) is the only urban centre of Narmada district which is spread over 15 km with municipal corporation class “C” as Urban Local Bodies. The Location map of the study area in Narmada district is given in Figure 1.

2. Objectives of the Study

The major objectives of development of DUDA GIS for proper planning and monitoring the Municipality activities using Geo-informatics Technology are follows:

- To create detailed and reliable database of entire municipality activities in GIS.
- To provide comprehensive e-governance solutions for facilitating and tracking the municipality activities.
- To identify deficiencies both quantitatively and geographically in the field of physical infrastructure, health, education, shelter and economy, enabling the municipality to plan in a holistic manner.
- To monitor allocation of funds to different areas, avoid duplication of grants, and organize the work in a comprehensive manner for balanced development.

3. Methodology

3.1. Satellite Data Used

In the present study, Indian Remote Sensing Satellite (IRS) LISS-III (24 m resolution) and LISS-IV (5.8 m resolution) data covering the study area have been used for preparation of various thematic layers of settlements, transport network, drainage, water bodies, thematic land use / land cover etc. The details of Satellite data products are given in Table 1.

Table 1: *Indian Remote Sensing Satellite (IRS) LISS-IV and LISS-III Data used for Rajpipla Town in Narmada District*

Satellite (Sensor)	Spectral Bands (µm)	Resolution (m)	Swath (km)	Path / Row	Date of pass
IRS LISS-IV	0.52 – 0.59 0.62 – 0.68 0.77 – 0.86	5.8	70 X 70	94 /57	17Mar-2015
IRS LISS-III		24	140 X 140	94/57	17Mar-2015

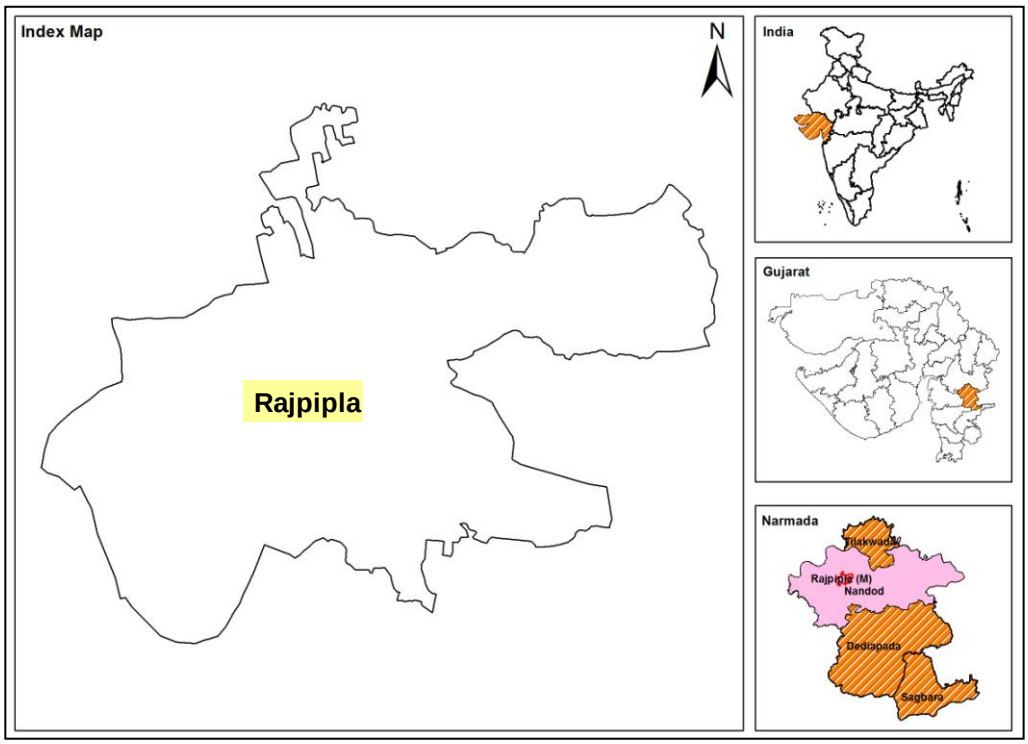

Figure 1: *Location of Rajpipla Town in Narmada district, Gujarat State*

Google image covering Rajpipla town in Narmada district was also used to study the land use pattern. The Goggle image covering Rajpipla in Narmada district is given in Figure 2 and IRS LISS-IV image covering Rajpipla town is given in Figure 3.

Figure 2: *Google image covering Rajpipla Town, Narmada District*

3.2. Departmental Data used

The municipal data related to various amenities and services, infrastructure etc. was collected from Rajpipla Municipal Corporation. Transport network and details about road conditions was collected from the Road and Building Department. The census data was also collected from the Rajpipla Municipal Corporation.

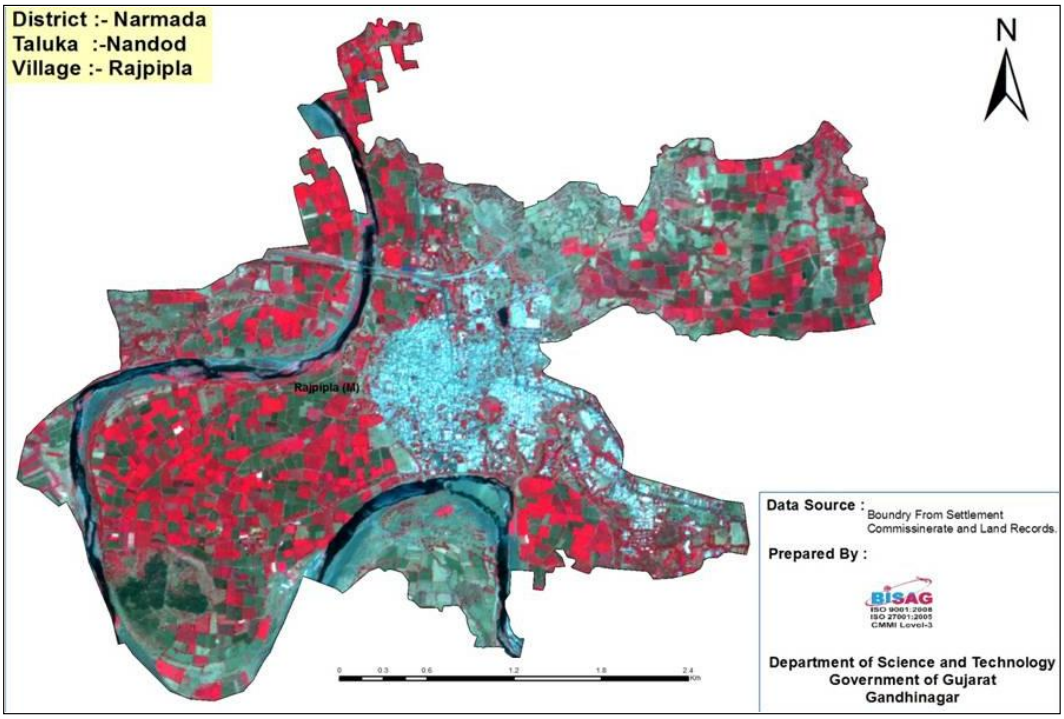

Figure 3: *IRS LISS-IV image covering Rajpipla Town, Narmada District*

3.3. Generation of Various Thematic Layers

Geographic Information System (GIS) is an important and efficient tool that can be used by local administrations for monitoring the Municipality developmental activities. In order to monitor the implementation of various town development schemes and to monitor the progress of various municipality activities, GIS layers and other associated thematic maps have been created for each of the wards and development activities in the Rajpipla town. The list of various GIS layers created as base administrative layers and other dependant layers for generation of Decision Support System for Rajpipla Municipality is as follows:

Taluka/ Block administrative boundary ii) boundary layers of various wards in Rajpipla town, iii) main road and minor roads road networks, iv) locations of villages, with their names, v) mapping of residential, commercial and industrial built-up areas, vi) census population data (2011) vii) Geographical locations (latitude, longitude) of various ongoing operational municipality works viii) demarcation of development plans and ongoing repairs or developmental works from the municipal corporation.

3.4. Concept of Decision Support System (DSS)

Decision Support System (DSS) is a computerized information system that supports decision making activities in a logical way based on scientific database. The useful information is compiled from the raw database to identify and solve problems and suggests appropriate decisions. The basic structure of a DSS consists of three components: database management, model base management, and user interface (Bani et al., 2009).

In order to make the process of monitoring government schemes and municipal activities more rational and transparent, geo-informatics based Municipality Decision Support System (DSS) has been developed by creating the database of all the municipal activities. The municipality DSS is a dynamic web-based system aimed at supporting decision makers take optimal decisions on various municipality activities such as resource prepositioning, gap analysis, prioritization, and resource optimization along with the day-to-day tasks to be accomplished by concerned officials. Using these geo-spatial databases, various municipality on-going and completed functional activities can be visualized and progress of the work can be monitored by the municipal authorities. The DSS is the state-of-the-art and is the most suitable solution for municipality activities. This is a Web based application built using .NET Framework 3.5 utilizing the GIS capabilities of an open source GIS Platform. This is an Object Oriented Programming model with loose coupling between various layers, which provides support for query and render the spatial data view, query and update capabilities so that users can update database. This also provides the facility to view and query the outputs in a tabular format as well as thematic map generator to visualize the various municipal activities on the thematic maps.

4. Results and Discussion

4.1. Satellite Data Analysis

The IRS LISS-IV data along with departmental maps was analyzed for creation of GIS database base of various thematic using open source GIS software. These maps were prepared on 1:5,000 scales for Rajpipla town. In the present study, two scenes of IRS-P6 LISS-IV (5.8 m resolution) data of January 2011 and March 2011 have been used for various thematic interpretations. The IRS satellite LISS-IV data have been extensively used for base map updating of settlement, transport network, drainage, water bodies, etc. in the town. The satellite data was also geo-referenced with the various departmental maps for urban land use classification like identification of residential, commercial, industrial areas etc. in the Rajpipla town.

4.2. Development Decision Support System (DSS) For DUDA

The major vision of the DUDA GIS was to develop a decentralized Ward Level e-Governance System and Web Based Monitoring System for the Municipality. This helps to monitor various activities of the municipality in dynamic and transparent mode. The DUDA GIS portal and boundaries of various wards and their numbers are given in Figure 4. This DUDA GIS portal includes all the GIS layers of most of the municipality activities which can be visualized as well as monitoring just by clicking the specific icons created on this portal.

4.3. Monitoring of Road Condition

Various infrastructures, amenities and services etc. was digitized using the data collected from Rajpipla Municipal Corporation. Transport network along with type of the road i.e. cement concrete and tar roads and details about road conditions was collected from the Road and Building Department. The roads with bad condition as well as work in progress and completed on these bad roads was also monitored using the DUDA GIS. The type of the road and condition of the road mapped from departmental data is given in Figure 5 and Figure 6.

4.4. Monitoring water Supply pipe lines and Source of water

The water supply sources like tube-wells and Elevated Storage Reservoirs (ESR) along with the location of sluice valves in the Rajpipla town were mapped from the data collected Rajpipla Municipal Corporation. The status of pipeline in terms of its diameter size, its length and their connectivity to water supply sources as well as sluice valves were also mapped in GIS environment. The status of pipe lines along with damage to pipe lines and the status of progress of repair work were mapped. In case of failure of water supply from one of the ESR to a particular locality, the alternate connection to nearby ESR along with diversion of water supply through another pipe line connection and alternate sluice valve locations were also mapped. The water supply sources, pipeline size along with location of sluice valves is given in Figure 7.

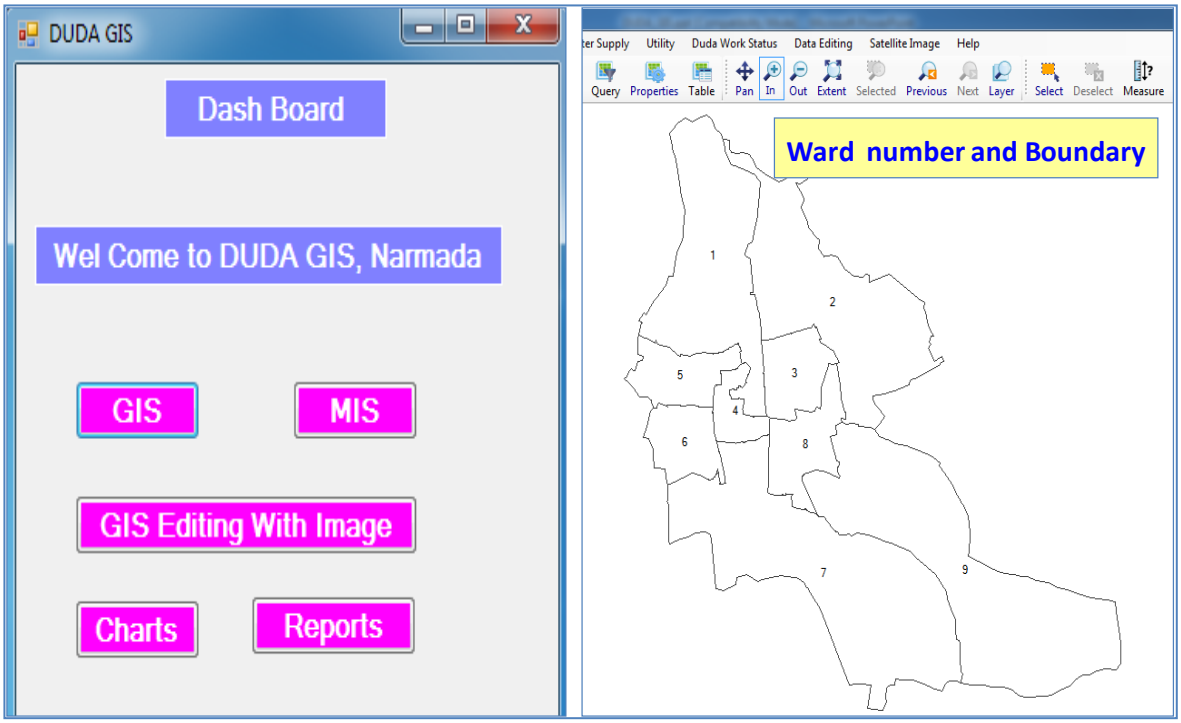

Figure 4: *DUDA GIS Portal and Ward boundaries of Rajpipla Town*

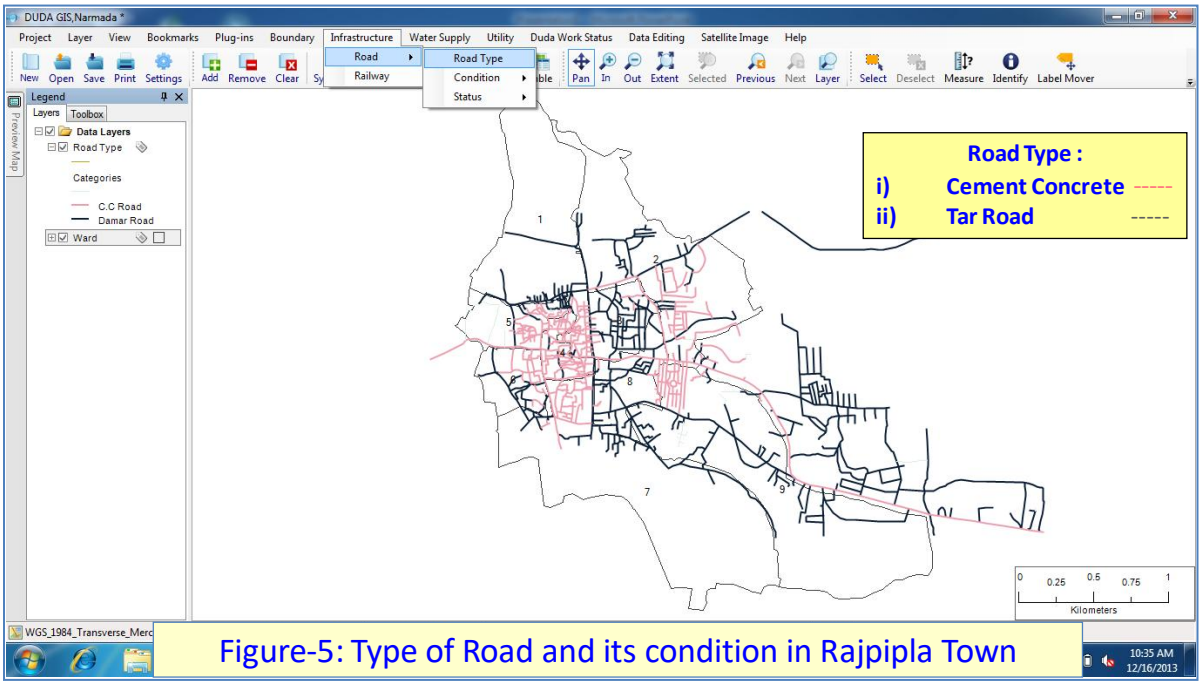

Figure 5: *Type of Road and its condition in Rajpipla town*

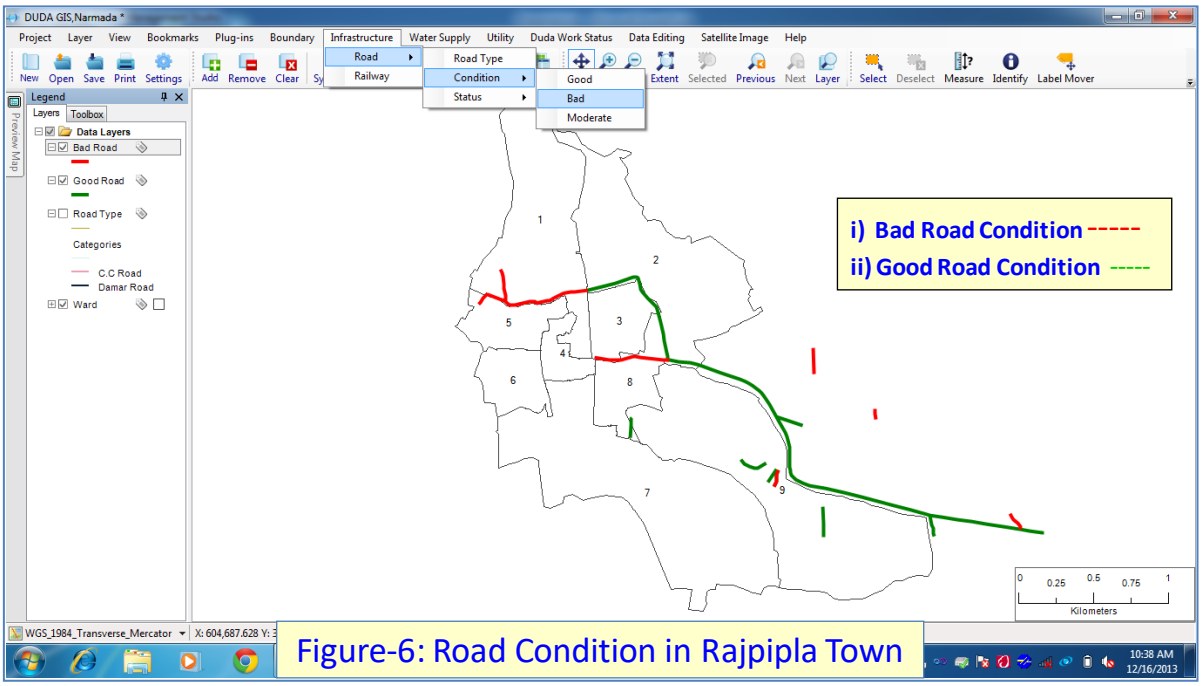

Figure 6: *Road condition in Rajpipla town*

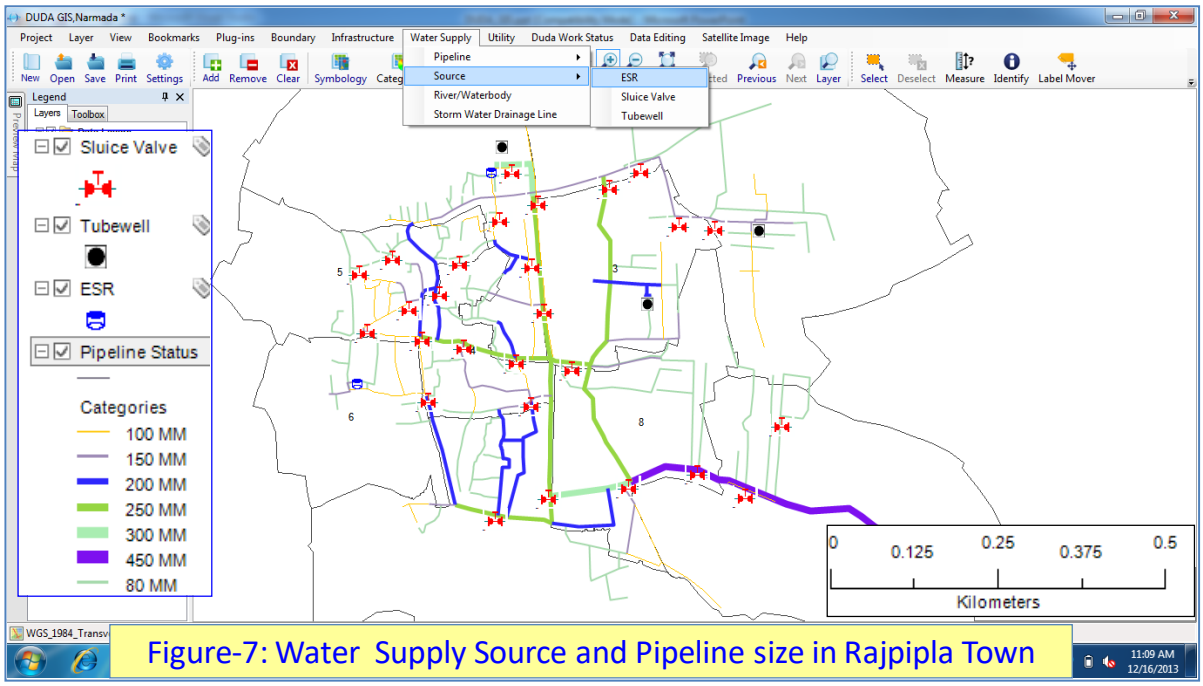

Figure 7: *Water Supply Source and Pipeline size in Rajpipla town*

4.5. Urban land use classification and Mapping for Tax Assessment

The urban built-up area in Rajpipla town was classified into residential, commercial and industrial areas in each Town Planning (TP) scheme and mapped along with the transport network. This classification was carried out essentially to assess the property tax which depends on the use of that particular built-up area. The city survey numbers were also linked with each of the built-up area. This has helped in accurate tax calculation depending on the type of property. This database has also helped to enumerate the properties based on query builder having tax dues more than certain cash limit during the particular financial year. The map of the classification of built-up area into residential, commercial and industrial areas is given in Figure 8. The results of query builder the properties having tax dues more than Rs. 1800 during financial year of 2013 is given Figure 9.

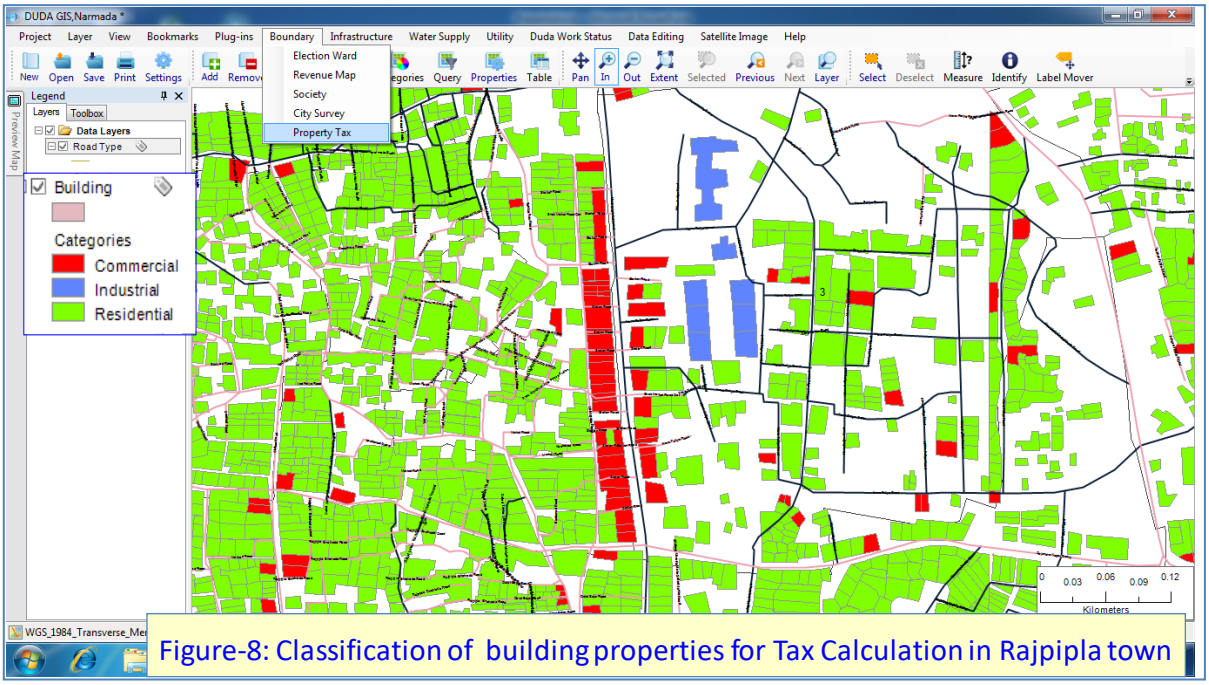

Figure 8: *Classification of building properties for tax calculations in Rajpipla town*

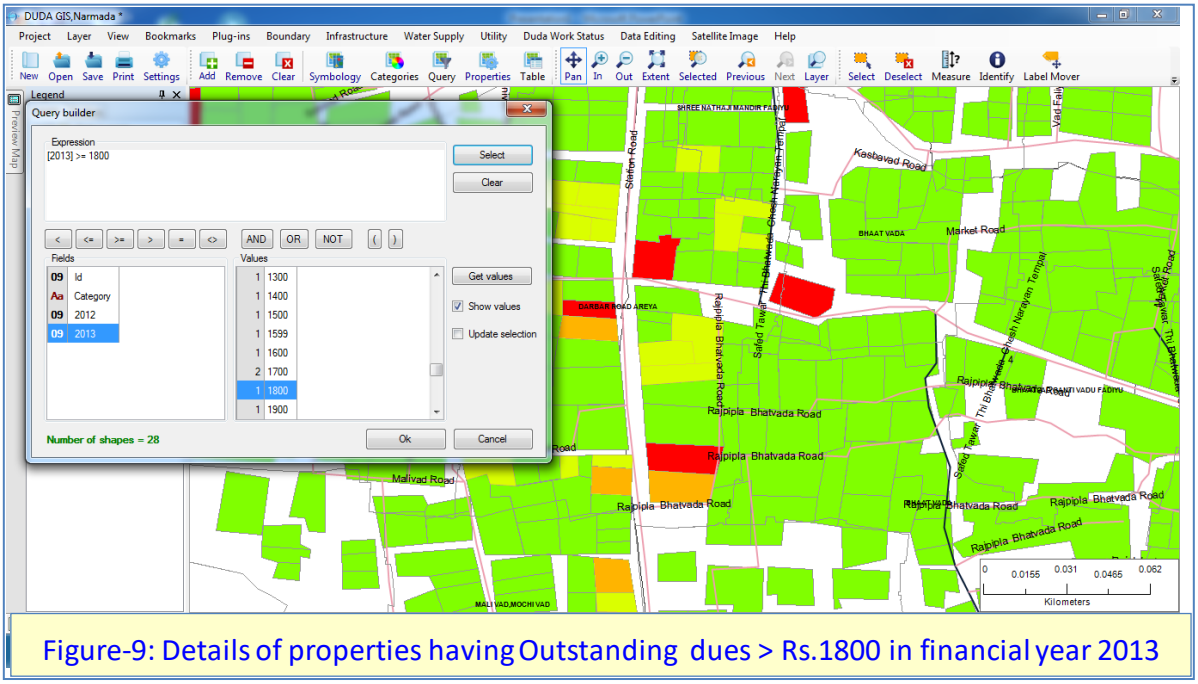

Figure 9: *Details of properties having outstanding dues> Rs. 1800 in financial year 2013*

4.6. Location based utility Mapping

The location of various utilities like primary health centers, educational institutes, Aanganwadies, Public Distribution govt. Shops etc. in various wards of Rajpipla town were mapped. Apart from these public utilities other utilities like location of solid waste containers, pay-and use toilets, waste dumping

sites and location of slum pockets were also mapped. The location of various public utilities in Rajpipla town is given in Figure 10.

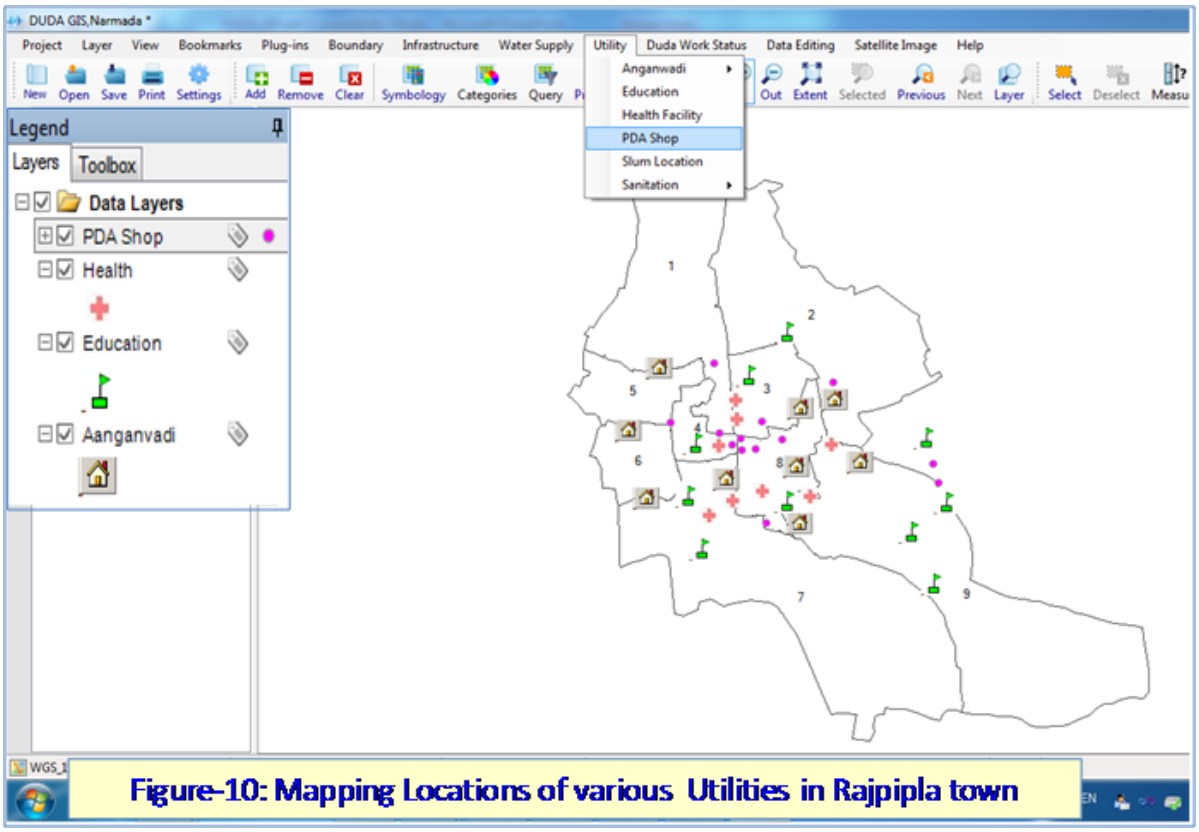

Figure 10: *Mapping locations of various utilities in Rajpipla town*

4.7. Monitoring Progress of Work and Fund Allocation Status

The DUDA Decision Support System (DSS) can effectively be used for monitoring the progress of the various works undertaken by the municipality. The query-cell developed in DSS can also be used to visualize status of funds allocation related to various municipal schemes and activities in various wards of the Rajpipla town by the concerned officials. Figure 11 shows the locations of sites in various wards where work is in progress and grants allocation status can be visualized by using the query-cell shown in Figure 12.

4.8. Major Achievements and Value added Services of the Project

The GIS Cell in DUDA is now effectively monitoring the various schemes, their completion schedule by the contractors and payment based on the satisfactory and timely completion of the work. This has helped to bring transparency in various activities of the municipality. This is one of the successful softwares for communication and dissemination of information related to municipality activities. The team work and participation of various levels of officials makes it sustainable and long lasting for monitoring activities of the municipality. The major achievements and value addition delivered to the beneficiary of the project are as follows:

- ❖ Linking of maps with Government Scheme has helped in development and Control of various municipal activities;
- ❖ It has effectively controlled duplication of work by bringing transparency;
- ❖ It has ensured equitable distribution of works and funds for various schemes;

- ❖ This effectively helped to Identify under developed areas by visualization of various developmental schemes and online supervision;
- ❖ It has helped in planning various future developmental activities.

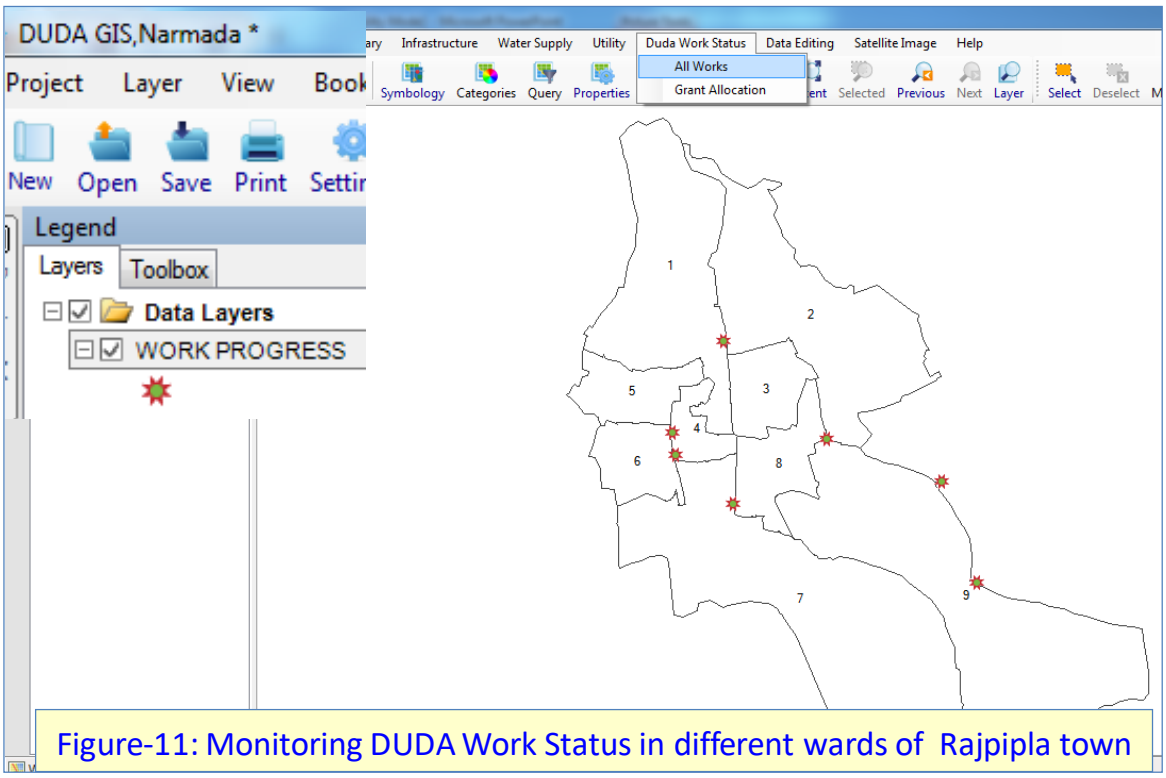

Figure 11: *Monitoring DUDA work status in different wards of Rajpipla town*

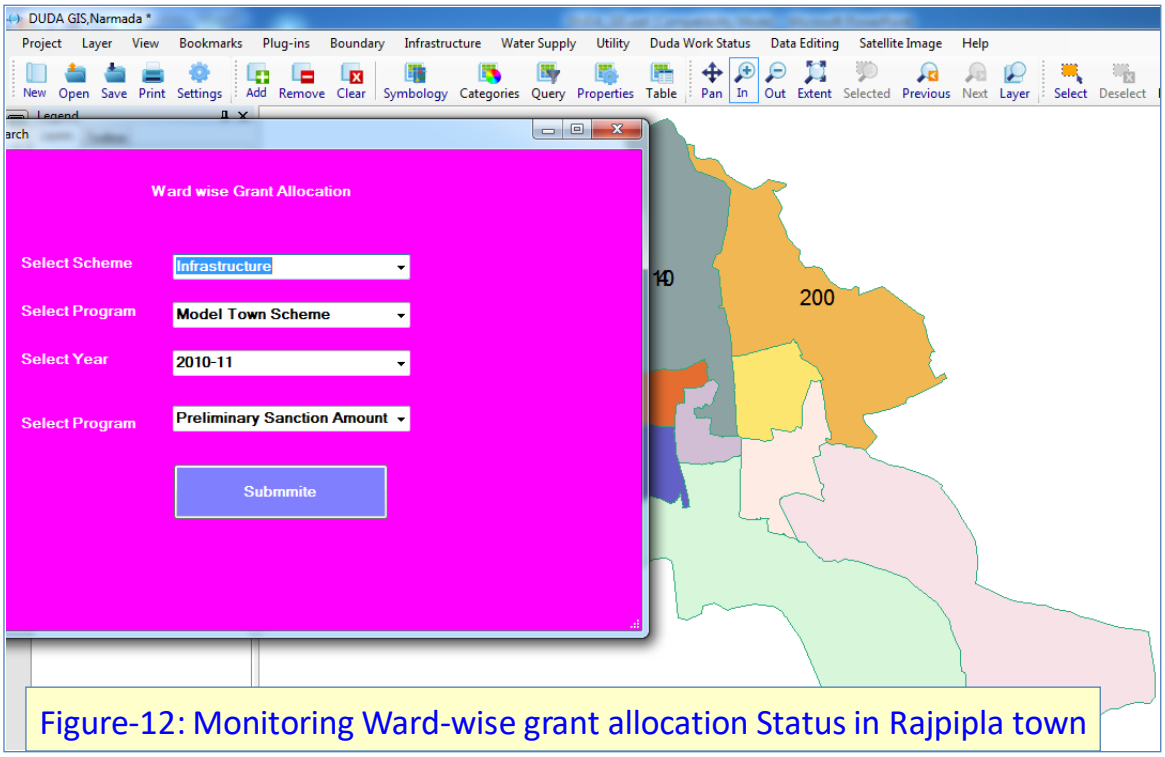

Figure 12: *Monitoring ward-wise grant allocations status in Rajpipla town*

4.9. Adaptability of DUDA GIS

- The DUDA has proactively decided to utilize this technology for the benefit of the people of the municipality with developing a well-defined institutional mechanism.

- The understanding of problems of middle level functionaries of various activities has helped to articulation of their needs and development of suitable GIS system.

- In addition to providing operational services to the departments for geospatial technology based information, developmental planning support and decision making tools for efficient utilization have also been developed in DUDA GIS.

4.10. Accountability of DUDA GIS

- DUDA GIS and MIS systems have been developed as per the specifications and requirements through understanding of various functionalities of municipal management functions.

- This DUDA GIS has helped to bring awareness from top level to bottom level functionaries of the department that has helped the directives from top level being successfully implemented.

- Essentially it has a 3-tier system of monitoring from top-level officials, middle-level and lower level functionaries bringing accountability at each level with transparency. This ensures continuity of services even when some of the officers are transferred.

4.11. Scalability of DUDA GIS

The major vision of the DUDA GIS was to develop a decentralized Ward Level e-Governance System and Web Based Monitoring System for the Municipality. This helps to monitor various activities of the municipality in dynamic and transparent mode. The system developed for the municipality of a town can be replicated for the larger towns and big cities with the help of detailed dataset from these towns using Geographic Information System (GIS). This will help the municipality to identify deficiencies both quantitatively and geographically in the field of physical infrastructure, health, education, shelter and economy, enabling the municipality to plan in a holistic manner. Even this system can be implemented in any other state of India for efficient management of the Municipality using e-Governance along MIS system.

Acknowledgments

The authors like to express their sincere thanks to Shri T.P. Singh, Director, Bhaskarcharya Institute for Space Applications and Geo-informatics (BISAG), Department of Science & Technology, Government of Gujarat, Gandhinagar 382007, and Team Members of BISAG, for fruitful discussions, suggestions and continuous cooperation in carrying out this project.

References

Abdul Kalam, A.P.J. 2014. A Vision of Citizen-centric e-Governance for India. Compendium of e-Governance Initiatives in India, pp. 3-7.

Abdul Muheet Chowdhary. 2014. Case Studies on e-Governance in India, 2013–2014. National Institute for Smart Government, www.nisg.org.

Bani, M.S., Rashid, Z.A., Hamid, K.H.K., Harbawi, M.E., Alias, A.B. Aris, M.J. 2009. The development of decision support system for waste management: a review. *World Academy of Science, Engineering and Technology*, 49, pp.161-168.

eGovernance Policy for the State of Gujarat (2014-2019). Department of Science & Technology, Government of Gujarat, November 2014, vibrantgujarat.com.

Ohri, A. and Singh, P.K. 2010. Development of Decision Support System for Municipal Solid waste management in India: A Review. *International Journal of Environmental Sciences*, 1(4), pp.440-453.

Parminder Jeet Singh, 2012. e-Governance in India: Existing context and possible scope for UNDP programing over 2013-18. IT for Change, July, 2012.

Urban Development Solutions. MapmyIndia, www.mapmyindia.com.

Cloud Publications
International Journal of Advanced Remote Sensing and GIS
2017, Volume 6, Issue 1, pp. 2171-2177
ISSN 2320 – 0243, Crossref: 10.23953/cloud.ijarsg.264

Research Article | Open Access

Lithologic Mapping using Remote Sensing Data in Abu Marawat Area, Eastern Desert of Egypt

Mohamed Abdelkareem[1], Ibrahim Othman[2], Kamal El Din G[1]

[1]Geology Department, South Valley University, Egypt
[2]Egyptian Company for Mineral Resources, Egypt

Publication Date: 30 May 2017

DOI: https://doi.org/10.23953/cloud.ijarsg.264

Abstract Remotely sensing data include Landsat-8 Operational Land Imager (OLI) and Advanced Spaceborne Thermal Emission and Reflection Radiometer (ASTER) data successfully delineated the alteration zone in Abu Marawat area. Image transformation technique was applied in the present study. Band ratio color composites (6/7, 6/5,*4/5, 5) and Principal Component Analysis (PCA) technique of Landsat-8 highlighted the alteration zone. Band ratio color composites ASTER bands 4/6, 4/2, and 4/3 in the R, G, and B, respectively, provided a significant results of alteration zone. Minimum Noise fraction technique (MNF) provided better results that clearly delineated the mineral potential area. Field data and previous works validated the alteration zones. The overall results showed the importance of image processing in showing the probable area of mineral resources.
Keywords *Remote sensing, image processing, alteration zone; Egypt*

1. Introduction

Advances in multispectral imaging systems include Landsat series and Advanced Spaceborne Thermal Emission and Reflection Radiometer (ASTER) allowed mapping the geologic and structural features in fine resolutions (e.g., Abdelkareem and El-Baz, 2015 & 2016 & 2017). Landsat sensors (e.g., Landsat-5 to Landsat-8) successfully delineated lithologic and mineral characteristics using visible NIR and SWIR bands (e.g., Abrams et al., 1983; Sabins, 1997; Ramadan et al., 2004). On February 11, 2013 the new Landsat Operational Land Imager (OLI) which aboard by Landsat-8 improved the spectral, radiometric and spatial resolutions of the acquired data. This sensor measures the reflected electromagnetic waves in nine bands and measures the Thermal wavelengths in two bands (TIR). Several studies were used the OLI in imaging the hydrothermal alteration minerals (Zhang et al., 2016; Pour and Hashim, 2015; Abdelkareem and El-Baz, 2016).

ASTER aboard the Earth observation system (EOS) Terra platform measures the Electromagnetic (EM) waves in 14 spectral bands. This sensor has the advantage to cover the SWIR which are significant to map several mineral groups include hydroxides, hydrates and carbonates (Abdelkareem and El-Baz, 2016). This allowed discriminating between key-alteration minerals such as kaolinite, smectite, alunite, and jarosite (Zhang et al., 2016; Yamaguchi and Naito, 2003; Pour and Hashim,

2012; Rowan et al., 2003; Hubbard and Crowley, 2005; Zadeh et al., 2014). These minerals of alteration zones appear on contact with ore deposits which occupied the center of the alteration zones. Analysis and integration of OLI and ASTER data are effective in predicting the occurrence of a certain group of minerals; Al-OH, Fe-OH and Mg-OH e.g., kaolinite, alunite, illite, muscovite, montmorillonite, chlorite, calcite, and dolomite (Azizi et al., 2010; Mars and Rowan, 2006; Rowan et al., 2006).

Several studies were carried out in the Central Eastern Desert of Egypt to map lithology and alteration zone (e.g., Sultan et al., 1986 & 1987; Gabr et al., 2010; Asran et al., 2012; Kusky and Ramadan, 2002). The aim of the present study is to apply OLI and ASTER data to map and highlight area of hydrothermal alteration zones as an indication of mineral resources in the arid regions.

2. Study Area

Abu Marawat area is located in the northern portion of the Central Eastern Desert of Egypt (Figure 1). Regionally, the geology of the studied area consists of ultramafic rocks (Serpentinite-talc-carbonate rocks) which represent the oldest geologic unit, overlain by island arc-related metavolcano-sedimentary sequences. These rock units overlain by Hammamat sediments and intruded by a variety of granitic rocks. These varieties cut by dykes and quartz veins that occur as a later phase of magmatic intrusion.

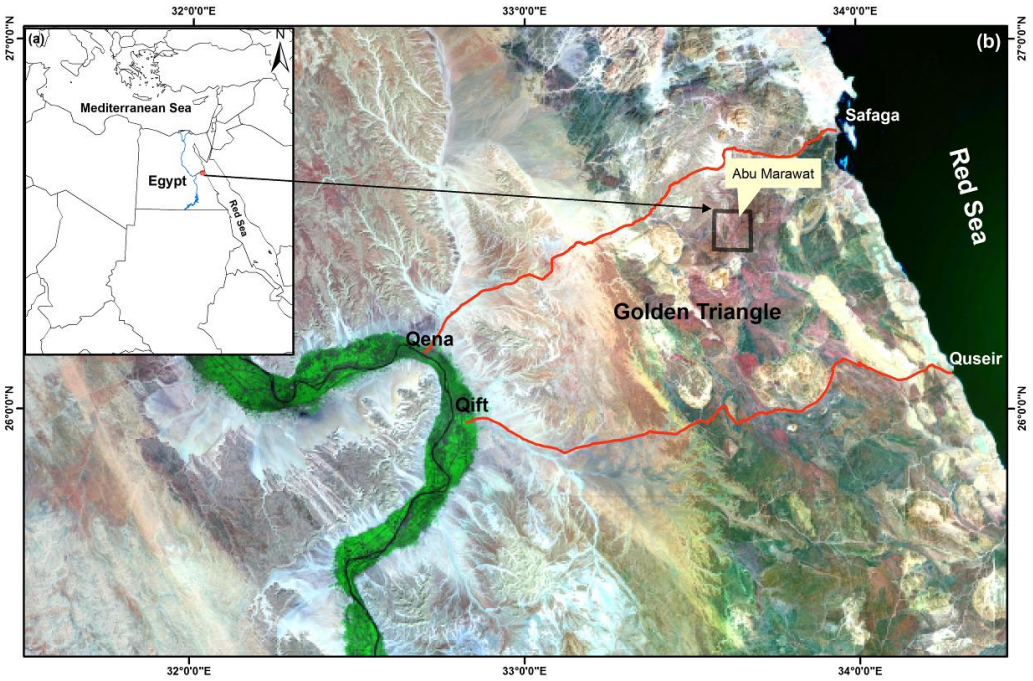

Figure 1: *Location map of the study area*

3. Data Used and Methods

Landsat-8 (OLI) and ASTER data were used in the present study. The OLI has nine optical bands and two bands measure the Thermal IR wavelengths. The OLI bands 2, 3, 4, 5, 6 and 7 are processed and transformed in the present study. The OLI sensor collect two sub-systems visible near infrared (VNIR); shortwave infrared (SWIR), and Thermal infrared (TIR). The spatial coverage of VNIR and SWIR is 30 m and, the TIR is about 60 m. Image enhancement, and transformations were used to delineate the areas of mineral alteration zone. In addition to OLI data, ASTER data which obtained in December

1999 by NASA and METT (Japan Ministry of Economic trade and industry) were used to highlight areas of hydrothermal alterations. The data were georeferenced to Universal Transverse Mercator (UTM). World Geodetic system 1984 (WGS 84) zone 36.

Band ratio represents a transformation technique that applies by dividing the digital numbers of one band by their corresponding pixels of another band (e.g., Mather, 2004). This helps to enhance the spectral differences between the variables on land surface (Goetz et al., 1983). This technique allowed discrimination between different rock types and highlighted areas rich in specific mineral compositions (Abrams et al., 1983; Sabins 1997; Abdelkareem and El-Baz, 2016; Gad and Kusky, 2006). In addition to band ratios, PCA was used to transform the components of the image into its principal components (Loughlin, 1991; Gomez et al., 2005). This transformation has the ability to highlight the similarities and differences in the used data. The output will be eigenvectors and eigenvalues of the matrix Covariance.

Minimum noise transformation technique also was used to segregate noise from the VNIR-SWIR ASTER Data. The advantage of this technique is to filter or remove those bands that contribute most to noise (Green et al., 1988; Boardman and Kruse, 1994). It is better technique than PCA in compressing and ordering data in relationship of their image quality. Where the PCA technique is yields linear transformations of the input data which subsequently amplify their variance, and the MNF transform yields linear transformation which subsequently reduce their noise fraction.

4. Results and Discussion

4.1. Landsat-8

Using band ratios 6/7, 6/5,*4/5, 5 in R, G, B (Figure 2a) allowed discriminating geologic units such as felsic varieties with pinkish color; however, the mafic-intermediate rocks discriminated in greenish color. This is because iron oxides and iron-bearing minerals are highlighted by band ratios 6/5,*4/5 (Sultan, 1986 & 1987). The alteration zones could be identified by their yellow/whitish yellow color. This composite discriminated the mineralized alteration zone in bright yellow tone whitish yellow colors from all the others rock units.

Using PCA transformation (Table 1), it is found that band 6 contributed more than the other bands. The eigenvalue of the first PC represents 95.24% of the total variance. This component have negative loading from all bands. The second principle component “PC2” displays contrast between the VNIR and SWIR bands. Noteworthy, PC3 displays contrast between band 6 (0.601736) and band 7 (-0.61628) that provides significant information on the OH-bearing minerals. In PC5, a contrast between band 4 (0.811358) and band 2 (-0.24045) that reveal the iron oxides in bright tone. In this transformation, the PC6 represents noise. Displaying PC3, PC4, and PC5 in R, G, and B, (Figure 2b) allowed discriminating mineralized alteration zone with bright tone (reddish white color).

Table 1: *Principal component analysis of VNIR/SWIR*

Eigenvector	Band 2	Band 3	Band 4	Band 5	Band 6	Band 7	Eigenvalue%
St. dev	783.03	1194.90	1636.59	2022.79	2514.65	2150.75	
PC 1	-0.17	-0.26	-0.37	-0.45	-0.57	-0.48	95.24
PC 2	0.25	0.34	0.42	0.44	-0.38	-0.55	3.31
PC 3	-0.29	-0.29	-0.12	0.27	0.60	-0.61	0.95
PC 4	0.41	0.45	0.03	-0.62	0.40	-0.29	0.43
PC 5	-0.38	-0.24	0.81	-0.37	0.01	-0.01	0.052
PC 6	0.71	-0.68	0.13	0.0002	0.026	-0.006	0.017

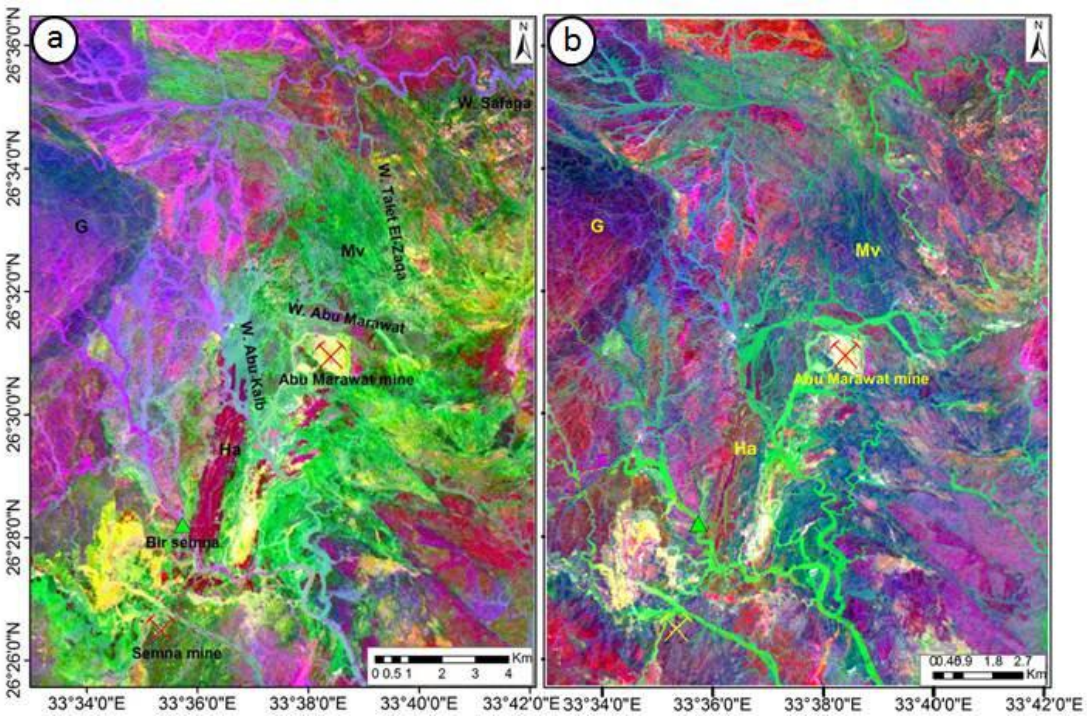

Figure 2: *(a) Band ratio composite image of 6/7, 6/5*4/5, 5 in R, G, and B. (b) False color composite of PC3, PC4, and PC5 in R, G, and B, respectively*

4.2. ASTER Data

Band ratio composite 4/6, 4/2, and 4/3 were used to enhance the spectral differences between altered and non-altered rocks. We apply band ratios 4/6 to highlight the aluminum hydroxide (Al-O-H), 4/2 and 4/3 for iron oxides. This based on that the spectral properties of hydrothermal alteration minerals are different from unaltered minerals. In areas of hydrothermal alteration, the OH- and iron bearing minerals are common. Therefore, using band ratios 4/6, 4/2, and 4/3 (Figure 3a) clearly highlighted the alteration minerals in bright white tone color.

The result of MNF technique which was applied on the VNIR-SWIR ASTER bands is shown in Figure 3b. This technique provides images with successive increasing noise level and decreasing image quality with increasing the fraction level (order). By examine the Minimum noise fraction output images; negated MNF4 represented the best component that highlighted the alteration zone clearly in white color (Figure 3b). Field examination (Figure 4) revealed the alteration zone and the detected sites are of high mineral potentials that represents the mine of Abu-Marawat.

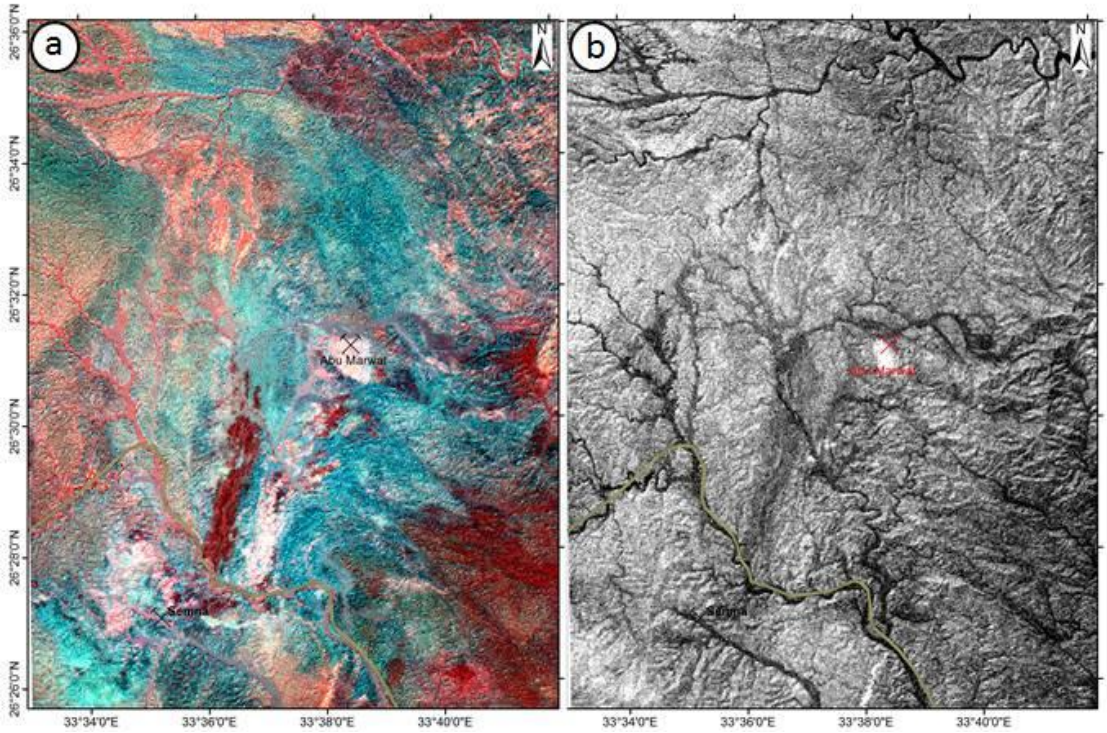

Figure 3: *(a) Band ratio composite image of 4/6, 4/2, 4/3 in R, G, and B. (b) MNF 4 of VNIR-SWIR ASTER bands*

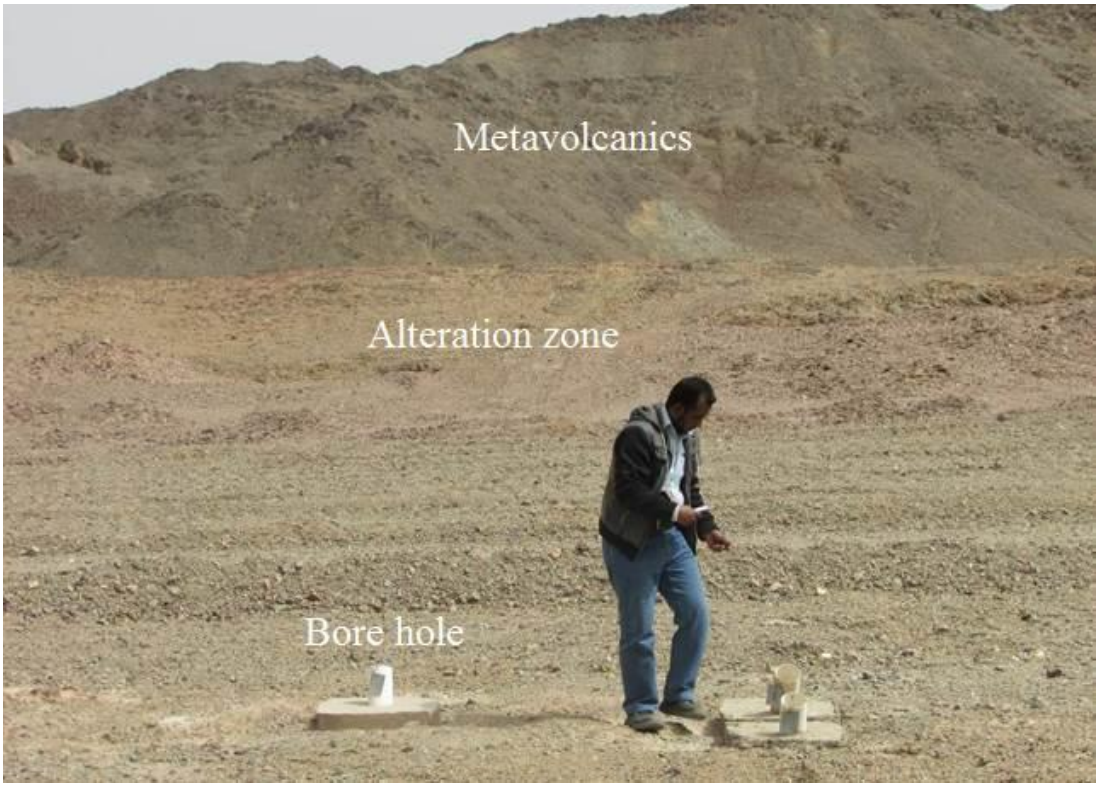

Figure 4: *Field photograph showing the alteration zone*

5. Conclusions

This article represents application of remote sensing data in arid region to characterize the hydrothermal alteration zone. OLI and ATER data clearly highlighted the potential area of hydrothermal alteration using image transformation technique. Applied the Minimum Noise Fraction provided better observation than band ratios and PCA in delineating the areas of hydrothermal alteration. In summary, applying remote sensing data is effective tool prior to any field investigations.

Acknowledgments

This article was funded by the South Valley University sector of Postgraduate Studies and Research.

References

Abdelkareem, El-Baz, F. 2016. Mapping hydrothermal alteration zone as a probable site of potential mineral resources in the Central Eastern Desert of Egypt using remotely-sensed data. *Geological Society of America Abstracts with Programs*, 48(7). doi: 10.1130/abs/2016AM-282399.

Abdelkareem, El-Baz, F. 2015. Analyses of optical images and radar data reveal structural features and predict groundwater accumulations in the central Eastern Desert of Egypt. *Arabian Journal of Geosciences*, 8, pp.2653-2666.

Abdelkareem, M. and El-Baz, F. Forthcoming 2017. Characterizing hydrothermal alteration zones in Hamama area in the central Eastern Desert of Egypt by remotely sensed data. *Journal of Geocarto International.* http://dx.doi.org/10.1080/10106049.2017.1325410

Abrams, M.J., Brown, D., Leple, L. and Sadowski, R. 1983. Remote sensing of porphyry copper deposits in Southern Arizona. *Economic Geology*, 78, pp.591-604.

Azizi, H., Tarverdi, M.A., and Akbarpour, A. 2010. Extraction of hydrothermal alterations from ASTER SWIR data from east Zanjan, northern Iran. *Advances in Space Research*, 46, pp.99-109.

Boardman, J.W. and Kruse F.A. 1994. Automated spectral analysis: a geologic example using AVIRIS data, north Grapevine Mountains, Nevada. In: *Proceedings, ERIM tenth thematic conference on geologic remote sensing*, 9-12 May 1994, San Antonio, Texas. Ann Arbor, MI: Environmental Research Institute of Michigan, pp.407-418.

Gabr, S., Ghulam, A. and Kusky, T. 2010. Detecting areas of high-potential gold mineralization using ASTER data. *Ore Geology Reviews*, 38, pp.59-69.

Gad, S. and Kusky, T. 2006. Lithological mapping in the Eastern Desert of Egypt, the Barramiya area, using Landsat thematic mapper (TM). *Journal of African Earth Sciences*, 44(2), pp.196-202.

Goetz, A.F.H., Rock, B.N. and Rowan, L.C. 1983. Remote sensing for exploration: an overview. *Economic Geology*, 78, 573-590.

Gomez, C., Delacourt, C., Allemand, P., Ledru, P. and Wackerle, R., 2005. Using ASTER remote sensing data set for geological mapping, in Namibia. *Physics and Chemistry of the Earth*, *parts A/B/C*, 30(1-3), pp.97-108.

Green, A.A., Berman, M., Switzer, P. and Craig, M.D. 1988. A transformation for ordering multispectral data in terms of image quality with implications for noise removal. *IEEE Transactions on Geoscience and Remote Sensing*, 26, pp.65-74.

Hubbard, B.E. and Crowley, J.K. 2005. Mineral mapping on the Chilean-Bolivian Altiplano using co-orbital ALI, ASTER and Hyperion imagery: Data dimensionality issues and solutions. *Remote Sensing of Environment*, 99, pp.173-186.

Kusky, T.M. and Ramadan, T.M. 2002. Structural controls in the Neoproterozoic Allaqi suture: An integrated field, Landsat TM, and radar C/X SIR SAR images. *Journal of African Earth Sciences*, 35, pp.107-121.

Loughlin, W.P. 1991. Principal component analysis for alteration mapping. *Photogrammetric Engineering and Remote Sensing*, 57, pp.1163-1169.

Mars, J.C. and Rowan, L.C. 2006. Regional mapping of phyllic- and argillic-altered rocks in the Zagros magmatic arc, Iran, using advanced spaceborne thermal emission and reflection radiometer (ASTER) data and logical operator algorithms. *Geosphere*, 2, pp.161-186.

Mather, P. 2004. *Computer Processing of Remotely-Sensed Images: An introduction*, 3rd Edition, Wiley, p.442.

Pour, A.B. and Hashim, M. 2015. Hydrothermal alteration mapping from Landsat-8 data, SarCheshmeh copper mining district, south-eastern Islamic Republic of Iran. Journal of Taibah University for Science, 9, pp.155-166.

Pour, A.B. and Hashim, M. 2012. Identifying areas of high economic-potential copper mineralization using ASTER data in the Urumieh-Dokhtar Volcanic Belt, Iran. Advances in Space Research, 49, pp.753-769.

Rowan, L.C., Mars, J.C. and Simpson, C.J. 2003. Lithologic mapping in the mountain pass, California area using Advanced Spaceborne thermal Emission and Reflection Radiometer (ASTER) data. Remote Sensing of Environment, 84, 350-366.

Rowan, L.C., Schmidt, R.G. and Mars, J.C. 2006. Distribution of hydrothermally altered rocks in the RekoDiq, Pakistan mineralized area based on spectral analysis of ASTER data. *Remote Sensing of Environment*, 104, pp.74-87.

Sabins, F.F. 1999. Remote sensing for mineral exploration. *Ore Geology Reviews*, 14, 157-183.

Sabins, F. 1997. *Remote sensing principles and interpretation*. 3rd ed. New York: W.H. Freeman and Company, p.494.

Sultan, M., Arvidson, R.E. and Sturchio, N.C. 1986. Mapping of serpentinites in the Eastern Desert of Egypt using Landsat Thematic Mapper data. *Geology*, 14, pp.995-999.

Sultan M., Arvidson R.E., Sturchio N.C. and Guinness, E.A. 1987. Lithologic mapping in arid regions with Landsat thematic mapper data: Meatiq Dome, Egypt. *Geological Society of America Bulletin,* 99(6), pp.748-762.

Yamaguchi, Y. and Naito, C. 2003. Spectral indices for lithologic discrimination and mapping by using the ASTER SWIR bands. *International Journal of Remote Sensing*, 24(22), pp.4311-4323.

Zadeh, M.H., Tangestani, M.H., Roldan, F.V. and Yusta, I. 2014. Sub-Pixel mineral mapping of a porphyry copper belt using EO-1 Hyperion data. *Advances in Space Research*, 53, pp.440-451.

Zhang Tingbin, Yi Guihua, Li Hongmei, Wang Ziyi, Tang Juxing, Zhong Kanghui, Li Yubin, Wang Qin and Bie Xiaojuan. 2016. Integrating Data of ASTER and Landsat-8 OLI (AO) for Hydrothermal Alteration Mineral Mapping in Duolong Porphyry Cu-Au Deposit, Tibetan Plateau, China. *Remote Sensing*, 8, p.890.

Cloud Publications
International Journal of Advanced Remote Sensing and GIS
2017, Volume 6, Issue 1, pp. 2178-2191
ISSN 2320 – 0243, Crossref: 10.23953/cloud.ijarsg.265

Research Article | Open Access

Morphometric Evaluation and Sub Basin Analysis in Hanur Watershed, Kollegal Taluk, Chamarajanagar District, Karnataka, India, using Remote Sensing and GIS Techniques

Siddaraju, K., Nagaraju, D., Bhanuprakash, H.M., Shivaswamy, H.M., Balasubramanian, A.

Department of Studies in Earth Science, University of Mysore, Manasagangotri, Mysore, 570006, Karnataka, India

Publication Date: 30 May 2017

DOI: https://doi.org/10.23953/cloud.ijarsg.265

Abstract The study area covers 1026 sq km comprising of 15 sub-watersheds, namely Saggiyam (SB-1), Mudoldoddi (SB-2), Halgapuram (SB-3), Deverabetta (SB-4), Mattugaudanadoddi (SB-5), Handgalli (SB-6), Manchepura (SB-7), Lokkanahalli (SB-8), Chinchalli (SB-9), Prakash palya (SB-10), Naripura (SB-11), Adugulpodu (SB-12), Ramayanadoddi (SB-13), Jodukara hatti (SB-14), Depudisahibradoddi (SB-15) which range in area from 16.87 to 180.02 sq km. Different morphometric parameters were evaluated to understand the drainage characteristics. The drainage pattern of these sub basins have been delineated using Geocoded FCC bands 2, 3 and 4, of IRS 1C and 1D (LISS 111+ PAN merged) on 1:50,000 scale and Survey of India Toposheets as reference. The morphometric parameters are computed using Arc Info and Arc View GIS software's. The drainage pattern of the study has shown dendritic to sub-dendritic drainage pattern with stream orders ranging from 4th to 5th order. The Drainage density ranges from 1.51 to 4.83 km/km^2 suggesting coarse to moderate drainage texture. The change in values of stream length ratio indicates their late youth stage of geomorphic development. The values of bifurcation ratio are ranging from 0.11 to 20.75 indicating that the study area is having strong structural control over the drainage pattern and all the sub basins fall under normal basin category. The values of form factor and circulatory ratio, suggest that the sub basins are elongated to circular in shape. Geographic Information System, when used with satellite images, could help in determining the morphometric parameters of watershed and river basins. It is concluded that remote sensing ground and GIS have been proved to be efficient tools in drainage delineation and updation.

Keywords *Morphometry; Dendritic; Drainage; Texture; Circularity Ratio; Elongation Ratio*

1. Introduction

Watershed is a basic hydrological unit; it helps in determining the runoff of the unit from the amount of total precipitation. Precipitation is a dynamic variable. It varies from one place to other and from time to time. Watershed management is necessary for low flow regions. Geoinformatics based morphometric calculation is a new technique used for watershed management. Geoinformatics is the combination of Remote Sensing, Geographical Information System and Global Positioning System (Bera, K. &

Bandyopadhyay, J., 2011). Morphometric analysis of watershed provides a quantitative description of the drainage system (Rao et al., 2010). The morphometric parameters are classified into three categories i.e. Linear, Relief and Arial morphometric parameters. Morphometric parameters have greater hydrological significances. More recent attempts on morphometric analysis using remote sensing techniques have been made by Rao et al., 2010; Kumar et al., 2010; Rekha et al., 2011; Pal. B. et al., 2012; Mishra et al., 2010, and Arun et al., 2005. The present study aims at the morphometric analysis on sub-basin level using remote sensing and GIS.

1.1. Study Area

The study area is spread over 1026 km^2. It comprises of fifteen sub-basins. This area is located between 770 51 to 770 301 East longitude and 110 451 to 120 151 North latitude. It is covered by 115 villages (Figure 1). The area is accessible by good road network. The morphometry based on remote sensing and GIS techniques can help in analyzing the hydrogeomorphic conditions of a basin (King, 1872; Foote, 1876; Rao et al., 1975; Mathur, 1977; Kale et al., 1990 and Malur and Nagedra, 1994). The study area enjoys a warm summer and dry winter. It is a semi-arid region with dry climate followed by very less humidity and scanty annual rainfall which is not exceeding 699 mm. Therefore, this area is considered to be one of the drought-prone zones of Chamarajanagar district, in Karnataka state.

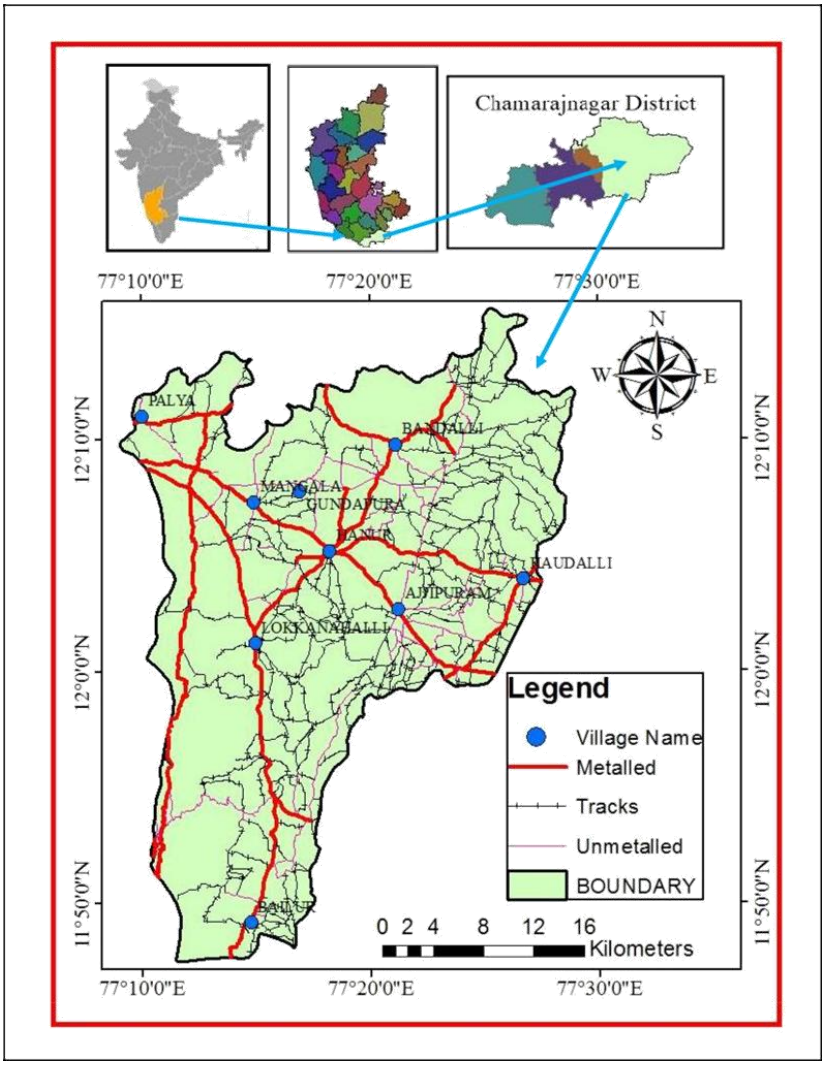

Figure 1: *Location Map of the Study Area*

1.2. Geology of the Area

This area falls into the Western Block of Proterozoic basins of Southern Karnataka. It comes under the semi-arid condition with weathered and fractured Charnockites, Hornblende/Amphibolite schist form the main aquifer in Hanur watershed. The weathered and fractured Charnockites, hornblende /Amphibolite schist gneisses occupying the total area and has limited recharge facilities. This area is a typical hard rock terrain.

2. Methodology

The drainage map (Figure 2) of the study area has been prepared from digital data of IRS 1C and ID of both LISS111 and PAN data of 2001. These satellite imageries had been geo-referenced and merged using image processing software ERADAS IMAGINE V.9.2 and the thus merged data were used in the present study. The drainage systems have been delineated using merged satellite data of geo-coded FCC of bands 2, 3, 4 on 1:50,000 scale and survey of India toposheets no- 57 H/4, 57H/7, 57H/8, 58E/1 and 58E/5 as reference. The morphometric parameters were computed using the formulae of different worker's presented in Table 1. For digitization; computation and output generation, the GIS software like Arc GIS V 9.2 was used.

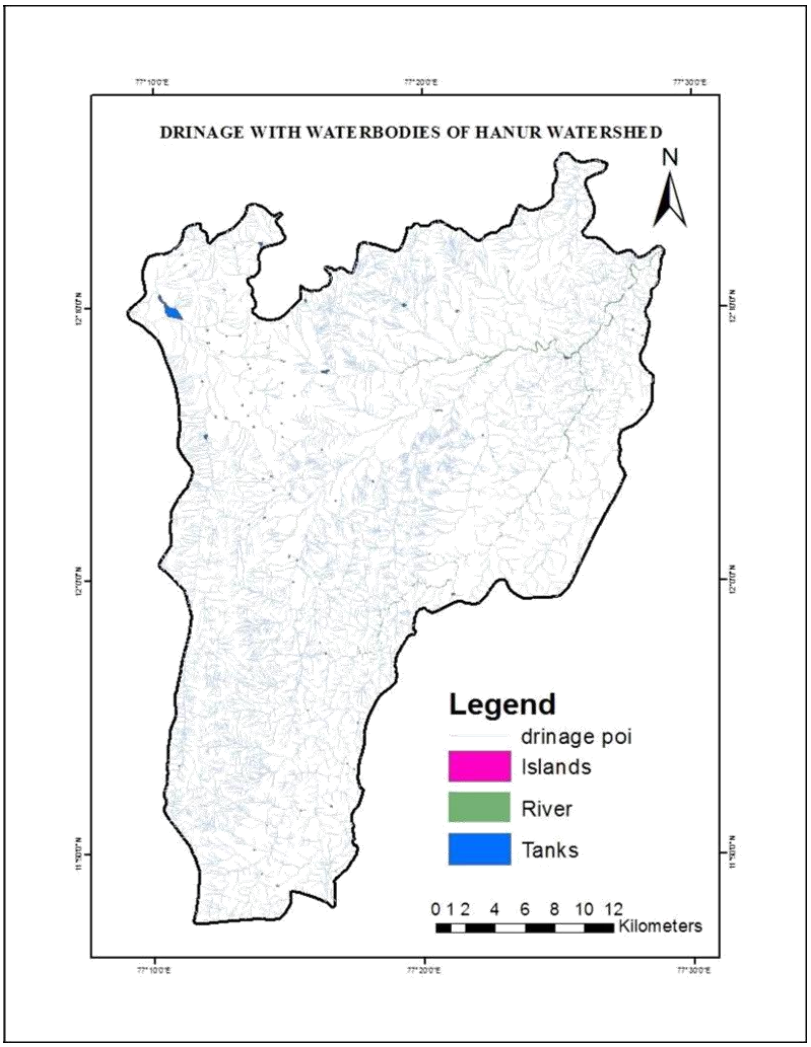

Figure 2: *Drainage Map of Study Area*

3. Basin Delineation

In the present study, the basin has been sub divided into 15 sub basins, which are named based on the important places at the outlet. They are namely Saggiyam (SB-1), Mudoldoddi (SB-2), Halgapuram (SB-3), Deverabetta (SB-4), Mattugaudanadoddi (SB-5), Handgalli (SB-6), Manchepura (SB-7), Lokkanahalli (SB-8), Chinchalli (SB-9), Prakash palya (SB-10), Naripura (SB-11), Adugulpodu (SB-12), Ramayanadoddi (SB-13), Jodukara hatti (SB-14), Depudisahibradoddi (SB-15) which range in area from 1026 sq km.

Table 1: *Methodology Adopted for Computations of Morphometric Parameters*

Sl. No.	Morphometric Parameters	Formula	Reference
1	Stream order	Hierarchical rank	Strahler 1964)
2	Stream Length(Lu)	Length of the stream	Horton 1945)
3	Mean stream Length (Lsm)	Lsm=Lu/Nu, where, Lsm= mean stream Length Lu=total stream length of order 'U' Nu= Total no of stream segments of order 'u'	Strahler (1964)
4	Stream Length Ratio	Rl=Lu/lu-1, where, RL= stream length Ratio Lu= the Total no stream length of order 'u' Lu-1= the total stream length of its next lower order	Horton (1945)
5	Bifurcation Ratio (Rb)	Rb=Nu/Nu+1, where, Rb=Bifurcation Ratio Nu= Total no of stream segments of order 'u' Nu+1= Number of segments of the next higher order	Schumn (1956)
6	Mean bifurcation ration ((Rbm)	Rbm= Average of bifurcation ratios of all orders	Strahler (1964)
7	Relief Ratio (Rh)	Rh=H/Lb, where, Rh=Relief Ratio H= Total relief (Relative relief) of the basin in kilometers, Lb=Basin Length	Schumn (1956)
8	Drainage Density (D)	D=Lu/A, where, D=drainage Density Lu= total stream length of all orders A= Area of the Basin (Km)	Horton (1945)
9	Stream Frequency (Fs)	Fs=Nu/A, where, Fs=stream Frequency Nu=total no. of stream of all orders A= Area of the Basin (Km)	Horton (1945)
10	Drainage texture (Rt)	Rt=Nu/p, where, Rt=Drainage texture Nu=total no. of stream of all orders, p=perimeter (Km)	Horton (1945)
11	Form factor (Rt)	Rf=A/Lb2, where, Rf=from Factor A= Area of the Basin (Km),Lb^2=square of basin length	Horton (1945)
12	Circularity Ratio (Rc)	Rc=4* pa/p2, RC=circularity ratio	Miller (1953)

		p!=p! value 3.14, A= Area of the Basin (Km), p=square of the perimeter(km)	
13	Elongation ratio (Re)	Re=2v (A/P!)/lb where, Re= elongation Ratio, A= Area of the Basin (Km), p!=p! value 3.14, Lb= Basin Length	Schumn (1956)
14	Length of overland flow	lg=1/D*2, where, Lg=Length of overland flow D=Drainage Density	Horton (1945)

4. Morphometry

According to Clarke (1966), morphometry is the measurement and mathematical analysis of the configuration of the earth surface, shape and dimensions of the landforms. The morphometric analysis is carried out through measurement of linear, areal and relief aspects of the basin and slope contribution (Nag and Chakraborty, 2003). The measurement of various morphometric parameters namely- stream order, stream length (Lu), mean stream length (Lsm), stream length ratio (RL) bifurcation ratio (Rb), mean bifurcation ratio (Rbm), relief ratio (Rh), drainage density (D), stream circulatory ratio (Rc), elongated ratio (Re), length of overland flow (Lg) has been carried out and the data are presented in Table 2. In the present study, the satellite remote sensing data has been used for updation of drainages and the updated drainages have been used for morphometric analysis.

4.1. Linear Aspects

The linear morphometric parameters include the stream order, stream length, mean stream length, stream length ratio and bifurcation ratio, which were determined and results have been presented in Table 2.

4.2. Stream Order

The designated stream order is the first step in the drainage basin analysis. In the present study, ranking of stream has been carried out based on the method proposed by Strahler (1964). The order wise stream numbers, area and stream length of the 15 sub basins are presented in Table 2. Out of these sub basins Halgapuram, Deverabetta, Mattugaudanadoddi, Handgalli, Lokkanahalli, Chinchalli, Naripura and Jodukarahatti are found to be of 5th order, in Table 2. It is noticed that the maximum frequency is in case of first order stream. It is also observed that there is a decrease in stream frequency as the stream order increases.

4.3. Stream Length

Stream lengths have been measured from the highest elevation of drainage divide to the mouth of the river with the help of GIS software. This has been computed based on the law proposed by Horton (1945) for all the sub-basins of the study area. Usually, the total number and length of stream segment will be maximum in first order streams this may decreases as the stream order increases. The Lokkanahalli, Jodukarahatti, Naripura and Handgalli sub basins show variation from general observation (Table 2). This may be due to flowing of streams from high altitude, change in rock type and moderately steep slopes and probable uplift across the basin (Singh and Singh, 1997; Vittala et al., 2004; Chopra et al., 2005).

4.4. Mean Stream Length

Mean stream length (Lsm) is a characteristic property related to the drainage network components and it associated basin surfaces (Strahler, A.N., 1964). This has been calculated by dividing the total stream length of an order (u) by the number of streams of segments in that order. The mean stream length values of sub basins are presented in Table 2. It is seen that, Lsm values exhibit much variation from 0.03 to 7.55. It is observed that Lsm values of Manchepura and Halgapuram sub basins indicate that Lsm of the given order is greater than that of the lower order and less than that of its next order.

4.5. Stream Length Ratio

Stream length ratio (RL) is the ratio of the mean length of one order to the next lower order of the stream segments. The RL values of the sub basins are presented in Table 2. The stream length ratio between the streams of different orders of the study area has shown some variation. This variation might be attributed to the variation in slope and topography, indicating the late youth stage of geomorphic development in the streams of the study area (Singh and Singh, 1997; Vittala et al., 2004).

4.6. Bifurcation Ratio

According to Schumn (1956), the term bifurcation ratio (Rb) may be defined as the ratio of the number of the stream segments of given order to the number of segments of the next higher order. Bifurcation ratio shows a small range of variation for different regions or for different environments except where the powerful geological control dominates (Strahler, 1975). The Rb values of study area are shown in Table 2. It is seen that the Rb values are not uniform from one order to next order. These differences are depending upon the geological and lithological development of the drainage basin (Strahler, 1964). In the study area, the higher values of Rb indicate a strong structural control in the drainage pattern whereas the lower values indicate that the sub-basins are less affected by structural disturbances (Strahler, A.N., 1964; Nag, 1998; Vittala et al., 2004; Chopra et al., 2005). The Rb values in the sub basins of the study area range from 0.11 to 20.75 indicating that all the sub-basins are falling under regular basin category.

Table 2: *Different Parameters Morphometric Analysis of Hanur Watershed, Kollegal Taluk, Chamarajanagar District*

			Stream Orders						Stream length (KM)					
Sl. no	Sub Basin	Stream order	Total no of 1st order	Total no of 2nd order	Total no of 3rd order	Total no of 4th order	Total no of 5th order	ΣNu	Total length in 1st order	Total length in 2nd order	Total length in 3rd order	Total length in 4th order	Total length in 5th order	ΣLu
1	Saggiyam	IV	52	23	10	15	0	100	27.39	11.21	8.90	6.90	0.00	54.40
2	Mudoldoddi	IV	40	18	7	12	0	77	22.50	10.22	8.51	3.90	0.00	45.13
3	Halgapuram	V	84	40	13	19	1	157	42.85	22.20	5.39	10.13	7.55	88.12
4	Deverabetta	V	85	44	17	1	1	148	39.15	25.21	10.71	0.32	8.50	83.89
5	Mattugaudanadoddi	V	95	41	24	5	1	166	41.38	19.12	12.20	2.39	4.51	79.61
6	Handgalli	V	210	96	47	37	2	392	100.69	47.15	23.35	15.33	8.69	195.21
7	Manchepura	IV	92	44	4	36	0	176	42.70	21.73	14.45	1.42	0.00	80.31
8	Lokkanahalli	V	427	169	106	83	4	789	194.88	71.96	46.14	34.15	20.80	367.93
9	Chinchalli	V	131	47	37	22	1	238	55.47	22.34	15.22	7.14	4.10	104.27

10	Prakash palya	III	37	20	9	0	0	66	16.47	7.87	2.26	0.00	0.00	26.60
11	Naripura	V	246	103	58	54	3	464	143.31	47.52	30.30	21.58	6.09	248.80
12	Adugulpodu	IV	254	113	49	36	0	452	91.82	34.43	12.94	12.83	0.00	152.02
13	Ramayanadoddi	IV	165	76	41	30	0	312	72.79	27.19	17.20	9.39	0.00	126.56
14	Jodukarahatti	V	460	189	113	61	4	827	186.97	70.63	41.43	19.61	19.45	338.09
15	Depudisahibradoddi	IV	51	30	4	6	0	91	24.57	11.18	1.56	2.77	0.00	40.08

Table Cont…

		Linear Parameters											
		Stream Length Ratio						Bifurcation Ratio					
Sl. no	Sub Basin	II/I	III/II	IV/III	V/IV	Basin area in (A)Kms	Basin Length (LB)	I/II	II/III	III/IV	IV/V	Mean bifurcation ratio	Length of over head (Lg)
1	Saggiyam	0.40	0.79	0.77	0	33.22	11.25	2.26	2.3	0.66	0	1.3	0.41
2	Mudoldoddi	0.45	0.83	0.45	0.00	28.80	6.07	2.22	2.57	0.58	0	1.34	1.28
3	Halgapuram	0.51	0.24	1.87	0.74	47.19	11.11	2.1	3.07	0.68	19	6.21	1.07
4	Deverabetta	0.64	0.42	0.02	26.53	55.25	6.65	1.93	2.58	17	1	5.62	1.32
5	Mattugaudanadoddi	0.46	0.63	0.19	1.88	52.18	12.38	2.31	1.70	4.80	5	3.45	1.31
6	Handgalli	0.46	0.49	0.65	0.56	106.16	15.10	2.18	2.04	1.27	18.5	5.99	1.09
7	Manchepura	0.50	0.66	0.09	0	47.67	11.38	2.09	11	0.11	0	3.3	1.19
8	Lokkanahalli	0.36	0.64	0.74	0.60	180.02	21.65	2.52	1.59	1.27	20.75	6.53	0.98
9	Chinchalli	0.40	0.68	0.46	0.57	56.42	12.82	2.78	1.27	1.68	22	6.93	1.08
10	Prakash palya	0.47	0.28	0	0	16.87	4.02	1.85	2.22	0	0	1.01	1.27
11	Naripura	0.33	0.63	0.71	0.28	108.01	14.94	2.38	1.77	1.07	18	5.8	0.86
12	Adugulpodu	0.37	0.37	0.99	0	64.10	22.98	2.24	2.3	1.36	0	1.47	0.84
13	Ramayanadoddi	0.37	0.63	0.54	0	50.82	12.2	2.17	1.85	1.36	0	1.34	0.80
14	Jodukarahatti	0.37	0.58	0.47	0.99	156.99	25.51	2.43	1.67	1.85	15.25	5.3	0.93
15	Depudisahibradoddi	0.45	0.13	1.77	0	19.39	5.23	1.7	7.5	0.66	0	2.46	0.97

Table cont….

		Aerial Parameters											
							Mean Stream length (Lsm)						
Sl. no	Sub Basin	Drainage Density	Stream Frequency (fs)	Form factor	Elongation Ratio	Circulatory ratio	I	II	III	IV	V	Drainage texture (Rt)	Perimeter
1	Saggiyam	4.83	3.01	0.26	1.88	0.49	0.52	0.48	0.89	0.46	0	3.43	29.13
2	Mudoldoddi	1.56	2.67	0.78	3.02	0.55	0.56	0.56	1.21	0.32	0	3	25.61
3	Halgapuram	1.86	3.32	0.38	2.70	0.44	0.51	0.55	0.41	0.53	7.55	4.28	36.67

4	Deverabetta	1.51	2.67	1.24	5.29	0.58	0.46	0.57	0.63	0.32	8.5	4.28	34.50
5	Mattugaudanadoddi	1.52	3.18	0.34	2.68	0.45	0.43	0.46	0.51	0.47	4.51	4.37	37.93
6	Handgalli	1.83	3.69	0.46	4.47	0.27	0.47	0.49	0.49	0.41	4.34	5.59	70.10
7	Manchepura	1.68	3.69	0.36	2.66	0.49	0.46	0.49	3.61	0.03	0	5.05	34.82
8	Lokkanahalli	2.04	4.38	0.38	5.29	0.48	0.45	0.42	0.43	0.41	5.2	11.51	68.50
9	Chinchalli	1.84	4.21	0.34	2.80	0.55	0.42	0.47	0.41	0.32	4.10	6.64	35.84
10	Prakash palya	1.57	3.91	1.04	2.67	0.43	0.44	0.39	0.25	0	0	2.99	22.06
11	Naripura	2.30	4.29	0.48	4.60	0.54	0.58	0.46	0.52	0.39	2.03	9.29	49.91
12	Adugulpodu	2.37	7.05	0.12	1.77	0.19	0.36	0.30	0.26	0.35	0	7.07	63.86
13	Ramayanadoddi	2.49	6.13	0.34	2.65	0.51	0.44	0.35	0.41	0.31	0	8.84	35.29
14	Jodukarahatti	2.15	5.26	0.24	3.91	0.35	0.40	0.37	0.36	0.32	4.86	11.10	74.44
15	Depudisahibradoddi	2.06	4.69	0.70	2.36	0.48	0.48	0.37	0.39	0.46	0	4.04	22.47

4.7. Aerial Aspects

The Aerial morphometric aspects include parameters like drainage density, texture ratio, stream frequency, form factor, circulatory ratio, elongation ratio and length of the overland flow. The values of these parameters have been evaluated and presented in Table 2 and discussed and interpreted, in the following sections.

4.7.1. *Drainage Density*

Horton (1932) introduced the term drainage density (Dd). It is an important indicator of the linear scale of land form elements in stream eroded topography. It is the ratio of total channel segment length of all orders within a basin to the basin area. The drainage density is expressed in terms of Km/Km^2. The drainage density indicates the closeness of spacing of channels, thus providing a quantitative measure of the average length of stream channel for the whole basin. It has been observed from drainage density measurement made over a wide range of geologic and climatic type that a low drainage density is more likely to occur in region of highly resistant and highly permeable subsoil material under dense vegetative cover and where the relief is low. High drainage density is the resultant effect of weak or impermeable subsurface material, sparse vegetation and mountainous relief. Low drainage density leads to coarse drainage texture while high drainage ranging density leads to fine drainage texture (Strahler, A.N., 1964). The drainage density (Dd) of study area is from 1.51 to 4.83 Km/Km^2 as shown in Table 2. The High drainage density indicates that the basin has highly impermeable land surface, steep slopes and limited vegetation cover and limited erosion.

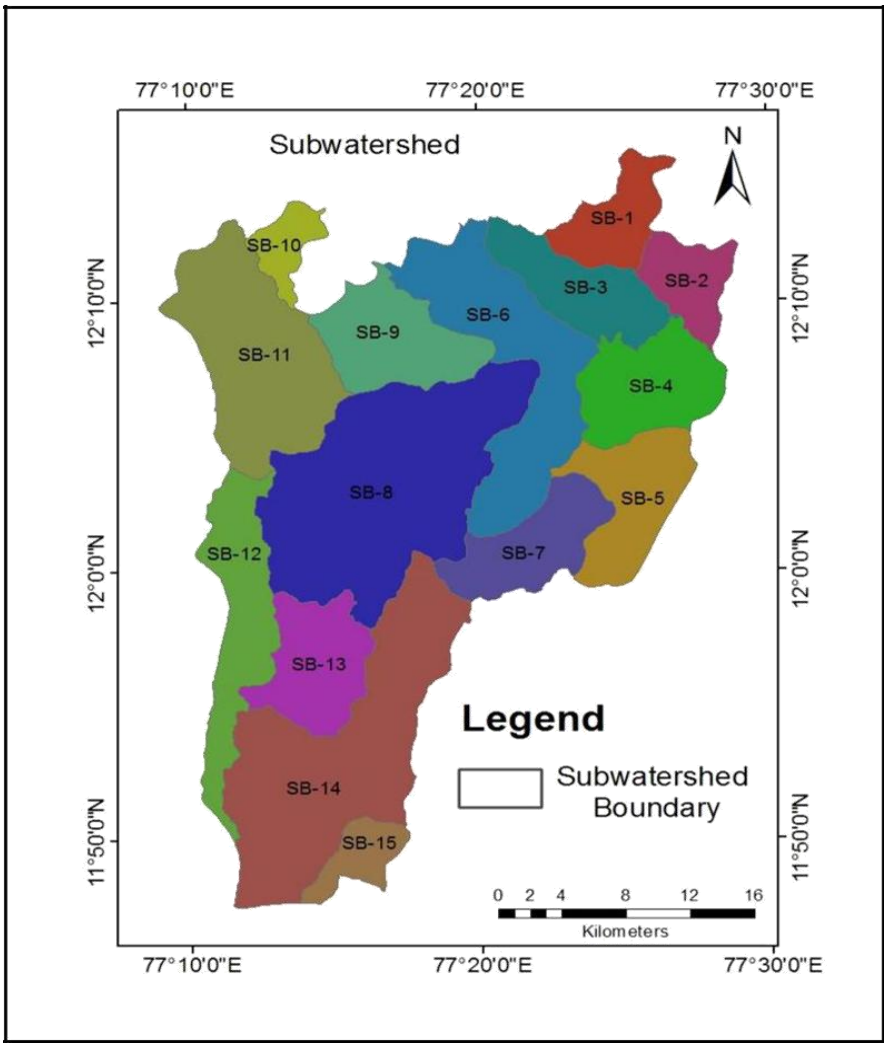

Figure 3: sub watershed Map of Hanur watershed

4.7.2. *Stream Frequency/Channel Frequency*

The total of stream segments of all orders per unit area is known as stream frequency (Fs) (Horton, 1932). It is possible to have basins of same drainage density with differing stream frequency and basins of the same frequency differing in their drainage density. The Fs values of the sub-basins of the study area are presented in Table 2. It is noted that the values of Fs vary from 2.67 to 7.05. It is also seen that the drainage density values of the sub-basins exhibit +ve correlation with the stream frequency suggesting that there is an increase in stream population with respect to increasing drainage density.

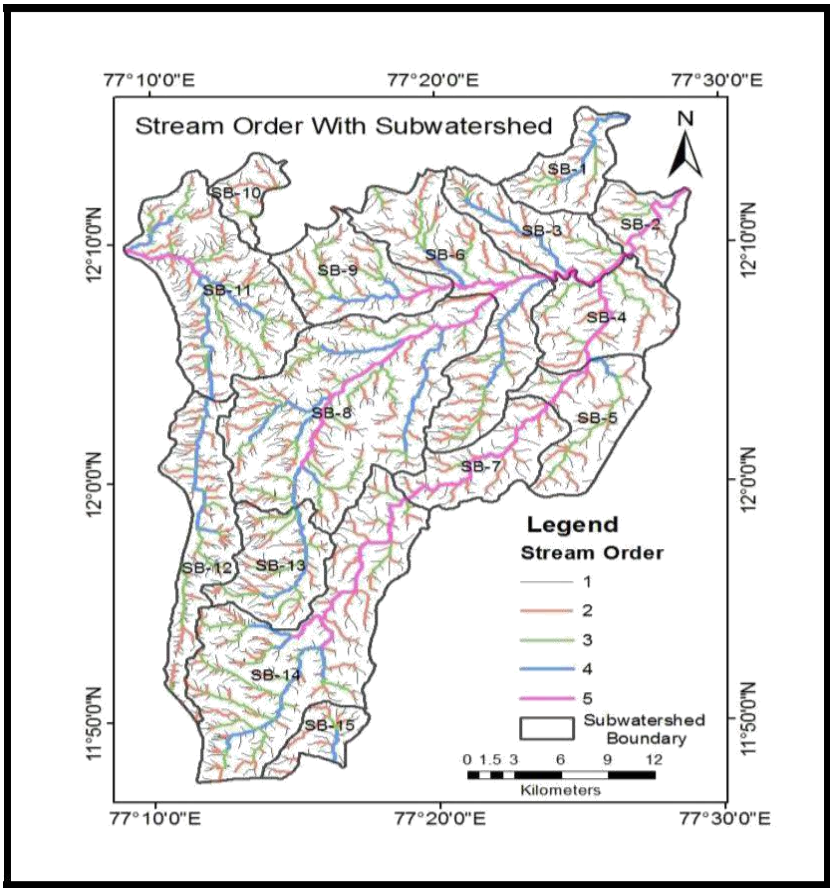

Figure 4: *Stream order with sub watershed*

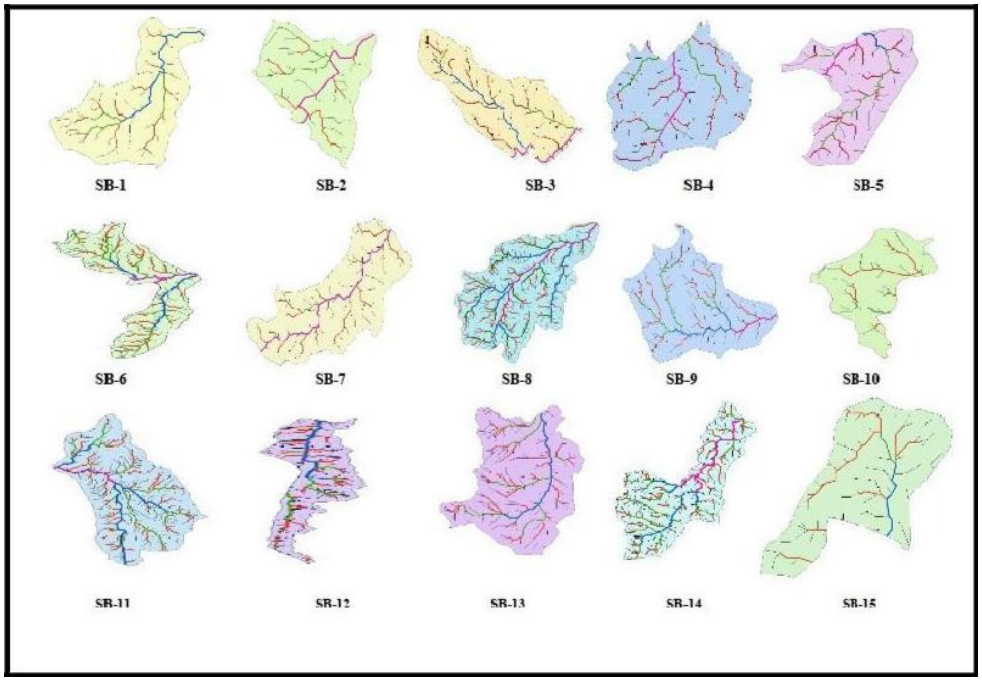

Figure 5: *Major 15 sub basins of Hanur Watershed*

Saggiyam (SB-1), Mudoldoddi (SB-2), Halgapuram (SB-3), Deverabetta (SB-4), Mattugaudanadoddi (SB-5), Handgalli (SB-6), Manchepura (SB-7), Lokkanahalli (SB-8), Chinchalli (SB-9), Prakashpalya (SB-10), Naripura (SB-11), Adugulpodu (SB-12), Ramayanadoddi (SB-13), Jodukara hatti (SB-14), Depudisahibradoddi (SB-15)

4.7.3. *Drainage Texture*

Drainage texture (Rt) is the total number of stream segments of all orders per perimeter of that area (Horton, 1945). It is one of the important concepts of geomorphology which depicts the relative spacing of drainage lines. Drainage lines are numerous over impermeable zones than permeable horizons. According to Horton (1945), infiltration capacity as a single important factor also influences the drainage density and stream frequency. The values of drainage texture ratio of the study area vary from 3.00-11.51. According to Smith (1950), five different drainage textures have been classified based on the drainage density. The drainage density less than 2 indicates very coarse, between 2 and 4 is related to coarse, between 4 and 6 is to moderate, between 6 and 8 is related to fine and greater than 8 is related to very fine drainage texture. In the study area Saggiyam, Mudoldoddi and Prakash palya sub basins have shown coarse and Halgapuram, Deverabetta, Mattugaudanadoddi, Handgalli, Manchepura and Depudisahibradoddi sub basins are moderate and Chinchalli and Adugulpodu sub basins have shown fine and Lokkanahalli, Naripura, Ramayanadoddi and Jodukarahatti sub basins have shown very fine drainage textures.

4.7.4. *Form Factor*

Form factor (Rf) may be defined as the ratio of the area of the basin and square of basin length (Horton, 1932). The value of form factor would always be greater than 0.78 for a perfectly circular basin. Smaller the value of form factor, more elongated will be the basin shape. Rf values of the study area are shown in Table 2. It is noted that the Rf values vary from 0.12 to 1.24. The values of 0.78 to 1.24 are seen in Mudoldoddi, Prakash palya and Deverabetta sub basins which indicates circular shape and remaining sub basins are of elongated in shape.

4.7.5. *Circulatory Ratio*

The circulatory ratio (Rc) is mainly concerned with the length and frequency of streams, geological structures, land use/land cover, climate, relief and slope of the basin. It is the ratio of the area of the basins to the area of circle having the same circumference as the perimeter of the basin. In the study area, the Rc values are ranging from 0.19 to 0.58. The values are more than 0.5 which indicates that they are more or less circular in shape and are characterized by the high to moderate relief and the drainage system are structurally controlled.

4.7.6. *Elongation Ratio*

Elongation ratio is the ratio between the diameter of the circle of the same area as the drainage basin and the maximum length of the basin. The elongation ratio values of the sub basins vary from 1.77 to 5.29. The elongation ratio values generally exhibit variation from 0.6 to 1.0 over a wide variety of climatic and geologic types. In the study area, all 15 sub basins are showing the elongation ratio greater than 1.0, indicating their lower relief.

5. Conclusion

From the Morphometric study, it is seen that the basin forms the dendritic to sub-dendritic drainage pattern with stream orders ranging from 4th to 5th orders. The Average bifurcation ratio is calculated for the watershed as 3.87. The value of Rb in the present case indicates that this watershed has

higher values of Rb indicating a strong structural control in the drainage pattern; the high drainage density indicates the presence of weak or impermeable subsurface material, sparse vegetation and mountainous relief. Drainage textures have been classified based on the drainage density. The drainage density less than 2 indicates very coarse, between 2 and 4 is related to coarse, between 4 and 6 is moderate, between 6 and 8 is fine and greater than 8 is very fine drainage texture. In the study area Saggiyam, Mudoldoddi and Prakash palya sub basins are coarse and Halgapuram, Deverabetta, Mattugaudanadoddi, Handgalli, Manchepura and Depudisahibradoddi sub basins are moderate and Chinchalli and Adugulpodu sub basins are fine and Lokkanahalli, Naripura, Ramayanadoddi and Jodukarahatti sub basin is very fine drainage textures. The Rf values vary from 0.12-1.24. The values of 0.78 to 1.24 are seen in Mudoldoddi, Prakashpalya and Deverabetta sub basins indicating that they are circular in shape and remaining sub basins are elongated in shape. In the study area, the Rc values are ranging from 0.19 to 0.58. The values are more than 0.5 which indicating that they are more or less circular in shape and are characterized by the high to moderate relief and the drainage system were structurally controlled. The elongation ratio values generally exhibit variation from 0.6 to 1.0 over a wide variety of climatic and geologic types. In the study area, all 15 sub basins showed the elongation ratio greater than 1.0 indicating that they have lower relief.

Acknowledgement

The author is grateful to the Department of Studies in Earth Science, University of Mysore, Mysore for permission to prepare this paper.

References

Chopra, R., Raman Deep. Dhiman and Sharma, P.K. 2005. Morphometric analysis of sub-watersheds in Gurdaspur district, Punjab using Remote sensing and GIS techniques. *Journal of the Indian Society of Remote Sensing*, 33(4), pp.531-539.

Clarke, J.I. 1966. *Morphometry from Maps, Essays in Geomorphology*. New York: Elsevier Publishing Company, pp.235-274.

Foote, R.B. 1876. The geological feature of the Southern Marhatta country and adjacent districts. *Memoirs of the Geological Survey of India*, X11(1), pp.70-164.

Gottschalk, L.C. 1964. Reservoir sedimentation. In: V.T., Chow (ed.), *Hand book of Applied Hydrology*. New York: McGraw Hill Book Company. Section 7-1.

Horton, R.E. 1945. Erosional development of streams and their drainage basins; Hydrophysical approach to quantitative morphology. *Geological Society of America Bulletin*, 56, pp.275-370.

Horton, R.E. 1932. Drainage basin characteristics. *Transactions- American Geophysical Union*, 13, pp.350-361.

Kale, V.S., Mudholkar, A.V., Phansalkar, V.G. and Peshwa, V.V. 1990. Stratigraphy of the Bhima Group. *Journal of the Palaeontological Society of India*, 35, pp.91-103.

Mahadevan, C. and Kazim Syed. 1947. The Bhima series and other rocks of Gulbarga districts. *Journal of Hyderabad Geological Survey*, 5, pp.1-60.

Mathur, S.M. 1977. Some aspects of stratigraphy and limestone resources of the Bhima basin. *The Indian Mineral*, 18, pp.59-64.

Nag, S.K. 1998. Morphometric analysis using remote sensing techniques in the Chaka sub basin, Purulia district, West Bengal. *Journal of the Indian Society of Remote Sensing*, 26(1&2), pp.69-76.

Nag, S.K. and Chakraborty, S. 2003. Influences of rock types and structures in the development of drainage network in hard rock area. *Journal of the Indian Society of Remote Sensing,* 31(1), pp.25-35.

Rao, J.L.H., Srinivasa Rao, C. and Ramakrishna, T.L. 1975. Reclassification of the rocks of Bhima basin, Gulbarga District, Mysore State. *Geological Survey of India Miscellaneous Publication*, 23(1), pp.177-184.

Schumn, S.A. 1956. Evolution of drainage systems and slopes in Badlands at Perth Amboy, New Jersey. *Geological Society of America Bulletin*, 67, pp.597-646.

Singh, S. and Singh, M.C. 1997. Morphometric analysis of Kanhar river basin. *National Geographical Journal of India*, 43(1), pp.31-43.

Smith, K.G. 1950. Standards for grading textures of erosional topography. *American Journal of Science*, 248, pp.655-668.

Strahler, A.N. 1964. Quantitative geomorphology of drainage basin and channel networks. In: V.T. Chow (ed.), *Handbook of Applied Hydrology*. New York: McGraw Hill Book Company, Section 4.

Vittala, S.S., Govindiah, S. and Honne Gowda, H. 2004. Morphometric analysis of sub-watersheds in the Pavagada area of Tumkur district, South India, using remote sensing and GIS techniques. *Journal of the Indian Society of Remote Sensing*, 32(4), pp.351-362.

Strahler, A.N. 1957. Quantitative analysis of watershed Geomorphology. *Transactions - American Geophysical Union*, 38, pp.913-920.

Mahadevaswamy, G., Nagaraju, D., Lakshmamma, S., Lone, M.S., Nagesh P.C. and Krishna, R. 2011. Morphometric analysis of Nanjangud taluk, Mysore District, Karnataka, India, using GIS Techniques. *International Journal of Geomatics and Geosciences*, 1(4), pp.721-734.

Malur, M.N. and Nagendra, R. 1994. Lithostratigraphy of Bhima basin (Central part) Karnataka, South India. *Journal of Paleontological Society of India*, 39, pp.55-60.

Miller, V.C. 1953. *A quantitative geomorphic study of drainage basin characteristics in the Clinch Mountain area Virginia and Tennessee*. Technical Report 3, Department of Geology, Columbia University, New York.

Ramesh, L. Dikpal, T.J. and Renuka Prasad. 2015. Evaluation of Morphometric Parameters Derived from Carto DEM and Aster GDEM with SOI Toposheets of Kumudvathi Watershed Basin, Karnataka, India. *International Journal of Advanced Remote Sensing and GIS*, 4, pp.1286-1294.

Tribhuvan, P.R. and Sonar, M.A. 2016. Morphometric Analysis of a Phulambri River Drainage Basin (Gp8 Watershed), Aurangabad District (Maharashtra) using Geographical Information System. *International Journal of Advanced Remote Sensing and GIS*, 5, pp.1813-1828.

Nagaraju, D. and Ravikumar. 2009. Drainage morphometric analysis of Gundlupet taluk, Chamarajanagar, District, Karnataka, India. *Journal of Ecotoxicology and Environmental Monitoring*, 19(2), pp.193-200.

Lakshmamma, Nagaraju, D, Mahadevaswamy, G., Siddalingamuthy, S. and Manjunatha, S. 2011. Morphometric analysis of Gundal watershed, Gundlupet taluk, Chamarajanagar district, Karnataka, India. *International Journal of Geomatics and Geo Sciences*, 1(4), pp.758-775.

Mohammad Subhan Lone, Nagaraju, D., Mahadevaswamy, G., Lakshamma and Siddalingamurthy, S. 2012. Morphometric Analysis of Heggadevana kote (H.D. Kote) taluk, Mysore District, Karnataka, India. *International Journal of Earth Sciences and Engineering*, 5(2), pp.288-293.

Siddalingamurthy, S., Nagaraju, D., Mahadevaswamy, G., Mohammad Subhan Lone, Lakshamma and Pankaja, G.V. 2012. Evaluation of Morphometric Parameters studies in Chamarajanagar taluk, Chamarajanagar district, Karnataka, India, Using Remote sensing and GIS techniques. *International Journal of Earth Sciences and Engineering*, 5(4), pp.524-531.

Nagaraju, D., Siddalingamurthy, S., Balasubramanian, A., Lakshamma and Sumithra. 2015. Morphometric analysis of Byramangala Watershed, Bangalore Urban District, Karnataka, India. *International Journal of Current Engineering and Technology*, 5(3), pp.2156-2164.

Cloud Publications
International Journal of Advanced Remote Sensing and GIS
2017, Volume 6, Issue 1, pp. 2135-2155
ISSN 2320 – 0243, Crossref: 10.23953/cloud.ijarsg.262

Research Article | Open Access

Comparative Analysis of Jordan Transverse Mercator (JTM) and Cassini-Soldner Projection (CASS)

Ibrahem Ahmad Gharaibeh[1], Mohd Sanusi S. Ahamad[1], Bassam Saleh Malkawi[2]

[1]School of Civil Engineering, Universiti Sains Malaysia, 14300 Nibong Tebal, Pulau Pinang, Malaysia
[2]Faculty of Engineering, Isra University, Amman, Jordan

Publication Date: 30 May 2017

DOI: https://doi.org/10.23953/cloud.ijarsg.262

Abstract Jordan uses two coordinate systems; one based on the Palestine 1923 Datum, Cassini-Soldner projection (CASS), and a more recent one called “Jordan Transverse Mercator” (JTM). The JTM Projection System is based on the “International Hayford 1927” Datum. The Department of Land and Survey (DLS) is responsible for managing the cadastral maps of Jordan. Maps in the Cassini-Soldner projection cover 17% of Jordan and maps in the JTM projection cover the rest of the country. This study is devoted to compare CASS with JTM in Jordan. Adopting a reference frame was done in Jordan to support development of a spatial data infrastructure (SDI). On the other hand, depending on affine adjustment process using ArcMap, version 10.2.2, CASS projection was transformed to JTM. In conclusion, the transformation from CASS to JTM, according to the method used in this study, gave accurate results of approximately 10cm. This is a potent result that encourages the transfer of all maps from CASS to JTM.
Keywords *JTM; CASS; Jordan network; Jordanian Geodetic Control Network; transformation*

1. Introduction

1.1. Map Projection Properties

The distortion properties of maps are typically classified according to what is not distorted on the map. Unfortunately, there is no perfect way of representing spherical polar coordinates on a flat map. Then, no map projection can serve all purposes. Each one is good at some characteristics but bad at others. Different kinds of distortions will be introduced depending on the projection method. Map projections are classified according to what is not distorted on the map. The most important are:

a) Correct Areas, representing areas correctly. Most projections stretch area features on the map. This stretching is usually not constant across the map, so those features are close to the poles on a world map. Example: Mollweide projection.

b) Equal Distance. No map projection can correctly represent distances between all points on the map. This is important to remember that compute distance is a common application of GIS

databases. For large scale mapping in a small geographic region, the errors are usually negligible. For national or global applications using small scale maps, the distances calculated by a GIS are not reliable unless the system compensates for the error introduced by Euclidean metric calculation at this scale. Moreover, equidistant projections do not display all distances correctly, but they can represent all distances accurately from one or two points to all other points, or along one or more lines. Example: Equidistant conic projection.

c) Correct Angles Conformal Projections. Angles and shapes of small areas are shown correctly on the map. Meridians and latitudes intersect at right angles. These projections are most useful in navigation. Example: Mercator projection.

1.2. The Universal Transversal Mercator (UTM) Reference System

One cartographic reference system that deserves more detailed study is the UTM system. It is one of the most common systems used around the world for large-scale mapping. It is based on a transverse cylindrical projection -Transverse Mercator- in which the cylinder touches the globe along a meridian. A different “local” meridian is chosen for different parts of the world. Distortions in distance, scale and shape along this tangent are very small. The UTM system consists of sixty zones of longitude.

Each zone has a width of 6 degrees longitude, 3 degrees in each direction from the tangent meridian. UTM zones are numbered sequentially from west to east, starting with one for the zone that covers 180°W to 174°W with central meridian 177°W. The zones are divided into rows, with a height of eight degrees. These are assigned letters from north to south, starting at 80° south with the letter C. No UTM zone is defined for regions beyond poles limits because distortion is very large.

Map scale is a ratio, the larger the distance on the ground, the smaller the map scale. For example, 1:1,000,000 scale map is a small scale map, 1 divided by 1 million is a very small number (0.000001). A 1:5,000 scale map is a large scale, 1 divided by 5,000 is a relatively larger number (0.0002). Thus, large scale maps focus on small areas while small scale maps show large areas.

1.3. Practical Considerations

Any large digital geodatabase project requires the integration of map information from many different sources. For that reason, a coordinate system and standard projection need to be chosen. Ideally, the reference system that is chosen should match the system used in other agency activities in the country. Most countries use a standard projection that is optimal for the national geographic information system.

Most GIS packages provide functions for transforming coordinates between different reference systems and for converting digital maps from longitude/latitude into a map projection or to change between projections. They also allow the user to select a geodetic datum and any other transformation parameters.

Projection and datum information are usually included in geographic maps. A problem with digital spatial data sets is that standard GIS formats do not necessarily store projection information explicitly. For example, a Department of Land and Survey (DLS) may obtain a geographic data set of roads or hydrology without any information about their map projection. If such data are combined with the digital cadastre maps, they may not match perfectly. Vertical integration is impossible unless the two data sets are brought into the same projection system (Division, 2009). Coordinates may be rigorously converted from one coordinate type to another as long as the metadata on the coordinates is known (Williamson et al., 2004).

1.4. The Jordanian Geodetic Control Network

Geodetic Control is a system of precisely determined geographic control points that serve as the reference for all mapping activities in a country, sometimes termed benchmarks. Jordan contains two main networks, Network 1 (Cassini) and Network 2 (JTM).

There are two existing local geodetic reference systems in Jordan: Cassini-Soldner projection and Jordan Transverse Mercator (JTM) coordinates. The first, second and third order control is maintained by RJGC while the fourth order and below is maintained by DLS. Maps in Cassini-Soldner projection cover 17% of Jordan and maps in JTM projection cover the rest of the country, (Figure 1). For heavily populated areas in Jordan, the Cassini-Soldner (PAL) projection is still in use, while desert areas and some cities use JTM projection. Continuing to work with two existing local coordinates in an international environment, where positioning, navigation and information systems relate to a global earth model, is becoming increasingly inefficient and difficult. This paper highlights the process of implementing one projection for managing, collecting, storing and applying spatial data. This will ensure compatibility across various geographic systems locally and globally. Kadir et al. (2003) highlight the importance of providing a homogeneous geodetic infrastructure as the basis for integration of spatial data for sustainable development decision making by reducing duplication and uncertainty.

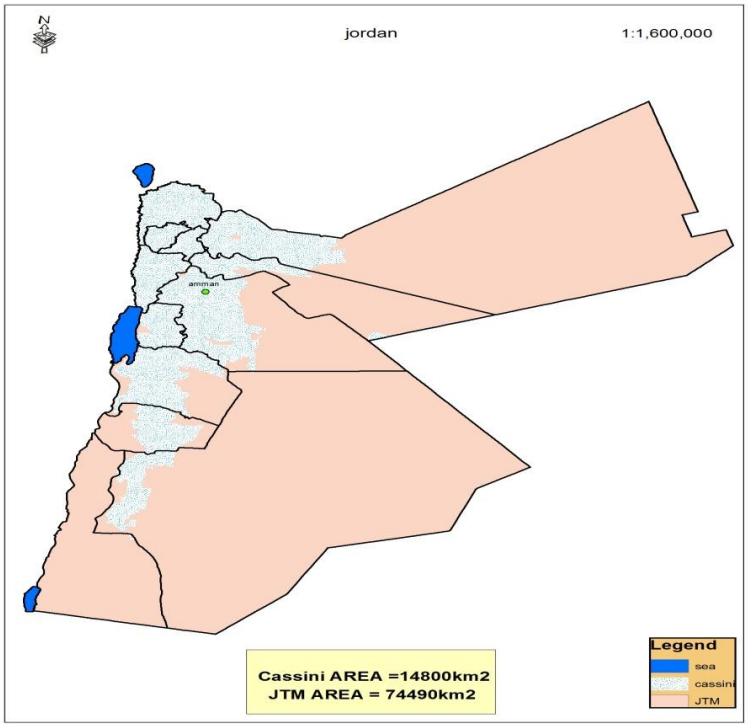

Figure 1: *JTM projection and Cassini projection*

1.4.1. *Network (CASS)*

Began in 1922 and was completed in 1956, (Figure 2). At the period of the British Mandate, the ruling triangulation was established and maintained by the Survey of Palestine. Apart from minor extensions in Trans-Jordan, the triangulation covered the area from the coast to the Jordan River Valley and from the Syrian border in the north as far south as Lat. 31°N. No permanent triangulation had been

established between this parallel and the Egyptian border. The Palestine major triangulation consisted of about 100 stations with sides of average length 15kms. The Survey of Palestine rectangular coordinates were computed on the Cassini projection. As this was not conformable, it was unsuitable for military survey purposes and a Transverse Mercator grid was therefore established to replace Cassini. The origin was a point at Jerusalem with geographical coordinates: — Lat. 31°44' 02.749". Long. 35°12'43.49". The Transjordan Triangulation Extension was initiated in 1937 by the Department of Lands and Surveys, Amman, and is based on the major triangulation of Palestine. Between Tiberias Lake and the Dead Sea, the network had 42 triangles 137M-178M. In 1941, the 36 New Zealand Survey Battery extended the Palestine triangulation down the eastern side of the Dead Sea in order to provide suitable mapping control points along the Palestine-Trans-Jordan border. This was eventually connected to the stations established by the South African Survey Company at the Gulf of Aqaba, (Gavish, 2005). Furthermore, it completed a circuit of triangulation called the Palestine-Trans-Jordan Chain (188M-211M).

The British Army contracted a civilian surveyor, Kolomoytzeff in 1942-1943 to observe a major triangulation connecting the Syrian Cadastral Primary Triangulation to the Existing work in Transjordan and it was a good network. The network had 42 triangles (1K-42K). In 1948, Jabalaltbeg Triangulation was initiated in the Jordanian-Saudi border area with 18 triangles (100TU-117TU).

In the period between 1945 and 1952, the North Eastern triangulation network was established to be the eastern facade of the South Eastern Mediterranean Network. Calculations were carried out by the Middle East Survey Directorate, and the number of network points was 22 points, holding the numbers 1A-22A. In the period between 1954 and 1955, the Jordanian-Iraqi Network has been established to unite the triangulation networks in the middle east region based on the European Datum ED 50 (global Ellipsoid), not like that used in the survey of Palestine (DLS, 2007).

In 1956, the U.S. Army Map Service (AMS) decided to eliminate all of the individual datums and grid systems of Europe, the Mid-East, and North Africa and to combine all into a single datum called the European Datum of 1950. The origin was at the Helmetturm (Helmert's Tower) in Pottsdam, Germany where: Φo = 52º 22' 51.446" North, Λo = 13º 03'58.928" East of Greenwich, and was referenced to the International 1924 ellipsoid where a = 6,378,388 m, and 1/f = 297. AMS converted all of the Palestine and Jordan surveys to the European Datum of 1950. The method used was a conformal transformation on the complex plane using UTM coordinates.

Local datum shift from Palestine 1928 Datum to European Datum 1950 is: $\Delta X = -76$ meters, $\Delta Y = +64$ meters, $\Delta Z = +442$ meters (Mugnier, 2008).

The Cassini–Soldner projection has many properties. There is no distortion in shape and area along the central meridian. Whereas on the other hand, the distortion increases with distance from the central meridian. Moreover, scale distortion increases with distance from the central meridian. Therefore, it is used primarily for large-scale mapping of areas near the central meridian. The extent on a spheroid is limited to 5° either side of the central meridian. Beyond that range, data projected to Cassini–Soldner may not project back to the same position. Transverse Mercator is often preferred due to the difficulty in measuring scale and direction on Cassini–Soldner (ESRI, 2015c).

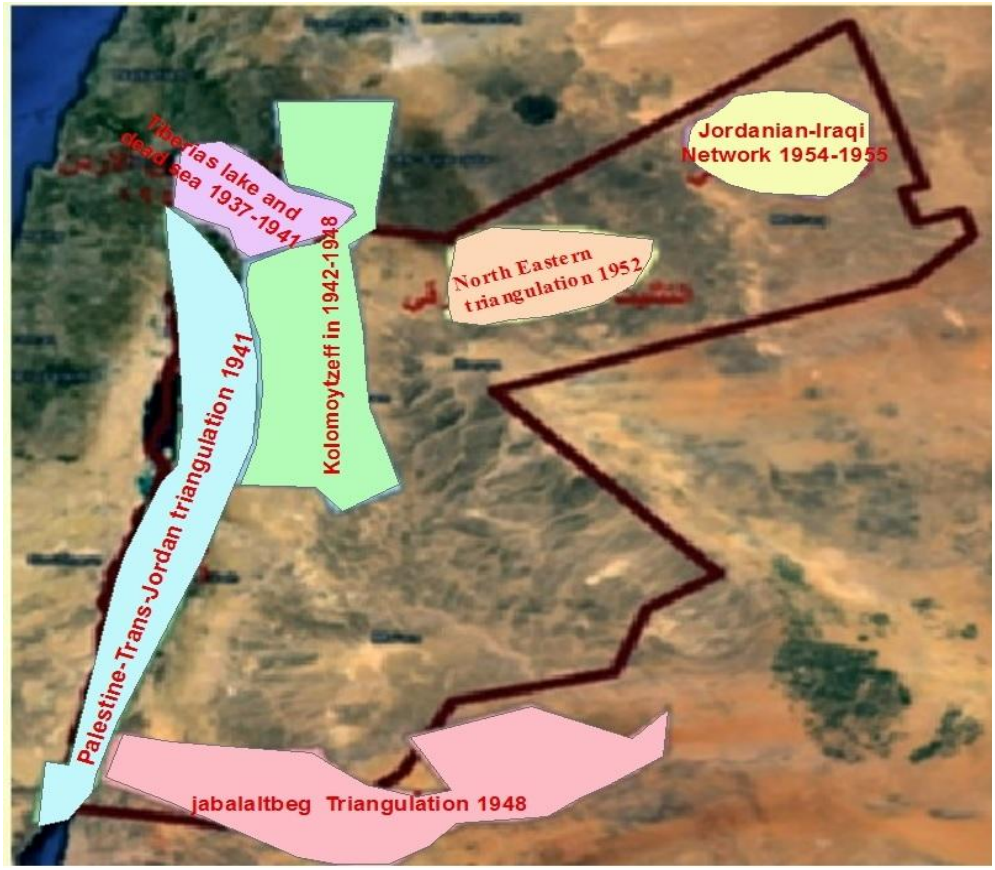

Figure 2: *All networks between 1937-1956 from RJGC*

1.4.2. *Network (JTM)*

Created by the Royal Jordanian Geographic Centre, is considered as a modern network and the most accurate in the world. It was completed in a record period of ten years and the number of the total points surpassed 2,000 points, with relative accuracy equivalent to 1:100000.

a) **First Order Control:** was carried out by the latest scientific methods at that time, where 14 points have been observed by satellite. By using the Doppler global ways, the number of points increased to be 87 points. Traverse network has been used to link the 14 Doppler points with 20km spacing between these points on average.

b) **Second Order Control:** at this stage, 10 points have been observed astronomically in addition to the astronomical points observed in the stage of First order control in order to make a geoid map. In addition, 519 new points were added where the distances between them ranged from 8-15 km. Consequently, the number of Second order control points became 529 points.

c) **Third Order Control:** at this stage, the densification of points has been increased, with a spacing of 4-8 km, and the number of these points reached to be more than 1,400 points.

Jordan used one UTM zone through the country. In fact, Jordan is located in two zones, 36-37, in the UTM system. Since the width of Jordan from west to east is less than 6 degrees, and each zone has a width of six degrees longitude, Jordan used one zone called JTM with a central meridian of 37°.

1.5. Linear distortions resulting from the use of various types of projections

Distortions that concern us here are the linear distortions resulting from the use of various types of projections (Figure 3).

a) **Cassini-Soldner Projection:** It is distinguished from other types of projections used in the kingdom like transverse Mercator that the linear distortion resulting from the use of Cassini-Soldner projection is directly related to the direction, and is expressed in the following equation.

$$DP = D_0\left(1 + \frac{COS^2 VE^2}{6R^2}\right)$$

$E^2 = (XA\text{-}X_0)^2 + (XB\text{-}X_0)^2 + (XA\text{-}X_0) - (XB\text{-}X_0)$
D0 = Length (longitude) on the surface of the ellipsoid
V = Deviation angle from the north (bearing)
R = The radius of the earth
E = Linear eccentricity

Where, the maximum value of the distortion is when cos V = 1 which means that the measured length of the line is located in the north-south. On the other hand, the lowest distortion value of the measured line is east-west cos V = 0

b) **Palestine Transverse Mercator (PTM):** the linear distortion resulting from the use of this projection is expressed in the following equation:

$$DP = D_0\left(1 + \frac{E^2}{6R^2}\right)$$

The distortion at a certain point does not change with the direction of the line, but this distortion increases as we move away from the central meridian because of the value of scale factor = 1

c) **Jordan Transverse Mercator (JTM):** the linear distortion resulting from the use of this projection is expressed in the following equations:

$$DP = D_0 \times K$$
$$K = K_0\left(1 + \frac{E^2}{6R^2}\right)$$

K is a scale factor at the points where the distance is measured. K_0 is a scale factor when the central meridian in this projection = 0.9998. One of the advantages of this system is that the distortion of the signal is changeable as we move away or closer to the central meridian.

The corrections of measured horizontal distances in Jordan are illustrated in Figure 4.

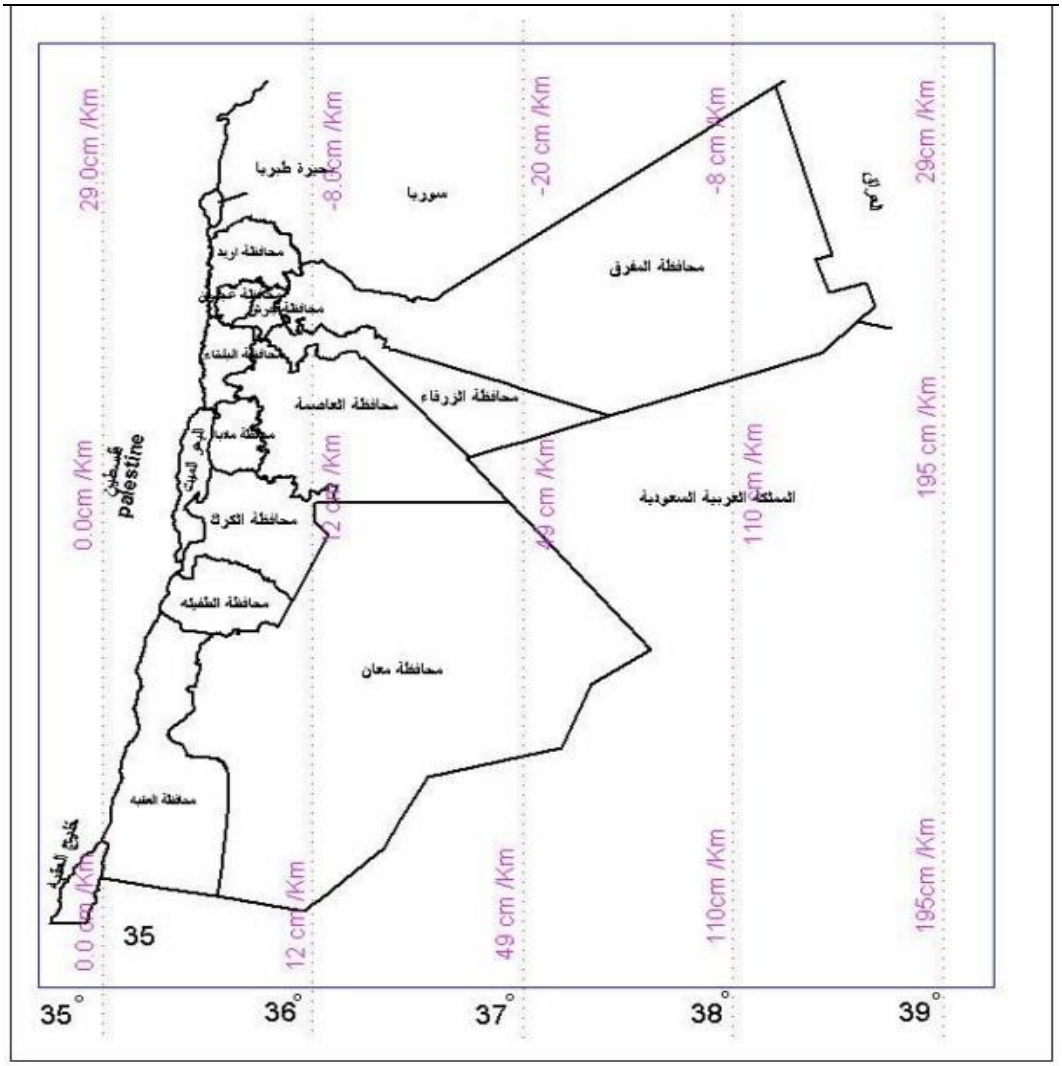

Figure 3: *Linear distortion in Cassini, Palestine PTM and JTM from DLS*

1.6. Defining Parameters for all Projections

Table 1: *All Projections Used in Jordan*

Projection Name	Jordan Transverse Mercator	Palestine Grid (Cassini)	Palestine Belt (Transverse Mercator)
Datum	Hayford Ellipsoid1909 JGD82	Palestine Spheroid Clarke 1880	Palestine Spheroid Clarke 1880
Central Longitude	37.0	35.212 080 55	35.212 080 55
Central Latitude	0.0	31.734 096 944 44	31.734 096 944 44
Scale Factor	0.9998	1	1
False Easting	500000	170,251.555	170,251.555
False Northing	-3000000	1,126,867.909	1,126,867.909

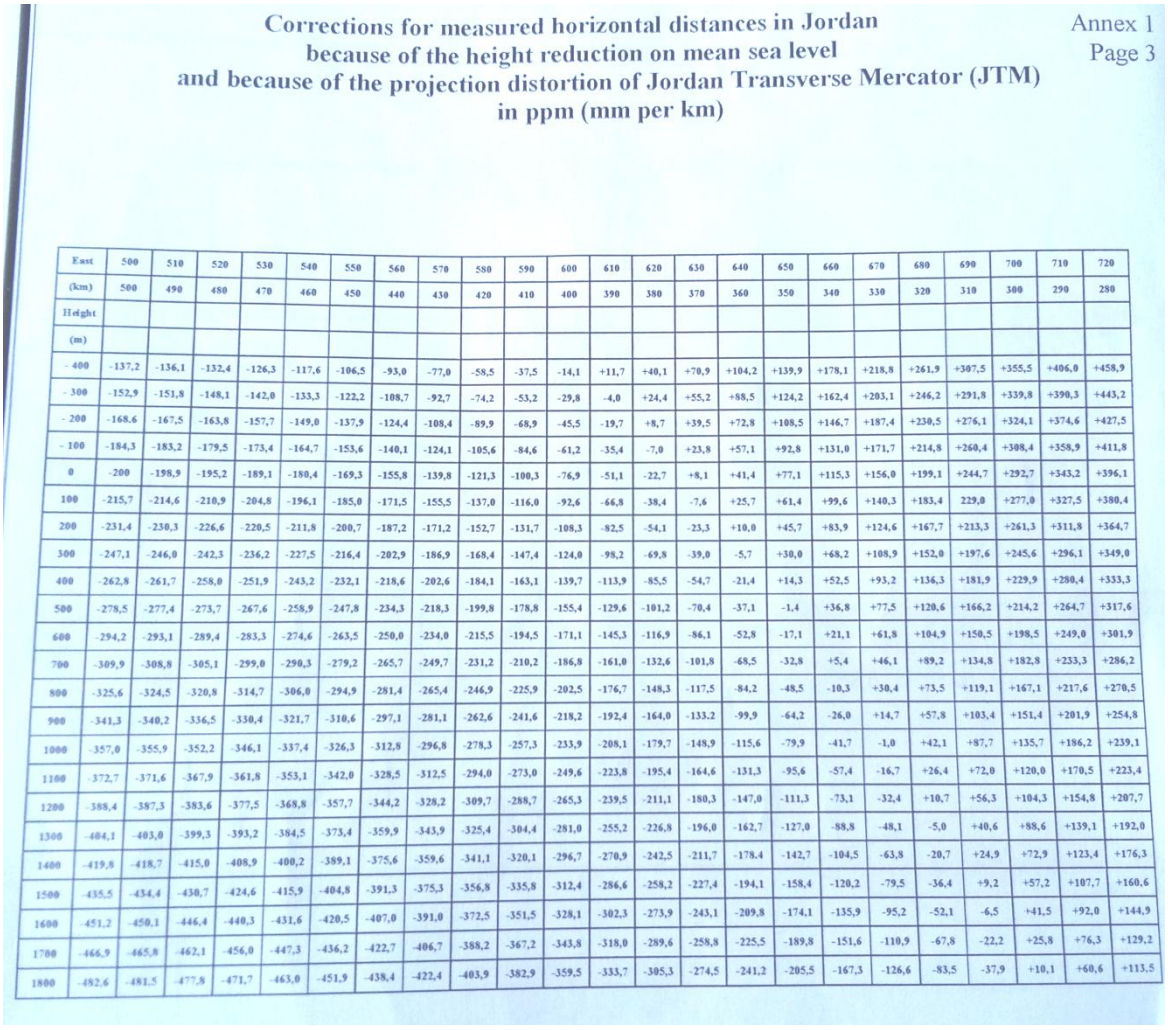

Corrections for measured horizontal distances in Jordan
because of the height reduction on mean sea level
and because of the projection distortion of Jordan Transverse Mercator (JTM)
in ppm (mm per km)

Annex 1
Page 3

East (km)	500	510	520	530	540	550	560	570	580	590	600	610	620	630	640	650	660	670	680	690	700	710	720
	500	490	480	470	460	450	440	430	420	410	400	390	380	370	360	350	340	330	320	310	300	290	280
Height (m)																							
- 400	-137,2	-136,1	-132,4	-126,3	-117,6	-106,5	-93,0	-77,0	-58,5	-37,5	-14,1	+11,7	+40,1	+70,9	+104,2	+139,9	+178,1	+218,8	+261,9	+307,5	+355,5	+406,0	+458,9
- 300	-152,9	-151,8	-148,1	-142,0	-133,3	-122,2	-108,7	-92,7	-74,2	-53,2	-29,8	-4,0	+24,4	+55,2	+88,5	+124,2	+162,4	+203,1	+246,2	+291,8	+339,8	+390,3	+443,2
- 200	-168,6	-167,5	-163,8	-157,7	-149,0	-137,9	-124,4	-108,4	-89,9	-68,9	-45,5	-19,7	+8,7	+39,5	+72,8	+108,5	+146,7	+187,4	+230,5	+276,1	+324,1	+374,6	+427,5
- 100	-184,3	-183,2	-179,5	-173,4	-164,7	-153,6	-140,1	-124,1	-105,6	-84,6	-61,2	-35,4	-7,0	+23,8	+57,1	+92,8	+131,0	+171,7	+214,8	+260,4	+308,4	+358,9	+411,8
0	-200	-198,9	-195,2	-189,1	-180,4	-169,3	-155,8	-139,8	-121,3	-100,3	-76,9	-51,1	-22,7	+8,1	+41,4	+77,1	+115,3	+156,0	+199,1	+244,7	+292,7	+343,2	+396,1
100	-215,7	-214,6	-210,9	-204,8	-196,1	-185,0	-171,5	-155,5	-137,0	-116,0	-92,6	-66,8	-38,4	-7,6	+25,7	+61,4	+99,6	+140,3	+183,4	229,0	+277,0	+327,5	+380,4
200	-231,4	-230,3	-226,6	-220,5	-211,8	-200,7	-187,2	-171,2	-152,7	-131,7	-108,3	-82,5	-54,1	-23,3	+10,0	+45,7	+83,9	+124,6	+167,7	+213,3	+261,3	+311,8	+364,7
300	-247,1	-246,0	-242,3	-236,2	-227,5	-216,4	-202,9	-186,9	-168,4	-147,4	-124,0	-98,2	-69,8	-39,0	-5,7	+30,0	+68,2	+108,9	+152,0	+197,6	+245,6	+296,1	+349,0
400	-262,8	-261,7	-258,0	-251,9	-243,2	-232,1	-218,6	-202,6	-184,1	-163,1	-139,7	-113,9	-85,5	-54,7	-21,4	+14,3	+52,5	+93,2	+136,3	+181,9	+229,9	+280,4	+333,3
500	-278,5	-277,4	-273,7	-267,6	-258,9	-247,8	-234,3	-218,3	-199,8	-178,8	-155,4	-129,6	-101,2	-70,4	-37,1	-1,4	+36,8	+77,5	+120,6	+166,2	+214,2	+264,7	+317,6
600	-294,2	-293,1	-289,4	-283,3	-274,6	-263,5	-250,0	-234,0	-215,5	-194,5	-171,1	-145,3	-116,9	-86,1	-52,8	-17,1	+21,1	+61,8	+104,9	+150,5	+198,5	+249,0	+301,9
700	-309,9	-308,8	-305,1	-299,0	-290,3	-279,2	-265,7	-249,7	-231,2	-210,2	-186,8	-161,0	-132,6	-101,8	-68,5	-32,8	+5,4	+46,1	+89,2	+134,8	+182,8	+233,3	+286,2
800	-325,6	-324,5	-320,8	-314,7	-306,0	-294,9	-281,4	-265,4	-246,9	-225,9	-202,5	-176,7	-148,3	-117,5	-84,2	-48,5	-10,3	+30,4	+73,5	+119,1	+167,1	+217,6	+270,5
900	-341,3	-340,2	-336,5	-330,4	-321,7	-310,6	-297,1	-281,1	-262,6	-241,6	-218,2	-192,4	-164,0	-133,2	-99,9	-64,2	-26,0	+14,7	+57,8	+103,4	+151,4	+201,9	+254,8
1000	-357,0	-355,9	-352,2	-346,1	-337,4	-326,3	-312,8	-296,8	-278,3	-257,3	-233,9	-208,1	-179,7	-148,9	-115,6	-79,9	-41,7	-1,0	+42,1	+87,7	+135,7	+186,2	+239,1
1100	-372,7	-371,6	-367,9	-361,8	-353,1	-342,0	-328,5	-312,5	-294,0	-273,0	-249,6	-223,8	-195,4	-164,6	-131,3	-95,6	-57,4	-16,7	+26,4	+72,0	+120,0	+170,5	+223,4
1200	-388,4	-387,3	-383,6	-377,5	-368,8	-357,7	-344,2	-328,2	-309,7	-288,7	-265,3	-239,5	-211,1	-180,3	-147,0	-111,3	-73,1	-32,4	+10,7	+56,3	+104,3	+154,8	+207,7
1300	-404,1	-403,0	-399,3	-393,2	-384,5	-373,4	-359,9	-343,9	-325,4	-304,4	-281,0	-255,2	-226,8	-196,0	-162,7	-127,0	-88,8	-48,1	-5,0	+40,6	+88,6	+139,1	+192,0
1400	-419,8	-418,7	-415,0	-408,9	-400,2	-389,1	-375,6	-359,6	-341,1	-320,1	-296,7	-270,9	-242,5	-211,7	-178,4	-142,7	-104,5	-63,8	-20,7	+24,9	+72,9	+123,4	+176,3
1500	-435,5	-434,4	-430,7	-424,6	-415,9	-404,8	-391,3	-375,3	-356,8	-335,8	-312,4	-286,6	-258,2	-227,4	-194,1	-158,4	-120,2	-79,5	-36,4	+9,2	+57,2	+107,7	+160,6
1600	-451,2	-450,1	-446,4	-440,3	-431,6	-420,5	-407,0	-391,0	-372,5	-351,5	-328,1	-302,3	-273,9	-243,1	-209,8	-174,1	-135,9	-95,2	-52,1	-6,5	+41,5	+92,0	+144,9
1700	-466,9	-465,8	-462,1	-456,0	-447,3	-436,2	-422,7	-406,7	-388,2	-367,2	-343,8	-318,0	-289,6	-258,8	-225,5	-189,8	-151,6	-110,9	-67,8	-22,2	+25,8	+76,3	+129,2
1800	-482,6	-481,5	-477,8	-471,7	-463,0	-451,9	-438,4	-422,4	-403,9	-382,9	-359,5	-333,7	-305,3	-274,5	-241,2	-205,5	-167,3	-126,6	-83,5	-37,9	+10,1	+60,6	+113,5

Figure 4: *Correction for measured horizontal distance in Jordan (JTM) (DLS)*

2. Methodology

2.1. Implementation and Adopting a Reference Frame to Support SDI

The concept of the SDI hierarchy, ranging from local through to global levels, needs to be built on a solid positional foundation. Without a good geodetic base, many of the problems regarding positional accuracy become more intelligible (Williamson et al., 2004).

a) Defining the distortion and homogeneity in the geodetic network, this network is computed in the Cassini-Soldner projection, which is not a conformal projection. Some triangulation points were observed by GPS (Global Positioning System). These points have coordinates in the Cassini-Soldner projection (from the office which is responsible for triangulations) and the field surveying provides its Cassini coordinates. The points are used to determine distortion and homogeneity in the geodetic network.

The triangulations are from three governorates: Irbid, Jarash, and Ajloun. We will take every one as a separate zone then we take them all together, we used Leica Geo office 8 software to calculate coordinates in different zones.

AJ0007	228985.6810	1197031.3170	0.0000
AJ0019	228983.5650	1195858.2780	0.0000
IR0704	231942.8230	1197734.0610	0.0000
JA0216	233223.945	1195025.495	0.0000
JA0219	233668.961	1194104.523	0.000

//observation depending on three zones//

aj0007	228985.4455	1197031.3544
aj0019	228983.3849	1195858.1782
IR0704	231942.7064	1197734.1473
ja0216	233223.5374	1195025.5146
ja0219	233668.5968	1194104.6619

//observation depending on Ajloun zone//

aj0007	228985.4455	1197031.3543
aj0019	228983.3849	1195858.1781
IR0704	231943.0139	1197734.2139
ja0216	233225.3833	1195026.2303
ja0219	233670.9110	1194105.4507

//observation depending on Irbid zone//

aj0007	228985.5394	1197031.0945
aj0019	228983.5827	1195858.1539
IR0704	231942.7064	1197734.1473
ja0216	233225.0528	1195026.5245
ja0219	233670.5691	1194105.8803

//observation depending on Jarash zone//

aj0007	228983.6221	1197030.6662
aj0019	228981.5136	1195857.6594
IR0704	231941.0119	1197733.3471
ja0216	233223.1205	1195025.4652
ja0219	233668.5610	1194104.7111

Table 2: *Comparison table for aj0007*

Triangulations No	aj0007	aj0007	aj0007	aj0007	**aj0007**
Zone	From office	three zone	Ajloun zone	Irbid zone	**Jarash zone**
x	228985.6810	228985.4455	228985.4455	228985.5394	**228983.6221**
y	1197031.3170	1197031.3544	1197031.3543	1197031.0945	**1197030.6662**

Coordinate Differences: if we match aj0007 from office with aj0007 from Jarash, we will see approximately 2 meters difference on coordinate.

Table 3: *Comparison table for aj0019*

Triangulations No	aj0019	aj0019	aj0019	aj0019	**aj0019**
Zone	From office	three zone	Ajloun zone	Irbid zone	**Jarash zone**
x	228983.5650	228983.3849	228983.3849	228983.5827	**228981.5136**
y	1195858.2780	1195858.1782	1195858.1781	1195858.1539	**1195857.6594**

Coordinate Differences: if we match aj0019 from office with aj0019 from Jarash, we will see approximately 2 meters difference on coordinate.

Table 4: *Comparison table for IR0704*

Triangulations No	IR0704	IR0704	IR0704	IR0704	**IR0704**
Zone	From office	three zone	Ajloun zone	Irbid zone	**Jarash zone**
x	231942.8230	231942.7064	231943.0139	231942.7064	**231941.0119**
y	1197734.0610	1197734.1473	1197734.2139	1197734.1473	**1197733.3471**

Coordinate Differences: if we match IR0704 from office with IR0704 from Jarash, we will see approximately 2 meters difference on coordinate.

Table 5: *Comparison table for ja0216*

Triangulations No	ja0216	ja0216	**ja0216**	**ja0216**	ja0216
Zone	From office	three zone	**Ajloun zone**	**Irbid zone**	Jarash zone
x	233223.945	233223.5374	**233225.3833**	**233225.0528**	233223.1205
y	1195025.495	1195025.5146	**1195026.2303**	**1195026.5245**	1195025.4652

Coordinate Differences: if we match ja0216 from office with ja0216 from Ajloun and Irbid zones, we will see approximately 2 meters difference on coordinate.

Table 6: *Comparison table for ja0219*

Triangulations No	ja0219	ja0219	**ja0219**	**ja0219**	ja0219
Zone	From office	three zone	**Ajloun zone**	**Irbid zone**	Jarash zone
x	233668.961	233668.5968	**233670.9110**	**233670.5691**	233668.5610
y	1194104.523	1194104.6619	**1194105.4507**	**1194105.8803**	1194104.7111

Coordinate Differences: if we match ja0219 from office with ja0219 from Ajloun and Irbid zones, we will see approximately 2 meters difference on coordinate.

Therefore, the network is not homogeneous and according to (Z. Alostah, and S. Alkhatib) the reasons for discrepancies in map-edges (in Department of Land and Survey) is the non-homogeneous network (Cassine).

Depending on the previous results, the Cassini-Soldner projection is non-homogeneous and JTM is homogeneous.

JTM

AJ0007	390576.8603	582439.4797	0.0000
AJ0019	390555.1000	581266.9639	0.0000
IR0704	393545.0590	583092.4975	0.0000
ja0216	394781.501	580363.538	0.0000
ja0219	395211.315	579435.654	0.0000
aj0007	390576.6255	582439.5210	0.0050
aj0019	390554.9182	581266.8671	0.2241
IR0704	393544.9438	583092.5858	0.0092
ja0216	394781.4384	580364.0430	0.0023
ja0219	395211.3637	579436.1142	0.0053

b) Geodetic Network Coverage: the JTM covers all Jordan while Cassini projection does not cover the eastern regions of the Kingdom (Figures 5 and 6).

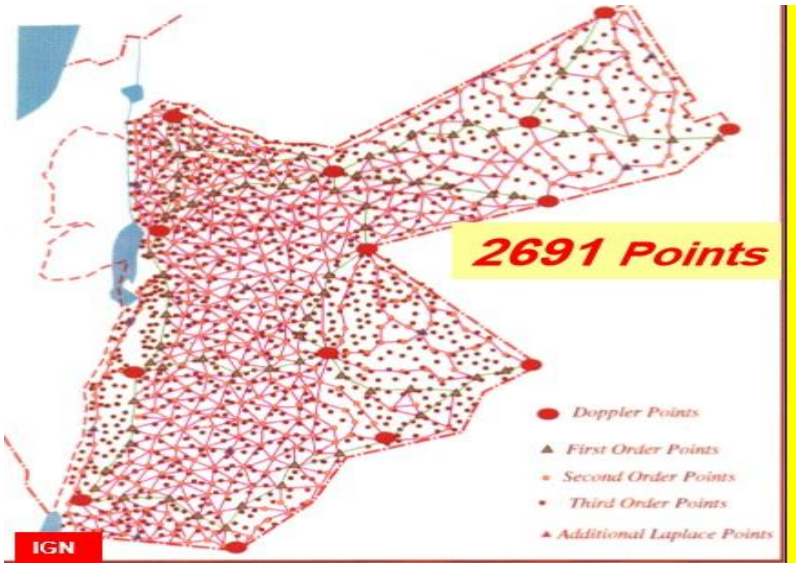

***Figure 5**: JTM Network*

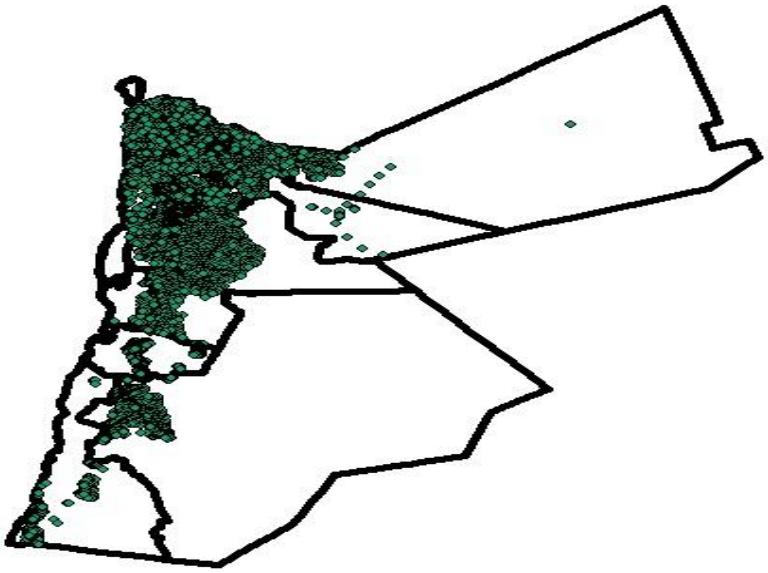

***Figure 6:** Cassini Network*

c) Jordan used one zone throughout the country. In fact, Jordan is located in the two zones 36-37 in the UTM system. Since the width of Jordan from west to east is less than 6 degrees, each zone has a width of six degrees longitude. Therefore, Jordan used one zone called JTM with the central meridian of 37°, while Cassini used two zones.

d) The national geodesic network, created by the Royal Jordanian Geographic Centre (RJGC), is considered as a modern network and the most accurate in the world. It was completed in a record period of ten years and the number of total points surpassed 2,000 points, with relative accuracy equivalent to 1:100000. In the 1930s and 1940s, the English army had established

several triangulation networks, which served as a basis for both topographic and cadastral surveying.

e) The geodetic network is computed and based on a non-conformal projection “Cassini-Soldner” while JTM is a conformal projection.

f) From 1978-1988 (new) the RJGC completed the national geodetic network (JTM) (1st, 2nd and 3rd order) while Cassini triangulation network began in 1922 and was completed in 1956 (old).

Depending on the previous points we will transform to JTM projection.

2.2. Transformation

Geodetic datum transformation is the determination of a mathematical relationship to be used in transforming a set of coordinates from one geodetic datum to another (Dawod and Alnaggar, 2000). There are many ways of modelling the transformation between two datums (ICSM, 2014), but those in common use include:

2.2.1. *Molodensky's method* is commonly used in Geographic Information Systems (GIS) and hand-held GPS receivers. The formulae are simple, assuming that the transformation between the local and global datums can be represented by 5 parameters: a shift at the origin (the earth's centre of mass) along the earth-centred Cartesian coordinate axes (ΔX, ΔY, ΔZ) and the difference between the local and global ellipsoids (semi-major axis and flattening). The origin shifts can be determined by an averaging of the same differences at each of the common points and the difference in ellipsoids is a simple subtraction of the ellipsoid parameters; the errors in Molodensky's formulae: 5 metres.

Table 7: *Advantages and disadvantages of Molodensky transformation*

Molodensky Transformation	
Advantages	*Disadvantages*
• Simple derivation	• Assumes internally consistent networks
• Simple application	• Limited accuracy
• Available in GIS packages and hand-held GPS	• Derivation requires ellipsoidal heights

2.2.2. *The 7-parameter method* assumes a similar relationship between the local and global datums. The common points are used in a Least Squares process to solve 7 parameters which represent the relationship between the two datums: origin shifts at the earth's centre of mass (ΔX, ΔY, ΔZ); rotations about each of the axes (Rx, Ry, Rz); and a scale change between the two systems, the errors in 7-parameter: 1-2 metres.

Table 8: *Advantage and disadvantage of 7-Parameter Transformation*

7-Parameter Transformation	
Advantages	*Disadvantages*
• Improved accuracy	• Assumes consistent geodetic networks
• Used in many GIS packages	• Moderately complex derivation & application

	• Requires ellipsoidal heights for both global and local positions
	• Accuracy limited by geodetic network consistency

The selection of a datum transformation method depends on the accuracy required and the number of commonly available points, the size of the area and the type of the network (3D or 2D or even 1D) (Mitsakaki, 2004).

We used ArcMap 10.2.2 and the parameter for JTM projection and Cassini projection depended on ArcMap (Table 9).

Table 9: *the parameter for JTM projection and Cassini projection depended on ArcMap*

Projection name	Palestine_1923_Palestine_Grid	Jordan_JTM
Authority	Custom	ESRI
Projection	Cassini	Transverse_Mercator
False_Easting	170251.555	500000.0
False_Northing	1126867.909	-3000000.0
Central_Meridian	35.21208055555556	37.0
Scale_Factor	1.0	0.9998
Latitude_Of_Origin	31.73409694444445	0.0
Linear Unit	Meter (1.0)	Meter (1.0)
Geographic Coordinate System	GCS_Palestine_1923	GCS_Jordan
Angular Unit:	Degree (0.0174532925199433)	Degree (0.0174532925199433)
Prime Meridian	Greenwich (0.0)	Greenwich (0.0)
Datum	D_Palestine_1923	D_Jordan
Spheroid	Clarke_1880_Benoit	International_1924
Semimajor Axis	6378300.789	6378388.0
Semiminor Axis	6356566.435	6356911.946127947
Inverse Flattening	293.4663155389802	297.0

Transformation depends on GIS package, arc 10.2.2 and we match the transformed zone with adjacent border because it's in JTM. By this way the error has been determined.

a) Depending on **Palestine_1923_To_WGS1984_1+ Jordan_To_WGS_1984** parameter, the error is approximately 5 meters (Figure 7).

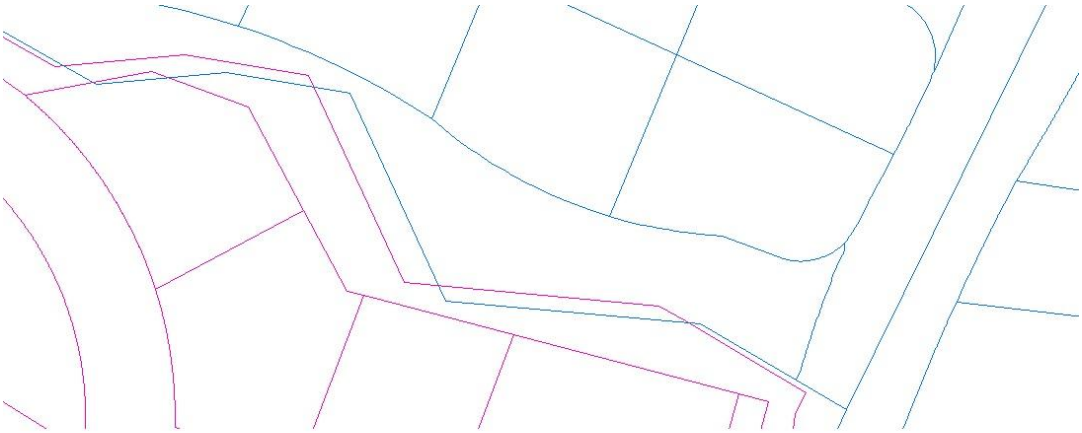

Figure 7: *The error depending on* ***Palestine_1923_To_WGS1984_1+ Jordan_To_WGS_1984*** *parameter*

b) Depending on **Palestine_1923_To_WGS1984_1X+ Jordan_To_WGS_1984** parameter, the error is more than 100 meters (Figure 8).

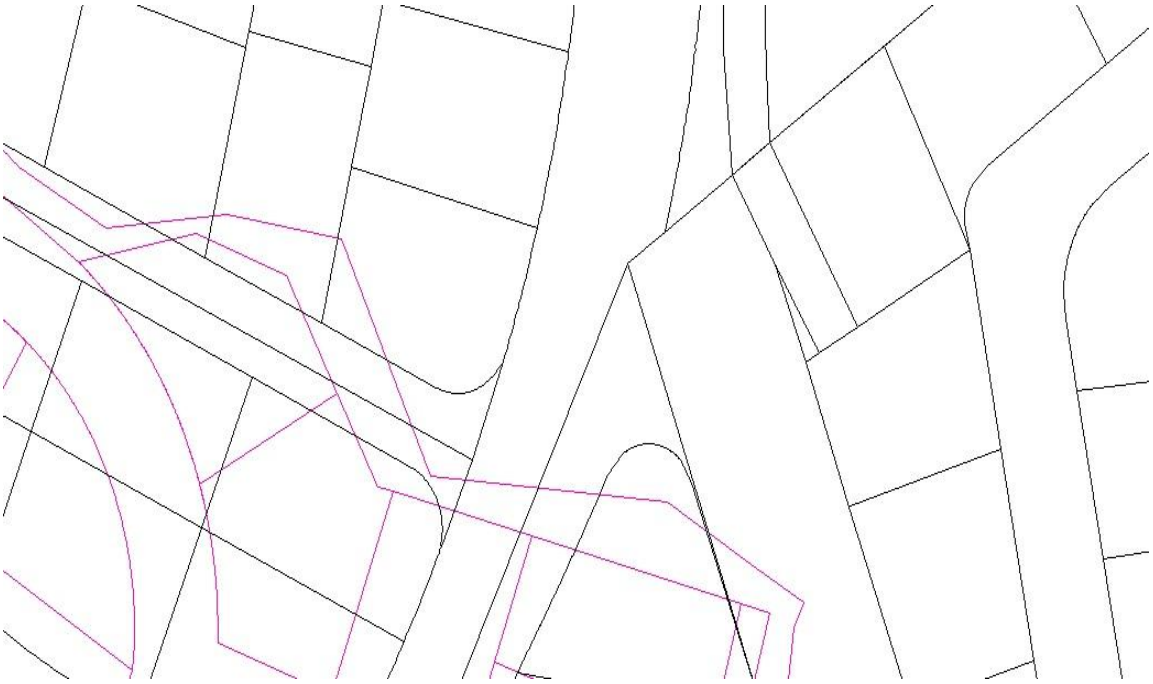

Figure 8: *the error depending on* ***Palestine_1923_To_WGS1984_1X+ Jordan_To_WGS_1984*** *parameter*

c) Depending on **Palestine_1923_To_WGS1984_2+ Jordan_To_WGS_1984** parameter, the error is approximately 10 meters (Figure 9).

Figure 9: *The error depending on* ***Palestine_1923_To_WGS1984_2+ Jordan_To_WGS_1984*** *parameter*

d) Depending on **Palestine_1923_To_WGS1984_2X+ Jordan_To_WGS_1984** parameter, the error is approximately 2.5 meters (Figure 10).

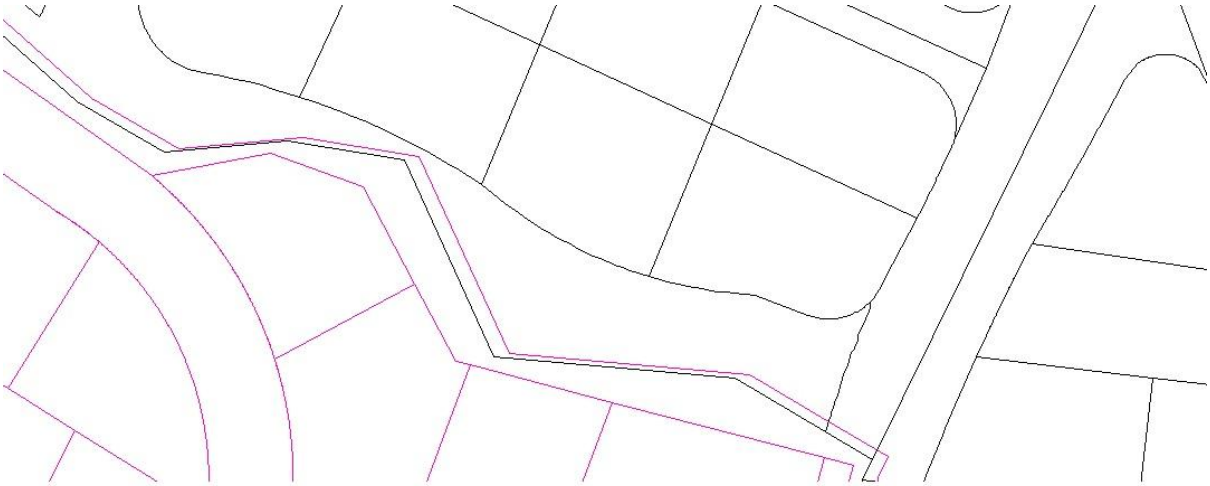

Figure 10: *The error depending on* ***Palestine_1923_To_WGS1984_2X+ Jordan_To_WGS_1984*** *parameter*

The (7 parameters) transformation will not suffice for high accuracy applications.

Table 10: *Errors (for transformation from Cass to JTM, used in arc 10.2.2)*

Parameter for transformation from Cass to JTM, used in arc 10.2.2 (Geographic Transformation)	Errors
Palestine_1923_To_WGS1984_1+ Jordan_To_WGS_1984	Approximately 5 meter
Palestine_1923_To_WGS1984_1X+ Jordan_To_WGS_1984	Approximately 100 meter
Palestine_1923_To_WGS1984_2+ Jordan_To_WGS_1984	Approximately 10 meter
Palestine_1923_To_WGS1984_2X+ Jordan_To_WGS_1984	Approximately 2.5 meter

2.2.3. ***Spatial Adjustment Transformations*** Transformations move or shift data within a coordinate system. For transformations, from and to locations of links are used to construct the transformation formulas. When creating links for transformations, you are trying to match the same location in the source and destination locations. Links do not have to start or end on features. The distance from and to locations can often be quite large. ArcMap supports three types of transformations: affine, similarity, and projective.

i) Affine Transformation

An affine transformation can differentially scale the data, skew it, rotate it, and translate it. Figure 11 illustrates the four possible changes.

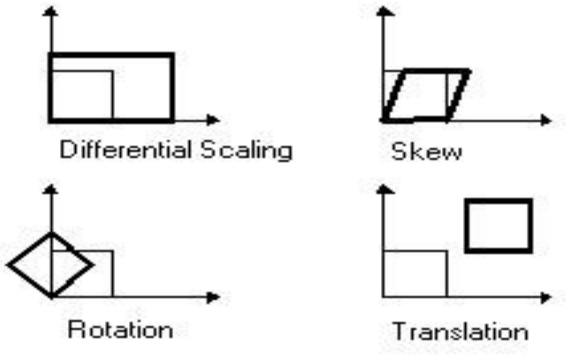

Figure 11: *The four possible changes of an affine transformation*

The affine transformation function is:

x’ = Ax + By + C
y’ = Dx + Ey + F

where x and y are coordinates of the input layer and x’ and y’ are the transformed coordinates. A, B, C, D, E, and F are determined by comparing the location of source and destination control points. They scale, skew, rotate, and translate the layer coordinates.

ii) Similarity Transformation

The similarity transformation scales, rotates, and translates the data. It will not independently scale the axes, nor will it introduce any skew. It maintains the aspect ratio of the features transformed, which is important if you want to maintain the relative shape of features.

The similarity transform function is

x’ = Ax + By + Cy’ = -Bx + Ay + F

where
A = s * cos t
B = s * sin t
C = translation in x direction
F = translation in y direction
and
s = scale change (same in x and y directions)
t = rotation angle, measured counterclockwise from the x-axis

iii) Projective Transformation

The projective transformation is based on a more complex formula that requires a minimum of four displacement links.

x’ = (Ax + By + C) / (Gx + Hy + 1)
y’ = (Dx + Ey + F) / (Gx + Hy + 1)

This method is used to transform data captured directly from aerial photography (ESRI, 2015B).

In this work, we used affine adjustment to transform from the Palestine projection to the JTM projection (see Figures 12, 13 and 14). For this purpose the area of the Kingdom was divided into blocks 12x12 km. Blocks are edge matched so that points transformed at or near the boundary of multiple blocks will not result in multiple differing solutions. Depending on our study, Badran and Abunoser villages have been transferred, more than 80 observed points by GPS (Global Positioning System) have been used, and any suspect data (observations) that may contain errors or blunders are removed during the adjustment process. These points were used to determine the transformation parameters between the CASS and JTM projections. What applies to this block can be applied to all Jordan. After we finish transformation, we will get a file for transformation parameters and it's an accurate and rigorous solution.

The cadastral map in Jordan is used as a base map for most purposes such as utilities, transportation, developments plans and land use planning. The Department of Lands and Survey (DLS) is the agency responsible for both the land registration and the cadastral surveying on a national level DLS consists of 12 central directorates (in the headquarters) and 34 land registration directorates distributed all over the kingdom plus 4 registration service offices. DLS is under the umbrella of the Ministry of Finance.

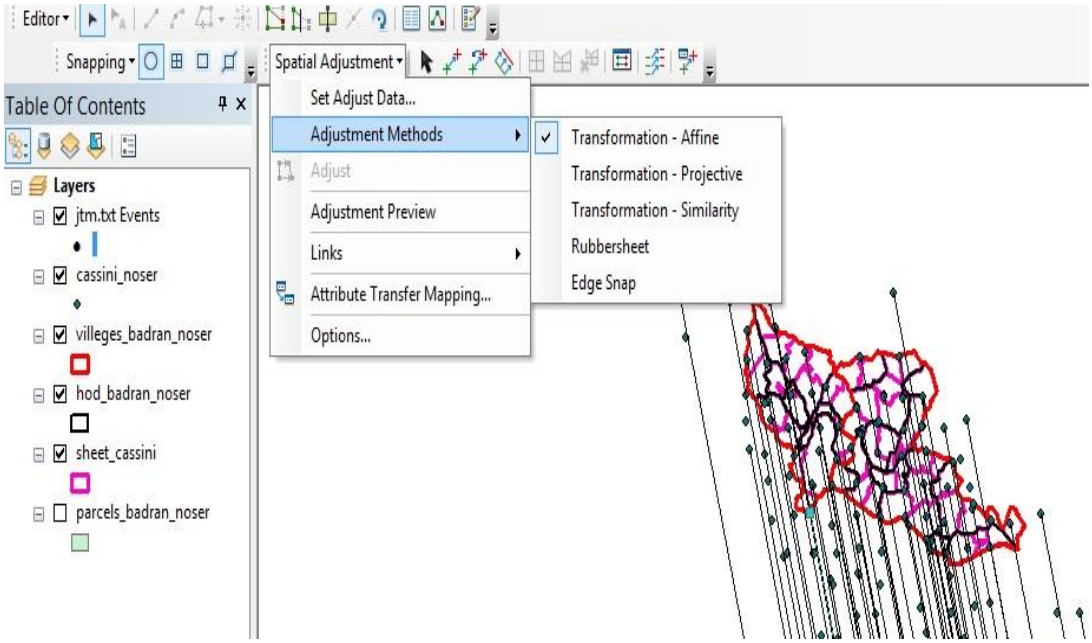

Figure 12: *Affine Adjustment Process*

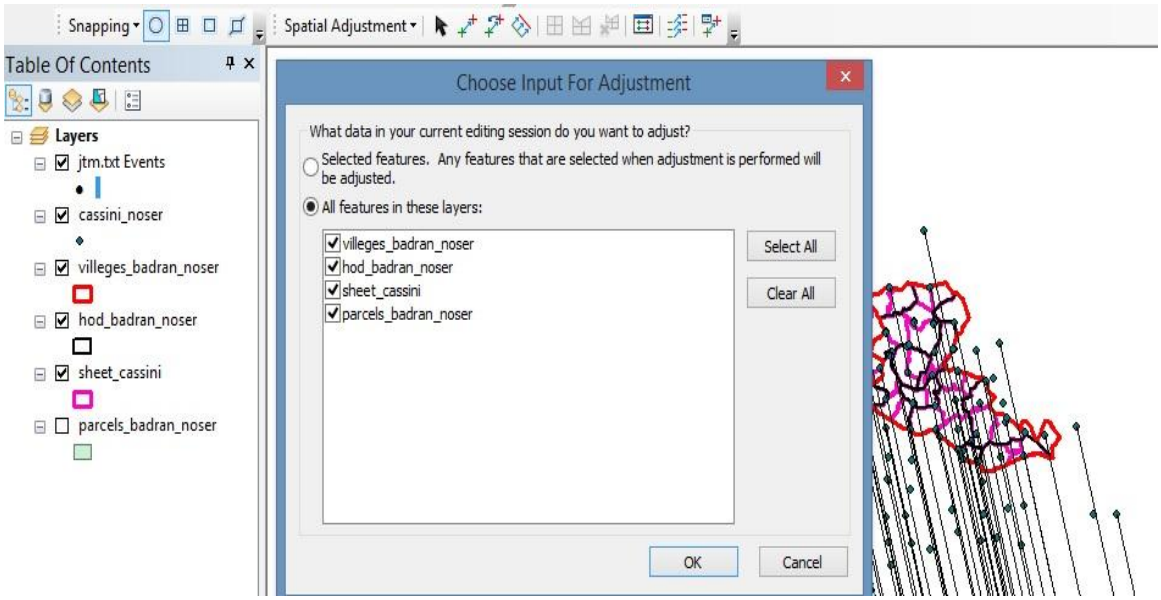

Figure 13: *Selected layers for Affine Adjustment Process*

The point we have used in transformation, in Cassini-Soldner projection and Jordan Transverse Mercator (JTM). The RMS Error is 0.108 meter Table 11.

Table 11: *The points were used to determine the transformation parameters between CASS and JTM projections*

id	X Source	Y Source	X Destination	Y Destination	Residual Error
70	236932.342	1162983.154	397953.507	548268.009	0.019167
66	238059.34	1163151.362	399083.154	548417.404	0.021836
12	237954.43	1162085.409	398960.511	547353.47	0.032299
35	239262.125	1162769.632	400279.4	548015.736	0.03598
52	231009.959	1167962.566	392115.136	553344.656	0.036372
50	237039.538	1163808.186	398074.433	549091.049	0.041181
7	238854.332	1163908.461	399890.646	549161.059	0.042089
32	234937.411	1161101.628	395927.574	546420.199	0.043251
46	239001.797	1161992.972	400006.182	547243.615	0.047444
40	231265.043	1167132.105	392356.349	552510.19	0.048618
24	230159.394	1168262.268	391269.712	553658.407	0.049704
17	239840.422	1164165.876	400880.874	549401.975	0.050494
21	235957.361	1161043.303	396946.409	546344.897	0.056255
25	237891.894	1164915.81	398945.145	550184.177	0.057839
49	229981.459	1167009.377	391070.937	552408.837	0.058137
11	232818.746	1161183.818	393810.563	546537.686	0.060566
65	237004.03	1164857.983	398056.418	550141.158	0.061973
36	238039.857	1160282.317	399015.908	545549.462	0.064502
30	229997.593	1166059.676	391071.254	551459.173	0.064508
33	236808.57	1166161.951	397882.735	551447.886	0.069579
63	237076.868	1161040.481	398065.705	546323.428	0.069797
39	243165.052	1161158.831	404154.861	546340.414	0.070088
55	240121.195	1161298.633	401113.848	546530.823	0.071542
34	241809.858	1160798.06	402793.896	546002.283	0.075225
29	231739.424	1166128.134	392813.947	551498.621	0.07985
27	236134.986	1164934.532	397188.752	550232.157	0.084909

2	233825.871	1162020.687	394831.444	547357.531	0.086189
68	238835.868	1160889.452	399821.924	546143.148	0.088038
28	235210.877	1163845.946	396246.627	549159.22	0.094924
51	232579.953	1166296.087	393657.151	551652.53	0.095516
19	244925.024	1157934.589	405860.82	543087.802	0.096019
48	234650.878	1163249.405	395676.773	548572.164	0.102339
60	238622.887	1160601.495	399604.195	545858.814	0.105039
67	240880.844	1160075.302	401853.018	545295.178	0.105621
53	234901.17	1164548.79	395948.668	549867.03	0.110886
1	232890.815	1162063.783	393897.23	547416.202	0.114077
5	234026.167	1162905.199	395046.417	548238.462	0.114235
4	230969.203	1164734.985	392020.667	550118.721	0.117021
44	234137.355	1163925.096	395174.57	549256.221	0.126696
10	233254.187	1163163.239	394278.834	548509.297	0.143883
3	231838.991	1163885.996	392875.906	549255.435	0.154067
47	233536.642	1165190.522	394595.004	550531.329	0.168158
61	230104.891	1163192.903	391130.851	548591.507	0.177628
20	232900.546	1165000.772	393955.834	550352.231	0.185131
14	226726.899	1169085.204	387851.65	554538.334	0.195029
45	235074.607	1166178.775	396149.144	551493.596	0.21568
6	236555.057	1168231.25	397663.551	553520.795	0.228909
43	228526.689	1170361.844	389672.469	555784.579	0.246911
				RMS	**0.108392**

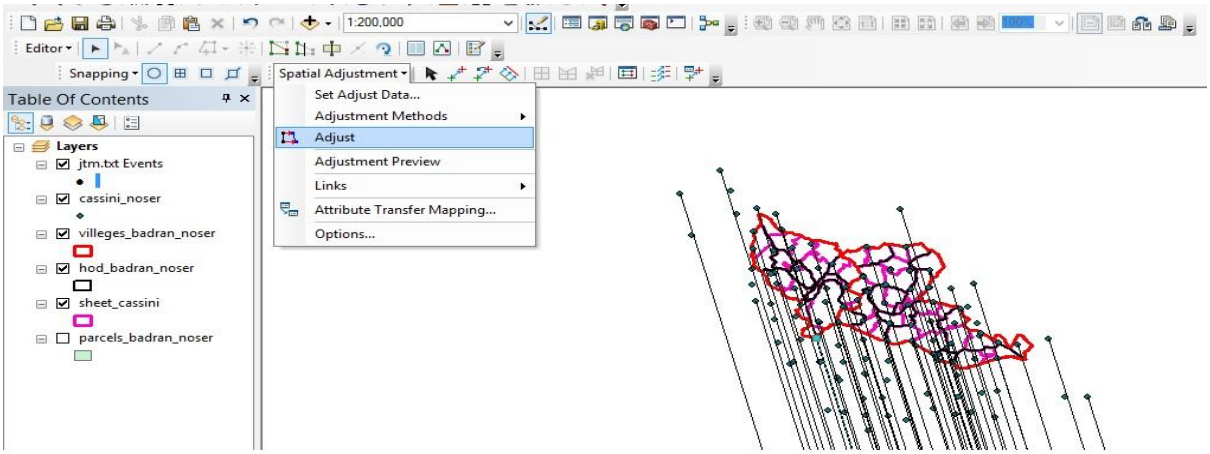

Figure 14: *Affine Adjustment Process after selected layer*

We match the transformed zone with the adjacent border because it's in JTM and its approximate match Figure 15.

Figure 15: *the result after applied an affine transformation process*

3. Results and Discussion

a) In this study, CASS was demonstrated as a non-homogeneous projection. On the other hand, the JTM was a homogeneous projection. Moreover, the JTM was more comprehensive than CASS, where JTM covers all Jordan while Cassini projection does not cover the eastern regions of the Kingdom.
b) Depending on GIS the package, ArcMap 10.2.2, the lowest error in transformation was approximately 2.5 meter, therefore, it not suitable for accurate data like cadastre and topographic maps.
c) Depending on Affine Adjustment (block 12*12 km), the RMS error was 10 cm, which is an adequate result and suitable for accurate data like cadastre and topographic maps.
d) The homogeneity, comprehensiveness, and accuracy of the JTM projection taken together to prove that the JTM projection is more suitable for surveying work than the CASS projection. This supports the Department of Land and Survey in Jordan to transform from CASS to JTM to build the Jordan Digital Cadastral Data Base (JDCDB).
e) According to this study, the discrepancies between organisations might be eliminated by using the JTM projection as one reference system in Jordan.

4. Conclusions

The ideas presented in this paper are so far just ideas - not official policy. However, the Department of Land and Survey proposes the development of building the Jordan Digital Cadastral Data Base (JDCDB). The original maps are in Cassini-Soldner projection which is a non-homogeneous datum and doesn't cover all Jordan using two zones (1922-1956). Therefore, transforming all the (20000) maps to JTM fulfils the overall goal of establishing JDCDB to participate in building National Geographic Information System (NGIS).

The JTM projection will have the flexibility to provide a stable spatial foundation for Jordan for the foreseeable future. Many users of the survey system seek stability in coordinates. This is an understandable desire given the limitations of spatial data processing today. JTM can provide a complete and adaptable coordinate system with the stability that users seek, because JTM is a uniform, precise, homogeneous geodetic network, and highly accurate, with 6° zones, a central meridian of 37° and scale factor in the central meridian of 0.9998. Moreover, the transformation from CASS to JTM, according to the method used in our study, gave accurate results of approximately 10cm. This encourages the transfer of all maps from Cass to JTM. Spatial data infrastructure (SDI)

depends on a base of the homogeneous network, and for the maximum benefit of the data, there should be no confusion about its positional accuracy, and in Jordan we are looking to build Jordan Spatial Data Infrastructure (JSDI).

References

Alostah, Z. and Alkhatib, S. 2005. Building Jordan Digital Cadastral Data Base (JDCDB) in the Department of Lands and Survey (DLS), In: *Proceedings of FIG Working Week*. Cairo, Egypt, 16-21 April 2005.

Dawod, G. and Alnaggar, D. 2000. Optimum geodetic datum transformation techniques for GPS surveys in Egypt. In: *Proceedings of Al-Azhar Engineering Sixth International Engineering Conference*. Cairo, Egypt: Al-Azhar University, pp.1-4.

Division, U.N. 2009. Handbook on geospatial infrastructure in support of census activities, Department of Economic and Social Affairs, Statistics Division, Series F No. 103. United Nations, New York.

DLS. 2007, Survey-Specification Dept. of land and survey of Jordan. Available at: http://10.66.6.56/ar/dlsDocuments/survey-spcification-2007.pdf

ESRI. 2015b. *ArcMap- About spatial adjustment transformations.* Available at: https://desktop.arcgis.com/en/desktop/latest/manage-data/editing-existing-features/about-spatial-adjustment-transformations.htm

ESRI. 2015c. *ArcGIS Help 10.1.* Available at: http://resources.arcgis.com/en/help/main/10.1%20/index.html#//003r0000001v000000. (Accessed: December 2015).

Gavish, D. 2005. *A survey of Palestine under the British Mandate*. Abingdon, United Kingdom: Psychology Press.

Grant, D. and Pearse, M. 1995. Proposal for a dynamic national geodetic datum for New Zealand. *IUGG General Assembly*, 2-14 July, Boulder, Colorado, USA.

ICSM. 2014. Geocentric Datum of Australia technical manual, version 2.4, http://www.icsm.gov.au/gda/gda-v_2.4.pdf. (Accessed: Dec. 2015).

Kadir, M., Ses, S., Omar, K., Desa, G., Omar, A.H., Taib, K. and Nordin, S. 2003. Geocentric datum GDM2000 for Malaysia: Implementation and implications. Seminar on GDM2000, Department of Survey and Mapping Malaysia, Kuala Lumpur, Malaysia.

Mitsakaki, C. 2004. Coordinate transformations. In: *Proceedings of FIG Working Week*. Athens, Greece, 22-27 May 2004.

Mugnier, C.J. 2008. Grids & Datums. *Photogrammetric Engineering & Remote Sensing*, 74(4), pp. 391-392.

Williamson, I.P., Rajabifard, A. and Feeney, M.E.F. 2004. *Developing spatial data infrastructures: from concept to reality*. Florida, United States: CRC Press.

Cloud Publications
International Journal of Advanced Remote Sensing and GIS
2017, Volume 6, Issue 1, pp. 2103-2113
ISSN 2320–0243, Crossref: 10.23953/cloud.ijarsg.237

Research Article | Open Access

Land-Use Land-Cover Change and Its Impact on Surface Runoff using Remote Sensing and GIS

Prakash, C.R.[1], **Sreedevi, B.**[2]

[1]Associate Professor, St. Martin's Engineering College, Secunderabad, India
[2]Principal Scientist, Directorate of Rice Research, Rajendranagar, Hyderabad, Telangana, India

Publication Date: 25 April 2017

DOI: https://doi.org/10.23953/cloud.ijarsg.237

Abstract Due to urbanization, the incessant growth and development occurring in the peri-urban region, has led to a significant transformations of land-use/ land-cover pattern especially in built-up areas. As a result, there has been an expansion of impervious land (concretization) which has significantly affected the surface runoff behavior in the urban realm. Scenarios like urban floods, water pollution and soil degradation are some of the major consequences of changes in runoff pattern. It calls for an objective assessment and the study temporal behavior of surface runoff pattern for taking up any preventive and/or curative measures. Timely and reliable information on surface runoff in spatial domain is a pre-requisite in this endeavor. Space-borne multispectral and multi-temporal measurements hold a great promise in analyzing land-use/land cover patterns and their temporal behavior, and its impact on the runoff in a timely and cost-effective manner. A study was taken up in Serilingampally Mandal of Rangareddy district, a peri-urban area of Hyderabad city, Telangana state for assessment and monitoring of surface runoff patterns using Landsat-MSS data and Resourcesat 2 LISS-IV data collected in 1975 and 2016, respectively through heads-up/on-screen visual interpretation approach. Initially, the information on land use/cover pattern was generated to assess the growth of the urban settlements. Subsequently the corresponding increase in surface runoff during the monsoon seasons (June-October) 1975 and 2016 were computed using SCS (Soil Conservation Service) curve number method. Results indicate a sharp increase in built up land from 0.91% to 69.36%. During the period 1975-2016 with consequent higher runoff to the tune of 27.5% as compared 1975 period.
Keywords *spectral measurements; landsat-MSS; resourcesat 2 LISS-IV; urbanization; surface runoff; soil conservation service curve number*

1. Introduction

Land is becoming a scarce resource due to population growth and industrialization. Due to this reason there is rapid change in land-use land cover in general and in urban areas in particular. The irregular growth in urban sprawl has caused a great impact on the fertile lands as well as it became a vital reason for many environmental problems, waste disposal and water pollution as specified by the U.N. Conference on Human settlement. Land-use and land-cover changes may have four major direct

impacts on the hydrological cycle and water quality: they can cause floods, droughts, and changes in river and groundwater regimes, and they can affect water quality (Rogers, 1994).

The process of urbanization has a considerable hydrological impact in terms of influencing the nature of runoff and other hydrological characteristics, delivering pollutants to rivers, and controlling rates of erosion (Goudie, 1990). The development of residential and commercial buildings increases imperviousness which reduces the time of runoff concentration so that peak discharges are higher and occur sooner after rainfall starts in catchments. The volume of runoff and flood damage potential will greatly increase. Moreover, the installation of sewers and storm drains accelerates runoff (Goudie, 1990). Therefore, the rainfall–runoff phenomenon in an urban area intends to be fairly dissimilar from that in natural conditions depicted in conventional hydrological cycles. Integration of urbanization with hydrological studies is made possible because both utilize land-use and land-cover data.

2. Background

The land-use and land-cover pattern of a region is an outcome of natural and socio-economic factors and their utilization by man in time and space. Hence, information on land-use and land-cover is essential for selection, planning and implantation of land-use and can be used to meet the increasing demands for basic human needs and welfare. This information also assists in monitoring the dynamic of land-use resulting out the changing demands of increasing population (Zubair, 2008).

There has been a significant change in land-use and land-cover for the past decade. For sustainability of the sprawl there needs to be a harmonic interaction with the nature. This can be possible by a proper monitoring and management of natural resources that are water and land. Alteration of the land-use and land-cover impacts the surface runoff behavior and leads to the scenarios like urban floods, water pollution, soil degradation and ground water.

3. Role of Remote Sensing and GIS

With multi-temporal analysis, remote sensing gives a unique perspective of how rural area evolves. “Remote sensing methods can be employed to classify types of Land- Use in a practical, economical and repetitive fashion, over large areas” (Natural Resource, Canada). The collection of remotely sensed data facilities the synoptic analysis of earth-system function, patterning and change at local, regional and global scales over time, such data also provide an important link between intensive localized ecological research and regional, national and international conversation and management of biological diversity.

Remotely sensed data and geographic information systems (GIS) have been identified as a powerful and effective tool in detecting urban growth (Harris & Ventura, 1995; Yeh & Li 1996, 1997). Digital as well as visual interpretation of the satellite based multi-resolution and multi-temporal data proves to be pivotal for understanding and monitoring urban transformation. GIS provides a multi-dimensional environment for visualization, manipulation and analyzing digital data from various inputs required for urban feature identification, change detection, and spatial database development. In hydrological and watershed modeling, remotely sensed data and GIS are found to be valuable for providing cost-effective data input and for estimating model parameters (Engman & Gurney, 1991; Drayton et al., 1992; Mattikalli et al., 1996). Thomas (2015) used RINSPE model implemented in ArcView GIS 3.3 environment to model for estimating runoff in the Olifants river catchment area in north eastern South Africa as surface runoff and entering into the subsurface as infiltration. In another study, Hong Quang Nguyen and Martin Kappas (2015) used Soil and Water Assessment Tool (SWAT) and Bridging Event and Continuous Hydrological (BEACH) models for estimating surface runoff and evapotranspiration in a tropical watershed in North Vietnam. While estimating the runoff in Vindhyachal region, part of Mirzapur district, Uttar Pradesh, northern India, Topno et al. (2015) observed an improvement in

estimated runoff accuracies by using a curve number (CN) model developed by the United States Department of Agriculture (USDA).

4. Study Area

The area of concern of the present study, Serilingampally, is a municipality and Mandal in Ranga Reddy district, Telangana, is bound by geo co-ordinates 17.414 to 17.517^{0}N and 78.283 to 78.414^{0}E and covers an area of approximately 101 sq. km (Figure 1). Due to its close proximity to Hitech City, Gachibowli, Nanakramguda, Manikonda and Kondapur, there has been a heavy influx of IT companies. As a result, it has witnessed an unprecedented growth and development in the infrastructure in the recent times. Lithologically, the test site consists of granite-gneiss complex. Hills, pediment, pediplain and valleys the physiographic units encountered in the test site. Coarse-textured red soils predominantly occur with inclusions of black soils in local depressions and low lying areas. The area enjoys semi-arid sub-tropical climate with average daytime temperature ranging from 25-30^{o}C during November to February and 40-45^{o}C during April-June. Annual precipitation ranges between 700-1000 mm yr^{-1} which is received mostly during July to October.

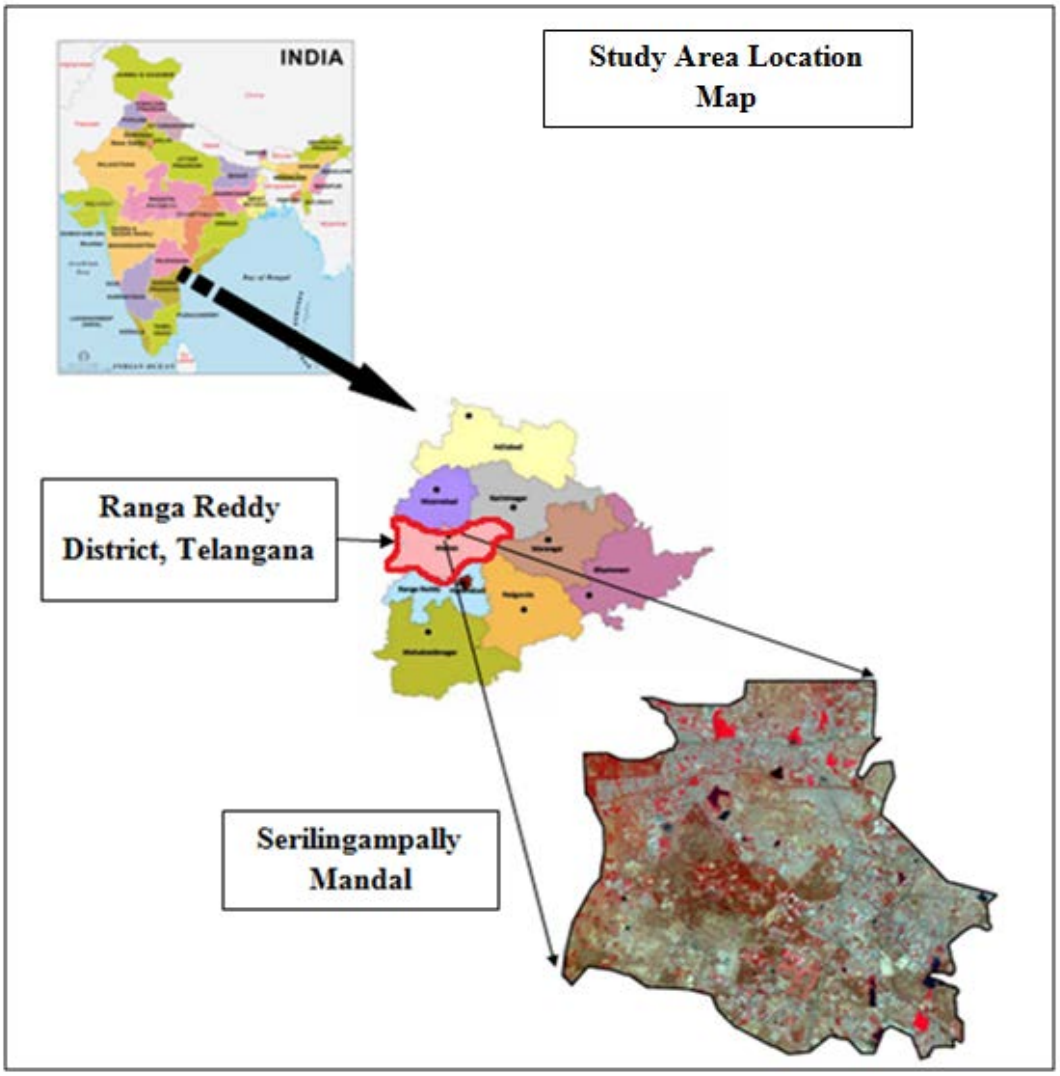

Figure 1: *Location map of the test site*

5. Database

The Landsat MSS and Resourcesat-LISS IV digital data with 80m and 5.8m spatial resolution, respectively were used for developing land use/ land cover maps of the test site. The specifications of the satellite sensor data used `are given in Table 1 and 2 respectively. Whereas Landsat MSS digital data was downloaded from United States Geological Survey (USGS) Database, Resourcesat LISS-IV data was procured from National Remote Sensing Center, Hyderabad. Survey of India topographical map at 1:25,000 scale was used for developing base map as well for data analysis. The information on relief was extracted from Carto-DEM. Hydrological Soil Group (HSG) map was derived from soil texture available in soil resources map collected from Telangana State Remote Sensing Center, Hyderabad. Mandal-wise precipitation data was obtained from Directorate of Economics and Statistics, Telangana. Ancillary information consists of cadastral maps and socio-economic data collected from Serilingampally Mandal office.

Table 1: *Specifications of Resourcesat-2 LISS IV sensor*

Specifications	LISS IV
No. of bands	1 (mono), 3 (MX)
Spectral bands (µm)	B2 0.52-0.59 B3 0.62-0.68 B4 0.77-0.86 B3-default band for mono
Resolution (m)	5.8
Swath (km)	70/23
Revisit (days)	5
Quantization	10-bit

Source:http://lps16.esa.int/posterfiles/paper1213/[RD13]_Resourcesat-2_Handbook.pdf

Table 2: *Specifications of MSS of Landsat-1*

Specifications	MSS
No. of bands	4
Spectral bands (µm)	B4 0.5-0.6 B5 0.6-0.7 B6 0.7-0.8 B7 0.8-1.1
Resolution (m)	80
Swath (km)	185
Revisit (days)	18
Quantization	6-bit

Source: http://gisgeography.com/usgs-earth-explorer-download-free-landsat-imagery/

6. Methodology

The methodology involves geo-referencing of digital temporal satellite data, generation of land use/ land cover map, derivation of hydrological soil groups from available soil map and integration the information on land use/land cover, hydrological soil group to estimate run off following USDA-Soil Conservation Service curve number approach (Figure 2).

To begin with, Landsat-MSS data was georeferenced to Survey of India (SOI) topographical maps at 1:50,000 scales on a Silicon Graphics (Octane)-based system by identifying adequate ground control points by using ERDAS/IMAGINE software by identifying well distributed ground control points identifiable on Landsat-MSS digital image and topographic maps. Similar exercise was done for geo-referencing Resourcesat-2 LISS-IV data with 6m spatial resolution using ground control points from

1:25,000 scale topographic maps. The digital output, thus generated, was used for land use/ cover mapping.

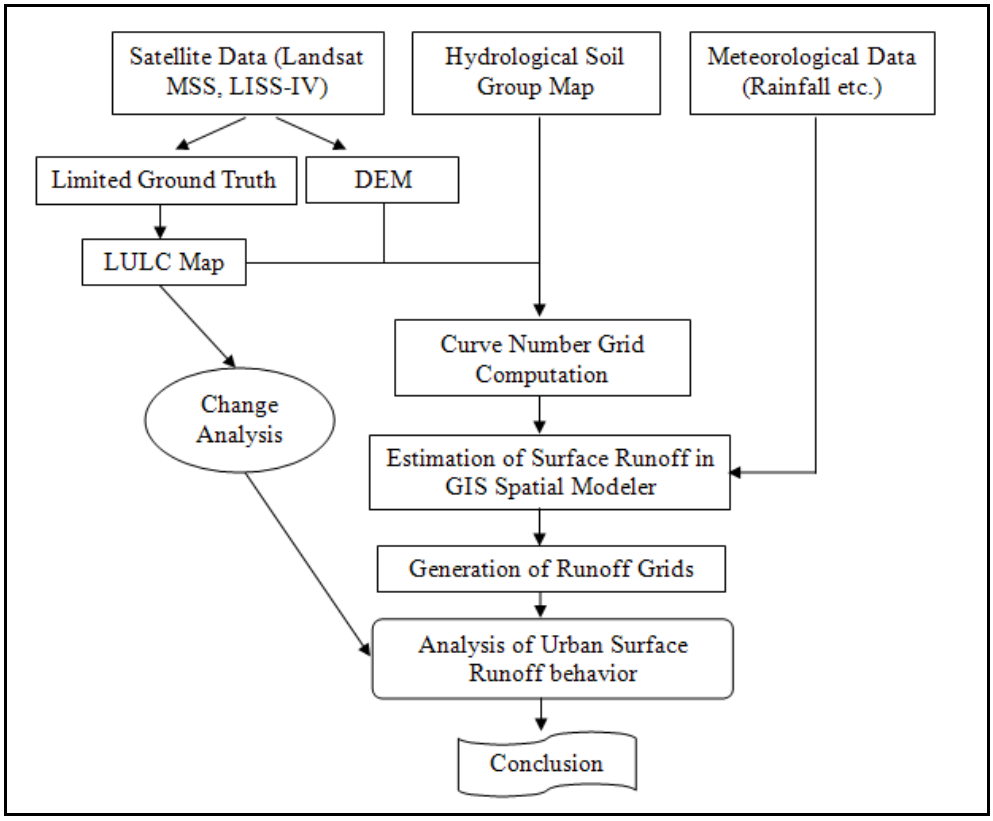

Figure 2: *Schematic diagram of the methodology*

6.1. Preliminary Visual Interpretation

Due to coarse resolution of Landsat-1 MSS data for the period land use/land cover mapping for 1975 was confined to 8 aggregate classes while high resolution LISS IV data could afford delineation of 14 distinct land-use/ land cover categories.

6.2. Ground Truth Collection

The parcels of land representing various land use/land cover classes as delineated during preliminary visual interpretation in each sample strip and located onto topographical maps, were physically located on the ground. Subsequently observations on various land use categories in each sample strip were made to correlate the image elements and their correspondence with land use/ cover categories. The location of each observation was recorded with help of a GPS receiver.

6.3. Map Finalization

To begin with, the digital Resourcesat-2 LISS-IV data was displayed onto colour monitor of the Silicon Graphics (Octane) - based system using ERDAS IMAGINE software and a blank vector layer was overlaid onto the image. The areas which were delineated as having land use/ land cover categories during preliminary visual interpretation were then located in the image and the boundaries were modified *vis-a-vis* ground truth collected during field visit. The vector coverage was generated for and use/land cover categories delineated from Landsat MSS and LISS-IV data delineated on the colour monitor of the Silicon Graphics (Octane) system using ERDAS/ IMAGINE software and its topology built. The area statistics for each land use/ land cover categories was generated.

6.4. Land Use/ Land Cover Change Analysis

A change analysis for the corresponding years was performed in the geo-spatial environment to prepare a change detection map. The vector coverage of use/land cover categories delineated from Landsat MSS and LISS-IV data were overlay and the transformation of land-use and land-cover classes from one to another was observed. The spatial extent of various land /land cover statistics of the changes in land use/ land cover categories over the period of time from 1975 to 2016 was generated.

6.5. Computation of Surface Runoff

There are numerous rainfall-runoff algorithms for simulating the hydrological cycle. We have used a Curve Number algorithm, a simplified and most applicable rainfall loss method, for runoff estimation. As mentioned earlier, the SCS (Soil Conservation Service) curve number method was developed by the Soil Conservation Service of United States Department of Agriculture (USDA).The primary reasons for its wide applicability and acceptability lies in the fact that it accounts for most runoff producing watershed characteristics (e.g. soil type, land use/treatment, surface condition and antecedent moisture condition (AMC). The amount of total direct runoff is estimated as follows:

$$Q = \frac{(P-0.2S)^2}{P+0.8S} \; (Q = 0 \; IF \; P \leq 0.2S) \text{.....(1)}$$

$$S = \frac{25400}{CN} - 254 \quad \text{.....(2)}$$

Where, Q is the precipitation excess (runoff) in mm (millimeters), S is the potential maximum retention in mm (millimeters) and CN is the SCS curve number.

It is amply clear from equations (1) and (2) that two main inputs that are required for computation of the surface runoff are: precipitation and curve number. The CN values are normally estimated using field survey data with reference to CN (under AMC II condition) tables published by USDA's SCS. The SCS has evolved the hydrological soil group code A, B, C, or D based on permeability and infiltration characteristics of soils. Group A soils are coarse, sandy, well-drained, with the highest rate of infiltration and the lowest potential for runoff. Group D soils, on the other hand, are heavy-textured, clayey, poorly drained soils, with the lowest rate of infiltration and highest potential for runoff. Group B and C soils are intermediate between groups A and D. We have prepared daily rainfall grids for the monsoon season (June-October) using IDW (Inverse Distance Weight) GIS tool for the years 1975 and 2016 and have resampled to suitable scale for a better spatial representation. The curve number grids were generated through an integrated GIS analysis of land-use, soil textural information (Figure 3) and hydro-DEM (Figure 4) under AMC II (normal condition).

A spatial model for simulating the rainfall-runoff phenomenon was developed using advanced map algebra functions in a GIS environment for preparing monthly surface runoff grids from which the total runoff during the monsoon period of the corresponding years was computed.

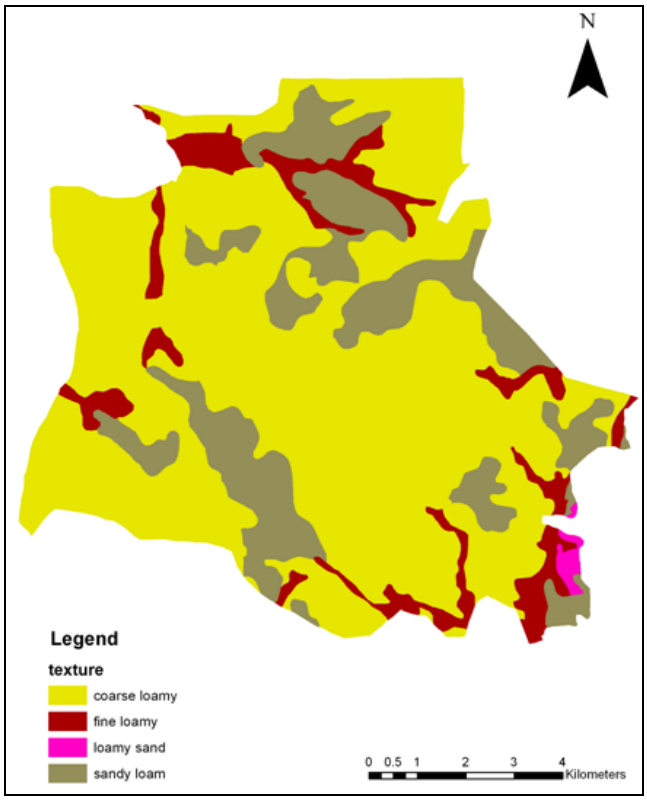

Figure 3: *Soil texture map of the test site*

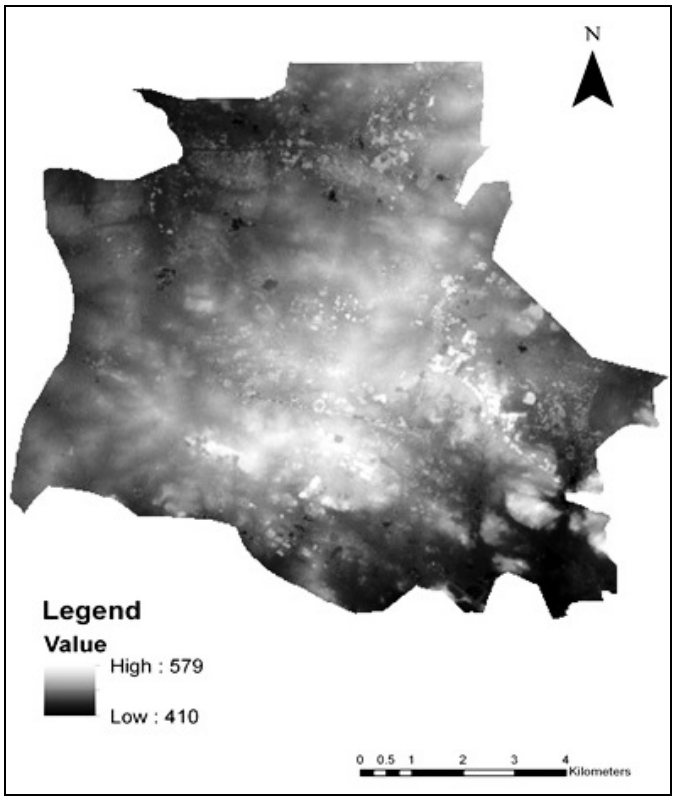

Figure 4: *DEM of the test site (values are in metres)*

7. Results and Discussion

Land use/land cover pattern as delineated from Landsat-MSS and Resourcesat-2 LISS-IV data were used to study its temporal behavior and the urban sprawl that has occurred in the test site. The corresponding increase in surface runoff due to development of impervious land (concretization) due to urbanization was assessed to provide the information to planners and decision makers for utilizing the land and water resources with a sustainable approach.

7.1. Land Use/Land Cover Scenario and Change Analysis

Landsat-MSS data could afford delineation of broad land use/land cover categories, namely agriculture, forest, scrubs, layouts recreational and water bodies (Figure 5). The land use/land cover map derived from LISS-IV data is appended as Figure 6. As evident from the map several sub-divisions within each land use/ land cover category delineated from Landsat_MSS data could be made. For example, within settlements medium dense settlements, dense settlements, apartments, and villas could be identified on LISS-IV image with 6m spatial resolution.

During the period 1975 to 2016 spanning over four decades, there have been remarkable changes in built-up land, cropland and scrubs. The built up land has expanded from 0.91% in 1975 to 69.36% in the year 2016. Conversely, the cropland has shrunken from (1.18% in 1975 to 4.22% in 2016). Similar trend has been observed in scrub which has decreased from 22.84% in 1975 to 5.67% in 2016 (Table 3 & 4).

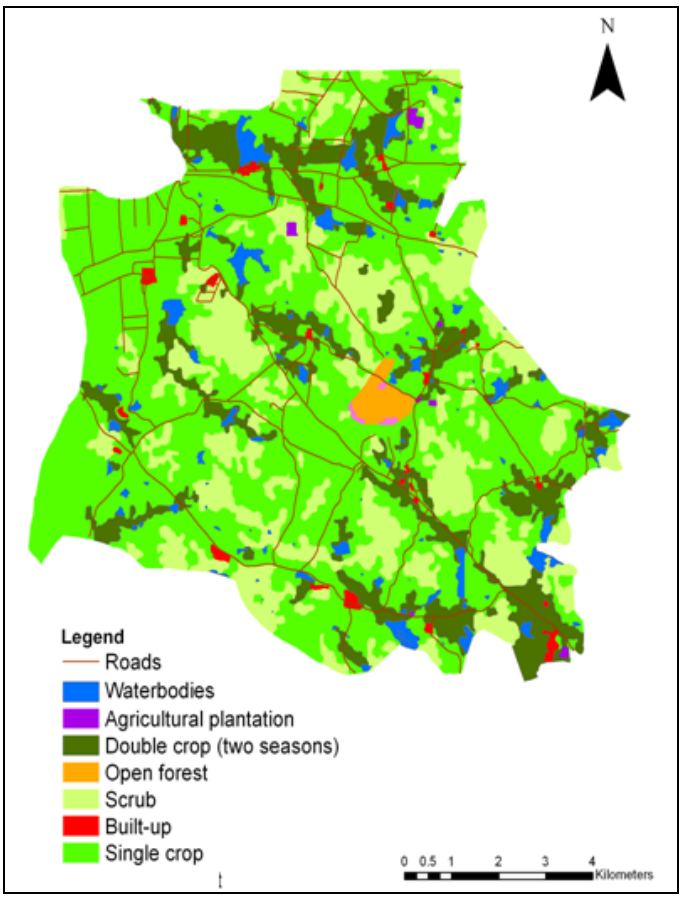

Figure 5: *LULC map of the study area derived from Landsat-MSS imagery*

Table 3: *Spatial extent of various land-use and land cover categories during 1975*

Land-use	Area (sq-km)	Percent Area (%)
Agricultural Plantation	0.25	0.26
Double Crop (two seasons)	13.09	13.52
Open Forest	1.02	1.05
Scrub	22.12	22.84
Built-up	0.89	0.92
Single crop	55.82	57.65
Water bodies	3.63	3.75

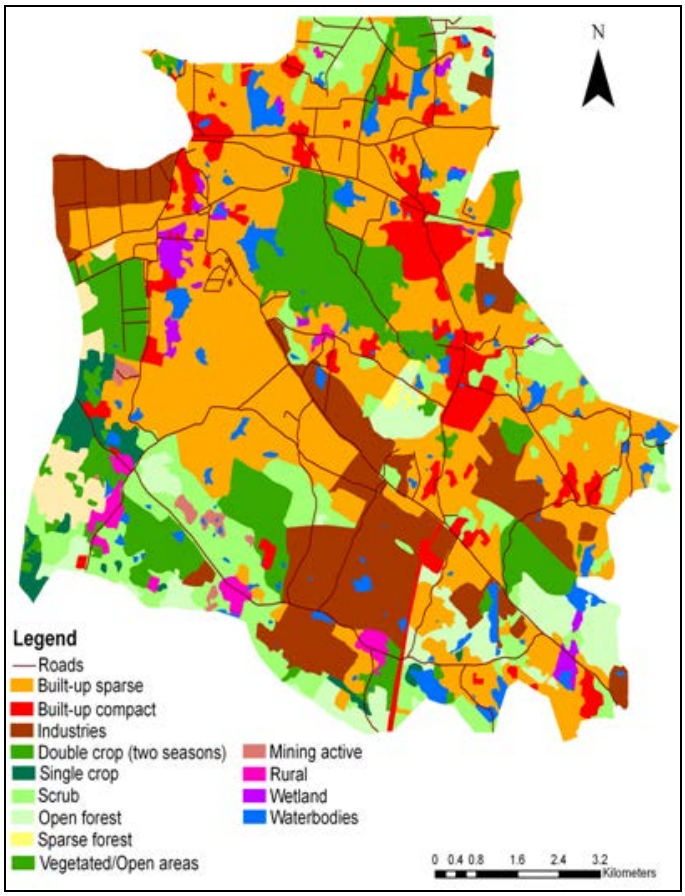

Figure 6: *LULC map derived from 2016 LISS-IV data*

Table 4: *Spatial extent of various land-use and land cover categories during 2016*

Land-use	Area(sq-km)	Percent Area (%)
Built-up compact	6.23	6.44
Built-up sparse	37.27	38.49
Double crop (two seasons)	0.89	0.91
Industries	12.86	13.29
Single crop	3.2	3.31
Mining active	0.44	0.45
Open forest	0.94	0.97
Rural	1.09	1.13
Scrubs	16.27	16.81
Vegetated/open areas	12.56	12.96

Water bodies	3.63	3.82
Wetlands	1.11	1.15

7.2. Urbanization and Runoff

As pointed out in section 7.1, the land use/land cover area statistics indicates an increase in built-up land from 0.91% in 1975 to 69.36% in 2016. Conversely, there has been a sharp decrease in cropland (71.18% in 1975 to 2.63% in 2016). Urban growth has led to increase in area under impervious cover which tends to increase surface flow. Runoff map for the month of June for the corresponding years are portrayed in Figure 7.

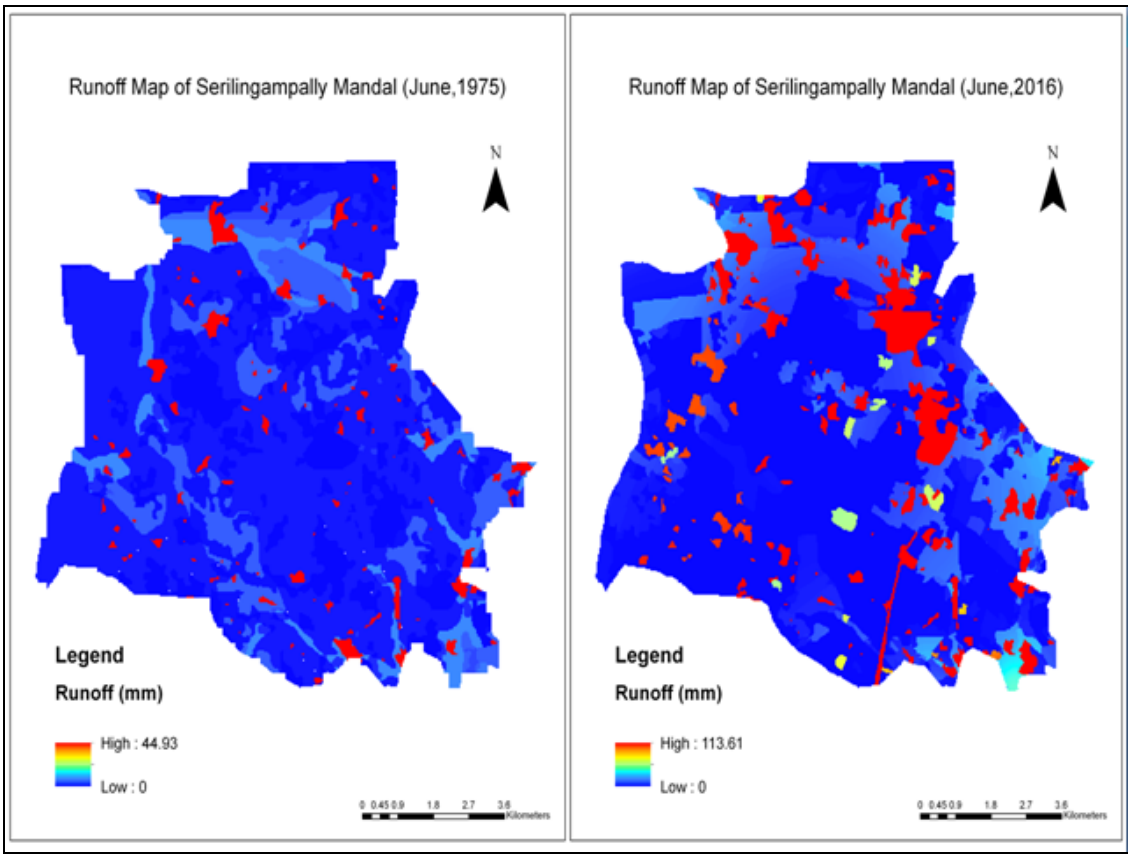

Figure 7: *Runoff map of Serilingampally Mandal for the month of June (1975, 2016)*

It is evident from the figure that there has been a significant increase in the built-up area over a period of four decades resulting in to corresponding increase in potential to overland flow represented in red patches for the built-up and water bodies in an integrated way. The runoff value is as high as 113.61 mm for the month of June in 2016 compared to 44.93 mm in 1975. It is observed that a total precipitation of 869.15 mm in 1975 monsoon has yielded a runoff of 312.30 mm while a precipitation of 870.73 mm in 2016 monsoon has contributed a runoff amounting to 398.26 mm. An overall increase in runoff of to the tune of 27.5% has been observed.

8. Conclusions

Alteration of the land-use and land-cover impacts the surface runoff behavior and leads to the scenarios like urban floods, water pollution, soil degradation and ground water. In order to assess the magnitude of the impact of land cover change on overland flow, a novel approach utilizing remote sensing, GIS and curve number model was used. The approach involves generation of information on

land use/land cover pattern and integrating it with soil texture, relief and precipitation using USDA-SCS curve model. The advantage of *a priori* knowledge of the area coupled with the ease of access to detailed ground truth enabled the visual interpretation of satellite data to study the land-use / land cover dynamics and generation of hydrological soil groups. The study demonstrates the role of urban growth on over land flows by way appreciable increase impervious cover with attendant decrease in infiltration. However, the role of quantum and intensity of rainfall pattern in the process cannot be overlooked.

Acknowledgements

C.R. Prakash, one of the authors, wishes to place on record his heartfelt gratitude to Prof. A. Jayasree, Director, Institute of Science and Technology JNTUH, Hyderabad for providing necessary facilities during the course of investigation. He is also grateful to wishes to Prof. K. Manjula Vani, Chairperson, Board of Studies, CSIT, IST and Head, Civil Engineering Department, JNTUH, Hyderabad for her encouragement in the study. Thanks are also due to Shri J. Venkatesh, Associate Professor and Head, CSIT, IST, JNTUH for timely help and evincing keen interest in the study.

References

Drayton, R.S., Wilde, B.M., & Harris, J.H.K. (1992). Geographic information system approach to distributed modeling. *Hydrological Processes, 6*, 36-368.

Engman, E.T., & Gurney, R.J. (1991). *Remote sensing in hydrology*. London: Chapman and Hall, London.

Goudie, A. (1990). *The human impact on the natural environment*, 3rd ed. Massachusetts: The MIT Press, Cambridge.

Harris, P.M., & Ventura, S.J. (1995). The integration of geographic data with remotely sensed imagery to improve classification in an urban area. *Photogrammetric Engineering and Remote Sensing, 61*(8), 993-998.

Mattikalli, N.M., Devereux, B.J., Richards, K.S. (1996). Prediction of river discharge and surface water quality using an integrated geographic information system approach. *International Journal of Remote Sensing, 17*(4), 683-701.

Nguyen, Hong Quang, & Martin Kappas. (2015). Modeling Surface Runoff and Evapotranspiration using SWAT and BEACH for a Tropical Watershed in North Vietnam, Compared to MODIS Products. *International Journal of Advanced Remote Sensing and GIS, 4*, 1367-1384.

Rogers, P. (1994). Hydrology and water quality. In W.B. Meyer, & B.L. Turner II (Eds.), *Changes in land use and land cover: A global perspective* (pp. 231-258). Cambridge: Cambridge University Press.

Thomas, A. (2015). Modelling of Spatially Distributed Surface Runoff and Infiltration in the Olifants River Catchment/Water Management Area Using GIS. *International Journal of Advanced Remote Sensing and GIS, 4*, 828-862.

Topno, A., Singh, A.K., & Vaishya, R.C. (2015). SCS CN Runoff Estimation for Vindhyachal Region using Remote Sensing and GIS. *International Journal of Advanced Remote Sensing and GIS, 4*, 1214-1223.

Yeh, A.G.O., & Li., X. (1997). An integrated remote sensing- GIS approach in the monitoring and evaluation of rapid urban growth for sustainable development in the Pearl River Delta, China. *International Planning Studies, 2*(2), 193-210.

Zubair, A.O. (2006). Change detection in land use and land cover using remote sensing data and GIS (A case study of Ilorin and its environs in Kwara state.), Department of Geography, University of Ibadan.

Cloud Publications
International Journal of Advanced Remote Sensing and GIS
2017, Volume 6, Issue 1, pp. 2192-2203
ISSN 2320 – 0243, Crossref: 10.23953/cloud.ijarsg.273

Research Article

Coastal Geomorphological and Land Use and Land Cover Study on Some Sites of Gulf of Kachchh, Gujarat, West Coast of India using Multi-Temporal Remote Sensing Data

Disha P. Nayak , Madhusudan H. Fulekar

School of Environment and Sustainable Development, Central University of Gujarat, Gandhinagar, 382030, Gujarat, India

Publication Date: 10 June 2017

DOI: https://doi.org/10.23953/cloud.ijarsg.273

Abstract The coastal rapid changes are monitored by Remote sensing (RS) and Geographical information (GIS) tools for the conservation and management. Aims of this paper are to monitor morphological, total vegetation, and water index changes in last two and half decades (1989, 2002, 2016) using Remote Sensing and GIS. The study area is rapidly changing at an alarming rate due to anthropogenic and natural activities. Morphological changes on study area are presenting major anthropogenic actions. Between 1989 and 2016 period, a tropical cyclone in 1998 caused a major change in mudflat area which reduced from 1143.97 to 459.07 km^2. More than fifty percent changes were observed in the built-up area and salt pan which increased from 9.18 to 18.17 km^2 and 51.55 to 90.32 km^2 respectively. The mangrove class increased from 180.63 to 296.5 km^2 showing better restoration and conservation practices of Gujarat government. The NDVI supports these results by increasing maximum positive index value from 1989 to 2016. This study indicates that Gulf of Kachchh coastal is undergone excessive pressure due to the rapid development of the surroundings artificial landscape, where socio-economic factors lead to changes in the near environment, as well as proliferative activities of salt production affecting the quality in the coastal ecosystem. For coastal conservation, the government introduced socio-economic activities, designing strict management policies and awareness programs for local communities about the importance of coastal for protection and management.

Keywords *Coastal conservation; Kachchh; Western region; LULC; Remote sensing*

1. Introduction

The coastal ecosystem is known as a unique environment where terrestrial, marine and atmosphere meet, interact and interplay with each other (Ramsar Convention Secretariat, 2010; Space Applications Centre, 2012). It provides various ecosystem services such as flood control, natural cycling of sediments and nutrients and water purification (Dagar, 2005; Zhang & Shao, 2013). Periodically interval shows rapid changes take place in its area morphology and productivity. In 1991, the Government of India (MoEF, 1991) declared tidal effects stretch the coastal area as Coastal Regulation Zone (CRZ). Coastal ecosystems are under pressure due to the anthropogenic activities and natural disasters. Increasing industries, urban population, and development process are the leading cause of the ecological destruction of coast area. In addition, natural disasters like flood, tsunami, and cyclone are also responsible for the higher rate of changes in this area (Balamurugan &

Aravind, 2015; Pascual-Aguilar et al., 2015). In order to evaluate and predict the ecological and geomorphological changes in coastal zones require immense individual sites studies, by the feature of complexities associated with them (Mani Murali & Dinesh Kumar, 2015). Despite great ecological value, coastal wetlands are graded at less priority for conservation and their rate changes remain limited and debated.

Therefore, monitoring and assessment of different classes of the ecosystem are a need for change detection. Remote sensing (RS) and Geographical information system (GIS) are an efficient and coast effective tool for a change detection of natural resources, reliable alternative to a ground survey that provides a useful source of information coverage (Ibharim et al., 2015; Nayak & Bahuguna, 2001). From the RS data inventorying, mapping, monitoring and recently for the management and development planning activities are proceeding for the optimal sustainable exploitation of natural resources (Klemas, 2012; Prasad et al., 2002). It is also beneficial in functioning relevant observations, which can bring out the impact of deforestation on global climate (McGuffie, 1995). To expose it from several decades monitoring and change detection concept has been widespread (Srivastava et al., 2012). RS data gives information about the changes in a time interval with better accuracy in short time. It also provides a better understanding the relationships and interactions of natural and man-made phenomena from multi-temporal data. From the LULC data, we can obtain information about the current sites cumulative output of the interactions between natural and man-made activities (Misra & Balaji, 2015; Srivastava et al., 2014). Hence, these tools are helpful to develop information sources and support judgment making process in a plethora of coastal zone applications.

Several studies have been carried out for LULC and related subjects in Gulf of Kachchh region. In comparison to other Gulf and coastal sites of Gujarat, Gulf of Kachchh is most productive by diverse habitat. It covered around 77% of mangrove area of Gujarat (Rodrigues et al., 2011). Previously this area was evaluated for biodiversity assessment of dominant plant communities along with the mangroves, seaweed, seagrass beds and dune vegetation mapped with accuracy by IRS data. This study helped in planning various management actions for protecting and conserve this ecosystem (Nayak & Bahuguna, 2001). Srivastava et al., (2014) evaluated mangrove forest change detection from 1994 to 2010 by hybrid classification approach using LISS-II and LIS-III imagery data in Mundra forest region. The study found total 11 classes showed significant change due to anthropogenic and sea level rise activities in the forest area. Nayak, Pandeya, & Gupta (1989) carried out a study on tidal wetland changes by Landsat MSS and TM data from 1975 to 1986 owing to the accessed use of fuel and fodder, and the proliferation of salt pan activities. Previously LULC study performed on hotspots of Gulf of Kachchh from 1977 to 2015 and from six class total 33 positives and 11 negative change discovered in this area. The major changes were found in mangrove, salt pans and built-up lands (Pasha, Reddy, Jha, Rao, & Dadhwal, 2016).

With this background, the present study performed to evaluate LULC change detection in a periodic interval from last two and half decades (1989, 2002, and 2016). The long term interval information also provides an interchange of various classes. Previous literature (Pasha et al., 2016) available for this region hotspot change within 6 class digitization. Further, more clarity in different class anthropogenic and natural pressure, we evaluated LULC, NDWI, NDVI, and data accuracy assessment for the study area. For the LULC total area classified in nine classes and total area change and percentage variability calculated by visual classification technique. Habitually occurring climatic variables changes, rapid growing industrialization and other local factors are key factors to perform this study. The present study aimed to generate an accurate database on land use/land cover and identify total vegetation and water index difference for 1989, 2002 and 2016 year.

2. Description of the Study Area

The Gulf of Kachchh (GK) region situated at the Arabian Sea-facing of western Indian site. The geographical location is 22.7443° N and 69.9550° E. It is included in the rich biodiversity area of the few coastal zones in the world. Around 77% of western Indian mangroves are covered by the Gulf of Kachchh. The essential components of this ecosystem are coral reefs and mangrove vegetation. The GK is having shallow depth around 60 m at the mouth to less than 20 near the head and covered 7350 sq. km enrich marine biodiversity area. It is semi-enclosed basin with a high tidal range of about 4 m at its mouth and 7 m at its head. The temperature of the region varies from 12 °C to > 36 °C. Humidity is higher in monsoon i.e. up to 80% while remaining year around 55 to 70 %. Alteration rainfall pattern is responsible for the higher vegetation diversity in this area. Annual maximum rainfall reported in 2011 from Jamnagar coast (605.0 mm), Okha and Dwarka (500.9 mm), Saurashtra received less than 630 mm, and the least amount reported from Mandvi to Bhachau (400.0 mm). The study area (Figure 1) shows that Gulf of Kachchh mainly covered by Kachchh and Jamnagar districts (Rodrigues et al., 2011; Coastal zones of India, 2012; SERCME, 2012)

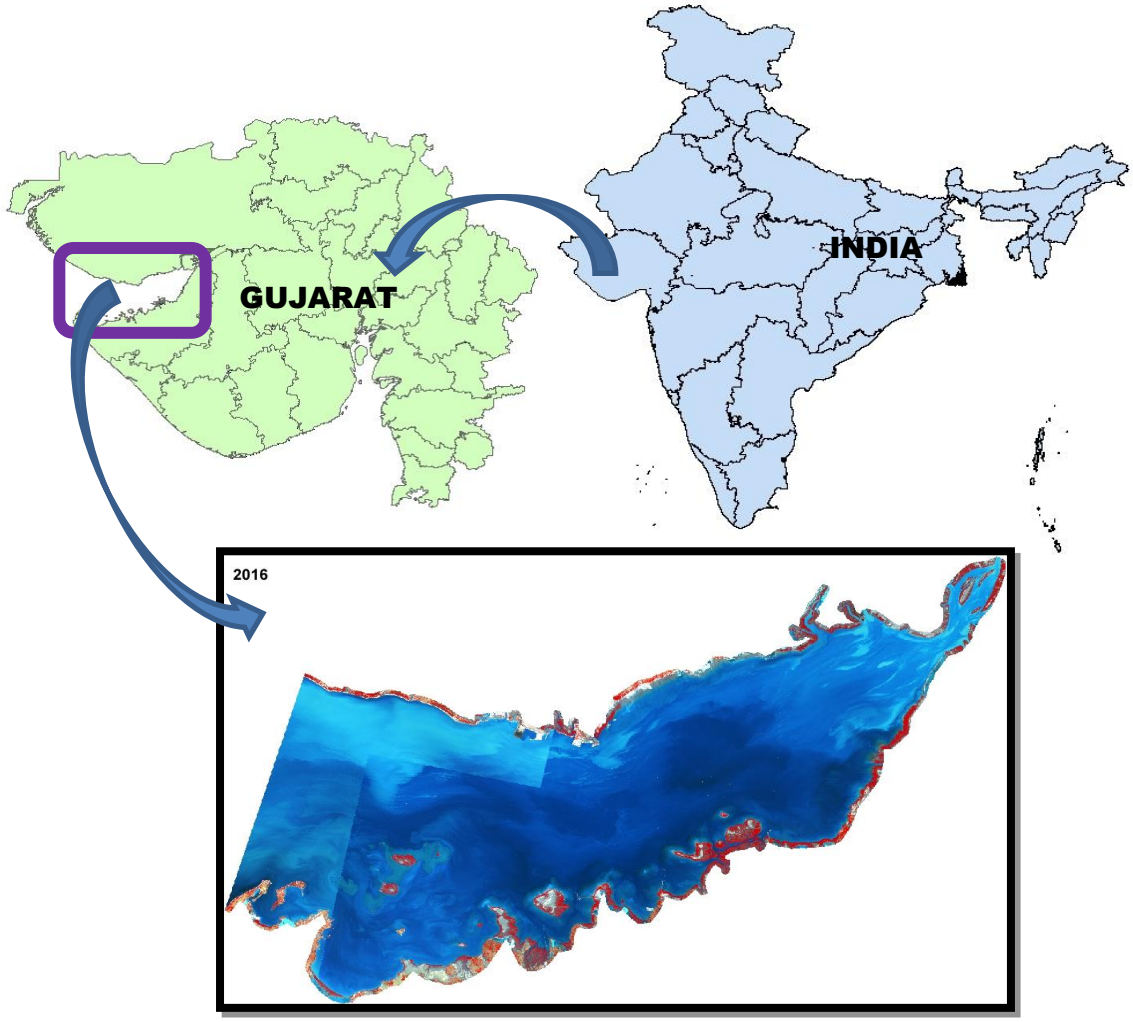

Figure 1: *Study Area*

3. Materials and Methods

3.1 Datasets used

In this study, we used three satellite images for each year (Table 1). The LANDSAT data was acquired from USGS, Earth Explorer (U.S. Department of the Interior U.S. Geological Survey).

Table 1: *Details of satellite data used in the study*

No	Satellite/Sensor	Pixel size	Spectral resolution	Swath width	Band used	Path/Row	Date
1	LANDSAT 5	30 m	Multispectral (6 bands)	185 km	1,2,3,4 B,G,R,NIR	150 / 044	Dec 17, 1989
						150 / 045	Dec 17, 1989
						151 / 044	Dec 24, 1989
2	LANDSAT 7	30 m	Multispectral (8 bands)	185 km	1,2,3,4 B,G,R,NIR	150 / 044	Dec 13, 2002
						150 / 045	Dec 13, 2002
						151 / 044	Dec 04, 2002
3	LANDSAT 8	30 m	Multispectral (11 bands)	185 km	2,3,4,5 B,G,R,NIR	150 / 044	Nov 09, 2016
						150 / 045	Nov 09, 2016
						151 / 044	Nov 16, 2016

3.2 Image data and pre-processing

Geographically rectified images were downloaded with UTM (Universal Transverse of Mercator) projection system; spheroid WGS 84 (World Geodetic System) and zone 42 North projection system were used for this study region. Further, images open in ERDAS 14 software and blue, green, red and near-infrared bands were stacked. Stacked layer images were mosaicked, and clipped with the reference boundary to extract out the study area. Subsequently, pan-sharpening of images was performed to enhance the resolution of images. The study area digitized at 1:25,000 and 1:50,000 scale using Arcgis 10.3 software. The digitized study area for 1989, 2002 and 2016 was converted in the vector format (.shp) which was used for change detection (Balasaraswathi et al., 2016; Misra & Balaji, 2015; Scopélitis et al., 2009).

3.3 Classification System for Land Cover

Study area classification provides a framework for categorizing information which can be extracted from image data. The images were classified according to NRSC classification Level II and it is important for the study and discernible from the data. Mainly nine classes were considered for land-cover classification i.e. barren land, built-up area, scrub, cropland, mudflat, mangrove, saltpan, sand beach and water bodies. Cropland includes lands with vegetation as well as land just after harvested crop. The Gulf area covered by major water body class.

3.4 Mapping of study area

In this study, various Land-use/Land-cover classes for the GK coastal covered area extracted from 2016, 2002 and 1989 Landsat imagery by digitizing the study area. For the change detection field studies were carried out in the approx 3-decade interval. Ground truth was collected with the help of False Color Composite (FCC) of specific locations of the study area. On screen digitization was embraced for the land cover mapping as the explanation of the finer type variation was possible. Steps included loading satellite data, rectification and restoration, image enhancement and information extraction. Arcgis 10.3 was used for visual interpretation and for assigning attributes to an individual polygon for various classes. LULC change detection was carried out by calculating the area of each

class. Further time interval variation calculated by using pivot table analysis for each class (Pasha et al., 2016; Srivastava et al., 2014).

3.5 Normalized Difference Vegetation Index (NDVI)

NDVI is used for calculation of vegetation indexed from the remotely sensed data. Vegetation index is a number which generated by some combination of remote sensing bands. In that near infra-red strongly reflectance and lower red light reflectance by vegetation and soil. It is calculated by,

NDVI = (NIR - RED) / (NIR + RED) (1)

where NIR is the near-infrared band response for a given pixel (band 4 (L4, L7) & band 5 (L8) and RED is the red response, (band 2 (L4, L7) & band 3 (L8). The resulting index can range from -1 to +1 in which vegetation surface gave positive, soil near about zero and water features have negative values (Hurley et al., 2014; Tucker, 1979).

3.6 Normalized Difference Water Index (NDWI)

Normalize Differences Water Index (NDWI) used for the assessment of the water resources, both regarding quality and quantity measurement. In remote sensing, NIR strongly absorbed by the water and green band gave an average reflectance of water features. The values of radiance or reflectance converted into the digital number and compared with other data sets for calculating water index. It is calculated by,

NDWI = (Green – NIR) / (Green + NIR) (2)

In this visible green and NIR band gave positive value for water; while soil and terrestrial vegetation have zero or negative values (McFeeters, 1996) The detailed methodology is shown in Figure 2.

3.7 Accuracy Assessment

Accuracy assessment is required for image classification study. Land cover maps derived from remote sensing and classification technique has some error. To derived land-cover maps and the supplementary resource statistics, the errors quantitatively explained in terms of classification accuracy. In the present study for accuracy assessment, error matrix method was used (Berberoğlu et al., 2010). For the assessment 90 points selected and could be assigned to each class on land cover maps, then the results were recorded in an error matrix. For the classified data overall accuracy and kappa coefficient were calculated in the accuracy assessment report. Percentage of overall accuracy measured for each class after image classification. The kappa coefficient expressed the proportionate reduction in error generated by a classification process compared with the error of a completely random classification (Bishop et al., 1975; Sharma et al., 2011; Srivastava et al., 2014)

$$\kappa = \frac{N\sum_{i=1}^{r} x_{ii} - \sum_{i=1}^{r}(x_{i+} \times x_{+i})}{N^2 - \sum_{i=1}^{r}(x_{i+} \times x_{+i})} \quad (3)$$

Where N is the total number of sites in the matrix, r is the number of rows in the matrix, x_{ii} is the number of observations in row i and column i, x_{i+} is the total row i and x_{i+} are the total for column i.

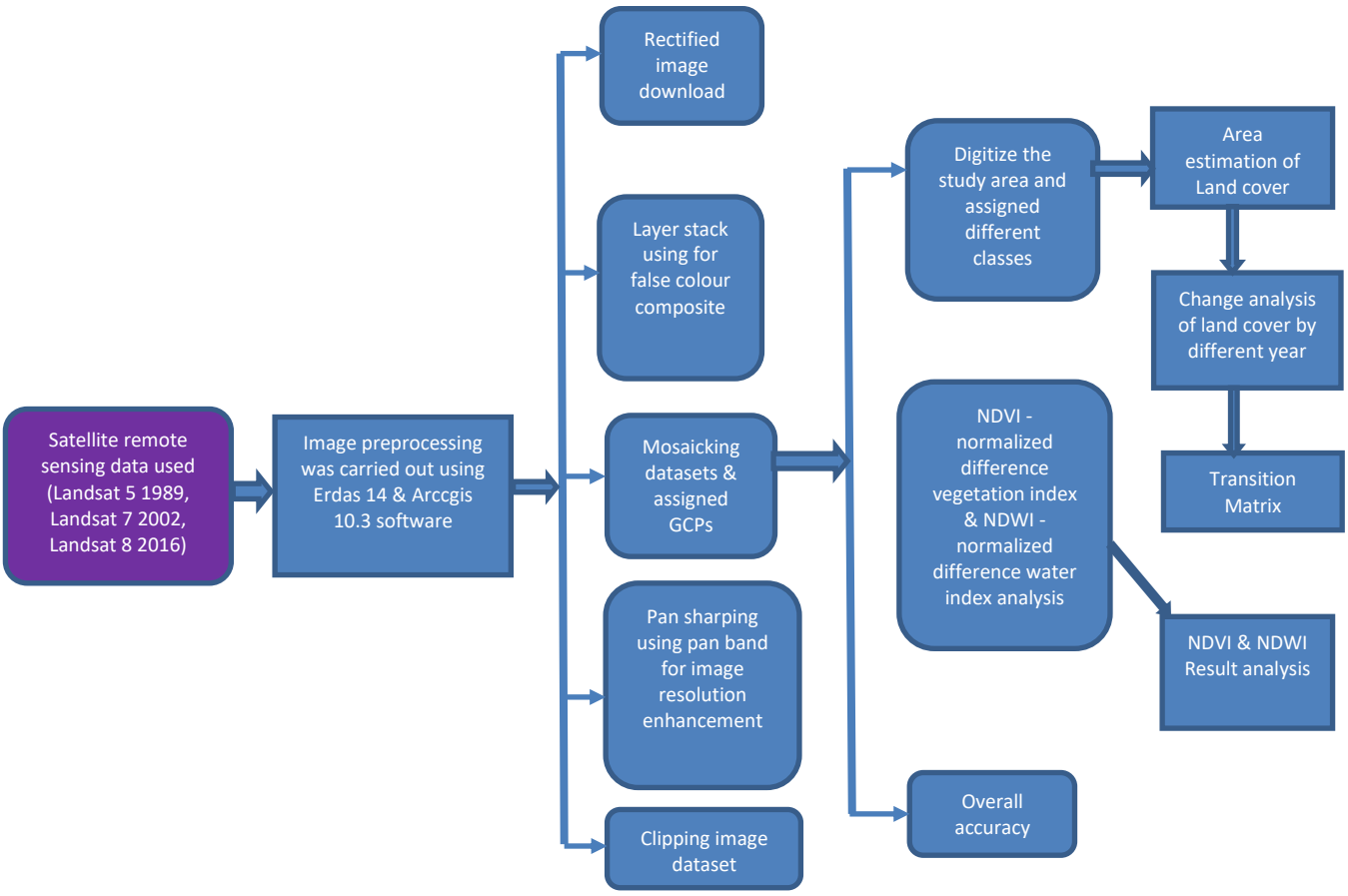

Figure 2: *Flow chart of the methodology used in the present study*

4. Results and Discussion

4.1 Land use and land cover change (LULC)

The LULC assessment was carried out for some of sites of Gulf of Kachchh in the year 1989, 2002 and 2016 from Landsat TM, ETM and OLI satellite image respectively. The classification maps produced by visual classification techniques are illustrated in Figure 3. The three satellites images have been classified into nine classes, namely 1) barren, 2) built-up, 3) cropland, 4) mangrove, 5) mudflat, 6) saltpan, 7) sand beach, 8) scrub, 9) water. Information derived from the analysis of satellite data pertaining to land use and land cover revealed that the major class covered by water body ranged from 76.33 % to 84.38 %. It showed around 8.05 % water level increased from 1989 to 2016. The estimated area as the percentage of total study area under this classification approach for barren 0.72 %, 0.59 %, 0.43 %; built-up 0.13, 0.15, 0.27; scrub 1.028 %, 1.24 %, 1.23 %; cropland 0.81 %, 0.88 %, 0.82 %; saltpan 0.77 %, 0.95 %, 1.36 %; mudflat 17.25 %, 8.76 %, 6.92 %; mangrove 2.72 %, 2.81 %, 4.47 %; sand beach 0.19 %, 0.22 %, 0.08 % obtained for 1989, 2002 and 2016 year respectively (Table 2). However, results obtained from this classification showed according to decade interval decreased barren, mudflat and sand beach area while, increased built-up and mangrove area. Therefore, the study indicates that barren and sand beach area may occupy by built-up area. Another significant change was observed for scrub and cropland area.

Table 2: *Decade interval Land-use/land cover area changes of Gulf of Kachchh sites*

	LULC change area km^2											
Year	Barren	Built-up	Scrub	Cropland	Saltpan	Mudflat	Mangrove	Sand beach	Water body	Total	% of Overall accuracy	Kappa coefficient
1989	48.09	9.18	68.22	54.34	51.55	1143.97	180.63	13.15	5061.85	6630.98	88.88	0.86
% of area	0.72	0.13	1.028	0.81	0.77	17.25	2.72	0.19	76.33			
2002	39.63	10.12	82.74	58.5	63.6	581.29	186.64	14.7	5593.76	6630.98	92.41	0.905
% of area	0.59	0.15	1.24	0.88	0.95	8.76	2.81	0.22	84.35			
2016	28.93	18.17	81.58	54.91	90.32	459.07	296.5	5.89	5595.61	6630.98	97.11	0.96
% of area	0.43	0.27	1.23	0.82	1.36	6.92	4.47	0.08	84.38			

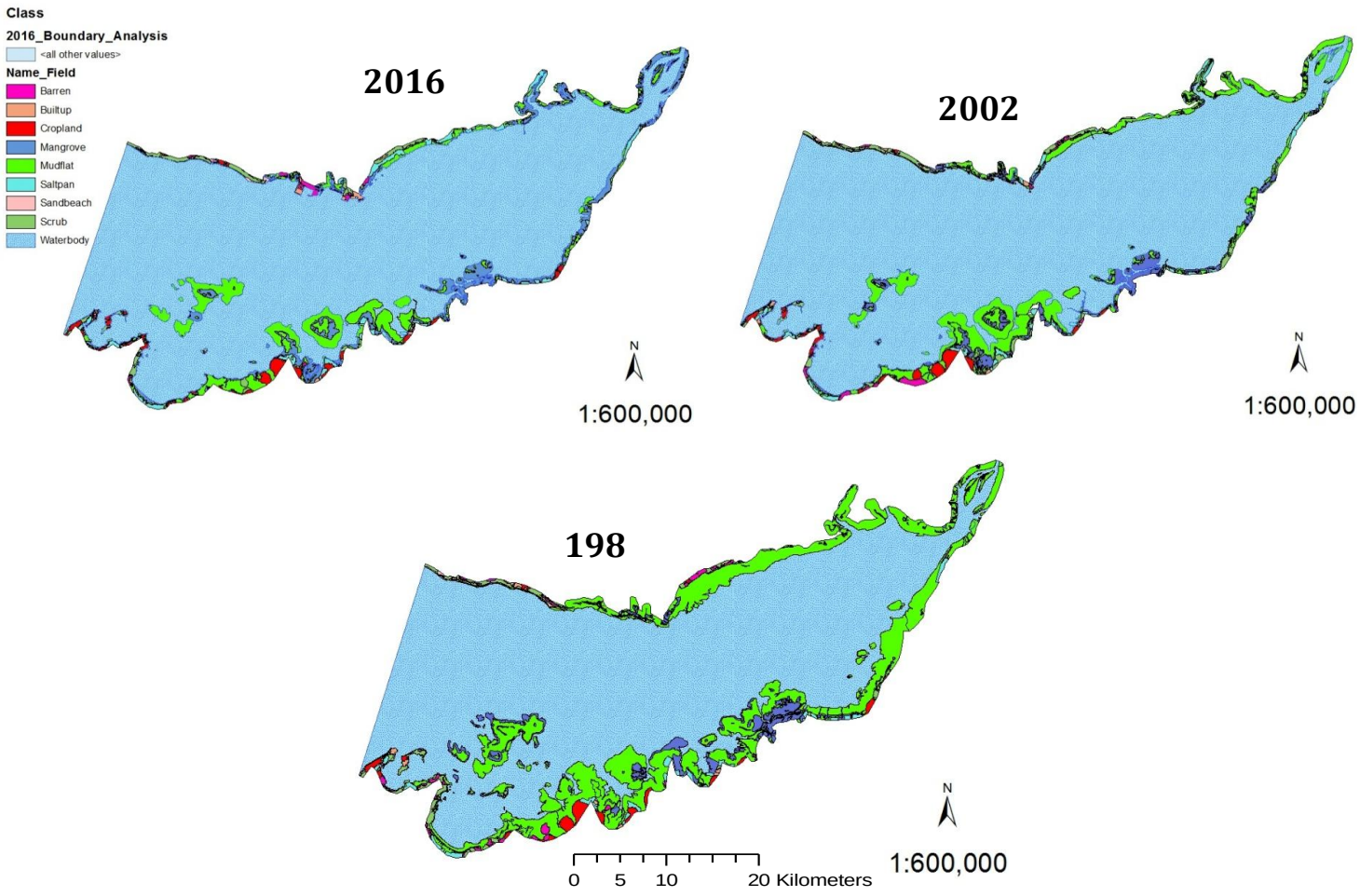

Figure 3: *Land use/land cover imagery 1989, 2002, and 2016*

In the cropland two different class included before and after harvested crops and scrub area also interlinked so, the varied changes observed at a different year. Due to 1998, ARB 02 cyclone effect on Gulf of Kachchh area mudflat observed drastic change and decrease the area from 8.49 % during 1989 to 2002 and 1.84 % from 2002 to 2016 (Ministry of Earth Sciences Govt. of India). In all sites mangrove area covered by *Avicennia marina* abundance along with some woody and grassy

halophytic communities at intertidal zone. Interestingly, the mangrove area increase from 180.63 to 296.5 km^2, i.e., 2.72 % to 4.47 % in two and half decade's interval. This was increased due to the major participation in the Government initiatives for conservation and sustainable development of this ecosystem. According to Pasha et al., (2016) around 130 km^2 mangrove plantation and restoration have been afforested by the Gujarat Forest department from the first 5-year plan to 1999. Gujarat is the largest producers of salt in India and occupied the second position to export in the world (Discovered India). This statement support to this study and we observed salt pan area increased from 51.55 km^2, 63.6 km^2 and 90.32 km^2 between three-decade intervals. Some of the sand beach areas are also converted into the salt pan, indicating, degrading sand area by changing environmental conditions. For all the three-year class variable changes represented in Figure 4. The LULC result observed a severe change occurs in a various class of coastal area due to anthropogenic and natural disasters activity. Rapid industrialization and urbanization also may affect this area productivity (Mahapatra et al., 2015; Nagendra et al., 2013; Srivastava et al., 2014).

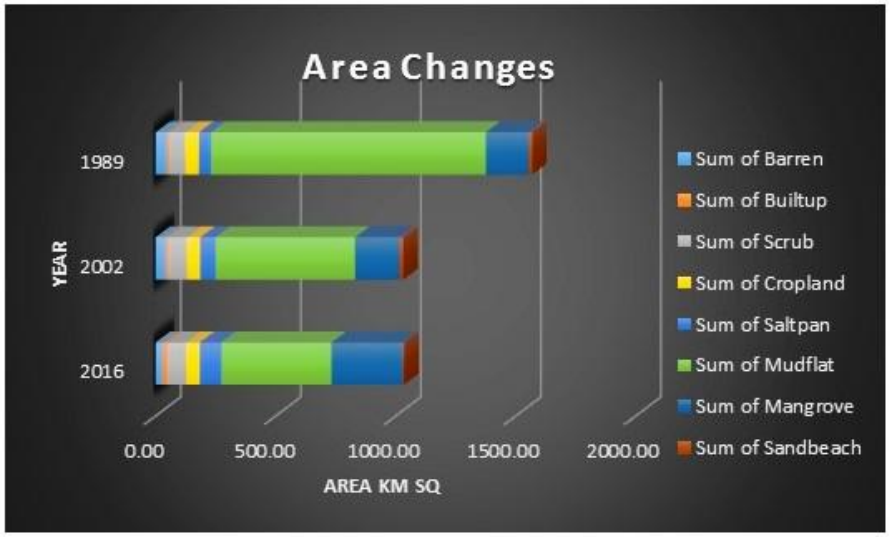

Figure 4: *Different class area change among three the different year 1989, 2002, and 2016*

4.2 Result of Normalize Vegetation Index (NDVI)

NDVI gave the information about vegetation cover from the remotely sensed imagery at a different year. It produced a result in the form of digital numbers by some combination of remote sensing band according to Eq. 1. Satellite images phenological differences identified among vegetation types. Here, the result of the index can range from -1 to +1. Vegetated surface gave positive value, the soil may have near zero and for water features negative value obtained (Defries & Townshend, 1994; Hurley et al., 2014). In our study, NDVI result presented non-significant variation between decade intervals. During 1989 to 2002 the positive range dropped down from 0.84 to 0.64, which indicate 23.80 % vegetation index decreased. For that 1998 tropical cyclone activities responsible for major affection in this area (Ministry of Earth Sciences Govt. of India). From 2002 to 2016 period showed increased range of vegetation index. On account of the government mangrove afforestation and conservation program active participation involved in it. The vegetation index range increased 30.43% having a range from 0.64 to 0.92. For all the three-year NDVI changes described in Figure 5.

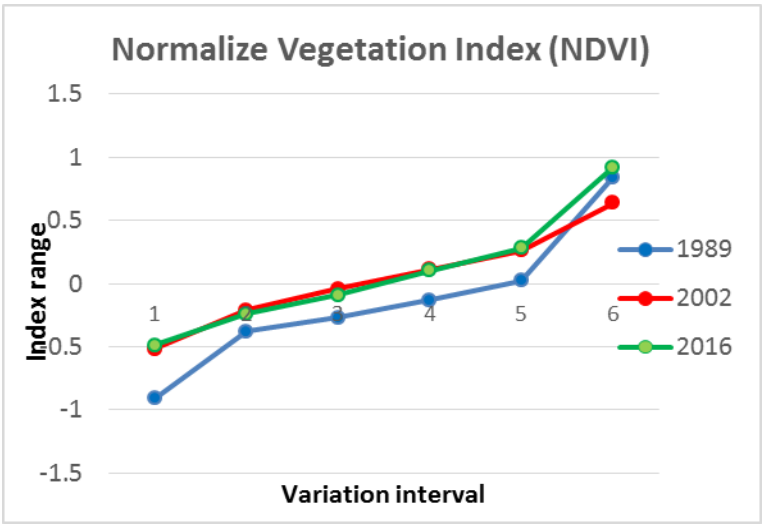

Figure 5: *Vegetation index range from -1 to +1. Total vegetation variability demonstrated for all three years 1989, 2002, and 2016*

4.3 Result of Normalize Water Index (NDWI)

The NDWI derived from the Green and NIR band, to increase the reflectance of water features by green light wavelength, decrease low reflectance of water features by NIR, and it also gives a high reflectance of NIR by terrestrial vegetation and soil features. The calculated NDWI from Eq. 2 gave positive value for water; while soil and terrestrial gave zero and negative values, owing to their higher reflectance of NIR than the green band (Alsaaideh et al., 2013; McFeeters, 1996). In our study NDWI 0.76, 0.56, and 0.77 maximum positive value obtained for 1989, 2002, and 2016 year respectively. The result showed that, from 1989 to 2002 water level decreased around 26.31 % and from 2002 to 2016 again increased around 27.27 %. Interestingly, the water level changes occurred since thirty year period attributable to the climate change effect and varied rainfall pattern in this area. Water level changes for all three years mentioned in Figure 6.

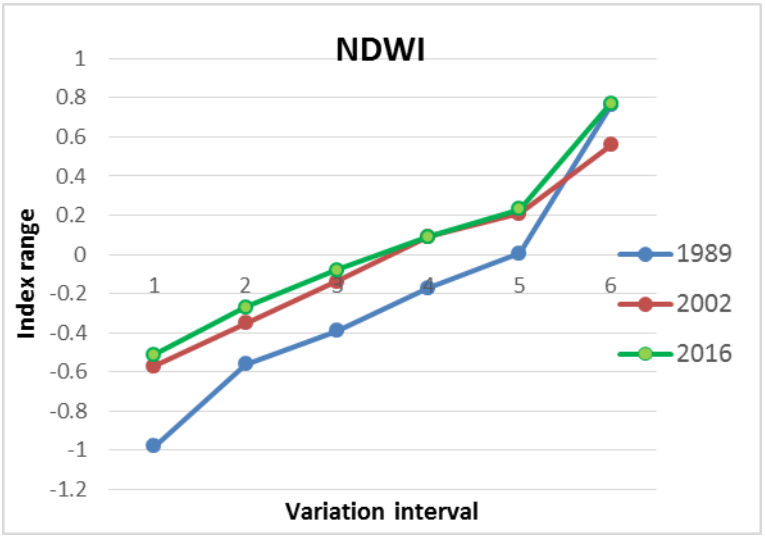

Figure 6: *Water index range from -1 to +1; a positive value indicates water level and zero or negative value refer soil and vegetation in the terrestrial land. Water level changes demonstrated for all three years 1989, 2002, and 2016*

4.4 Accuracy assessment

Accuracy assessment was done by error matrix and kappa coefficient calculated for each year using Eq. 3. The overall accuracy analysis indicated the highest accuracy obtained for 2016 image followed by 2002 and 1989. The overall accuracy 97.11 %, 92.41 % and 88.88 % and kappa coefficient 0.96, 0.90 and 0.86 obtained for 2016, 2002 and 1989 years respectively (Table 2). The kappa statistics represented clear picture and accuracy of visual classification. It showed in the year 2016 lesser error found in individual class digitizing process. OLI sensor gave a clearer picture in compared with ETM and TM satellite imagery. A higher difference of kappa value (0.06) and overall accuracy percentage (4.7 %) was observed between 2002 to 2016 intervals. This result indicates that classified land-cover maps for different years have sufficient accuracy for change detection. Moreover, heterogeneity of different classes present in the study area and their classification accuracies obtained is in fair agreement for each year. Although the classified result has some error in 2002 and 1989 image classes but overall it shows good results in terms of overall accuracy and kappa coefficient for change detection evaluation.

5. Conclusions

The coastal ecosystem known to be Kidney of Earth and its role in the environment functions are undebatable. It is the most productive ecosystem and enriches source of flora fauna diversity. Protection and conservation of the coastal ecosystem are essential because it works as a natural ecological barrier against natural disasters. Coastal assimilation, monitoring, and evaluation climate change impacts need to conserve it. For that, the present study performed by RS and GIS coast effective techniques to understand the dynamic changes in the study sites In this study we found the rapid growth of industrialization for salt production may responsible for ecological degradation. Although mangrove is a crucial link of marine ecology; in recent decades, several mangroves is being destroyed due to anthropogenic activities. The study also indicates the climate change and natural disasters adverse effect on the study area. The impact of sea level rise and changes in natural conditions causes the decrease in ecological diversity. This approach, as well as products thereby created, have the likely to make it easier for managers and practice persons with a simple practical understanding of RS to produce information on conservation status regularly, rapidly and quite economically, with reasonable levels of accuracy, which can be useful for adaptive management of protected areas as well as in their geographic context. For that our strong recommendation to the Government of India and the Ministry of Environment and Forests (MoEF) is that the coastal ecosystem is a sensitive zone and need to be protected for environment services.

References

Alsaaideh, B., Al-Hanbali, A., Tateishi, R., Kobayashi, T. and Hoan, N.T. 2013. Mangrove Forests Mapping in the Southern Part of Japan Using Landsat ETM+ with DEM. *Journal of Geographic Information System*, *5*(8), pp.369-377.

Balamurugan, G. and Aravind, S.M. 2015. Land use land cover changes in pre- and postearthquake affected area using geoinformatics - Western Coast of Gujarat, India. *Disaster Advances*, *8*(4), pp.1-14.

Balasaraswathi, P., Srinivasalu, S. and Management, O. 2016. *Change detection analysis of coastal zone features in Cuddalore District, Tamilnadu using Remote sensing and GIS techniques*. IOSR *Journal of Applied Geology and Geophysics*, *4*(5), pp.1-8.

Berberoğlu, S., Akin, a., Atkinson, P. M. and Curran, P.J. 2010. Utilizing image texture to detect land-cover change in Mediterranean coastal wetlands. *International Journal of Remote Sensing*, *31*(11), pp.2793-2815.

Bishop, Y.M., Fienberg, Stephen E. and Holland, P.W. 1975. *Discrete Multivariate Analysis*. (1, Ed.). New York, USA: Springer-Verlag.

Dagar, J. 2005. Ecology, management, and utilization of halophytes. *Bulletin of the National Institute of Ecology*, *15*(January 2005), pp.81-97.

Defries, R.S. and Townshend, J.R.G. 1994. NDVI-derived land cover classifications at a global scale. *International Journal of Remote Sensing*, *15*(931144751), pp.3567-3586.

Discovered India, http://www.discoveredindia.com/gujarat/salt-industry-in-gujarat.htm

Hurley, M. a, Hebblewhite, M., Gaillard, J.-M., Dray, S., Taylor, K. a, Smith, W.K. and Bonenfant, C. 2014. Functional analysis of normalized difference vegetation index curves reveals overwinter mule deer survival is driven by both spring and autumn phenology. *Philosophical Transactions of the Royal Society of London*. Series B, Biological Sciences, *369*(1643), p.15.

Ibharim, N.A., Mustapha, M.A., Lihan, T. and Mazlan, A.G. 2015. Mapping mangrove changes in the Matang Mangrove Forest using multi-temporal satellite imageries. *Ocean & Coastal Management*, 114, pp.64-76.

Klemas, V. 2012. Remote Sensing of Coastal and Ocean Currents: An Overview. *Journal of Coastal Research*, 28(3), pp.576-586.

Mahapatra, M., Ramakrishnan, R. and Rajawat, A.S. 2015. Coastal vulnerability assessment of Gujarat coast to sea level rise using GIS techniques: a preliminary study. *Journal of Coastal Conservation*, 19(2), pp.241-256.

Mani Murali, R. and Dinesh Kumar, P.K. 2015. Implications of sea level rise scenarios on land use /land cover classes of the coastal zones of Cochin, India. *Journal of Environmental Management*, 148, pp.124-133.

McFeeters, S.K. 1996. The use of the Normalized Difference Water Index (NDWI) in the delineation of open water features. *International Journal of Remote Sensing*, 17(7), pp.1425-1432.

McGuffie, K. 1995. Global climate sensitivity to tropical deforestation. *Global and Planetary Change*, 10(1–4), pp.97-128.

Misra, A. and Balaji, R. 2015. A study on the shoreline changes and Land-use/land-cover along the south Gujarat coastline. Procedia Engineering, 116(1), pp.381-389.

Ministry of Earth Sciences Govt. of India, http://www.imdahm.gov.in/

MoEF. 1991. Declaration of Coastal Stretches as Coastal Regulation Zone (CRZ). Notification, S.O. no. 114(E), 19 February. Ministry of Environment and Forests, New Delhi, p.14.

Nagendra, H., Lucas, R., Honrado, J. P., Jongman, R.H.G., Tarantino, C., Adamo, M. and Mairota, P. 2013. Remote sensing for conservation monitoring: Assessing protected areas, habitat extent, habitat condition, species diversity, and threats. *Ecological Indicators*, 33, pp.45-59.

Nayak, S. and Bahuguna, A. 2001. Application of remote sensing data to monitor mangroves and other coastal vegetation of India. *Indian Journal of Marine Sciences*, 30(4), pp.195-213.

Nayak, S., Pandeya, A. and Gupta, N.C. 1989. Application of satellite data for monitoring degradation of tidal wetlands of the Gulf of Kachchh, Western India. *Acta Astronautica*, 20(C), 171-178.

Pascual-Aguilar, J., Andreu, V., Gimeno-Garc??a, E. and Pic??, Y. 2015. Current anthropogenic pressures on agro-ecological protected coastal wetlands. *Science of the Total Environment*, pp.503-504, pp.90-199.

Pasha, S.V., Reddy, C.S., Jha, C.S., Rao, P.V.V.P. and Dadhwal, V.K. 2016. Assessment of Land Cover Change Hotspots in Gulf of Kachchh, India Using Multi-Temporal Remote Sensing Data and GIS*. Journal of the Indian Society of Remote Sensing*, 44(6), pp.905-913.

Prasad, S.N., Ramachandra, T.V., Ahalya, N., Sengupta, T., Kumar, A., Tiwari, A.K. and Vijayan, L. 2002. Conservation of wetlands of India - A review. *Tropical Ecology*, 43(1), pp.173-186.

Ramsar Convention Secretariat. 2010. *Coastal management: Wetland issues in Integrated Coastal Zone Management,* p.52.

Rodrigues, R.S., Mascarenhas, A. and Jagtap, T.G. 2011. An evaluation of flora from coastal sand dunes of India: Rationale for conservation and management. *Ocean and Coastal Management*, 54(2), pp.181-188.

Scopélitis, J., Andréfouët, S., Phinn, S., Chabanet, P., Naim, O., Tourrand, C. and Done, T. 2009. Changes of coral communities over 35 years: Integrating in situ and remote-sensing data on Saint-Leu Reef (la R??union, Indian Ocean)*. Estuarine, Coastal and Shelf Science*, 84(3), pp.342-352.

Sharma, C.S., Behera, M.D., Mishra, A. and Panda, S.N. 2011. Assessing Flood Induced Land-Cover Changes Using Remote Sensing and Fuzzy Approach in Eastern Gujarat (India)*. Water Resources Management*, 25(13), pp.3219-3246.

Space Applications Centre. 2012. Coastal Zones of India, pp.1-609.

Srivastava, P.K., Han, D., Gupta, M. and Mukherjee, S. 2012. Integrated framework for monitoring groundwater pollution using a geographical information system and multivariate analysis*. Hydrological Sciences Journal,* 57(7), pp.1453-1472.

Srivastava, P.K., Han, D., Rico-Ramirez, M.A., Bray, M. and Islam, T. 2012. Selection of classification techniques for land use/land cover change investigation. *Advances in Space Research*, 50(9), pp.1250-1265.

Srivastava, P.K., Mehta, A., Gupta, M., Singh, S.K. and Islam, T. 2014. Assessing impact of climate change on Mundra mangrove forest ecosystem, Gulf of Kutch, western coast of India: a synergistic evaluation using remote sensing*. Theoretical and Applied Climatology*, pp.685-700.

*S*tate of Environment Report on Coastal and Marine Environment Gujarat state*.* 2012. Gandhinagar, Gujarat.

Tucker, C.J. 1979. Red and photographic infrared linear combinations for monitoring vegetation. *Remote Sensing of Environment*, 8(2), pp.127-150.

U.S. Department of the Interior U.S. Geological Survey, https://earthexplorer.usgs.gov/

Zhang, L. and Shao, H. 2013. Direct plant-plant facilitation in coastal wetlands: A review. *Estuarine, Coastal and Shelf Science*, 119, pp.1-6.

Cloud Publications
International Journal of Advanced Remote Sensing and GIS
2017, Volume 6, Issue 1, pp. 2274-2280
ISSN 2320 – 0243, Crossref: 10.23953/cloud.ijarsg.289

Methodology Article

Road Network Impedance Factor Modelling Based on Slope and Curvature of the Road

Prabhakar Alok Verma[1], Kislay Kumar[2], Sameer Saran[1]

[1]Geoinformatics Department, Indian Institute of Remote Sensing-ISRO, Dehradun, Uttrakhand, India
[2]Department of Information Technology, Institute of Engineering & Management, Kolkata, Bengal, India

Publication Date: 31 July 2017

DOI: https://doi.org/10.23953/cloud.ijarsg.289

Abstract Travelling in hills like Himalaya is very time-consuming due to presence of high slope and curvature in the road. Travel time is also affected by condition of the road i.e. surface roughness, rut depth, pavement conditions etc. However, for this research paper only slope and curvature is considered. To plan the journey in proper way, exact time required for travelling plays key role for any person. Google is providing best route to travel and estimated time required between source and destination. This travel time estimate by Google is up to the mark in plain region but not satisfactory in hills. Because road transportation network in hills contains a lot of curvature and slope of the network in also very high and varying due to undulating terrain of the mountains. Therefore, in this research a technique is proposed to calculate better travel time estimate. Proposed technique considers natural obstacles to the travel speed in the hills like slope and curvature. In this a network model is proposed which assigns average driving speed to the road segment, and this driving speed is calculated by percentage rise in the slope & radius of curvature of the road segment. Model takes road network and raster image of slope in degrees. Open source tools and languages (Python, GDAL, and QGIS) are used to make this model. Results of proposed network model are near to the ground truth value.
Keywords *Curvature; GIS; Impedance; Python*

1. Introduction

Significant modelling of any real world phenomenon requires proper representation of the object. Geographic information system (GIS) provides facility to represent real world. But over the year's real world has become very complex to model properly using any information system (Sadeghi-Niaraki et al., 2011). Better representation allows us to use GIS tools and produce accurate outputs. One of the GIS tool is network analysis tool, which is having functionalities to calculate optimum path, closest facility, service area etc. based on the impedance of the network. Road networks are geometric networks, a geometric network is composed of nodes and edges where nodes are junction points and edges are road segments. According to Lupien et al., (1987) network is a line graph composed of links & nodes where links represent linear channels of flow, and nodes represent connections of links. For each real world road network, direction and impedance must be assigned with each edge to calculate travel cost/time (Husdal, 1999). Transportation planning requires network analysis in situations like finding the shortest path, service area within a specified travel cost (Husdal, 1999).

Impedance factor of road network plays a key role to get accurate output of network analysis. Hence, attempt to make more accurate modelling under different conditions is being carried out by researchers across the world since last two decades. Chunithipaisan et al., (2004) used distance as the mono-dimensional variable, Leonard et al., (2000) used speed as mono-dimensional variable, Shadewald et al., (2001) used traffic as mono-dimensional variable to model impedance factor of road network. Various researches are available where multiple variables including environmental conditions are used to model the impedance factor. Thirumalaivasan et al., (1997) used volume of traffic, type of road, road width, number of junctions, turns etc. to model the impedance factor. From the earlier researches, it can be concluded that mono-dimensional variable based impedance factor modelling is not capable of modelling the real world. Multiple variables can help to model impedance factor in an accurate way, but required variables changes from one ecosystem to another ecosystem. E.g. for high population zone, dominating variables can be traffic, road width, vehicle count per hour, for less population region dominating variables can be road width, road condition, environmental condition and for hilly region with less population or traffic dominating variable can be road width, slope of the road, road condition, curvature of bends, distance between two bends, environmental condition etc.

Since travel time in hilly region is high compared to plan region due to non-availability of straight and plane roads. This study is focused to incorporate natural limitations to the speed or impedance factor. The objective of this study is to calculate impedance for each segment of road based on slope and curvature at the bends. Also condition of speed limit as per the government rules is to be incorporated.

One possible form of impedance factor is average driving speed on the road which will give us optimum travel time in case of any route. Driving speed/impedance factor is mostly calculated based on length, width, type and traffic on the road. But if the road network belongs to hilly area where a lot of ups & downs and steep curvatures are present. In such kind of scenario apart from the mentioned criteria effect of slope and curvatures should also be considered to calculate optimum impedance. In this research slope and curvatures of the road network are considered to calculate average driving speed, since traffic is very low in my study area so this factor is neglected.

1.1. Study Area and Data Sets

The study area includes one of the state of India, Uttarakhand. Geographical area of this state is around 53,483 sq. kms. This state is mostly covered by Himalayan hills. Yearly average temperature of study region is around 25^0 C, pleasant weather and natural beauty attracts tourists from whole India.

Table 1: *Datasets*

Data	Source
DEM	30 m spatial resolution Cartosat data
Road network	Downloaded from OSM

Table 1 shows the dataset used to carry out this research. Road network was downloaded from OpenStreetMap (OSM) and digitization errors were removed to make it usable for my research. Cartosat DEM having 30m resolution is used to calculate slope of the road segments.

2. Methodology

In this research, curvature and slope of the road are the limiting factor to the average driving speed. Slope is derived from satellite derived DEM whereas curvature of the road is calculated using the vector data of road network.

2.1. Radius of Curvature of the Road

Minimum three points are required to calculate radius of curvature, this is clear from the equation of the circle:

$(x-a)^2 + (x-b)^2 = r^2$

Where x, y are the coordinates of the points and a, b are the coordinates of the centre of the circle & r is the radius of circle.

For this research entire road network is divided in multiple segments bends in the road network is identified based on the change in angle between two successive segments, in my case if change in angle is more than 45 degrees then it considered as bending. Similarly, all such segments participating in a bend are stored and circular regression is done to calculate the radius of curvature. Finally, radius of curvature is stored in attribute table of the participating segments of the bend.

2.2. Circular Regression

Suppose (x_1, y_1), (x_2, y_2), (x_3, y_3),……,(x_n, y_n) are the middle points of segments participating in the bend. Then equation of circle becomes:

Consider $R = r^2 - a^2 - b^2$

$$
\begin{aligned}
&R + 2ax_1 + 2by_1 = {x_1}^2 + {y_1}^2 \\
&R + 2ax_2 + 2by_2 = {x_2}^2 + {y_2}^2 \\
&R + 2ax_3 + 2by_3 = {x_3}^2 + {y_3}^2 \\
&\ldots\ldots\ldots\ldots\ldots\ldots\ldots \\
&R + 2ax_n + 2by_n = {x_n}^2 + {y_n}^2
\end{aligned}
$$

$$
\overbrace{\begin{pmatrix} x_1 & y_1 & 1 \\ x_2 & y_2 & 1 \\ . & . & . \\ x_n & y_n & 1 \end{pmatrix}}^{A}
\overbrace{\begin{pmatrix} 2a \\ 2b \\ R \end{pmatrix}}^{X}
=
\overbrace{\begin{pmatrix} {x_1}^2 + {y_1}^2 \\ {x_2}^2 + {y_2}^2 \\ . \\ {x_n}^2 + {y_n}^2 \end{pmatrix}}^{B}
\quad \ldots \text{ eq. (1)}
$$

$AX = B$

$X = A^{-1}B$

Solving eq. (1) will give a, b and r.

This information is updated in attribute table.

Using the radius of curvature, maximum allowed speed is calculated from the condition of toppling. Since dynamics of the moving body on the curve suggest the condition at which it will topple. For a moving body on a curve, the condition for toppling of the body can be expressed as:

$v \leq \sqrt{Fr/m}$ … eq. (2)

Where F is force acting on the body (gravitational force in this case), r is the radius of curvature and m is mass of the body.

Eq. (2) leads to maximum allowed velocity as:

$v = \sqrt{r\,\mathrm{g}\tan\theta}$ … eq. (3)

Where g is gravitational acceleration, θ is across slope angle of the road segment.

Using the equation 3 and radius of curvature, maximum allowed speed is calculated at the bends and updated in the attribute table of road network.

2.3. Slope of the Road

Slope of whole study area is calculated in degrees from the Cartosat DEM using QGIS software. Road network is overlaid over the slope image and corresponding slope values for road segments were filled in attribute table of road network.

A relationship is established between slope of the road and maximum allowed speed as per the Indian Road Congress (IRC). From the established relationship speed corresponding to slope of segments is updated in the attribute table of road network.

Table 2 shows then terrain classification as per IRC and table shows the allowed speed type and terrain of the road.

Table 2: *Terrain Classification*

Terrain classification	Cross Slope (%)
Plain	0 - 10
Rolling	10 - 25
Mountainous	25 - 60
Steep	>60

Table 3: *Design Speed in km/hr as per IRC (ruling and minimum)*

Type	Plain	Rolling	Hilly	Steep
NS & SH	100-80	80-65	50-40	40-30
MDR	80-65	65-50	40-30	30-20
ODR	65-50	50-40	30-25	25-20
VR	50-40	40-35	25-20	25-20

The website of the national highways authority of India (www.nhai.org) gives the classes as:

1. Expressways
2. National highways
3. State highways
4. Major district roads
5. Rural and other roads
6. Other road classes

On the basis of regression model for the speed and slope provided by IRC, following relationship says that velocity and slope of the road are exponentially related.

$v = 59.825\, e^{-0.016\, s}$ … eq. (4)

Where v is speed and s is the slope of the road segment.

Let's say speed from the slope is denoted by v_s and speed from radius of curvature is denoted by v_r , then final speed or impedance factor (v_f) for a road segment is:

$v_f = min(v_s, v_r)$ … eq. (5)

2.4. Calculation of Time from Point A to Point B

Suppose A and B are the points/locations for which travel time need to calculated, there are n road segments between A & B, then:

Travel time = $\frac{d_1}{v_1} + \frac{d_2}{v_2} + \cdots + \frac{d_n}{v_n}$ … eq. (6)

Where d_n $is\ the\ legth\ and\ v_n is\ final\ speed\ of\ road\ segment\ for\ n = 1,2,3 \ldots \ldots n)$

3. Results and Discussion

To perform validation of the proposed technique road segment from Rishikesh, Uttarakhand to Deoprayag, Uttarakhand (as shown in Figure 1) was taken. Total length of the segment is 74.018 kilometers, and it consists only hilly region where roads are very steep and curvy. The figure below shows the actual scenario of the road segment.

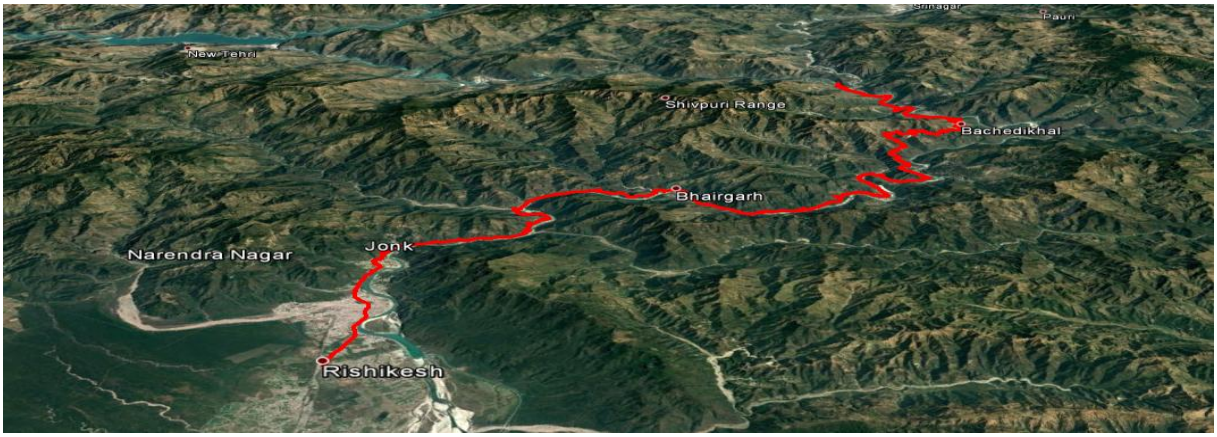

Figure 1: *Road Segment*

FID	Shap	X	Y	slope	f_vel	len	time
0	Polyli	268765.2	3337403.5	38.182	32.47	4.4709	0.008
1	Polyli	268755.8	3337417.5	63.353	21.70	29.802	0.082
2	Polyli	268737.9	3337481.1	75.011	18.01	103.52	0.344
3	Polyli	268722.3	3337542.4	69.967	19.52	23.584	0.072
4	Polyli	268710.6	3337604.8	75.135	17.98	104.27	0.347
5	Polyli	268709.4	3337681.9	62.038	22.17	51.897	0.140
6	Polyli	268713.3	3337731.7	58.775	23.35	48.941	0.125
7	Polyli	268731.1	3337775.7	60.445	22.74	54.826	0.144
8	Polyli	268749.5	3337802.5	50.457	26.68	14.542	0.032
9	Polyli	268735.1	3337827.7	89.630	14.25	45.166	0.190
10	Polyli	268723.6	3337852.9	83.501	15.72	14.920	0.056
11	Polyli	268732.7	3337874.4	83.501	15.72	31.830	0.121
12	Polyli	268750.6	3337902.8	60.731	22.64	35.785	0.094

Figure 2: *The Overall Structure of the Data Stored in Shapefile Format*

Figure 2 shows the overall structure of the data stored in shapefile format. “X” and “Y” are the coordinates of midpoints of the line segment, “slope” is the slope (in degrees) corresponding to that segment as per Cartosat DEM, “f_vel” is the final allowed velocity for each segment, “len” and “time” are the length (in meters) of the segment and time (in minutes) required to cover length of the corresponding segment respectively.

Finally, total time required to cover the desired road from Rishikesh to Devprayag using proposed technique is coming as 207.49 minutes or 3 hrs 27 minutes. This time is much more realistic to cover this distance. As per the Google map, time required to travel same route is around 2 hrs. Covering 74 km distance in plain region is possible but it is nearly impossible to cover 74 km in complex terrain of Himalaya. So, proposed technique is giving much more realistic results.

4. Conclusions

The calculated travel time considering the impedance factor proposed is subsequently greater and more realistic than the estimated travel time given by the Google Maps for same route. This shows that to determine impedance factor, curvatures and slopes plays an important. There can be other factors also like traffic, road condition, weather etc. However, it is assumed that roads are of good condition, hilly regions are less traffic prone.

References

Chunithipaisan, S., James, M. P. and Parker, D. 2004. Online network analysis from heterogeneous datasets - Case study in London train network. *Map Asia Conference, Beijing, China.* Available from: https://www.geospatialworld.net/article/online-network-analysis-from-heterogeneous-datasets-case-study-in-london-train-network/.

Husdal, J. 1999. Network analysis - network versus vector - A comparison study. *Unpublished working paper, University of Leicester, UK.*

Leonard, J. D. and Oliveira, M. A. R. C. E. L. O. 2000. Towards an area wide service measure. Proceedings of the Fourth International Symposium on Highway Capacity Transportation Research Board National Research Council, Hawaii, USA.
Available from: http://gulliver.trb.org/publications/circulars/ec018/ec018toc.pdf.

Lupien, A. E., Moreland, W. H. and Dangermond, J. 1987. Network analysis in geographic information-systems. *Photogrammetric Engineering & Remote Sensing,* 53(10), pp.1417-1421.

Sadeghi-Niaraki, A., Varshosaz, M., Kim, K. and Jung, J. J. 2011. Real world representation of a road network for route planning in GIS. *Expert Systems with Applications,* 38(10), pp.11999-12008.

Shadewald, J. K., Hallmark, S. and Souleyrette, R. R. 2001. Visualizing system-wide economic impacts of transportation projects. *Journal of Urban Planning and Development,* 127(4), pp.158-168.

Thirumalaivasan, D., and Guruswamy, V. 1997. Optimal route analysis using GIS. Available from: http://www.gisdevelopment.net/application/Utility/transport/utilitytr0004a.htm.

Cloud Publications
International Journal of Advanced Remote Sensing and GIS
2017, Volume 6, Issue 1, pp. 2223-2233
ISSN 2320 – 0243, Crossref: 10.23953/cloud.ijarsg.281

Research Article

Land Use/Land Cover Change Study of District Dehradun, Uttarakhand using Remote Sensing and GIS Technologies

Varun Rawat and Mansi Puri

Department of Computer Science, DIT University Dehradun, Uttrakhand, India

Publication Date: 22 July 2017

DOI: https://doi.org/10.23953/cloud.ijarsg.281

Abstract The present study illustrates an integrated approach of geospatial technologies, i.e., remote sensing and GIS for assessment of land use/cover dynamics of a district of the Uttarakhand State viz., the Dehradun. Landsat satellite imageries of three different years, i.e., Landsat Thematic Mapper (TM) of 1994, 1999 and 2016 were acquired by USGS Earth Explorer and quantified the land use/cover changes in district Dehradun for a period of more than two decades. Supervised Classification methodology has been employed using Maximum Likelihood Technique in ERDAS 9.3. The images of the study area were categorized into six different land us/land cover classes, viz., vegetation area (in 61.47% area), agricultural land (17.61%), built-up area (6.82%), barren area (5.91%), sediment area (5.67%) and area under water body (2.53%). The results indicate that during the last twenty two years (1994-2016) the vegetation area, built-up area, barren land and sediment area have been increased about 163.67 km^2, 110.78 km^2, 83.69 km^2 and 78.55 km^2, respectively, while the agricultural land and water body have been decreased about 366.78 km^2 and 67.91 km^2, respectively. The approach adopted in this study has clearly demonstrated the potential of remote sensing and GIS techniques in measuring the change pattern of land use/cover.
Keywords *Change detection; Geospatial Technologies; Remote Sensing; GIS; District Dehradun*

1. Introduction

The land is one of the most important natural resources as life and various development activities are based on it. Land cover is a fundamental parameter describing the Earth's surface. This parameter is a considerable variable that impacts on and links many parts of the human and physical environments (Torrens and Alberti, 2000; Barnes et al., 2001). Land use refers to human activities which are directly related to the land (Epstein et al., 2002). Land use involves the management and modification of natural environment or wilderness into built environment such as fields, pastures, and settlements. Land use/land cover (LULC) changes are driven by natural forces or by human land uses. Thus, it involves both the natural and the human dimensions. Information on LU/LC is important to support planning and sustainable management of natural resources and socio-economic development (Rawat et al., 2013a; b; Zubair et al., 2006).

The land is one of the most important natural resources, as life and various development activities are based on it. Land-cover change has been identified as one of the most important drivers of changes in the ecosystem and their services.

Locally, the land cover changes due to an environment or climatic factors determine the vulnerability of people to climatic perturbations and thus affect the decisions on land use by people. Globally, on the other hand, the land cover changes significantly affecting the functioning of Earth's system. Hence, information on land use/land cover is essential for the selection, planning and implementation of land use and can be used to meet the increasing demands for basic human needs and welfare. This information also assists in monitoring the dynamics of land use resulting out of changing demands of increasing population. Changes in land cover by land use patterns, affects biodiversity, water and other processes that come together to affect climate and biosphere. Changes in LU/LC now have become the central component in current strategies for managing of the land use pattern in any area (Abdelhamid et al., 2006; Ye Bai et al., 2008; Lo Yang et al., 2002; Cohen et al., 2006; Heuvelink and Burrough et al., 2002).

LU/LC change detection is very essential for better understanding of landscape dynamic during a known period of time having sustainable management (Kiefer et al., 1987; Zhang et al., 2011) and to asses loss and ecosystem disturbances (Rawat, 2016). LU/LC change is a widespread and accelerating process, mainly driven by natural phenomena and anthropogenic activities, which in turn drive change that would impact natural ecosystem. Timely and precise information about LULC change detection of Earth's surface is extremely important for understanding relationships and interactions between human and natural phenomena for better management of decision making (Pontius and Malanson et al., 2005; Jokar et al., 2013).

Research conducted in Ethiopia has shown that there were considerable LULC changes in the country during the second half of the 20th. Timely and precise information about LULC change detection of Earth's surface is extremely important for understanding relationships and interactions between human and natural phenomena for better management of decision making (Krivoruchko and Redlands et al., 2005). Recent LU/LC studies in the Uttarakhand State in Central Himalaya reveals that due to population pressure, towns are growing indiscriminately on the highly fertile agricultural lands (Rawat et al., 2013a;2013b;2013c;2013d; 2014)

The present study aims to demonstrate application of geospatial technologies, i.e., remote sensing and GIS in land use/ land cover study and to define its dynamics since the last few decades.

2. Material and Methodology

2.1. Study Area

The study area, viz., district Dehradun is one of the total thirteen districts of the Uttarakhand state (Figure 1) where the capital of the State –Dehradun lies. District Dehradun, encompassing an area of 3088.50 km^2, extends in between 29^o 57'56.44" N to 31 ^{o}1'127.13" N Latitudes and 77^o 38'19.57" E to 78.1424.53" E Longitudes. The elevation of the district varies in between 288 m to 3096 m from the mean sea level. Attitudinally about one-third part (i.e., 32.43% area) of the district lies in between 600m to 1200m relief region while a small part (3.55% area) lies in the relief zone more than 2400m. The district has 6 development blocks, 6 tehsils and 771 villages with population of 5, 69,578 having a population density of 184 persons/km^2 (SH, 2011)

2.2. Data Process and Data Use

The LANDSAT is a scientific program which is operated by NASA and USGS, which offers the longest global record of Earth's surface. The satellite data used in the present study includes the imagery of LANDSAT-5 "TM", LANDSAT-7 "ETM" And LANDSAT-8 "OLI" & "TIRS" Sensor.

The LANDSAT-5 imagery is of February 1994, LANDSAT-7 imagery is of March 2000, and LANDSAT-8 is of February 2016 with the resolution of 30m nominal and panchromatic resolution is 15m. Map projection used in "UTM" datum "WGS84" and UTM zone is 44.

2.3. Software used

In this study, ERDAS IMAGINE-9.3 remote sensing application with raster graphics editor abilities designed by ERDAS is used. ERDAS IMAGINE is aimed primarily at geospatial raster data processing and allows the user to prepare, display and enhance the digital image for mapping use in GIS or software.

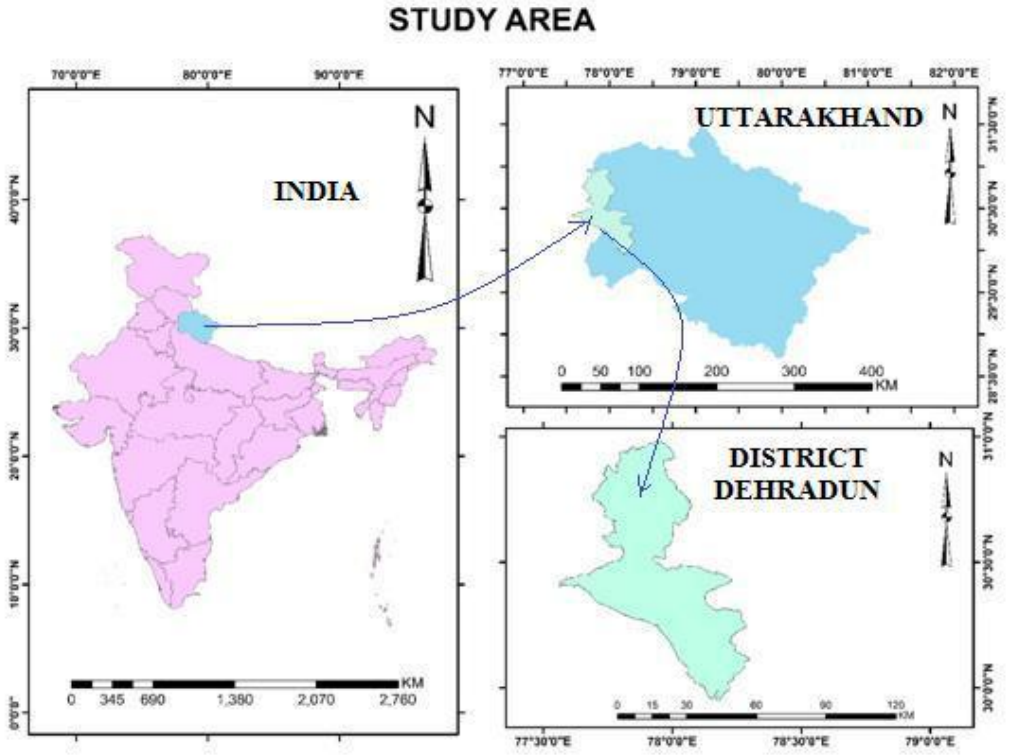

Figure 1: *Location map of the study area, viz., Dehradun District*

2.4. Image Classification

Multispectral classification is the process of sorting pixels into a finite number of individual classes or categories of data, based on their data file values. If a pixel satisfies a certain set of criteria, the pixel is assigned to the class that corresponds to that criterion. This process is also referred to as image segmentation. Depending on the type of information to be extracted from the origin data, classes may be associated with known features on the ground or may simply represent areas that look different to the computer. An example of a classified image is a land cover map, showing vegetation, bare land, pasture, urban and so forth. In this study we have used supervised image classification map, one common application of remotely-sensed images to land management is the creation of maps, vegetation type, or other discrete classes by remote sensing software. The flow chart (Figure 2) illustrates methodology used in this paper which includes data used and different steps of data processing.

2.5. Accuracy Assessment

In the context of information extraction by image analysis, accuracy measures the agreement between a standard assumed to be correct and a classified image of unknown quality (Singh et al., 2013). The accuracy of image classification is most often reported as a percentage correction. The consumer's accuracy (CA) is computed using the number of correctly classified pixels to the total number of pixels assigned to a particular category.

It takes errors of the commission into account by telling the consumer that, for all areas identified as category X, a certain percentage are actually correct. The producer's accuracy (PA) informs the image analyst of the number of pixels correctly classified in a particular category as a percentage of the total number of pixels actually belonging to that category in the image. Producer's accuracy measures errors of the omission.

2.6. Error Matrix

One of the most common means of expressing classification accuracy is the preparation of a classification error matrix. Error matrices compare, on a category by category basis, the relationship between known reference data (ground truth) and the corresponding result of an automated classification. Such matrices are square, with the number of rows and columns equal to the number of categories whose classification accuracy is being assessed. Overall accuracy is computed by dividing the total number of correctly classified pixels by the total number of reference pixels. The accuracies of individual categories can be calculated by dividing the number of correctly classified pixels in each category by either the total number of pixels in the corresponding row and column. Producers accuracies result from dividing the number of correctly classified pixels in each category (on the major diagonal) by the number of training set pixels used for other categories (the column total). User accuracy is computed by dividing the number of correctly classified pixels in each category by the total number of pixels that were classified in that category (the row total).

3. Results and Discussion

3.1. Land use/Land Cover

LULC categories for three different years (i.e., 1994, 2008 and 2016) were assessed using remote sensing and GIS techniques. The results are presented in Figure 3 and Table 1. A brief account of year wise discussion of these results is presented in the following paragraphs.

3.1.1. LULC in 1994- The satellite image of the study area, classification of different LULC of district Dehradun for the year 1994 is presented in Figure 3 (left). In 1994 about 1734.15 km^2 which accounts for 56.17% of the total district area was under vegetation cover, about 910.45 km^2 which accounts for 29.48% was under agricultural land, about 99.76 km^2 which accounts for 3.23% was under built up area, about 98.76 km^2 which accounts for 3.20% was under barren land, about145.98 km^2 which accounts for 4.73% was in water body and the remaining about 98.45 km^2 which accounts for 3.19% of the total district area was under sediment area (Table 1).

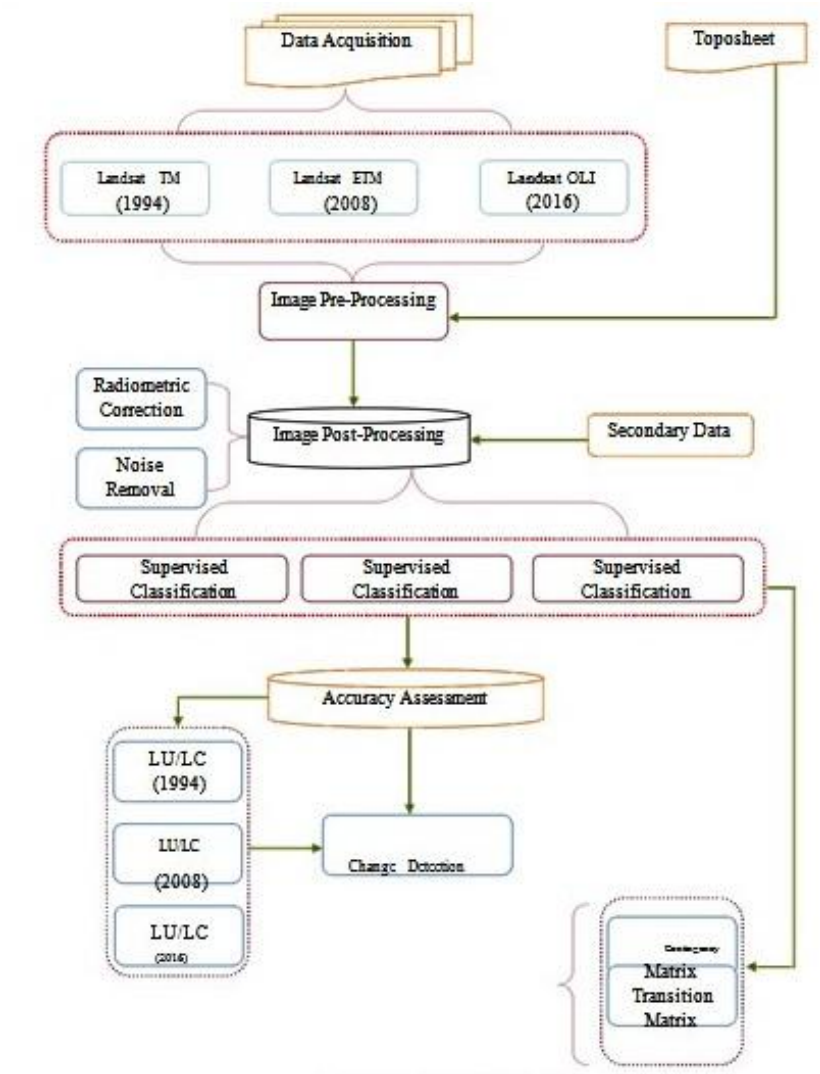

Figure 2: *Methodology Chart*

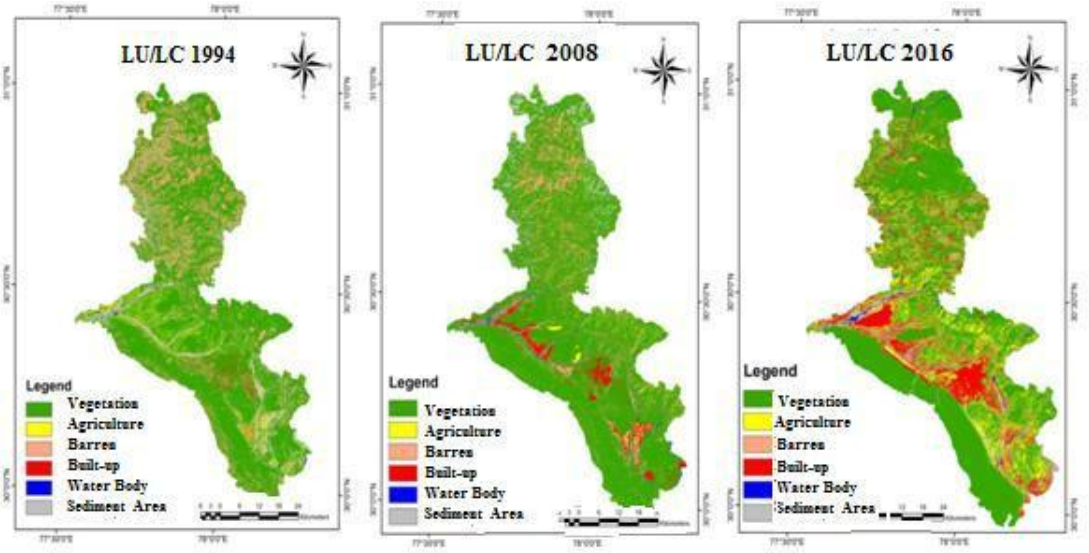

Figure 3: *Land use/Land Cover in 1994, 2008 and 2016 in district Dehradun*

Table 1: *Land use/Land Cover pattern in district Dehradun in 1994*

Land Category	Area(1994)		Area (2008)		Area (2016)	
	in km^2	in %	in km^2	in %	in km^2	in %
Vegetation Cover	1734.15	56.17	1805.89	58.49	1897.82	61.47
Agricultural Area	910.45	29.49	793.59	25.70	543.67	17.61
Barren Land	98.76	3.20	116.09	3.76	182.45	5.91
Built-up Area	99.76	3.23	130.55	4.23	210.54	6.82
Water Body	145.98	4.73	125.46	4.06	78.07	2.53
Sediment Area	98.45	3.19	115.97	3.76	175.00	5.67

3.1.2 LULC in 2008 - Figure 3 *(middle)* depicts the geographical distribution of LULC of district Dehradun for 2008. During 2008 in Dehradun district, the total area under agricultural land was about 793.59 km^2 which accounts for 25.70% of the total district area. Built-up area was 130.55 km^2 which accounts for 4.23%, vegetation area was 1805.89 km^2 which accounts for 58.49%, barren land was 116.09 km^2 which accounts for 3.76%, water body was 125.46 km^2 which account for 4.06% and sediment area was about 115.97 km^2 which accounts for 3.76% of the total district area (Table 1).

3.1.3 LULC in 2016 - Figure 3 *(left)* depicts the geographical distribution of LULC of district Dehradun for 2016. During 2016 in Dehradun district the total distribution of the agriculture area was about 543.67 km^2 which accounts for 17.61% of the total district area, built-up area is 210.54 km^2 which accounts for 6.82%, vegetation area was1897.82 km^2 which accounts for 61.47%, barren land was 182.45 km^2 which accounts for 5.91%, water body was 78.07 km^2 which accounts for 2.53% area of the district (Table 1).

3.2. LULC Change Detection

LULC change detection in district Dehradun was done for three different periods. These are 1994 to 2008, 2008 to 2016 and 1994 to 2016. Results are presented in Figure 4 and Table 2. A brief discussion of these LULC change is presented in the following paragraphs.

3.2.1. Change Detection during 1994-2008 - Figure 4 depicts the status of LULC change in district Dehradun during 1994 to 2008 which reveals that during this period, the vegetation area, built up area, barren land and sediment area have been increased about 71.74 km^2, 30.79 km^2, 17.33 km^2 and 17.52 km^2, respectively; while the agricultural land, and water bodies have decreased about 116.86 km^2 and 20.52 km^2, respectively.

3.2.2. Change Detection During 2008-2016 - Since 1994 to 2008 there has been an increase of 91.93 km^2 of area in vegetation area, 66.36 km^2 in barren land, 79.99 km^2 in built-up area and 59.03 km^2 of area in sediment area, and decrease of about 249.92 km^2 in agricultural area and 47.39 km^2 in water body.

3.2.3. Change Detection During 1994-2016 - Over all during the last 22 years (1994 to 2016), there has been an increase of 163.67 km^2 in vegetation area, 83.69 km^2 in barren land area, 110.78 km^2 in built-up area and 76.55 km^2 in sediment area, and decrease of 366.78 km^2 in agricultural area and 67.91 km^2 in area under water body. From these data, it can be inferred that the built-up and vegetation area is increasing while the water body as well as agriculture area is continuously decreasing in district Dehradun.

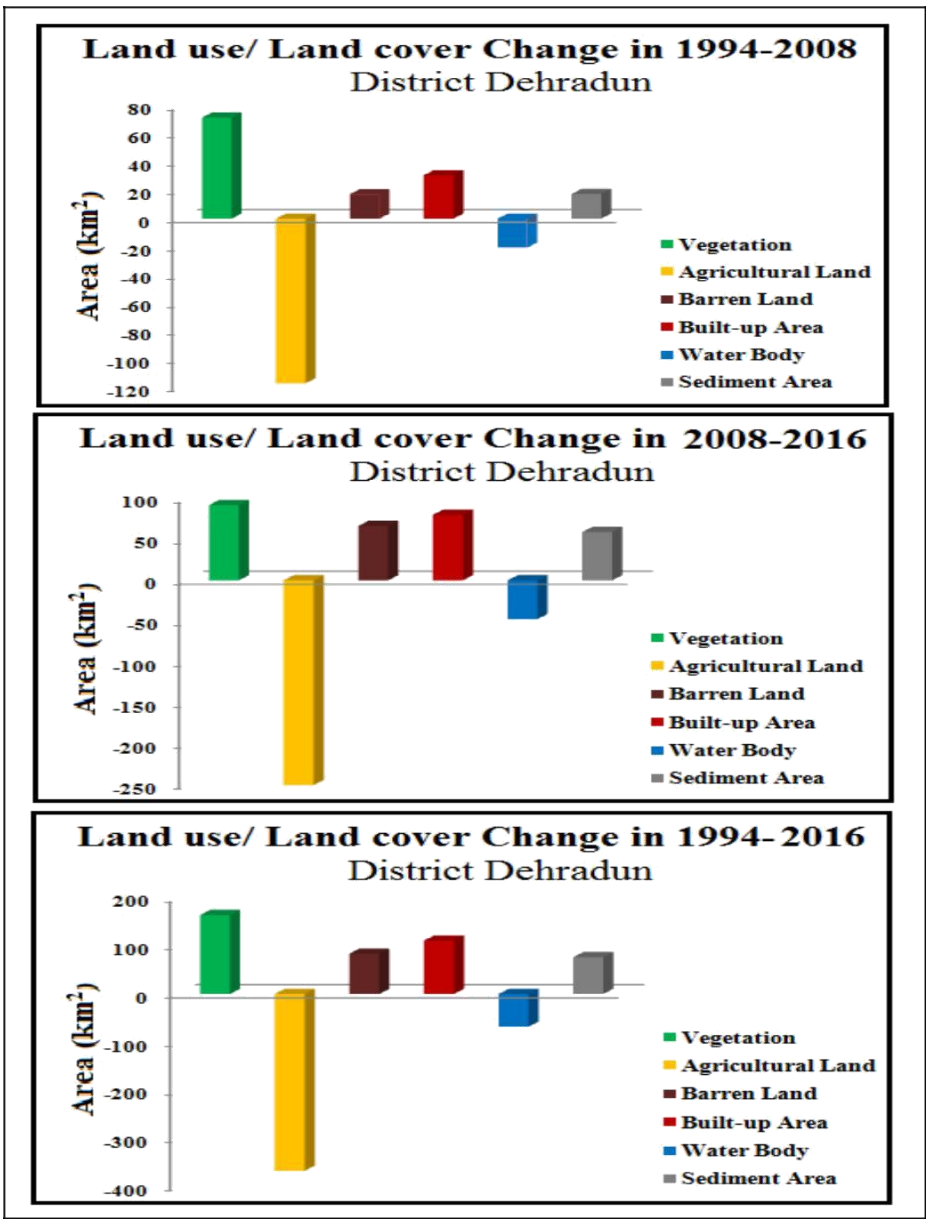

Figure 4: *Bar diagramme showing changes in LU/LC during 1994-2008 (upper), 2008-2018 (middle) and 1994-2016 (lower) in the Dehradun district*

Table 2: *LULC change in district Dehradun during different periods*

Land Category	1994-2008	2008-2016	1994-2016
	km^2	km^2	km^2
Vegetation	71.74	91.93	163.67
Agricultural Land	-116.86	-249.92	-366.78
Barren Land	17.33	66.36	83.69
Built-up Area	30.79	79.99	110.78
Water Body	-20.52	-47.39	-67.91
Sediment Area	17.52	59.03	76.55

3.3. LULC Change Matrix

How much LULC has been changed from one category of land to another category? To define this problem, Change Matrix was calculated for different durations, i.e., 1994-2008 (Table 3), 2008-2016 (Table 4) and 1994-2016 (Table 5). A brief account of these Change Matrices is given in the following paragraphs.

3.3.1. Change Matrix 1994 and 2008 - In district Dehradun, during 1994-2008, about 97.01 km^2 agricultural land area, 2.12 km^2 sediment area and 0.85 km^2 barren land area was converted in to vegetation area; about 12.65 km^2 agricultural land and 0.65 km^2 barren land was converted into agricultural area; about 17.08 km^2 agricultural area and 3.01 km^2 vegetation area was converted in to barren area; 12.67 km^2 vegetation area and 12.77 km^2 agricultural area and 6.21 km^2 barren land area was converted into built-up area; about 1.1 km^2 sediment area was converted into water body; and 21.62 km^2 area of water body was converted in to sediment area (Table 3).

Table 3: *Comparative Matrix between 1994 and 2008*

Category	Vegetation	Agriculture	Barren Land	Built-up	Water Body	Sediment	**1994**
Vegetation	1705.83	12.65	3.01	12.67	0	0	**1734.16**
Agriculture	97.01	783.59	17.08	12.77	0	0	**910.45**
Barren	0.85	0.65	96.36	6.21	0	0	**104.07**
Built-up	0	0.00	0	98.90	0	0	**98.90**
Water Body	0	0.00	0	0.00	124.36	21.62	**145.98**
Sediment	2.12	0.00	0	0.00	1.1	95.30	**98.52**
2008	**1805.81**	**796.89**	**116.45**	**130.55**	**125.46**	**116.92**	

3.3.2. Change Matrix 2008 and 2016 - In district Dehradun, during 1994-2008, about 164.92km^2 agricultural land area and 8.05km^2 barren land area was converted in to vegetation area; about 29.85km^2 vegetation area and 1.25 km^2 barren land area was converted into agricultural land area; about 67.32 agricultural land area and 10.21 agricultural land area was converted into barren land; about 40.25 km^2 forest area , 47.32 km^2 agricultural area and 2.02 km^2 barren land area was converted into built up area; about 70.13 km^2 area of water body was converted into sediment area; and about 13.03 km^2 sediment area was converted into water body (Table 4).

Table 4: *Comparative Matrix between 2008 and 2016*

Category	Vegetation	Agriculture	Barren Land	Built-up	Water Body	Sediment	**2008**
Vegetation	1725.30	29.85	10.21	40.25	0	0	**1805.6**
Agriculture	164.92	512.57	67.32	47.32	0	0	**792.13**
Barren Land	8.05	1.25	105.08	2.02	0	0	**116.40**
Built-up	0	0.00	0	120.45	0	0	**120.45**
Water Body	0	0.00	0	0.00	65.32	70.13	**135.45**
Sediment	0.9	0.00	0	0.00	13.02	101.87	**115.79**
2016	**1899.17**	**543.67**	**182.61**	**210.04**	**78.34**	**172.00**	

3.3.3. Change Matrix 1994 and 2016 - In district Dehradun, over all within the last 22 years (i.e., during 1994-2016) about 237.66 km^2 area of agricultural land, 0.98 km^2 area of barren land and 0.25 km^2 sediment area was converted in to vegetation area; about 10.25 km^2 vegetation area and 0.36

km^2 barren land area was converted into agricultural land; about 76.32 km^2 agricultural land area and 9.21 km^2 vegetation area was converted into barren land area; about 48.32 km^2 vegetation area, about 63.21 km^2 agricultural area and 0.25 km^2 barren land area was converted into built-up area; about 11.25 km^2 sediment area was converted into water body; and about 78.25 km^2 water body area was converted into sediment area (Table 5).

Table 5: *Comparative Matrix between 1994 and 2016*

Category	Vegetation	Agriculture	Barren Land	Built-up	Water Body	Sediment	**1994**
Vegetation	1660.25	10.25	9.21	48.32	0	0	**1728.00**
Agriculture	237.66	533.21	76.32	63.26	0	0	**910.45**
Barren Land	0.98	0.36	97.25	0.25	0	0	**98.84**
Built-up	0	0.00	0	98.65	0	0	**98.65**
Water Body	0	0.00	0	0.00	67.58	78.25	**145.83**
Sediment	0.25	0.00	0	0.00	11.25	87.25	**98.75**
2016	**1899.14**	**543.82**	**182.78**	**210.48**	**78.83**	**165.50**	

4. Conclusions

The study conducted in one of the districts of the Uttarakhand state in the Central Himalaya, viz., Dehradun advocates that multi-temporal satellite data are very useful to detect the changes in LULC quickly and accurately. The study reveals that the major landuse in the Dehradun district are vegetation cover in 61.47% (1897.82 km^2) area, agricultural land in 17.61% (543.67 km^2) area, built-up area 6.82% (210.54 km^2) area, barren land 5.91% (182.45 km^2) area, sediment area 5.67 % (175 km^2) area and water body 2.53 % (78.07 km^2) area. During the last 22 years (1994 to 2016), there has been an increase of about 163.67 km^2 areas in vegetation cover, 83.69 km^2 of area in barren land, 110.78 km^2 in built-up area and 76.55 km^2 in sediment area; and decrease of about 366.78 km^2 in agriculture area and 67.91 km^2 in water body. The study depicts that due to indiscriminate sprawl in built-up area the district, about 48.32 km^2 vegetation areas, 63.21 km^2 agricultural areas and 0.25 km^2 barren land area was converted into built-up area during the last two decades. Thus, increasing population pressure is putting tremendous pressure on the land use and land cover in district Dehradun. The approach adopted in this study has clearly demonstrated the potential of GIS and remote sensing techniques in measuring the change in LULC pattern.

Acknowledgement

Authors are thankful to the Director, Centre of Excellence for NRDMS in Uttarakhand, Department of Geography, Kumaun University SSJ Campus Almora for extending laboratory facility and to Er. Pawan Kumar for technical assistance in data processing.

References

Abdelhamid, A. 2006. Urban Development and Planning in the Occupied Palestinian Territories: Impacts on Urban Form. The Conference on Nordic and International Urban Morphology: Distinctive and Common Themes, Stockholm, Sweden.

Barnes, K.B., Morgan, I., Roberge, J.M. and Lowe, M.C. 2001. Sprawl Development: Its patterns, Consequences, and Measurement. *Towson University*, Towson.

Cohen, B. 2006. Urbanization in developing countries: Current trends, future projections, and key challenges for sustainability. *Technology in Society*, 28(2), pp.63-80.

Epstein, J., Payne, K. and Kramer, E. 2002. Techniques for mapping suburban sprawl. *Photogrammetric Engineering & Remote Sensing*, 63(9), pp.913-918.

Heuvelink, G.B.M. and Burrough, P.A. 2002. Developments in statistical approaches to spatial uncertainty and its propagation. *International Journal of Geographical Information Science*, 16(2), pp.111-113.

Jokar Arsanjani, J., Helbich, M. Kainz, W. and Darvishi Boloorani, A. 2013. Integration of logistic regression, Markov chain and cellular automata models to simulate urban expansion. *International Journal of Applied Earth Observation and Geoinformation*, 21, pp.265-275.

Kiefer Lillesand, T. 1987. *Remote sensing and image interpretation*. 5th ed. New York: John Wiley & Sons. p.721.

Krivoruchko, K., Crawford, C.A.G. and Redlands, C.A. 2005. Assessing the uncertainty resulting from geoprocessing operations. In: Maguire, D.J. Batty, M. and Goodchild, M.F. (eds.) *GIS Spatial Analysis, and Modeling*. Redlamds, CA: ESRI Press, pp.67-92.

Lo, C.P. and Yang, X. 2002. Drivers of land-use/land-cover changes and dynamic modeling for the Atlanta, Georgia metropolitan area. *PE & RS-Photogrammetric Engineering & Remote Sensing*, 68(10), pp.1073-1082.

Pontius, G.R. and Malanson, J. 2005. Comparison of the structure and accuracy of two land change models. *International Journal of Geographical Information Science*, 19(2), pp.243-265.

Neelam Rawat, Asha Thapliyal, Saurabh Purohit, Govind Singh Negi, Sourabh Dangwal, Santosh Rawat, Ashok Aswal and Kimothi, M.M. 2016. Vegetation Loss and Ecosystem Disturbances on Kedargad Mandakini Subwatershed in Rudraprayag District of Uttarakhand due to Torrential Rainfall during June 2013. *International Journal of Advanced Remote Sensing and GIS*, 5, pp.1662-1669. doi: 10.23953/cloud.ijarsg.50

Rawat, J.S., Kumar, M. and Biswas, V. 2013a. An integrated approach of remote sensing and GIS for land use/cover change detection: a case study of Bhimtal Tourist Town (India). *Bulletin of Environmental and Scientific Research,* 2(23), pp.1-6.

Rawat, J.S., Biswas, V. and Kumar, M. 2013b. Changes in land use/cover using geospatial techniques-A case study of Ramnagar town area, district Nainital, Uttarakhand, India. *The Egyptian Journal of Remote Sensing and Space Sciences*, 16, pp.111-117.

Rawat, J.S., Manish, K. and Pathak, R.N. 2013c. Spatio temporal dynamics of Almora town Area, India. *International Journal of Advanced Remote Sensing and GIS,* 2(1), pp.425-432.

Rawat, J., Vivekananda Biswas and Manish Kumar. 2013d. Quantifying Land Use/Cover Dynamics of Nainital Town (India) Using Remote Sensing and GIS Techniques. *Asian Journal of Geoinformatics*, 13(2), pp.6-12.

Rawat, J.S., Manish Kumar and Vivekananda Biswas. 2014. Land use/cover dynamics using multi-temporal satellite imagery - A case study of Haldwani town area, district Nainital, Uttarakhand, India. *International Journal of Geomatics and Geosciences*, 4(3), pp.536-543.

CH. 2011. Census Handbook 2011.

Singh, A., Singh, S., Garga, P.K. and Khanduri, K. 2013. Land Use and Land Cover Change Detection: A Comparative Approach using Post Classification Change Matrix Function Change Detection Methodology of Allahabad City. *International Journal of Current Engineering and Technology*, 3(1), pp.142-148.

Torrens, P.M. and Alberti, M. 2000. Measuring sprawl. Working paper no. 27, Centre for Advanced Spatial Analysis, University College, London.

Ye, B. and Bai, Z. 2008. Simulating land use/cover changes of Nenjiang County based on CAMarkov model. *Computer and Computing Technologies in Agriculture*, I, pp.321-329.

Zhang, R., Tang, C., Ma, S., Yuan, H., Gao, L. and Fan, W. 2011. Using Markov chains to analyze changes in wetland trends in arid Yinchuan Plain, China. *Mathematical and Computer Modelling*, 54(3), pp.924-930.

Zubair, A.O. 2006. Change detection in land use and land cover using Remote Sensing data and GIS, A case study of Ilorin and its environs in Kwara State. M.Sc. Thesis, Department of Geography, University of Ibadan.

Cloud Publications
International Journal of Advanced Remote Sensing and GIS
2017, Volume 6, Issue 1, pp. 2234-2245
ISSN 2320 – 0243, Crossref: 10.23953/cloud.ijarsg.283

Case Study

Monitoring Urbanization and Comparison with City Master Plans using Remote Sensing and GIS: A Case Study of Lahore District, Pakistan

Faisal Nadeem

PUCIT, University of the Punjab, Lahore, Pakistan

Publication Date: 24 July 2017

DOI: https://doi.org/10.23953/cloud.ijarsg.283

Abstract Urbanization Growth, one of the core issue in the developing countries, has negative impacts on the cities. The rapid urbanization has become a common phenomenon for developing countries across the globe. This, according to popular notions especially among economists, is a good sign because rapid urbanization indicates economic development. According to the UN-Habitat, half of humanity now lives cities, and that the urban population will increase to 60% within next two decades. For developing countries, experiencing rapid urbanization, the inability of the existing social infrastructure to meet the growing needs emanating from urbanization, pose a major challenge for governments, with Pakistan as no exception. Lahore as the capital of Punjab Province and as the 2nd largest city of Pakistan is the largest growth pole and undergone rapid urbanization, infrastructure and social transformation. In this study detect the changes of urban sprawl and urban growth in Lahore district. Urban growth starts from a small point and after that it spreads in different directions. The growth pattern varies from one urban place to another and it is necessary to study such phenomenon for appropriate urban planning. Urban growth can be mapped, measured and modeled by using remote sensing data and GIS techniques along with several statistical measures. The outcome of this study gives a difference between the proposed land use in the master plan and existing land use. To overcome this rapid urbanization, need a detailed strategic development planning and effective master planning. For this purpose, master plan prepare and then implemented to achieve better results like economic development, utilities services and to make a better cities for living.
Keywords *GIS; urbanization; land use; urban planning; remote sensing; master plan*

1. Introduction

Urban growth defined as the process of increasing density of population within a town or city. Urban growth continues to create unhealthy and dehumanizing environments (air pollution, stress, isolation, lack of community, etc.). The growth pattern varies from one urban place to another and it is necessary to study such phenomenon for appropriate urban planning. Urbanization has undergone dramatic changes in most of the developing countries as a result of unplanned and irregular urban growth which needs to be analyzed and understood for future planning purpose. Such unplanned growth has been facilitated by rapid development in communication and new economic opportunities mostly found in the surrounding regions of an urban Center. This kind of growth later on takes different patterns in different directions and shapes. Especially, Pakistan belongs to under developed countries. So, major cities of Pakistan have been growing with high growth rate from last three decades because

mostly population migrated to cities for better living, lifestyle and employment opportunities. After migration, they were settled permanent in the cities. Lahore becomes the 2nd metropolitan city in Pakistan and 27th largest city in the world (demographia). Agriculture land very rapidly changes into urban land due to high growth of population. Spatial Patterns of Urban Development and Growth are two in which one is Lateral Growth Pattern and other Vertical Growth Pattern. In lateral growth pattern, land has available for conversion to urban land while Vertical Growth has lack of land available for conversion to urban land, City grows upward, high population density for example Hong Kong, Tokyo etc. In this study mapped and measured urbanization and urban growth by using remote sensing and GIS techniques along with several statistical techniques. In this research study, Satellite Images of Landsat TM and ETM were tacking at different time (2001, 2006, 2011 and 2016) for temporal analysis. These imageries were supervised classified to monitoring the urban extent in different directions. A measure of pattern which follow by urban growth. The results have shown that the city and it's surrounded has high degree-of-freedom, extended growth and urban growth follow the lateral growth pattern. The area of Lahore city has very high population growth rate and urban growth was increased 32% in last 16 years from 2001.

2. Area of Study

The Lahore is the second largest metropolitan city of Pakistan and capital city of the province of Punjab. It is located 31°32′59″ N, 74°20′37″ E (WGS) and Lahore district covered area 1,772 km^2. Lahore has an economic, political, transportation, entertainment, and educational center of Pakistan. Economically Lahore city with an estimated total nominal GDP of $58.14 billion (Lahore fact sheet). It is situated at a height of 208-217 m above the mean sea level, near the river Ravi. This study was consisting on Lahore District.

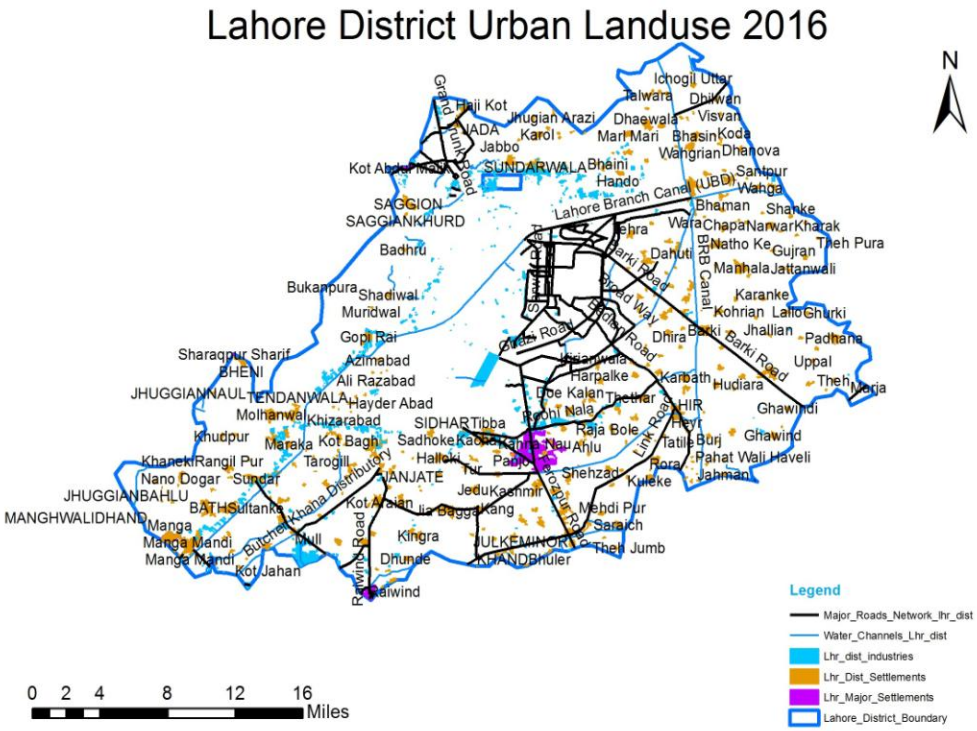

Figure 1: *Area of Study*

3. Process and Methods of Remote Sensing Data

First of all, there is so many techniques for land use detection in GIS like some of the major techniques include unsupervised classification, supervised classification, combination of classified images, and radar images comparison etc. When detecting a land use about an area then clearly know the technique which is used. In this research, the supervised classification technique was used. Remote sensing data source was satellite images. Which were tacking at four different time for spatial temporal Analysis of urbanization. Satellite images were download from USGS Glovis as following time as given in the Table 1. Different layers of Satellite Image bands (1, 2, 3, 4, 5, and 7) were stacking using ERDAS IMAGINE software. Boundary of Lahore District was clipped by using clip tool on stacked images. After clipping the stacked images then have to make the classification. Classification techniques can be broadly divided into two types: supervised classification and other is unsupervised classification. In supervised classification, Spatial Analyst has already known about the class ground reality While in Unsupervised classification, Spatial Analyst has not known about any class ground reality. Used the supervised classification in this study. The Maximum Likelihood Classification tool is the main classification method. A signature file, which identifies the classes and their statistics, is a required input to this tool. For supervised classification, the signature file is created using training samples through the Image Classification toolbar.

After the supervised classification, apply NDVI (Normalized difference vegetation index) which is a simple graphical indicator that can be used to analyze remote sensing measurements, typically observed contains live green vegetation or not in the image. The NDVI is calculated from these measurements. NDVI = (NIR-VIS) / (NIR+VIS), Where VIS and NIR stand for the spectral reflectance measurements acquired in the visible (red) and near-infrared regions.

Table 1: *Data Time Period*

Sr. No.	Data Type	Date	Scale
1	Landsat Image	2001-09-30	30 m TM
2	Landsat Image	2006-09-05	30 m TM
3	Landsat Image	2011-06-09	30 m TM
4	Landsat Image	2016-11-05	30 m TM

4. Spatial Urban Growth Pattern of the City

Table 2: *Spatial Growth Change in Landuse of Lahore City*

Year	Urban Area (hectare)	Agriculture Area(hectare)	Other Land use(hectare)	Change in Urban Area	Variation
2001	54490	83674	92506	23.23%	-
2006	70780	78145	81745	30.69%	07.46%
2011	89107	54490	87073	38.63%	15.04%
2016	108006	33619	89045	46.82%	23.60%

Urban Growth of Lahore city commenced from 2001, total area of urban city being just 54490 hectare which is 23.23% of the total area (230670 hectare). Due to rapidly increase in urban growth, urban area covered 70780 hector and 30.69% of the total area in 2006. Similarly in 2011, the urban area covered 89107 hectare which is 38.63%. While now in 2016, the urban area covered 108006 hector and 46.82%. In 16 years, total change in the urban land was increased up to 23.6%. It is a very large change in the urban built up land. These spatial urban growth measured by using satellite images and GIS techniques and tools which is describing in Table 2.

From Figure 2(a) and 2(b), Lahore district in 2016 shows different land use (urban land, water channels, open land and vegetation/ agriculture land). Land use classification planning has different phases

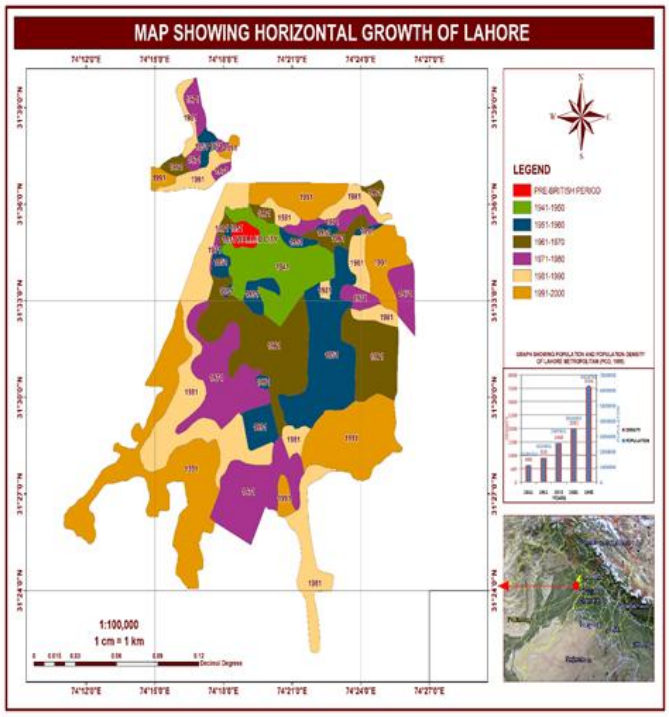

Figure 2(a): *Lateral urban growth map of Lahore from Pre-British to 2000*

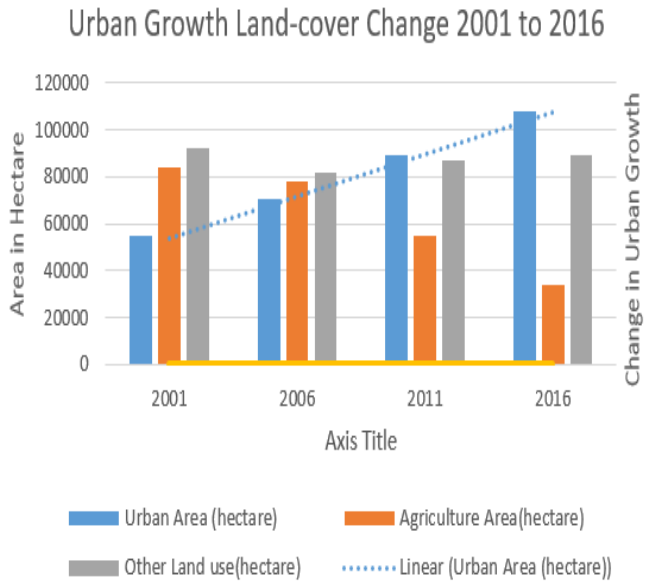

Figure 2(b): *Land cover change 2001 to 2016*

5. Urban Growth and Land Cover Maps of the City Comparison with the Master Plan

Urban Growth and land cover change can be detection with the help of different Classified raster Land use maps given below. Master Plan provides the guidelines for the future expansion of the city with recommendations in all sectors of Urban Planning i.e. land Development, housing, transportation, community facilities, public utilities, infrastructure, environment and institutional framework. Lahore Development Authority (LDA) is responsible for preparation and approval of Master plan of Lahore.

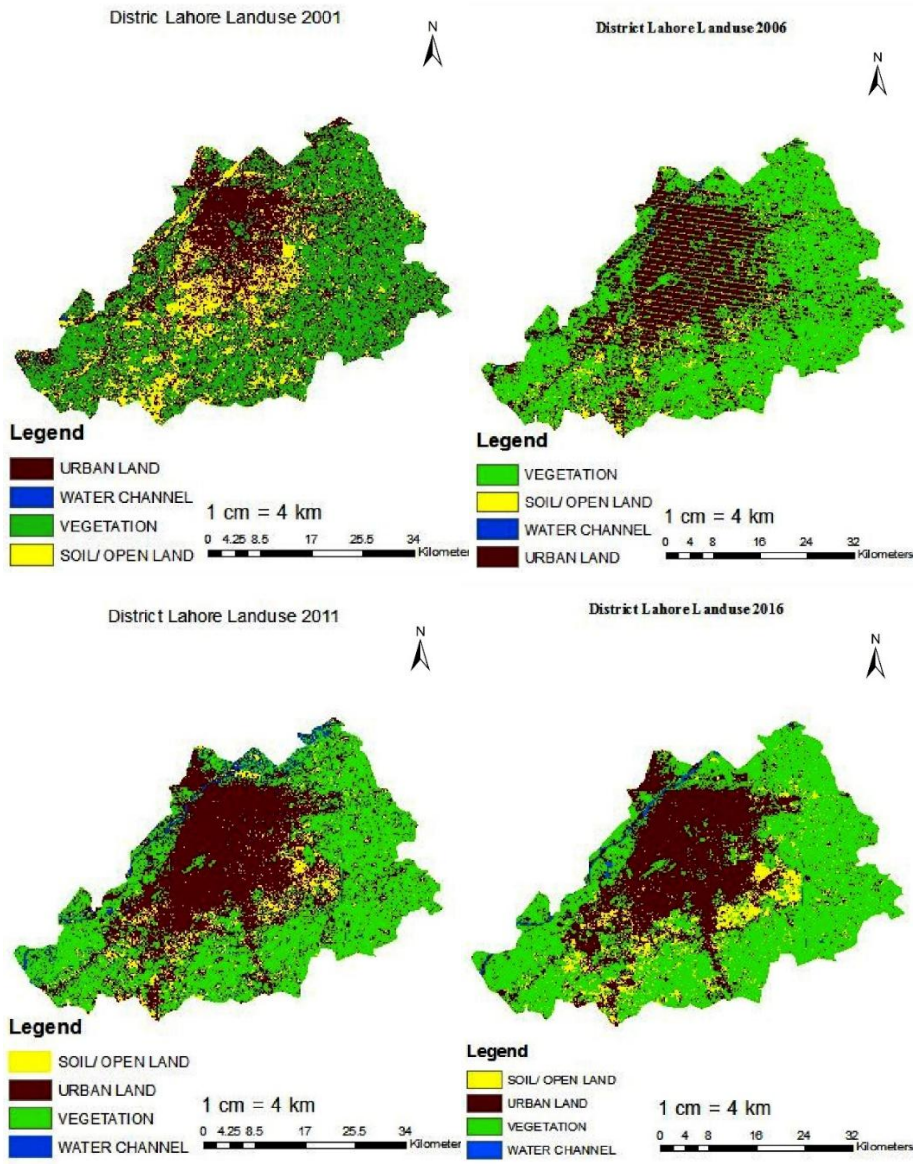

Figure 3: *Classified maps shows land use of different classes from 2001, 2006, 2011 and 2016*

5.1. First Master plan prepare with the name of "Greater Lahore-1966". It was Prepared under 2nd five year National Plan (1960-65) by Housing and Physical Planning (H&PP) Department, Govt. of Punjab. Adopted by the LMC under Municipal Administration Ordinance-1960 and notified on 13 July 1972. According to Planning Concept, 24 km Green belt was proposed around the core Urban Area, Three

Industrial Sites were proposed. Along the Green Belt, Circular Railway Line was proposed connecting all three proposed Industrial Sites. Expansion was proposed in North, South-West and South-Eastern parts of the cities.

5.2. Second Master plan was "LAHORE URBAN DEVELOPMENT AND TRAFFIC STUDY 1980". Integrated Urban Development & Transport Infrastructure Plan up to 2000 was prepared by Halcrow Fox UK, a World Bank Consultant. Future growth was planned in the South and Southwest axis, with adequate Transport Infrastructure. Structure Plan Roads were proposed.

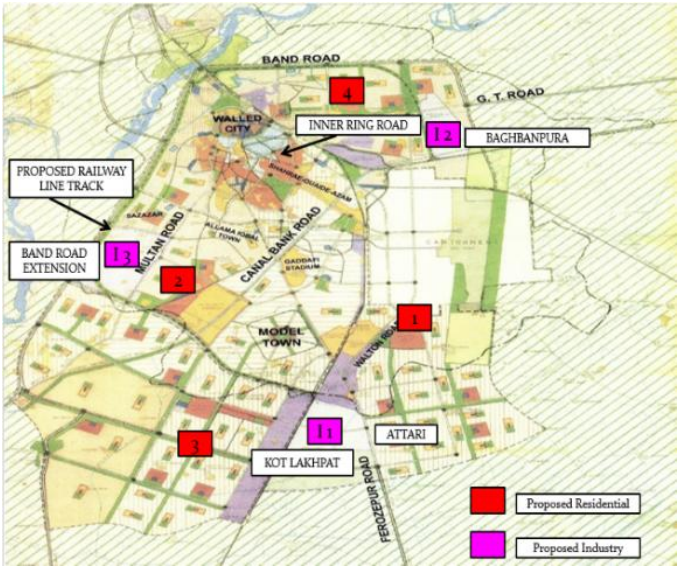

Figure 4: *Master Plan for Greater Lahore-1966*

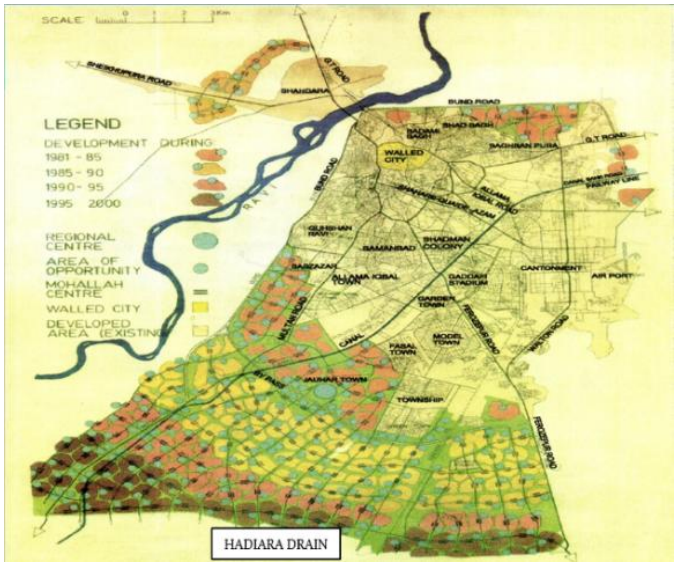

Figure 5: *Lahore Urban Development and Traffic Study 1980*

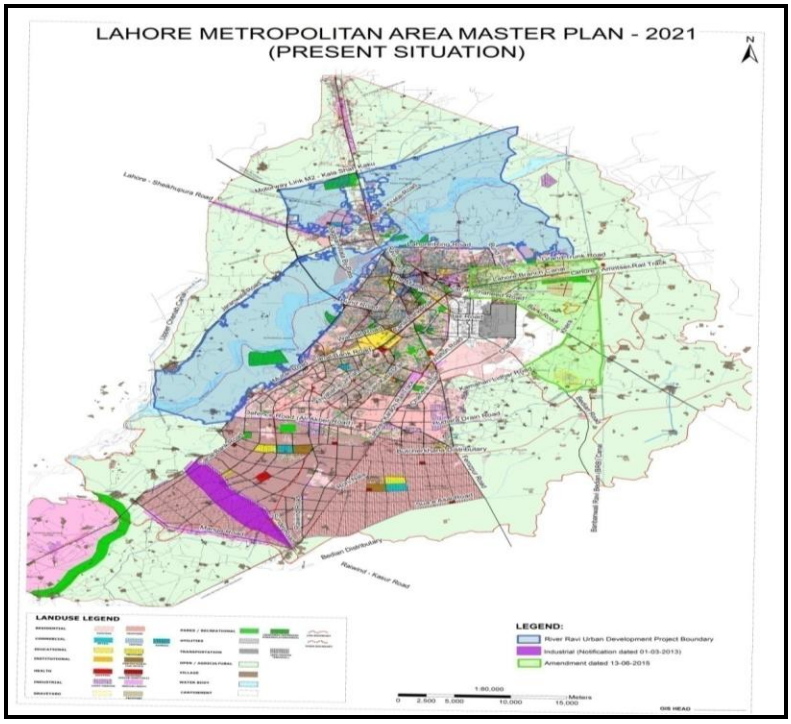

(a)

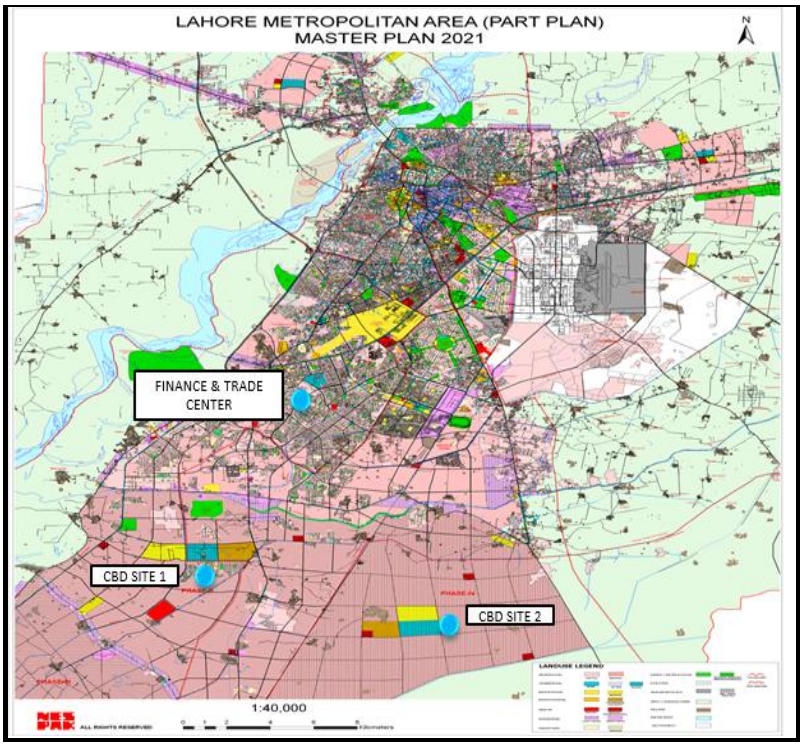

(b)

Figure 6(a) and (b): *IMPL-2021 shows present situation (b) IMPL-2021 shows different Land use*

5.3. Third Master Plan was "INTEGRATED MASTER PLAN OF LAHORE – 2021". The study was conducted by NESPAK and approved by District Assembly, CDGL in Oct 2004. This Master Plan designate different land uses and provide guideline for expansion of Lahore City up to year 2021.Urban Planning proposal were Expansion of Residential area in South West of Hadiara drain as Phase-II, Phase-III, Phase-IV, Establishment of Chunian Industrial Estate Near Bhai Pheru along Multan Road with 1 km Buffer zone, Establishment of Environmental Protection Zone (EPZ) and Industrial area along Sundar-Raiwind Road. For Business and Commercial Activities Trade and Finance Center in Johar Town measuring about 1400 Kanal is proposed to be developed. 200 Hectors area is proposed for development of Business District towards South of Hadiara Drain on both sides of Railway Lines. Three parks have been proposed along the river side to explode the river, recreational potential and to introduce boating, fishing and water game facilities. Besides a multi propose river site development zone, river view city comprising of commercial, recreational, and residential uses has been proposed in the areas bounded by three bridges vice versa Lahore bypass bridge, Sagain Bridge and old Ravi Bridge.

6 Urbanization Analysis result Comparison with Master Plan IMPL-2021

When Urbanization Analysis Land Use results compared with Master plan IMPL-2021 a major difference found between them. From following pie charts shows existing urbanization 2016 and expected in 2021. Urban land use in 2016 is 47% of the total land use while in IMPL-2021 proposed is 31%. There are 16% increase in urban land use before five years; it was a dramatic increased change in urbanization.

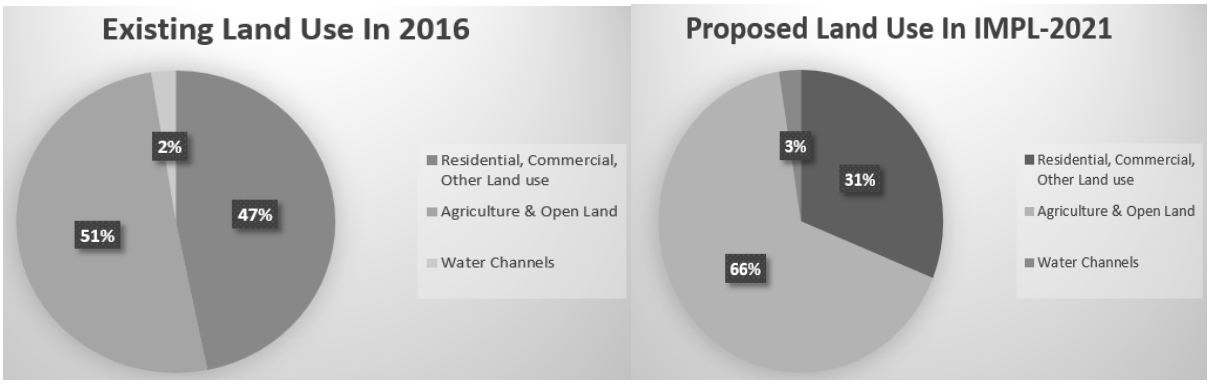

Figure 7: *Different Land Use comparison between Existing and proposed Land Use in IMPL-2021*

7. Integrated Strategic Development Plan (ISDP) - 2035, Lahore Division

Since the Integrated Master Plan 2021 for Lahore was prepared in 2004, rapid urbanization of the City of Lahore and its surrounding towns has changed its economic & socio-economic characteristics and urban form. The urban area of Lahore has expanded much beyond the limits of defunct metropolitan corporations, resulting in unregulated urban sprawl and has even expanded up to the urban areas of Sheikhupura and Kasur.

8. Planning Strategies for Lahore City

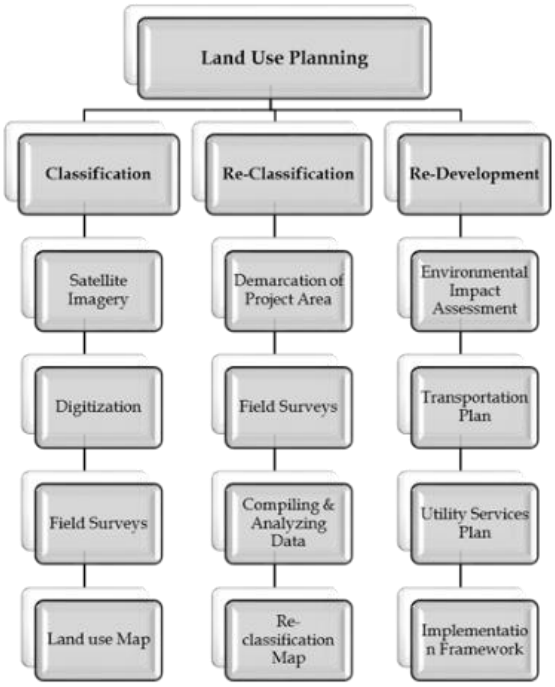

Figure 8: *Landuse Classification Planning*

The estimated population of Lahore is around nine million, whereas the population of Lahore Division is estimated to be close to 15 million, further expected to double in next twenty five years. This implies, if the current trend of unplanned and unregulated growth has to continue, another Lahore City will be required to accommodate additional population of future, with poor quality of life and services delivery. Moreover, due to reliance on outdated estimates and secondary data, the requirements of future urban Lahore cannot be worked out. Development scenario of Lahore Division has been changed since some recent years due to:

1. Rapid Urbanization Economic boom
2. Load on Infrastructure & Services
3. Environmental degradation
4. Housing Shortage
5. Inadequate public transport and Transport Management
6. Rapid Urbanization (Population growth @ 4% per annum)
7. Land Speculation
8. Illegal housing development (Katchi Abadis, Slums etc.)
9. Development in contravention of Master Plan provisions
10. Intermingle of industries with residential areas
11. Lack of utility services (Physical infrastructure, Health, Education, Water supply etc.)
12. Encroachment on roads
13. Inadequate parking facilities
14. Growing environmental degradation Un-employment
15. Lack of skilled labor
16. Inadequate vocational training centers/ institutes

17. Overlapping of functions (Authorities & Agencies)
18. Lack of coordination between government service provider departments.
19. Inadequate land-fill sites
20. High security risk
21. Governance & Implementation weakness

With all these core issues, there are need of Conventional Master Planning, Structure Planning, Outline Development Planning, Landuse Classification Planning, Strategic Development Planning and Regional Planning.

9. Recommendations

Urbanization presents one of the key challenges and, at the same time, opportunities in the new millennium. Urbanization is taking place at a rapid pace and is beyond the effective control of most government across the world. Even in jurisdictions where growth control boundaries have been implemented, such as Portland, such boundaries have been repeatedly revised to meet the demands for growth. The scale and complexity of urban problems are increasing everywhere. All cities must plan ahead to enable a sustainable future in the rapidly changing urban environment. Cities must review their strategic plans to develop better economic, social and environmental future. Those cities that fail to plan ahead and execute the pans will not be competitive in the globalized world. Urban economies are contributing significantly more too national exchequer and at the same time have become key employment markets. Cities indeed are important engines of economic growth and provide significant economies of scale in the provision of jobs, housing and services. In addition to spatial and physical expansion and lack of reliable data & studies on the existing profile of the City and Region, the Institutional set up of services delivery and Governance in Punjab and Lahore has undergone major changes during past few years, which requires carrying out of preparation of a master plan. The previous master plans and studies kept narrow focus on land use planning and lacked strategic vision and focus on economic development, environmental conditions, financial and implementation arrangements.

City boundary should be defined and control the uneven growth of urbanization. Basic facilities should be provided in surroundings of Lahore city so that migration of peoples should be minimized. While multi-stories buildings culture promote in the city. Urban sprawl has already spread to extreme lengths around the world, fortunately it can be stopped and its effects can be reversed. Doing so, however, will require cooperation from homebuyers, property developers, and government officials alike. Especially focus on the implementation of Master plan to achieve desired objectives of development and planning of the city.

10. Conclusion and Results

The study demonstrates measure and monitor urbanization in Lahore district and its environs, using remote sensing and GIS techniques. This method can be easily implemented using GIS to facilitate the measurement of urbanization for land use change detection and comparison of different Maser plans. There is a significant change (23.16%) in the last 16 years. These values indicate that there is an increase in urban sprawl and the urban growth tends to be more dispersed over a period of time. With the development of urban utility and service facilities around the city centers, urban sprawl would mainly impact on natural resources, i.e., agricultural land, water bodies, forest and fringe ecology. So the wisdom lies in how effectively the urban growth is planned and governed without hampering the natural resources and disturbing the green agro-rural setup.

The future scope of this work would look into generating the images of further sprawl under different scenarios to understand new threat to urban-agro ecosystem. This will judiciously demonstrate the application of geospatial technology in studying the dynamics of urban sprawl in Pakistani cities and elsewhere. Make Master plan for long term period and implemented for urbanization control in a better manner so that improved urban governance; Improved economic productivity & financial sustainability (through a proposed revenue collection/generation system which incorporates efficiency, transparency and accountability, and identification of buoyant sources of municipal tax revenue etc.); efficient land use planning & growth management; improved mobility & accessibility across region for work/education and recreation including focus on non-motorized transportation; improved access to basic services & public amenities including establishment of standards for municipal service delivery; improved urban environment including adaptation to the impacts of climate change and energy conservation. Similarly urban land use classes (built-up land, vegetation, water channels etc.) separately management with the help of Master plans.

The ISDP-2035 will make areas self-sustainable by enhancing their economic development and at the same time, providing solutions to upcoming issues. The Scope of ISDP will entail Formulation of vision, analysis of existing situation, identification of issues, Regional economic development plan, and comprehensive and regional land use plan, Strategies for all sectors like housing, transportation, and environment. Strategic short, medium and long term projects, Institutional framework, Public consultation and strongly Implementation Mechanism.

References

[1] Eiman A. Mohammed, Hanan M. Alawad, Khalid A. Elsayed Zeinelabdein and Abdelhafiz G. Ali. 2015. Urban expansion and population growth in Omdurman city, Sudan using geospatial technologies and statistical approaches. *American Journal of Earth Sciences*, 2(1), pp.1-7.

[2] Praveen Kumar Mallupattu and Jayarama Reddy Sreenivasula Reddy. 2013. Analysis of Land Use/Land Cover Changes Using Remote Sensing Data and GIS at an Urban Area, Tirupati, India. *The Scientific World Journal*. doi: http://dx.doi.org/10.1155/2013/268623.

[3] Ather Ashraf, Muhammad Imran and Anam Shahbaz. 2015. Protecting Agricultural Land in Developing Countries: A Case Study from Lahore, Pakistan. *International Journal of Advanced Remote Sensing and GIS*, 4, pp.1181-1194. doi: https://doi.org/10.23953/cloud.ijarsg.106.

[4] Ashraf M. Dewan and Yasushi Yamaguchi. 2009. Using remote sensing and GIS to detect and monitor land use and land cover change in Dhaka Metropolitan of Bangladesh during 1960–2005. *Environ Monit Assess*, 150, pp.237-249. doi: 10.1007/s10661-008-0226-5.

[5] Kalyani, P. and Govindarajulu, P. 2013. A multi-scale Urban Analysis using Remote Sensing and GIS. *GeoInformatica*, 3, pp.1-11.

[6] Rizwan Hameed and Obaidullah Nadeem. 2008. Challenges of Implementing Urban Master Plans: The Lahore Experience. *International Journal of Social, Behavioral, Educational, Economic, Business and Industrial Engineering,* 2(12), pp.1297-1304.

[7] Praveen Kumar Rai, Sweta, Abhishek Mishra and Mohammad Onagh. Multi-seasonal Irs-1c Liss III Satellite Data for Change Detection Analysis and Accuracy Assessment: A Case Study. *Journal of GIS Trends*, 2, pp.13-19.

[8] Mahesh Kumar Jat, Garg, P.K. and Deepak Khare. 2008. Monitoring and Modelling of Urban Sprawl Using Remote Sensing and GIS Techniques. *International Journal of Applied Earth Observation and Geoinformation*, 10, pp.26-43.

[9] Paul, S. and Dasgupta, A. 2013. Spatio-temporal analysis to quantify urban sprawl using Geoinformatics. *International Journal of Advances in Remote Sensing and GIS*, 1(3), pp.264-278.

[10] Earth Observatory. Measuring Vegetation (NDVI & EVI). Avaliable from: https://earthobservatory.nasa.gov/Features/MeasuringVegetation/measuring_vegetation_2.php

[11] U.S. Geological Survey. USGS Global Visualization Viewer ("classic"). Avaliable from: https://glovis.usgs.gov/

[12] U.S. Geological Survey. USGS Global Visualization Viewer ("classic"): About Browse Images Avaliable from: https://glovis.usgs.gov/AboutBrowse.shtml

[13] Lahore Development Authority (LDA). 2013. Integrated Strategic Development Plan for Lahore Region 2035 (ISDP-35). Avaliable from: https://www.lda.gop.pk/images/stories/RFQ_for_ISDP_35.pdf

[14] GOP, 2014: Punjab Portal, Technical Report, Government of Punjab, Pakistan. [Online] http://www.punjab.gov.pk/, Accessed on 17 Sep. 2014.

[15] Jat, M.K., Garg, P.K. and Khare, D. 2008. Monitoring and Modelling of Urban Sprawl Using Remote Sensing and GIS Techniques. *International Journal of Applied Earth Observation and Geoinformation*, 10(1), pp.26-43.

[16] Yuan, H., Van Der Wiele, C.F. and Khorram, S. 2009. An Automated Artificial Neural Network System for Land Use/Land Cover Classification from Landsat TM Imagery. *Remote Sensing*, 1(3), 243-265.

[17] Pakistan Bureau of Statistics, Census Report 1998. Available from: http://www.pbs.gov.pk/content/demographic-indicators-1998-census

[18] Malczewski, J. GIS-Based Land-Use Suitability Analysis: A Critical Overview. Progress in Planning. 2004. 62; 3–65.

[19] Falahatkar, S., Soffianian, A.R., Khajeddin, S.J., Ziaee, H.R. and Ahmadi, N.M. Integration of Remote Sensing Data and GIS for Prediction of Land Cover Map. Geomatics and Geosciences. 2011. 1 (4) 847–864.

[20] Lunetta, R.S., Knight, J.F., Ediriwickrema, J., Lyon, J.G. and Worthy, L.D. Land-Cover Change Detection Using Multi-Temporal {MODIS} {NDVI} Data. Remote Sensing of Environment. 2006. 105 (2) 142–154.

[21] MOF, 2014: Pakistan Economic Survey 2012–13, Agriculture Division Technical report, Ministry of Finance, Islamabad, Pakistan. [online]. http://www.finance.gov.pk/survey_1213.html, Accessed on 17 Sep. 2014.

Cloud Publications
International Journal of Advanced Remote Sensing and GIS
2017, Volume 6, Issue 1, pp. 2325-2342
ISSN 2320 – 0243, Crossref: 10.23953/cloud.ijarsg.298

Research Article

A Study on Urban Flood Vulnerability in Vrishabhavathi Valley Watershed, Bengaluru, Karnataka using AHP, GIS and RS Techniques

Meena Y.R.[1], Anil K. Gupta[2]

[1]School of Engineering and Technology, Jain University, Global Campus, Jakkasandra, Rural Bengaluru, Karnataka, India - 562112
[1]Research Resource Centre (RRC), Visweswaraya Technological University, Belagavi, India- 590018
[2]Department of Civil Engineering, Dr. Ambedkar Institute of Technology, Bengaluru - 560056

Publication Date: 12 August 2017

DOI: https://doi.org/10.23953/cloud.ijarsg.298

Abstract Urban flood problems are common in urban areas. These are due to heavy rainfall, adverse topographical conditions and anthropogenic factors, lead to destruction of drainage, damage to buildings, and even loss of life and property. To control such problems, systematic urban flood studies are necessary. The present study focused on the mapping and spatial analysis of urban flood vulnerability in Vrishabhavathi valley watershed, Bengaluru using AHP, GIS and remote sensing techniques. Some of the causative factors for flooding considered are rainfall, slope, drainage density, land use, building density, road density, non-existing natural drainage and non-existing Lake. Each thematic map of these factors was converted into raster maps. Numerical weight and ranking scores were assigned to each element factor according to fundamental scale of Analytical Hierarchy Process (AHP) technique. Urban Flood Vulnerability Zone (UFVZ) map was computed using weighted overlay analysis of GIS technique and classified into five categories, viz., very low, low, moderate, high and very high flood zone classes. UFVZ map was compared with the flood prone locations exist in Bengaluru city to assess the accuracy of result. Plot of flood prone locations on flood vulnerability zone map shows that, 50% of flood prone locations found under moderate flood vulnerability zone class and comparatively very less of flood prone locations 28% found in high zone class. The result depicts the fact that, urban flood vulnerability is highly influenced by anthropogenic factors than natural factors in urban environmental study area. The predicted flood vulnerability zones are found to be good agreement with known flood prone locations data.
Keywords *AHP technique; Geographic information system; Remote sensing; Urban flood*

1. Introduction

Urban floods are caused by a localized heavy rainfall. Flood disaster is considered a major natural hazard due to its devastating effects on the affected area. Floods are increasing both in urban and rural areas due to natural and manmade causes. Heavy rainfall is one of the major natural causes. In urban areas, inadequate capacities of drains, encroachment of drain boundary, dispose of solid wastes and debris in to drains, asphalting or concreting of roads giving no scope for percolation of water, are the important causes (SUDA, 2007). Bengaluru (the study area) is one of the cities of India. The cosmopolitan nature of the city has resulted in the migration of people from other states. Buildings

and pavement area has been increased to 45.19% in 2005 from 27.30% in 1973 in Bengaluru. Author Ramachandra T.V, analysis revealed that the wetland numbers have declined from 51 in 1973 to 17 in 2007 and the number of lake water bodies reduced from 159 in 1973 to 93 in 2007. A case study of urban flood in Bengaluru reported that improper solid waste management, encroachment of drains boundary, siltation of sewers are leading to urban flood (Ramachandra et al., 2009). The recent study on urban flooding impacts on climate change says rainfall intensity is increasing in Bengaluru (Mujumdar, 2012). Rapid urbanization requires the integration of flood risk management into regular urban planning and governance (Jha et al., 2012). From the above reviews, it is required to study flood vulnerability analysis for sustainable urban flood management.

In the present paper, urban flood vulnerability of Bengaluru using GIS (Geographical Information System) and AHP (Analytical Hierarchy Process) techniques has been studied. Various factors both natural and anthropogenic that causes urban flood were selected for preparing Urban Flood Vulnerability Zone (UFVZ) map. All these factors are integrated into urban flood vulnerability maps using GIS techniques. Prioritization (Determining the relative merits of members of a set of alternatives) and ranking (putting set of alternatives in order from most to least desirable) process of selected factors are employed by AHP techniques. The AHP is a structured technique for analyzing complex decisions where multiple decision criteria involved, based on mathematics. It was developed by Thomas L. Saaty in the 1970s (Saaty, 1992). AHP has particular application in group decision making and is used around the world in a wide variety of decision situations in many fields (Forman et al., 2001).

AHP has been applied to numerous areas of the world. AHP technique has been used to obtain urban flood vulnerability and risk map in Eldoret municipality, Uasin Gishu County, Kenya and the proposed AHP approach is reliable up to 92% of accuracy level in his study (Ouma et al., 2014). AHP method in Northern Philippines, applied for the municipality of Enrile, Pinacanauan river basin to assess floodplain risk (Siddayao et al., 2014). AHP method has been applied to assess flood vulnerability in Austria, Italy and Germany (MOVE, 2011). Ramu et al., (2014) presented AHP technique to find out potential zones of ground water in Mysore taluka, Karnataka, India and result compared with the collected borewell sample data, given 95% of accuracy. AHP method to prepare landslide hazard zones of the Coonoor and Ooty, part of Kallar watershed, The Nilgiris, Tamil Nadu, India (Abdul Rahamana, et al., 2014). Siddayao et al., (2014) analyzed the various disaster criteria used in nine different research paper work (all nine studies have a reasonable Consistency Ratio less than 0.1) related to flood studies adopting AHP as the methodology for decision support system. This shows the power and versatility of AHP in multiple criteria for disaster analysis.

AHP as an multi criteria analysis approach has been used for solving various flooding problems. Author Willet used AHP to select the optimal flood control projects for the Grand River and Tar Creek in Miami, USA (Willet et al., 1991). In India, flood risk analysis using AHP and mapped by GIS has been applied to the Kosi River Basin (Sinha et al., 2008). A two-dimensional diffusive overland flow model to simulate inundation status in northern Taiwan, and further used GIS to illustrate the area and depth of inundation (Chen, et al., 2004). Based on the inundation map, they developed a model to evaluate the possible damage from floods by using grey AHP (Chen et al., 2004). The above reviews shows that AHP is mostly applied in natural environments and not in developed urban areas. The present study focuses on the mapping and spatial analysis of urban flood vulnerability in Vrishabhavathi valley watershed, Bengaluru using advanced technology of remote sensing, GIS and AHP for the planning and management of urban flood.

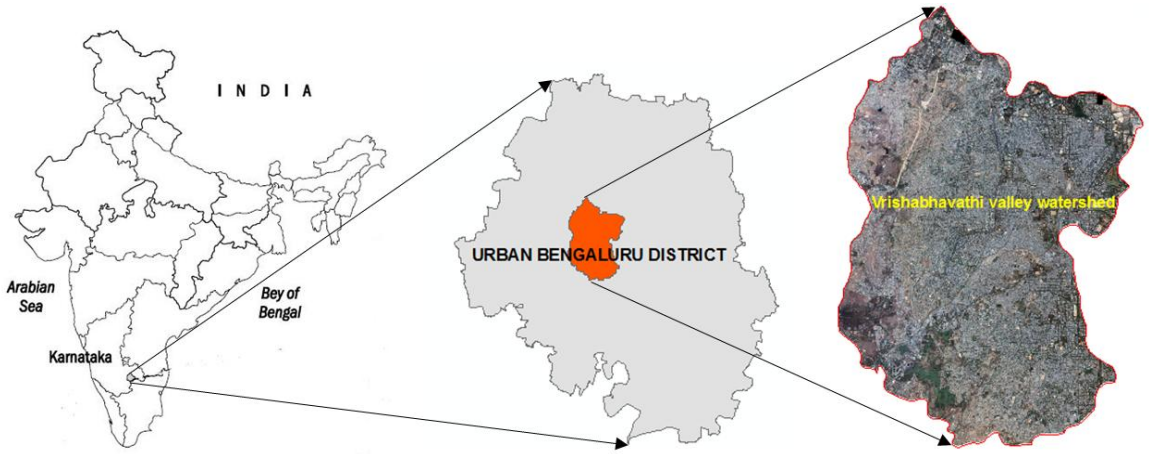

Figure 1: *Location map of the study area*

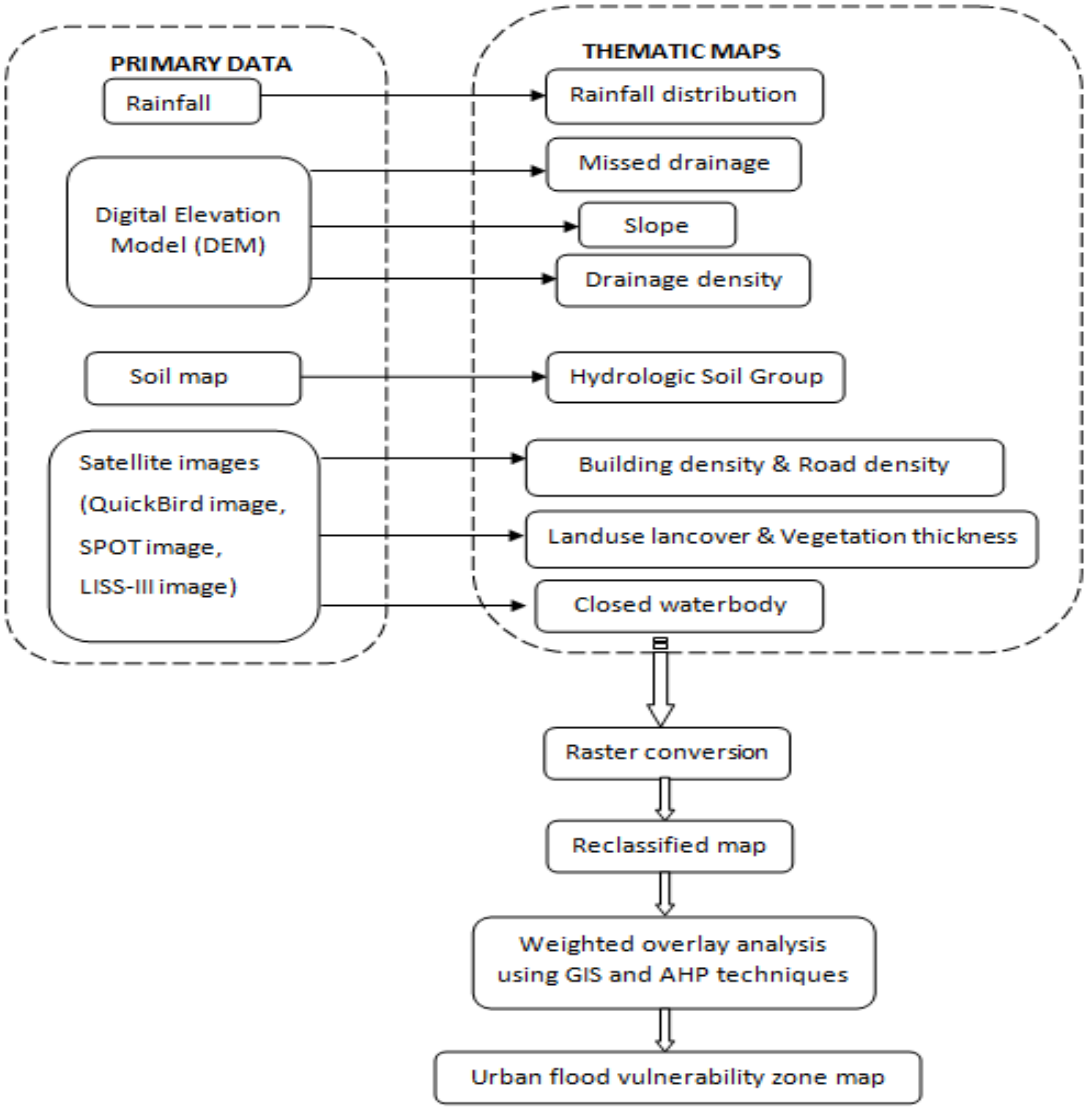

Figure 2: *Flow chart for delineating the flood vulnerability zones*

1.1. Study Area

Vrishabhavathi watershed is located in Bengaluru district and covers a surface area of 350Km^2. A part of the watershed lies in the urban area of Bengaluru city covering around 92.51Km^2. The basin stretches from west to east between longitudes 77^0 23' E to 77^0 35' E and from south to north between latitudes 12^0 45' N to 13^0 03' N (Figure 1). The study area has a semi-arid subtropical climate with mild summers and cold winters. The normal annual average rainfall is about 950mm in a period about 52 days. A major portion (i.e. about 70%) of it is during South – West monsoon period (May to August). Lithologically Vrishabhavathi watershed is characterized by the presence of xenolith and migmantites which are found in small patches. In general the area of study is characterized by red soil, the source rock being undoubtedly gneiss. Locally the soil may be lateritic, red clayey, red loamy or sandy in nature. The topography of the study area is undulating to plain. The relief of the area is 800m above the mean sea level.

2. Methodology

The study has been conducted based on the primary data which have been collected from concerned department. The study has considered eight parameters for the mapping of urban flood vulnerability zone, Vrishabhavathi valley watershed in Bengaluru. The methodology adopted for the present study is shown in Figure 2. The eight factors that have significant influence to induce occurrence of urban flood considered are rainfall, slope, drainage density, land use, building density, road density, non-existing natural drainage and non-existing Lakes.

There are 6 rain gauge stations located in the study area namely Bengaluru palace, Bengaluru city railway station, Bengaluru municipal office, Bengaluru Lalbagh, Uttarahalli and Kengeri. For each rain gauge stations maximum annual rainfall depth was calculated for different return periods based on Gumbel's rainfall distribution method. Gumbel's distribution is most commonly used for modeling storm rainfalls and maximum flows (Subramanya, 2008). This method is used to model the distribution of the maximum (or minimum) of a number of samples of various distribution. This distribution might be used to represent the distribution of the maximum level of a river in a particular year if there was a list of maximum values for the past ten years. It is useful in predicting the chance that an extreme earthquake, flood or other natural disaster occurrence. The potential applicability of the Gumbel distribution is to represent the distribution of maximal values. In hydrology the Gumbel distribution is used to analyze sample of a random variables as monthly and annual maximum values of daily rainfall and river discharge volumes and also to describe droughts (Burke et al., 2010).

The extreme annual rainfall depth for 50 years return period was calculated from 43 years daily rainfall data for each rain gauge station as shown in Table 1. It can be observed that, there is high rainfall at Bengaluru lalbagh and Bengaluru Municipal Office rain gauge station and comparatively low rainfall at Kengeri and Uttarahalli rain gauge station. The daily rainfall data of urban Bengaluru for 43yrs from 1970 to 2012 was collected from Indian Meteorological Department, Bengaluru. The annual maximum rainfall values were geo-spatially interpolated using Inverse Distance Weighted (IDW) method to obtain rainfall distribution map in Arc GIS 9.3 software. To predict a value for any unmeasured location, IDW uses the measured values surrounding the prediction location. The measured values closest to the prediction location have more influence on the predicted value than those farther away. IDW assumes that each measured point has a local influence that diminishes with distance. It gives greater weights to points closest to the prediction location and the weight diminishes as a function of distance, hence the name inverse distance weighted.

Table 1: *Maximum annual rainfall depth for various raingauge stations*

Return period (T), year	Annual Maximum Rainfall (X_T), mm					
	Bengaluru municipal	Bengaluru railway station	Bengaluru palace	Bengaluru Lalbagh	Uttaralli	Kengeri
2	83.40	81.15	76.06	79.95	73.72	73.40
5	110.40	107.52	101.09	108.55	96.70	93.08
10	128.28	124.98	117.67	127.47	111.92	106.11
25	150.86	147.04	138.61	151.39	131.15	122.58
50	167.61	163.40	154.15	169.13	145.42	134.79

Slope map of study area was developed using DEM (Digital Elevation Model) of 3m resolution in Arc GIS software. DEM raster data was collected from STUP Consultants Pvt. Ltd., Bengaluru. Drainage density is a measure of how well or how poorly a watershed is drained by stream channels. Natural drainage vector map was collected from Karnataka State Remote Sensing Application Centre (KSRSAC), Bengaluru. Drainage density map was prepared from the natural drainage map using line density tool in Arc GIS software. The land use and land cover (LU/LC) map was prepared using LISS III (Linear Image Self scanning System) scanner image data freely downloaded from Bhuvan website (Bhuvan.nrsc.gov.in) and image is the source of IRS (Indian Remote Sensing) satellite. LISS III image has 23.5m spatial resolution and image sense captured for the date 13th February 2012. LU/LC analysis was done by supervised image classification method using maximum likelihood classification algorithm. 51 training sites of ground truth data were collected to train the images using global positioning system (GPS). LULC classes were defined into 5 classes namely buildings, roads, open ground, vegetation and water body based on how these classes encourages and diminishes the overland flow. The overall classification accuracy of 91.67% was assessed by Kappa matrix method.

Urban density plays a guiding role in city planning, land management and environmental protection. Building density also called building coverage ratio, refers to the ratio of the total standing area of all the buildings to the total interest area (Xian-Zhang et al., 2006; Bratsolis et al., 2016). To get the building density distribution information, Quick Bird image of high resolution 0.6m was collected from STUP Consultants Pvt. Ltd., Bengaluru. The building density map was prepared by visual image interpretation method. Based on contribution of building density towards impact of flood, the map is grouped into very low, low, moderate, high and very high. Very High category includes more congested building plots and very small gap between buildings. High category includes an area has many dwellings on a small amount of land and planned layout area. In the moderate category, building construction rising up and open land sites are more. Low category includes detached big buildings on a larger land and relatively large distance between buildings. Very low category includes water body or vegetated land or stadium or bus terminals with isolated buildings.

The road density refers to length of road for every square kilometer of area. The poor road density is an indicator of highly unsustainable situation of a city. Drainage is one of the primary components of road. The primary purpose of a road drainage system is to remove water from the road and its surroundings and to avoid water logging problem on road. Roads in urban areas are classified into expressway, arterial road, sub-arterial road, collector road and local road as per code of IRC-69 (Indian Road Congress, 1977). For the study purpose, expressway, arterial road and sub-arterial road classes are considered. The road data was extracted from the Bangalore city development plan (CDP)

map-2021 and from toposheets of SOI (Survey of India). Natural drainages and lakes are an essential part of living in an urban area, as drainage reduces flood damage by carrying water away and lake water body acts as flood storage reservoir. Non-existing drains and lakes were extracted by overlaying the existing (2016 year) water body and natural drainage map on the old (KSRSAC-1989) water body and drainage map.

Various factors include both natural and anthropogenic factor, causes flood in urban area. The eight factors that have significant influence to induce occurrence of urban flood are selected. They are rainfall, slope, drainage density, land use, building density, road density, non-existing natural drainage and non-existing Lakes. These eight factors were used for integration to delineate Urban Flood Vulnerability Zone (UFVZ) map in study area. GIS technique was applied for generating new thematic data layer of each factor. All thematic maps were reclassified and proper weight given based on their relative importance to urban flood vulnerability as per the Satty's Analytical Hierarchy Process (AHP). The AHP process introduced by Thomas Saaty in the year 1980, which is an effective tool for dealing with complex decision making and aid the decision maker to set priorities and make the best decision. The AHP considers a set of evaluation criteria and a set of alternative options among which the best decision is to be made. The AHP generates a numerical weight or priority (relative importance) for each evaluation criterion according to the decision maker's pair wise comparisons (Comparing each other, relative importance to the goal, two at a time in the hierarchy) of the criteria. Decision makers use the AHP fundamental scale in assigning the weights. It is the essence of the AHP that, decision maker's judgment can be used in performing the evaluation (Saaty, 2008). Each subclass is analyzed independently. Numerical priorities are calculated for each of the decision alternatives. Higher the assigned weight, more important the corresponding criterion. Higher the score, better the performance of the option with respect to the considered criterion.

Table 2: *Continuous weightage scale of Satty's Analytical Hierarchy Process (AHP)*

1/9	1/8	1/7	1/6	1/5	1/4	1/3	1/2	1	2	3	4	5	6	7	8	9
Extreme		Strong		Moderate		slight		Equal		Slight		Moderate		Strong		Extreme
LEAST IMPORTANT ←																→ MORE IMPORTANT

Table 3: *Percentage of influencing factor based on Saaty's Analytical Hierarchy Process (AHP)*

Influencing factor	value	Saaty's scale (in Fraction)	Saaty's scale (in Decimal)	% Influence = (Satty's scale/sum)*100	Relative influence value
Rainfall	High	1	1	36.76	37
Slope	↓	1/2	0.50	18.38	19
Drainage density		1/3	0.33	12.13	12
Landuse		1/4	0.25	9.19	9
Building density		1/5	0.20	7.35	7
Road density		1/6	0.17	6.25	6
Non-existing natural drainage		1/7	0.14	5.15	5
Non-existing lakes	Low	1/8	0.13	4.78	5
			Sum = 2.72		

By integrating different thematic maps in GIS software's weighted overlay analysis tool, the Urban Flood Vulnerability Zone (UFVZ) map was prepared and classified. The results in Table 2 shows the procedure of assigning weightage for each factor based on the relative importance of it in contributing flood. The value 9 in the table shows highest important while 1/9 shows the least important and 1 shows the equal weight of a factor. Based on these weightage criteria, each factor in the study has been classified and Table 3 shows the weightage assigned for eight factors for the study. Weightage for the subclass of each factor has been determined as mentioned in Table 4.

Table 4: *Assigned weight according to Satty's Analytical Hierarchical Process (AHP)*

Influencing factor	Class interval	Urban flood vulnerability level	Satty's scale (in Fraction)	Satty's scale (in Decimal)	% Influence = (Satty's scale/sum) *100	Relative influence value
Rainfall, mm	140-146	Very low	1/9	0.11	6.18	6
	146-152	Low	1/7	0.14	7.87	8
	152-158	Moderate	1/5	0.20	11.24	11
	158-164	High	1/3	0.33	18.54	19
	164-170	Very high	1	1	56.18	56
				Sum=1.78		
Slope,%	0-1	Very High	1	1	45.45	45
	1-3	High	1/2	0.50	22.73	24
	3-5	Moderate	1/5	0.20	9.09	9
	5-10	Low	1/7	0.14	6.36	6
	10-15	Low	1/7	0.14	6.36	6
	15-30	Very low	1/9	0.11	5.00	5
	Above 30	Very low	1/9	0.11	5.00	5
				Sum=2.20		
Drainage density, Km^{-1}	0-0.25	Very High	1	1	56.18	56
	0.25-0.50	High	1/3	0.33	18.54	19
	0.50-0.75	Moderate	1/5	0.20	11.24	11
	0.75-1.00	Low	1/7	0.14	7.87	8
	1.00-1.27	Very low	1/9	0.11	6.18	6
				Sum=1.78		
Landuse	Buildings	Very High	1	1	56.18	56
	Roads	High	1/3	0.33	18.54	19
	Open ground	Moderate	1/5	0.20	11.24	11
	Vegetation	Low	1/7	0.14	7.87	8
	Water body	Very low	1/9	0.11	6.18	6
				Sum=1.78		
Building density	Congested building	Very High	1	1	56.18	56
	Small gap between buildings	High	1/3	0.33	18.54	19
	Well planned area	Moderate	1/5	0.20	11.24	11

	Industrial area	Low	1/7	0.14	7.87	8
	Detached buildings	Very low	1/9	0.11	6.18	6
				Sum=1.78		
Road density, Km^{-1}	0-1.41	High	1	1	65.36	65
	1.41-2.82	Moderate	1/3	0.33	21.57	22
	2.82-4.23	Low	1/5	0.20	13.07	13
				Sum=1.53		
Non-existing drainages, Km^{-1}	0-0.1	Low	1/3	0.33	24.81	25
	0.1-0.69	High	1	1	75.19	75
				Sum=1.33		
Non-existing lakes	Non-existing lake catchment	High	1	1	75.19	75
	existing lake catchments	low	1/3	0.33	24.81	25
				Sum=1.33		

Table 5: *Flood vulnerability zone wise distribution of flood prone locations*

Flood hazard zones	Area coverage, Sq. Km	Area , %	No. of flood prone locations
Very low (Zone-1)	6.48	7	2
Low (Zone-2)	19.43	21	2
Moderate (Zone-3)	38.85	42	14
High (Zone-4)	24.05	26	8
Very high (Zone-5)	3.7	4	2
	∑92.51	∑100	∑28

3. Results and Discussion

As mentioned in the methodology the selected eight factors of thematic maps have been generated using GIS techniques and integrated by weighted overlay analysis to produce Urban Flood Vulnerability Zone (UFVZ) map of study area. The detailed discussion of each factor is shown below.

3.1. Rainfall

Heavy rainfall is one of the major causes of urban flood. The amount of runoff is related to the amount of rain a region experiences. For study area the maximum annual rainfall for 43 years was calculated using Gumbel's distribution for 6 rain gauge stations. The calculated maximum annual rainfall values were then spatially interpolated using Inverse Distance Weighted (IDW) method to obtain rainfall distribution map as shown in Figure 3. Major study area of 67% receives heavy rainfall of about 158 to 169mm. The coverage area experienced heavy rainfall is at South East Basavanagudi region, Vijaynagar, Laggere, Yashwantpur region at North of the study area.

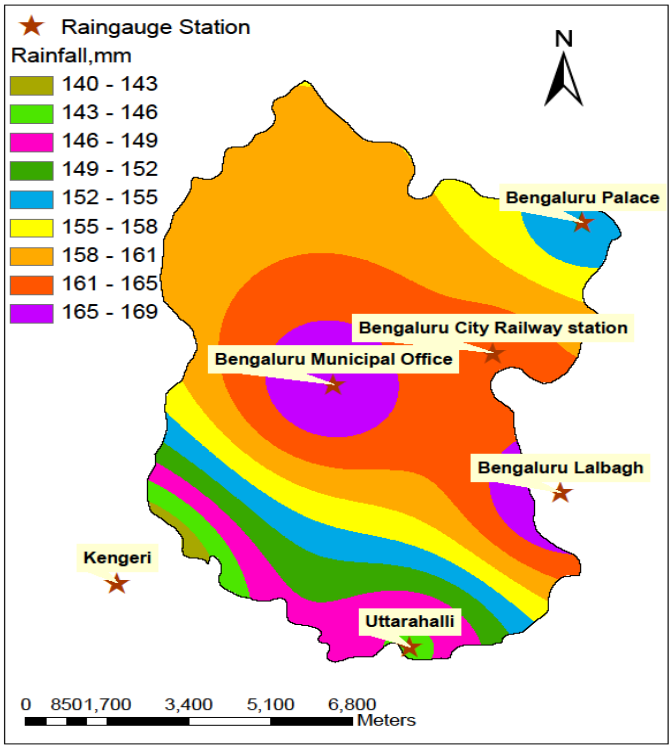

Figure 3: *Rainfall distribution map of study area*

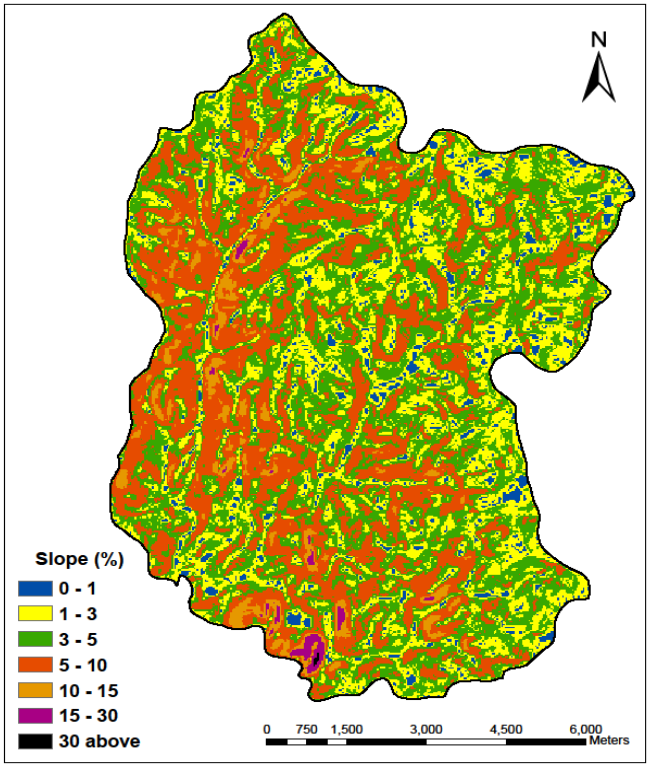

Figure 4: *Slope map of study area*

3.2. Slope

Slope plays an important role in controlling the surface runoff reaching a particular place. Steep slope generates more velocity than smaller slopes and hence can dispose the runoff faster. For flat to gentle slope, runoff gets stored over an area and disposes out gradually over a time. Therefore low gradient slopes at lower reaches are highly vulnerable to flood occurrence compared to high gradient slopes. Steeper slopes shed out the surface runoff faster while flat terrains are susceptible to water logging. Figure 4 shows the slope map of study area. In Vrishabhavathi valley watershed, area coverage on both side of the drainages found to be 5-15% steep slope and very little area less than 1% of study area is occupied by very high steep slope above 15%. Flat to gentle slope 0-5% can be seen in upland and upstream of valleys covers 64% of study area and is more susceptible to water logging.

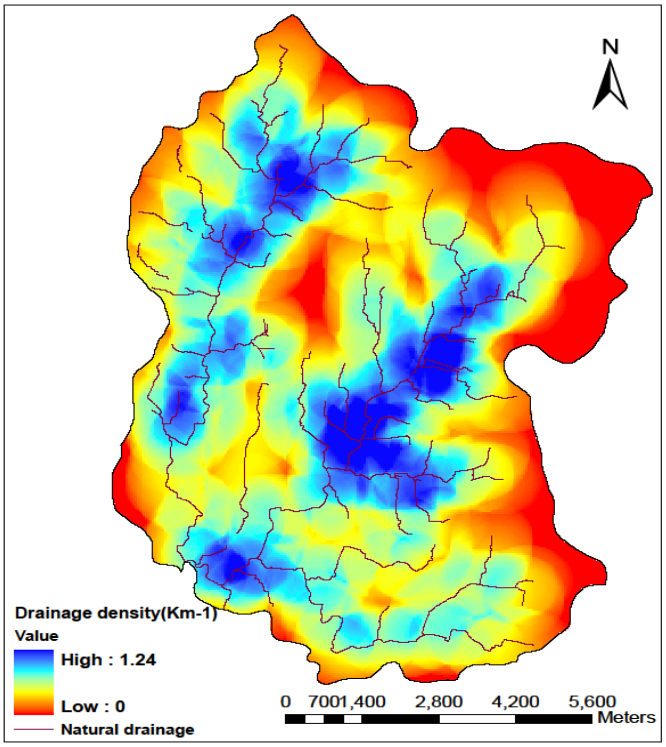

Figure 5: *Drainage density map of study area*

3.3. Drainage Density

Drainage density is the ratio between the total length of the channel in a drainage basin and the area drained by them. The effect of drainage density on runoff volume is associated with the time during which the runoff remains in the watershed. Low drainage density allows for long residence time, therefore, obstruction mechanisms have more time to discharge out the water from a watershed. The drainage density map of study area is shown in Figure 5. The maximum value of drainage density found in the study area is 1.24 Km/Km^2.

3.4. Land Use Land Cover

The land use and land cover (LU/LC) of an area is also one of the primary concerns in flood hazard mapping. Land use types like buildings, road decreases the water penetration capacity of the soil. The

existing land use classes of the area were reclassified into five groups in order of their capacity to decrease the rate of flooding. The major land use types in the study area are buildings, roads, open ground, vegetation and water body. The land use land cover map of study area is shown in Figure 6. Buildings area alone comprises around 53% of study area. There is significant less percentage coverage of vegetation (12%) and water body (3%).

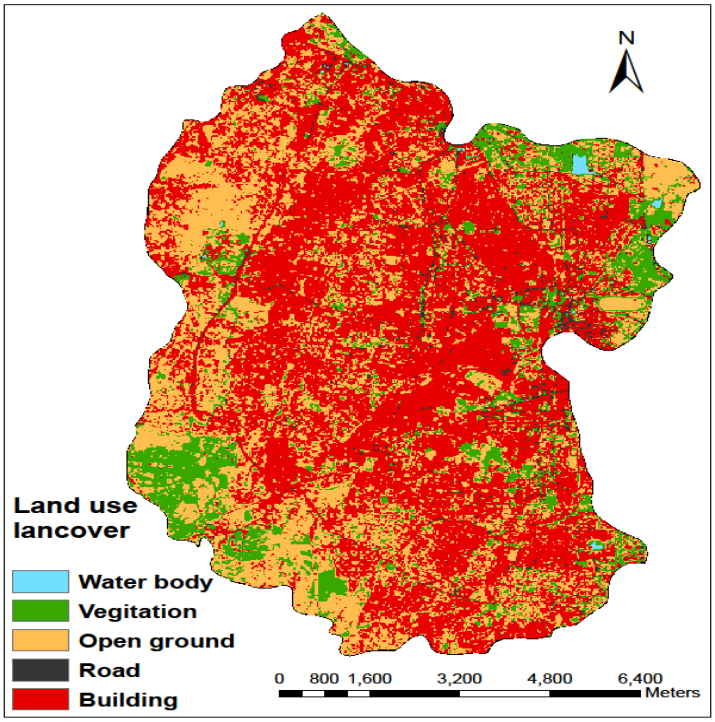

Figure 6: *Land use and land cover map of study area*

3.5. Building Density

Urban building density is an important indicator for quality assessment in aspects of urban design, planning, land management and environmental protection. Measuring urban form and compactness of cities becomes more important for understanding the spatial urban structure to intervene accordingly for sustainable urban development (Kotharkar et al., 2014). Cities are extremely complex ecosystems. Physical assets such as offices, hospitals, schools and transit systems are often concentrated in small spaces and interact with large and diverse populations including commuters, tourists and residents. This density can intensify the impact of storm floods, disease outbreaks and other events. Many a time urban floods are result of not a natural calamity, it's due to an anthropogenic activities (Mukherjee, 2016). Impervious cement cover (buildings) is not capable to soak up water. This excess water is directed to nearby streams which then overflow due to the excess amount of water. The building density map was prepared by visual image interpretation method. Based on contribution of building density towards impact of flood, the map is grouped into very low, low, moderate, high and very high as shown in Figure 7. Very high class zone can be seen in the old and early developed area surrounding very close to the city centre. High class zone category area spread little far from the city centre and just after the very high category area. Moderate class zone category can be found more in outskirt of city. Low class zone category includes detached big buildings on a larger land and relatively large distance between buildings. More of very low category is found in remote area from the city centre.

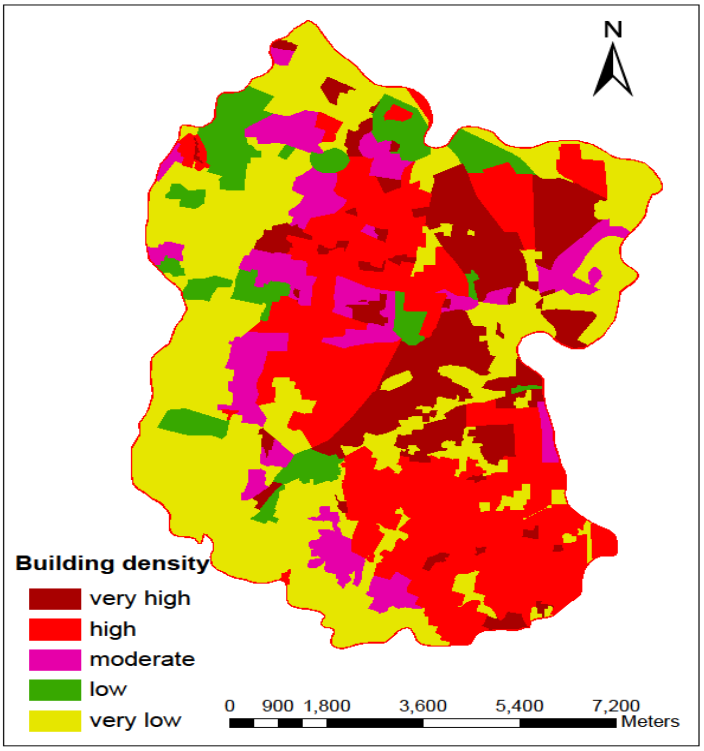

Figure 7: *Building density map of study area*

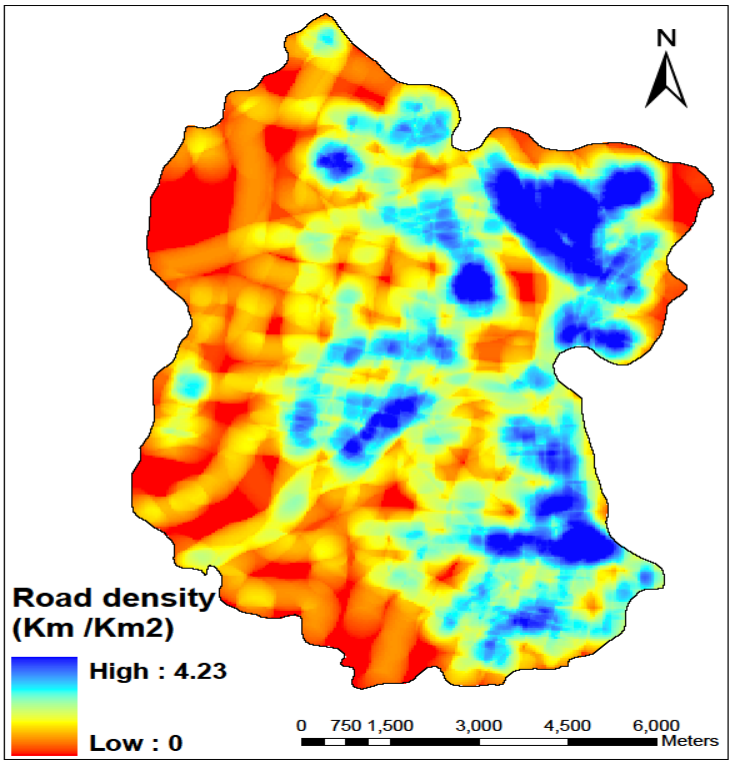

Figure 8: *Road density map of study area*

3.6. Road Density

Road density is the ratio of total road length to the total land area. The impact of road density is important in several aspects. Unplanned road construction decays the physical setup of a city. High road density usually dewater the surroundings but caused waterlogged problem due to heavy pressure small and giant size vehicles on road and leads traffic congestion (Roy et al., 2016). The urban road classes for the study, ring road, primary urban road, major and minor urban road are accounted as arterial and sub-arterial roads according to land use zoning classification map of Bangalore.

Arterial and sub-arterial roads such as ring road, primary urban road, major and minor urban road of urban Bengaluru (study area) were accounted as road vector data input for producing road density map of the study area. The urban road density map is shown in Figure 8. The maximum road density of study area is 4.23km/km^2.

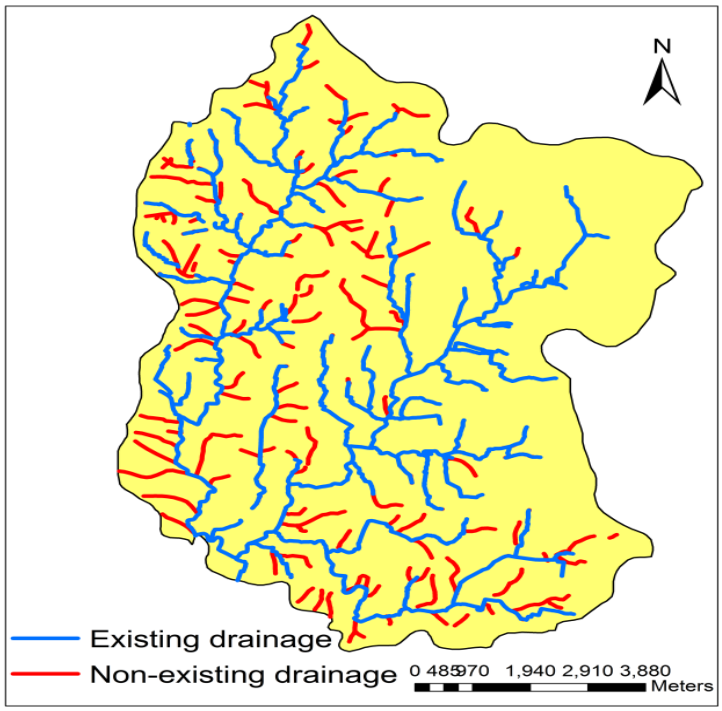

Figure 9: *Non-existing natural drainage map of study area*

3.7. Non-existing Natural Drainage

The importance of natural drainage systems cannot be overemphasized. Natural storm water drainages encroached, filled up, diverted are caused obstruction to the smooth flow of water creating severe water logging in the Dhaka city, Bangladesh every year during monsoon (Mowla et al., 2013). Non-existing natural drainage map of study area is shown in Figure 9. Non-existing drainage density map was generated and the maximum non-existing drainage density value found is 0.69. The map was reclassified into two groups. Non-existing drainage area as one group and remained area as another group. A considerable amount of 33% of study area is under the group of non-existing drainage area. Few tributaries of complete drainage way length and some tributaries of starting upstream drainage way have not been existed in the study area. New built up area was found when verified with field visit and Google earth images.

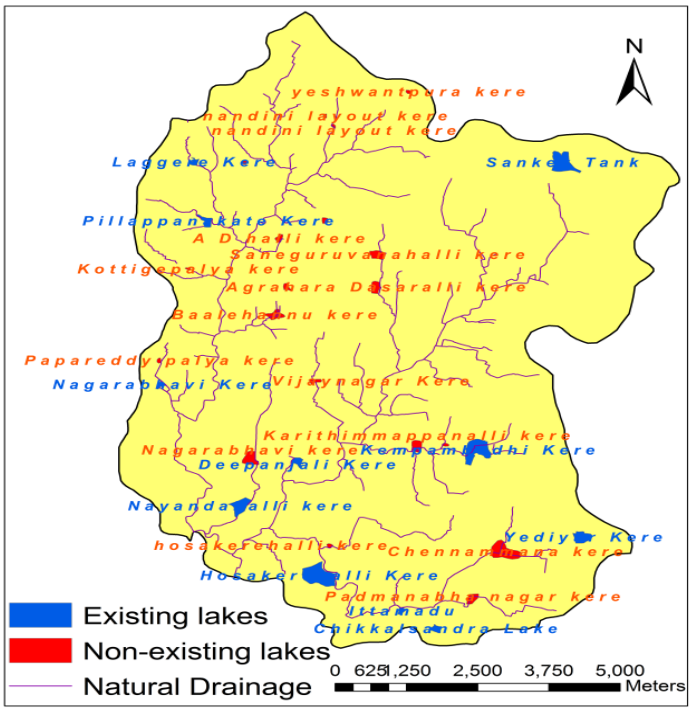

Figure 10: *Non-existing lake water body map of study area*

3.8. Non-existing Lakes

A lake water body serves as natural drainage system and prevents flooding. In Chennai city, on 12th September 2013, areas around the tanks were not waterlogged. Many roads with lack of storm water drain, where water bodies had facilitated runoff. Many areas escaped from inundation in Chennai city due to their proximity to water bodies. In many layouts in the suburbs (Chennai city) where storm water drains were accorded the least priority, water bodies served the purpose (Lopez, 2016). Non-existing lakes water body map of study area is shown in Figure 10. Present study reveals that, Vrishabhavathi valley study area had 30 lakes in the year 1989 and now in the year 2017, 11 lakes are alive but most of the alive lakes are sewage fed and eutrophicated. Lakes being vanished due to encroachments and closed lakes have been converted to park/play ground/stadium/community space.

3.9. Mapping of Urban Flood Vulnerability Zone (UFVZ)

Flood vulnerability is the process of determining the degree of susceptibility of a given place for flooding. The flood vulnerability zones for the study area were generated through the integration of various thematic maps viz. rainfall, slope, drainage density, land use, building density, road density, non-existing natural drainage and non-existing Lakes using weighted overlay analysis. The “Weighted Overlay” is a tool built inside ArcGIS software and this tool has been used to perform an overlay analysis. The weighted overlay tool overlays several raster using a common measurement scale and weights each according to its important. The result of overlay analysis has been classified into five class zones as very low, low, moderate, high and very high zones as shown in Figure 11. From the resultant urban flood vulnerability zone map, it has been showed that, 6.48Km^2 area is having very low, 19.43 Km^2 area is having low, 38.85 Km^2 area is having moderate, 24.05 Km^2 area is having high and 3.7 Km^2 area is having very high flood vulnerability zone. The study depicts that 42% of vast area comes under moderate flood vulnerability zone.

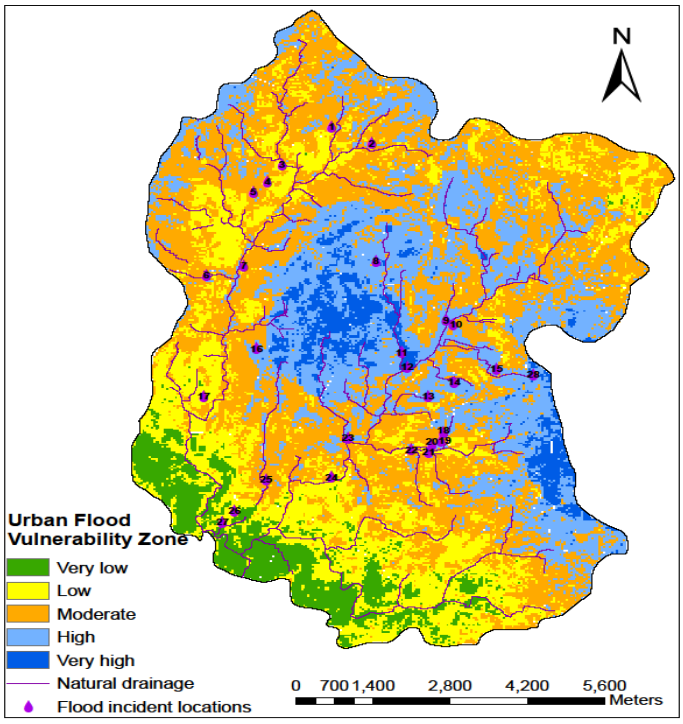

Figure 11: *Urban flood vulnerability zone map of study area with flood prone locations*

Flood vulnerability zone map was compared with the flood prone locations found in Bengaluru city to assess the accuracy of result. Flood prone locations in Vrishabhavathi Valley watershed study area were surveyed by author and identified based on local information, news of flooding in newspapers and other available literature that recorded the past events of flood prone areas. Besides this information, BBMP (Bruhat Bengaluru Mahanagara Palike) the Bengaluru municipal city corporation as well identified, documented and reported the flood prone locations found in Bengaluru city from reconnaissance survey based on history of flood, the severity of inundation and the time of inundation during 2011 (BBMP, 2011). Totally 28 number of flood prone locations have been found in the Vrishabhavathi Valley watershed study area Figure 11. These flood prone locations were numbered and overlaid on the flood vulnerability zones map. The percentage covering area of each flood zone classes are shown in Table 5 along with number of known flood prone locations fall on each zone. The resulted UFVZ shows 50% of flood prone location numbers i.e. 14 out of 28, lies within the moderate flood vulnerability zone class. This implies that anthropogenic factors (land use, building density, road density, non-existing drainages and non-existing lakes) have much influence to flood vulnerability in the urban study area rather than natural factors (rainfall, slope and drainage density) even though more weightage assigned to natural factors (Table 3) because of flood is a natural disaster. Study depicts that anthropogenic factors are more influenced to a flood disaster in urban environment. Supporting the result, in small area five flood prone locations numbered 18, 19, 20, 21 and 22 is found very closely (Figure 11) and flood events being reoccurred every monsoon, majorly due to the two lakes closed (Karithimmappanahalli lake converted to park and Azad Nagar lake using as automobile stand) in that area (Figure 11). Similarly flood prone locations numbered 1, 8 and 25 is found very proximity to the two closed lakes in nandini layout area; saneguruvanahalli closed lake and Nagarbhavi closed lake respectively. Flood prone locations numbered 28b (Bhakshi Garden-Cottonpete) and 15 (Nagamma Nagara near Minerava Mill) lies on very high building density class zone and low road density class zone and that locations are the slum area where very narrowed and

haphazard road network with no proper storm water drains. Flood prone locations numbered 14 (Jagajeevan Ramanagara) and 13 (Goripalya-Guddadahalli) found at very high building density class zone area. Flood prone locations numbered 4, 5 (Laggere) and 16 (Moodalapalya) lies upon non-existing drainage area. Flood prone locations numbered 26 and 27 even though lies under very low building density class zone, blockage of road side chamber inlet due to silt and solid waste causes flood events. 68% (19 no.) of flood prone locations found along Vrishabhavathi valleys and closed to drainage.

4. Conclusions

Delineating the Urban Flood Vulnerability Zone (UFVZ) in Vrishabhavathi valley watershed of Urban Bengaluru using AHP, GIS and remote sensing techniques can aids in quick decision-making for sustainable urban flood management. Each thematic maps namely rainfall, slope, drainage density, land use, building density, road density, non-existing natural drainage and non-existing lakes were assigned with proper weightage through AHP technique and then integrated by weighted overlay analysis tool in GIS, to prepare the UFVZ map of study area. The map showed 42% of study area is prone to moderate flood vulnerability. The result of present study has been compared with the known flood prone locations to assess the accuracy of result. 50% of flood prone locations found under moderate flood vulnerability zone class and comparatively very less 36% flood prone locations found in high and very high zone class. The results indicate that, in urban environmental study area, the flood disaster is more influenced by anthropogenic impacts.

The proposed methodology would be suitable for mapping flood vulnerability zones through Analytical Hierarchy Process (AHP) approach. The present paper shows a simple and cost effective empirical method for delineating flood vulnerability zones using remote sensing and GIS from the available data. The present work identified zones required for urban flood disaster management. The study can also aids for planning future urban flood projects in the study area in order to ensure sustainable urban flood management.

Acknowledgements

The authors sincerely express their gratitude for technical support and necessary data provided by Karnataka State Remote Sensing Application Center (KSRSAC), Bengaluru; IMD (Indian Meteorological Department), Bengaluru and STUP Consultants Pvt. Ltd., Bengaluru. The authors are grateful to all the professors of Jain University for their keen interest in the study and suggestions provided during discussions.

References

Abdul Rahamana, S., Aruchamy, S. and Jegankumar, R. 2014. Geospatial approach on landslide hazard zonation mapping using multicriteria decision analysis: a study on Coonoor and Ooty, part of Kallar Watershed, The Nilgiris, Tamil Nadu. *International Archives of the Photogrammetry, Remote Sensing,* 8, pp.1417-1422.

Bratsolis, E., Cahrou, E., Tsenoglou, T. and Vassilas, N. 2016. Automated building block extraction and building density classification using aerial imagery and lidar data. *Journal of Earth science and Engineering,* 6(1), pp.1-9.

Bruhat Bengaluru Mahanagara Palike (BBMP) - Hebbal Valley. 2011. Preparations of revised detailed project report for remodeling of primary and secondary storm water drains in four major catchment areas in core Bangalore city. Available from: http://218.248.45.166:8092/vssIFMS/Files/WO-1--30577815-Detailed_Estimate.pdf.

Burke, E. J., Perry, R. H. J. and Brown, S. J. 2010. An extreme value analysis of UK drought and projections of change in the future. *Journal of Hydrology,* 388, p.131.

Chen, S. P. and Wang, R. Y. 2004. Analyzing hazard potential of typhoon damage by applying grey analytic hierarchy process. *Natural Hazards,* 33(1), pp.77-103.

Forman, E. H. and Gass, S. I. 2001. The analytical hierarchy process - an exposition. *Operations Reasearch,* 49(4), pp.469-487.

Jha, A. K., Bloch, R. and Lamond, J. 2012. Cities and Flooding: A Guide to Integrated Urban Flood Risk Management for the 21st Century. *The World Bank,* pp.46-49. Available from: http://hdl.handle.net/10986/2241.

Kotharkar, R., Bahadure, P. and Sarda, N. 2014. Measuring compact urban form: a case of Nagpur City, India. *Sustainability,* 6, pp.4246-4272.

Lopez, A. X. 2016. Waterbodies Serve as Natural Drainage System, Prevent Flooding In Chennai. Available from: http://www.thehindu.com/news/cities/chennai/water-bodies-serve-as-natural-drainage-system-prevent-flooding-in-chennai/article5117644.ece.

Methods for the Improvement of Vulnerability Assessment in Europe (MOVE). 2011. Handbook of vulnerability assessment in Europe - European Commission DG Environment. Collaborative project-Grant agreement No. 211590.

Mowla, Q. A. and Islam, M. S. 2013. Natural drainage system and waterlogging in Dhaka: measures to address the problems. *Journal of Bangladesh Institute of Planners,* 6, pp.23-33.

Mujumdar, P. P. 2012. Urban floods: implications of climate change. *Internatinal Conference on Environmentally Sustainable Urban Ecosystem - Integrated Landuse Planning and Water Resource Management,* IIT Guwahati, pp.2-11.

Mukherjee, D. 2016. Effect of urbanization on flood - a review with recent flood in Chennai, India. *International Journal of Engineering Sciences and Research Technology,* 5(7), pp.451-455.

Ouma, Y. O. and Tateishi, R. 2014. Urban flood vulnerability and risk mapping using integrated multi-parametric AHP and GIS: methodological overview and case study assessment. *Water,* 6, pp.1515-1545.

Ramachandra, T. V. and Mujumdar, P. P. 2009. Urban floods: case study of Bangalore. *Journal of the National Institute of Disaster Management,* 3(2), pp.1-97.

Ramu, M. B. and Vinay, M. 2014. Identification of ground water potential zones using GIS and Remote Sensing Techniques: A case study of Mysore taluk-Karnataka. *International Journal of Geomatics and Geosciences,* 5(3), pp.393-403.

Roy, R. and Md. Kutubuddin, D. 2016. Seasonal waterlogging problem in a mega city: a study of Kolkata, India. *Journal* of Research In Humanities and Social Science, 4, pp.1-9.

Saaty Thomas, L. 2008. Relative measurement and its generalization in decision making: why pairwise comparisons are central in mathematics for the measurement of intangible factors - the analytic hierarchy process. *Review of the Royal Academy of Exact, Physical and Natural Sciences, Series A: Mathematics,* 102(2), pp.251-318.

Saaty, T. L. 1992. The Analytic Hierarchy Process. Springer - McGraw Hill International.

Siddayao, G. P., Valdez, S. E. and Fernandez, P. L. 2014. Analytic Hierarchy Process (AHP) in spatial modeling for flood plain risk assessment. *International Journal of Machine Learning and Computing,* 4(5), pp.450-457.

Sinha, R., Bapalu, G. V., Singh L. K. and Rath, B. 2008. Flood risk analysis in the kosi river basin, north bihar using multi-parametric approach of Analytical Hierarchy Process (AHP). *Journal of Indian Socio Remote Sensing,* 36, pp.335-349.

State Urban Development Authority (SUDA). 2007. *Urban disaster management training programme,* Mysore, Karnataka, India, pp.20-32.

Subramanya, K. 2008. Engineering Hydrology. 4th ed. New Delhi, India*:* McGraw-Hill, p.197, pp.308-316.

The Indian Road Congress (IRC). 1977. Space standards for roads in urban areas. Available from: https://thelibraryofcivilengineer.files.wordpress.com/2015/09/irc-69-1977-space-standards-for-roads-in-urban-areas.pdf.

Willet, K. and Sharda, R. 1991. Using the analytic hierarchy process in water resource planning: Selection of flood control projects. *Journal of Socio Economic Planning Science,* 25, pp.103-112.

Xian-Zhang, P., Qi-Guo, Z., Chen, J., Liang, Y. and Sun, B. 2008. Analyzing the variation of building density using high spatial resolution satellite images: the example of Shanghai City. *Sensors*, 8(4), pp.2541-2550.

Zhang, L., Wang, J., Bai, Z. and Chunjuan, L. V. 2015. Effects of vegetation on runoff and soil erosion on reclaimed land in an opencast coal-mine dump in a loess area. *CATENA,*128, pp.44-53.

Cloud Publications
International Journal of Advanced Remote Sensing and GIS
2017, Volume 6, Issue 1, pp. 2253-2266
ISSN 2320 – 0243, Crossref: 10.23953/cloud.ijarsg.287

Research Article

Hydrological Simulation using Process Based and Empirical Models for Flood Peak Estimation

Arnab Saha[1], Praveen K. Thakur[2], Arpit Chouksey[3]

[1]Research Fellow, Uttarakhand Technical University, Dehradun 248007, India
[2&3]Scientist, Water Resources Department, Indian Institute of Remote Sensing, Dehradun 248001, India

Publication Date: 28 July 2017

DOI: https://doi.org/10.23953/cloud.ijarsg.287

Abstract This study introduces about the parameterization of hydrological modelling for Asan and Song river basin the whole Doon Valley. SWAT an empirical hydrological model, VIC a physical hydrological model and HEC-HMS a semi distributed hydrological model are used for flood peak generation at predetermined locations. The land cover mapping of Doon Valley was attempted using remotely sensed images of Landsat and Google Earth imagery. The specific objectives are hydrological modelling for peak flow hydrograph generation, to observe LULC change scenarios between 1995, 2005 and 2014 year, comparison and validation of the simulated runoff using three different hydrological models (VIC, SWAT and HEC-HMS). The VIC model performance was found good and a close agreement between the observed and simulated values was obtained for 2014 LULC map. Model performance was also found good for other subbasins. The various input parameters are the meteorological data, discharge and sediment data were processed as per requirement of the SWAT model. The model was calibrated for the year 2006 to 2010. The Hydrological modeling indicates that the curve number is most influence parameter into the total discharge. Land use and vegetative cover play an important role in watershed runoff and stream flow discharge patterns over time, including peak flows. Increased human interventions have caused rapid transitions in land cover, adversely affecting the watershed processes and hydrological cycle in the long run. It may be concluded that the impact of land cover changes are most pronounced during low flows and that during high flows, role of land cover becomes comparatively less.
Keywords *Coefficient of determination; Hydrological modelling; HEC-HMS; LULC; SWAT; VIC*

1. Introduction

Hydrology is defined as the science dealing with the movement of water over and under the land surface and a hydrological model can be defined as a mathematical representation of the flow of water and its constituents on some part of the land surface or sub-surface environment. Hydrologic modeling has been going on for at least 150 years. Over the last century, land use land cover (LULC) in the lower Himalayan region shifted from perennial, cropping, fallow land to built-up area. Historical LULC change impacted the annual water balance in many basins by decreasing annual evapotranspiration (ET), water yield and increasing runoff (Yong et al., 2015).

Recent expansion of the industry and urbanization may lead to future LULC changes from needed plantation to urban (Garg et al., 2012; Engman et al., 1996). The little change in LULC, affects the

hydrological processes and lastly the water balance. In matter of comfort and development, human being keeps on changing the environment especially LULC resulting in huge urbanization that significantly influence hydrologic variations (Bradford et al., 2007). The continuously changing environment makes it necessary to realize and compute various hydrological components for competent water resource management. The water resources management requires a systems approach that includes not only all of the hydrological components, but also the interactions, links, consequences, relations and implications among these components (Islam et al., 2014). A thorough knowledge and understanding of the different hydrological phenomena and hydrological cycle as a whole is required in studying the implications of these changes (Bhattacharya et al., 2013).

In this regard, the hydrological modeling technique can help to gain an understanding of the hydrological system in order to provide reliable information for managing water resources in a sustained manner at smaller scale and larger scale (Kiriwongwattana & Garg, 2013). In this study, Variable Infiltration Capacity (VIC) semi-distributed hydrological model, SWAT (Soil and Water Assessment Tool) a physical based semi distributed hydrological model and HEC-HMS (Hydrological Engineering Corporation - Hydrologic Modeling System) a semi distributed hydrological model has been used for hydrological simulation.

1.1. Study Area

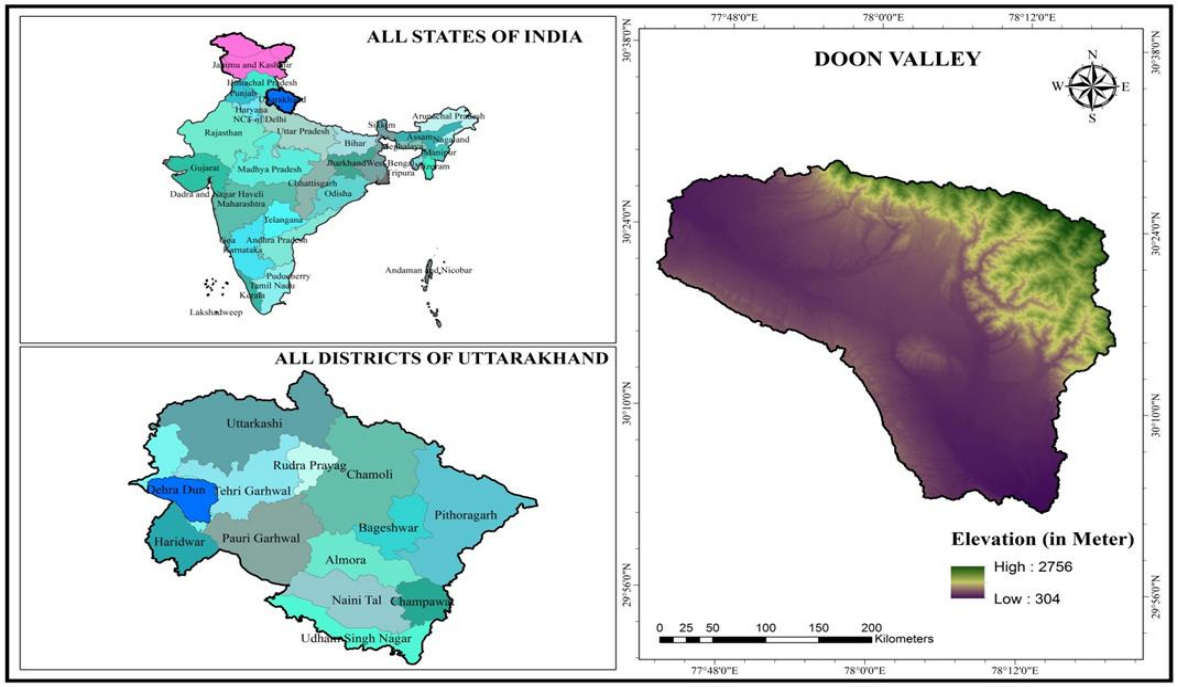

Figure 1: *Study area map of Doon Valley*

Valley is situated in Dehradun district of Uttarakhand, it is lying geographically between 29°50 N-0°30 N Lat. and 77°35-78°20 E long. Maximum length of Doon valley is 80 km and 25 km in width. In the Sub Himalayan region it is considered as one of the largest ‘duns’. River Ganga flows in eastern and river Yamuna flows in western side of Doon Valley. Two rivers, Song and Asan river systems drained in Doon Valley. These rivers receiving water through a number of perennial and non-perennial streams originated in Lesser Himalayan rocks in north and Siwalik in south direction and finally contribute to the discharges of Ganga and Yamuna River in east and west, respectively (Dudeja et al., 2011). The

Dehra-Asarori water divide, running NE-SW from Clement Town, Dehradun city to Rajpur, separates the NW flowing river Asan from SE flowing river Song. Generally temperature of this area is temperate Depending upon the altitude of the area temperature varies greatly from tropical to severe cold. The district is hilly so that temperature variations possible because of difference in elevation. Summer is pleasant in hilly regions but in the Doon, the heat is often intense, although not too much temperature as in the plains of the adjoining district. During the summer months, the temperature varies between 36°C and 16.7°C. The winter months are colder with the maximum and minimum temperatures moving from 23.4°C and 5.2°C respectively. The average rainfall of the area is 2073.3 mm. Most of the annual rainfall in this area is achieved during the months from June to September and the rainiest months are July and August (Singh et al., 2013).

1.2. Data and Materials

ISRO GBP LULC 1995, 2005, 2014 developed by Indian Institute of Remote sensing, Dehradun was used for mapping land cover in the region. Originally the map was prepared for 14 classes at a scale of 1:50, 000 but as the extent was limited to Indian region only, the map was reclassified and recoded to 9 classes as present in Global land use land cover map so that it can be merged with it and facilitate information for Asan and Song watershed (Doon Valley) extending beyond Indian boundary. ASTER Global Digital Elevation Model (GDEM) was used in the present study. Cloud free Satellite data of Landsat 5 dated 17-Nov-1994, 18-Feb-1994, 10-Jun-1994 & 27-Mar-1996 and Landsat 8 dated 13-Mar-2014, 23-Oct-2014 and 12-Feb-2015 with special resolution of 30m for the year 1994, 1996, 2014 & 2015 corresponding to the study area were downloaded from the global land cover facility (GLCF) website to quantify the changes in the land use/land cover type of the area and to analyse its impact on surface runoff and sediment. Digitized soil maps of Doon Valley lying in India were obtained at 1:50,000 scale. Soil mapping for Indian region has been done by NBSSLUP (National Bureau of soil survey and Land use planning), Nagpur. Some of the associated soil properties were also derived from it. Daily metrological data such as rainfall, minimum and maximum temperature, pan evaporation data were obtained from Automatic Weather Station (AWS), Dehradun and National Institute of Hydrology (Roorkee). The daily rainfall was used as an input to the ArcSwat Model, HEC-HMS Model, and VIC Model. The maximum and minimum temperature was used to calculate potential evapotranspiration (El-Sadek and Salem, 2015).

2. Methodology

Variable Infiltration Capacity (VIC) model is a grid-based macroscale hydrological model designed to represent surface energy and hydrological fluxes for large river basins (Terrestrial Hydrology Research Group, Princeton University, 2007). Most important characteristic of this model include sub-grid variability in surface vegetation classes, soil moisture storage capacity and drainage from the lower soil moisture zone also known as base-flow. VIC model contain a Routing model which is based on linear transfer function to simulate stream flow for basin (Liang et al., 1994). VIC model run on VIC tool that was developed as a part of the ISRO-GBP project on LULC dynamics and impact of human inversion in Indian River basins. The input layers required for the model are Terrain (Elevation, Slope, Flow Direction), LULC, Vegetation properties (LAI, Albedo, Root Distribution, Canopy Resistance), Soil properties (Layer-wise physical texture and hydraulic properties), River discharge data, Meteorological inputs from downscaled GCM (Precipitation, Temperature). The input files which are used to calibrate and validate VIC model are grid files (Latitude, Longitude, Grid number, Run grid, Soil_1, Soil_2, Slope, Elevation, Rain), soil database file (describe the characteristic of the soil layers for each grid), vegetation parameter file (contains land cover characteristics on a monthly average basis), forcing file (daily maximum and minimum temperature (in ^{0}C) and daily precipitation (in mm)) and global parameter file as input in VIC tool, the model runs if it stops at any place encountering error in any of

missing file the model will restart. The VIC model runs in CYGWIN rather than in the tool. The VIC tool has an added feature that can generates a tabular analysis of output fluxes. Primary input files required to run Routing model are Flux file (containing fluxes of surface runoff, evapotranspiration, base flow, soil moisture), Flow direction file, Fraction file (contains fraction of each grid), Station location file (contains details of row and column in the grid shape file) and unit hydrograph file. Calibration has been done by adjusting the infiltration parameters and the base-flow parameters at which non-linear base-flow takes place. The soil parameters have been altered since VIC primarily considers the infiltration capacity curve and nonlinear base-flow curve that occurs predominant at the lower layers of the soil. The process continues until the simulated stream flow is almost equal to pragmatic stream flow at given outlets.

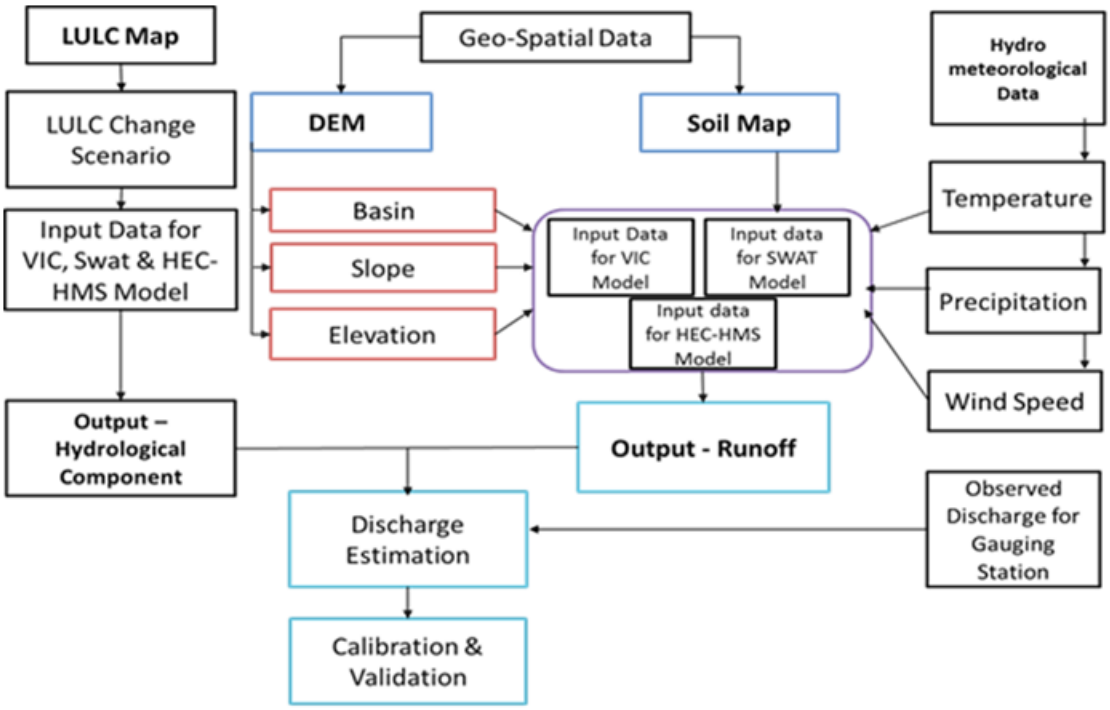

Figure 2: *Methodology flowchart of three different hydrological models*

The steps which are followed to set-up the model and input database in SWAT model are watershed delineation using source DEM, land use, soil types and climate data (Merwade & Rajib, 2014). A few additional inputs are required for running the model are management data, soil data, soil chemical data, manning's roughness coefficient and in stream water quality parameters (Betrie et al., 2002). These input files were set up and edited as per the requirements and objective of the project. Finally, the ARCSWAT model runs to simulate the various hydrological components. Calibration is done to minimize the difference between simulated and observed stream flows. In the present study the ARCSWAT model was calibrated for the year 2006-2010 based on the observed discharge and sediment data and the model was validated for monthly and daily surface runoff for the year 2006 to 2010.

Hydrologic Engineering Centre-Hydrological Modelling System (HEC-HMS) is design to simulate the hydrologic process of dendritic watershed systems. Curve Number are used for loss estimation in HEC-HMS model, it is prepared by the combination of LULC and soil map. HEC-HMS model is running

from 1 July to 1 August of 2006 year, and 29 July to 1 August of 2010 and 2012. Curve Number (CN) and initial abstraction are used for sensitivity analysis in year 2006.

3. Results and Discussion

As per the objectives, the Asan and Song River basin was delineated and various thematic maps were generated as per the requirement of the SWAT, HEC-HMS and VIC model. The various database related to climate and soils were also prepared as per the requirement of the model. Various hydrological components like surface runoff, sediment yield, Evapotranspiration (ET), PET were simulated on daily, monthly and yearly basis. The predictions of the model for weekly and monthly surface runoff and sediment yield were compared with the measured counterparts (Kumar et al., 2013). The performance of the model was also evaluated using statistical and graphical methods to decide the capability of the model in simulating the runoff and sediment yield from the Asan & Song basin. Land use/land cover change scenario and its impact on the hydrological regime is also presented and discussed in this paper.

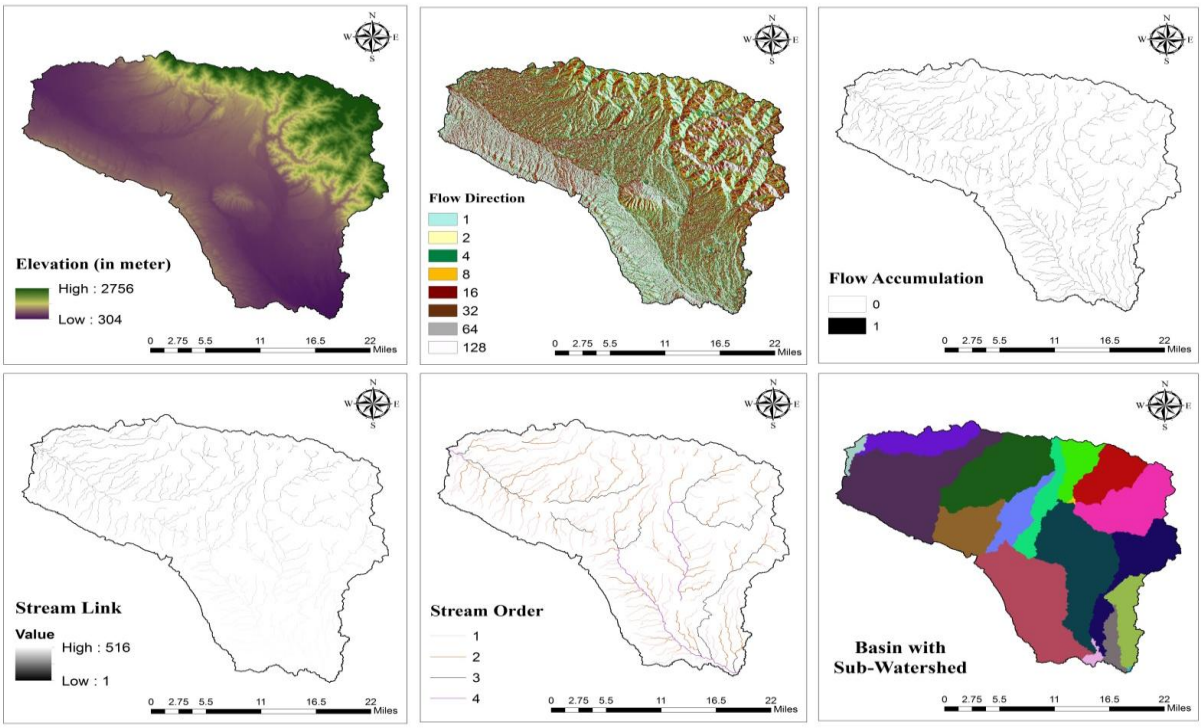

Figure 3: *Watershed delineation of Doon Valley*

Basin boundary and drainage characteristics of the watershed were derived in ArcMap10.1 software using Aster Global Digital elevation model (250m & 30m) as major input. The following operations were fill sinks, flow direction, flow accumulation, stream link, stream order, catchment polygon processing, drainage line processing, watershed and sub-watershed. Flow direction map is derived from fill sink map and subsequently a flow accumulation map is derived from it. Stream definition is derived from this flow accumulation by specifying the maximum threshold area for delineating drainages. A sub-watershed for each delineated stream is then extracted. To extract the basin boundary, an outlet at Paonta station in the Asan river basin and Rishikesh station in the Song river basin was defined. Finally, a basin for the defined outlet is delineated along with the river network. It

can further subdivide basin into desired number of sub-watersheds by specifying various outlets where the gauging station exists along the extracted (Dadhwala et al., 2010).

In order to prepare the LULC map for Asan & Song Basin, the downloaded FCC of Landsat TM and Landsat ETM satellite image for the year 1995, 2005 and 2015 were subsetted to extract the area of interest and classified with supervised classification method using maximum likelihood classifier as discussed and presented. In order to check the accuracy of the classified images accuracy analysis was also carried out using accuracy assessment classifier of Erdas imagine 2014 using ground truth information collected from field (Baishya et al., 2006).

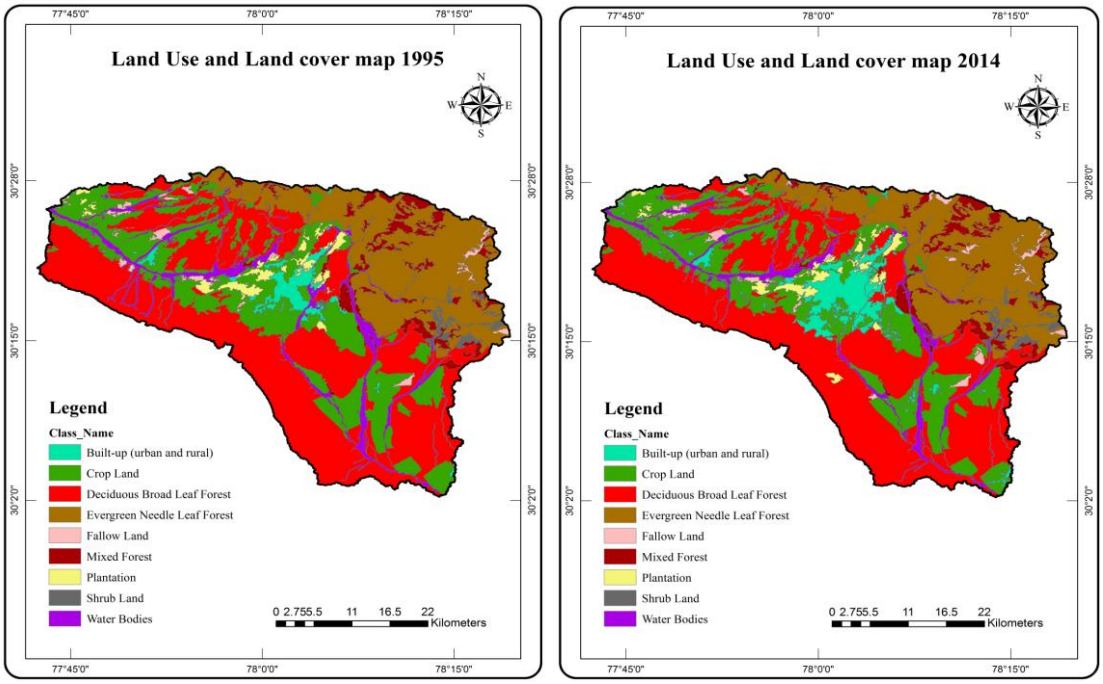

Figure 4: *LULC map of 1995 and 2014 year of Doon Valley*

Table 1: *Change detection matrix for 1995-2014*

	Water bodies	Evergreen leaf forest	Deciduous leaf forest	Mixed forest	Shrub land	Plantation	Crop land	Fallow land	Built-up
	1	2	3	4	5	6	7	8	9
Water bodies	114.88	1.58	11.83	8.02	0.19	0.39	4.53	0.31	6.77
Evergreen leaf forest	1.26	317.29	0.55	3.71	1.11	0.01	0.45	5.13	0.58
Deciduous leaf forest	5.05	0.41	684.6	0.49	0.26	2.29	9.04	1.39	6.6
Mixed forest	0.02	4.19	0.43	85.25	0	0	0.94	2.51	1.15
Shrub land	0.17	0.82	0.09	2.59	17.07	0	0	0	0.75
Plantation	0.24	0	0.13	0.78	0	31.1	2.49	0.07	5.44
Crop land	2.95	0.42	5.43	0.14	0	1.45	247	2.81	45.87
Fallow land	0.25	0.6	0.75	0.03	0.02	0.07	2.46	21.53	1.71
Built-up	0.13	0.05	0.05	0.04	0.02	0.17	0.52	0	47.36
Total	**124.95**	**325.36**	**703.86**	**101.05**	**18.67**	**35.5**	**267**	**33.75**	**116.2**

To see the change in LULC of hydrological regime of Doon valley watershed mainly in built-up area change detection technique adopted. For this purpose in Erdas imagine 2014 change detection matrix has been prepared. In 2014 total 68 km2 built-up area increased from 1995 and the main contribution of cropland almost 60% contributions. In the LULC change detection matrix, urban areas increased, becoming the dominant LULC type and continuously extending into around the city (Sun et al., 2013). In summary, the selected areas experienced rapid LULC change, especially urbanization, from 1995 to 2014.

A. VIC Model

The preliminary comparisons of simulated and observed daily stream flows are presented for two outlets location. The coefficient of determination showing agreement between the trends of simulated and observed stream flow records (Bhattacharya et al., 2015; Liang et al., 1996). LULC map of 2014 and rainfall data was used 2006 to 2010 for simulation and validation. Coefficient of determination is 0.732 for 2014 year. There are no heavily changes in simulation data. No consistency in the simulation results was observed which implies the need for model calibration. The time series of the observed and simulated daily monthly surface runoff. An attempt was also made to calibrate for monthly sediment for the period January-December, 2006 to 2010. For this calibration, the slope of the sub-basin, this is one of the most sensitive parameter for sediment load. Several simulation runs were then applied until a goodness-of-fit between observed and simulated flow was obtained. In order to compare the simulated values with the observed values coefficient of determination (R2).

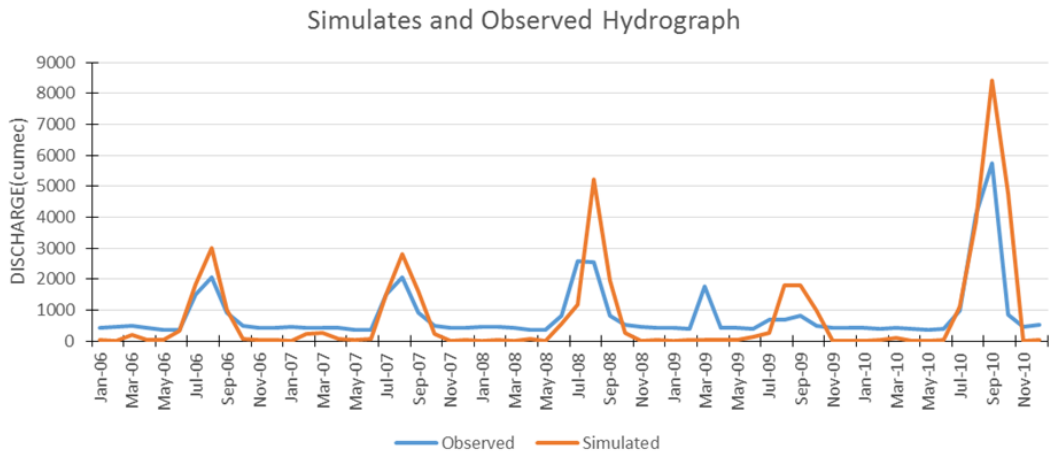

Figure 5: *Monthly mean simulated & observed runoff relationship for Doon Valley watershed (LULC 2014) using rainfall data 2006-2010*

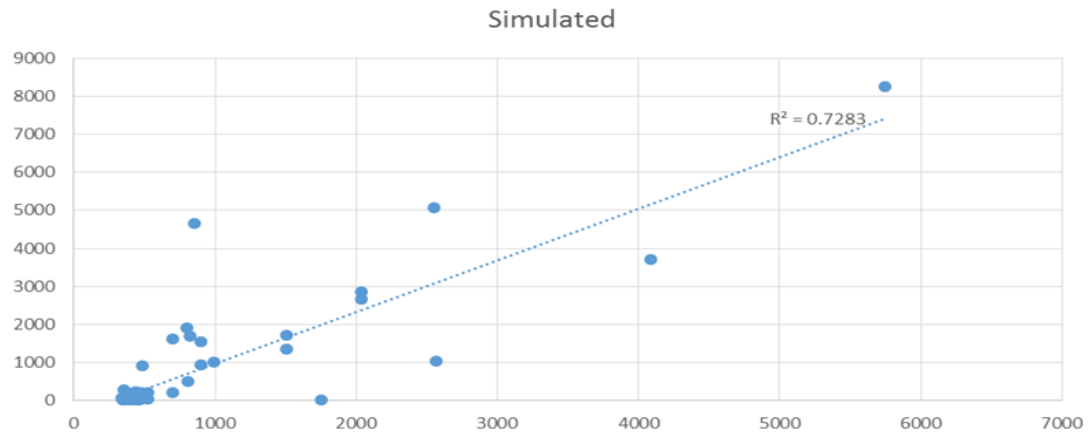

Figure 6: *Simulated and observed runoff relationship for Doon Valley watershed 2006-2010*

B. SWAT Model

The preliminary comparisons of simulated and observed daily stream flows are presented for 32 outlets location for this watershed simulated for whole watershed area Asan and Rishikesh together. The coefficient of determination showing agreement between the trends of simulated and observed stream flow records (Dadhwala et al., 2010). LULC map of 2014 and rainfall data was used 2006 to 2010 on monsoon season for simulation and validation. Coefficient of determination is 0.781 for 2014 year. Model simulated runoff is only for 2006 to 2010 year on monsoon season. After calibrating the result it can observed that in below graph rainfall was increased in June to September season. That reason, water yield and sediment yield were also increased in June to September. Fluctuations rate of average monthly basin values for evapotranspiration was also seen in this season.

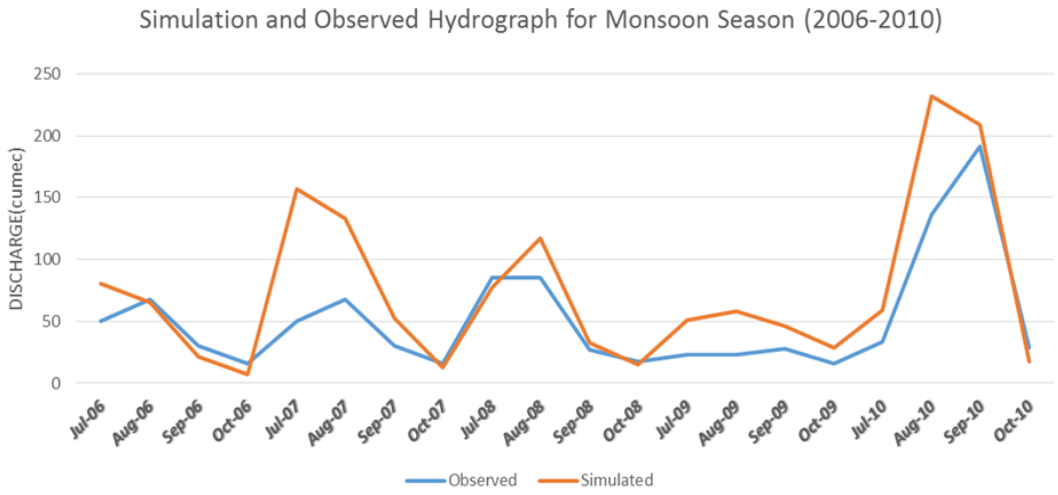

Figure 7: *Peak discharge for LULC 2014 using rainfall data 2006-2010 on monsoon season*

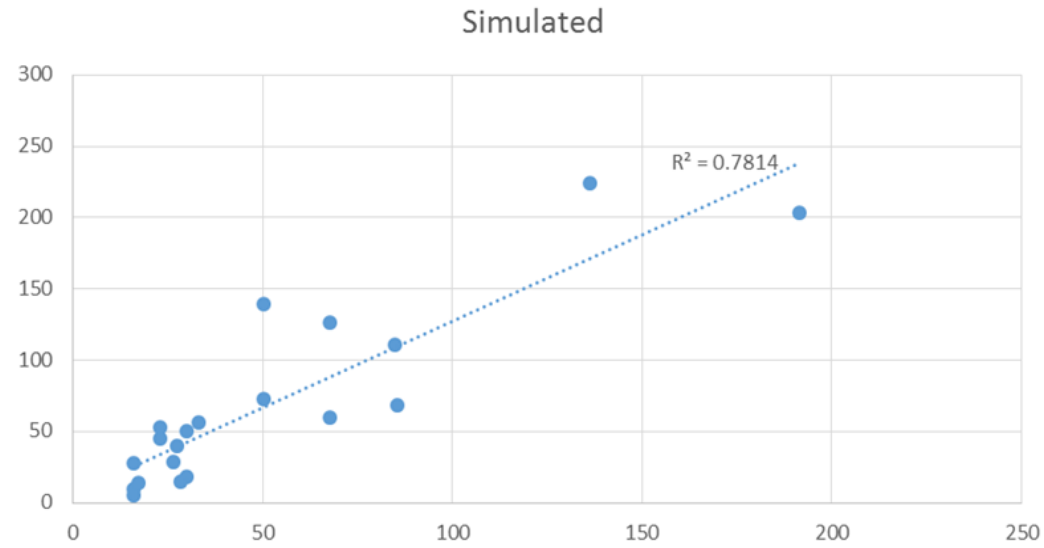

Figure 8: *Simulated and observed runoff relationship for Doon Valley watershed 2006-2010 on monsoon season*

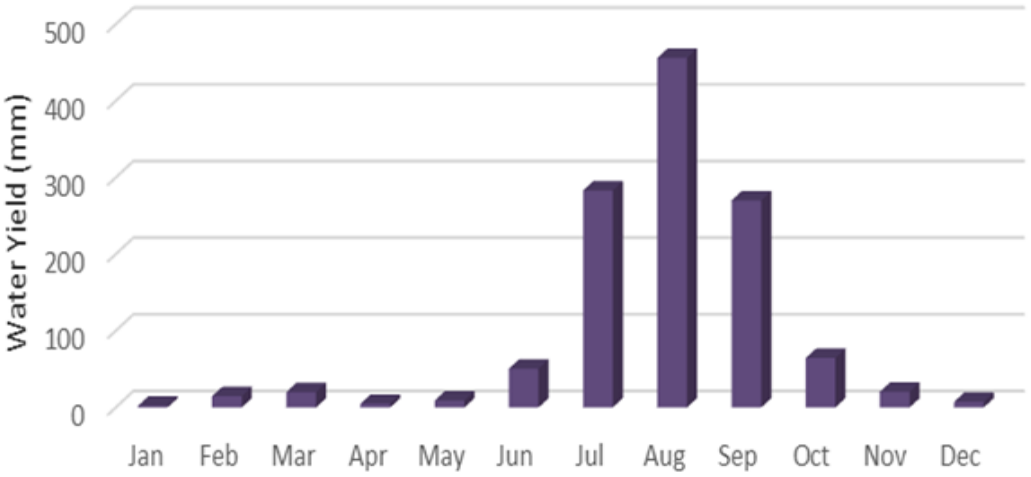

Figure 9: *Average monthly basin values for rain (mm) from 2006-2010*

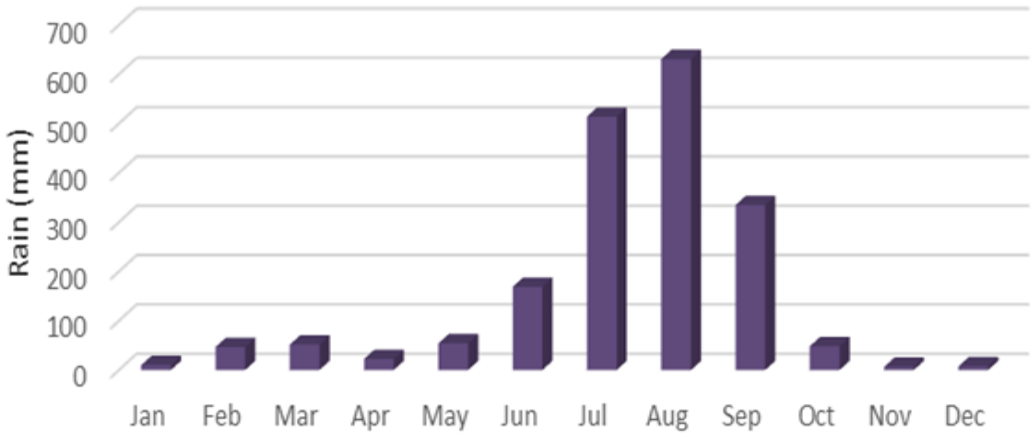

Figure 10: *Average monthly basin values for water yield (mm) from 2006-2010*

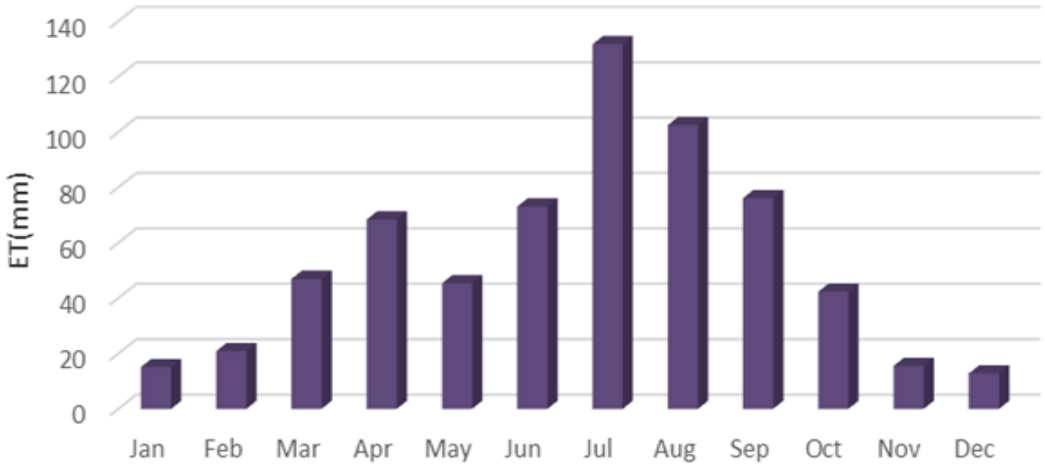

Figure 11: *Average monthly basin values for evapotranspiration (mm) from 2006-2010*

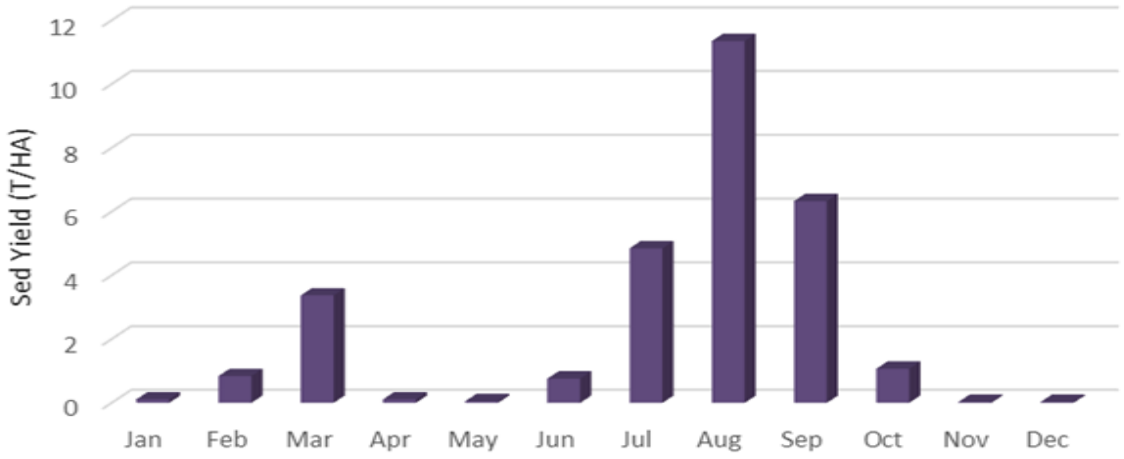

Figure 12: *Average monthly basin values for sediment yield (T/Ha) from 2006-2010*

C. HEC-HMS Model

HEC-HMS is a model primarily designed to assess and evaluate short term climate and land cover changes on basin hydrology (Mishra et al., 2010). It therefore essentially ignores the effect due to human induced activities. The Asan and Rishikesh basin contains several storage reservoirs and diversion structures and the observed stream flows are thus bias and are not really appropriate for the purpose of calibration. This may be a reason of disagreement between observed and simulated discharge (Dadhwal et al, 2010). During low flows, reservoirs come into play and store most of the river waters whereas during high flows a reservoir has to throw out all waters coming into it once filled. This may be the possible reason of overestimation during low flows and underestimation during high flows. LULC 2005 map and TRMM 2006 rainfall data was used 1st July-1st August, 2006 for simulation and calibration. Coefficient of determination is 0.659 for 2006 year (Jul-Aug).

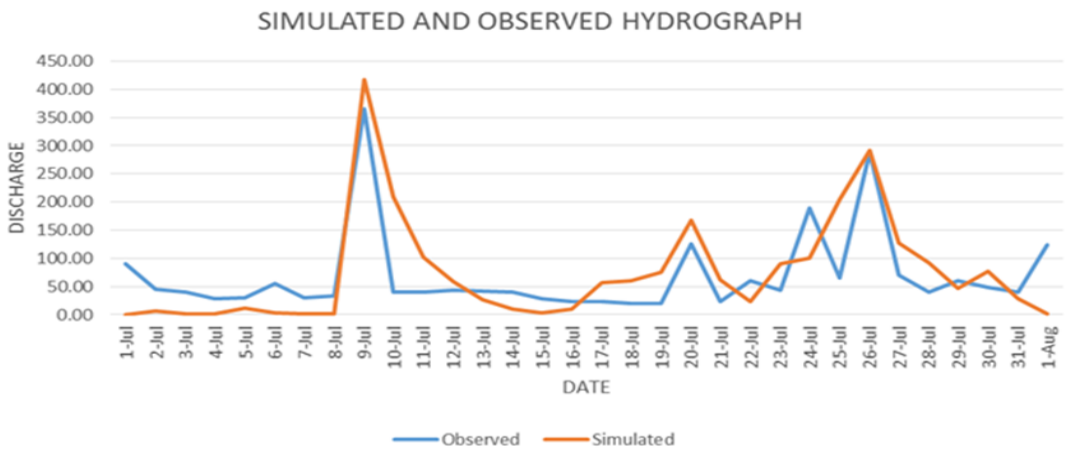

Figure 13: *Simulated and observed runoff relationship for Doon Valley watershed 1st Jul-1st Aug, 2006*

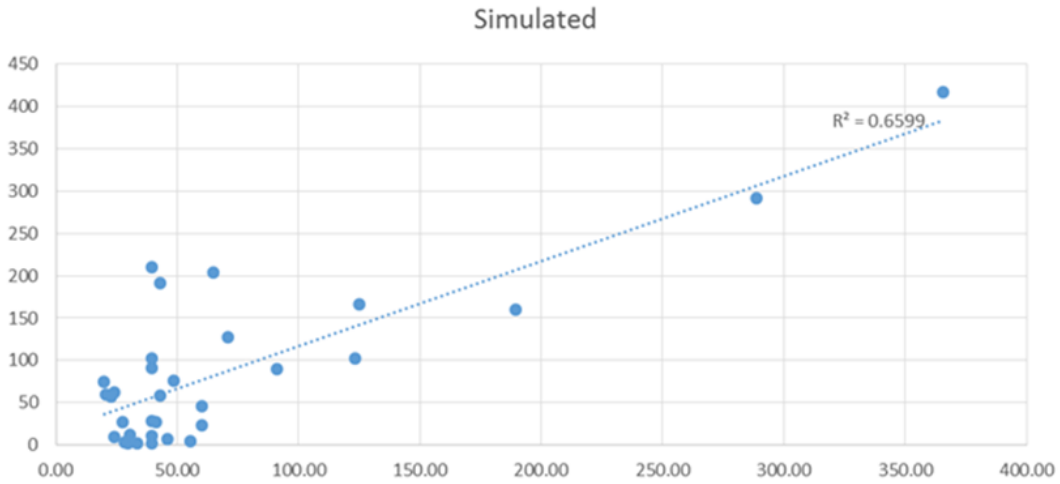

Figure 14: *Runoff relationship for Doon Valley watershed 1st July-1st August, 2006*

Table 2: *Comparison between two models yearly average simulated discharge*

Year	VIC model simulated discharge (cumec)	SWAT model simulated discharge (cumec)	Observed discharge (cumec)
2006	18.05	19.64	23.21
2007	18.76	32.96	22.95
2008	25.62	24.72	28.28
2009	13.84	17.55	20.66
2010	50.27	44.96	45.86

Table 3: *Comparison between two models simulated highest peak discharge*

Year	VIC model highest peak discharge (cumec)	SWAT model Highest peak discharge (cumec)	Observed highest peak discharge (cumec)
2006	212.25	280.98	240.64
2007	449.89	401.46	241.64
2008	705.78	651.23	534.88
2009	188.96	150.56	101.92
2010	1485.88	1088.63	1062.48

4. Conclusion

Distributed hydrological modelling offer a competent solution to appraise long term hydrological changes by allowing quantification fluctuations in stream flow patterns. Observed LULC changed scenario between 1995, 2005 and 2014 using maximum likelihood supervised classification method. Due to frequent occurrence of hydro-meteorological conditions such as floods, droughts and cyclones in recent times indicates a shift in the hydrological response of the basin ascribed to land cover changes. This study attempts to model the hydrological response of Asan and Song river basin using physically based, distributed VIC, SWAT and HEC-HMS models and assess land cover change impacts on stream flow at various points along the river. Pre-calibration and comparison of observed and simulated stream flow was done for year of 2006-2010 using 2014 LULC Map. The coefficient of determination before calibration was found 0.732 for VIC model, for SWAT model it was found to be 0.781 and for HEC-HMS model it was found to be 0.769. The relative increment in stream flow was found high in the months of July to October in all sub-basins. It is concluded that the impact of land cover changes is most noticeable during low flows.

Acknowledgement

The authors would like to thanks Indian Institute of Remote Sensing, ISRO, Dehradun, Uttarakhand, India. Special thanks given to Dr. S. P. Aggarwal, Dr. Vaibhav Garg and Dr. Bhaskar Nikam, Water Resources Department, IIRS, Dehradun. Thanks are also given to the Uttarakhand Technical University.

References

Baishya, B. 2006. Modelling of hydrological components and impact of land use/land cover change on hydrological regime. M.Tech. thesis, Andhra University, Andhra Pradesh, India. pp.34-37.

Betrie, G. D., Xuan, Y. and Griensven, A. V. 2002. ArcGIS interface for Soil and Water Assessment Tool (SWAT). UNESCO-IHE, Delft, Netherlands, Blackland Research and Extension Center and Spatial Sciences Laboratory, Texas A & M University, pp.1-65.

Bhattacharya, T., Aggarwal, S. P. and Garg, V. 2013. Estimation of water balance components of Chambal river basin using a macroscale hydrology model. International Journal of Scientific and Research publications, 3(2), pp.1-6.

Bhattacharya, T., Raju, P.V. and Hakeem, A. 2015. Climate change impact on snowmelt runoff modelling for Alaknanda river basin. Journal of Environment and Earth Science, 5(11), pp.56-67.

Bradford, A., Noor, R. and Whiteley, H. R. 2007. Ecological flow assessment for Hanlon creek Ontario: use of synthesized flows with range of variability approach. *Canadian Water Resources Journal,* 32(2), pp.111-128.

Chinnayakanahalli, K., Kroeber, C., Hill, R., Tarboton, D. G., Olson, J. and Hawkins, C. 2006. The Multi-Watershed Delineation Tool: GIS Software in Support of Regional Watershed Analyses. Utah State University, pp.1-39.

Dadhwal, V. K., Aggarwal, S. P. and Mishra, N. 2010. Hydrological simulation of Mahanadi river basin and impact of land use/land cover change on surface runoff using a macro scale hydrological model. The International Archives of the Photogrammetry, Remote Sensing and Spatial Information Sciences, 37(Part 7B), pp.165-170.

Dudeja, D., Bartarya, S. K. and Biyani, A. K. 2011. Hydrochemical and water quality assessment of groundwater in Doon Valley of outer Himalaya, Uttarakhand, India. Environmental Monitoring and Assessment, 181(1), pp.183-204.

El-Sadek, A. and Salem, E. 2015. Impact of ridge-furrow water harvesting system on faba bean (Vicia faba L.) production under rainfed conditions in Matrouh, *Egypt. Annals of Agricultural Science,* 60(1), pp.61-66.

Engman, E. T. 1996. Remote sensing applications to hydrology: future impact. *Hydrological Sciences,* 41(4), pp.637-647.

Garg, V., Khwanchanok, A., Gupta, P. K., Aggarwal, S. P., Kiriwongwattana, K., Thakur, P.K. and Nikam, B. K. 2012. Urbanisation effect on hydrological response: A case study of Asan river watershed, India. Journal of Environment and Earth Science, 2(9), pp.39-50.

Islam, S. M., Kamila, A., Jana, S. and Paul, A. K. 2014. Estimation of land surface temperature of Chilika lagoon watershed and its dependence on terrain properties. Indian Journal of Geography and Environment, pp.78-98.

Kiriwongwattana, K. R. and Garg, V. 2013. Urbanization effect of watershed hydrology: A case study of Asan river watershed. *Proceeding - Science and Engineering*, pp.616-629.

Kumar, P., Shrivastava, R., Thakur, P. K. and Shankar, V. 2013. Sediment yield estimation of Gambar watershed using semi distributed modelling approach. Proceedings of the Fortieth National Conference on Fluid Mechanics and Fluid Power, 12-14 December, 2013, NIT Hamirpur, Himachal Pradesh, India, 298, pp.1530-1539.

Liang, X., Lettenmaie D. P., Wood E. F. and Burge S. J. 1994. A simple hydrologically based model of land surface water and energy fluxes for general circulation model. *Journal of Geophysical Research: Atmosphere,* 99(7), pp.415-428.

Liang, X., Lettenmaier, D. P. and Wood, E. F. 1996. One-dimensional statistical dynamic representation of subgrid spatial variability of precipitation in the two-layer variable infiltration capacity model. *Journal of Geophysical Research,* 101(D16), pp.21, 403-22.

Merwade, V. and Rajib, A. 2014. Setting up a SWAT model with ArcSWAT. [Online]. [Accessed 12 June 2017] Available from: http://docplayer.net/27149702-Setting-up-a-swat-model-with-arcswat.html

Mishra, N. 2008. Macroscale hydrological modelling and impact of land cover change on stream flows of the Mahanadi river basin. M.Tech. thesis, Andhra University, Andhra Pradesh, India. pp.1-100.

Singh, O., Arya, P. and Choudhary, B. S. 2013. On rising temperature trends at Dehradun in Doon valley of Uttarakhand. India. Journal of Earth System Science, 122(3), pp.613-622.

Sun, Z., Li, X., Fu, W., Li, Y. and Tang, D. 2013. Long-term effect of land use/land cover change on surface runoff in urban areas of Beijing, China. Journal of Applied Remote Sensing, 8(1), pp.084596.

Terrestrial Hydrology Research Group, Princeton University. 2007. [Online]. Available from: http://hydrology.princeton.edu/models.php.

Yong, L. G., Hong, T. Q., Yi, H. M., Yang, H. and Ruby, L. L. 2015. Projected changes in mean and interannual variability of surface water over continental China. *Science China Earth Science,* 58(5), pp.739-754.

Cloud Publications
International Journal of Advanced Remote Sensing and GIS
2017, Volume 6, Issue 1, pp. 2267-2273
ISSN 2320 – 0243, Crossref: 10.23953/cloud.ijarsg.288

Research Article

Predicting Potential Habitat Distribution of *Rauwolfia serpentina* an Important Medicinal Plant using Maxent Modeling in Doon Valley, Uttarakhand State, India

Neelam Rawat, Kishor Kandpal, Saurabh Purohit, Govind Singh, Durgesh Pant

Uttarakhand Space Application Centre, Dehradun, Uttarakhand, 248001, India

Publication Date: 31 July 2017

DOI: https://doi.org/10.23953/cloud.ijarsg.288

Abstract The growing demand and dependencies of people for herbal care is time need. Among the list of various used herbal plants, *Rauwolfia serpentina* (Apocynaceae) is an important and due to relief of various central nervous system disorders. The root of this plant has been used in the treatment of hypertension or as a sedative and tranquillizing agent. This plant is variously used in Ayurveda, Unani system of medicine and Homeopathy for various disease ailments. Predicting potential geographic distribution of the species is important from species occurrence and habitat restoration point of view. This paper hearsay the results of a study carried out in the Dehradun valley in India (Dehradun surrounding forest area) on potential distribution modeling for *Rauwolfia serpentina* using Maxent model. The Worldclim bioclimatic variables, slope, aspect, elevation, and the FSI forest type data and 100 spatially well-dispersed species occurrence points were used to predict the potential distribution of *Rauwolfia serpentina* in ca. nearly 1277 km^2 of Doon valley study area. Jackknife test was used to evaluate the importance of the environmental variables for predictive modeling. Maxent model was highly accurate with a statistically significant AUC value of 88.5. The approach could be promising in knowing the eventing the potential distribution of medicinal plant species and thus, can be an effective tool in species restoration and conservation planning.

Keywords: *Dehradun; Jackknife; Maxent; Medicinal and aromatic plant; Potential distribution; Rauwolfia serpentina*

1. Introduction

The habitat restoration of species is one of the successful ecological engineering measures for the species rehabilitation and habitat conservation (Polak and Saltz, 2011). Knowledge on the distribution of species is often a pre-requisite to rehabilitate the species in any ecosystem (Barik and Adhikari, 2011; Franklin et al., 2009). The species-environment analysis relationship has always been a central issue in ecology and biogeography (Guisan and Zimmerman, 2000; Haines, 1925). The application of remote sensing and Geographic Information System (GIS) provides several useful input variables such as vegetation type and density, biome landscape or eco-region maps and for geospatial database creation, data integration and modeling (Turner et al., 2003; Kushwaha, 2011, Irfan-Ullah et al., 2006).

Models predicting the potential geographic distribution of species are important for a variety of applications in conservation biology with a number of statistical models to simulate the spatial distribution of plant species invasive species, species diversity and impact of climate change (Ferrier et

al., 2002; Graham et al., 2004, Kumar and Stohlgren, 2009; Adhikari et al., 2012, Peterson et al., 2003; Thuiller et al., 2005, Graham et al., 2006, Thomas et al., 2004; Saran et al., 2010).

Maximum entropy (Maxent) model is a species distribution model (SDM) originating from the statistical mechanics (Phillips et al., 2004; Jaynes, 1957). This environmental model for predicting the potential distribution of species has several advantages; it requires only species presence (or occurrence) data and environmental information (Elith et al., 2011). The presence modeling methods simply require a set of known occurrences together with predictor variables such as topography, climate, soil, biogeography etc. that make use of both continuous and categorical data and incorporate the interactions between the variables (Phillips and Dudik, 2008, Phillips et al., 2006).

Rauwolfia serpentina (L.) Benth. ex Kurz.(Family:*Apocynaceae*), is widely distributed in the foothills of Himalayan range, up to the elevation of 1300-1400 m and in the sub-Himalayan tract from Punjab eastwards to Nepal, Sikkim and Bhutan, in Assam, in the lower hills of Gangetic plains, Eastern and Western Ghats, in some parts of central India and in the Andamans. The natural reserves of this plants are declining as a result of over harvesting, IUCN has kept this plant under endangered status, and it is listed in CITES Appendix II. The National Medicinal Plants Board (NMBP), Govt. of India has also placed this plant among 32 plants identified and prioritized for cultivation, development, formulating schemes and guidelines for financial assistance because of their high demand. *Rauwolfia serpentina* is an erect evergreen perennial under shrub with a cluster of branches (2- 6) arising from the root, attains a height up to 75 cm. to 1 m under cultivation, rootstock is long, irregularly, nodular and yellowish.It prefers clay-loam to silt-loam soils with plenty of humus and rich in nitrogenous and organic matter with good drainage. The plant requires slightly acidic to neutral soils for good growth with medium to deep well drained fertile soils. Alkaline soils are not suitable for commercial cultivation. Generally, organic cultivation is practiced. It grows well in frost-free tropical to sub-tropical situations under irrigation. It grows luxuriantly well where the rainfall is 2500 mm or more. The major alkaloid present in root, stem and leaves of the plant is reserpine varies from 1.7 to 3.0%. The root barks has more than 90% of the total alkaloids in roots. The minor alkaloids present in the plant are Ajmalicine, ajmaline, isoajmaline, ajmalinine, chandrine, rauwolfinine, renoxidine, rescin-namine, reserpiline, reserpin, reserpinine, sarpagine, serpentine, serpentinine, tetraphyllicine, yohimbine, 3-epi-ayohimbine. The root contains ophioxylin, resin, starch and wax (Sastri, 1990).

Therefore, extend and availability of this important medicinal plants becomes necessary and the present study is designed for predicting the potential habitat distribution of *Rauwolfia serpentina* in Dehradun valley of Uttarakhand using Maxent modeling.

1.1. Study Area

Dehradun valley is situated in lesser Himalaya of Uttarakhand State, India. The Dun Valley occupies an area of 1277 km^2, and is bounded by Shivalik hills in the south and Lesser Himalayas in the north. It receives a mean annual rainfall of 2051 mm. The temperature ranges from 2°C in winter to 42°C in summer. Dun valley is a forested landscape with forests, agriculture, settlements, orchards and tea gardens. The principal forest types are: (i) Moist Bhabar-Dun Sal Forest (3C/C2bi), (ii) Lower Himalayan Moist Temperate Forest (12C1), (iii) Himalayan Subtropical Pine Forest (9/C1), and (iv) Northern Dry Mixed Deciduous Forest (5B/C2) (Champion and Seth, 1968). *Shroea robusta, Terminalia tomentosa, Anogeissus latifolia, Mallotus philippensis, Dalbergia sissoo, and Acacia catechu* are some of the important tree species in the Valley.

2. Materials and Methods

The dataset used for the present study are the Forest Survey of India (FSI) forest type map based on Champion and Seth classification. The Environmental variables and species occurrence data Nineteen bioclimatic variables (Hijmans et al., 2005; Corvellec and Hultman, 2012) with 30 seconds (ca. 1 km) spatial resolution, downloaded from WorldClim dataset (www.worldclim.org), were used to find out the most influential variables associated with *Rauwolfia serpentina* distribution. The Advanced Spaceborne Thermal Emission and Reflection Radiometer (ASTER) Digital Terrain Model (DTM) with 30 m resolution, was used to generate the slope, aspect and elevation data layers. A total of 100 species occurrences were recorded randomly in the study area. A hand-held Global Positioning System (GPS) receiver with ±5 m positional accuracy was used to acquire the species occurrence geocoordinates. Spatial modeling: Erdas 11 and ArcGIS 10.2 were used to create the spatial data layers. The categorical data were re-sampled to 1 km spatial resolution using nearest neighbor re-sampling technique. The 70% of selected data used for training and the rest 30% for testing. A total of 100 runs were set for model building (Flory et al., 2012). Other values were kept as default. The area under the Receiving Operator Curve (AUC) was used to evaluate model's goodness-of-fit and model with highest AUC value was considered as the best performer. The Jackknife procedure was used to assess the importance of the variables. The final potential species distribution map had a range of values from 0 to 1 which were regrouped in to three classes of potential habitats viz., 'High potential' (>0.55), 'Moderate potential' (0.38-0.55), 'Less potential' (0.2-0.38).

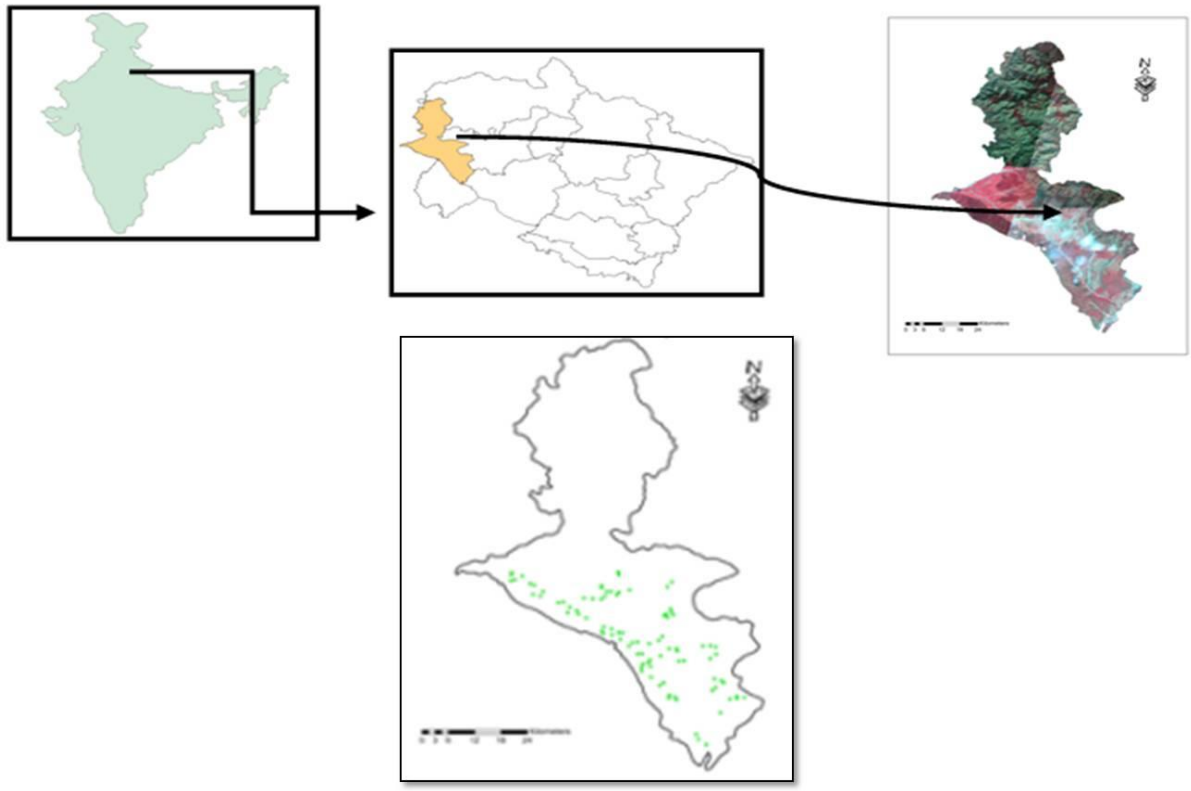

Figure 1: *Study area location map of present study*

3. Results and Discussion

The Jackknife evaluation results indicated forest type, slope, isothermality and meantemperature of driest quarteras main factors influencing *Rauwolfia serpentina* distribution. The percent contribution values given in are only heuristically defined; they depend on the particular path that the Maxent code uses to get to optimal solution. These results were consistent with the Jackknife evaluation. The model output provided satisfactory results with the given set of training and test data, the final model had high accuracy with an AUC value of 88.5. It is important to note that AUC values tend to be lower for species that have broad distribution scope (Mcpherson and Jetz, 2007; Evangelista et al., 2008).

Table 1: *Environmental variables used in the study and their percentage contribution*

Code	Environmental variables	Percent contribution	Permutation importance
Bio1	Annual mean temperature		
Bio2	Mean diurnal range (mean of monthly max. and min. temp.)		
Bio3	Isothermality ((Bio2/Bio7) ×100)	10.9	2.9
Bio4	Temperature seasonality (standard deviation ×100)		
Bio5	Maximum temperature of warmest month		
Bio6	Minimum temperature of coldest month		
Bio7	Temperature annual range (Bio5–Bio6) ◦		
Bio8	Mean temperature of wettest quarter ◦C		
Bio9	Mean temperature of driest quarter	0.9	0.7
Bio10	Mean temperature of warmest quarter		
Bio11	Mean temperature of coldest quarter		
Bio12	Annual precipitation	1.6	1.2
Bio13	Precipitation of wettest period		
Bio14	Precipitation of driest period	0.2	0.9
Bio15	Precipitation seasonality (CV)	0.6	8
Bio16	Precipitation of wettest quarter		
Bio17	Precipitation of driest quarter		
Bio18	Precipitation of warmest quarter		
Bio19	Precipitation of coldest quarter	5	41.9
SLO	Slope	19.9	10.1
Ftype	Forest type	61	34.2

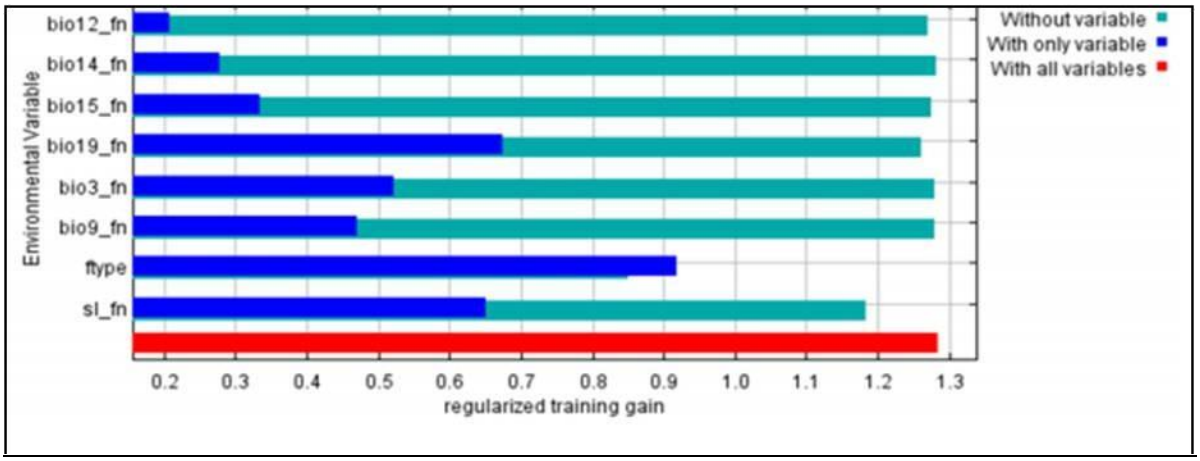

Figure 2: *The Jackknife test for evaluating the relative importance of environmental variables*

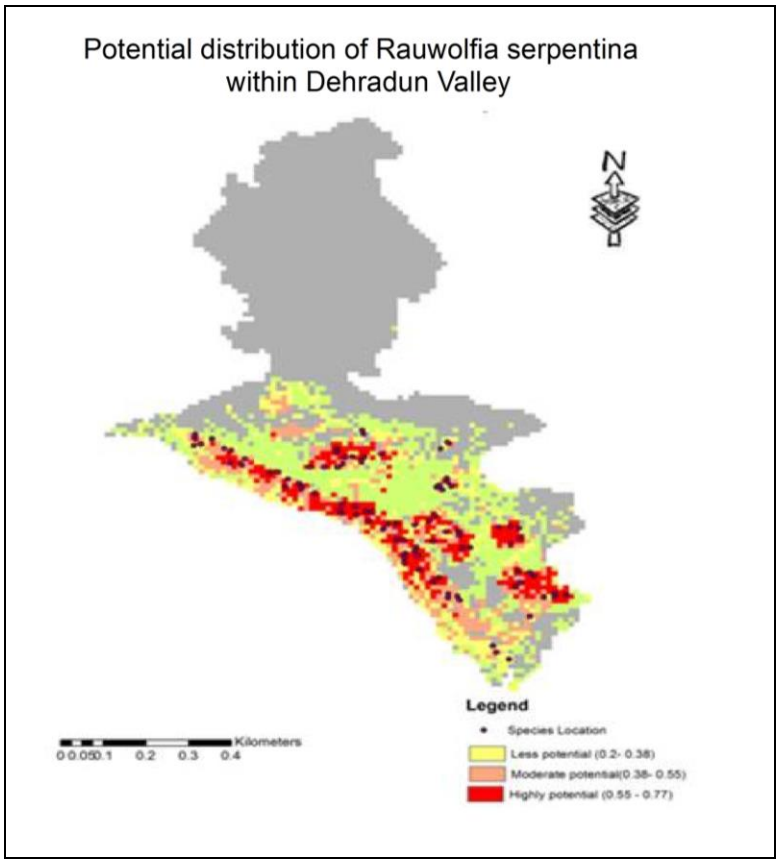

Figure 3: *Predicted potential distribution of Rauwolfia serpentina within dun valley*

As evident from the Figure 2, the eastern part of Dun valley, in general, has higher potential than the western part for *Rauwolfia serpentina*, which could primarily be attributed to the Forest types in this part of the Valley, especially Sal dominated areas. The model results showed that an area of 231.46 km^2 has high potential area. Approximately 254.50 km^2 area showed moderate potential while 234.39 km^2 area showed less potential. Our results support the statement that the predicted potential

distribution areas through Maxent modeling almost always appear as over-estimated compared to realized niche of the species, i.e. the habitat. Since Maxent model considers only niche-based presence data, it predicts the species fundamental niche rather than realized niche (Pearson, 2007; Kumar and Stohlgren, 2009). In reality, a species might have failed to disperse due to geographic barriers, human disturbance or associated competitive species. The method is certainly promising in predicting the potential distribution of other medicinal plant species and can be a valuable tool in species conservation planning and climate change-species distribution studies.

References

Adhikari, D., Barik, S. K. and Upadhaya, K. 2012. Habitat distribution modelling for reintroduction of Ilex khasianaPurk, a critically endangered tree species of northeastern India. *Ecological Engineering,* 40, pp.37-43.

Barik, S. and Adhikari, D. 2011. Predicting geographic distribution of an invasive species Chromolaena odorata L. (King) and HE Robins in Indian subcontinent under climate change scenarios. In: *Invasive alien plants: an ecological appraisal for the Indian subcontinent,* Bhatt, J.R., Singh, J.S., Tripathi, R. S., Singh, S.P. and Kohli, R.K. (Eds.), pp.328.

Corvellec, H. and Hultman, J. 2012. From “less land filling” to “wasting less” Societal narratives, socio-materiality, and organizations. *Journal of Organizational Change Management,* 25(2), pp.297-314.

Elith, J., Phillips, S. J., Hastie, T., Dudík, M., Chee, Y. E. and Yates, C. J. 2011. A statistical explanation of MaxEnt for ecologists. *Diversity and Distributions,* 17(1), pp.43-57.

Evangelista, P. H., Kumar, S., Stohlgren, T. J., Jarnevich, C. S., Crall, A. W., Norman, J. B. and Barnett, D.T. 2008. Modelling invasion for a habitat generalist and a specialist plant species. *Divers Distrib,* 14, pp.808-817.

Ferrier, S., Drielsma, M., Manion, G. and Watson, G. 2002. Extended statistical approaches to modelling spatial pattern in biodiversity in northeast New South Wales. II. Community-level modelling. *Biodiversity and Conservation,* 11(12), pp.2309-2338.

Flory, A. R., Kumar, S., Stohlgren, T. J. and Cryan, P. M. 2012. Environmental conditions associated with bat white nose syndrome mortality in the north-eastern United States. *Journal of Applied Ecology,* 49, pp.680-689.

Franklin, M. N., Mackie, T. T. and Valen, H. 2009. Electoral change: Responses to evolving social and attitudinal structures in Western countries. *ECPR Press - Classics,* pp.490.

Graham, C. H., Ferrier, S., Huettman, F., Moritz, C. and Peterson, A. T. 2004. New developments in museum-based informatics and applications in biodiversity analysis. *Trends in Ecology and Evolution,* 19, pp.497-503.

Graham, I. D., Logan, J., Harrison, M. B., Straus, S. E., Tetroe, J., Caswell, W. and Robinson, N. 2006. Lost in knowledge translation: time for a map? *Journal of Continuing Education in the Health Professions,* 26(1), pp.13-24.

Guisan, A. and Zimmermann, N. E. 2000. Predictive habitat distribution models in ecology. *Ecological Modelling,* 135(2), pp.147-186.

Haines, H. H. 1925. The Botany of Bihar and Orissa. London: Adlard and Son & West Newman Ltd.

Hijmans, R. J., Cameron, S. E., Parra, J. L., Jones, P. G. and Jarvis, A. 2005. Very high resolution interpolated climate surface for global land areas. *International Journal of Climatology,* 25, pp.1965-2198.

Irfan-Ullah, I. and Ruhe, G. 2006. Towards comprehensive release planning for software product lines. *International Workshop on Software Product Management,* Minneapolis, USA, pp. 51-56.

Jaynes, E. T. 1957. Information theory and statistical mechanics. *Physical Review,* 106(4), pp.620.

Kumar, S. and Stohlgren, T. J. 2009. Maxent modeling for predicting suitable habitat for threatened and endangered tree Canacomyrica monticola in New Caledonia. *Journal of Ecology and the Natural Environment,* 1(4), pp.094-098.

Kushwaha, S. P. S. 2011. Remote sensing of invasive alien plant species. In: Bhatt, J. R., Singh, J. S., Tripathi, R. S., Singh, S.P. and Kohli, R.K. (Eds.), Invasive Alien Plants – An Ecological Appraisal For the Indian Sub-continent. *CABI,* Oxfordshire, pp.131-138.

Mcpherson, J. M. and Jetz, W. 2007. Effects of species' ecology on the accuracy of distribution models. *Ecography,* 30, pp.135-151.

Pearson, R. G. 2007. Species' distribution modeling for conservation educators and practitioners. *Synthesis - American Museum of Natural History*, New York, USA, Available from: http://ncep.amnh.org.

Peterson, G. D., Cumming, G. S. and Carpenter, S. R. 2003. Scenario planning: a tool for conservation in an uncertain world. *Conservation Biology,* 17(2), pp.358-366.

Phillips, S. J. and Dudík, M. 2008. Modeling of species distributions with Maxent: new extensions and a comprehensive evaluation. *Ecography,* 31(2), pp.161-175.

Phillips, S. J., Anderson, R. P. and Schapire, R. E. 2006. Maximum entropy modeling of species geographic distributions. *Ecological Modelling,* 190(3), pp.231-259.

Phillips, S. J., Miroslav, D. and Schapire, R. E. 2004. Maxent software for species distribution modeling. Available from: http://cs.princeton.edu/~schapire/Maxent/.

Polak, T. and Saltz, D. 2011. Reintroduction as an ecosystem restoration. *Conservation Biology,* 25(3), pp.424-427.

Saran, S., Joshi, R., Sharma, S., Padalia, H. and Dadhwal, V. K. 2010. Geospatial modelling of brown oak (Quercus semecarpifolia Sm.) habitats in the Kumaun Himalaya under climate change scenario. *Journal of the Indian Society of Remote Sensing,* 38, pp.534-547.

Sastri, B. N. 1990. The Wealth of India: A Dictionary of Indian Raw Materials and Industrial Products; Raw Materials, Vol. II, and Industrial Products, Part II, covering letter "C." *Publications and Information Directorate, Council of Scientific and Industrial Research,* New Delhi, India. pp.427.

Thomas, C. D., Cameron, A., Green, R. E., Bakkenes, M., Beaumont, L. J., Collingham, Y. C. and Hughes, L. 2004. Extinction risk from climate change. *Nature,* 427(6970), pp.145-148.

Thuiller, W., Richardson, D. M., Pysek, P., Midgley, G. F., Hughs, G. O. and Rouget, M. 2005. Niche-based modeling as a tool for predicting the risk of alien plant invasions at a global scale. *Global Change Biology,* 11, pp.2234-2250.

Turner, B. L., Kasperson, R. E., Matson, P. A., McCarthy, J. J., Corell, R. W., Christensen, L. and Polsky, C. 2003. A framework for vulnerability analysis in sustainability science. *Proceedings of the National Academy of Sciences,* 100(14), pp.8074-8079.

Cloud Publications
International Journal of Advanced Remote Sensing and GIS
2017, Volume 6, Issue 1, pp. 2343-2359
ISSN 2320 – 0243, Crossref: 10.23953/cloud.ijarsg.299

Research Article

Monitoring of Agricultural Drought using Satellite based Drought Severity Index over Andhra Pradesh State of India

Chandrasekar K.[1], Lingala Sneha[2], Ramana K.V.[1], Rao P.V.N[1]

[1]National Remote Sensing Centre, Hyderabad, Telangana, India
[2]Jawaharlal Nehru Technological University, Kakinada, Andhra Pradesh, India

Publication Date: 16 August 2017

DOI: https://doi.org/10.23953/cloud.ijarsg.299

Abstract Several indices both conventional and satellite based are used in drought monitoring and assessment. In this study, a satellite derived Drought Severity Index (DSI) was used to monitor and assess the agricultural drought over Andhra Pradesh state, India from 2002 to 2012. The components of DSI are the Normalize Difference Vegetation Index (NDVI) and Evapotranspiration. The NDVI and evapotranspiration products of MODIS were used in this study to derive the DSI. The DSI is expected to capture the drought event that has been reported in the state between 2002 and 2012 and provide a quantitative measure of severity. The analysis showed that the DSI was having a larger variance during June due to the large variation in the onset of monsoon. The DSI variance was low in the predominantly irrigated districts. The spatial cumulative seasonal DSI captured the drought affected districts during the reported drought years. When the seasonal cumulative DSI was correlated with seasonal rainfall, it showed a strong relation with the current month rainfall in the rainfed crop growing districts. The annual DSI showed strong positive correlation with the annual Net Primary Productivity. This study clearly shows that the DSI was able to discern the drought affected regions in the state of Andhra Pradesh, India during the study period.
Keywords *Drought; Drought Severity Index; ET; NDVI; Standardized Vegetation Index*

1. Introduction

Under the changing climate scenario, drought events may become more frequent and severe in nature (Dai et al., 2004). Drought is one of the major natural disasters which impair the food production leading to unemployment, malnutrition, migration, conflicts and environmental degradation. Though prediction of drought is neither accurate nor precise, it is critical to monitor and assess drought through timely and reliable weather information, including seasonal forecasts, to aid decision makers. This information, if properly applied, can reduce the impact of drought and other extreme climate events (Wilhite and Svoboda, 2000). Several indices are used to assess and monitor drought from local to global scale. However due to the multi-disciplinary character of drought, a single unique definition of drought does not exist; but is subject to the domain of interest of the observer (Wilhite and Glantz, 1985; Maracchi and Sivakumar, 2000; Tate and Gustard, 2000). Drought indices may use parameters which are meteorological, hydrological, spectral, agricultural and social in nature. Ideally, a drought index integrates large amounts of data, such as precipitation, snowpack, stream flow and other water supply indicators, to monitor drought severity in a comprehensive framework and to measure how much the climate in a given period has deviated from historically established normal condition

(Narasimhan and Srinivasan, 2005; Mu et al., 2013). The American Meteorological Society (1997) suggests that the time and space processes of supply and demand are the two basic processes that should be included in an objective definition of drought and thus, in the derivation of a drought index (Heim, 2002). Mu et al. (2013) reviewed various drought indices like Palmer Drought Severity Index (PDSI) (Palmer 1965; Alley, 1984), United States Drought Monitor (USDM) (Svoboda, 2002), and Evaporative Drought Index (EDI) among other indices. The relative strengths and weaknesses of these indices were discussed and concluded that most of them were designed to detect meteorological and/or hydrological drought without incorporating vegetation responses into drought. Except the USDM and the EDI which use both reanalysis meteorological data and remotely sensed data (Svoboda et al., 2002; Yao et al., 2010), most drought indices use reanalysis meteorological data that contain substantial uncertainties (Zhao et al., 2006; Chen and Bosilovich, 2007; Gao et al., 2010; Mu et al., 2013). To overcome these limitations, Mu et al. (2013) developed a remotely sensed global Drought Severity Index (DSI). DSI was derived using satellite derive Evapotranspiration (ET), Potential Evapotranspiration (PET) and Normalized Difference Vegetation Index (NDVI) to identify and monitor drought.

In India, organizations like the Central Research Institute for Dry Land Agriculture (CRIDA), Hyderabad, provide information on drought conditions and their mitigation measures during the season. The India Meteorological Department monitors the meteorological parameter while the Central Water Commission provides the latest storage status of the major water bodies of the country. A project called National Agricultural Drought Assessment and Monitoring System (NADAMS), operational since 1989 and presently being carried out by Mahalanobis National Crop Forecast Centre (www.ncfc.gov.in) has been using satellite derived indices like NDVI, Normalized Difference Water Index (NDWI), Vegetation Condition Index (VCI), meteorological, crop and field parameters to provide agricultural drought information in terms of prevalence, severity and persistence at state, district and sub-district level for India. However, development of a unified index for drought severity assessment by integrating data from different sources is an important challenge. Use of a process based indicator like the DSI which describes the actual process taking place on the ground will provide the realistic condition of the crops in the field. Towards this objective the DSI proposed by Mu et al. (2013) was used to monitor the drought condition in the state of Andhra Pradesh, India during the time period of 2002-2012. The DSI will be evaluated on how best it is able to identify the reported drought year between 2002-2012, quantify the severity of drought and address the drought in a near real time basis. It was also envisaged to find the relation between the DSI with the monthly rainfall and Net Primary Productivity over the study area.

1.1. Study Area and Data Used

Study Area

The region chosen for this study is the erstwhile state of Andhra Pradesh in India presently bifurcated into two states namely Andhra Pradesh and Telangana. For this study the two states Andhra Pradesh and Telangana will be called with its erstwhile name of Andhra Pradesh. The Andhra Pradesh state had a total geographical area of 27.44 million hectares. It has a vegetation types ranging from the forested districts in the north to the dry arid districts in the south offering diverse agro-climatic condition. The state gets its major share of rainfall (68.5%) during the four southwest monsoon months (June to September). The southern arid district received as low as 300 mm while the northern forested districts receive over 1000 mm of rainfall during the monsoon. The majority of the crops (65% of the 13.02 million hectare) that are grown during the monsoon season rely on the monsoon rainfall for its sustenance (Mishra, 2005). Almost 45% of the state is prone to drought according to Seth (1998).

This study uses the districts of this state as the study unit which is approximately 4000-5000 km². Some of the major crops grown in the state are paddy, groundnut, cotton, chilli, maize and millets among other crops. Figure 1 shows the study area of the erstwhile state of Andhra Pradesh, India.

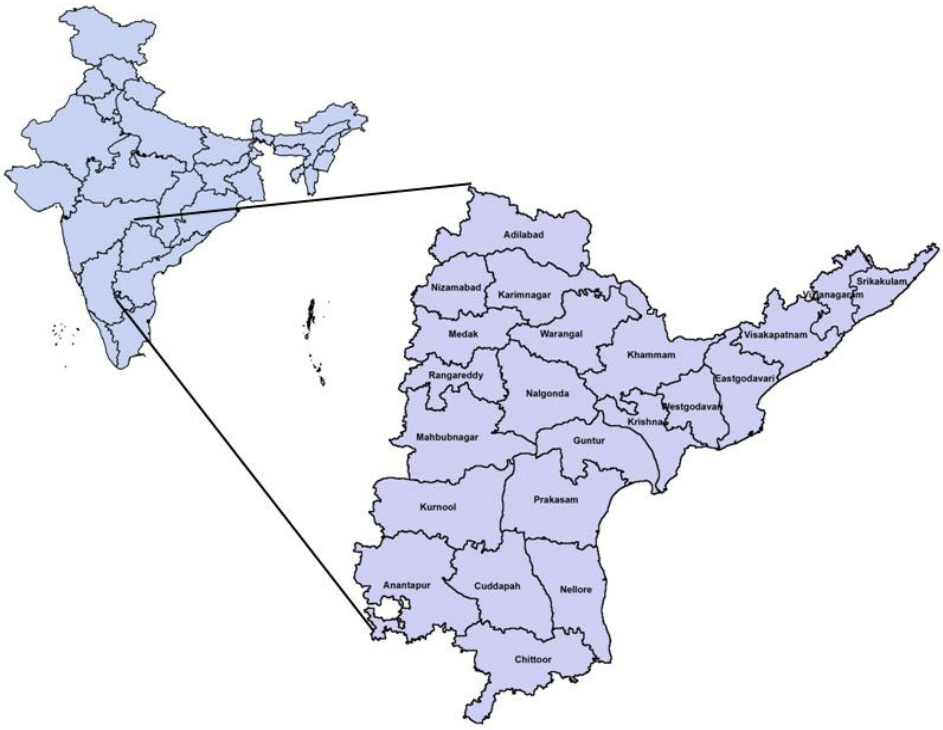

Figure 1: *Study area - the erstwhile state of Andhra Pradesh, India*

1.2. The Normalized Difference Vegetation Index

The Normalized Difference Vegetation Index (NDVI) is the most widely used vegetation index for its long legacy, simplicity and robustness. It has been extensively used for assessing and monitoring vegetation dynamics, biomass production, changes in vegetation conditions and many more (Tucker et al., 1985; Hielkema et al., 1986; Prince and Tucker, 1986; Kogan, 1990). The Moderate Resolution Imaging Spectroradiometer (MODIS) sensor onboard Terra and Aqua satellite has been providing spectral information in 36 spectral bands since 1999 and 2002 respectively. MODIS Vegetation Index 16 day's products at multiple spatial resolutions have been providing consistent spatial and temporal information on vegetation canopy greenness, canopy structure and other biophysical parameters. This study uses the Terra MODIS Vegetation Index (VI) 16 day (MOD13A2) products for its analysis. The theoretical basis, algorithm description, product specification and quality assurance of the MODIS VI product is provided in the MODIS Vegetation Index User Guide (Didan et al., 2015) (http://vip.arizona.edu). The VI products downloaded from LADDS DAAC (https://ladsweb.nascom.nasa.gov) web page were processed using the open source software (QGIS), to derive the NDVI. The cloud contaminated and erroneous pixels were eliminated by using the quality assurance flag of NDVI. The NDVI data from the first fortnight of June 2002 till the second fortnight of April 2013 were used in the analysis.

1.3. Evapotranspiration

The amount of water lost to the atmosphere from the soil surface as evaporation and through vegetation as transpiration combined together is called Evapotranspiration (ET). Evapotranspiration is an important component of the hydrological cycle which is responsible for the mass and heat transfer into the atmosphere. Since the amount of ET depends on the imbalance in the soil-water-atmospheric continuum, it helps in assessing the moisture deficit over a region which in turn will help us in assessing the drought condition. This study uses the MODIS Global Terrestrial ET (MOD 16) products which were derived using the Mu et al.'s improved ET algorithm (2011). The algorithm theoretical basis and the details of the ET product are provided in www.ntsg.umt.edu/project/mod16 web page and also in Mu et al. (2007). Mu et al. (2007, 2011) integrated the Penman-Monteith equation (Monteith, 1965) with the Priestley-Taylor (1972) method to estimate the Potential Evapotranspiration, while the global remotely sensed actual ET was derived using the Penman-Monteith equations. The main input parameter for the Penman-Monteith equations are the meteorological variables, remotely sensed vegetation parameter of Leaf Area Index (LAI) (Myneni et al., 2002), fraction of photo synthetically active radiation (FPAR) (Los et al., 2000). It provides the day and night cumulative ET estimates.

The limitations with the MOD16 products are i) it uses a static MODIS land cover map, ii) wind and precipitation are not used in the calculations of ET, iii) the relative humidity influence on saturated soil and standing water and canopy intercepted water are not considered and iv) the meteorological inputs to this product is coarse. Several studies have attempted the validation of global evapotranspiration product (MOD16) using flux tower and Large Aperture Scintillometer (LAS) measurements (Ramoelo et al., 2014; Tang et al., 2015). The results show that the 8-day MOD16 actual ET product tends to underestimate at higher ET levels and overestimate at low ET levels. Under irrigated condition MOD16 tends to underestimate significantly. Though there are limitations in using MOD16 ET data, it provides a spatial time series data which is readily available for the entire globe for over a decade. Tang et al. (2015) points out that the temporal pattern of ET estimate matches with the LAS and flux tower values. In this study the Moisture Adequacy Index (MAI) which is used in the derivation of Drought Severity Index (DSI) is the ratio of actual ET to Potential ET. This ratio helps in cancelling out the common error in actual ET and PET thus reducing the uncertainty in the MOD16 product for the use in DSI.

1.4. The Gross Primary Production and Net Primary Production

Primary productivity is defined as the rate at which the sun's energy is transformed into biomass through plants photosynthesis or chemosynthesis. The primary productivity can be Gross Primary Productivity (GPP) which is the total amount energy converted as biomass which includes the energy consumed by the plant for respiration while the Net Primary Productivity (NPP) is the net amount of energy consumed by the plant resulting in dry plant biomass. NPP gives an idea on the amount of energy that is consumed by the plant resulting in the carbon dioxide assimilation. It represents the availability of carbon in the form of plant material for consumption as food, fuel and feed (Abdi et al., 2014). In this study the MODIS Gross Primary Production (GPP) and Net Primary Production (NPP) product (MOD17) were used which provides estimates of vegetation GPP and NPP at consistent spatial and temporal resolutions for global vegetated land areas (Running et al., 1999). The algorithm theoretical basis and the details of the MOD17 GPP/NPP product can be had from 'User's Guide - Daily GPP and Annual NPP (MOD17A2/A3) Products, NASA Earth Observing System MODIS Land Algorithm (Running and Zhao, 2015) (http://www.ntsg.umt.edu/sites/ntsg.umt.edu/files/modis/MOD17UsersGuide2015_v3.pdf). The MOD17 GPP/NPP product has been widely validated and applied to regional and global scales (Turner et al., 2005, 2006; Heinsch et al., 2006; Zhao and Running, 2010). It is a known fact that during drought year the NPP is expected to reduce due to

abiotic stresses. The MOD17 GPP/NPP product was used in this study for comparison against the DSI as a surrogate measure of vegetation activity and associated NPP response to different drought scenarios during various time periods.

1.5. Rainfall Data

Rainfall forms an important input for any vegetation and drought studies. In this study, the Climate Prediction Centre's (CPC) RFE2.0 daily accumulation rainfall estimates product was used, which was downloaded from its FTP site (ftp://ftp.cpc.ncep.noaa.gov/fews/S.Asia /data/). It provides the southern Asian region daily rainfall estimates in millimeters with a resolution of 0.1° x 0.1°. The inputs for the rainfall estimate include Global Telecommunication System (GTS) station data, as well as geostationary infrared cloud top temperature fields and polar orbiting satellite precipitation estimate data from SSM/I and AMSU-B microwave sensors. All satellite data are first combined using a maximum likelihood estimation method, and then GTS station data is used to remove bias. Warm cloud precipitation estimates are not included in RFE 2.0 estimates (www.cpc.ncep.noaa.gov/ products/fews/RFE2.0_desc.shtml). The data was provided in binary format which was imported using commercial image processing software and rainfall data was extracted for the Andhra Pradesh state and its districts which were used in the analysis.

1.6. The Drought Severity Index

The remotely sensed Drought Severity Index (DSI) has two components namely 1. The vegetation condition component which helps in detecting the vegetation health and vigour and 2. The evapotranspiration deficit component which helps in detecting the moisture stress in the crop. Since the causative and the manifestation indicators are combined in a single index called the DSI, it clearly helps in addressing the drought holistically.

For the vegetation health/vigour monitoring purpose, MODIS Vegetation Index has been used. The long term VI data (2002-2012) was used to drive the standardized NDVI (Z_{NDVI}) also called the Standardized Vegetation Index (SVI) for each composite period (monthly) during the classified growing season at each grid cell which is given in equation 1.

$$Z_{NDVI} = \frac{\mathrm{NDVIi} - \overline{\mathrm{NDVI}}}{\sigma_{NDVI}} \quad \ldots (1)$$

The SVI allows visualization of relative vegetation greenness in terms of 'greenness probability' through the use of a probability estimate, which suggests comparison over time periods that are longer than the archival imagery. The value of the SVI ranges between zero and one ($0 < SVI < 1$). Zero is the baseline condition in which a pixel NDVI value is lower than all possible NDVI values for that week in other years and *vice versa* (Peters et al., 2002).

Evapotranspiration has a commanding roll in the transportation of energy and mass into the atmosphere. The rate of ET is actually controlled by the vapour pressure deficit in the atmosphere and the moisture availability in the soil water reservoir. When the supply component of soil water is unlimited the ET takes place at its potential rate which is known as the Potential Evapotranspiration (PET). Hence, the ratio of the ET versus the PET can indicate the amount of water stress that exists in the region. This ratio of actual ET to PET is also called the Moisture Adequacy Index (MAI) (Drought Manual, 2009) which is expressed in percentage. MAI is critical in ascertaining the agricultural drought condition. For each monthly period, the ratio of actual ET to PET is derived as given in equation 2.

$$\text{MAI} = \frac{\text{ET}}{\text{PET}} \quad \ldots (2)$$

The temporal standard deviation of MAI (σ_{MAI}) and MAI average (MAI) were then computed on a grid cell basis over the available satellite record (2002 - 2012). The standardized MAI (Z_{MAI}) was then calculated using equation 3.

$$Z_{MAI} = \frac{\text{MAIi} - \overline{\text{MAI}}}{\sigma_{MAI}} \quad \ldots (3)$$

The standardized NDVI (Z_{NDVI}) and standardized MAI (Z_{MAI}) were summed as given in equation 4 to give a Z value.

$$Z = Z_{MAI} + Z_{NDVI} \ldots (4)$$

The standardization of the Z value would provide the remotely sensed DSI as given in equation 5.

$$DSI = \frac{Z - \overline{Z}}{\sigma} \quad \ldots (5)$$

The DSI ranges from unlimited negative value to positive values. Negative DSI indicating drier conditions while positive DSI indicating wetter conditions. It is always suggested that to have sufficiently longer database so that the DSI derived represents the realistic ground conditions.

2. Results and Discussion

2.1. Variance of the DSI in the Irrigated and Rainfed Crop Growing Districts

Figure 2a and 2b shows the DSI values during the Kharif season (May to November) plotted for the years from 2002 to 2012 for few predominantly irrigated crop growing districts (*viz* East and West Godavari, Krishna and Guntur) and predominantly rainfed crop growing districts (*viz.* Ananthpur, Prakasam, Mahabubnagar and Kurnool) of Andhra Pradesh state respectively. The DSI usually ranges between -1.5 to +1.5 where -1.5 indicates extreme drought while +1.5 indicates extremely wet conditions. It can be observed from Figure 2a and 2b, that only during the month of June the DSI varied widely between -1.5 to +1.5 under both irrigated crop and rainfed crop growing districts. The variation of the DSI between maximum and minimum was much less in all the remaining months. The large variations of the DSI in the month of June can be attributed to the variation in the onset of monsoon and the variations in the amount of rainfall received during this month. Table 1 gives the monsoon onset date and rainfall deviation of the three meteorological sub-divisions of Andhra Pradesh along with the DSI values of the districts under study. The years 2003, 2009, 2011 and 2012 showed negative DSI deviation in all the districts. Though the rainfall received in June 2003 was normal, the negative deviation in 2003 was due to the carryover effect of the huge deficit in the previous year's (2002) seasonal rainfall which resulted in drought that year. The previous year's (2002) seasonal rainfall deviation in Coastal Andhra, Telangana and Rayalaseema were -25%, -22 and -33 respectively. In the years 2009, 2011 and 2012, the majority of the state experienced poor rainfall in June resulting in negative DSI. During other months of the season the dynamic range of the DSI was not as large as observed during June. It was ranging between -0.5 to +0.5. The variation was the least during the month of August followed by July and September. The variation demonstrates that the DSI is sensitive to the rainfall during these months.

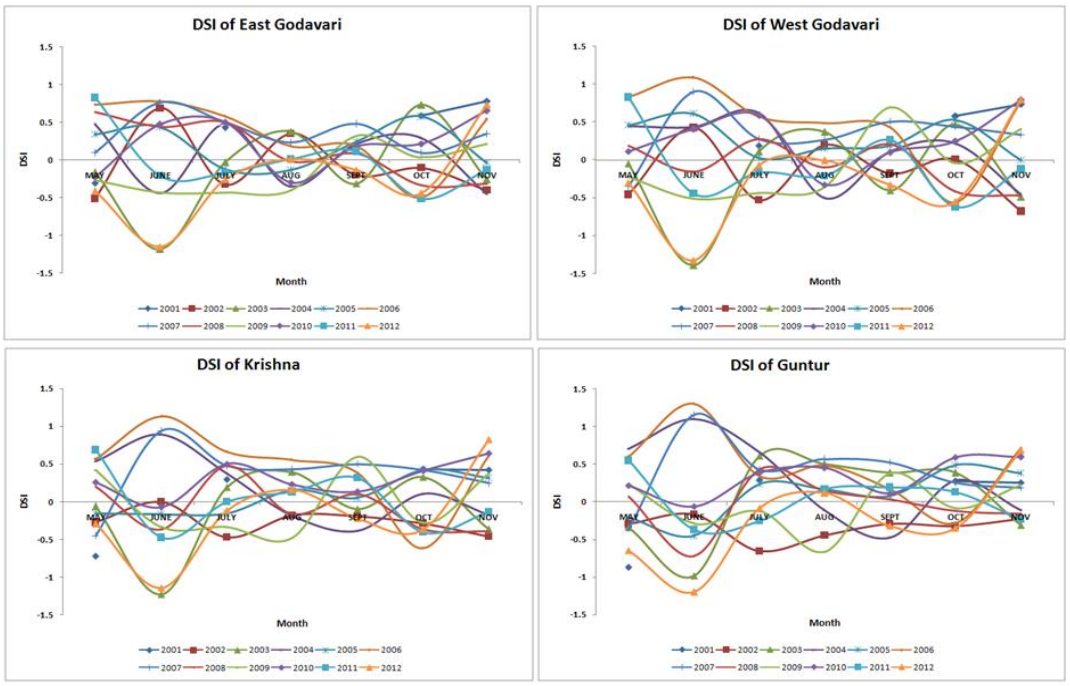

Figure 2a:*The DSI during Kharif season from 2001-2012 for predominantly irrigated crop growing districts*

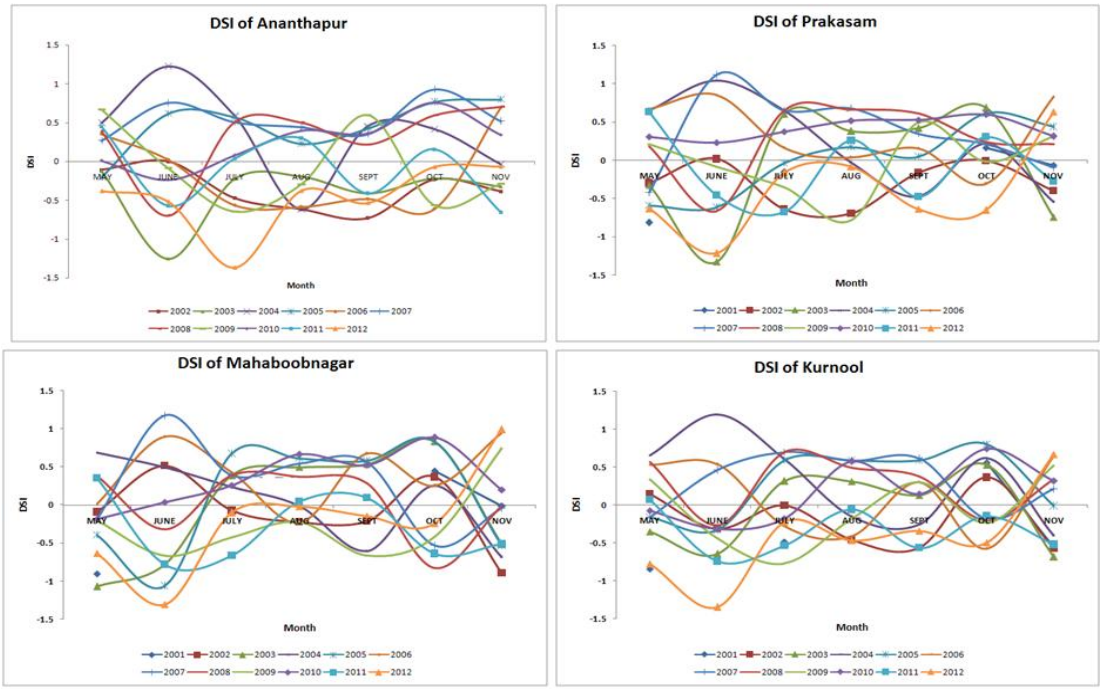

Figure 2b: *The DSI during Kharif season from 2001-2012 for predominantly irrigated crop growing districts*

Figure 3 shows the monthly variance of the DSI, for the typical irrigated and rainfed crop growing districts of Andhra Pradesh during 2002-2012. It can be observed that the variance of the DSI was the highest during the month of June in both the irrigated and rainfed crop districts. In the irrigated crop growing districts the variance of DSI was low in the month of July, August and September in the Kharif

season. During Rabi cropping season the variance was low in December, January and February. The values of variance among districts were also very close during these periods. The variance of the DSI was high during the month of June due to the variation in the onset and amount of monsoon rainfall. During the months of October and November, which is the transition period between the Kharif and Rabi cropping seasons, the variance increased. The harvest of the Kharif crop takes place during these months. Any staggering during the sowing month will also reflect in the harvesting months and hence the higher variance in October and November. The variance of the DSI was also high during the summer months of March, April and May when there is a large uncertainty in rainfall and crops.

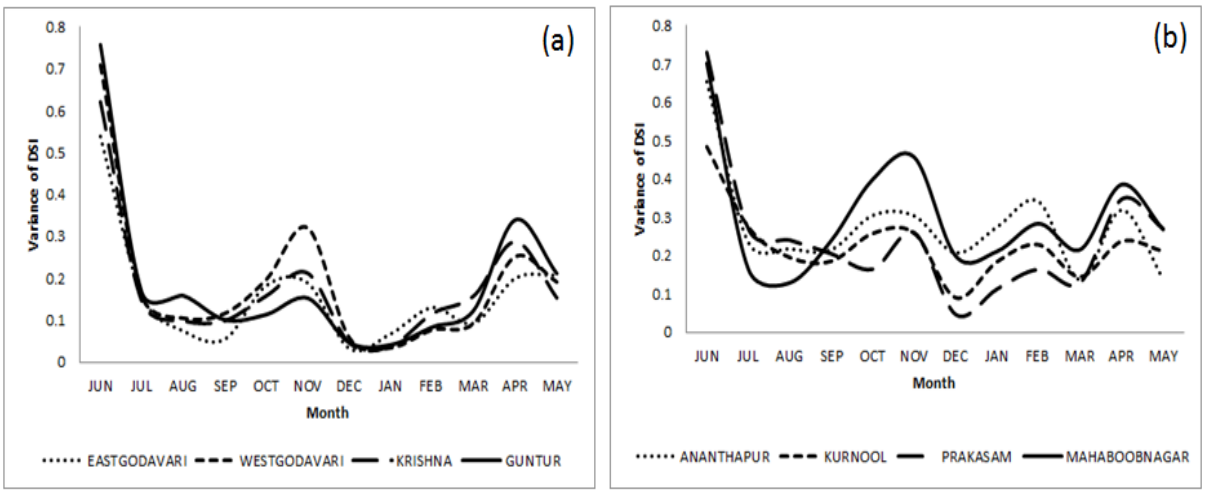

Figure 3: *The variance of the DSI during 2002-2012 for (a) irrigated crop growing district and (b) rainfed crop growing districts*

Table 1: *The monsoon onset dates, rainfall deviations and the DSI during June month for few typical districts*

Year	Monsoon onset day over Andhra Pradesh	Rainfall deviation during June over Met-sub divisions of AP			District average DSI during June							
		Rayala seema	Telangana	Coastal Andhra	East Godavari	West Godavari	Krishna	Guntur	Mahabubnagar	Kurnool	Prakasam	Ananthpur
2002	10th June	31	2	7	0.687	0.424	-0.002	-0.171	0.517	-0.312	0.017	-0.003
2003	15th June	20	-11	-5	-1.183	-1.393	-1.225	-0.983	-0.782	-0.645	-1.330	-1.255
2004	10th June	-53	-55	9	-0.437	0.436	0.894	1.102	0.499	1.196	1.045	1.222
2005	21st June	-1	-26	-22	0.438	0.609	-0.166	-0.452	-1.061	-0.329	-0.614	0.615
2006	24th June	57	-24	15	0.774	1.089	1.131	1.299	0.898	0.538	0.857	0.024
2007	14th June	285	26	159	0.762	0.902	0.940	1.156	1.176	0.459	1.118	0.757
2008	10th June	-35	-8	-16	0.440	-0.155	-0.368	-0.719	-0.315	-0.269	-0.662	-0.697
2009	26th June	5	-52	-46	-0.428	-0.514	-0.333	-0.289	-0.664	-0.437	-0.082	-0.086
2010	14th June	57	-24	39	0.469	0.405	-0.071	-0.061	0.036	-0.316	0.230	-0.237
2011	16th June	-24	-41	-27	-0.210	-0.447	-0.474	-0.372	-0.780	-0.742	-0.457	-0.572
2012	18th June	-48	-14	-22	-1.146	-1.327	-1.144	-1.199	-1.309	-1.347	-1.216	-1.369

The rainfed crop growing districts also showed larger variance in the DSI during the months of June, October, and November and during summer months. The low variance was observed in July, August and September during Kharif, and in December and January during Rabi. It is clearly seen that the coherence of variance values among districts observed during low variance months in irrigated crop growing districts was not observed in the rainfed crop growing districts. There was larger variation of

variance among the district throughout the season. This analysis demonstrates that the DSI is sensitive to the variations in the onset of monsoon and the amount of rainfall received during each month, which results in variations in the NDVI and the evapotranspiration. It also clearly distinguishes between the irrigated crop growing districts which has lower DSI variance and rainfed crop growing districts by registering larger variance during the cropping season.

2.2. Response of the DSI to Rainfall

Since the DSI was found to be sensitive to the onset of monsoon rainfall and had a greater variance in the rainfed crop growing districts, it was appropriate to establish the strength of relationship between the rainfall and the DSI. A correlation analysis was carried out between the rainfall and the DSI from the year 2002 to 2012. Table 2 shows the district wise correlation of the DSI to the rainfall of the current month and the previous month. It was observed that the DSI had a higher correlation with the current month rainfall when compared with the previous month rainfall. The SVI which is one of the two components of the DSI is a function of the NDVI. It is proven that the NDVI as a standalone index has a lagged response to rainfall. In a study over Andhra Pradesh on a satellite based NDVI response to rainfall, the NDVI lags rainfall by two months in most of the districts (Chandrasekar et al., 2006).

Table 2: *Correlation between DSI vs current and one month lagged rainfall*

S. No.	Districts	Correlation coefficient		Percent irrigated cropped area
		Current Rainfall	One month Lag	
1	Adilabad	0.711	0.167	17.94
2	Ananthpur	0.791	0.324	15.93
3	Chittoor	0.717	0.143	47.51
4	Cuddapah	0.757	0.000	41.80
5	East Godavari	0.528	0.127	60.35
6	Guntur	0.488	0.295	63.79
7	Karimnagar	0.744	0.153	83.20
8	Khammam	0.691	0.163	47.77
9	Krishna	0.600	0.392	51.05
10	Kurnool	0.777	0.041	29.79
11	Mahabubnagar	0.724	0.315	38.73
12	Medak	0.745	0.298	43.24
13	Nalgonda	0.643	0.292	61.13
14	Nellore	0.629	0.061	78.98
15	Nizamabad	0.757	0.138	88.04
16	Prakasam	0.623	0.144	36.85
17	Rangareddy	0.681	0.407	41.19
18	Srikakulam	0.646	-0.102	50.33
19	Vishakhapatnam	0.643	0.094	39.98
20	Vizianagaram	0.791	0.050	44.18
21	Warangal	0.745	0.160	72.03
22	West Godavari	0.550	0.338	85.94

However, the SVI is an estimate of the ‘probability of occurrence’ of the present vegetation condition. Peters et al. (2002) in a study over the Great Plains states from North Dakota to Texas compared the SVI with the US Drought Monitor (DM) outputs and found that the SVI reflects short-term vegetative response to weather conditions while the DM maps show both short term and long-term drought conditions. The SVI map will show areas of relatively good or poor vegetation status and will show

changes more quickly than the DM maps. This could be the reason for the immediate response of the DSI to rainfall despite having the NDVI as a component. The highly irrigated delta districts of Guntur (r=0.488), Krishna (r=0.60), East Godavari (r=0.528) and West Godavari (r=0.55) were having low correlation coefficients. Since these delta districts are in the tail reach of the river basin, the reservoirs which supply irrigation water get filled up with a lag. Because of this the irrigated crop calendars in these districts have a lag with monsoon rainfall and hence the poor relation with rainfall.

Figure 4 shows the cumulative DSI (June to November) of the state of Andhra Pradesh from 2002 to 2012. It can be observed from the Figure 4 that the DSI was negative in most of the districts of the state in the years 2002, 2003, 2009, 2011 and 2012. Based on the analysis of historic rainfall it was found that the years 2002, 2003, 2009, 2011 and 2012 were meteorological drought years with deficient rainfall. In all the other years the DSI was positive if the districts had experienced normal to excess rainfall.

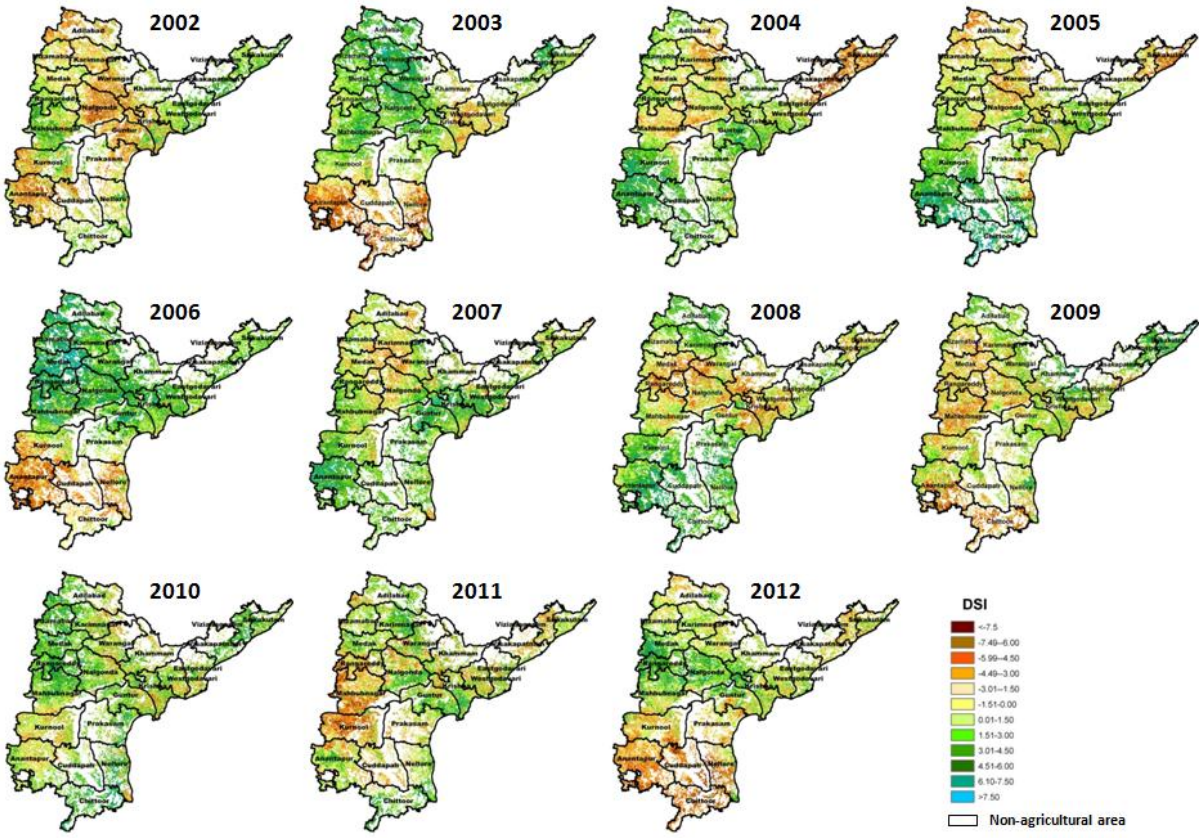

Figure 4: *Cumulative DSI (Jun-Nov) of Kharif cropping season in the state of Andhra Pradesh*

The district average cumulative DSI was extracted for each district for all the years under study and was plotted against the district cumulative rainfall of the corresponding period. It can be observed from Figure 5a & 5b that whenever there is deficient cumulative rainfall during the season there is a negative DSI and vice versa. The conformity between the positive or negative cumulative rainfall events to the positive or negative cumulative DSI respectively is more pronounced in the rainfed crop growing districts (Figure 5b) rather than in the irrigated crop growing districts (Figure 5a). This clearly brings out that the DSI is sensitive to the rainfall events.

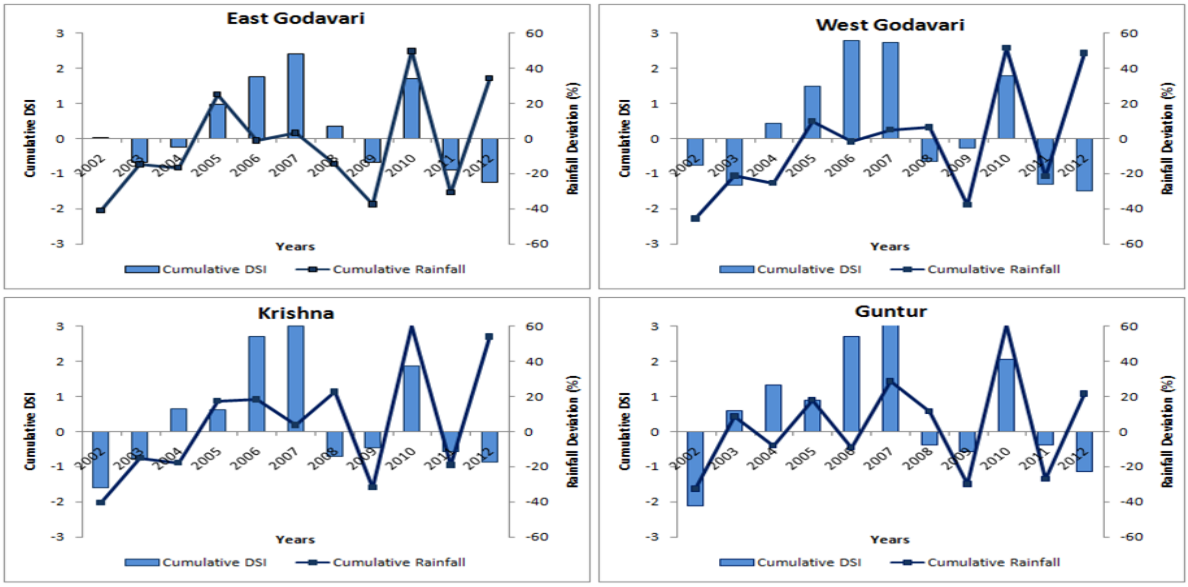

Figure 5a: *Cumulative rainfall plotted against cumulative DSI during Kharif cropping season (Jun-Nov) in irrigated crop growing districts*

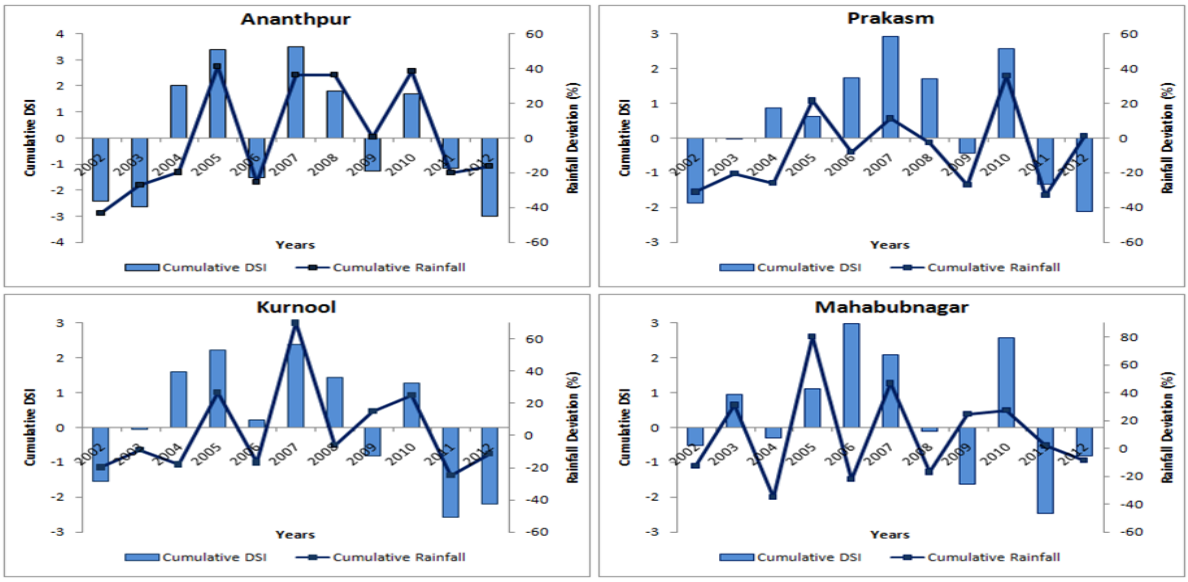

Figure 5b: *Cumulative rainfall plotted against cumulative DSI during Kharif cropping season (Jun-Nov) in rainfed crop growing districts*

2.3. Relation between the DSI and the NPP

The Net Primary Productivity (NPP) refers to the production of organic compounds from atmospheric or aquatic carbon dioxide (CO_2) by plants, principally through the process of photosynthesis (photosynthesis minus autotrophic respiration) (Pei et al., 2013). Studies by Zhao and Running (2010) showed that large-scale drought events have reduced the global NPP. Xiao et al. (2009) have found that most of the drought events which occurred in China had reduced the NPP and the Net Ecosystem Productivity (NEP) in large parts of the drought affected areas. Extreme droughts can impact the terrestrial productivity in a significant way and can reduce the sink strength at sub-continental scale

(Ciais et al., 2005; Reichstein et al., 2007; van der Molen et al., 2011). Since the NPP is directly related to drought, it was found appropriate to find the relation between the DSI and the NPP over the study area. This study used the MOD17 GPP/NPP product as a surrogate measure of vegetation activity/productivity and associated the NPP response to drought, for comparison against the DSI. The DSI and the NPP results should be correlated, especially for water supply-constrained regions (Nemani et al., 2003) through vegetation moisture constraints on canopy transpiration; net photosynthesis and CO_2 exchange (Mu et al. 2013).

Figure 6a and 6b shows the plot of the annual DSI along with the annual NPP of few typical districts of the study area. It can be observed that the DSI closely followed the annual NPP for all the years except 2011. The DSI was having low negative values during 2002, 2003, 2009 and 2012 and the annual NPP was also low during these years compared to its mean for each district. The annual NPP during a good monsoon year was above 0.7 PgC/year for the irrigated crop growing districts while it was around 0.5 PgC/yr for the rainfed crop growing districts. The higher annual DSI did not always result in higher NPP on the contrary lower negative annual DSI consistently resulted in lower annual NPP irrespective of whether it was an irrigated or rainfed crop growing district.

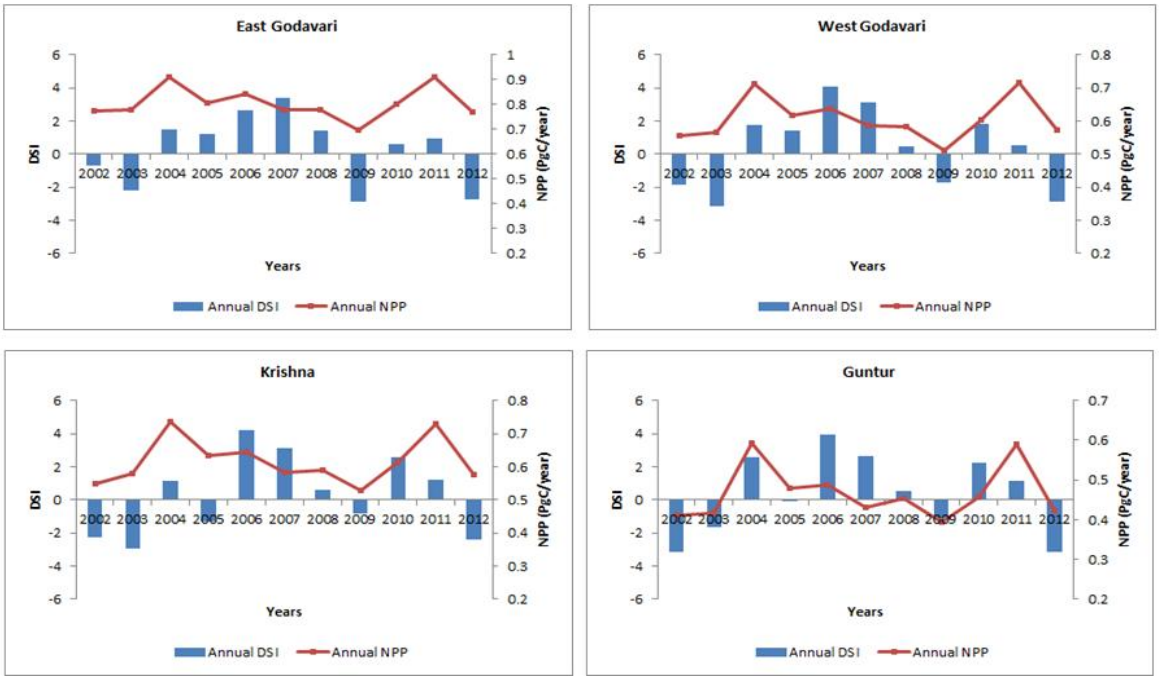

Figure 6a:*Annual DSI and corresponding NPP in irrigated crop growing districts of Andhra Pradesh*

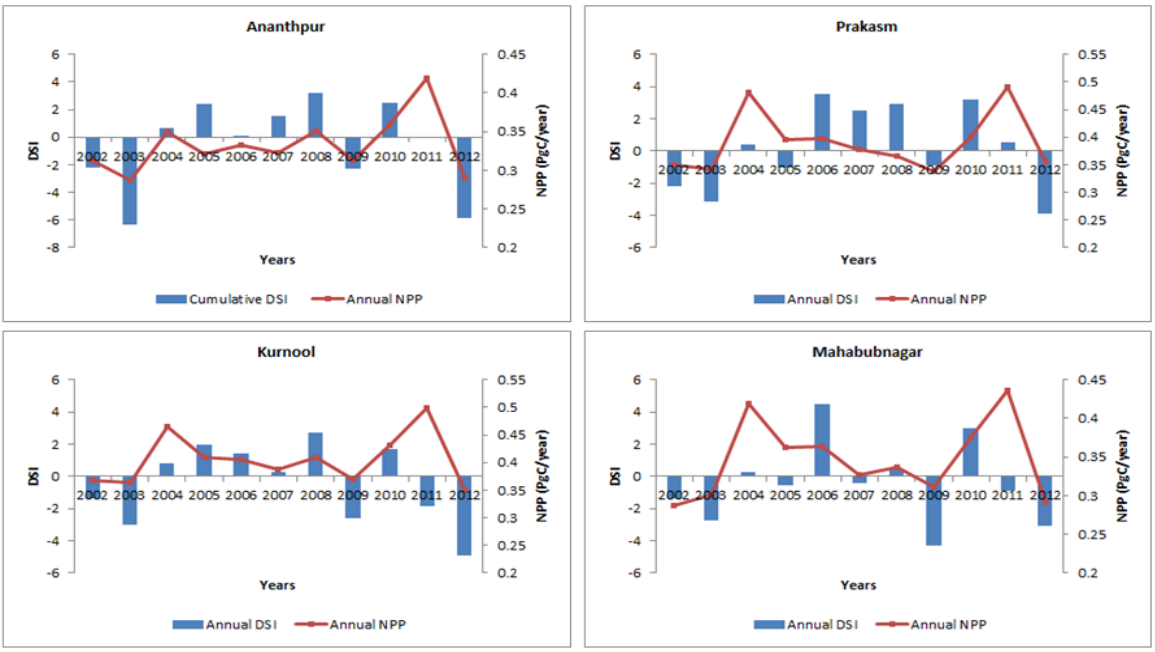

Figure 6b: *Annual DSI and corresponding NPP in rainfed crop growing districts of Andhra Pradesh*

Table 3 shows the correlation coefficient of the annual DSI against the annual NPP. It can be observed that most of the districts were having strong relation between the DSI and the NPP. The correlation coefficient was the highest in the districts of Ananthpur (0.88), Khammam (0.78), Kurnool (0.77), Adilabad (0.75), Rangareddy (0.74), Vizianagaram (0.74), Medak (0.73) and Chittoor (0.72). Majority of the cropped area in these districts are rainfed crop as the percent irrigated cropped area was less than 50% of the total cropped area (Table 3). The low correlation coefficient was observed in the districts of Prakasam (0.39) and Nellore (0.46) as these two districts are predominantly northeast monsoon (October to December) dependent districts. The DSI has also captured all the reported drought years which are 2002, 2003, 2009 and 2012. The DSI recorded the negative values in all these years in all these districts. This clearly indicates that the DSI was able to discern the drought year very clearly in the state of Andhra Pradesh.

Table 3: *Correlation coefficient of annual DSI versus annual NPP*

S. No.	Districts	NPP	% Irrigated cropped area
1	Adilabad	0.75	17.94
2	Ananthpur	0.88	15.93
3	Chittoor	0.72	47.51
4	Cuddapah	0.65	41.80
5	East Godavari	0.62	60.35
6	Guntur	0.62	63.79
7	Karimnagar	0.51	83.20
8	Khammam	0.78	47.77
9	Krishna	0.42	51.05
10	Kurnool	0.77	29.79
11	Mahabubnagar	0.65	38.73
12	Medak	0.73	43.24
13	Nalgonda	0.82	61.13

14	Nellore	0.46	78.98
15	Nizamabad	0.69	88.04
16	Prakasam	0.39	36.85
17	Rangareddy	0.74	41.19
18	Srikakulam	0.66	50.33
19	Vishakhapatnam	0.63	39.98
20	Vizianagaram	0.74	44.18
21	Warangal	0.69	72.03
22	West Godavari	0.62	85.94

3. Conclusions

The DSI is a function of standardized ratio of ET to PET and standardized NDVI. This enables the DSI to be sensitive to water availability and also the vegetation stress condition in the region. The negative DSI values represent drier than normal conditions and positive values represent relatively wet conditions. The spatial average monthly DSI for each year was plotted for each district. It was observed that the dynamic range was large in the month of June. The variance plot showed that in the month of June, the DSI was having larger variance. The variance was also high during the transition period between two cropping seasons and during summer. It was also observed that the variance was low in the predominantly irrigated crop growing districts compared to the rainfed crop growing districts. The spatial pattern of the cumulative seasonal DSI clearly captured the drought affected districts during the reported drought years. When the seasonal cumulative DSI was correlated with the seasonal rainfall, the DSI showed a very strong relation with the current month rainfall in all the districts. It was also observed that in delta districts with predominant irrigated crop, the DSI vs rainfall relation was poor as the delayed crop calendar in the irrigation command does not synchronize with the rainfall distribution during the cropping season. The Net Primary Productivity (NPP) of a region gets greatly reduced due to the incidents of drought. In this study the MOD17 GPP/NPP product was used as a surrogate measure of vegetation activity/productivity and associated the NPP response to drought, for comparison against the DSI. When the annual DSI was plotted along with the annual NPP, it was observed that the DSI co-varied with the NPP in all the years and study. It also captured all the reported drought years by recording negative values during those years. When correlated with the NPP, most of the district showed very strong relation with the DSI. This study over Andhra Pradesh state of India reveals that the DSI could discern the problem area within the time scale considered. The DSI was able to provide a quantitative degree of severity of the drought in a region and hence DSI can be one of the important drought indicators for early assessment of drought.

Acknowledgements

The authors would like to place on record their immense gratitude to Dr. Y.V.N. Krishna Murthy, Director, National Remote Sensing Centre (NRSC), ISRO, Hyderabad for his inspiring guidance and encouragement. Grateful thanks also go to all my colleagues and the administrative staffs for their support and cooperation.

References

Abdi, A. M., Seaquist, J., Tenenbaum, D. E., Eklundh, L. and Ardö, J. 2014. The supply and demand of net primary production in the Sahel. *Environmental Research Letter*, 9, pp.1-11.

Alley, W. M. 1984. The drought severity index: Limitations and assumptions. *Journal of Climate and Applied Meteorology*, 23, pp.1100-1109.

American Meteorological Society. 1997. Meteorological drought - Policy statement. *Bulletin of American Meteorological Society*, 78, pp.847-849.

Chandrasekar, K., Sesha Sai, M. V. R., Jeyaseelan, A. T., Dwivedi, R. S. and Roy P. S. 2006. Vegetation response to rainfall as monitored by NOAA-AVHRR. *Current Science*, 91, pp.1626-1633.

Chen, J. and Bosilovich, M. J. 2007. Hydrological variability and trends in global reanalyses. Conference on Climate Variability and Change, San Antonio, USA. Available from: https://ams.confex.com/ams/87ANNUAL/techprogram/paper_119754.

Ciais, P., Reichstein, M., Viovy, N., Garnier, A., Ogee, J., Allard, V., Aubinet, M., Buchmann, N., Bernhofer, C. and Carrara, A. 2005. Europe-wide reduction in primary productivity caused by the heat and drought in 2003. *Nature*, 437, pp.529-533.

Dai, A., Trenberth, K. E. and Qian, T. 2004. A global data set of palmer drought severity index for 1870-2002: relationship with soil moisture and effects of surface warming. *Journal of Hydrometeorology*, 5, pp.1117-1130.

Didan, K., Munoz, A. B., Solano, R. and Huete, A. 2015. MODIS Vegetation Index User's Guide. Vegetation Index and Phenology Lab. The University of Arizona. Available from: https://vip.arizona.edu/documents/MODIS/MODIS_VI_UsersGuide_June_2015_C6.pdf.

Manual for drought management. 2009. Department of Agriculture and Cooperation, Ministry of Agriculture. *Government of India,* New Delhi, India.

Gao, H., Tang, Q., Ferguson, C. R., Wood, E. F. and Lettenmaier, E .F. 2010. Estimating the water budget of major U.S. river basins via remote sensing. *International Journal of Remote Sensing*, 31, pp.3955-3978.

Heim, R. R. 2002. A Review of Twentieth Century Drought Indices Used in the United States. *Bulletin of American Meteorological Society*, pp.1149-1165.

Heinsch, F. A., Zhao, M. and Running, S. W. 2006. Evaluation of remote sensing based terrestrial productivity from MODIS using regional tower eddy flux network observations. *IEEE Transactions on Geoscience and Remote Sensing*, 44, pp.1908-1925.

Hielkema, J. U., Prince, S.D. and Astle, W. L. 1986. Rainfall and vegetation monitoring in the Savanna zone of the Democratic Republic of Sudan using the NOAA-AVHRR. *International Journal of Remote Sensing*, 7, pp.1499-1514.

Kogan, F. N. 1990. Remote sensing of weather impacts on vegetation on non-homogeneous areas. *International Journal of Remote Sensing*, 11, pp.1405-1419.

Los, S. O., Collatz, G. J., Sellers, P. J., Malmstro, C. M., Pollack, N. H., Defries, R. S., Bounoua, L., Parris, M. T., Tucker, C. J. and Dazlichi, D.A. 2000. A Global 9-yr Biophysical Land Surface Dataset from NOAA AVHRR Data. *Journal of Hydrometeorology*, 1, pp.183-199.

Maracch, G. and Sivakumar, M. V. K. 2000. Handbook of GIS Applications in Agrometeorology. *World Meteorological Organization,* Geneva, Switzerland.

Mishra, P. K. 2005. Guidelines for rainfed production system and management. Drought Management. Sharma, K. D. and Ramasastri, K. S. ed. *Allied Publishers Private Limited,* pp.387-398.

Monteith, J. L. 1965. Evaporation and Environment. 19th Symposia of the Society for Experimental Biology. *University Press, Cambridge,* 19, pp.205-234.

Mu, Q., Zhao, M. Kimball, J. S., McDowel, N. G. and Running, S.W. 2013. A Remotely sensed global terrestrial drought severity index. *Bulletin of the American Meteorological Society,* 94, pp.83-98.

Mu, Q., Heinsch, F. A., Zhao, M. and Running, S. W. 2007. Development of a global evapotranspiration algorithm based on MODIS and global meteorology data. *Remote Sensing of Environment*,111, pp.519-536.

Mu, Q., Zhao, M. and Running, S. W. 2011. Improvements to a MODIS global terrestrial evapotranspiration algorithm. *Remote Sensing of Environment*, 115, pp.1781-1800.

Myneni, R. B., Hoffman, S., Knyazikhin, Y., Privette, J. L., Glassy, J. and Tian, Y. 2002. Global products of vegetation leaf area and fraction absorbed PAR from year one of MODIS data. *Remote Sensing of Environment*, 83, pp.214-231**.**

Narasimhan, B. and Srinivasan, R. 2005. Development and evaluation of soil moisture deficit index (SMDI) and evapotranspiration deficit index (ETDI) for agricultural drought monitoring. *Agriculture and Forest Meteorology*, 133, pp.69-88.

Nemani, R. R., Keeling, C. D., Hashimoto, H., Jolly, W. M., Piper, S. C., Tucker, C. J., Myneni, R. B. and Running, S. W. 2003. Climate-driven increases in global terrestrial net primary production from 1982 to 1999. *Science,* 300, pp.1560-1563.

Palmer, W. C. 1965. Meteorological drought. U.S. *Weather Bureau Research Paper,* 45, p.65.

Pei, F. L. X, Liu, X. and Lao, C. 2013. Assessing the impact of drought on net primary productivity in China. *Journal of Environmental Management,* 114, pp.362-371.

Peters, A. J., Elizabeth, A., Shea, W., Ji, L., Vliia, A., Hayes, M. and Svoboda, M. D. 2002. Drought Monitoring with NDVI-Based Standardized Vegetation Index. *Photogrammetric Engineering and Remote Sensing*, 68, pp.71-75.

Priestley, C. H. B. and Taylor, R. J. 1972. On the assessment of surface heat flux and evaporation using large scale parameters. *Monthly Weather Review,* 100, pp.81-92.

Prince, S. D. and Tucker, C. J. 1986. Satellite remote sensing of rangelands in Botswana. *International Journal of Remote Sensing*, 7, pp.1555-1570.

Ramoelo, A., Majozi, N., Mathieu, R., Jovanovic, N., Nickless, A. and Dzikiti, S. 2014. Validation of global evapotranspiration product (MOD16) using flux tower data in the African Savanna. South Africa. *Remote Sensing,* 6, pp.7406-7423.

Reichstein, M., Ciais, P., Papale, D., Valentini, R., Running, S. and Viovy, N. 2007. Reduction of ecosystem productivity and respiration during the European summer 2003 climate anomaly: a joint flux tower, remote sensing and modelling analysis. *Global Change Biology,* 13, pp.634-651.

Running, S. W., Baldocchi, D. D., Turner, D. P., Gower, S. T., Bakwin, P. S. and Hibbard, K. A. 1999. A global terrestrial monitoring network integrating tower fluxes, flask sampling, ecosystem modeling and EOS satellite data. *Remote Sensing of Environment,* 70, pp.108-127.

Running, S. W. and Zhao, M. 2015. User's Guide. Daily GPP and Annual NPP (MOD17A2/A3) Products NASA Earth Observing System MODIS Land Algorithm, Version 3.0. Available from: http://www.ntsg.umt.edu/sites/ntsg.umt.edu/files/modis/MOD17UsersGuide2015_v3.pdf.

Seth, S. M. 1998. Drought characterization in sub-humid climatic region. CS (AR)-13/98-99, National Institute of Hydrology. *Jalvigyan Bhawan,* Roorkee, Uttarakhand.

Svoboda, M. 2002. The Drought Monitor. *Bulletin of the American Meteorological Society*, 83, pp.1181-1190.

Tang, R., Shao, K., Li, Z. L., Wu, H., Tang, B. H., Zhou, G. and Zhang, L. 2015. Multiscale Validation of the 8-day MOD16 Evapotranspiration Product Using Flux Data Collected in China. *IEEE Journal of Selected Topics in Applied Earth Observations and Remote Sensing*, 8, pp.1478-1486.

Tate, E. L. and Gustard, A. 2000. Drought definition: a hydrological perspective. In: Drought and Drought Mitigation in Europe. Vogt, J. V. and Somma, F. ed. *Kluwer Academic Publishers,* The Netherland, pp.23-48.

Turner, D. P., Ritts, W. D., Cohen, W. B., Gower, S. T. and Running, S. W. 2006. Evaluation of MODIS NPP and GPP products across multiple biomes. *Remote Sensing of Environment,* 102, pp.282-292.

Turner, D. P., Ritts, W. D., Cohen, W. B., Maeirsperger, T., Gower, S. T. and Kirschbaum, A. 2005. Site-level evaluation of satellite-based global terrestrial gross primary production and net primary production monitoring. *Global Change Biology*, 11, pp.666-684.

Tucker, C. J., Vanprac, C., Sharman, M. J. and Van Ittersum, G. 1985. Satellite remote sensing of total herbaceous biomass production in the Senegalese Sahel: 1980-1984. *Remote Sensing of Environment*, 17, pp.233-249.

Van der Molen, M. K, Dolman, A. J., Ciais, P., Eglin, T., Gobron, N. and Law, B. E. 2011. Drought and ecosystem carbon cycling. *Agriculture and Forest Meteorology,* 151, pp.765-773.

Wilhite, D. A. and Svoboda, M. D. 2000. Drought early warning systems in the context of drought preparedness and mitigation. In: Wilhite, D. A., Sivakumar, M. V. K. and Wood, D. A. *Proceedings of an Expert Group Meeting,* Lisbon, Portugal.

Wilhite, D. A. and Glantz, M. H. 1985. Understanding the drought phenomenon: The role of definitions. *Water International,* 10, pp.111-120.

Xiao, J., Zhuang, Q, Liang, E., Shao, X., McGuire, A. D., Moody, A., Kicklighter, D. W. and Melillo, J. M. 2009. Twentieth-century droughts and their impacts on terrestrial carbon cycling in China. *Earth Interactions,* 13, pp.1-31.

Yao, Y., Liang, S., Qin, Q. and Wang, K. 2010. Monitoring drought over the conterminous United States using MODIS and NCEP Reanalysis-2 data. *Journal of Applied Meteorology and Climatology,* 49, pp.1665-1680.

Zhao, M. S. and Running, S. W. 2010. Drought-induced reduction in global terrestrial net primary production from 2000 through 2009. *Science,* 329, pp.940-943.

Zhao, M., Running, S. W. and Nemani, R. R. 2006. Sensitivity of Moderate Resolution Imaging Spectroradiometer (MODIS) terrestrial primary production to the accuracy of meteorological reanalysis. *Journal of Geophysical Research,* 111, p.G01002.

Cloud Publications
International Journal of Advanced Remote Sensing and GIS
2017, Volume 6, Issue 1, pp. 2246-2252
ISSN 2320 – 0243, Crossref: 10.23953/cloud.ijarsg.284

Research Article

Estimation of PM10 Distribution using Landsat 7 ETM+ Remote Sensing Data

Ajay Roy[1], Anjali Jivani[2], Bhuvan Parekh[2]

[1]MCA Department, D. D. University, Nadiad, India
[2]Department of CSE, The Maharaja Sayajirao University of Baroda, Vadodara, India

Publication Date: 24 July 2017

DOI: https://doi.org/10.23953/cloud.ijarsg.284

Abstract Remote sensing imagery is a rich source of information with applications in varied fields. Monitoring of environment pollution is one of them. The work presented in this paper is focused on estimation of the ambient concentration of pollutant using remote sensing. Particulate Matter with particle sizes less than 10 microns (PM10) is estimated for the study area Vadodara. Landsat 7 ETM+ data of different wavelength has been processed and analyzed for the relationship with coincident ground station PM10 data. The radiance values observed by the satellite and its difference with the radiance calculated after atmospheric correction for the same pixel is considered as a measure to estimate PM10. This difference, called path radiance is calculated and correlated with the ground station PM10 values. Using regression analysis on the calculated data and the ground station PM10 data, the algorithm for PM10 estimation is generated and PM10 map is generated for the study area. The algorithm shows good results for the test data. Pollution estimation through remote sensing is an efficient technique as it can be carried out in less time. Estimation and analysis for larger area is possible using remote sensing approach. The 30 meter resolution of Landsat satellite makes it more suitable for local and regional study.
Keywords: *Landsat ETM+; PM10; Remote Sensing*

1. Introduction

Air pollution is a major problem causing damage to human, animal, crops and water bodies (Kampa and Castanas, 2008; Kanakiya et al., 2015). Respirable Suspended Particulate Matter (RSPM) also known as particulate matter 10 (PM10) are particles with size less than 10 microns (Husar et al., 1981; Ayub and Sharma, 2011). The ambient concentration of PM10 is measured under the National Ambient Monitoring Program (NAMP) by Pollution control board under which, the data is collected for selected stations of the city periodically. Remote sensing can be effectively used to estimate the concentration of PM10 for air quality. The atmosphere affects satellite images of the Earth's surface in the solar spectrum (Lillesand and Kiefer, 1980; Saleh and Hasan, 2014). Hence, different algorithms applied to find about accurate concentration of PM10 particulate from the captured image from satellite of any given area.

Many scientists have used different algorithm to find out PM10 level in different areas of world using satellite image. Li et al., (2015) has used aerosol optical thickness (AOT) based Particulate Matter study. Lim et al., (2007) has used Landsat data for PM10 distribution. Emili et al., (2010) has used

SEVIRI and MODIS sensors for the study using AOD. In the present study, an algorithm has been proposed to estimate the distribution of PM10 using Landsat 7 ETM+ remote sensing imagery. This investigation is unique and differs from most previous studies in term of high data resolution, PM10 and temporal-spatial distribution capability. Most previous works used MODIS (low resolution) or ASTER data (high resolution). The low resolution (250 m) is not appropriate for small-area study (Gyanesh et al., 2010; Techarat, 2013). The availability of Landsat ETM+ is better in comparison with ASTER data.

The main objective of the research study is to test the suitability of the proposed algorithm for mapping PM10 using Landsat satellite images. In situ measurements were required for algorithm validation. PM10 data have been collected simultaneously during the satellite Landsat overpass the study area, which was recorded by GPCB at ground stations of the study area. An algorithm was developed to determine the PM10 concentration on the earth surface. The efficiency of the proposed algorithm was determined based on the correlation coefficient (R^2) and root-mean-squares deviation, RMS. The radiance generated through this process is compared with the radiance before atmospheric correction to calculate the atmospheric path radiance, based on which the estimation of the PM10 is carried out. Finally, the PM10 map was generated using the proposed algorithm. The PM10 map was classified using QGIS and color-coded for visual interpretation.

2. Methodology

2.1. Study Area

The study was carried out in the Vadodara city and suburbs. Vadodara is located in the Gujarat state between $73^0$2' to $73^0$18' Eastern longitudes and $22^0$12' to $22^0$24' Northern latitude. Vadodara city and Nandesari town has many industries mainly chemicals, petrochemicals and biotechnology. With the industrial and urban development, the level of pollution has also been raised high (GPCB, 2010). The monitoring of pollutants is primarily required to initiate its control. The traditional method of its measurement is time consuming process. Also, the data may be collected only for selected locations identified as ground stations.

2.2. Data Acquisition

Landsat 7 ETM+ temporal data has been selected for the study from 2003 to 2014 of October month. There are other satellites available like MODIS, NOAA-AVHHR, ASTER and others. However, the spatial resolution of Landsat is 30 m for reflective bands, which is good compared to other satellites like MODIS. The temporal resolution of Landsat ETM+ is also reasonable. It is available since 1999, and follows a 16 days cycle. The Imagery of the study area was selected using USGS EarthExplorer interface. 14 Scenes for the dates with no cloud cover were ordered through USGS ESPA on demand interface. These higher level products included surface reflectance products which are atmospherically corrected using 6S method. Ground measurements of PM10 recorded at six locations of Vadodara were collected from GPCB office for the selected dates.

2.3. Data Processing

Satellite records the radiance of the surface received at sensor. The recorded radiance does not represent the true radiance of the surface. It is attenuated by aerosol and Particulate Matters. In order to get the true radiance, the recorded values need to be corrected using the sensor calibration values and then remove the noise added due to the atmospheric scattering. In several application of remote

sensing, this noise is normally removed from the image during preprocessing. Instead, this noise was used to quantify and estimate the PM10 concentration in the air in the present study.

The total signal at the sensor consists of three components: (a) Reflected radiation from the viewed pixel, (b) Radiation from the neighborhood (c) Atmospheric Path Radiance. The atmospheric path radiance is the result of backscattering to space by particles and molecules in the atmosphere (Yoram, 1993). Based on path radiance an algorithm was derived to estimate the PM10 concentration in the study area.

The following equation was used to calculate the path radiance (Chuvieco and Huete, 2010)

$$L_{p,\lambda} = L_{\lambda} - \frac{\rho_{\lambda} ESUN_{\lambda} (\cos\theta)^2}{\pi\, d^2} \qquad \ldots (1)$$

Where $L_{p,\lambda}$is the atmospheric path radiance (W/m^2/sr) for band λ, L_{λ} is at sensor radiance for band λ, ρ_{λ} is surface reflectance of band λ, $ESUN_{\lambda}$ is irradiance arriving at the top of atmosphere (W/m^2) in band λ, θ is the angle of incidence (degree), d is the correction factor for Earth-sun Distance, J is Julian day.

$$d = 1 + 0.01674\ \sin(2\pi(J - 93.5)/365) \qquad \ldots (2)$$

The recorded values of the image are known as Digital Number (DN). The following equation is used to convert Digital Numbers (DNs) back to radiance (L_{λ}):

$$L_{\lambda} = Gain * DN + Bias \qquad \ldots (3)$$

Where L_{λ} is the cell value as radiance, DN is the cell value digital number, gain is the gain value for a specific band, bias is the bias value for a specific band. The gain and bias values are available in the metadata file of the Landsat image.

After processing these remote sensing data, (a) Reflected radiation from the viewed pixel and (c) Atmospheric Path Radiance was calculated for selected stations remote sensing imagery. A relationship between the Path radiance and the ground station PM10 values has been established using regression analysis.

The surface reflectance was taken from the Landsat 7 ETM+ Surface Reflectance Product received through ESPA on demand interface of USGS. The surface reflectance products were already atmospherically corrected (Schmidt et al., 2013). So the radiance calculated using the atmospherically corrected data and the radiance before atmospheric correction quantifies as path radiance (eq. (1)). The path radiance was calculated for band 1, 2, 3, 4, 5 and 7 of Landsat data.

3. Results and Discussion

After processing, the derived path radiance values for all bands were analyzed for suitability of the algorithm based on their sensitivity to PM10. Using SPSS, Principal Component Analysis was performed for reduction of independent variables. The correlation for band 1, 3 and 4 was 89%, 47% and 47% respectively. Thus, the sensitivity of blue, red and NIR band to the ambient pollution has been ascertained by the results. Band 1 (blue) explains 61% of variance with eigenvalue 2.44 and 98% variance is explained with cumulative effect of the three bands. Techarat (2013) has given the PM10 algorithm for landsat images using the path radiance of band 3. It is evident with the present

study that confirms the sensitivity of band 3. However, band 1 and band 4 have marginal effect of PM10 on the radiance reaching the satellite, which is evident from the results. Multiple linear regression analysis between the calculated band values and ground station PM10 data was performed using SPSS 17. The coefficient of determination (R^2) of the regression model was 0.89, which indicates a good model fit. The following algorithm was derived for PM10 estimation using the regression analysis.

$$PM10 = (-46.60 * L_{p,1}) - (0.374 * L_{p,3}) - (8.021 * L_{p,4}) + 1943.24 \quad \ldots (4)$$

Where $L_{p,1}$, $L_{p,3}$ and $L_{p,1}$ are path radiance of band 1, 3 and 4 respectively. The model was evaluated with test data which shows good results. The PM10 distribution map for the study area was generated using the derived algorithm using QGIS software ver. 2.18.7. The map was classified in 5 classes for visual interpretation. The PM10 map shows a good match with the available ground station average PM10 data. The month average data recorded by GPCB for October 2015 is 82 for Gotri and 72 for GPCB office station respectively, which matches with the derived PM10 classified map results.

Table 1: *Test data results for different ground station values and Landsat ETM+ Scene values*

Station	PM10 (µg/m^3)	PM10 Estimated (µg/m^3)
GPCB Office	51.00	44.21
GPCB Office	84.00	88.97
Gotri	83.00	96.50

Research on using remote sensing based PM10 estimation has been done using different sensors and methods. Commonly used approach for PM10 estimation is Aerosol Optical Thickness based retrieval using remote sensing. However, AOT input requires complex calculation and ancillary data. Atmospheric correction is normally applied to remote sensing images before using them for specific applications. The present study has been carried out using the selected Landsat images October month of the year 2003 to 2014. Similar study has to be carried out using the data of different months of the year to take seasonal variations into consideration.

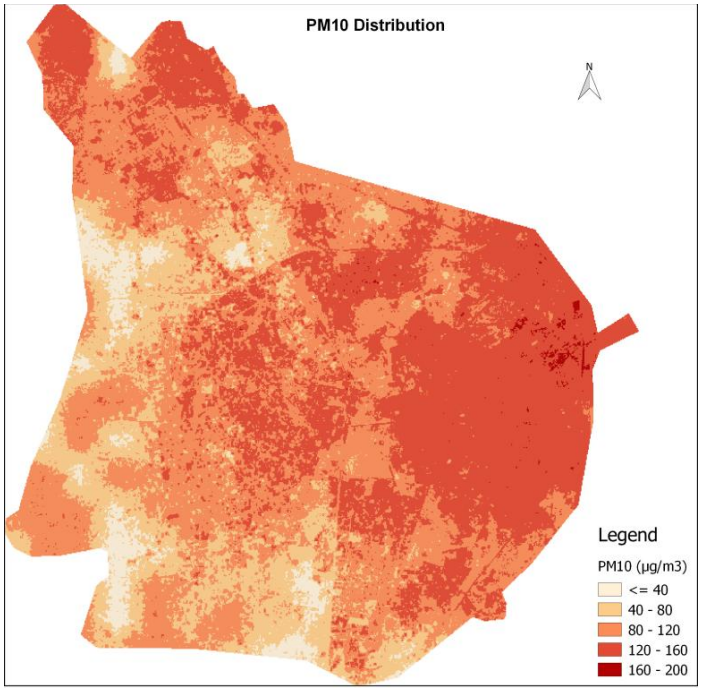

Figure 1: *PM10 classification map generated using the algorithm for Landsat ETM+ image of 16-Oct-2015 Vadodara city*

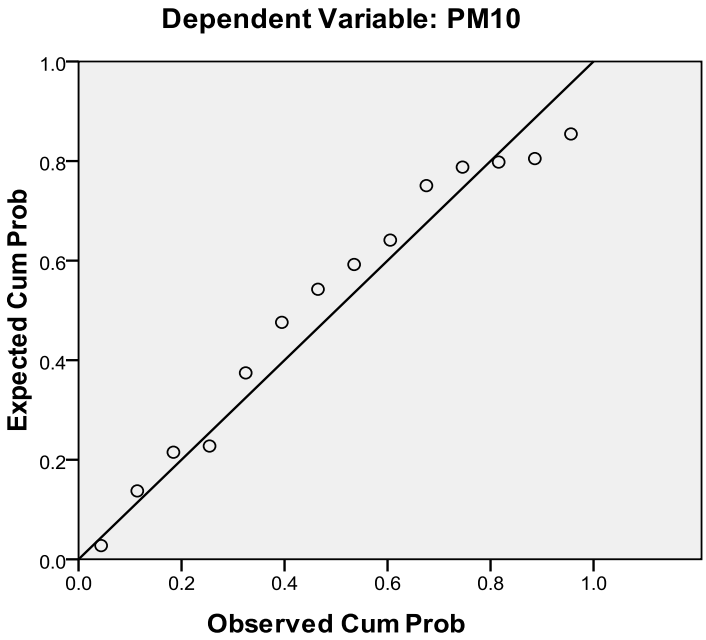

Figure 2: *Normal P-P plot of regression standardized residual*

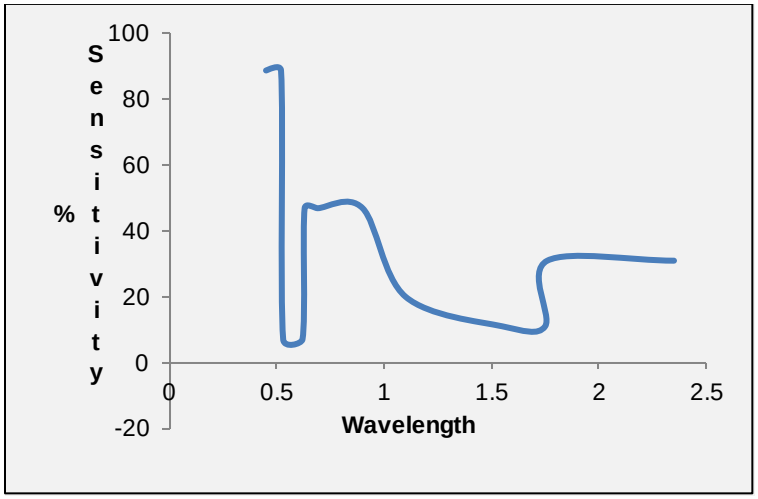

Figure 3: *Observed sensitivity plot for PM10 in different wavelength range of Landsat ETM+ sensor*

Techarat (2013) suggested that Landsat TM/ETM+ data can successfully be used as inputs of the derived algorithm to map the spatial distribution of PMs and SO2 concentrations with high efficiency. The Landsat ETM+ data should be used because they have high resolution, availability spatially and temporally, and easy to get (Techarat, 2013; Sotoudeheian and Arhami, 2014; Wang et al., 2017). The atmospheric correction, which is generally taken as preprocessing in remote sensing applicaions, has been effectively used for pollution distibution mapping (Marcello et al., 2016). The derived equation can be used for PM10 distribution mapping using Landsat ETM+ data for the study area. The remote sensing approach will save time taken in ground measurements. However, it will not give precise results, but good results for the purpose of estimation (Matthew et al., 2013). The main advantage is the entire study area may be covered for the distribution mapping based on the availability of Landsat ETM+ data for the desired time.

References

Ayub, S. and Sharma, S.K. 2011. Particulate matter emission from thermal power plant: parent material, formation mechanism, health concerns, control devices - a review. *Global Journal Engineering and Applied Sciences,* 1(3), pp.2249-2623.

Chuvieco E. and Huete A., 2010: *Fundamentals of satellite remote sensing.* Florida, United States: CRC Press-Taylor & Francis, p.418.

Emili, E., Popp, C., Petitta, M., Riffler, M. and Zebisch, M. 2010. PM10 remote sensing from geostationary SEVIRI and polar-orbiting MODIS sensors over the complex terrain of the European Alpine region. *Remote Sensing of Environment,* 114(11), pp.2485-2499.

Gujarat Pollution control Board. 2010. Status of Ambient Air Quality Monitoring (AAQM) in main places of Gujarat.

Gyanesh, C., Xiaoxiong, X., Taeyoung, C. and Amit, A. 2010. Monitoring on-orbit calibration stability of the Terra MODIS and Landsat 7 ETM+ sensors using pseudo-invariant test sites. *Remote Sensing of Environment,* 114(4), pp.925-939.

Husar, R. B., Holloway, J. M. and Patterson, D. E. 1981. Spatial and temporal pattern of eastern U.S. haziness: a summary. *Atmospheric Environment,* 15(10), pp.1919-1928.

Kampa, M. and Castanas, E. 2008. Human health effects of air pollution. *Environment Pollution,* 151(2), pp.362-367.

Kanakiya, R. S., Singh S. K. and Shah, U. 2015. GIS application for spatial and temporal analysis of the air pollutants in urban area. *International Journal of Advanced Remote Sensing and GIS,* 4(1), pp.1120-1129. doi: https://doi.org/10.23953/cloud.ijarsg.102

Li, L., Yang, J. and Wang, Y. 2015. Retrieval of high-resolution atmospheric particulate matter concentrations from satellite-based aerosol optical thickness over the Pearl River Delta Area, China. *Remote Sensing,* 7(6), pp.7914-7937.

Lillesand, T. M. and Kiefer, R. W. 2015. Remote Sensing and Image Interpretation. 7th ed. John Wiley and Sons, New York, USA. pp.488.

Lim, H. S., MatJafri, M. Z., Abdullah, K. and Mohd. Saleh, N. 2007. PM10 retrieval in urban area from space. In: Shen, S. S. and Lewis, P. E. (eds.) Algorithms and Technologies for Multispectral, Hyperspectral, and Ultraspectral Imagery XIII, 65651Z, Orlando, Florida, USA.

Marcello, J., Eugenio F., Perdomo, U. and Medina, A. 2016. Assessment of atmospheric algorithms to retrieve vegetation in natural protected areas using multispectral high resolution imagery. *Sensors,* 16(10), pp.1624.

Saleh, S. H. A. and Hasan, G. 2014. Estimation of PM10 concentration using ground measurements and Landsat 8 OLI satellite image. *Journal of Geophysics and Remote Sensing,* 3, pp.120.

Schmidt, G. L., Jenkerson, C. B., Masek, J., Vermote, E. and Gao, F. 2013. Landsat ecosystem disturbance adaptive processing system (LEDAPS) algorithm description (2013-1057). *U.S. Geological Survey,* 6, pp.19.

Sensors, M. J., Millet, D. B. and Marshall, J. D. 2013. Remote sensing of exposure to NO_2: satellite versus ground based measurement in a large urban area. *Atmospheric Environment,* 69, pp.345-353.

Sotoudeheian, S. and Arhami, M. 2014. Estimating ground-level PM10 using satellite remote sensing and ground-based meteorological measurements over Tehran. *Journal of Environmental Health Science and Engineering,* 12, pp.122.

Techarat, P. 2013. Mapping predictive ambient concentration distribution of particulate matter and sulfur dioxide for air quality monitoring using remote sensing. Thesis, Doctorate of Philosophy, Department of Environment Study and Engineering,University of Regina, Canada.

Wang, C., Chen, S., Li, D., Liu, W., Yang, J. and Wang, D. 2017. A Landsat-based model for retrieving total suspended solids concentration of estuaries and coasts. *Geoscience.* [Online]. Available from: doi:10.5194/gmd-2016-297.

Yoram, J. K. 1993. Aerosol optical thickness and atmospheric path radiance. *Journal of Geophysical Research,* 98(D2), pp.2677-2692.

Cloud Publications
International Journal of Advanced Remote Sensing and GIS
2017, Volume 6, Issue 1, pp. 2281- 2291
ISSN 2320 – 0243, Crossref: 10.23953/cloud.ijarsg.291

Research Article

Susceptibility Assessment of Rainfall-induced Shallow Landslides using a GIS-supported Deterministic Analysis – A Pilot Study

Santanu Sarma, Parag Jyoti Dutta, Ranjan Bikash Borgohain

Department of Geology, Cotton University, Guwahati – 781001, Assam, India

Publication Date: 3 August 2017

DOI: https://doi.org/10.23953/cloud.ijarsg.291

Abstract The landscape of Guwahati city (Assam) is characterized by a number of residual hills (eighteen) scattered in and around the main urban areas. The geology of all these isolated hills is the same, comprising an overburden of soil (weathered mantle) over bedrocks of porphyritic granite, quartzo-feldspathic gneiss, migmatites and schistose rocks. Shallow landslides in the form of soil slips are regular phenomena in these hills during the monsoons which are triggered by spells of high intensity rainfall. The Narakasur hill which lies in the heart of the city was selected as a small sample area for deterministic landslide susceptibility analysis to forecast the spatial occurrence of rainfall-induced shallow landslides. A grid-based slope-stability analysis was incorporated with the GIS spatial functions adopting the “infinite-slope” geometry to balance the resisting and the driving forces acting on the sliding mass. Landslide susceptibility is expressed by Safety Factor.Input data for the analysis includes topographic slope, soil thickness, water table depth and material strength properties. The effect of Safety Factor values, arising due to variation in material properties and water table conditions, was shown over the study area. Safety factors were calculated for three different water table depth scenarios assuming that soil is completely dry, completely saturated with water and an intermediate condition. Based on the calculated values of the Safety Factor the area was divided into stable, critical and unstable zones.Comparing the results with the shallow landslide inventory map, it has been observed that more than 70% agreement between predicted shallow landslide susceptibility and the inventory.

Keywords *Infinite-slope; Kriging; Regolith; Safety factor; Slope angle*

1. Introduction

Shallow landsliding is common on natural hillslopes mantled with a layer of colluvium or residual soil and are often triggered by rainfall to mobilize into debris flows (Salciarini et al., 2006). Infiltration of rainfall leads to increases in pore water pressures in the near subsurface that reduces the shear strength of the colluvial mass (Terzaghi, 1943).

Landslide susceptibility is the likelihood of a landslide occurring in an area on the basis of local terrain conditions (Brabb, 1984). The spatial probability of landslides, also known as susceptibility, is the probability that a region will be affected by landslides given a set of terrain conditions. The aim of the shallow landslide hazard analysis is to create a quantitative susceptibility map using adeterministic model to show the landslide susceptibility in the study area through the application of Geographic Information System (GIS). For very shallow, translational landslides; the infinite slope model yields

extremely good results (Bromhead, 1992).For landslide susceptibility mapping, the infinite slope model is used to calculate Safety Factors in the prevailing condition. This 'deterministic model' is used for deriving landslide susceptibility map of the study area by calculation the pixel based safety factors. To prepare a shallow landslide susceptibility map, the analysis is restricted to the shallow (2.4 m) failures that commonly form debris flows. The analysis uses shear-strength values for all of the soil units, a slope map prepared from a Digital Elevation Model (DEM) and the landslide inventory database.

The thematic maps of the parameter were generated using field data and GIS techniques. Landslide hazard zonation map at the disposal helps to take necessary landslide preventive measures and make the local people and authority aware about the possible hill failures.

1.1. Study Area

The study area being at a center of Guwahati, the capital city of Assam, is becoming a major dwelling area with constructions of houses, huts and associated infrastructure on hill slopes. A large scale alteration of hill slopes due to increase settlement, constructions and quarrying is noted in the study area. The fast construction practice leads to destabilization of hill slopes and cause landslides.

The study area, Kalapahar (Narakasur) hill, is located in the center of Guwahati, the capital city of the state of Assam, extending from 91º 44' 30" E to 91º 47' 09" E longitude and 26º 08' 28" N to 26º 09' 39" N latitude covering an area of 6.255 km^2 (Figure 1). Narakasur is one of the nineteen residual hills within the Guwahati Municipal Corporation (GMC) limits, which are low to moderately high (50 – 410 m above MSL) with a general E-W trend. These hills are the erosional remnants of the Precambrian Basement Gneissic Complex (BGC) of the Meghalaya Plateau. It falls within the Survey of India Toposheet Nos. 78N/12 and 78 N/16 of 1:50,000 scale. The maximum and minimum elevation of the area is 260 m and 54 m respectively from the MSL.

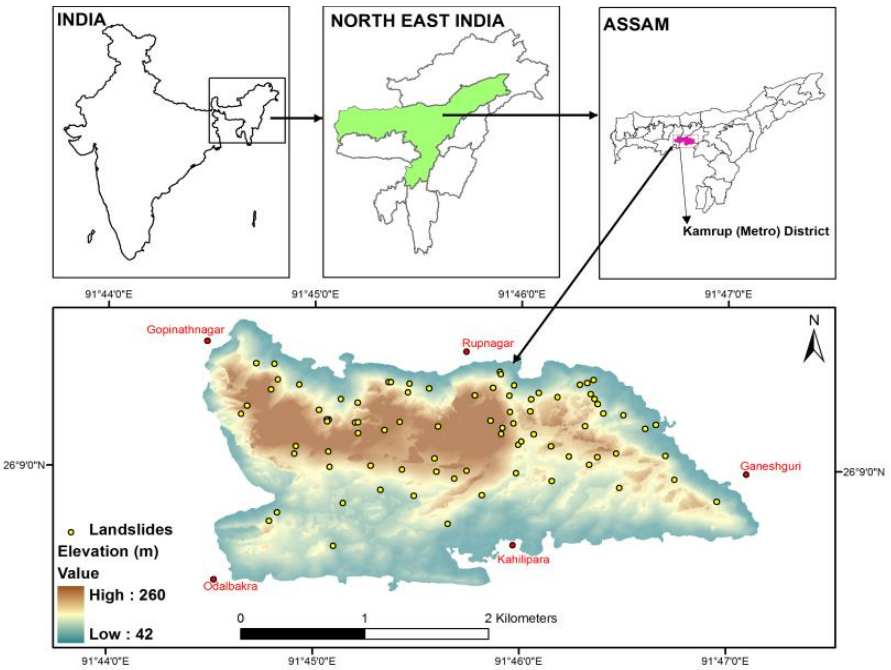

Figure 1: *Location map of the Study area*

Lithologically the area is comprised mainly of Quartz of eldspathic Gneiss and Porphyritic Granite of Precambrian time capped by loose soil and intensely weathered materials (regolith). The climate of the study area is predominantly tropical with average annual temperature ranging from 6°C to 38.0°C and experience heavy/incessant rainfall during the monsoon extending from June to September every year with 1,717.7 mm average yearly rainfall and 128 average rainy days per year.

A total of 82 scars of landslides of small magnitudes in the Narakasur Hill were mapped during the field survey carried out in the years 2011-2014 (Figure 2). There are no records of the triggering dates of these failures. As per the classification of Cruden and Varnes (1996), three types of failures were observed: (1) incipient translational slides, where the displaced mass has limited movement; (2) translational soil slides, where the mass has moved exposing the failure surface and (3) roto-translational slides, only adjacent to road-cuts. Among the three, type (2) failures are predominant in the study area. A shallow depth (1.0 – 1.5 m) of the sliding surface below the ground is a characteristic of these failures. Landslide bodies have lengths typically lower than 10 m, and volumes lower than 100m^3. Most of these have occurred on hillslopes with a gradient of 30°-45°. The landslide incidence in the study area has increased in the recent years due to anthropogenic activities which inflicts loss of property and life (Bhusan and Goswami, 2010).

Figure 2: *Few landslide sites in the field*

2. Methodology and Database

Creation of quantitative hazard maps where the degree of hazard is express by the Safety factor is the objective of this large scale landslide hazard analysis (scales larger than 1:10,000). Safety Factor (SF) is the ratio between the forces that causes the slope failure and those that prevent the slope from failing. SF-values larger than 1 indicate stable slope conditions, and SF-values smaller than 1 indicate unstable slope condition. At SF=1 the slope is at the point of failure. For the Safety Factor calculation different models are available. In this study an infinite slope model is used which can be used in GIS. This is a one dimensional model that describes the slope stability of slopes with an infinitely large

failure plane. SF calculation in this model can be done on a pixel basis. The pixels in the parameter maps can be considered as homogeneous units and the effect of the neighboring pixels is not considered. The model can be used to calculate the stability of each individual pixel, resulting in a hazard map of safety factors. The safety factor is calculated according the formula proposed by Brunsden and Prior (1984).

$$SF = \frac{c' + (\gamma - m\gamma_w)\, z \cos^2\beta \tan\varphi'}{\gamma z \sin\beta \cos\beta} \quad \ldots (1)$$

Where,
c' = Effective cohesion (Pa= N/m^2)
φ' = Effective angle of shearing resistance (°)
γ = Unit weight of soil (N/m^3)
γ_w = Unit weight of water (N/m^3)
z = Depth of failure surface below the surface (m)
z_w = Height of water table above failure surface (m)
$m = z_w/z$ (dimensionless)
β = slope surface inclination (°)

On this study the average safety factors are calculated for different conditions of saturation using the infinite slope model. In evaluating *SF* using Eq.1, the unit weight of slope material (γ) was assigned the value of 11kN/m^{3}in dry condition and 16kN/m^{3}in complete saturation condition, which is consistent with the average dry and wet unit weights of soil units in the study area. Unit weight of water (γ_w) was taken as 10kN/m^3. The factor of safety was then calculated by inserting values for material strength parameters (Effective Angle of Internal Friction and cohesion), thickness of the regolith and slope angle in Eq.1 for each cell in the model.

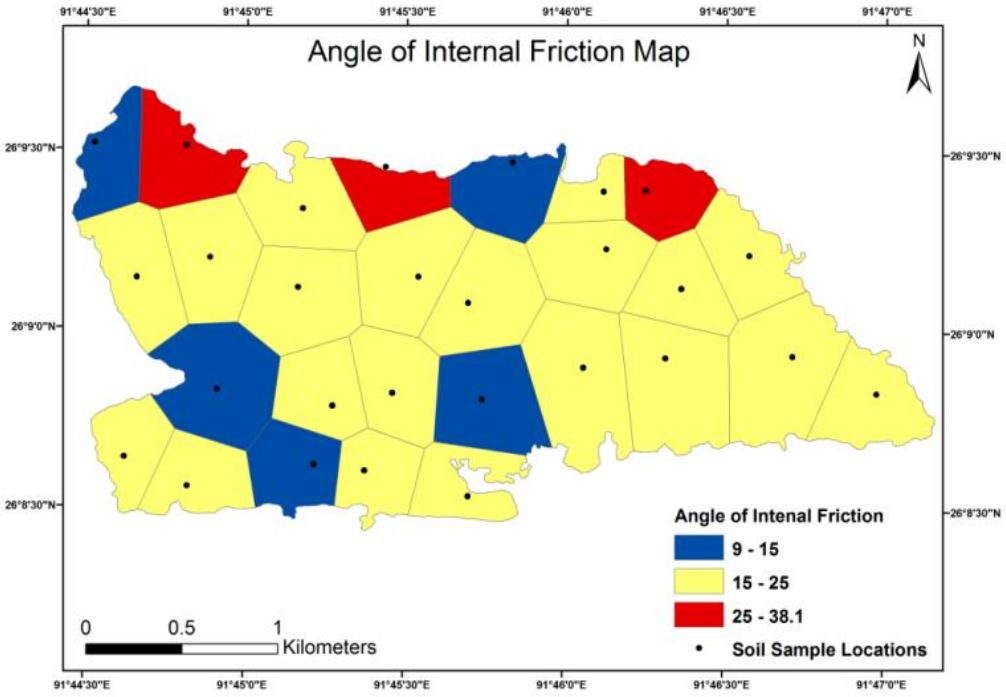

Figure 3: *Effective cohesion map*

For the representative soil sample collection, the study area of Narakasur hill was dividing into 28 square grids of 500m x 500m dimension. Undisturbed and disturbed subsurface soil samples were collected by manual augur boring from 28 field locations one from each grid. Due to the vertical homogeneity of the soil profile, the soil cores were collected from a depth of 1m from the ground surface for a good representation of the soil horizon. The entire population of soil samples covers all the land use types across the study area and equally distributed between the two bedrock types, namely QFG and PG.

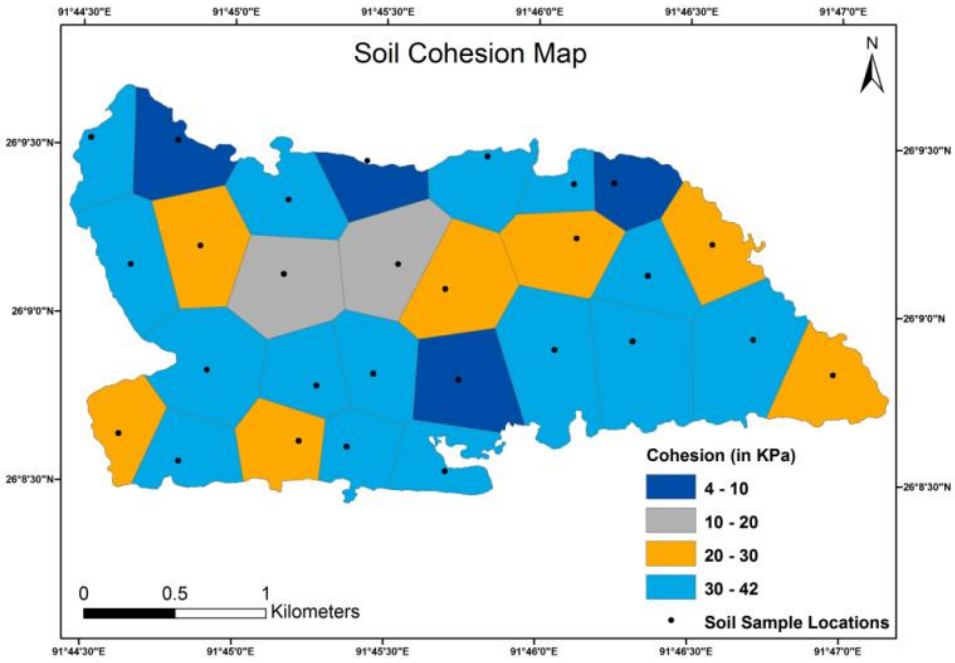

Figure 4: *Effective angle of internal friction map*

Geotechnical laboratory testing was conducted on soil samples collected from 28 field locations for the shear strength parameters (Effective Cohesion (c') and Effective Angle of Internal Friction (ϕ')). Shear strength parameters were measured by direct shear tests and Consolidated Undrained (CU) Triaxial Compression tests. Cohesion and angle of internal friction were calculated from the Stress – Strain Curves and Mohr Stress Circle plotted from the results of the test. Soil geotechnical properties were determined according to American Society for Testing and Materials (ASTM) procedures, 1988. Peak friction angle (φ') and effective cohesion (c') have a standard deviations of 5° and 4.6 kPa respectively. φ' is on the average (mean) of 25°, while c' of 2.5 kPa. The results of effective cohesion and angle of internal friction are plotted in the map (Figure 3 and 4) to show the representative area of influence of each value.

The regolith thickness represents a key data for the shallow landslide analysis, but its determination is not always simple.Measurment of regolith thickness (Depth-to-Bedrock), where no profile sections were exposed, was carried out at 160 point locations, by the knocking pole method;where an pointed iron spear (rod) was pierced into the soil until it reached bed rock (Uchida et al., 2008; Kuriakose et al., 2009). Three situations can arise with this method, 1) a representative surface to bedrock measurement, 2) an underestimate, measured only to a rubble layer and 3) a local overestimate, caused by cracks in the bedrock. Care was taken to minimize these errors. Percussion was done until

the bed rock was reached which could be recognized by the sound of the knocking pole. In addition to the measured samples, few zero-depth points were marked so as to represent the bare rock areas. The locations of these zero-depth points were determined to be bare rock areas both based on field work and the land use/land cover map. Further, in 477 locations the soil thickness was measured in unlined dug wells by measuring tape (Figure 5a).

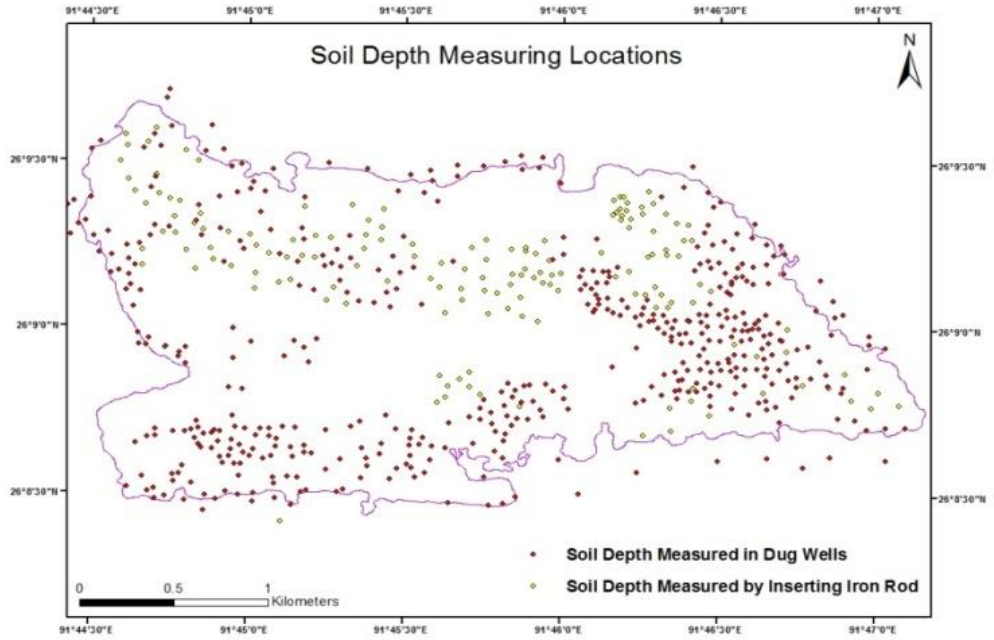

Figure 5a: *Measuring locations of soil depth*

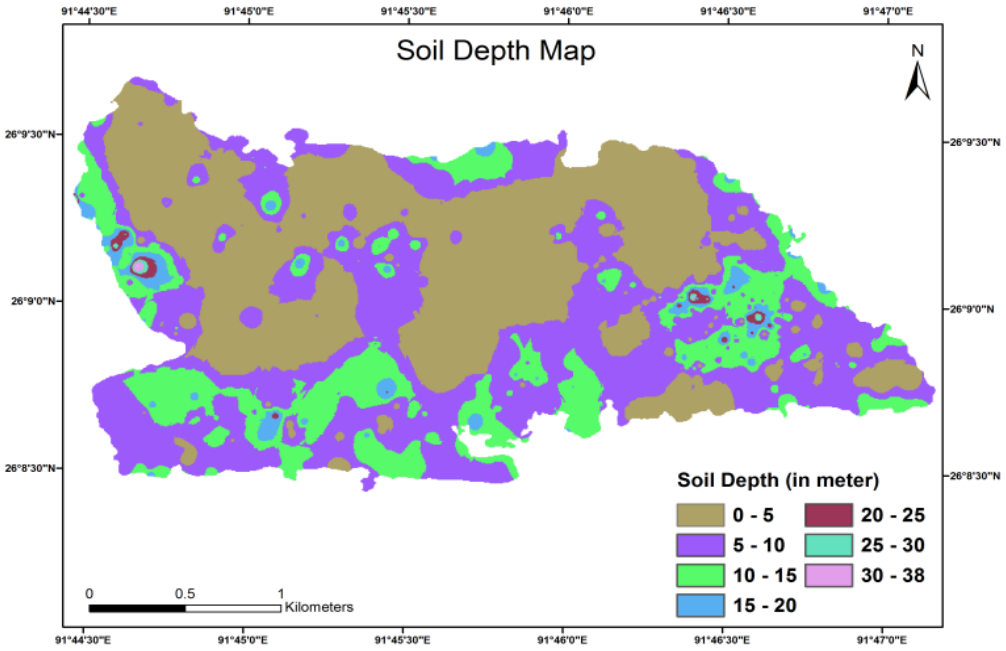

Figure 5b: *Interpolated depth-to-bedrock map*

A continuous prediction grid of Depth-to-Bedrock (DTB) was created by interpolating the 637 point measurements through Regression Kriging on a 5m × 5m block size (Figure 5b), using auxiliary environmental predictors of elevation and LS Factor (Hengl, 2007). The Regression Kriging module of SAGA GIS was used to perform the interpolation. Block Kriging has the advantage of reducing Kriging estimation variance since spatial variability smaller than the block size is averaged out. The accuracy was assessed by comparing the values of the root mean square error (RMSE), RMSE normalised by the observation range (NRMSE) and coefficient of determination (R^2) between the observed and estimated values of soil depth at the validation data locations. A higher R^2 indicated a better fit between the observed and estimated values, while lower values of RMSE and NRMSE indicated better estimation accuracy.

2.1. Slope Angle

The slope angle is one of the most important factors in landslide studies, as it strongly controls the shear forces acting on hillslopes and the water distribution (Catani et al., 2013). Slope angle (in degree) of the terrain derived from the 5m DEM generated from the point elevations derived from the Total Station survey. Slope map is derived in raster format with 5m x 5m grid using the 3D extension of ArcGIS. The slope angles of the study area vary from 0.0021° (Flat) to 85° with mean slope at 16° (Figure 6). The slope angle was categorized into five categories vis. 0° – 5°, 5° – 15°, 15° – 30°, >45° while determining the Safety Factor map.

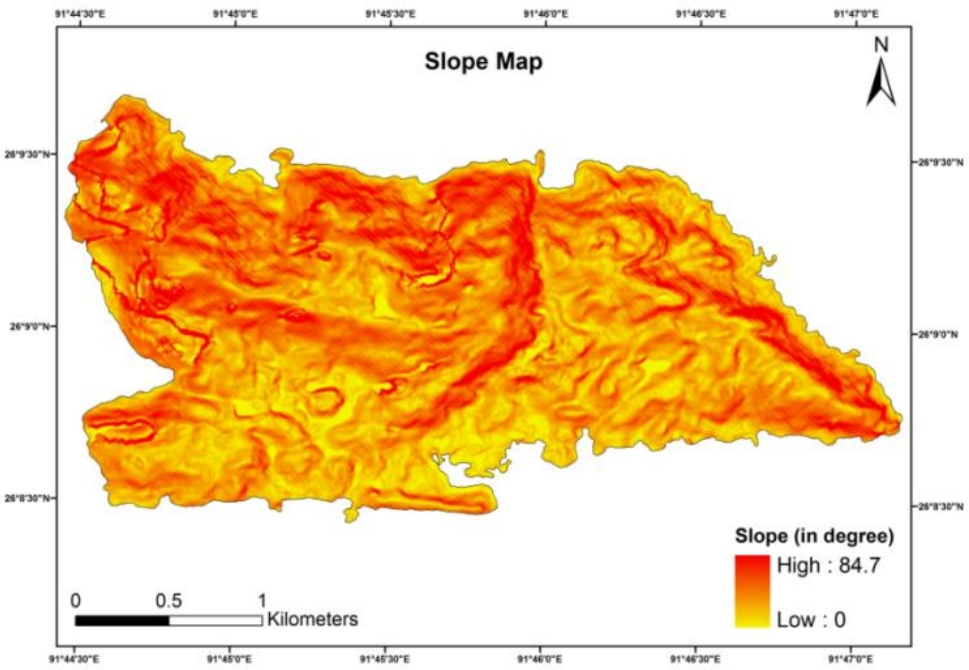

Figure 6: *Slope angle map*

Practically the entire study area of Narkasur Hill is covered by a layer of regolith. Only the area with steep slope (>45) regolith cover is normally absent and bed rock is exposed. In this study the stability of the regolith layer is calculated. This means that the depth of the possible failure plane is taken at the contact of the regolith layer and the underlying bed rock.

Raster layers of 5x5mgrid cell of various parameters were created in GIS environment, which are projected in WGS84 UTM 46N projection system. Raster calculator is used to determine the Safety Factor using the Eq.1. Final safety factor map is a raster map with pixel wise safety Factor values.

3. Results and Discussion

As rainfall is the main triggering factor in the occurrence of the shallow landslides within the study area, safety factor maps are created for different scenarios; varying from dry to complete saturation condition. In order to know the percentage of area in stable, critical and unstable condition the SF maps generated for different GW scenario are classified into three classes:

Unstable = safety factor lower than 1

Critical = safety factor between 1 and 1.5

Stable = safety factor above 1.5

3.1. Dry Condition

Safety factors are calculated for the regolith under the assumption that the soil is completely dry. In that case the parameter *m* is equal to zero as z_w is 0 and unit weight of soil (γ) is taken as 11,000 N/m^3. A completely dry situation is a very rare occurrence in a tropical region such as Assam, which receives quite a lot of rainfall each year. In any case, the map showing the Safety Factor in dry condition (F_{dry}), gives the most stable situation.

In this scenario 0.099 sq. km (1.56%) area, 0.358 sq. km (5.66%) area and 5.798sq. km (91.48%) area are classified as unstable, critical and stable respectively (Figure 7a).

3.2. Completely Saturated Condition

The next scenario, the SF values are evaluated for a condition in which the soil is completely saturated with water. This is a situation attain after a long duration low intensity rainfall, which is very common in this part of the region. It will give the most pessimistic estimation of slope stability, with only one triggering factor involved (rainfall leading to high water tables).

When soil is in complete saturation, the *m* factor is equal to 1. This means that the water table is at the surface. The unit weight of soil (γ) is considered to be 16,000 N/m^3 in wet condition.

In this scenario 0.838 sq. km (13.23%) area, 1.081 sq. km (17.06%) area and 4.335 sq. km (68.4%) area are classified as unstable, critical and stable respectively (Figure 7b).

3.3. Other Groundwater Scenarios

Using the formula and the input files created for SF calculation, a number of scenarios can be calculated using some other saturation value. SF values are calculated for the following saturation conditions.

In 15% saturation condition where m value is equal to 0.15 and unit weight of soil (γ) is considered to be 14,000 N/m^3. In this scenario 0.207 sq. km (3.26%) area, 0.538 sq. km (8.49%) area and 5.51 sq. km (86.94%) area are classified as unstable, critical and stable respectively (Figure 7c).

In 50% saturation condition where m value is equal to 0.5 and unit weight of soil (γ) is considered to be 14,000 N/m^3. In this scenario 0.366 sq. km (5.77%) area, 0.737 sq. km (11.62%) area and 5.152 sq. km (81.3%) area are classified as unstable, critical and stable respectively (Figure 7d).

After computing the SF values for four different scenarios, they are compared in the Table 1.

Table 1: *Unstable, critical and stable area under different groundwater scenarios*

Scenario	Unstable		Critical		Stable	
	Area in sq.km	%	Area in sq.km	%	Area in sq.km	%
Dry Condition	0.099	1.56	0.358	5.66	5.798	91.48
15% Saturation	0.207	3.26	0.538	8.49	5.51	86.94
50% Saturation	0.366	5.77	0.737	11.62	5.152	81.30
Complete saturation	0.838	13.23	1.081	17.06	4.335	68.40

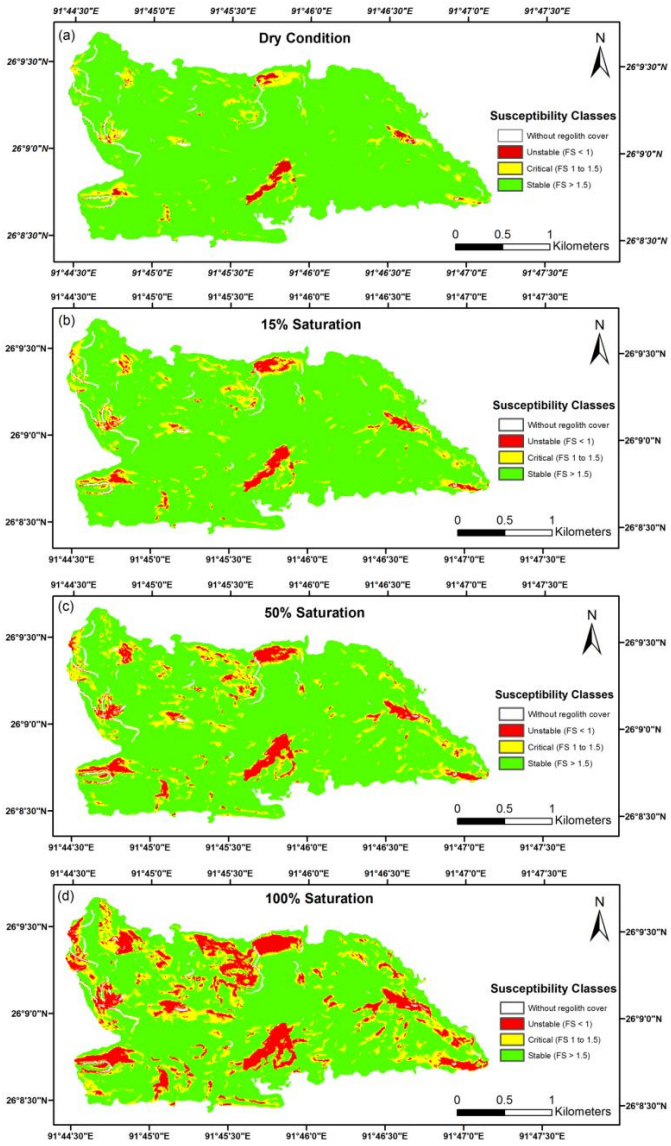

Figure 7: *Safety factor maps in different groundwater scenario*

4. Conclusion

The present study demonstrates a case study for landslide susceptibility mapping/zoning in a part of the Guwahati city landscape comprised of residual hills with Precambrian basement rocks, which is prone to frequent landslide occurrences during the annual monsoon season. The susceptibility mapping exercise was carried out by applying deterministic model.

The application of a Deterministic or physically based model namely the Factor of Safety (FS) for landslide susceptibility mapping is to evaluate the actual physical conditions and processes leading to landslides over the study area. Deterministic methods are used for local-scale analyses, either with GIS (mainly the 1-D infinite slope stability model) or without GIS (usually applied on 2-D vertical sections with circular or elliptic sliding surfaces). In this study, the infinite slope stability model is used in conjunction with GIS to calculate Factor of Safety (FS) maps for dry and saturated conditions. This is a one dimensional model that describes the slope stability with an infinitely large failure plane. FS computation in this model is done on a pixel basis. The pixels in the parameter maps can be considered as homogeneous units and the effect of the neighbouring pixels is neglected. The model can be used to calculate the stability of each individual pixel, resulting in a susceptibility map of safety factors. The length-to-depth ratio of most landslides in the study area is greater than 10 and can be considered as shallow and consequently, the infinite slope stability model is considered as a valid option.

Acknowledgement

The authors acknowledge to the Natural Resources Data Management System (NRDMS), Department of Science and Technology (Govt. of India), New Delhi, for providing financial support to carry out the work (Sanction Order No. NRDMS/11/2001/012).

References

Bhusan, K. and Goswami, D. C. 2010. Landslide hazard zonation of the Narakasur Hill, Guwahati, Assam. *Journal of Indian Geological Congress,* 2(2), pp.91-104.

Brabb, E. E. 1984. Innovative approaches to landslide hazard and risk mapping. *Proceedings of the 4th International Symposium on Landslides,* Ontario, Canada, 1, pp.307-324.

Bromhead, E. N. 1992. The Stability of Slopes. 2nd Ed. London, United Kingdom: Spon Press - Taylor and Francis Group, p.416.

Brunsden, D. and Prior, D. B. 1984. Slope Stability. New York*:* Wiley*,* p.620.

Catani, F., Lagomarsino, D., Segoni, S. and Tofani, V. 2013. Landslide susceptibility estimation by random forests technique: sensitivity and scaling issues. *Natural Hazards and Earth System Sciences,* 13, pp.2815-2831.

Cruden, D. M. and Varnes, D. J. 1996. Landslide types and processes. In: Turner, A. K. and Schuster, R. L. (ed.) *Landslides: investigation and mitigation*. Washington D.C., USA: National Academy Press*,* pp.36-75.

Hengl, T. 2007. A practical guide to geostatistical mapping of environmental variables. *European Commission, Joint Research Centre and Institute for Environment and Sustainability,* Luxemburg.

Kuriakose, S. L., Devkota, S., Rossiter, D. G. and Jetten, V. G. 2009. Prediction of soil depth using environmental variables in an anthropogenic landscape, a case study in the Western Ghats of Kerala, India. *Catena,* 79, pp.27-38.

Salciarini, D., Godt, J. W., Savage, W. Z., Conversini, P., Baum, R. L. and Michael, J. A. 2006. Modeling regional initiation of rainfall-induced shallow landslides in the eastern Umbria Region of central Italy. *Landslides*, 3, pp.181-194.

Terzaghi, K. 1943. Theoretical Soil Mechanics. New York*:* Wiley*,* p.532.

Uchida, T., Tamura, K. and Mori, N. 2008. A simple method for producing probabilistic shallow landslide hazard maps using soil thickness dataset. *European Geosciences Union General Assembly,* Vienna, Austria, p.10.

Cloud Publications
International Journal of Advanced Remote Sensing and GIS
2017, Volume 6, Issue 1, pp. 2377-2394
ISSN 2320 – 0243, Crossref: 10.23953/cloud.ijarsg.302

Research Article

Geographic Information System Based Solution for Location Allocation Problem for Finding High Quality Service Locations

Hari Shankar, Monika

Department of Geoinformatics, Indian Institute of Remote Sensing, Dehradun, Uttarakhand-248001, India

Publication Date: 19 August 2017

DOI: https://doi.org/10.23953/cloud.ijarsg.302

Abstract Location-Allocation Problem (LAP) is a combinatorial optimising network problem which has been widely studied by operational researchers due to its many practical applications. In real life, it is usually very hard to present the customer's demands in a precise way and thus they are estimated from historical data. There are so many types of the methods like exact, heuristic and metaheuristic methods to solve this problem to get the optimal and near optimal solutions. In this study, a metaheuristic approach is applied in GIS environment which gives quick and near optimal solution. To achieve this, one case study based on supply and demand of milk from Vita Distributors to Vita Booths in Hisar City, Haryana have been performed. In this study, the effectiveness and robustness of the metaheuristic algorithm was tested over a GIS geodatabase based network dataset consisting of road network (line features) and facility and customers locations (point features). The performance of the algorithm was also checked for two types of impedance factors i.e. time and distance. The results of this location-allocation problem are very much satisfactory in term of minimization of total transportation cost in providing high quality service locations (Vita Booths) for milk distribution.
Keywords *Metaheuristic algorithm; Network Analysis; Optimization; Transportation GIS*

1. Introduction

Decision making is one of the main ability of human being that differs them from the other creatures. Now, decision making and analysis is an important part of management sciences, and it is perhaps as old as history of mankind. In many real-world problems, the decision maker likes to pursue more than one target or consider more than one factor or measure. Such a desire transforms the decision making problem to a multi-objective decision making problem. There are many decision making problems whose information is spatially (geographically) distributed. These kinds of decisions are called location decisions.

Location decisions are now a major part of operations research and management science (named location science). Facility location is a branch of operations research related to locating or positioning at least a new facility among several existing facilities in order to optimize (minimize or maximize) at least one objective function (like cost, profit, revenue, travel distance, service, waiting time, coverage and market shares). From application point of view there is no limitation for location science. Many application areas including public facilities, private facilities, military environment, business areas and national and international scopes can be seen in the related literature.

1.1. Background

In most scientific disciplines, software plays an important role for solving the real life problems and implementation of any concept. In field of transportation GIS, the examples of these real life problems are optimal path problem, location-allocation problem, minimum spanning tree problem, supply-demand problem, vehicle routing problem, travelling salesman problem, postman problem, maximum flow problem etc. In this study, the location-allocation problem is solved using GIS over a road transportation network in which GIS helps to find out the best suitable location for establishing a facility and identifying the total service area of the facility.

Transportation road network is defined as a system of interconnected point and line features through which resources flow. The network properties like connectivity, position & weights of network features, and direction of flow of resources over the network decided the type of the road network. The connectivity among the network elements is overall responsible to perform the network analysis based on the weight function (cost factor) of the features and direction of flow of resources from one element to another. The weight function represents basically the transportation cost from one location to another location over a network, and in GIS it is commonly known as the impedance factor. The transportation cost (impedance factor) can be calculated with respect to travel distance or travel time or any other factor which is directly or indirectly responsible for transportation cost between the geographical locations.

Location-Allocation Problem (LAP) is to locate a set of new facilities in an area of interest in order to satisfy the customer demands and minimizing total transportation cost from customer locations to facilities and vice versa. This problem arises in many practical urban settings where facilities provide homogeneous services such as the identification and location of ATMs, malls, warehouses, distribution centers etc. Many models have been presented for the solution of LAP, and numerous algorithms have been designed for these models, involving branch-and-bound algorithms, simulated annealing, Tabu search, heuristic and metaheuristic which is proved to obtain the best results when the number of facilities to locate is large.

1.2. Geographic Information System (GIS)

Geographic Information System (GIS) is a computer based system including hardware and software for collection, storage, manipulation, analysis and visualization of geographical data representing some geographic phenomenon on the Earth. The geographical data or geospatial data or geo-referenced data consists of spatial and non-spatial (attribute) information of the geographical features. GIS technology has a unique capability to integrate common database operations and spatial analyses with the visualization and geographic analysis benefits offered by maps. These abilities distinguish GIS from other information systems.

We commonly think of a GIS as a single, well-defined, integrated computer system. However, this is not always the case. A GIS can be made up of a variety of software and hardware tools which are useful to solve the real life problems. The basic idea behind the GIS Tool is to solve the specific problem using that tool for which it is developed. At the time of development of GIS tool for a specific problem, is to first understand that specific problem and then convert the problem into mathematical form (equation/inequalities) using certain method/algorithm. After that write the programme of these mathematical equations/inequalities using compatible programming language, and then develop the GIS tool for that specific problem. Finally, in reverse way this developed tool will help you to get the solution of that specific problem. GIS software is basically the integration of these tools to provide a smoothly operating, fully functional geographical data processing environment.

GIS has a unique capability in order to optimize the solution of network related problems in an efficient way. This study shows the optimization of Location-Allocation problem in an urban area which is based on the metaheuristic algorithm.

1.3. Topology

Topology is a famous term in mathematics which deals with the relationships among the features (elements). In GIS topology deals with the spatial relationship (connectivity, continuity and containment) of geographical features (point, line and polygon), and the relationships among the geometric features remains invariant under certain transformations. Topology is fundamentally used to ensure data quality and to aid in data compilation.

Geospatial topology studies the rules concerning the relationships between the points, lines, and polygons that represent the features of a geographic region. For example, where two polygons represent adjacent counties, typical topological rules would require that the counties share a common boundary without any gap or overlapping.

1.4. Location-Allocation Problem

Location-Allocation Problem (LAP) is consisting of two words location and allocation and are known as the elements of the problem. Locations are the places to put the central facilities, also called facility point, and allocation are the places where material demand is required and is also called customer location. LAP is basically locating the facilities and allocating the demands to the facilities. Its objective is to find locations for facilities and allocate customers (demands) to them in order to minimize the total transportation cost. In short, Location Allocation determines the optimal locations of a service in order to serve the population in the most efficient manner. Graphically it can be shown in Figure 1.

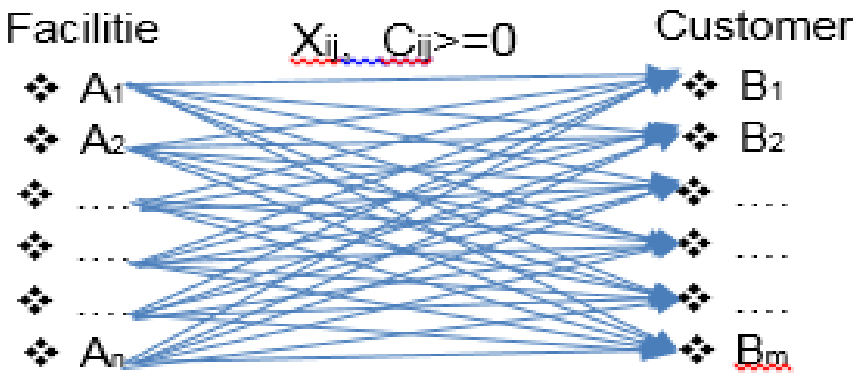

Figure 1: *Graphical representation of LAP*

In this representation there are n facility points and n demand points which are geographically scattered. Where Xij is the quantity transported from ith facility location to jth customer location and Cij is the per unit transportation cost from ith facility location to jth customer location. Meta-heuristics techniques, which are more efficient search approaches for larger and more complicated problems than heuristics methods, are used in this study.

1.5. Location-Allocation Problem Types

Based on actual requirement of supply and demand of a material from facility points to demand points, the following types of Location-Allocation Problems (LAPs) are given below:

Minimize Impedance: In this type of the LAP, the facility points are located in such a way that the total weighted cost (demand allocated to the facility multiplied by the impedance to the facility) between customer location and facility location is minimized. This problem basically reduces the total transportation costs of delivery of items to the outlets or the total travel distance/time to reach the chosen facility point.

This problem type handles the demand based on the following criteria:

The demand locations are allocated to the facility according to the facility's impedance (distance/time) cut-off value. Within the facility's impedance cut-off value, demands are allocated to the facility, and outside the facility's impedance cut-off value, demands are not allocated to that facility. A demand point inside the impedance cut-off value of two or more facilities has all its demand weight allocated to the nearest facility only.

Minimize Facilities: This problem describes that the facilities are located in such a way that as many demand points as possible are allocated to all facilities within the impedance cut-off. In addition to this the total number of facilities required to cover all demand points is minimized. Minimize Facilities problem is the same as Maximize Coverage but with the difference of the less number of located facilities.

The points below describe demands handled by Minimize Facilities problem:

Any demand point outside the impedance cut-off of all the facilities is not allocated. A demand point inside the impedance cut-off of one facility has all its demand weight allocated to that facility. A demand point inside the impedance cut-off of two or more facilities has all its demand weight allocated to the nearest facility only.

1.6. Mathematical Formulation of Location-Allocation Problem

Let $M = \{M_i : 1 \le i \le m\}$ is a set of 'm' facility (supply) locations and $N = \{N_j : 1 \le j \le n\}$ is a set of 'n' demand (customer) locations. Consider a_i $(1 \le i \le m)$ is the quantity available at supply (facility) location i, and b_j $(1 \le j \le n)$ is the quantity required at the demand (customer) location j.

In order to model the location-allocation problem, the following indices, parameters, and decision variables are used:

(x_i, y_i) = coordinates of facility location i, $1 \le i \le m$

(l_j, k_j) = coordinates of customer locations j, $1 \le j \le n$

C_{ij} = per unit transportation cost for delivering goods/material to customer j from facility i, $1 \le i \le m$ & $1 \le j \le n$.

D_{ij} = distance between the ith facility point and jth customer point, $1 \le i \le m$ & $1 \le j \le n$

X_{ij} = quantity transported from ith facility to jth customer

$$z_{ij} = \begin{cases} 1 & \text{if customer j is allocated to facility i} \\ 0 & \text{otherwise} \end{cases}$$

The decision variable representing number of customer locations assigned to ith facility is:

$$\eta_i = \sum_{j=1}^{n} b_j z_{ij} \quad where\, 1 \le i \le m$$

The objective function to minimize the total transportation cost can be written as:

$$Z = minimize \sum_{i=1}^{m} \sum_{j=1}^{n} X_{ij}\, C_{ij} D_{ij}$$

Subject to the following constraints:

$$\sum_{i=1}^{m} a_i = \sum_{j=1}^{n} b_j \qquad (1)$$

$$\sum_{i=1}^{m} z_{ij} = 1 \qquad \forall\ j \qquad (2)$$

$$z_{ij} = \{0,1\} \qquad \forall\ i\ \&\ j \qquad (3)$$

$$X_{ij} \ge 0 \qquad \forall\ i\ \&\ j \qquad (4)$$

$$C_{ij} \ge 0 \qquad \forall\ i\ \&\ j \qquad (5)$$

$$\sum_{j=1}^{n} X_{ij} \le a_i \qquad \forall\ i \qquad (6)$$

$$\sum_{i=1}^{m} X_{ij} \le b_j \qquad \forall\ i \qquad (7)$$

$$\sum_{i=1}^{m} z_{ij} = b_j \qquad \forall\ i \qquad (8)$$

The constraint (1) assumes that the total supply is equal to the total demand, while constraints (2) assure that every customer is assigned with any of the facility. Constraint (3) is domain constraint while the constraints (4) and (5) are representing the quantity transported and transportation cost respectively. Constraints (6) is called supply constraint and (7) is called demand constraint.

2. Objectives and Questions

The main purpose of this study is to solve the location-allocation problem using metaheuristic algorithm over the Hisar city of Haryana state, and also to observe the performance of the algorithm. The sub-objectives of the study are:

- To create the digital database of Hisar City, Haryana in GIS environment for the solution of Location-Allocation problem.
- To create the topology and network dataset in order to optimize the results of Location-Allocation problem.
- To perform the network analysis and find out the solution of Location-Allocation problem under various real life situations like:
  - ✓ To determine the optimal vita distributors location for vita booths
  - ✓ To determine the optimal vita booths location for vita distributors
  - ✓ To minimize the vita distributors in order to fulfil the demands of vita booths
  - ✓ To maximize the total coverage of the vita distributors in order to serve the maximum vita booths.

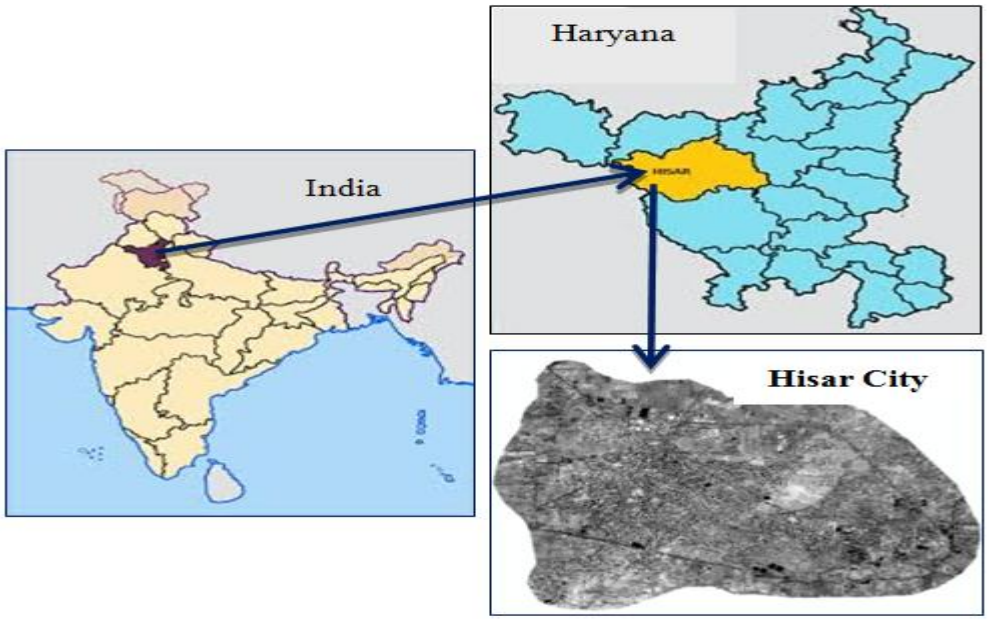

Figure 2: *Study area (Hisar City, Haryana, India)*

Under this study the main research question over the optimality of results are: i) what are the essential attribute information of the network features required for the solution of LAP in GIS environment? ii) What are the essentially required attributes of the Network Dataset to optimize the result of LAP?

3. Study Area

In this study, Hisar City of Hisar district in Haryana state, India is identified as the study area. The study area is located between parallel 29°6'49"N to 29°11'57"N and meridian 75°40'53"E to 75°48'19"E in the western part of Haryana state, and at an average elevation of 215 m from mean sea level. It covers total area of 82.8648 km^2 and Figure 2 shows the geographical extent of the study area.

To perform the analysis we have digitized only vita distributors, vita booths and roads layers in our database of the study area.

4. Literature Review

Farahani et al. (2010) and Farahani et al. (2012) reviewed the recent efforts and development in multi-criteria location problems in three categories including bi-objective, multi-objective and multi-attribute problems and their solution methods. They have studied so few chapters or sections in different books but they have not seen any comprehensive review papers or book chapter that can cover it. Yanga et al. (2007) investigated location-allocation problem under fuzzy environment. Consequentially, chance constrained programming model for the problem to seek the approximate best solution of the model was designed and some properties of the model were investigated using Tabu search, genetic and fuzzy simulation algorithms.

Sha and Huang (2012) proposed an emergency blood supply scheduling model, in which they proposed a multi-period location - allocation model, and give the heuristic algorithm based on Lagrangian relaxation. Finally, they tested this algorithm over an example case study in the context of Beijing. A multi-criteria analysis based study on Nawabwip Municipality, West Bengal, India for Location-allocation of urban waste disposal sites, was done by Paul (2012).

Hongzhong et al. (2007) studied the general facility location problems and identify models used to address common emergency situations, such as house fires and regular health care needs and then then analyzed the characteristics of large-scale emergencies and propose a general facility location model that is suited for large-scale emergencies. Hussey et al. (1996) had studies the selection of landfill sites and associated problem particularly in the field of public health using geographic information system (GIS) based on parameters given by European Union Landfill directives. Curtin (2007) analyzed the network data structures and network location problems using GIS. Brimberg et al. (2000) and Brimberg et al. (2005) have compared the heuristics for solving multisource uncapacitated weber problem and also suggested the improvements for the solution. The study was extended by Brimberg et al. (2006) and Talbi (2009) for solving continuous field location-allocation problem for fixed cost of zones and implemented metaheuristics. They have also proposed the decomposition strategies for large-scale continuous location-allocation problems.

A constrained form of the classical Weber problem was investigated by Butt et al. (1996). In this problem, new facilities have been located in the presence of convex polygonal forbidden regions such that the sum of the weighted distances from the new facility to ‘n’ existing facilities is minimized. Silva et al. (2008) presented a comparative study of genetic algorithms (GA) and ant colony optimization

(ACO) applied the online re-optimization of a logistic scheduling problem based on the simulation. Silva et al. (2009) studies a Hub location problem which generally involve three simultaneous decisions to be made: the optimal number of hub nodes, their locations and the allocation of the non-hub nodes to the hubs.

Abdollahi Demneh et al. (2011) examined the emergency services facility location problem focusing on lose due to service delay. They have considered delay as a function of distance between the server and the customer. They formulated the problem as a mathematical model and then solve it efficiently for a numeral example. Hajipour et al. (2014) proposed a novel soft-computing approach based on the vibration theory called vibration damping optimization (VDO) to solve the Redundancy Queuing-Location-Allocation Problem. They developed a multiobjective version of the VDO called multiobjective VDO (MOVDO) based on the fast nondominated sorting and crowding distance concepts in the literature and the performance of the proposed MOVDO was statistically compared with the nondominated sorting genetic algorithm and multiobjective simulated annealing.

5. Materials and Methods Used

In this study, the used materials and adopted methodology are described below which perform vital role to achieve the assigned objectives.

Figure 3: *Quick Bird image of study area*

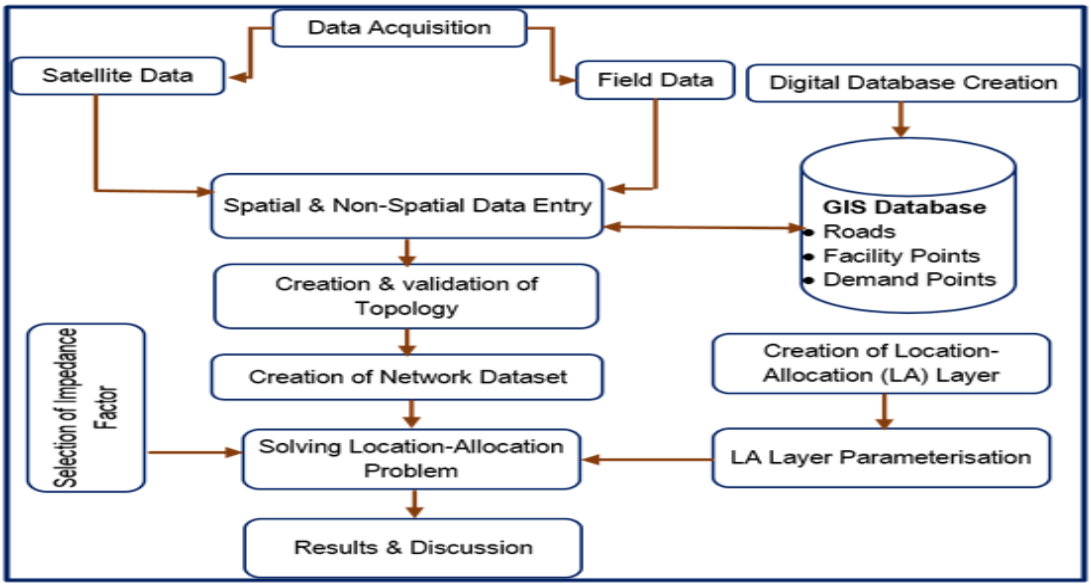

Figure 4: *Methodological flow chart*

5.1. Material Used

Satellite Data: To create the digital database of the study area for the purpose of Location allocation problem, a high spatial resolution Quick Bird satellite data (Figure 3) is used in this study. Quick Bird satellite is a polar satellite and launched on October 2001 and has a revolution time of 93.4 minutes around the Earth. The images collected by this satellite have spatial resolution of 0.61 m (panchromatic) and 2.5 m (multispectral). The multispectral images consist of four bands in the blue (0.45–0.52 µm), green (0.52–0.60 µm), red (0.63–0.69 µm) and near-infrared (0.76–0.89 µm) wavelength regions, and panchromatic images has a spectral band of 0.45–0.90 µm. In this study, a merged product (0.61 m spatial resolution) of multispectral (2.5 m) and panchromatic (0.61 m) images dated June 3, 2011, was used for capturing geographical features (point & line) of the study area.

Field Data: To perform the location-allocation problem, we have also acquired attribute information of features (point & line) from the field. We have collected attribute information of Road features (road type, road name and allowed speed limit), Facility/Supply Point features (Facility name, coordinates, type of available material/goods) and Demand Points features (Name, coordinates, type of demanded material/good).

Software Used: In this study, we have used ESRI desktop product ArcMap 10 software for digital GIS database creation, spatial & non-spatial data entry & editing, topology creation, network data set creation and solving the location-allocation problem.

5.2. Method Used

In this study, the method used to perform the solution of LAP is shown in the flow chart shown in Figure 4.

First of all, we have prepared the digital GIS database in ArcGIS software which contains three types of the feature classes namely Roads (line), Vita Distributors which supply the milk, and Vita Booths which takes milk from Vita Distributors, and collected attribute information about these feature classes

from the field. The coordinate system of database and satellite image was kept same i.e. WGS 84 datum, UTM projection and 43N zone. After that, we have entered the spatial data into all the feature classes by means of digitization over a satellite image. Once the data entry part is over, we have checked the digitization errors in the database and also corrected them by data editing tools.

Subsequently we have created topology of the database to remove remaining topological errors by creating various topological rules. And then a geo-database based network dataset was created using all the layers of database in GIS environment and decided different connectivity rules among different features, driving directions for easy access, turns and attributes of network dataset for optimal calculation.

For finding optimal allocation (demand) for each location (facility), we have decided the parameters of Location-Allocation layer and impedance factor. Finally, the analysis was performed and final results were generated.

In this study, we have considered two types of the bidirectional (From-to or FT and to-From or TF) impedance factors (cost functions) i.e. travel distance (meters) and travel time (minutes). For distance impedance, we have taken length of the road (shape_length) which is same along both the directions i.e. from-to (along the digitization direction) and to-from (opposite to the direction of digitization).

The time impedance factor was calculated using the road length (m) and speed limit of the road (km/h). It is not necessary that this impedance will be same along both the directions (FT and TF), so we have calculated it along both the directions separately using the following formula:

$$FT\_Time\_\text{minutes} = \frac{0.06 * SHAPE\_Length\,(m)}{FT\_Speed\,(km/hr)}$$

$$TF\_Time\_\text{minutes} = \frac{0.06 * SHAPE\_Length\,(m)}{TF\_Speed\,(km/hr)}$$

6. Results and Discussion

The results obtained are divided into different parts and discussed below:

6.1. Digital Database for LAP

The GIS database of the Hisar City (study area) was created in ArcGIS software. The database contains various feature classes (line & point) like roads, vita distributors and vita booths as shown in the Figure 5. In this database there are total 7556 roads having total shape length of 657652.4 meters, 3 vita distributors and 25 vita booths. After completing the GIS database, the topology of entire database was created to remove the topological errors of the database.

6.2. Network Dataset

The network dataset is basically a plate form where all the feature classes connect with each other and is essential to perform the solution of location-allocation problem in ArcGIS software. The network dataset was created using all the feature classes of the database where we have assigned the connectivity policy among different features, driving directions over the roads, turns at roundabouts, and created impedance factors for optimal path calculation. The created network dataset is shown in Figure 6.

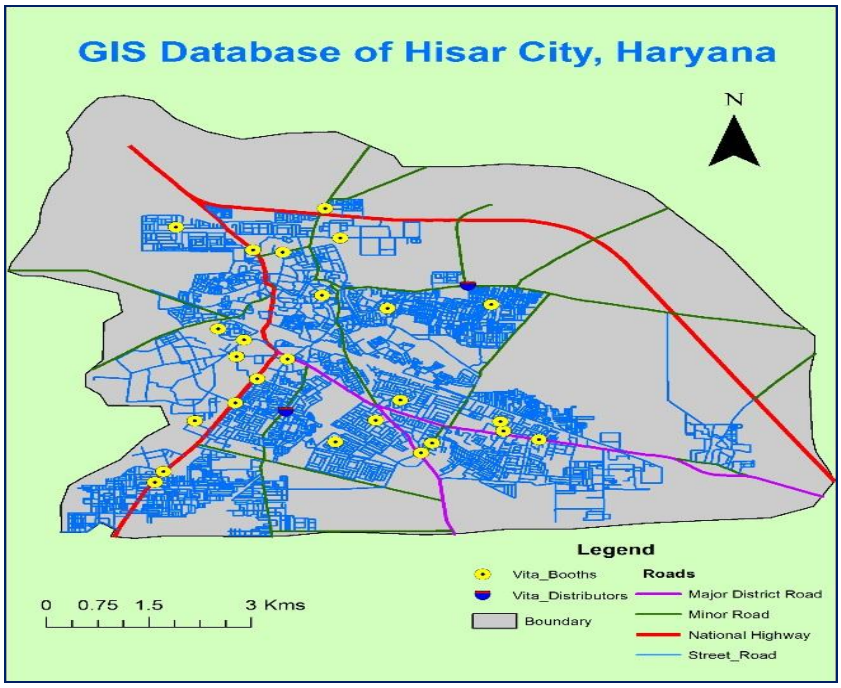

Figure 5: *GIS database of study area*

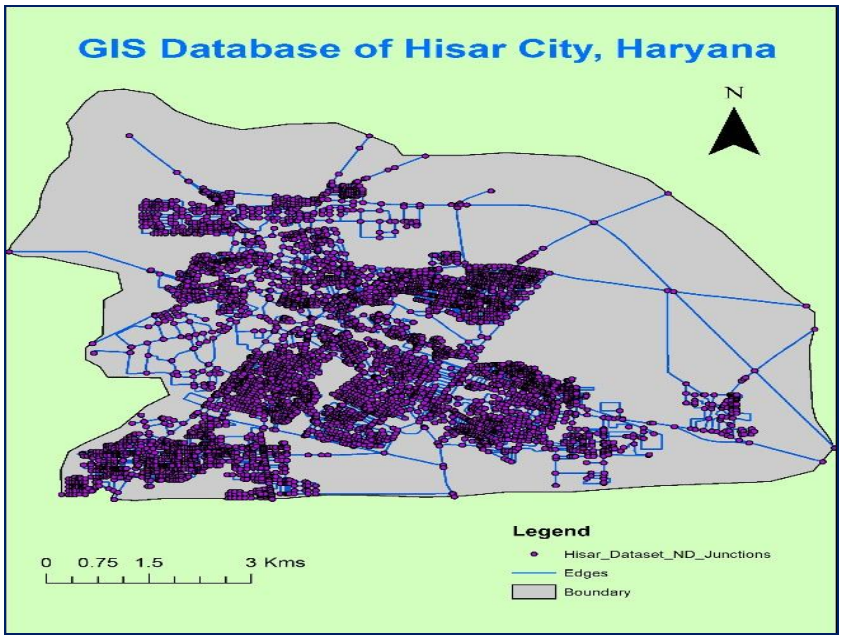

Figure 6: *Network dataset of GIS database*

In this GIS Network dataset we have created two types of impedance factors i.e. travel time (minutes) and travel distance (meters) for the calculation of optimal path. At the end of the creation of network dataset, there is another point feature layer, known as junction layer. These junctions are created at the intersection locations of line (road) features and stored in a separate layer.

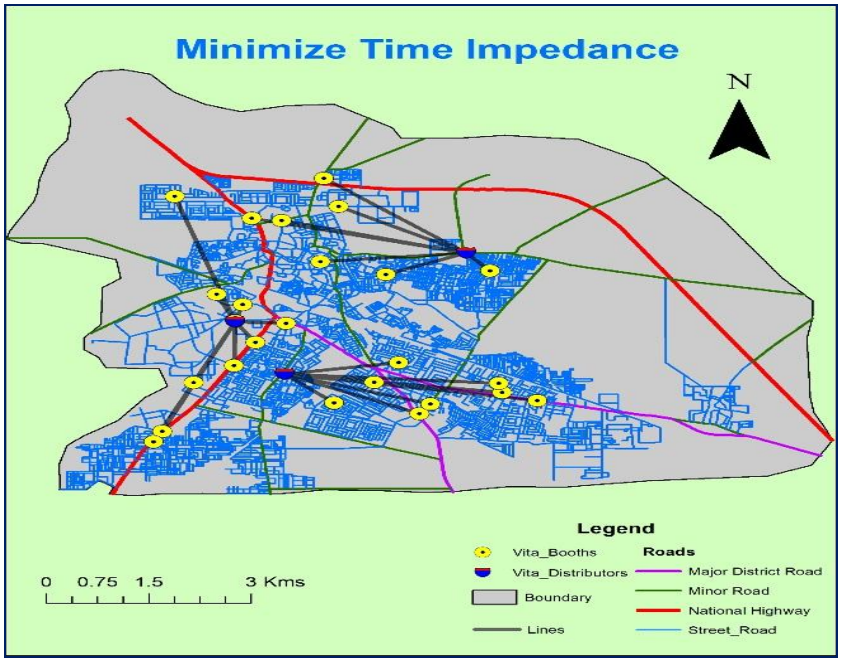

Figure 7: *Minimize time impedance*

6.3. Solutions of LAP

For finding out the solution of location allocation problem, we have considered the Vita distributors as the facility locations and vita booths as the demand locations where the material is to be allocated. The solution of LAP is assessed based on the different parameters in order to optimize the transportation cost in terms of driving time and travel distance. These are:

6.3.1. *Minimize Impedance*

In this case, the main objective is to minimize the total delivery cost of milk from vita distributor locations to vita booth locations. This type of problem is often called the P-Median problem. Here the solution of location allocation problem is shown based on two types of the impedance factors i.e. driving time and travel distance which are direct indicator of transportation/delivery cost.

Time Impedance: In this case the travel time impedance is minimized from vita booths (demand point) to vita distributors (facilities). In order to allocate all the vita booths with vita distributors, 7.3 minutes of cut-off time impedance was decided.

The optimal allocation of all the vita booths with the nearest vita distributors is shown in Figure 7.

Table 1: *Attribute information of facilities*

Name	Weight	Capacity	DemandCount	Total_Travel_Time	TotalWeighted_Travel_Time
PLA, Vita Plant	1	3000	8	44.121187	44.121187
HAU, Vita Plant	2	3800	10	29.155849	29.155849
Rajeev Nagar, Vita Plant	3	5000	7	31.571005	31.571005

Table 2: *Attributes of allocated vita booths with the vita distributors*

Name	DemandID	FacilityID	Total_Travel_Time	Total_Driving_Distance
GJU, Shopping Complex Booth - Rajeev Nagar, Vita Plant	5	1	5.816293	3635.202403
Civil Hospital Booth - Rajeev Nagar, Vita Plant	6	1	6.259657	3691.88064
New Police Line - Rajeev Nagar, Vita Plant	19	1	5.497048	3664.806116
Auto Market - Rajeev Nagar, Vita Plant	20	1	5.896906	3450.556872
Indira Colony - Rajeev Nagar, Vita Plant	23	1	2.726035	1499.747716
Shiv Nagar - Rajeev Nagar, Vita Plant	24	1	1.288921	671.33881
Multani Chowk - Rajeev Nagar, Vita Plant	25	1	4.086144	2351.788713
Jawahar Nagar Booth - HAU, Vita Plant	1	2	1.427966	720.470109
HAU Gate No 4 Booth - HAU, Vita Plant	2	2	2.231802	1327.080783
Bostal Jail, Vita Booth - HAU, Vita Plant	3	2	4.617836	3126.486009
Azad Nagar Booth - HAU, Vita Plant	4	2	5.0434	3434.77756
Municipal Corp. Gate - HAU, Vita Plant	11	2	2.02229	1010.818897
Court Complex - HAU, Vita Plant	12	2	4.185531	2098.630267
Old Court Complex - HAU, Vita Plant	17	2	1.649277	847.301843
Sector 14 - HAU, Vita Plant	18	2	7.081286	4340.194446
Madhuban Park - HAU, Vita Plant	21	2	0.85349	426.398144
Near Panchayat Bhawan - HAU, Vita Plant	22	2	0.042971	21.138628
Vidyut Nagar 1 - PLA, Vita Plant	7	3	6.698953	4105.622279
Vidyut Nagar 2 - PLA, Vita Plant	8	3	6.949732	4228.817161
MC Colony - PLA, Vita Plant	9	3	4.561222	2579.305336
Vidyut Nagar 3 - PLA, Vita Plant	10	3	7.291001	4569.339835
Sector 16-17 - PLA, Vita Plant	13	3	3.064557	1538.101387
Sector 13 P-II - PLA, Vita Plant	14	3	4.214814	2445.850537
ITI Chowk - PLA, Vita Plant	15	3	5.428648	3320.060153
Jindal Hospital - PLA, Vita Plant	16	3	5.91226	3379.070952

The attributes information of facilities layer is shown in Table 1. Here the weights and capacity (in litres) of all vita distributors is decided according to their importance. We have considered that all the vita booths are having same importance so the demand weight is same for all the vita booths i.e. 1 in this case. The total travel time & weighted travel time of all the assigned customers (vita booths) to each facility is shown in Table 1. Out of 25 vita booths 8 are allocated to PLA Vita Plant, 10 are allocated to HAU, Vita Plant and 7 are allocated to Rajeev Nagar Vita Plant.

The allocation detail of all the vita booths with the vita distributors and total travel time and distance from every vita booth to the concerned vita distributor is shown in Table 2.

Table 3: *Attribute information of facilities*

Name	Weight	Capacity	Demand Count	Total_Driving_Distance	TotalWeighted_Driving_Dista
PLA, Vita Plant	1	3000	8	25669.770816	25669.770816
HAU, Vita Plant	2	3800	10	17311.508486	17311.508486
Rajeev Nagar, Vita Plant	3	5000	7	18755.850515	18755.850515

Table 4: *Allocation of vita booths with vita distributors*

Name	DemandID	FacilityID	Total_Driving_Distance	Total_Travel_Time
GJU, Shopping Complex Booth - Rajeev Nagar, Vita Plant	5	1	3580.877611	6.358947
CMI Hospital Booth - Rajeev Nagar, Vita Plant	6	1	3691.88064	6.259657
New Police Line - Rajeev Nagar, Vita Plant	19	1	3575.708008	5.578961
Auto Market - Rajeev Nagar, Vita Plant	20	1	3393.624985	6.109048
Indira Colony - Rajeev Nagar, Vita Plant	23	1	1490.43175	2.729333
Shiv Nagar - Rajeev Nagar, Vita Plant	24	1	671.33881	1.288921
Multani Chowk - Rajeev Nagar, Vita Plant	25	1	2351.788713	4.086144
Jawahar Nagar Booth - HAU, Vita Plant	1	2	720.470109	1.427966
HAU Gate No 4 Booth - HAU, Vita Plant	2	2	1327.080783	2.231802
Bostal Jail, Vita Booth - HAU, Vita Plant	3	2	3126.486009	4.617836
Azad Nagar Booth - HAU, Vita Plant	4	2	3434.77756	5.0434
Municipal Corp. Gate - HAU, Vita Plant	11	2	1010.818897	2.02229
Court Complex - HAU, Vita Plant	12	2	2098.630267	4.185531
Old Court Complex - HAU, Vita Plant	17	2	847.301843	1.649277
Sector 14 - HAU, Vita Plant	18	2	4298.406245	7.232638
Madhuban Park - HAU, Vita Plant	21	2	426.398144	0.85349
Near Panchayat Bhawan - HAU, Vita Plant	22	2	21.138628	0.042971
Vidyut Nagar 1 - PLA, Vita Plant	7	3	4105.622279	6.698953
Vidyut Nagar 2 - PLA, Vita Plant	8	3	4228.817161	6.949732
MC Colony - PLA, Vita Plant	9	3	2579.305336	4.561222
Vidyut Nagar 3 - PLA, Vita Plant	10	3	4569.339835	7.291001
Sector 16-17 - PLA, Vita Plant	13	3	1538.101387	3.064557
Sector 13 P-II - PLA, Vita Plant	14	3	2445.850537	4.214814
ITI Chowk - PLA, Vita Plant	15	3	2962.202012	5.905003
Jindal Hospital - PLA, Vita Plant	16	3	3240.532268	6.456886

Distance Impedance: The optimal allocation of vita booths based on distance (in meters) as a impedance factor with a cut-off value 4800 meters was studied. The allocation of all vita booths with concerned vita distributor is shown in Figure 8.

The attributes (like total sum of driving distances from each vita booths to the assigned facility, facility weights, no. of vita booths assigned to a vita distributor) of vita distributors layer are shown in Table 3.

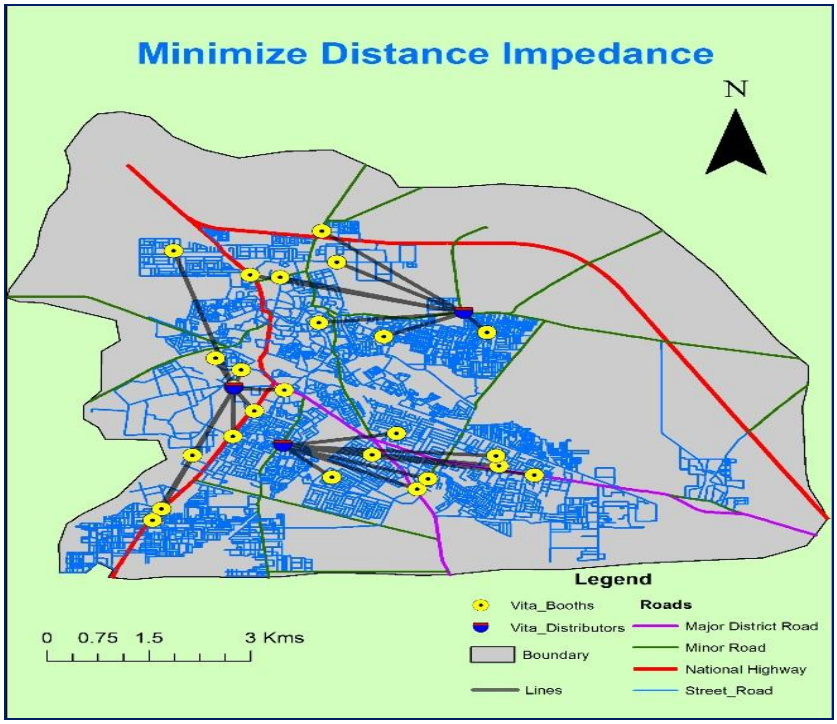

Figure 8: *Minimize distance impedance*

The driving distances and travel time from each vita booths to solution facility is shown in Table 4. The allocation of all vita booths is also mentioned in 'name' field.

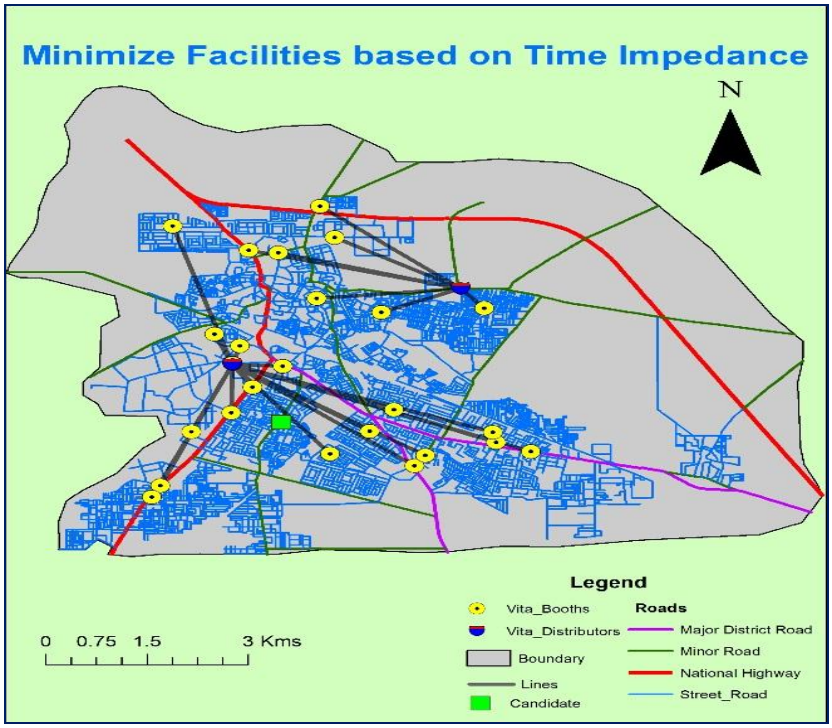

Figure 9: *Solution of minimize facilities problem*

6.3.2. *Minimize Facilities*

There are total 3 vita distributors which are serving all the 25 vita booths. To assign the optimal use of facilities, this number of facilities can be minimized and the total manufacturing cost can also be reduced for the business purpose. The problem was solved with 8 minutes of cut-off value of time impedance and it is found that only facilities are sufficient to serve all the demand points (vita booths) as shown in Figure 9. The serving facilities are shown by vita distributors feature and the facility which can be removing from the solution is shown by candidate feature in the Figure 9.

Table 5: *Attribute of facilities*

Name	FacilityType	Weight	Demand Count	Demand Weight	Total_Travel_Time
PLA, Vita Plant	Candidate	1	0	0	0
HAU, Vita Plant	Chosen	2	18	18	80.253799
Rajeev Nagar, Vita Plant	Chosen	3	7	7	31.571005

Table 6: *Allocation of vita booths to vita distributors*

Name	Facility ID	Demand ID	Total_Travel_Time	Total_Driving_Distance
Auto Market - Rajeev Nagar, Vita Plant	1	20	5.896906	3450.556872
Azad Nagar Booth - HAU, Vita Plant	2	4	5.0434	3434.77756
Bostal Jail, Vita Booth - HAU, Vita Plant	2	3	4.617836	3126.486009
Civil Hospital Booth - Rajeev Nagar, Vita Plant	1	6	6.259657	3691.88064
Court Complex - HAU, Vita Plant	2	12	4.185531	2098.630267
GJU, Shopping Complex Booth - Rajeev Nagar, Vita Plant	1	5	5.816293	3635.202403
HAU Gate No 4 Booth - HAU, Vita Plant	2	2	2.231802	1327.080783
Indira Colony - Rajeev Nagar, Vita Plant	1	23	2.726035	1499.747716
ITI Chowk - HAU, Vita Plant	2	15	5.92121	3781.417365
Jawahar Nagar Booth - HAU, Vita Plant	2	1	1.427966	720.470109
Jindal Hospital - HAU, Vita Plant	2	16	6.404822	3840.428164
Madhuban Park - HAU, Vita Plant	2	21	0.85349	426.398144
MC Colony - HAU, Vita Plant	2	9	5.053784	3040.662548
Multani Chowk - Rajeev Nagar, Vita Plant	1	25	4.086144	2351.788713
Municipal Corp. Gate - HAU, Vita Plant	2	11	2.02229	1010.818897
Near Panchayat Bhawan - HAU, Vita Plant	2	22	0.042971	21.138628
New Police Line - Rajeev Nagar, Vita Plant	1	19	5.497048	3664.806116
Old Court Complex - HAU, Vita Plant	2	17	1.649277	847.301843
Sector 13 P-II - HAU, Vita Plant	2	14	4.707376	2907.207749
Sector 14 - HAU, Vita Plant	2	18	7.081286	4340.194446
Sector 16-17 - HAU, Vita Plant	2	13	6.593385	3543.545618
Shiv Nagar - Rajeev Nagar, Vita Plant	1	24	1.288921	671.33881
Vidyut Nagar 1 - HAU, Vita Plant	2	7	7.191515	4566.979491
Vidyut Nagar 2 - HAU, Vita Plant	2	8	7.442294	4690.174373
Vidyut Nagar 3 - HAU, Vita Plant	2	10	7.783563	5030.697047

The facility name and type, facility weights, no. of allocated vita booth with the concerned facility and total sum of travel times from each vita booth to assigned facility are shown in Table 5.

The driving distances and travel time from each vita booths to solution facility is shown in Table 6. The allocation of all vita booths is also mentioned in 'name' field.

7. Conclusions

The crux of this study is to solve the location-allocation problem using metaheuristic algorithm. In order to achieve the objective we have comprehensively studied the allocation of demand points with the

supply points, and the same was applied for allocation of the veta distributors to the veta booths for the easy access of milk in order to minimize the impedance factor with respect to travel distance or travel time.

In this study, the effectiveness and robustness of the metaheuristic algorithm was tested over a GIS geodatabase based network dataset consisting of road network (line features) and facility & customers locations (point features). The performance of the algorithm was also checked for two impedance factors i.e. time and distance. The results of this location-allocation problem are very much satisfactory in term of minimization of total transportation cost in providing high- quality service to the veta distributors.

Recommendations

In this study we have solved the single objective location allocation problem which can be solved for multi-objective function too in future.

References

Abdollahi Demneh, S.M., Ghandehari, M. and Ketabi, S. 2011. A Location-allocation model for loss minimization in large-scale emergency situation. *Interdisciplinary Journal of Contemporary Research in Business,* 3(8), pp.954-964.

Brimberg, J. and Salhi, S. 2005. A continuous location-allocation problem with zone-dependent fixed cost. *Annals of Operations Research,* 136, pp.99-115.

Brimberg, J., Hansen, P. and Mladenovic, N. 2006. Decomposition strategies for large-scale continuous location-allocation problems. *IMA Journal of Management Mathematics,* 17, pp.307-316.

Brimberg, J., Hansen, P., Mladenovic, N. and Taillard, E.D. 2000. Improvements and comparison of heuristics for solving the uncapacitated multisource Weber problem. *Operations Research,* 48, pp.444-460.

Butt, S.E. and Cavalier, T.M. 1996. An efficient algorithm for facility location in the presence of forbidden regions. *European Journal of Operational Research,* 90, pp.56-70.

Curtin, K.M. 2007. Network analysis in geographic information science: review, assessment, and projections. *Cartography and Geographic Information Science,* 34(2), pp.103-111.

Farahani, R.Z., Asgari, N., Heidari, N., Hosseininia, M. and Goh, M. 2012. Covering problems in facility location: a review. *Computers and Industrial Engineering,* 62, pp.368-407.

Farahani, R.Z., Seifi, M.S. and Asgari, N. 2010. Multiple criteria facility location problems: a survey. *Applied Mathematical Modelling,* 34, pp.1689-1709.

Hajipour, V., Khodakarami, V. and Tavana, M. 2014. The redundancy queuing-location-allocation problem: a novel approach. *IEEE Transactions on Engineering Management,* 61(3), pp.534-544.

Hongzhong, J., Fernando, O. and Dessouky, M. 2007. A modeling framework for facility location of medical services for large-scale emergencies. *IIE Transactions*, (39), pp.1-41.

Hussey, V. Dodd, V. and Dennison, G.J. 1996. Locating a landfill site for Dublin using geographic information systems. *Proceedings of International Civil Engineering, Munic,* 115(3), pp.125-133.

Paul, S. 2012. Location allocation for urban waste disposal site using multi-criteria analysis: a study on Nabadwip Municipality, West Bengal. *International Journal of Geomatics and Geosciences,* 3, pp.74-88.

Sha, Y. and Huang, J. 2012. The multi-period location-allocation problem of engineering emergency blood supply systems. *Systems Engineering Procedia,* 5, pp.21-28.

Silva, C.A., Sousa, J.M.C. and Runkler, T.A. 2008. Rescheduling and optimization of logistic processes using GA and ACO. *Engineering Applications of Artificial Intelligence,* 21(3), pp.343-352.

Silva, M.R. and Cunha, C.B 2009. New simple and efficient heuristics for the uncapacitated single allocation hub location problem. *Computers and Operations Research,* 36(12), pp.3152-3165.

Talbi, E.G. 2009. Metaheuristics: from design to implementation. Wiley, p.624.

Yanga, L., Jib, X., Gaoa, Z. and Lia, K. 2007. Logistics distribution centers location problem and algorithm under fuzzy environment. *Journal of Computational and Applied Mathematics,* 208, pp.303-315.

Cloud Publications
International Journal of Advanced Remote Sensing and GIS
2017, Volume 6, Issue 1, pp. 2306-2324
ISSN 2320 – 0243, Crossref: 10.23953/cloud.ijarsg.296

Case Study

Runoff Depth Estimation using SCS-CN Method in Jhargram Community Development Block - A Remote Sensing and Geographic Information System Approach

Santanu Pani[1], Abhisek Chakrabarty[2]

[1]Research Scholar, Vidyasagar University, Medinipur, West Bengal
[2]Assistant Professor, Vidyasagar University, Medinipur, West Bengal

Publication Date: 11 August 2017

DOI: https://doi.org/10.23953/cloud.ijarsg.296

Abstract Jhargram Community Development blocks which is situated on a watershed divider of Kansabati river basin and Dulung river basin. At a glance the area is suffering for water resource in some of the major parts. Surface runoff is one of the most important indicators of surface water availability, ground water recharge, soil practice etc. In this regard, estimation of runoff is highly needed for water resource planning, management and environment impact analysis. And Geographical Information System (GIS) and Remote Sensing (RS) techniques are used to calculate the runoff depth, it is one of the most time consuming way in recent days. The US Department of Agriculture (USDA), Soil Conservation Service Curve Number (SCS-CN) method which is the most widely used method is very effective in this study. In fact, the model is a quantitative description of land use-land cover and soil complex characteristics of a watershed and their impact on surface water flow. ERDAS Imagine 2014 and ArcGIS 10.1 are the platform which generate the input maps like sub watershed & micro watershed delineation, drainage map, soil map & hydrological soil map, classification of land use/ land cover, elevation & slope map, Rainfall map, area calculation for each class. The rainfall map is prepared from the rainfall data of different stations. After sequentially used the equations of SCS-Curve Number method the different years from 2010 to 2014, the final prioritization map has been generated which shows the value of runoff depth from high to low. Similarly, there has been shown the runoff-rainfall relationship over the last five years. Wherever the runoff depth is high, the infiltration rate is low due to soil and slope. With seeing the results of this case study, this can be used for further management of water resources as well as water scarcity of this area.

Keywords *GIS; Remote sensing; Runoff; SCS-CN*

1. Introduction

The runoff curve number (also called a curve number or simply CN) is an empirical parameter used in hydrology for predicting direct runoff or infiltration from rainfall excess. The curve number method was developed by the USDA Natural Resources Conservation Service, which was formerly called the Soil Conservation Service or SCS - the number is still popularly known as a "SCS runoff curve number" in the literature. The runoff curve number was developed from an empirical analysis of runoff from small catchments and hill slope plots monitored by the USDA. It is widely used and is an efficient method for

determining the approximate amount of direct runoff from a rainfall event in a particular area (Wikipedia).

In this study, I have customized existing SCS-CN hydrological model which considers parameters like slope, catchment size, vegetation, drainage density and drainage length. In order to study land use/land cover type I have generated unsupervised classification and the soil map which is collected from National Bureau of Soil Survey-Land Urbanization Practices input to Soil Conservation System (SCS) model rainfall-runoff estimation.

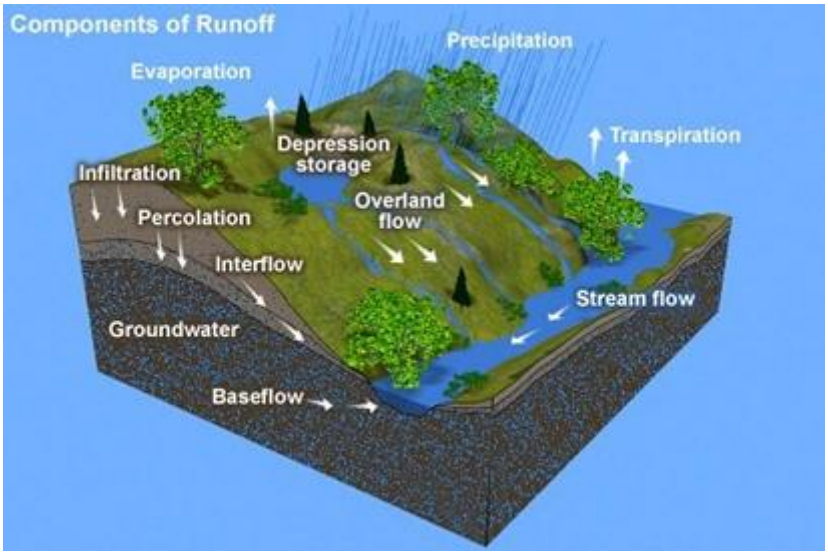

Figure 1: *Concept of water cycle system*

1.1. Objectives of Study

- To determine the quantity and rate from surface water flow.
- To deal with many watersheds related problems and it also focuses the needful decision for management.
- To validate the groundwater prospect zones with getting the run off maps.
- How effective and reasonable to generate run off estimation maps from SCS-CN method over the years using Remote Sensing and GIS technique.

1.2. Location of the Study Area

Jhargram police station serves this block. Headquarters of this block is at Jhargram. Total geographical area of this block is approximately 554 Sq. km. The maximum and minimum temperature varies from 45º C to 10º C and the average normal rainfall 1570 mm. The Jhargram block area covers the parts of two watersheds. The major watershed indicates Kasai river which is the main river flowing in the northern side of the block. And the minor watershed indicates Dulung River which flows south eastern side of the block.

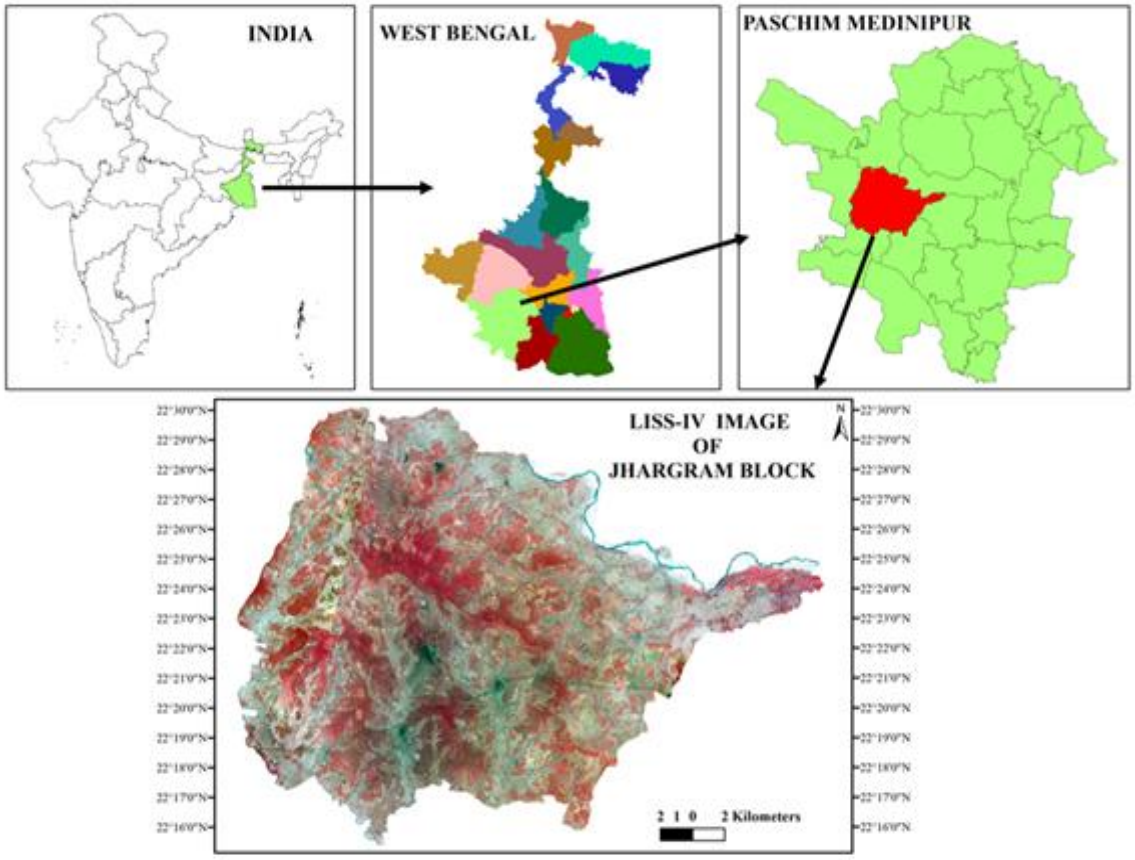

Figure 2: *Location of the study area*

2. Materials and Methods

A number of selective datasets are used for this study such as toposheets, soil map, DEM, satellite images from different sources. Topo maps are collected from Survey of India at the scale of 1:50000 were used for locations, to delineate watersheds and as a reference for all the thematic layers. Soil map is collected from National Bureau of Soil Survey (NBSS-LUP). LISS-IV satellite data of November 2012 was collected from NRSC, Hyderabad to prepare land use/land cover layer and to prepare drainage map as a reference of ASTER data and the ASTER Digital Elevation Model data downloaded from www.usgsearthexplorer.com website to generate major water basins, slope steepness, drainage channels. The monthly rainfall data was provided by Department of Irrigation, West Bengal and it is used after assigning the average annual rainfall.

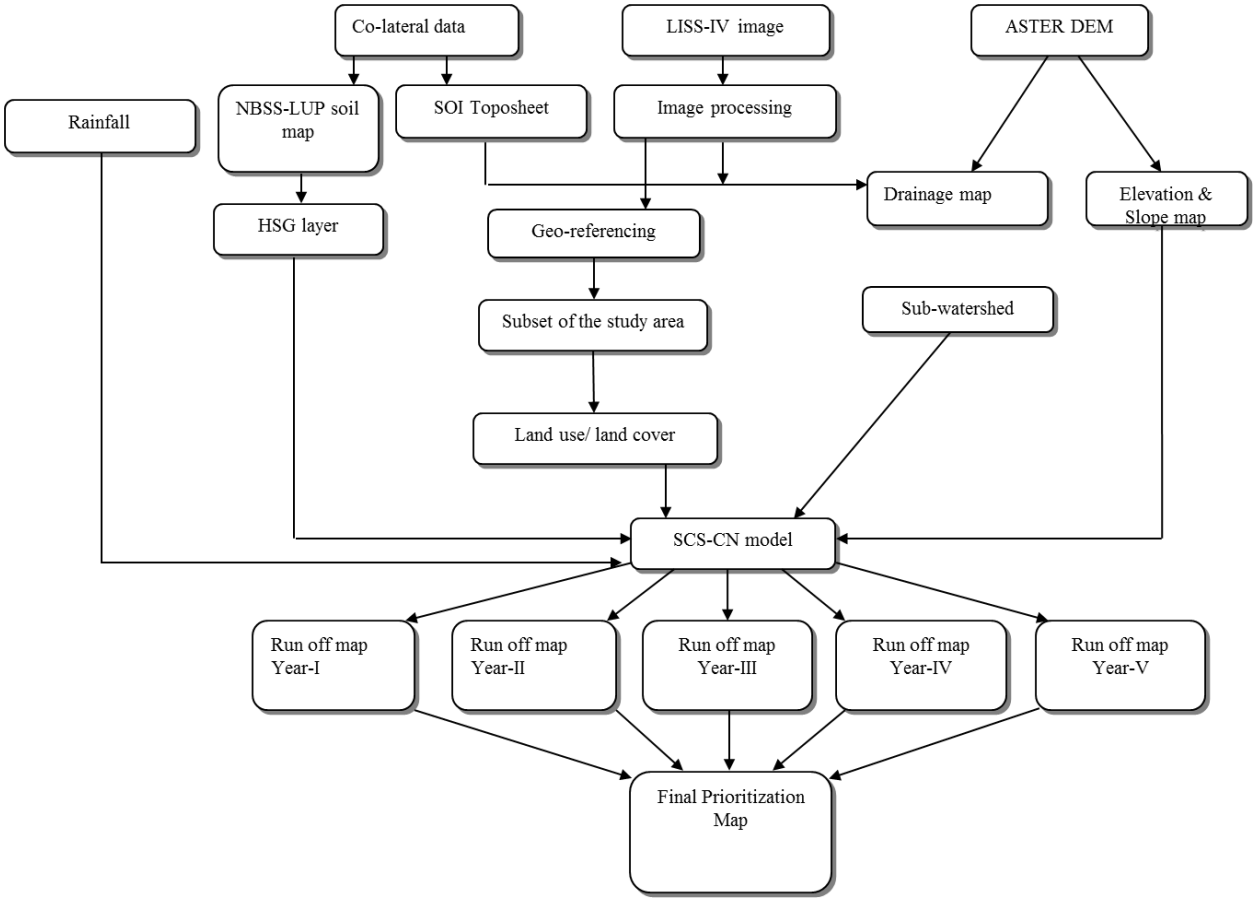

Figure 3: *Flow chart of methodology*

2.1. Generation of Various Types of Thematic Layers

After rectifying the base map is initially prepared from Toposheet (1:50000) provided by SOI. Moreover, the authentication of toposheet is very helpful for checking the location, land use/land cover map preparation, contour and drainage lines preparation and rectifying the other ancillary data. All the work completed through Arc GIS and ERDAS Imagine environment.

2.1.1. *Preparation of Soil Map and Hydrological Soil Map*

NBSS-LUP soil map was rectified with toposheets, block boundary and satellite data in ERDAS Imagine. The soil divisions are digitized in Arc GIS environment. There are five categories of soil identified by NBSS. These are Fine loamy ulti paleustalfs (W069), Fine loamy typic ustifluvents (W065), Fine loamy aeric ochraqualfs (W069), Fine aeric ochraqualfs (W070), and coarse loamy typic haplustalfs (W067).

Group A: Low runoff and high water transmission

Group B: Moderate infiltration and well runoff

Group C: Moderate runoff and poor infiltration capability

Group D: Very poor water transmission and high runoff

After analyzing the characters of different soil groups, the NBSS soil map has been categorized and merged with respect to the character of different Hydrological Soil Group (HSG) in GIS environment. Fine loamy ulti paleustalfs and Coarse loamy typic haplustalfs are converted into HSG – C which has low infiltration rate and high downward moment of water according to USDA, Fine loamy typic ustifluvents and Fine loamy aeric ochraqualfs are categorized into HSG – A which has the character of low runoff potentiality and high infiltration capability due to the contains of sand, Fine aeric ochraqualfs soil comes under HSG – D which has very low infiltration and high runoff potentiality. As a result of urbanization, the soil profile may be considerably altered and the listed group classification may no longer apply. In these circumstances, use the following to determine HSG according to the texture of the new surface soil, provided that significant compaction has not occurred (Brakensiek and Rawls 1983).

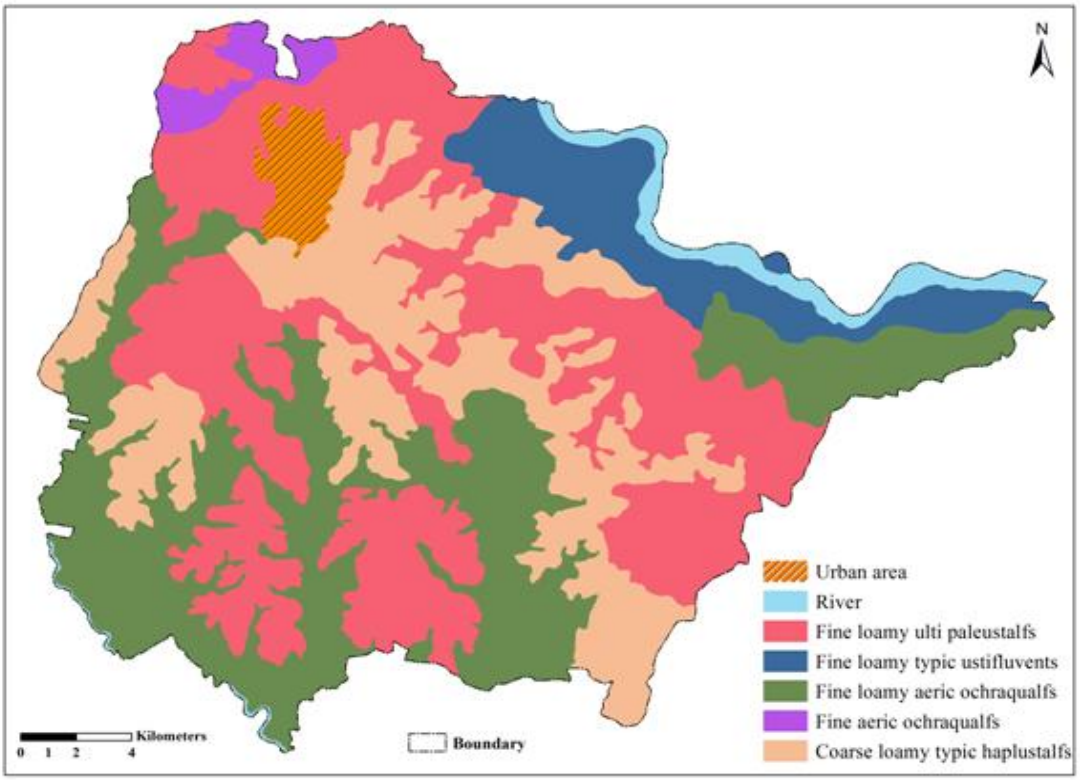

Figure 4: *Soil map*

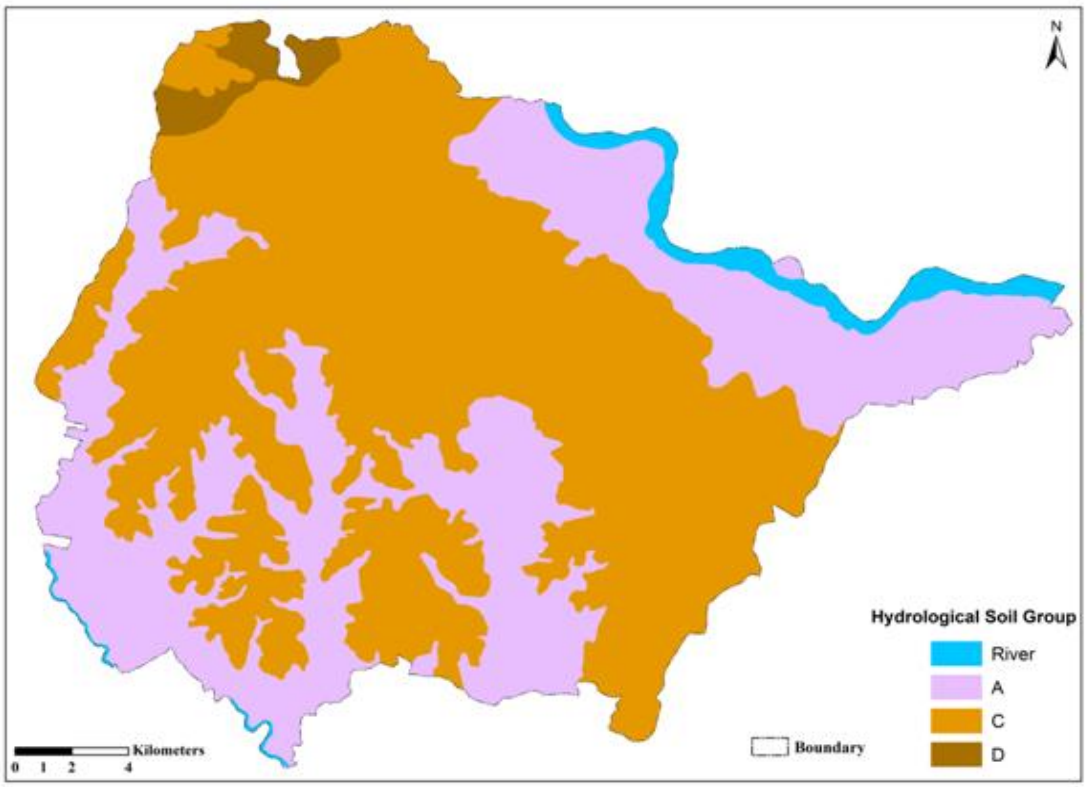

Figure 5: *Hydrological soil map*

2.1.2. *Preparation of LULC and Overlay on Hydrologic Soil Group (HSG)*

The land use/land cover classes have been identified using LISS-IV satellite data and toposheets used as a reference. With the visual interpretation technique, the classes have been found; Agricultural land, Forest, Scrub land, Mixed settlement (settlement mixed with vegetation), Water bodies, River, Social forestry and Urban area. It is very needful to show that the different land use classes have the different impacts on runoff systems. Like urban areas have the high runoff capabilities due to infrastructures as well as concrete areas and less soil. Other side, agriculture land has the less runoff those urban areas.

The final layout has been generated in Arc GIS interface. Final land use/ land cover map was prepared to attach with the Curve Number for each land use classes area falling under different HSG. It was for that the USDA defines the different curve number in different soil group for different land use features. As per the perfection of land use classification the result will be more accurate for selecting the curve numbers and in that case the result of the runoff is more accurate for the watershed.

In case of urban landscape (there is one urban area which is Jhargram township) there is impervious area which leads to connected drainage systems directly from rainfall and some other areas in the township they do outlet on to lawns where minimum infiltration occurs due to impervious land. Actually the slope and height of the township are highest in Jhargram block so that the minimal infiltration occurs against very high surface flow. Several factors, such as the percentage of impervious area and the means of conveying runoff from impervious areas to the drainage system, should be considered in computing CN for urban areas (Rawls et al., 1981).

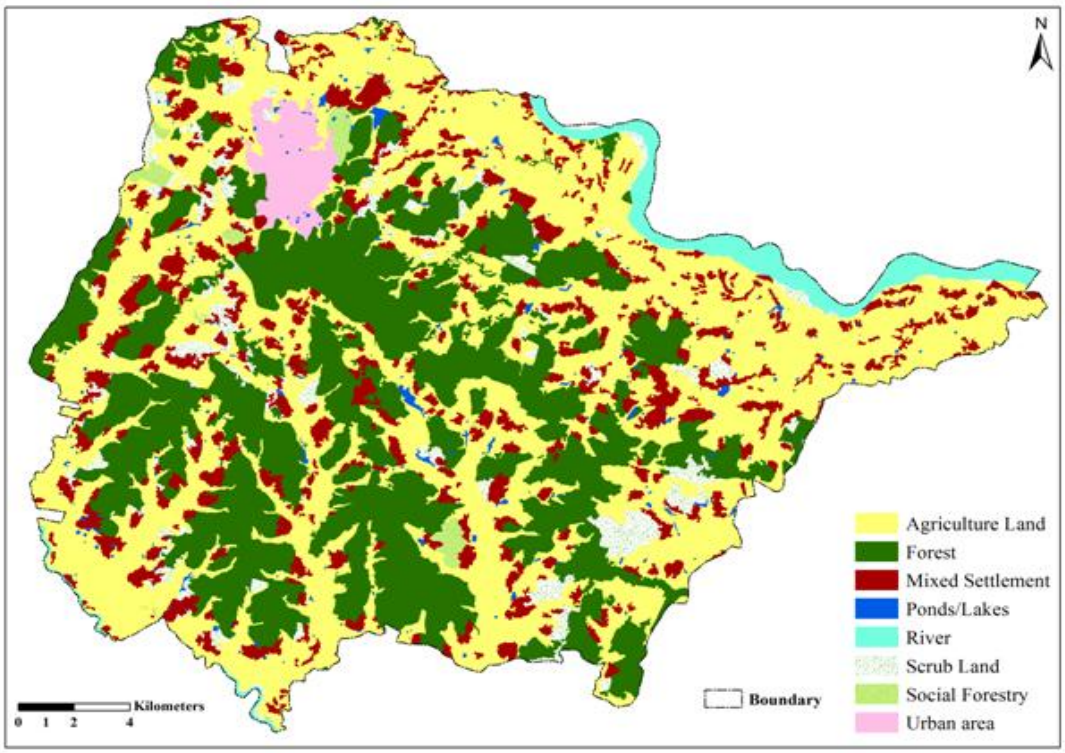

Figure 6: *Land use/land use map*

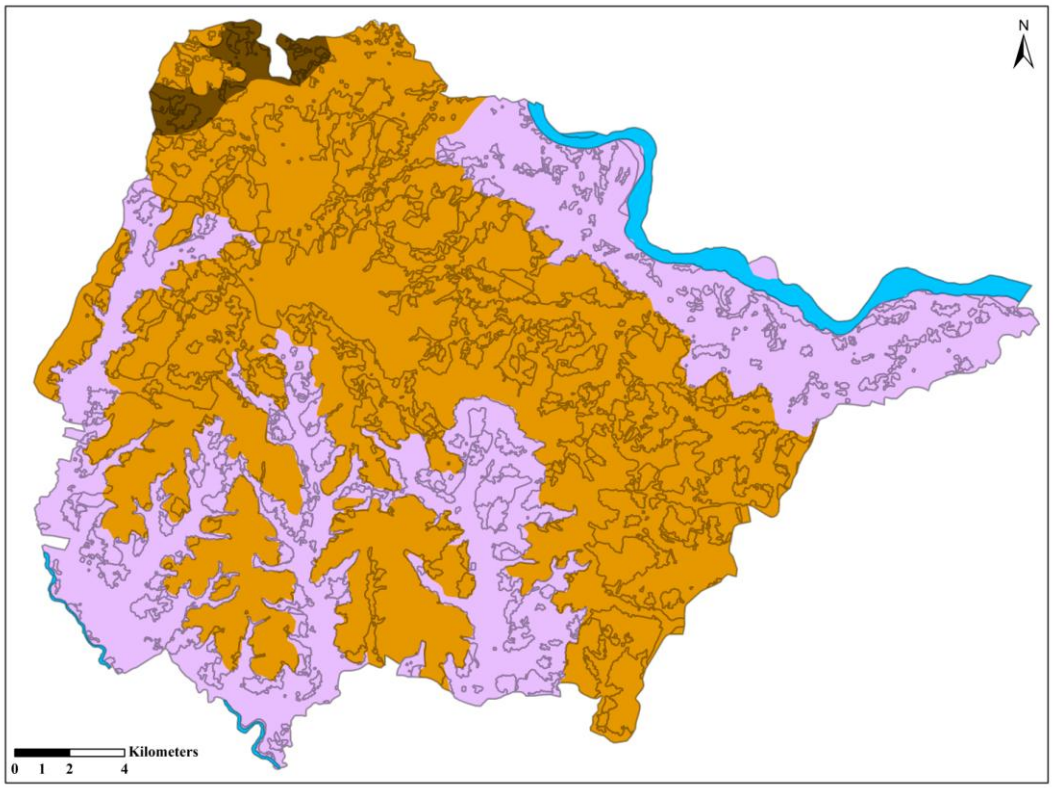

Figure 7: *Overlay of HSG and LULC*

2.1.3. *Elevation and Slope Map*

After processed the ASTER DEM in Arc GIS, the slope map was prepared and took the reference from toposheets. There are five zones (less than 45 meter, 45 – 60, 60 – 75, 75 – 100 and more than 100 meters) have been classified from the Digital Elevation Model. The highest peak of this block is 141 meter which lies at the southern part of Jhargram town. DEM proves the powerful tool and same like the conventional surveys and relief shading with one additional benefit of it providing a powerful analytical perspective. It provides the idea of terrain of the study area. The DEM emerges the degree of slope. Higher the degree of slope, higher the surface flow and soil erosion. The slope steepness map was categorized by five classes that is less than 2 degrees to 37 degrees. The steepest slope zone is within 11 to 37 degree which lies in the north and central zone of the block.

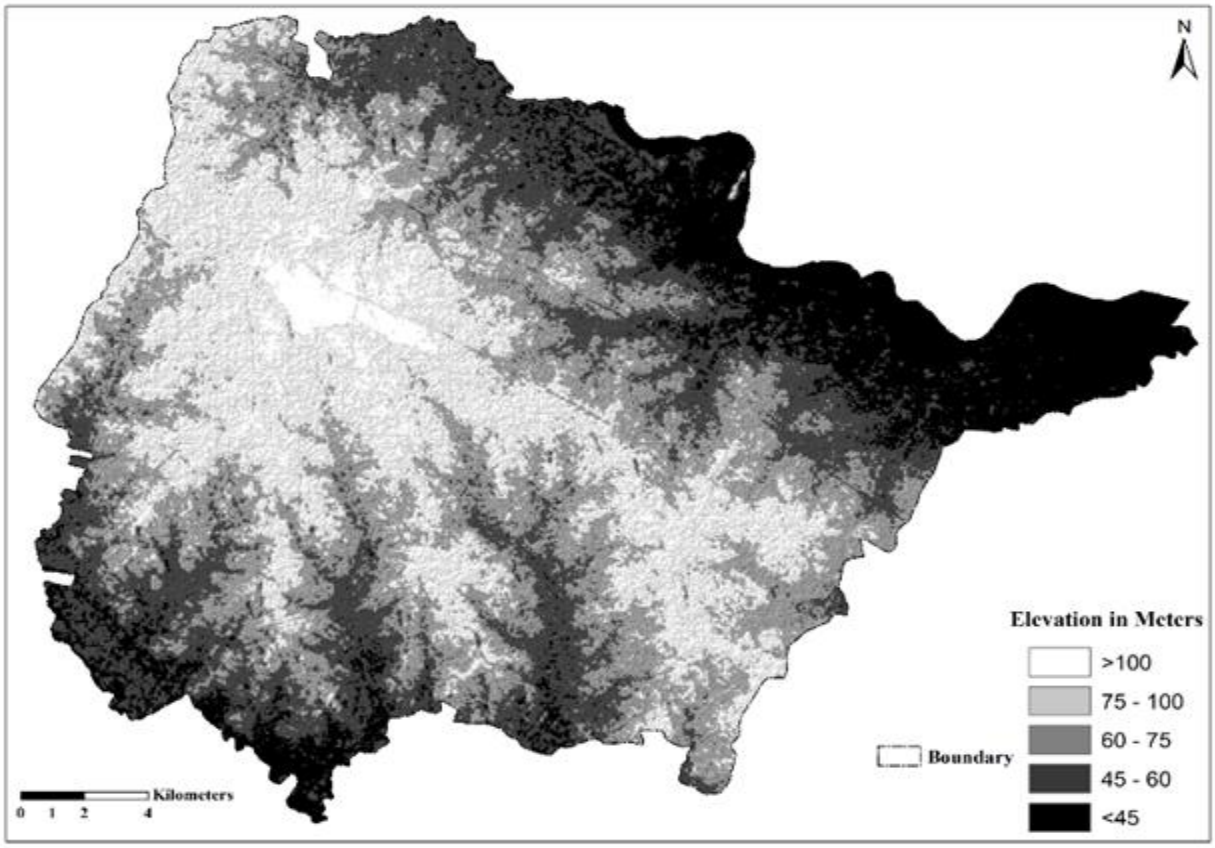

Figure 8: *Elevation map*

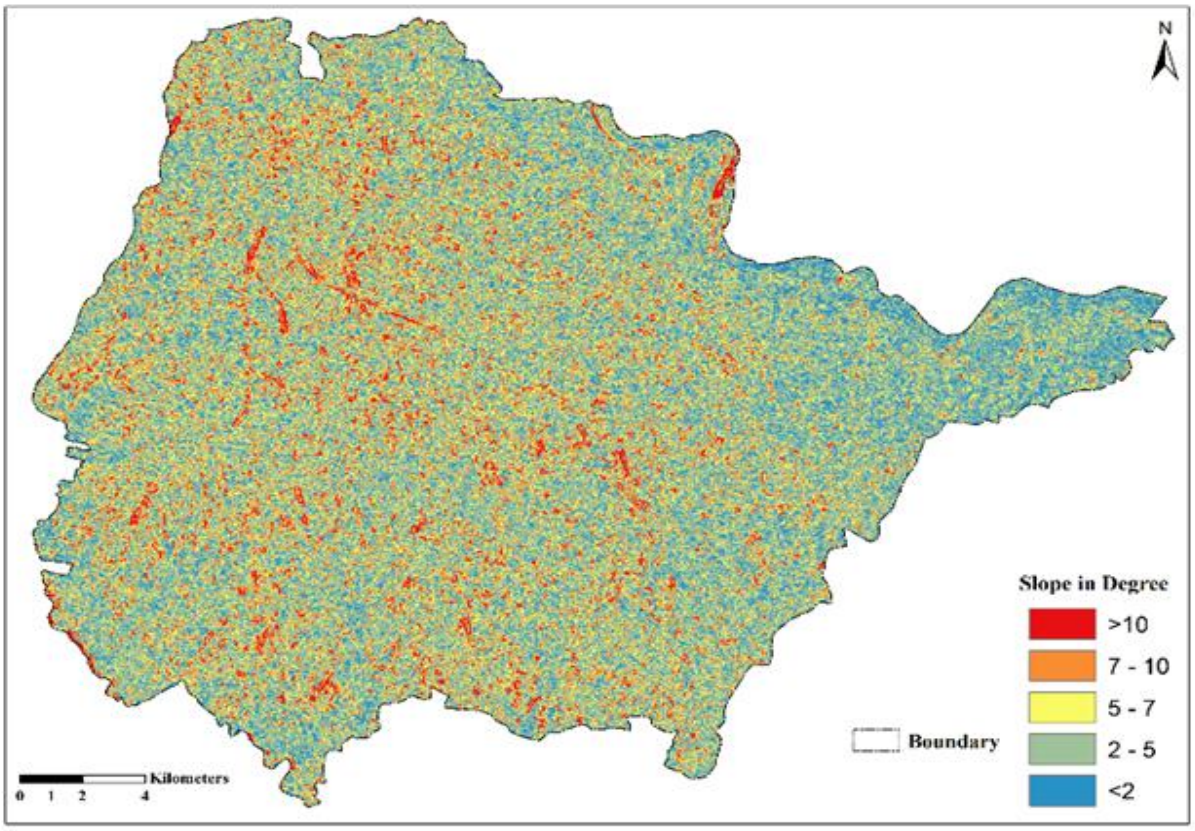

Figure 9: *Slope map*

2.1.4. *Preparation of Drainage and Watershed Demarcation*

The drainage channels were extracted in Arc GIS from the ASTER 30-meter DEM. The SOI toposheets used to reference for the drainage layer. In this context LISS-IV satellite image used to validate the stream channels mainly 1st order streams by interpreting the moisture content specially in the valley fill areas because LISS-IV has the high resolution to identify those features. This block is situated with covering some parts of the two watershed area. One is Kansabati watershed and another one is the Dulung watershed. Stream order is followed by the Strahler (1952) stream ordering technique in a hierarchical sequence and it helps to create the micro watersheds of that area. The ASTER DEM and the Dendritic drainage pattern help to extract the sub watersheds through ArcGIS environment. The 1st order streams helps to figure out the micro water basins from sub water sheds. There are 53 micro watersheds were showed out of 14 sub watersheds as per the drainage pattern and texture. Out of 53 micro watersheds there are 24 micro watersheds are under Kansabati river basin and the remaining micro watersheds are under Dulung basin area. The drainage basin properties and pattern depend on the number of classes i.e. nature, distribution, features. The number of quantitative features of a basin and its stream channels can be divided into linear aspect, aerial aspect and shape parameters. The details of micro watersheds are given below.

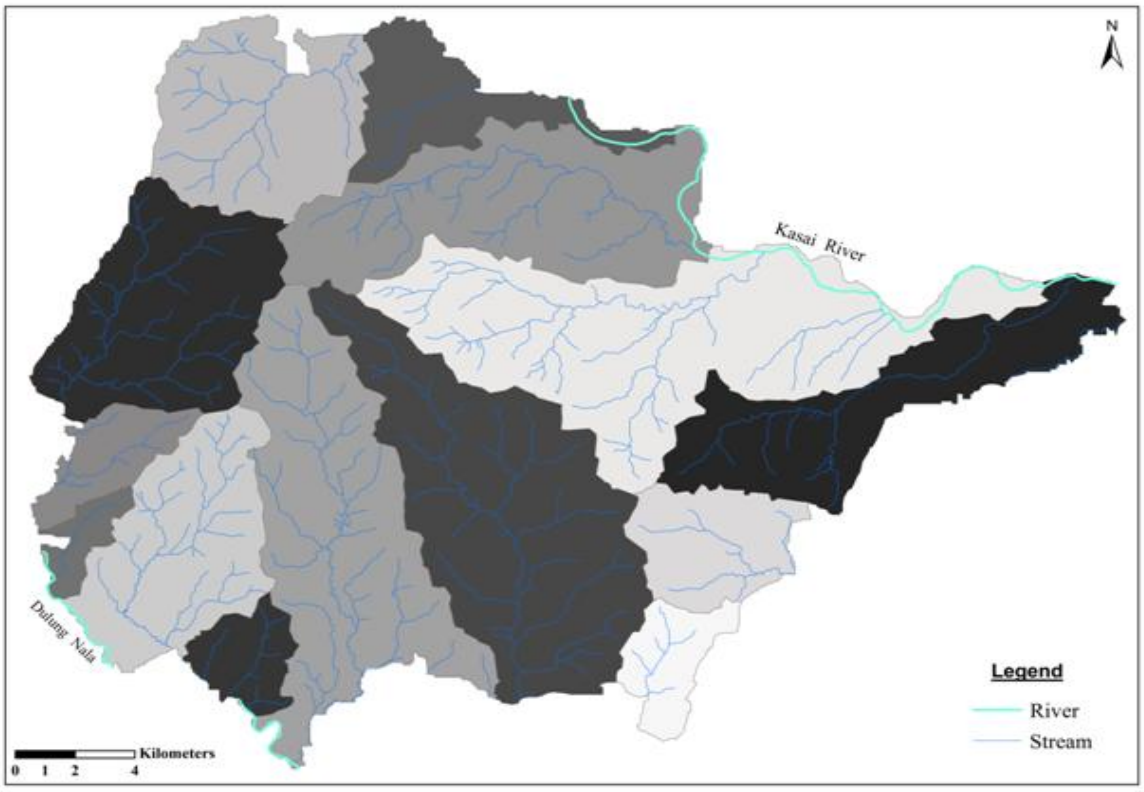

Figure 10: *Sub-watershed*

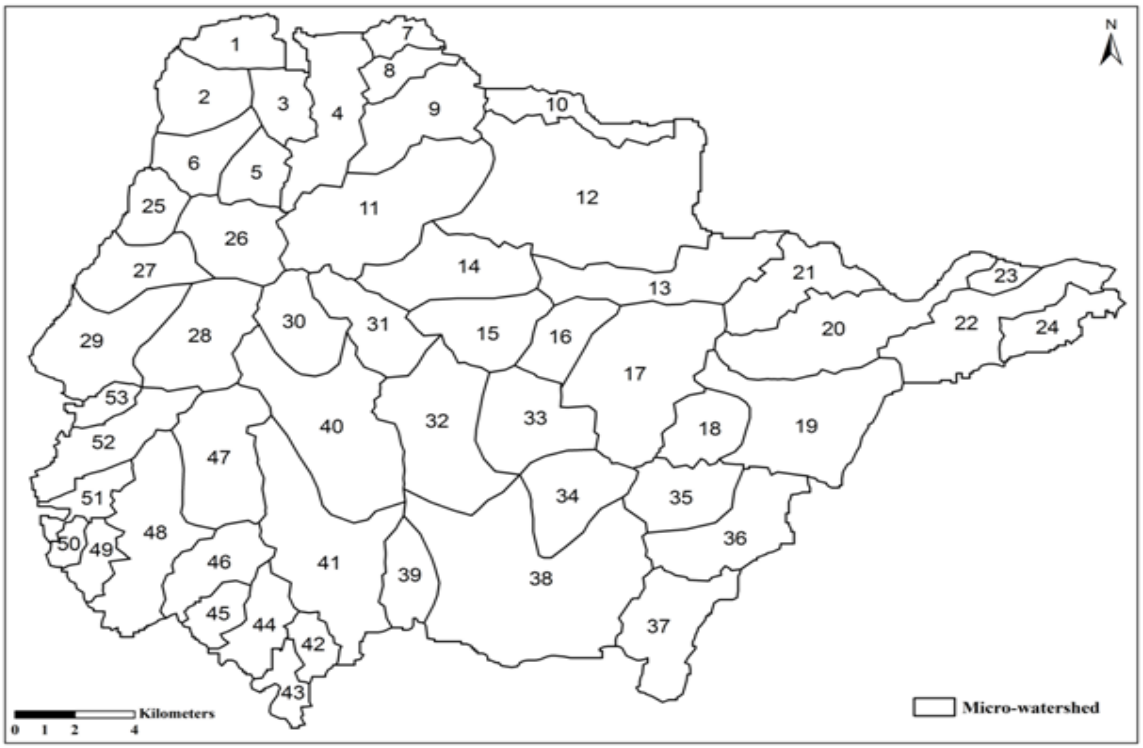

Figure 11: *Micro-watershed*

2.1.5. *Rainfall Map*

From the Irrigation department of West Bengal the rainfall data is collected. There are four rainfall zones according to its variation of average rainfall in a year and the rainfall measurement stations. Considering the nearby rainfall stations the rainfall boundaries has been simplified with the micro watersheds (MWS). The Pathra zone has the highest rainfall (1538.50 mm) and the Jhargram zone has the lowest rainfall (1427.32 mm) in comparing with other zones. The distribution of rainfall of this block is shown below.

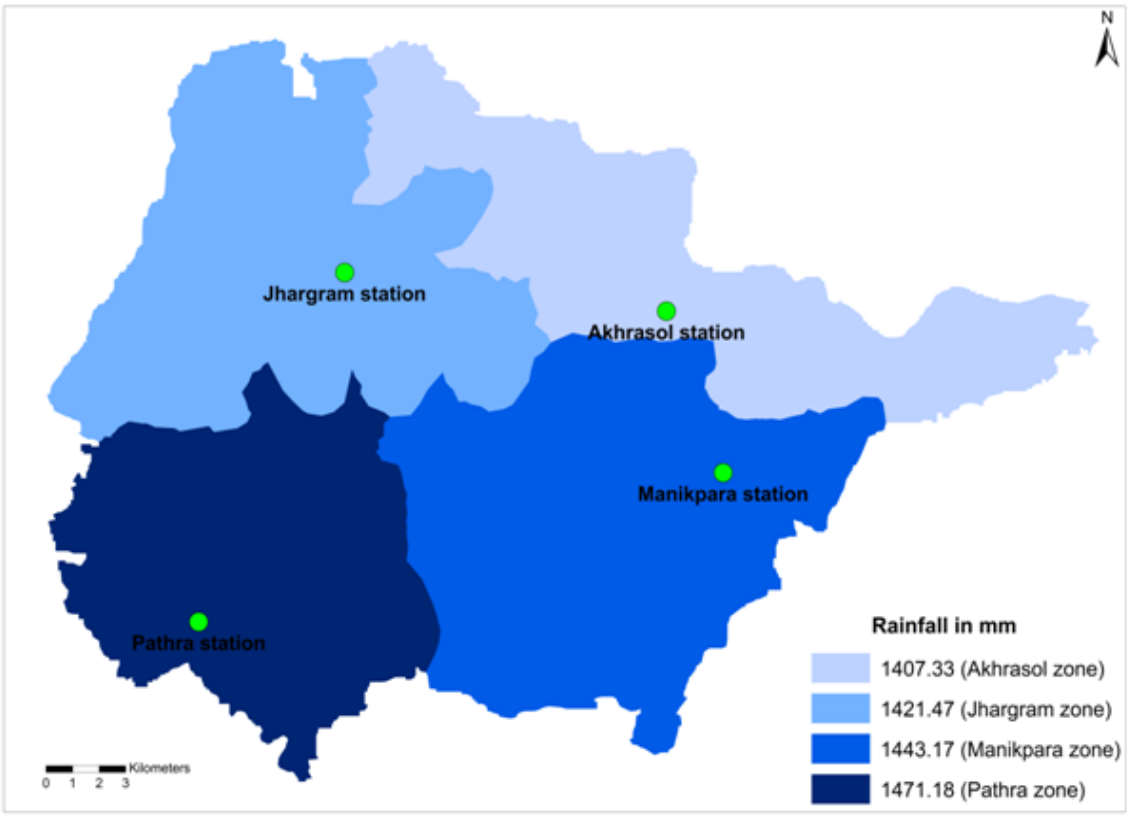

Figure 12: *Variation of rainfall in different zones*

A rainfall boundary has been drawn according to the rainfall stations and the variation of the rainfall with keeping in mind the 53 micro watersheds. It produces four rainfall zones which are Jhargram zone, Akhrasol zone, Manikpara zone and Pathra zone. According to the rainfall the Manikpara and Jhargram zone get the highest amount of rainfall and naturally it occurs the high amount of runoff with the impact of the permeability of soil

2.2. Estimation of Runoff of using SCS-CN Method

United States Department of Agriculture (USDA) addressed the most affecting and widely used method first issued by Soil Conservation Service (SCS) in 1975 to estimation of run-off in small watersheds. After that it has been incorporated with current research works and other changes in Technical Release 55 (TR- 55). It acts also rural to urban areas equally to estimate the discharge and volume of storm runoff in a watershed. The SCS Runoff Curve Number method has described its method in detail in 1985 and the equation is

$$Q = \frac{(P-Ia)}{P-Ia} + S$$

Where,
Q = runoff
P = rainfall
S = potential maximum retention after runoff begins
Ia = initial abstraction

Initial abstraction (Ia) is all losses before runoff begins. It includes water retained in surface depressions, water intercepted by vegetation, evaporation, and infiltration. Ia is highly variable but generally is correlated with soil and cover parameters. Through studies of many small agricultural watersheds, Ia was found to be approximated by the following empirical equation:

$$Ia = 0.3S$$

By removing Ia as an independent parameter, this approximation allows use of a combination of S and P to produce a unique runoff amount. Substituting equation 2-2 into equation 2-1 gives:

$$Q = \frac{(P - 0.3\,S)}{(P + 0.7\,S)}$$

2.2.1. *Generating CN Value*

Curve Number ranges from 0 to 100, whose values were developed from annual flood rainfall–runoff data from the literature for a variety of watersheds generally less than one square km in area (USDA SCS, 1972) for different combinations of land use and soil. After the division of micro watersheds, the HSG map and LULC map have been selected for intersection and created merged polygon into each watersheds using spatial analyst tools. As per the description from USDA each soil group has its own CN value for the different types of land use type with different hydrologic conditions. Considering the instruction, the appropriate CN values have been assigned for each land use/ land cover classes. To compute the CN values of the different micro watersheds as follows:

$$CN = (\Sigma\ (CNi * Ai))/A \ldots (2)$$

Where,
CN = Weighted curve number for the watershed
CNi = Curve number for specific land use feature
Ai = Area of the specific land use feature failing in the specific HSG
A = The total area of the micro watershed

Table 1: *Hydrologic Curve Numbers (AMC-II) in Indian condition for different land use/ land cover classes (based on USDA SCS, 1972)*

Land use/land cover classes	CN values		
	HSG-A	HSG-C	HSG-D
Agricultural Land	55	69	83
Forest	36	60	79
Mixed settlement	59	74	86
Ponds/Lakes	94	94	94
River	94	94	94
Scrub land	35	56	77
Social forestry	43	65	82
Urban area	68	79	89

2.2.2. *Estimation of S*

S is the potential maximum retention after runoff begins. Basically it defines the watershed storage of runoff. It depends on the characteristics of the Soil-Land-Vegetation (SVL) complex. According to SCS the value of S is calculated by this formula:

$$S = 25400/CN - 254 \ldots (1)$$

This should be noted that the value of CN always varies within 0 to 100, whose values were developed from annual flood rainfall-runoff data from the literature for a variety of watersheds generally less than one square km in area (USDA SCS, 1972) for different combinations of land use and soil. The dataset has been arranged from the specific classes which is suitable in Indian conditions.

2.2.3. *Runoff Depth Measurement*

USDA Soil Conservation Service (SCS) adopted the CN method for estimating the storm runoff event but here it was used for annual average runoff depth in each watershed. The basic assumption of the SCS curve number is that, for a single storm event, potential maximum soil retention is equal to the ratio of direct runoff to available rainfall. This relationship, after algebraic manipulation and inclusion of simplifying assumptions, results in the following equations (USDA-SCS, 1972).

$$Q = (P - 0.3\,S) / (P + 0.7\,S) \ldots (3)$$

After assigning the curve number for each land use feature, the weighted curve number for each watershed has been calculated that is defined as S, means potential maximum retention. The S value stands on the unique combination of soil hydrologic group, land use/ land cover and antecedent moisture condition to define each Hydrologic Response Unit (HRU). But here the Antecedent Moisture Condition (AMC) was not used because in this study it has been focused on annual average runoff condition of the block not any particular event, day or month. Initially, the study watershed was decomposed into sub watersheds and subsequently, sub watershed was delineated into Hydrologic Response Unit (HRU) (Maidment, 1991), which involves the aggregation of areas located with a unique combination of soil and land use regardless of their spatial position in the watershed in the GIS environment. Each and every HRU has been simply added to obtain the surface flow in every micro watershed.

After that the S has been used for runoff depth determination. The value of P means Precipitation should be always higher than the calculated value of 0.3S then the result will be meaningful otherwise the value of Q (Runoff) will be 0. In this content, the value of Q was estimated in every micro watershed and observed the ranges according to the variation of runoff depth in that specific year.

3. Results and Discussion

The above outputs of the last five years from 2010 to 2014 depict the overall schematic view of runoff in Jhargram block. In this study the main focus is on the highest & low runoff zones because this decides the water scarcity zones as well as the water resource monitoring system. Starting from the year 2010, the minimum runoff depth is 703.16 (MWS-22) and the high runoff depth is 970.45 (MWS-14). As per the rainfall there are 13 high runoff zones, 8 low runoff zones and 32 medium zones. In 2011, there are 19 high runoff zones, 13 low runoff zones and 21 moderate runoff zones. The highest Q is 1599.26 (MWS-14) and the lowest rate of Q is 1300.19 (MWS-23). In 2012, there are 18 micro watersheds with high runoff, 10 micro watersheds with low runoff and 25 micro watersheds with moderate runoff. In this year, the highest Q is 1298.85 which happen in MWS-2 and the lowest one is 979.77 happening in MWS-50. In this way, the runoff of 2013 says there is a highest runoff 1898.55 which is in the area of MWS-36 and the lowest one is 1615.32 which are in the area of MWS-24. In the year 2014, the highest Q is 1079.10 which are in the area of MWS-1 and the lowest Q is 809.48 which are in the area of MWS-23. All runoff maps of the different years are superimposed and generate a prioritization map that tells the overall figure of surface flow.

In the overall scenario of Runoff of five years, it clearly shows that the highest runoff zones are in the gentle slope areas where the soil is coarse loamy and fine loamy type. In the sense of Hydrological soil group, the C group is dominating in those zones which contain the low infiltration and moderate to well-draining system. The average values MWS 1, 2, 3, 4, 11, 14, 15, 16, 31, 29, 36, 37, these twelve micro watersheds are the high runoff priority zones and MWS 7, 10, 20, 21, 22, 23, 42, 43, 44, 45, 49, 50, these twelve micro watersheds are under the low priority zone. The remaining 29 micro watersheds are the medium range runoff priority. But the noticeable thing is that the medium priority zone has the facility for both the surface flow and the percolation process.

A raster choropleth map (Figure-18) shows the density of the runoff depth in the entire area on the basis of its priority in different micro watersheds where the priority zones is clearly visible from low to high. The medium and low runoff happens in most of the valley fills and the two main river basin areas (Kangsabati River and Dulung River). Where the drainage density and degree of slope increases, the runoff also increases. The urban area (Jhargram) including the large village (Manikpara) is affected from this. According to USDA, here Hydrologic Soil Group C and D covered areas which are the form of have the high surface flow due to the nature of soil. The HSG-C is the form of coarse loamy typic haplustalfs & Fine loamy ulti paleustalfs and HSG-D is the form of Fine aeric ochraqualfs soil. These soils have the poor water infiltration capacity rate rather than runoff. And these areas have the high drainage density and very gentle slope. So in the rainy season generally the runoff increases.

Table 2: *Runoff depth in each micro watershed in the past 5 years*

MWS	VQ_2010	VQ_2011	VQ_2012	VQ_2013	VQ_2014
1	925.28	1567.96	1200.16	1842.46	1079.10
2	924.00	1566.63	1298.85	1841.11	1077.81
3	914.22	1556.33	1288.79	1830.69	1067.86
4	902.71	1544.15	1276.92	1818.35	1056.12
5	878.45	1518.27	1251.78	1792.08	1031.33
6	882.35	1522.44	1255.83	1796.33	935.32
7	800.98	1341.25	1174.09	1715.41	953.34
8	803.83	1345.33	1178.07	1719.55	957.26
9	849.10	1486.55	1121.17	1759.80	901.21
10	732.94	1376.00	1008.02	1650.58	886.89
11	962.52	1590.27	1229.43	1861.12	1011.49
12	860.55	1498.97	1133.14	1772.46	912.97
13	884.06	1424.28	1157.61	1798.19	937.07
14	970.45	1599.26	1237.92	1870.38	1019.76
15	940.52	1565.12	1205.77	1835.18	1008.49
16	900.20	1532.68	1269.62	1804.71	1010.69
17	810.26	1543.86	1180.27	1816.18	961.11
18	820.89	1555.63	1191.51	1828.22	972.11
19	874.22	1413.72	1147.38	1787.46	927.00
20	715.96	1358.16	1090.58	1632.55	869.63
21	739.29	1382.63	1014.52	1657.28	893.34
22	703.16	1344.63	1077.39	1618.84	856.59
23	755.23	1300.19	1030.80	1673.98	809.48
24	900.89	1541.16	1274.00	1615.32	1053.25
25	874.68	1414.22	1147.87	1787.97	927.47
26	851.35	1489.00	1123.52	1862.29	903.52
27	847.32	1414.61	1119.29	1757.81	900.37
28	855.91	1421.95	1128.29	1767.34	908.21
29	932.60	1508.51	1203.84	1841.39	1042.20
30	849.14	1586.59	1121.21	1859.84	1001.25
31	953.17	1579.61	1219.40	1850.14	1017.73
32	830.26	1465.94	1101.38	1738.76	981.79
33	884.42	1424.66	1157.98	1798.58	1037.44
34	802.66	1435.43	1172.23	1707.53	953.25
35	841.56	1478.33	1113.26	1851.41	993.44
36	906.39	1524.63	1257.95	1898.55	1037.41
37	913.69	1534.04	1276.71	1803.03	1000.31
38	850.50	1488.07	1122.63	1761.35	902.65
39	853.07	1490.87	1125.32	1764.20	905.29
40	834.76	1500.89	1206.12	1843.82	986.44
41	870.95	1410.21	1143.98	1783.89	923.65
42	882.07	1322.15	1155.54	1696.03	835.04
43	707.91	1349.66	1082.28	1623.93	861.42
44	871.60	1310.91	1044.66	1684.60	824.32
45	879.48	1319.37	1052.85	1693.21	832.39
46	865.08	1403.87	1137.86	1777.44	917.62
47	845.94	1483.10	1117.85	1756.28	997.95
48	852.70	1490.46	1124.93	1763.79	904.91

49	708.31	1350.08	982.70	1624.36	861.83
50	705.48	1347.08	979.77	1621.33	858.95
51	858.66	1496.93	1131.16	1770.37	911.03
52	805.45	1416.17	1153.93	1687.77	935.38
53	802.48	1423.16	1136.89	1869.25	918.76

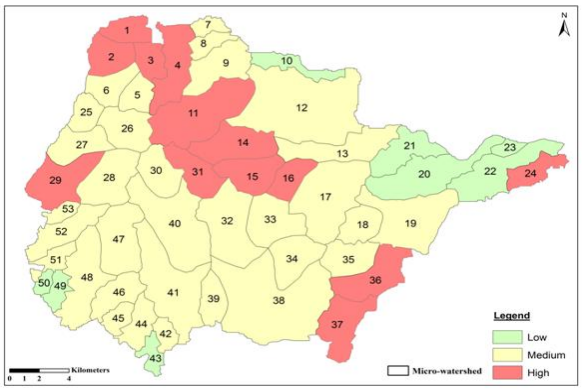

Figure 13: *2010*

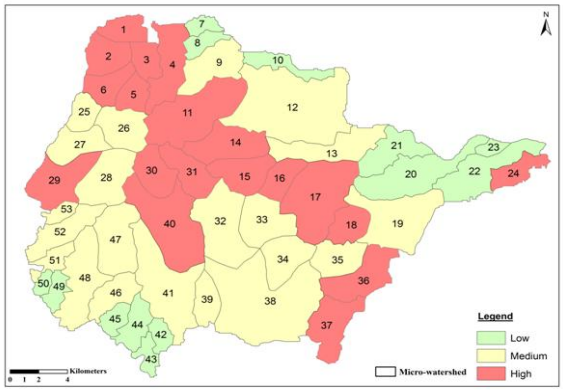

Figure 14: *2011*

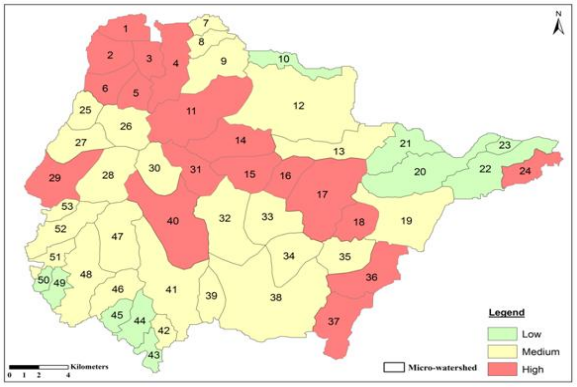

Figure 15: *2012*

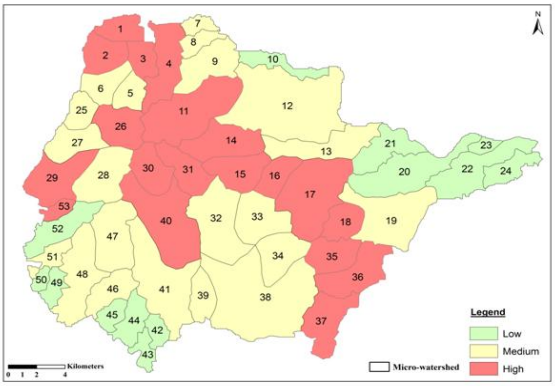

Figure 16: *2013*

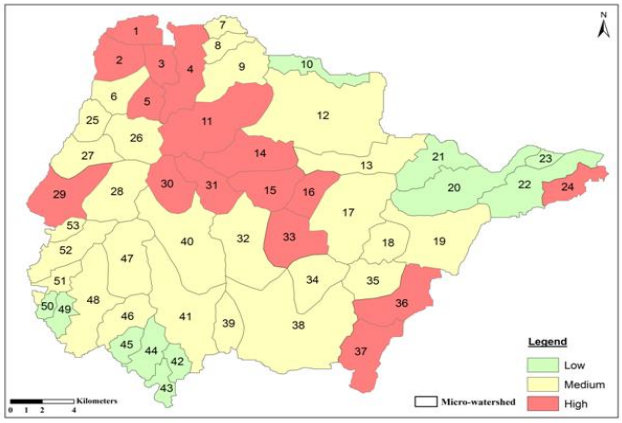

Figure 17: *2014*

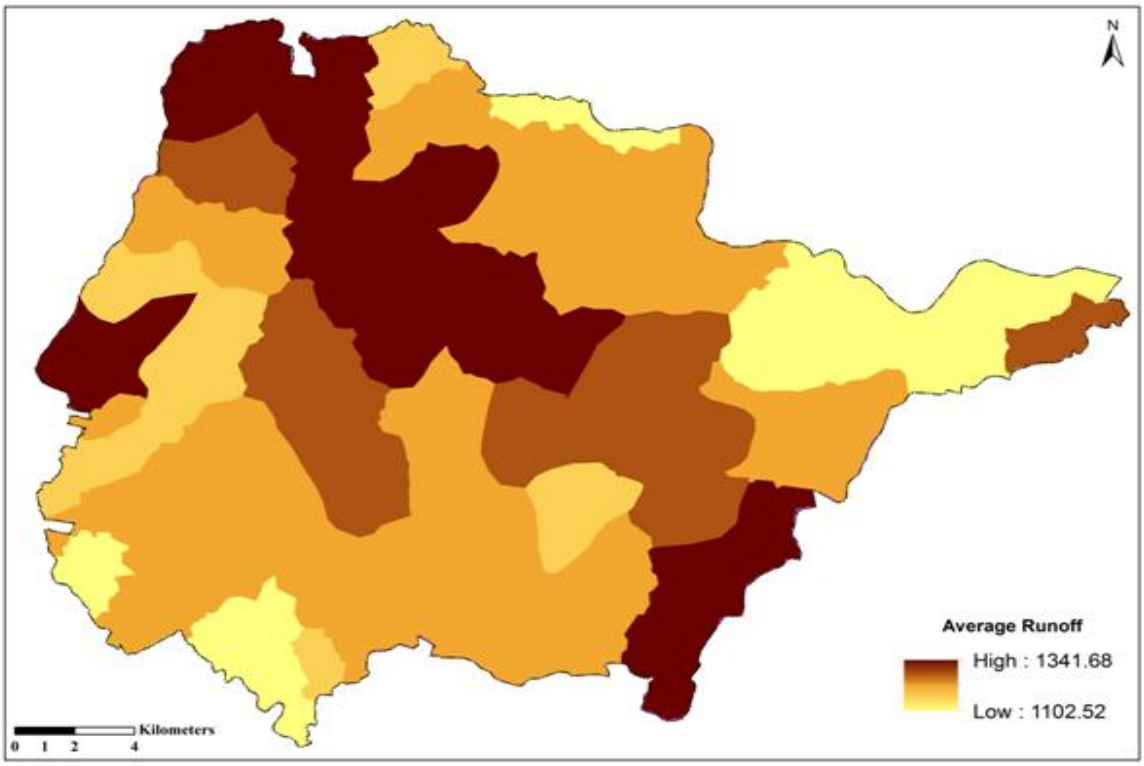

Figure 18: *Prioritization map of Runoff depth in mm*

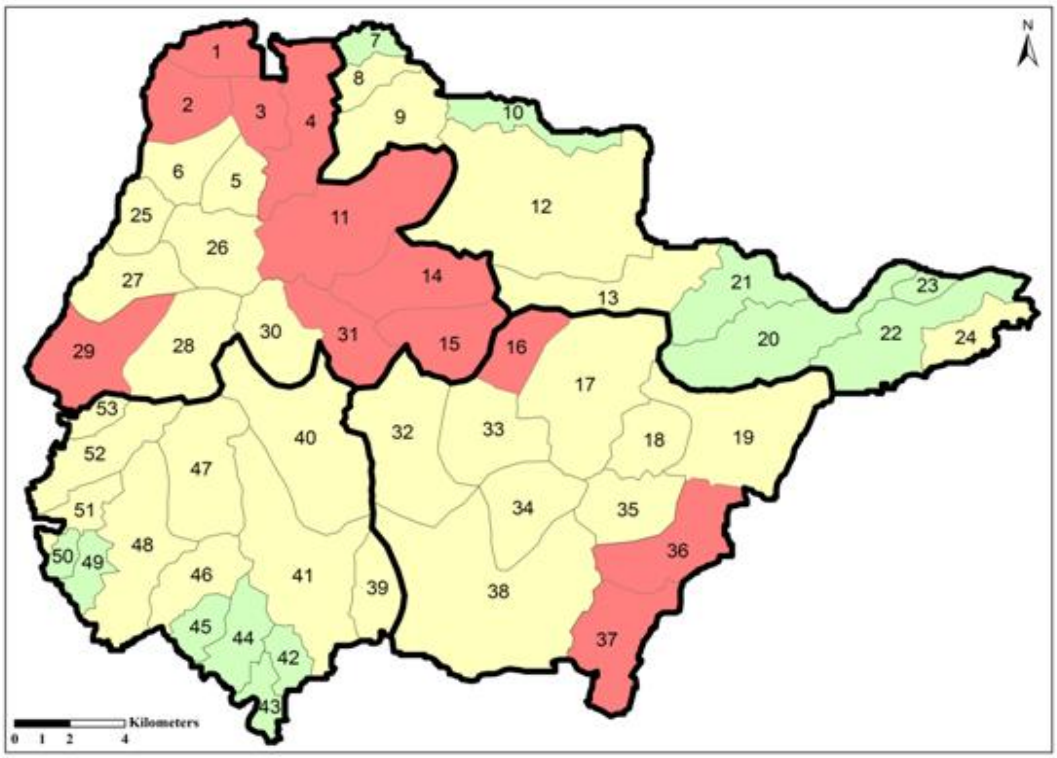

Figure 19: *Rainfall zone wise distribution of average-runoff*

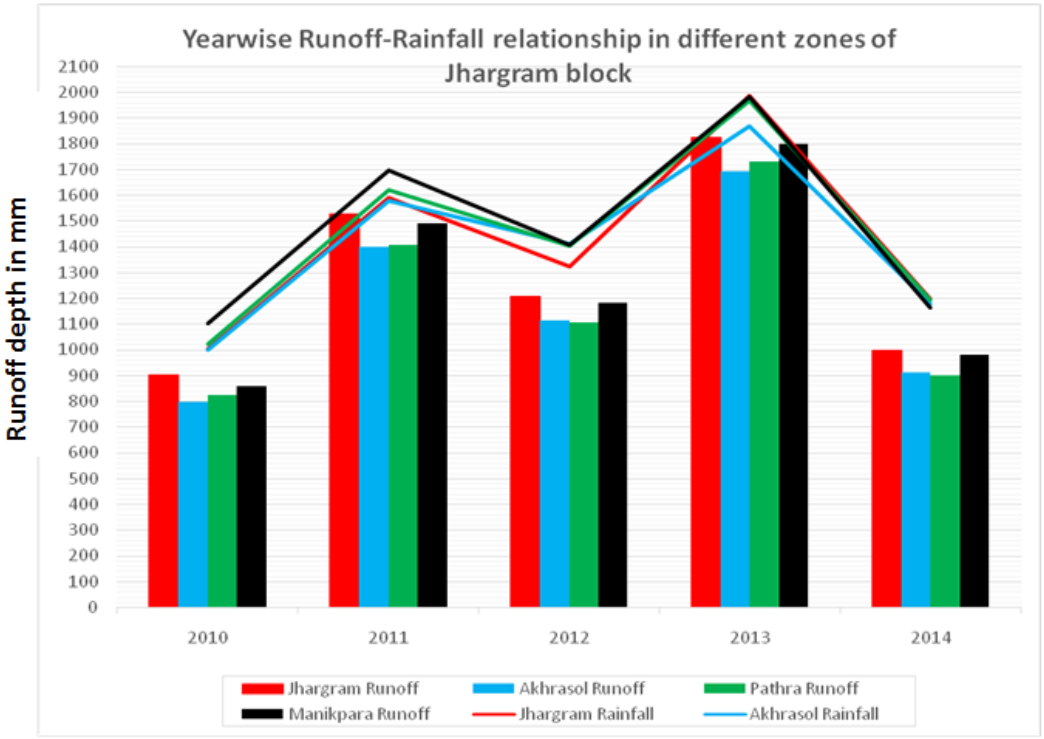

Figure 20: *5 years variation of runoff-rainfall*

4. Conclusion

It is very important to analyze Runoff in this study area which is useful for the protection of water resource and maintaining the water quality. In this study the value of runoff is not calculated seasonally because it is assumed that the maximum runoff occurs in the rainy season (June to August) and average rainfall data from different stations is used to estimate the depth of runoff. The above figures show that higher the rainfall occurs, higher the runoff depth. In this regard, due to the permeability of soil and degree of slope impact on the surface water flow despite of having huge rainfall in the different zones. As mentioned earlier the Jhargram block is situated covering with watershed divider and also with the part of two watersheds (Kangsabati River and Dulung River). In the monsoon season the basin faces the strong surface flow excepts some micro watersheds which is caused by different soil formulation and slope, but in the pre-monsoon period there is the crisis of water in the entire area. On the other hand, the study also shows the groundwater prospect zones. Where the high runoff occurs, the groundwater prospect will be poor. This needs to be planned scientifically by creating different water harvesting structures (check dam, rain water harvesting) and comprehensive treatment for controlling massive surface runoff to feed the water crisis area for better development.

References

Ahmad, I., Verma, V. and Verma, M. K. 2015. Application of curve number method for estimation of runoff potential in GIS environment. *International Conference on Geological and Civil Engineering,* Singapore, 80, pp. 16-20.

Al-Jabari, S., Abu Sharkh, M. and Al-Mimi, Z. 2009. Estimation of runoff for agricultural watershed using SCS curve number and GIS. *International Water Technology Conference,* Egypt, pp.1213-1229.

Al-Sabbagh, M. 2001. Surface runoff modelling using GIS and remote sensing - case study in Malewa Catchment, Naivasha, Kenya. *International Institute for Aerospace Survey and Earth Sciences,* Enschede, The Netherlands.

Brakensiek and Rawls. 1983. Appendix A, Hydrologic Soil Groups. Urban Hydrology for Small Watersheds TR-55 (210-VI-TR-55, Second Ed., June 1986). Available from: http://geology.wwu.edu/rjmitch/hydro_soil_groups.pdf

Chowdary, V. M., Desai, V. R., Gupta, M. and Jeyaram, A. 2012. Runoff simulation using distributed hydrological modeling approach, remote sensing and GIS techniques: a case study from an Indian agricultural watershed. *International Archives of the Photogrammetry, Remote Sensing and Spatial Information Sciences,* Melbourne, Australia, pp.203-207.

Gajbhiye, S. 2015. Estimation of surface runoff using remote sensing and geographical information system. *International Journal of u- and e- Service, Science and Technology,* 8(4), pp.113-122.

Kamuju, N. 2015. Rainfall-runoff estimation and comparative analysis using advanced geospatial digital hydrological modelling tools, ArcCN-Runoff and ArcSWAT. *International Journal of Geo informatics and Geological Science,* 2(4), pp.1-6.

Khatun, S. 2016. Estimation of surface runoff and its seasonality of Kushkarni river basin. *International Research Journal of Earth Sciences,* 4(5), pp.1-10.

Kiran, V. S. S. and Srivastava, Y. K. 2014. Micro watershed level water resource management based on three years runoff estimation using remote sensing and GIS techniques for Simlapal Block, Bankura, West Bengal, India. *International Journal of Earth Sciences and Engineering,* 7(10), pp.80-92.

Maidment, D. R. 1991. GIS and hydrologic modelling. In: *Proceedings of the First International Conference/Workshop on Integrating Geographical Information Systems and Environmental modelling*, *Boulder, Colarado.* Cary North Carolina: Oxford Univ. Press.

Pierson, S. M., Rosenbaum, B. J. and Mckay, M. D. 2008. Strahler stream order and straler calculator values in NHD Plus. Available from: ftp://ftp.horizon-systems.com/NHDPlus/NHDPlusV1/NHDPlusExtensions/SOSC/SOSC_technical_paper.pdf.

Pradhan, R., Pradhan, M. P., Ghose, M. K., Agarwal, V. S. and Agarwal, S. 2010. Estimation of rainfall runoff using remote sensing and GIS in and around Singtam, East Sikkim. *International Journal of Geomatics and Geosciences,* 1(3), pp.466-476.

Rawls, W. J., Shalaby, A. and McCuen, R. H. 1981. Evaluation of methods for determining urban runoff curve numbers. *Trans. Amer. Soc. Agricul. Eng.,* 24(6), pp.1562-1566.

United States Department of Agriculture. 1986. *Urban Hydrology for Small Watersheds.* Technical Release 55 (TR-55). 2nd ed. Natural Resources Conservation Service, Conservation Engineering Division. Available from: https://www.nrcs.usda.gov/Internet/FSE_DOCUMENTS/stelprdb1044171.pdf.
Wikipedia. *Runoff curve number*. Available from: https://en.wikipedia.org/wiki/Runoff_curve_number.

Cloud Publications
International Journal of Advanced Remote Sensing and GIS
2017, Volume 6, Issue 1, pp. 2367-2376
ISSN 2320 – 0243, Crossref: 10.23953/cloud.ijarsg.301

Case Study

Application of GIS in Panchayati Raj System in India: A Case Study of Naugaon Village, Uttarakhand, India (An Initiative of G-governance)

Saurabh Kaushik, K.C. Kandpal, Arvind Pandey

Kumaun University, Nainital, Uttarakhand, India

Publication Date: 19 August 2017

DOI: https://doi.org/10.23953/cloud.ijarsg.301

Abstract Panchayati Raj system is autonomous body of self-governance which deals with all aspect of village. Villages are the basic unit of administration, it is necessary to provide adequate power to villagers so that they have real sense of “Swaraj”. In this Present study Geographical Information Systems (GIS) technique has been used as problem solving tool to solve a real world problem which can influence villagers life’s directly. For the fulfillment of this objective filed survey has been carried out at Naugaon village, then long discussion with Sarpanch of village helps to identify problem of the village which can be solved with GIS technique. Shortage of water supply in some agriculture field has been treated as research problem. To solve this problem site suitability of water tank and canal has been done using GIS to provide adequate water supply to agricultural field. So in this way GIS can be used for scientific planning and decision making at village level.
Keywords *Geo-spatial Technology; Site Suitability and G-Governance*

1. Introduction

Panchyati Raj system has been in existence since long in India. Village panchayat consisting of village elders were autonomous local self-governance bodies which deal with all aspects of village. Considering villages as the basic unit of administration, it was necessary to provide adequate power to villagers so that they have real sense of “Swaraj”. In India the panchayat raj now functions as a system of governance in which gram panchayat are the basic unit of local decentralization. The system has three levels: gram panchayat (village level), Mandal parishad, or block samiti or panchayat samiti (block level), and zilaparishad (district level), it was formalized in 1992 by the 73rd amendment to the Indian constitution.

Government of India in 2006 with an intention to transform the governance landscape by ensuring participation of citizens in policy making and providing ease of access to information to the citizens, introduced the National e-Governance Plan (NeGP) in 2006. E-Government is not about ‘e’ but about ‘government’; it is not about computers and websites, but about services to citizens and businesses (Second Administrative Reforms Commission Report, Government of India, 2008). Now this era is shifting from e-governance to g-governance to bring wide range of benefits. GIS (Geographic Information System) is computer based system or tool in which we store, analyze, Retrieve and extract information out of Geospatial data.

The governance process, which involves the use of geo-information and communication technologies (Singh, 2009). G-governance is initiative to enable better planning processes, delivery systems, and increasing transparency and efficiency in the national-level decision-making and reaching developmental benefits to citizens in a unique manner. The application of Geographic information system could serve the needs of natural resources management, public distribution policy and other planning activities as spatial decision support systems. Participatory, decentralized and transparent governance could be efficiently achieved with G-governance or GIS based governance.

1.1. Role of Remote Sensing and GIS in Panchayati Raj System

Remote sensing (RS) is a science of obtaining information with distance. RS can be used to derive accurate information with high spatial and temporal resolution (Adham et al., 2016). A GIS is a tool for collecting, storing, and analyzing spatial and non-spatial data (Mati et al., 2016). In simplest term GIS is problem solving tool which solve real world problem and give alternative solution. This study is pioneer in order to implement GIS on village level to solve problem faced by villager in daily life with the help GIS technique.

Role of GIS in Panchayati System

Geographic information system could be used to support decision making at village level and national level. Scientific planning and monitoring of Natural resource could be efficiently achieved with this emerging technology. Integration of information and efficient management of data in digital form can provide basis for planning, resource management and public distribution. This technology is capable of giving voice to local people, to the extent of putting local people on a more equal footing with external experts and decision-makers, such as claimed for P-GIS used in land reform in South Africa (Michael, 2003)

Challenges in Implementing GIS Based Technology

- Majority of communities are illiterate/semi-literate living in adverse conditions. With the scarcity of resources and basic needs, using GIS and IT for database generation may seem luxurious
- Political resistance to local empowerment
- Participation in training programmes could be negligible because of overlap with their occupational calendar

Nowadays Government of India has started initiative of Digital India which aims at improved online structure to provide government services to citizens. Nationwide projects namely Village information system and Empowerment of Panchayati Raj Institution system aims at creation of digital data base (Land record, population data, Economic record) and asset mapping. Digital Database (spatial and non-spatial) can improve scientific planning and decision making. GIS has to play vital role in maintenance and creation of Digital Database of every city, Village, public and private organization. In this present study GIS has been applied on the village level therefore study attempts to give irrigation facility through site suitability of canal and water tank. Majority of population of village is engaged in agricultural activities, so increase in agricultural productivity will eventually help in overall economic perspective. This study is an example how GIS could be used for betterment of society and its efficiency in resource management and public distribution policy.

Study Area and Data

The study area of this project is Naugaon village which situated in Bageshwar district of state Uttarakhand. Bageshwar district is a hilly region-amidst Shiwalik range and high Himalaya (Figure 2). Bageshwar district characterized by average annual temperature of 20.4°c and evenly distributed rainfall. Most of the rainfall is convectional and occurs in summer season. According to Koppen climate classification this region comes under Cfa category. The areal extent of study area is 79°33'28" E and 79°33'46" E longitude and 29º 33' 28" N and 29º 53' 50" N latitude (Figure 1).

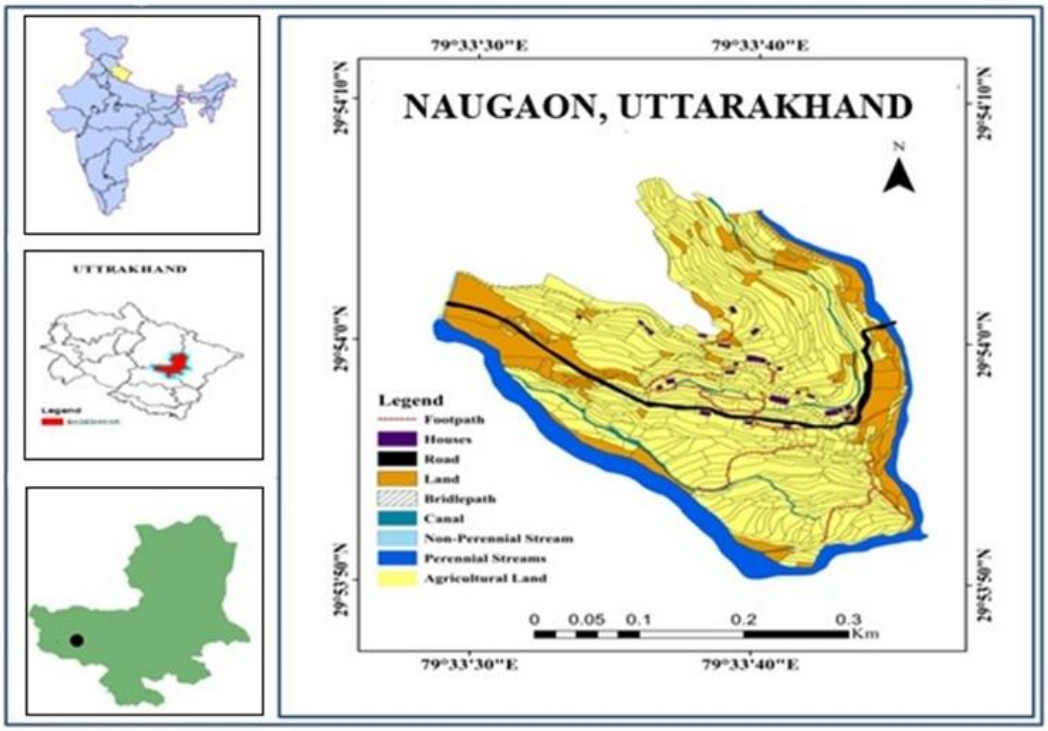

Figure 1: *Overview of study area*

The village is present at altitude of around 1315 meters above mean sea level. Economic condition of that region is low, majority of population engaged in primary activities such as agriculture, animal husband ring, cattle rearing etc.

Figure 2: *Physiography of study area*

Figure 2 is showing overall physiography of study area. Terrace farming has been practiced there and major crops are Barley, Ragi, Rice, and wheat which is mainly consumed within family of farmer, Development in agriculture activities could lead to overall development of region.

Data Used

The following data has been used for study (Table 1).

Primary Data: This data has been collected during field survey which includes GPS point of various entities which can't be identified on Google earth imagery. Population data of village has been collected to create digital Database of village.

Secondary Data: The secondary data include shape file and Base map of village provided by NRDMS Uttarakhand. Other than this Google earth and SRTM DEM has been used for updating village map.

Table 1: *Data used in study*

Data	Source	Specification
Base map	Revenue department	Every minute information is available
Shape files	COE NRDMS	Information of study area in different layer of 1959
Field data	Field survey	Primary data about house owner and number of family member
Google earth image	Hybrid	High resolution satellite image
Digital elevation Model	Bhuvan portal	30meter resolution DEM

2. Methodology

The methodology of present study has following phase:

2.1. Meeting with Ministry of Panchayati Raj and Rural Development on Role of GIS in Rural Development

This study primarily concerned with application of GIS technique at village level which can influence villager's life directly, Moreover to use GIS as a problem solving tool to solve a given problem. First of all meeting with ministry of Panchayati raj members has been conducted by Natural Resource Data Management System (NRDMS) Uttarakhand, to discuss work of ministry on rural development using GIS. After long discussion with representatives of ministry they reveal that till date no one has done GIS implementation at village level to solve their daily life problem. So this study could be beginning or pioneer of GIS implementation as tool which can solve daily life problem and capable of giving alternative solution of problem. So this study is pioneer with objective of solving village level problem with use of GIS.

2.2. Field Survey, KII and Problem Identification

Map of Naugaon village has been provided by NRDMS Uttarakhand. This map of Naugaon village has been prepared by the NRDMS in 2000, so with the help of Google earth and field survey final map as LULC of village has been prepared. Most stimulating and challenging part of this study is to find out the problem of village which can be solved with GIS. Field survey has been carried out in order to identify difficulty which can be sorted with means of geo-spatial technology. Personal observation and discussion with "Sarpanch" of village on each aspect helps to identify the problem. Naugaon village

has facilities such as school, Hospital, Post office and Police station in defined range as stated in government rule, however in some Agriculture field there's a shortage of water (Figure 3). This shortage of water has great significance because majority of village population is engaged in agricultural activities. To get rid of this problem construction of water tank and canal indeed this could be capable of providing water to agriculture field. The site suitability of canal and water tank has been considered as a research problem. As this research problem shows application of GIS at village level and problem solving tool for real life problem.

Figure 3: *Water shortage in Canal*

2.3. Site Suitability of Water Tank and Canal

First of all land use and land cover has been prepared with data provided by NRDMS Uttarakhand and data collected during field survey has been used to update feature of map. Land cover land use map show how much of land is cover by what type of natural phenomena or how it is used by man. LU/LC is prerequisite in many project of Remote sensing and GIS because it give us broad idea of what type of activities is running in that region, or if we took LU/LC map of different year we can easily identify what changes has occur in certain period of time. Site suitability analysis in GIS is used to find best place or location for something. The approach behind site suitability is rule based mapping in which we define certain condition of it and then if they will meet we have result of most suitable site. In site suitability Analysis we can have result in two form one is based on Boolean logic and another one is based on heuristic approach (knowledge based). Boolean logic gives result in form of 0 or 1 but in the heuristic approach we rank all the factors responsible for site suitability and give suitability to every location in form of high, medium, low suitable. In this study both approach has been adopted for comparative analysis of results.

2.4. Heuristic Approach for Site Suitability

This approach is also known as knowledge based approach because in this approach analyst rank all those factor which play significant role in influencing site suitability of that entity. The most important factor is Land use land cover map which has several layers such as canal, river, barren land, houses, brdidlepath, agriculture land and road. Suitable weights have been assigned to each thematic feature after considering their characteristics (Kumar et al., 2008) as shown in (Table 2). In this method weightage has been given to barren and location nearest to river. As LULC map shows (Figure 4.1) barren land present on North West direction at high elevation of study area. Advantage of constructing water tank on this side could be understood in two ways, Firstly barren land has no use, or may be with water availability it would become fertile after some time. Another advantage is that location is that it is nearest to river which will result in less expenditure in construction of water tank and supply of water.

Table 2: *Ranks given to LU/LC layers*

FID	Name	Rank
0	Road	2
1	Canal	3
2	River	4
3	House	2
4	Bridle path	2
5	agriculture	3
6	barren	5

Table 3: *Ranks given to distance from river*

FID	Distance (m)	Rank
0	10	5
1	20	4
2	30	3

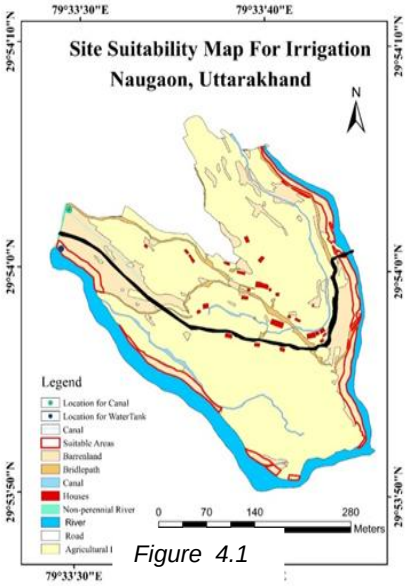

Figure 4.1

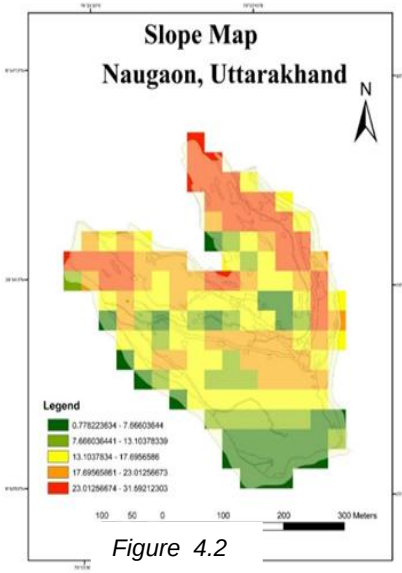

Figure 4.2

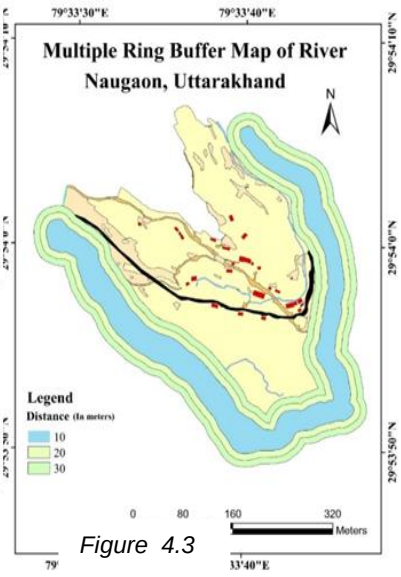

Figure 4.3

Figure 4: 4.1: *Site suitability map for irrigation Naugaon, Uttarakhand;* **4.2:** *Slope map Naugaon, Uttarakhand;* **4.3:** *Multiple ring buffer map of river Naugaon, Uttarakhand*

Another significant parameter which influence suitable site for water tank and canal are slope and distance from river. Buffer map as shown (Figure 4.3) on both side of river has been generated on both side of river using Arc GIS and weightage has been given to its nearest location. Slope map as shown in (Figure 4.2) has been generated in Arc GIS to analyze slope factor for suitable site of water tank and canal. Then union of these factors create new polygon where condition meet, for this first of all addition of both ranks required in new field (Rank final) with the help of field calculator then again new field (suitability) is added, finally area of high, medium and low suitability can be identified through query operation in which we state that final rank >=8 IS Highly suitable for water storage tank and final rank >=5 And final rank <8 is moderately suitable and remaining ones come under category of low suitable. We have result in form of every area has some sort degree for suitability of water storage tank but objective of site suitability analysis is to give particular location for that third factor of slope is used and put a point to particular location which has moderate slope or capable of serving water to barren land.

For suitability of canal as we can see in LULC map we need to locate canal at highest elevation point of barren which is capable of serving whole barren region, if location of canal would at highest point no power required to supply water it will flow to whole region due to gravitational force.

2.5. Boolean Logic (Method) for Site Suitability

Boolean logic gives output in form of 0 and 1, same factors are responsible for site suitability of water tank and canal but here analyst doesn't need to each factor, output can be generated by query operation such as river distance =10 and name = barren Result is generated as we can see in the map suitable site for water tank in form of polygon, same as in heuristic approach we could find particular location using third factor of slope where slope is moderate that site is much suitable for water storage tank.

3. Results and Discussion

The site suitability map for irrigation facilities with Boolean approach as shown (Figure 5.2) is showing best location for water tank and canal which is including three factors namely LULC, distance from river and slope of area.

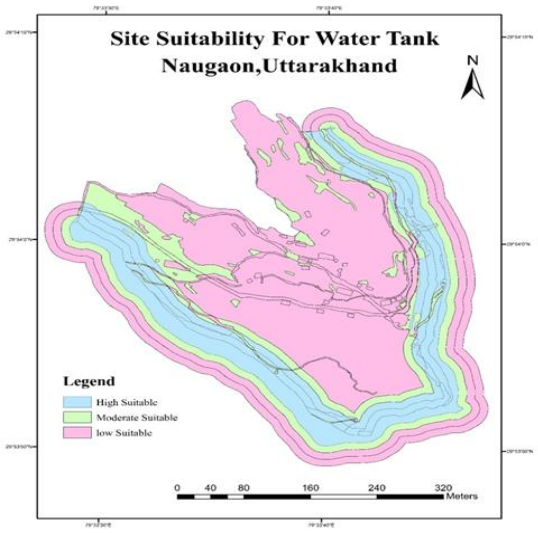

Figure 5.1

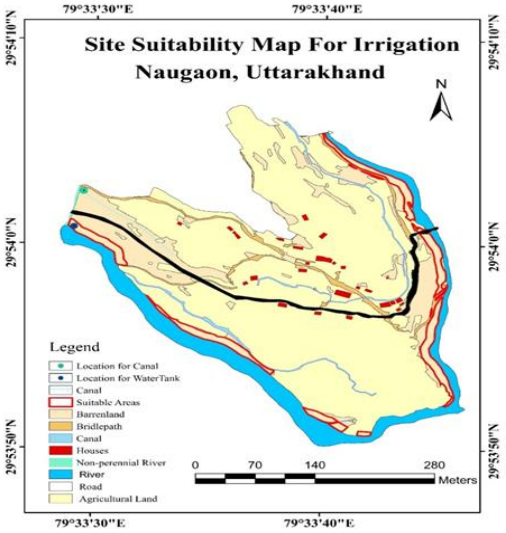

Figure 5.2

Figure 5: 5.1: *Site suitability for water tank Naugaon, Uttarakhand;* **5.2:** *Site suitability map for irrigation Naugaon, Uttarakhand*

The result is exact up to our expectation because water tank is closet to river and located at barren land which has two advantages. Firstly less expenditure indeed for water supply to water tank and second one is that we are using waste land which has no use right now or with the availability of water there are some chances for conversion of this barren land to agriculture land. Canal is located at highest point of barren land which is capable of serving water to whole barren land with force of gravity no external force is required. Total area under high suitability for water tank with Booleans approach is 6374.49 square meter

In the heuristic approach map as shown (Figure 5.1) degree of suitability for water tank to each location, but location of high suitability in both approach is almost same because we have given weightage to river and barren land then consider slope. Table is showing how much of area is under which category of suitability for water tank.

At present several national wide projects (EPRIS, SISDIP and VIS) are ongoing for application of GIS at village level for decentralizes planning. This present study is also step forward in the same direction. The overall objective of this project is to implement geographic information system technique on grass root level to solve village level problem. As we study this technique as a problem solving technique for real world and through this project we can directly influencing common people through GIS technique. To solve village level problem with GIS, in depth field observation played vital role. GIS can be used as a spatial decision support system for scientific and decentralize planning. With the help of GIS Digital base of each village could be generated which helps in efficient planning and resource management. This present study is attempt in same direction. To Use GIS as tool for rural development present case study is significant example. For fulfillment of objective field survey has been carried out and long

conversation with Sarpanch of that village we found that there is seasonal shortage of water supply to agricultural field so this project is all about providing irrigation facilities to agriculture fields.

As mentioned above result of this study is per expectation. With first interface of prepared updated map of Naugaon the first idea strikes in my mind that there should be some water storage tank near the river. Water from water tank need to be supplied to canal which is located at the highest elevation point of village which can be capable of serving water to all agriculture fields without external force required to supply water. Site suitability analysis for water tank and canal with help of two approaches shows almost same result however the main advantage of heuristic approach is that this approach provide alternative of highly suitable area for water tank. Result in form of polygon of suitability which range from higher to lower suitable site. However there should be particular location for water tank for.

In comparison to heuristic method, Boolean approach gives result for highest suitable site for water tank and canal. With the help of Boolean method exact site could be marked. The discussion part must contain how can we implement this project to real world or there is any economic viability of this project on ground, so know that we must know about total expenditure required for constructions of canal and water tank because this is hilly area of we have to make sustainable solution which is capable of tackling every problem.

At present time application of GIS on village level has great significance. Village information system and Empowerment of panchayati Raj system is nationwide project in India. Their major focus is on creating digital database of village which will play pivotal role in planning and decision making.

4. Conclusion

Geospatial technology or spatial science provides integrated tools for solving real world problem. Geospatial technology could be a very significant tool for efficient and transparent governance. Public distribution or resource management could be another example of Geospatial technology at grass root level. This study is pioneer in respect of GIS implementation at village level. Efficiency of geospatial technology on grass root level could be summarized using following points given below:

- GIS can be used in scientific planning and decision making.
- In this study GIS has been used to solve Real world which can influence villager's life directly.
- This study shows application of GIS at grassroots level.
- This study is an attempt toward decentralize planning using geospatial technology.
- Geospatial technology could be use to develop To develop comprehensive web portal as per PRIs and stakeholders needs for decentralized planning, governance, outreach to the citizens and data dissemination

Acknowledgment

I would like to acknowledge NRDMS Uttarakhand for providing all necessary data and thanks to Sarpanch of village for cooperating with us and providing all essential information.

References

Adham, A., Riksen, M., Quesar, M. and Ritsema, C. 2016. Identification of suitable sites for rainwater harvesting structures in arid and semi-arid regions: A review. *International Soil and Water Conservation Research*, 4(2), pp.108-120. doi.org/10.1016/j.iswcr.2016.03.001

Mati, B., De Bock, T., Malesu, M., Khaka, E., Oduor, A., Nyabenge, M. and V. Oduor. 2006. Mapping the potential of rainwater harvesting technologies in Africa. A GIS overview on development domains for the continent and ten selected countries Technical Manual, 6, p.126.

Kumar, G.M., Agarwal, A.K. and Bali, R. 2008. Delineation of potential sites for water harvesting structures using remote sensing and GIS. *Journal of the Indian Society of Remote Sensing,* 36(4), pp.323-334.

Michael, M. K. 2003. Seeking good governance in participatory-GIS: A review of processes and governance dimensions in applying GIS to participatory spatial planning. *Habitat International,* 27(4), pp.549-573. doi: 10.1016/S0197-3975(03)00005-5

Promoting e-Governance. 2008. The SMART Way Forward, Eleventh Report - Second Administrative Reforms Commission, Government of India, New Delhi, India.

Singh, P. K. 2009. G-Governance in India: Search for a Suitable Framework and Research Directions. *GSDI-11 Conference Proceedings,* Rotterdam, The Netherlands.

Cloud Publications
International Journal of Advanced Remote Sensing and GIS
2017, Volume 6, Issue 1, pp. 2292-2296
ISSN 2320 – 0243, Crossref: 10.23953/cloud.ijarsg.294

Research Article

Decadal Change in Glacier Area in the Chorabari Sub Watershed

Asha Thapliyal[1], Anju Panwar[1], Sanjeev Kimothi[2]

[1]Uttarakhand Space Application Centre, Dehradun, Uttarakhand, India
[2]Swami Rama Himalayan University, Dehradun, Uttarakhand, India

Publication Date: 4 August 2017

DOI: https://doi.org/10.23953/cloud.ijarsg.294

Abstract This area looks at glacier area change in Chorabari Sub Watershed for 1962-1990 and 2000-2016 periods. Study area of Chorabari Sub Watershed extends between the latitudes of 28º-31ºN to longitudes 77º-81°E. Chorabari Sub Watershed is the part of Mandakini basin and it has total number of 40 glaciers covered an area of 81.64 km^2 with the ice reserve of 5.9856 km^2. The reduction in the glacier area has been observed on the lateral side of Chorabari glacier and not on the snout position. Overall reduction in the basin glacier area was observed 1.23 km^2 during the year 1990 to 2016. In addition, this paper describes a method for estimating the ice surface elevation changes using the SRTM (2000) and elevation data generated from topographic maps (1962) to quantify the ice thickness change for the 1962-2000 periods.
Keywords *Glacier; Ice thickness; Moraine-dammed lakes; Sub-watershed*

1. Introduction

Himalayan glaciers are the major source of water as it lies over almost 6000 glaciers and occupied by an aerial extent of 20000 km^2. They can affect the supply of water to a large number of people in the Indian subcontinent. This is almost half of the glacier-covered area in the region and it suggests that the glaciers are losing an average 0.4% area per year (Bolch et al., 2010, 2012; Yong et al., 2010; Bhambri et al., 2011; Kulkarni et al., 2011; Bahuguna et al., 2007). In the other side the variation of glaciers are uncontrolled and they can be the major risk prone zone for various types of calamities especially in the context of climate change scenario. Most of these studies related to glacier retreat in Himalaya are attributed to climatic variations or global warming (Bhutiyani, 1999; Kulkarni et al., 2002a, 2005; Kulkarni et al., 2007; Bhutiyani et al., 2008; Hasnain, 2008). Glaciological studies carried out by various researchers in the Himalayas suggest that many of the glaciers are in a state of retreat due to climate forcing (IPCC report 2010).

The Himalayan region is one of the most vulnerable and complex region. Recent climate changes patterns have had significant impact on high-mountain glacial environment. This region has the past of natural devastations i.e. various landslides and flash flood in the past. The earlier studies enlightens that the formation and expansion of moraine-dammed lakes, creating a potential danger from dammed lake outburst floods are the result of rapid melting of snow/ice and heavy rainfall (Dobhal et al., 2013).

The aim of this paper is to identify the general trends of glacier area change using change - detection method based on multi-temporal satellite data for 1976-2014 time intervals. We used NDSI image differencing and change vector analysis methods.

1.1. Study Area

The study area is the part of Mandakini river basin. The Study area lies between the latitudes of 28º-31ºN to longitudes 77º-81°E. The upper part of the sub-watershed is covered by two glaciers i.e. Chorabari and Companion glacier shown in Figure.1. The Chorabari glacier is the major glacier and origin of Mandakini River. Total area of Chorabari glacier is around 4.23 km^2, and length of the glacier is 7 km approx. Companion glacier covered around 3.59 km^2 and length of this glacier is around 5.79 km. Thickness of the glacier is around 30 meters (98ft) to 75 meters (246ft), terminus of the Chorabari glacier is Chorabari Tal. The study area lies between 53N and 53J SOI sheets.

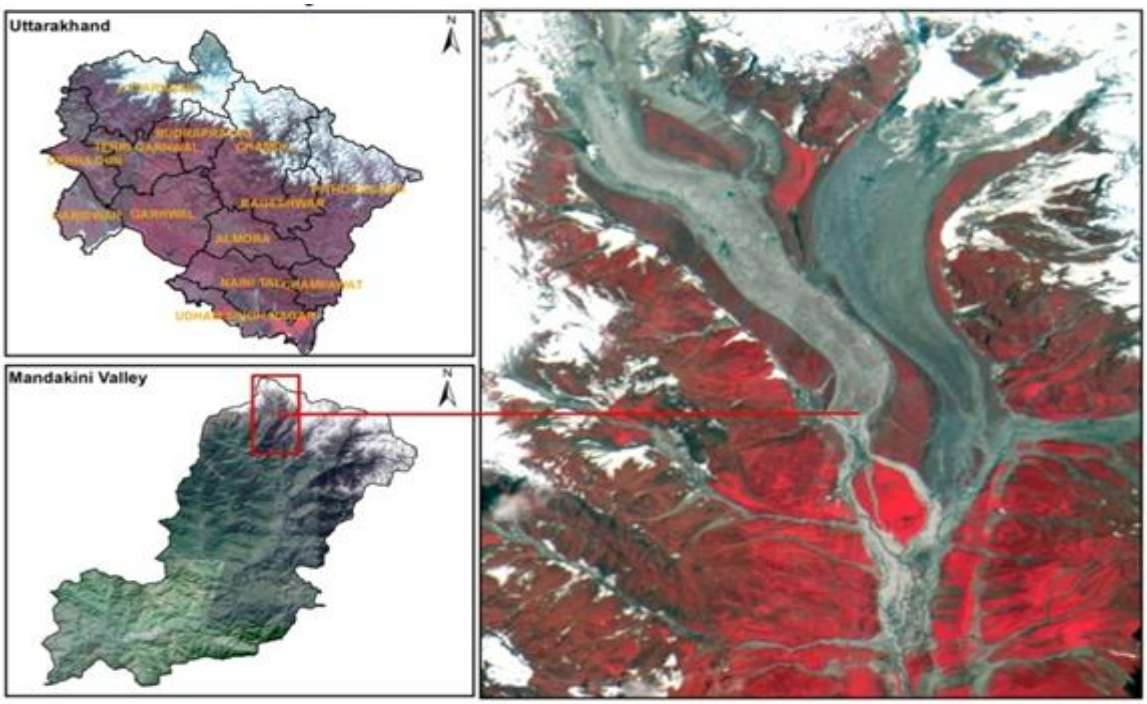

Figure 1: *Study area locating Chorabari sub-watershed in Uttarakhand Himalaya, India*

1.2. Physiography of the Mandakini River Basin

The Mandakini River basin lies between latitude 300 15'N and 300 45'N and longitude 780 48'E and 790 20' E, comprising an area of 2250 km^2. The elevation in the basin ranges from 640 to 6940 m asl. Mandakini is the main river of the Mandakini valley, which is a major tributary of Alaknanda River and originates from the Chorabari Glacier, located just 2 km upstream from Shri Kedarnath shrine. The major tributary of this river is Madhyamaheshwar, whereas smaller tributaries include Laster Gad, Helaun Gad, Kakra Gad, Kyunja Gad, Kyar Gad, Ghasta Gad, Markanda Ganga, Kali Ganga and Vasuki Ganga. The valley has complex topography having high mountain chains with glacierised basin in the north and fluvial terraces in the central and lower parts. The Chorabari and Companion are two largest glaciers besides a few other small glaciers. The area has a couple of high altitude lakes which are directly fed by snow/ ice melt and rain water.

1.3. Geology of the Region

The upper part of the sub-watershed is covered by two glaciers i.e. Chorabari and Companion glacier besides a few other small glaciers including ice apron, hanging glaciers, Glacierete and cirque

glaciers. The Chorabari glacier is the major glacier and origin of Mandakini River. Total area of Chorabari glacier is around 4.23 km^2, and length of the glacier is 7 km approx. Companion glacier covered around 3.59 km^2 and length of this glacier is around 5.79 km. The area has a couple of high altitude lakes which are directly fed by snow/ ice melt and rain water. Geomorphologically this area comes under valley glaciers and highly dissected hills and valley with moraines and piedmont slopes.

1.4. Glaciers of the Region

The majority of the glaciers in Mandakini basin are mountain glaciers with simple basins with their major source of recharge being from snow or avalanches. Glaciers in this region generally occur above the elevation of 3800 m asl. The distribution of glaciers in area is maximum of southwest and southeast aspect (15 and 12 in respectively). The north and west aspect glaciers are nil and rest on other aspects are few glaciers in number. The glaciated area in the Mandakini River basin extends from 30º 35' N to 30º 49' N latitude to 78° 59' E to 79° 22' E longitude. The basin has a total number of 40 glaciers occupying an area of 81.64 sq km with the ice reserve of 5.9856 km^3. The largest glacier recognized in this basin is Chorbari glacier which occupies 8.34 km^2 with the ice reserve of 0.7441 km^3. Four grid of SOI sheets and 17 grids of 3'x3' are mapped on 1:10,000 scale.

2. Methodology

In this study the multi temporal satellite imageries acquired over the Chorabari Sub Watershed. Based on image interpretation using multi temporal satellite imageries glacier morphological layer is generated and update for different years such as 1962, 1976, 1990, 2010 and 2016. The glacier inventory and glacier lake with details of the glacier features has been prepared using multi temporal satellite data and ancillary data.

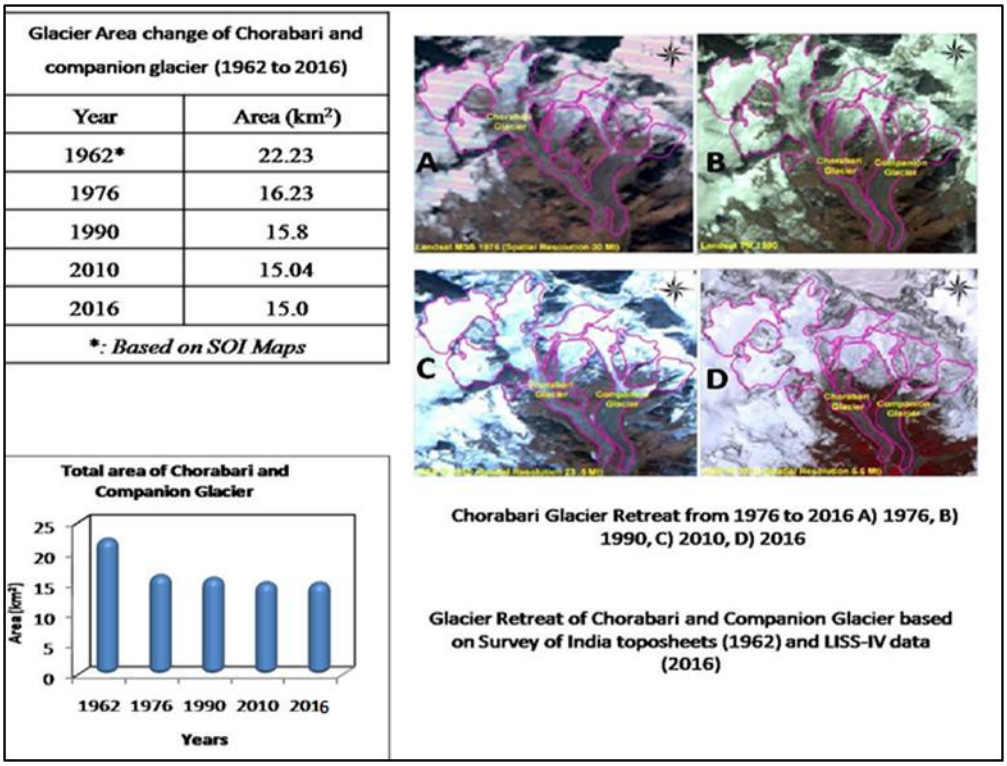

Glacier Area change of Chorabari and companion glacier (1962 to 2016)

Year	Area (km^2)
1962*	22.23
1976	16.23
1990	15.8
2010	15.04
2016	15.0

*: Based on SOI Maps

Chorabari Glacier Retreat from 1976 to 2016 A) 1976, B) 1990, C) 2010, D) 2016

Glacier Retreat of Chorabari and Companion Glacier based on Survey of India toposheets (1962) and LISS-IV data (2016)

Figure 2: *Chorabari Glacier retreat from 1976 to 2016 A) 1976, B) 1990, C) 2010, D) 2016*

2.1. Data Integration and Analysis

In the present work integration of Satellite Data and SOI Top sheets by geometric correction was done for the Chorabari Sub Watershed. The glacier boundary and glacial area was digitized on multi-temporal satellite and change area Analysis was done.

3. Results and Discussion

3.1. Change in Glacier Area

Based on image interpretation using multi temporal satellite imageries glacier morphological layer is generated and update for different years such as 1962, 1976, 1990, 2010 and 2016. The glacier inventory and glacier lake with details of the glacier features has been prepared using multi temporal satellite data and ancillary data. For long term change monitoring, Survey of India (SOI) topographical maps of 1962 at 1:50 000 scales have been used as reference maps. The Chorabari glacier retreat was observed from year 1976 to 2016 shown in Figure 2.

The following observations are:

- Total glacier area has been observed from 1962 to 2013, maximum changes has been observed during 1962 to 1976 period . In 1962 the total glacier area of Chorabari and Companion has been found 22.23 km^2 which has reduced up to 16.23 km^2 in 1976 and thus the overall reduction is 6 km^2.

- The retreat rate was very less from 1976 to 1990 period. The overall reduction in the glacier area was noticed 0.43 km^2.

- The overall reduction in the glacier area from 1990 to 2013 was also found very slow, which is only 1.23 km^2.

- In 1962 it has been observed that Chorabari glacier is the single glacier but in 1976 onwards fragmentation has been started from the snout position which was clearly visible in year 1990.

- In 1990 total glacier has been fragmentated into two seprate glacier. i.e Chorabari and companion glacier Srivastava et al., 1994 has reported the total area of Chorabari glacier is 12.28 km^2 and companion glacier is 2.12 km^2 which is 14.39 km^2as the total glacier area, which is approximately similar to our observation in year 1990.

- The reduction in the glacier area has been found on the lateral side of chorabari glacier not on the snout position.

In Chorabari glacier retreat is estimated and maximum change in the glacier was noticed during 1962-1976 period. The reduction in the glacier area was very slow from year 1990 to 2016, which is only 1.23 km^2.

References

Bahuguna, I. M., Kulkarni, A. V., Nayak, S., Rathore, B. P., Negi, H. S. and Mathur, P. 2007. Himalayan glacier retreat using IRS 1C PAN stereo data. *International Journal of Remote Sensing,* 28, pp.437-442.

Bhambri, R., Bolch, T., Chaujar, R. and Kulshreshtra, A. C. 2011. Glacier changes in the Garwal Himalaya, India, from 1968 to 2006 based on remote sensing, *Journal of Glaciology,* 57, pp.543-556.

Bhutiyani, M. R. 1999. Mass-balance studies on Siachen Glacier in the Nubra valley, Karakoram, Himalaya, India, *Journal of Glaciology,* 45(149), pp.112-118.

Bhutiyani, M. R., Kale, V. S. and Pawar, N. J. 2008. Changing stream flow patterns in the rivers of north western Himalaya: Implications of global warming in the 20th century. *Current Science,* 95(5), pp.618-626.

Bolch, T., Yao, T., Kang, S., Buchroithner, M. F., Scherer, D., Maussion, F., Huintjes, E. and Schneider, C. 2010. A glacier inventory for the western Nyainqentanglha Range and the Nam Co Basin, Tibet, and glacier changes 1976-2009. *The Cryosphere,* 4, pp.419-433.

Bolch, T., Kulkarni, A., Kaab, A., Huggel, C., Paul, F., Cogley, G., Frey, H., Kargel, J. S., Fujita, K., Scheel, M., Stoffel, M. and Bajracharya, S. 2012. The state and fate of Himalayan Glaciers. *Science,* 336, pp.310-314.

Dobhal, D. P., Gupta, A. K., Mehta, M. and Khandelwal, D. D. 2013. Kedarnath disaster: facts and plausible causes. *Current Science,* 105(2), p.25.

Hasnain, S. I. 2008. Impact of climate change on Himalayan glaciers and glacier lakes. *Lake Conference,* pp.1088-1091.

Intergovernmental Panel on Climate Change. 2010. IPCC Statement on the melting of Himalayan glaciers Geneva.

Kulkarni, A. V., Mathur, P., Rathore, B. P. and Kumar, M. 2002a. Effect of global warming on snow ablation pattern in the Himalayas. *Current Science,* 83(2), pp.120-123.

Kulkarni, A. V., Rathore, B. P., Mahajan, S. and Mathur, P. 2005. Alarming retreat of Parbati glacier, Beas basin, Himachal Pradesh. *Current Science,* 88(11), pp.1844-1850.

Kulkarni, A. V., Philip, G., Thakur, V. C., Sood, R. K. and Chandra, R. 2007. Glacier inventory of the Satluj Basin using remote sensing technique. *Himalayan Geology,* 20(2), pp.45-52.

Kulkarni, A. V., Rathore, B. P., Singh, S. K. and Bahuguna, I. M. 2011. Understanding changes in Himalayan cryosphere using remote sensing technique. *International Journal of Remote Sensing,* 32, pp.601-615.

Yong, N., Yili, Z., Linshan, L. and Jiping, Z. 2010. Glacial change in the vicinity of Mt. Qomolangma (Everest), central high Himalayas since 1976. *Journal of Geographical Sciences,* 20, pp.667-686.

Cloud Publications
International Journal of Advanced Remote Sensing and GIS
2017, Volume 6, Issue 1, pp. 2395-2415
ISSN 2320 – 0243, Crossref: 10.23953/cloud.ijarsg.307

Case Study

Conventional and Unconventional Urban Planning and Design Approach, a Way-out to Increase the Green Cover and to Reduce Temperature Variation in the Cities - Case Study Dehradun City

Jugmohan Singh

Associate Member, Institute of Town Planners of India (ITPI), 4-A, Ring Road, I.P. Estate, New Delhi -110002
Empanelled Member, Cogent Training Research Development Consultants Pvt. Ltd, Jaipur Rajasthan
Life Time Membership Administrative Staff College of India (ASCI) Bella Vista, Hyderabad
Joint Secretary, Uttarakhand Regional Chapter, Institute of Town Planners of India (ITPI) 2017-2018

Publication Date: 11 September 2017

DOI: https://doi.org/10.23953/cloud.ijarsg.307

Abstract In the last few decades, most of cities in India have seen rapid growth of industrialization and urbanization. This rapid growth in urbanization has lead to unplanned development of urban areas, by large scale cutting of trees, converting agricultural land into human habitation and deforestation. This has affected adversely on general environment and maintaining ecological balance. The escalated urbanization, associated with environmental degradation, has generated a debate on how much urban green space has been lost due to the urbanization process. Integrated means of addressing the ecological and environmental, economic and social concerns are still neglected in the framework of development. The increase in built up mass is increasing the temperature variation and UHI effect within the city & is also decreasing infiltration and evapo-transpiration of water which has directly increased the surface runoff and has lead to water logging in urban areas. Most of cities in India are now facing the problem of water logging & urban heat island effect; these problems are very common in most of the metropolitan cities like Mumbai, Delhi, Bangalore, Gurugram (Gurgaon). The unplanned development has increased water logging and flood like situation, during rainy season traffic movement gets hampered due to submersion of roads under water, the houses in low lying area of the cities get partly submerged and if not planned other cities in future are going to face the similar problems, the balance between open spaces and built up area has to be maintained. Therefore for sustainable development of any city it is important to maintain a balanced built up mass arrangement. Urban Planners, Geographers, Environmentalists have to adopt various conventional and unconventional urban planning designs and plans to increase the depleting green cover (open spaces) & to reduce temperature variation within Cities.
Keywords *Environment; Geographers; Green cover; Urbanization*

1. Introduction

Urbanization in India began to accelerate after independence. Population residing in urban areas in India has increased, according to 1901 census; the urban population was 11.4%. This count increased to 28.53% according to 2001 census, and crossing 30% as per 2011 census, standing at 31.16%. According to a survey by UN State of the World Population report in 2007, by 2030, 40.76% of country's population is expected to reside in urban areas. As per World Bank, India, along with China,

Indonesia, Nigeria, and the United States, will lead the world's urban population surge by 2050 (Kavitha and Gayathri, 2017). Rapid rise in urban population, in India, is leading to many problems like increasing slums, decrease in standard of living in urban areas, also causing environmental damage water logging, UHI effect etc. When a settlement grows in any city, it goes through various interactions of its physical components such as forest, green cover, air, water bodies etc. These fast growing cities not only need to accommodate the pressure of urbanization, but they should also to measure the issues of environment arising due to fast infrastructure development. The rapid growth of cities is eating up the open spaces, green cover and is thus affecting the ecological balance of the area.

Figure 1: *Increasing built up mass and decreasing green cover*

Dehradun city is not different than other Indian cities in the context to urban sprawl and its negative impacts; it has undergone rapid economic development and urbanization over past decades after becoming the interim capital of Uttarakhand in the year 2000. Dehradun city is going through a phase of rapid development; the growth in population has increased urban sprawl in all possible directions of the city, as the city was not much familiar with the concept of vertical development therefore the urban sprawl has mainly been horizontal in nature. This horizontal and unplanned development of the city has led to deforestation, decreases in green, open spaces, water bodies & increased in pollution etc.

As per the records maintained by an NGO "citizen for green doon" more than 30000 trees has been cut in Urban Area of the Dehradun in last 15 years. The decreasing green cover, deforestation, decreasing open spaces, increasing temperature & pollution has degraded the environment and ecological balance of the region. A city once know for soothing climate and better environmental conditions has now turned into a 31st most polluted city in the world (wikipedia.org). This negative growth is very alarming in nature and needs deep analytical analysis and due consideration of urban planners.

The whole study is has been phased into three subdivisions:

1. To observe the reduction of forest/green cover in the city & its impacts
2. Reduction of green/open spaces and its effect on temperature variation in within city area
3. Mitigation strategies and policies to increase green cover of the city with the help of conventional and unconventional methods of urban planning and design

1.1. Increasing Build up Mass (Concrete Jungle) and Decreasing in Green Cover of Dehradun City

After the declaration of Dehradun city as the interim capital of the Uttarakhand state, there has been a major change in land use adding to its deforestation has increased, open and green spaces have decreased in the city. The escalated urbanization, associated with environmental degradation, has generated a debate on how much urban green space has been lost due to the urbanization process. Integrated means of addressing the ecological and environmental, economic and social concerns are still neglected in the framework of development. As a result, large areas of urban green space are

declining rapidly, and causing numerous environmental problems. However, both environmental awareness and environmental legislation (setting of standards etc.) have advanced considerably in recent years, but enforcement is lagging almost everywhere. Now, it is well recognized that urban green/open spaces plays an important role in the social and natural sustainability of a city.

Urbanization has led to unprecedented reduction in agriculture open spaces, and vegetation. Due to this unprecedented reduction in the all these we have to face tremendous problems regarding to environment. The impact of reduction of green cover on air, water and society is negative. It has caused air pollution, variation in temperature, increased urban heat island effect and many other negative effects in the city. WHO has declared Dehradun city as 31st most polluted city in the world based on how much fine particulate matter (PM 2.5) they have in the air and Dehradun PM Count is beyond 100. (wikipedia.org).

About 114% growth in urban population since 1991 and 230% growth in urban buildup area have been observed since 1982 in Dehradun city (UUDP 2007). Dehradun city is highly vulnerable to urban climate change mostly due to anthropogenic activities. The annual maximum, annual minimum and annual mean temperatures at Dehradun city have positive trends of change. Overall it has warmed significantly and annual mean temperature has increased about 0.47°C during the 41 year period (1967-200). Per decade increase in annual mean temperature was found to be 0.12°C which is about four times more than the global increase in temperature. The time period during 1967-1987 has less intensity of temperature growth than the time period of 1988-2007 (UUDP-2007). Dehradun city will result into fatal effects on natural ecosystems. Below given data clearly indicates how green cover has decreased with passage of time in Dehradun city (Omvir Singh et al., 2013).

Table 1: *Decreasing Green cover in the Dehradun city*

Year	Agriculture	Tea garden	Forest	Total green cover
1998	14983.32	1119.068	12238.89	28341.278
2003	13763.17	1126.97	10586.874	25477.014
2008	12469.37	1089.97	9780.908	23340.248
2013	10340.75	1029.43	9821.195	21191.375

Urban Growth assessment using CA Markov Model: a case study of Dehradun City.

Table 2: *Data of tree felling/cutting in the urban areas of Dehradun*

Year	Private Green Trees	Private Dead Trees	Private Dangerous Trees	Public Dangerous Trees	Public Green Trees	Public Dead Trees	Total
2000	297	75	0	0	51	0	423
2001	460	191	26	1	6	1	685
2002	611	183	13	0	249	0	1056
2003	389	28	0	2	10	6	435
2004	439	6	3	0	6	0	454
2005	333	72	30	1	148	105	689
2006	181	72	38	0	251	0	542
2007	135	73	66	91	3839	64	4268
2008	118	99	48	0	214	42	521
2009	426	86	326	46	3911	984	5779
2010	177	196	276	98	217	706	1670
2011	224	73	383	268	2396	114	3458
2012	803	198	960	339	467	60	2827
2013	517	269	572	74	734	118	2284
2014	635	178	669	678	2508	755	4911
2015	158	30	648	84	24	5	950
Total							30,002

Citizen for Green Doon, Dehradun.

After becoming interim capital of Uttarakhand the buildup mass has increasing drastically as shown in images comparatively (Year 1986, 1998, 2011). With the passage of time and decreasing in the forest area, open spaces and water bodies in Dehradun city. In the images the urban sprawl is represented by red color which has increased & the water bodies which are shown by blue as well as forest which are shown by dark green and green cover which is shown by light yellow has decreased with time at an alarming pace.

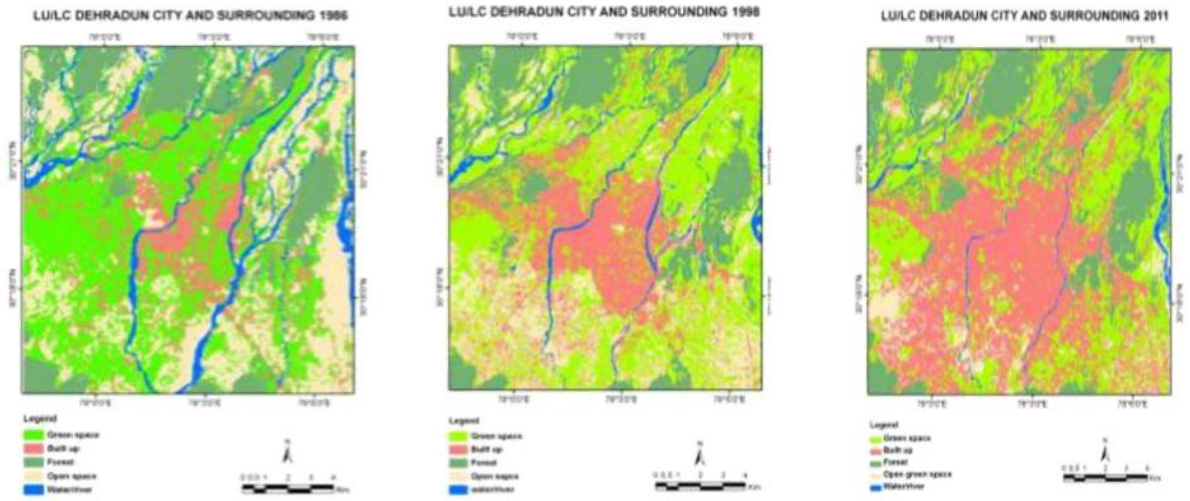

International Journal of Advanced Remote Sensing and GIS.

Figure 1: Unplanned urbanization leading to environment degradation of Dehradun city

The analysis of the satellite imaginary of Dehradun city and Its Environment for the Year 1986, 1998 and 2011 by (International Journal of Advanced Remote Sensing and GIS) clearly indicates that on the

one hand area under green cover, water bodies & forests has decreased and on the other hand built up mass has increased rapidly.

Table 3: *Development of built up area in Dehradun city during 1982-2004*

Type of urban land use	Built up area (hac)	Built up area (ha)	Growth in Built up area (%)
Residential	1588.8	4071.8	156.3
Commercial	81	341.4	321.5
Industrial	113.4	383.4	238.01
Govt. & semi govt. Buildings	267.2	479.6	79.5
Facilities & services	802.2	915.4	14.1
Orchards & gardens	205.7	728.4	254.1
Open spaces & parks	156	581.9	274.1
Tourism & Transportation	203	822	304.9
Rivers and Nalas	331.5	1179.3	255.7
Undefined land use	55	3058.8	5461.5
Total	3802.8	12565	230.1

Uttaranchal Urban Development Plan, 2007.

As of today the concrete jungle is continuously increasing and green cover and open spaces are decreasing, the unplanned growth is creating misbalance in built up mass arrangement in proportion to the green cover and open space ratio, which is effecting the overall environment and sustainable growth of the city. Dehradun city being the part of the Smart city project list has to do the interventions to enhance Sustainable environment & Health. This horizontal, unplanned and haphazard growth will affect the city in various ways, some of the factors are briefly describe below.

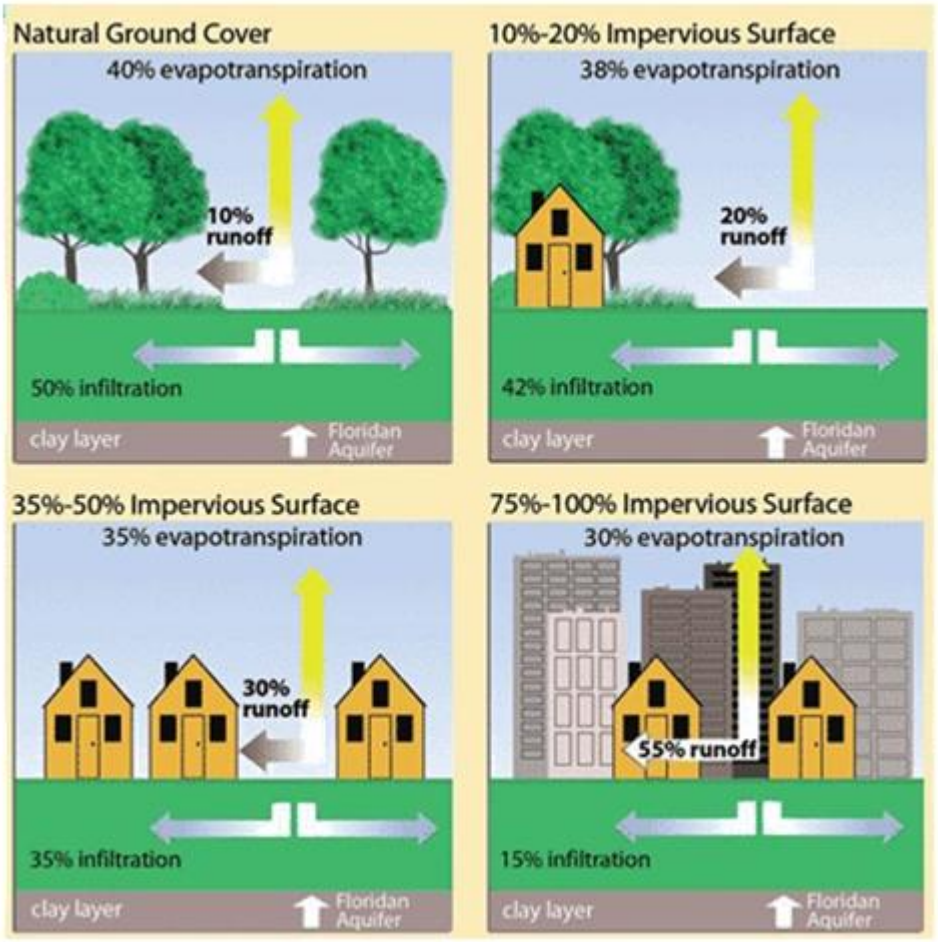

Figure 2: *Development and its effects*

1.2. Effect of Decreasing Green Cover and Increasing Built up Area

Massive urbanization and land use change has decreased infiltration, green and open spaces, evaporation & has increased the surface runoff which has lead to water logging in cities. Due to the insufficient percolation or seepage of water into the ground, water table also gets affected and therefore the surface runoff has increased in most of the urban areas, which has increased the risk of floods & Water logging. In the above given figure one can easily understand that how urbanization affects various environmental parameters.

Unplanned development & urban Sprawl has also lead to increase in unwanted Population Growth, increase in migration from rural to urban areas, decrease in water quality, increase in Erosion and Sedimentation, increase in Sewage Overflows, increase in Waterborne Pathogens, increase in Pesticides content in water and soil, Decrease in air quality, Decrease in life expectancy and reducing health inequality, Decreasing levels of physical activity and health, Decreasing psychological health and mental well-being, Negative effect on land and property values Impact on local economic regeneration, Decrease habitat areas, Decrease in population of some protected species, Decreasing species movement.

Climate change is another factor which increases with the urbanization in any city. For e.g. Heat amelioration or heat island: An urban heat island (UHI) is a city that is significantly warmer than its surrounding rural areas due to human activities. UHI is most noticeable during the summer and winter. The main cause of the urban heat island effect is from the modification of land surfaces. Waste heat generated by energy usage is a secondary contributor. As the density of population in core area grows, it tends to expand its area and increase its average temperature. The less-used term heat island refers to any area, which is consistently hotter than the surrounding area.

The UHI decreases air quality by increasing the production of pollutants such as ozone, and decreases water quality as warmer waters flow into area streams and put stress on the ecosystem. There are several causes of an urban heat island (UHI); for example, dark surfaces absorb significantly more solar radiation, which causes urban concentrations of roads and buildings to heat more than suburban and rural areas during the day.

Other causes of a UHI are due to geometric effects. The tall buildings within many urban areas provide multiple surfaces for the reflection and absorption of sunlight, increasing the efficiency with which urban areas are heated. This is called the "urban canyon effect". UHIs have the potential to directly influence the health and welfare of urban residents. Increased temperatures have been reported to cause heat stroke, heat exhaustion, heat syncope, and heat cramps.

Figure 3: *Locations*

1.3. Temperature Variation within the City Limits

Most of the times UHI effect is used to indicate, the temperature variation of city in comparison with surrounding rural areas, but in this case study temperature devices were used to detect temperature variation within Dehradun city limits. In this case study the variations in temperature within city limits have been studied, to confirm that there can be the temperature variation within the city limits because of unplanned built-up mass arrangement. To validate temperature variation within the city limits temperature device were installed at seven different locations randomly.

Table 4: *Recorded temperature variation in degree Celsius*

Location	11.5.2016 / 3 pm	12.5.2016 / 1pm	13.5.2016 / 1pm	14.5.2016 / 4pm	17.5.2016 / 5pm	23.05.2016 / 1pm	26.05.2016 / 2pm	01.06.2016 / 12.3	03.06.2016 / 1pm	08.06.2016 / 12.3 pm
House No-238 East Patel Nagar, Near Ramlila Ground, Dehradun	35	36	36	39	39	37	37	36	37	34
House No- 243, Loharwala, Sirmour Marg, Kishan nagar Chowk, Dehradun	35	35	34	38	38	35	35	35	35	33
Bhimtal, Subash Nagar, Post Office, Mobhewala, Dehradun	33	30	34	35	34	34	35	35	35	32
Astle Hall, Near Orient Cinema, Rajpur Road, Dehradun	34	34	36	37	39.5	36	37	35	35	35
Kolagarh, Near Kolagarh Post Office, Near FRI, Dehradun	33	35	35	36	37	37	37	36	35	33
Wadia institute of Himlayan Geology, GMS Road, Dehradun	31	30	33	35	34	34	34	31	32	30
House no 57, Near Gurukul School, Dharampur Dhanda, Dehradun	33	33	34	35	34	35	36	34	36	30
Google	32	33	35	37	38	36	38	34	34	31
Highest	35	36	36	39	39.5	37	38	36	37	35
Lowest	31	30	33	35	34	34	34	31	32	30
Difference	4	6	3	4	5.5	3	4	5	5	5

To collect, analyze & detect the variation in temperature at various locations within the city limits, temperature recording devices were provided free of cost to members and contact number of all persons where collected saved in the mobile. To make data collection & communication with member's easier whatsapp group under the name of "research members" was created and members were added

in the whatsapp group. The members were instructed about the location for installation of the devices and they were trained how to check the temperature. The members were told to note down the temperature in Degree Celsius scale instead of Fahrenheit scale for easy compilation and analysis of the data. The members were also instructed not to install the devices in the rooms; all the devices were installed outside of the house because room temperature which is subjected to various factors always differs from outside temperature. Temperature data of Dehradun was also collected from internet (http://www.accuweather.com) for comparison purposes. Temperature data was collected for once in a day for approximately 10 days. The details of the recorded temperature are given below in the table.

Analysis of the table clearly indicates the following:

- There is continuous temperature variation in the city limits.
- The temperature variation is between 3 degree Celsius to 6 degree Celsius.
- The lowest temperature was usually recorded in areas like
    1) Wadia institute of Himalayan Geology, GMS Road, Dehradun.
    2) Hous no 57, Near Gurukul School, Dharampur Dhanda, Dehradun.
    3) Bhimtal, Subash Nagar, Post Office, Mobhewala, Dehradun.
- The highest temperature was usually recorded in areas like
    1) House No-238 East Patel Nagar, Near Ramlila Ground, Dehradun,
    2) Kolagarh, Near Kolagarh Post Office, Near FRI, Dehradun.
    3) House No- 243, Loharwala, Sirmour Marg, Kishan nagar Chowk, Dehradun &
    4) Astle Hall, Near Orient Cinema, Rajpur Road, Dehradun.
- The temperature was recorded high in the densely populated areas with more built-up mass, which clearly indicates that built up mass effects the overall environment of the area.
- Temperature variation within the city spatially confirms the UHI effect at micro level.
- The areas with less green cover spatially are comparable hotter than the areas with less green cover.
- Built up area effects the micro environment of that region, for e.g. one of the location like Kolagarh is surrounded by green area in the sides but due to higher density along with built up area in that specific area is more which leads to higher temperature. Micro level temperature variation is very much dependent on the built of mass arrangement & density of that area.

Therefore, we can say that UDI affects is different for different areas of city based on the spatial growth in specific area. In the below given figures one can understand how urban built up mass arrangement effects the temperature variation in the city.

The impact of built up mass effects the heat absorption, the area with more built up area will be warmer than the surrounding area, but if studied on the micro level one can easily calculate variation in temperature in the city.

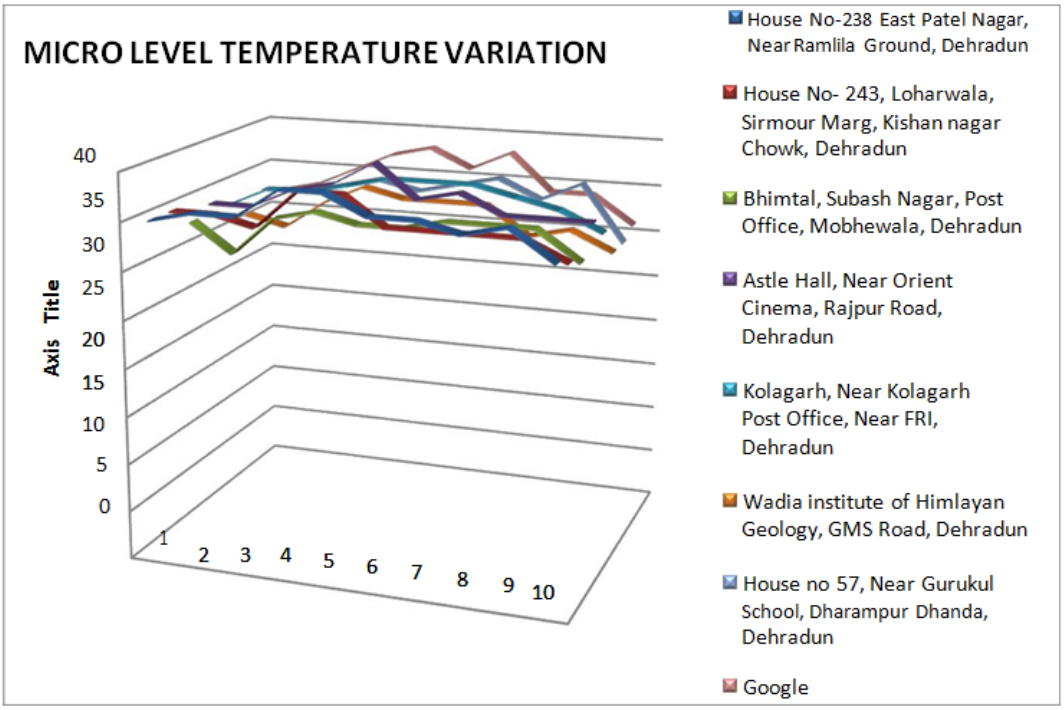

Figure 4: *Micro level temperature variation*

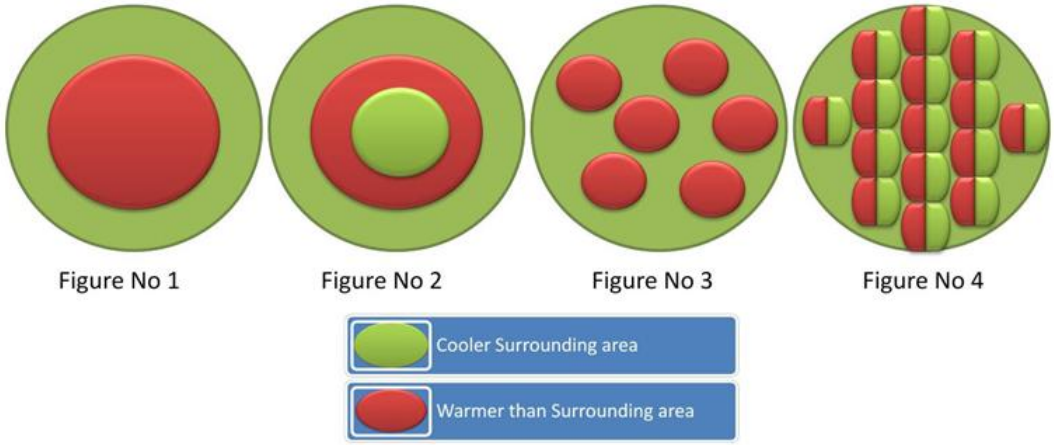

Figure 5: *Landscape planning patterns and its impacts*

Warmer core and cooler surrounding (Figure 1): In this pattern the growth is mostly concentrated in the core area of the city, which effects the environment of the city core area thus leading to warmer core and cooler surroundings.

Cool core area, central warm and cool peripheral areas (Figure 2): In this pattern as the core, outer surrounding is cool and the central area is warmer. This happens when the core area is preserved, most of the development has occurred in the central part of the city.

Scattered development (Figure 3): In this pattern the built up mass percentage is different all around the city, in some part is more and in some part its less, thus the areas with more built area are

comparably warmer than the other areas. The micro level temperature difference in Dehradun city is because of the difference in buildup mass arrangement which shows that effect can be different in different parts of Dehradun city.

Planned development (Figure 4): (Solution) planned development is the key for balanced Built up arrangement, in the figure no 4 the Built-up mass arrangement is planned and balanced, this kind of arrangement is possible in planned area. This type of built up mass arrangement decreases the temperature variation possibilities. The green area and open spaces are spatially located. It's not only about the total area under green cover and open space; it's about spatial placement of the green and open spaces.

Urban planning and design recommendations to create balanced built up mass arrangement to decrease the UHI impact.

Planning, design and orientation: As almost all Indian cities are facing the common issues of increasing environmental degradation. There is need to have strong policy and regulatory framework to increase urban environment sustainability. To moderate the environmental impacts of urbanization, sustainable ways of planning are required. Urban centre's by its form play a significant role in mounting urban heat island. Green city modules such as street orientation in lines with sun direction and wind direction not only help reduce the impact, but also slow down the gas emissions from artificial cooling systems. Further green spaces within the urban set-up ensures cooling effect and better public interaction spaces, apart from psychological supports in reducing human stress levels.

Effective land use planning: It is essential to implement effective Land Use planning. Green cities practices and effective land use reduces the impacts of urban sprawl by encouraging compact, mixed-use developments and promotes higher urban densities without affecting the quality of life. During the formation of master plan, city development plan, zonal plans should consider the planner should consider and promote and open and green spaces.

Landscape planning according to the recorded temperature statics: City landscape planning has to be correlated to the temperature variation statics for remarkable results; the temperature variation can be taken a right tool for implementing landscape planning. For e.g. if we are planning to plant trees shrubs or have planned to do any kind of landscaping in the city then the right way is to plan the plantation drives etc according to the temperature statics, the landscape planning has to be done in the areas which are hotter in comparison with the other areas in the surrounding. The landscape planning will be more fruitful if it is scientifically planned to decrease the temperature variation in the Dehradun city.

Time to adopt vertical development to save land and green spaces: Urban sprawl should be discouraged by practicing higher development densities with green roof tops. Urban sprawl has to be restricted & the unplanned growth patterns have to be checked. The zonal plans have to be strictly enforced. As the valley lies in the highest seismic Zone IV and Zone V making it more vulnerable to earthquakes therefore. Under such circumstances high rise buildings are not advisable under normal procedures of construction techniques. But with the increase in the technological advancement like earth quake resistant building construction techniques etc high rise building can be constructed.

Public transport: All Cities should majorly use public transportation to reduce fossil fuel consumption & vehicular emissions. The proximities of basic transportation mode should be in walk able distance. There is need to introduce smart, sustainable and green public transport.

Subsidiary materials: As the unbalanced and unplanned growth in terms of build up mass in Dehradun city is increasing as a result of which the evapo-transpiration, infiltration is decreasing , and surface runoff in increasing, therefore there is urgent need to use to porous material like porous concrete, interlocking tiles etc to cover open space like footpath, pathways tracks etc. The Buildings should be painted with light colors to reflect more light and absorb less light for eg (light color Plastic paints, emulsion paints, white wash), concrete structures without paint absorbs more heat and increase heat island effect.

Figure 6: *White roofs helps in increasing the albedo effect*

White roofs: Painting rooftops white has become a common strategy to reduce the heat island effect. In cities, there are many dark colored surfaces that absorb the heat of the sun in turn lowering the albedo. White rooftops allow high solar reflectance increasing the albedo of the city or area the effect is occurring. Therefore city dwellers should use white color to paint their roof tops

Vinyl sheets: Vinyl roofs provide an energy- efficient roofing option due to their inherently light coloring. While the surface of a black roof can experience a temperature increase of as much as 90 degrees under the heat of the full sun, a white reflective roof typically increases only 5–14 degrees Celsius. Vinyl membranes can also be used in waterproofing applications for roofing. This is a common technique used in association with green, or planted, roofs.

Spatial placement of green spaces: Open spaces have to be should be spatially distributed (Recreational space, Organized green) other common open spaces, the spaces have to be equally distributed across the city. Planned development is the key for balanced Built up arrangement, the Built-up mass arrangement is planned and balanced, This type of built up mass arrangement decreases the temperature variation possibilities and increase green cover in the city. The green area and open spaces are spatially located. It's not only about the total area under green cover and open space; it's about spatial placement of the green and open spaces.

Two dimensional landscape planning: The urban planner and designers have to carefully plan the green and open spaces; for long we have only concentrated on horizontal landscaping, a new

approach of vertical landscaping has also to be adopted to increase the green cover in the city. As per U&RDPFI in a green city about 25-35 % out of total area should be earmarked as recreational and open spaces within the Green City. So if we want to attain this criterion in our city and turn Dehradun into a green Doon we have to start implementing two dimensions landscape planning.

Figure 7: *Vertical landscaping a way forward to increase green covers in the future cities*

Vertical Landscaping

As we know the land resource in urban area is becoming scarce, rare and costly, therefore in future it will become difficult to keep large open space in urban area. But with vertical growth and vertical landscaping can be increased and land resource can be save.

What's the best way to deal with urban air pollution/urban smog? An intriguing solution to this problem is vertical gardens that scale up buildings. Several such projects have already sprung up around the world, in places like Italy and Mexico. Now, an Italian architecture firm called Stefano Boeri Architetti is planning to build the first one in Asia, specifically in Nanjing, China.

The firm is planning to build two towers laden with greenery, known as a Vertical Forest or the Nanjing Green Towers, in Nanjing's Pukou District. Due to be completed in 2018, the towers would be covered in 600 tall trees, 500 medium-sized trees, and 2,500 cascading plants and shrubs. In total, this would cover an area of 6,000 square meters (64,600 square feet).

Roof gardening/green roofs: Green roofs are another method to decrease the urban heat island effect and increases green cover in the city. Green roofery is the practice of having vegetation on a roof; such as having trees or a garden. The plants that are on the roof increase the albedo and decrease the urban heat island effect. In urban areas, due to escalating population, more land area is brought under the construction of houses; therefore there is hardly any space for landscaping. Especially in multistoried buildings, roof gardening is the only way to grow fruits and vegetables by using the pots and containers. This practice is known as container gardening. Psychiatrist recommends that working in garden refresh the body and mind by reliving harsh stresses. Gardens become the integral part of the family life benefited by the supply of toxic free fresh fruits and vegetables.

Figure 8: *utilization of Bonsai trees, bushes and shrubs on roof top gardening*

Use bonsai trees, bushes and shrubs: These types of trees or plants are very small in size and cover less space. So we can easily adopt these types of plants to cover open or small spaces effectively in our house. This will also help in increasing the green cover in the city.

Figure 9: *Plantation and installed variety of bonsai trees in and around the urban concrete structures*

Designing of housing units around the trees: The unfortunate reality of urbanization is that trees get in the way. Trees improve the air you breathe, cut your energy bills with their shade, provide homes for wildlife, and add beauty and value to your house. In fact, landscaping can add approximately 10 to 20 percent more value to a property especially landscaping that includes mature trees. Commercial areas with trees also attract more customers (and they stay longer and spend more money). The urbanization has led to tree cutting because trees are not kept as the part of the building design. Trees are usually cut to make way for construction and then unused/left over space are demarcated as the area for landscaping just to sake of building bye laws. Urban Planners, Architects & Urban designers in India have to change their mind set tree conservation has to be taken into account. The existing trees have to be agglomerated into the design. We have design the infrastructure around the trees, Existing they have to be the part of the design.

Figure 10: *Designing of housing units around the trees to decrease deforestation*

Plantation on dead walls/grass paved walls: (Vertical Greenery Systems (VGS)A well designed and maintained Green Wall can significantly enhance a building's appearance - whether it's to add a new aesthetic dimension, disguise a car park, refresh a tired façade or add color and texture to a complete wall or section. A green wall in an urban area can help improve local air quality, both by absorbing carbon dioxide and releasing oxygen, and by trapping dust and other pollutants. By adding a layer of insulation (both thermal and acoustic) green walls absorb sound - making a positive impact for both the building's occupants and the local environment. The grass paved walls look very attractive and can increase the green cover immensely. Just presume that all the walls are grass paved. The time has come when we have to think about this, thigh cost of the land in the urban areas makes it difficult to keep large chunks of land for parks and green spaces, but if we can adopt the idea of vertical plantation we will be able to increase the green cover of any city.

Figure 11: *Plantation on dead walls/grass paved walls to increase green cover*

Figure 12: *Cut out for skylight; Landscaping in Courtyard; Plantation in Shaft Area*

Plantation on balconies: The plantation can be done in any space kept open in a building for e.g. the plantation can be done in balconies of the building. The space left for balcony can be beautifully landscaped. The addition of the soft element will enhance the beauty of the space will also enrich the view.

Other ideas for vertical landscaping and internal landscaping which if adopted can increase the green cover in the city.

Horizontal Landscaping

Figure 13: *Planned Plantation of trees in and around urban and semi urban areas*

Planting trees in cities: Planting trees around the city can be another way of increasing albedo and decreasing the urban heat island effect. Trees absorb carbon dioxide and provide shade. It is recommended to plant deciduous trees because they can provide many benefits such as more shade in the summer and not blocking warmth of winter. trees can be installed in public area, cremation grounds, schools, median, graveyards, setback area, area left for road widening, low lying areas, low lying areas, flood prone area, plantation in the road margins, play grounds, open space, recreational spaces, etc.

Green parking lots/Green Parking lots to produce electricity: Green parking lots use surfaces other than asphalt and concrete to limit the impact urban heat island effect. In recent days there has been a huge Popularity of Solar Groves in the parking area: According to a Wall Street Journal report published in September 2012, “From Long Island to the Arizona desert, developers is covering their

parking lots with canopies of solar panels. These way parking lot owners get to double up on their use of underutilized land and to offset their utility bills at the same time. And very little stands between most parking lots and the sun, so they can produce plenty of power.

Figure 14: *Revitalization car parking space for increasing green cover and energy production*

Prevention of existing park and gardens: Careful planning prior to undertaking work can help prevent irrevocable damage to a cultural landscape. Professional techniques for identifying, documenting, evaluating and preserving cultural landscapes have advanced during the past 25 years and are continually being refined. Preservation planning generally involves the following steps: historical research; inventory and documentation of existing conditions; site analysis and evaluation of integrity and significance; development of a cultural landscape preservation approach and treatment plan; development of a cultural landscape management plan and management philosophy; the development of a strategy for ongoing maintenance; and preparation of a record of treatment and future research recommendations.

Figure 15: *Optimum utilization and revitalization of existing park and available open spaces to increase green cover*

Optimum utilization and revitalization of existing park and available open spaces: The open spaces which are not properly utilized should be redesigned for optimum utilization and beautification. There are various open spaces in the city which are not properly designed nor properly maintained. There are available spaces in the city which are either being used to through garbage or are encroached or being used for informal parking, all these spaces have to be utilized for eg the space beneath the flyovers, setbacks etc

Plantation of tree and shrubs in median and road side: Plants along median strips reduce vehicular glare and prevent accidents and also increase some green cover in the city. It is important to plant trees in road margin area available to increase the green cover of the city. Plantation on road side increases the aesthetics of the ROW and also helps in decreasing the pollution due to vehicle and also helps decreasing the temperature variation.

Figure 16: *Plantation of tree and shrubs in median and road side*

Plantation in setback spaces and road widening spaces: The setback spaces and area left open for road widening in future should be used optimally to install the plants, shrubs and trees, this will increase the green cover of the city and will also help in avoiding encroachment of the open spaces. The open spaces are usually encroached first. The plantation of the trees, plants, shrubs will help in curbing the menace of encroachment.

Figure 17: *Plantation of shrubs and trees in setback spaces & road widening spaces to increase green cover*

Figure 18: *Plantation along river/streams/nalas to increase the green cover*

Plantation along river/streams/nalas: I have always been astounded at the amazing power of trees and plants to provide so many benefits to our environment and communities. Forested stream banks act like a sponge, filtering out excessive nutrients, sediment, and other pollutants that run off from the land that would be damaging if they entered a stream. Shrubs and trees are also able to prevent stream bank erosion by anchoring the soils, keeping the banks stable and excess sediment out of the stream. Buffers can even help to mitigate flooding/water logging by absorbing and slowing down surface runoff. River front development programs should mostly include increasing the green cover and open spaces near the river banks.

As a potential two major tributaries Bindal and Ripana River are traversing through Dehradun city, unplanned vacant land which not being used and are being encroached by public has to be stopped the spaces on both sides of the river have to be utilized to increase the green cover of the city. The various tributaries and nalas which are the part of the catchment area have to be properly planned and green cover has to be increased. Encroachment along the banks has to be stopped. The banks of the both the rivers from the upfront point Anarwala of Bindal river & kailaghat ghas mandi upfront point of Rispana river till the merging/conflux point Doudwala, Mothorrowala. The River Front development of both the rivers will increase the green cover in the city; will also help in balancing build up mass arrangement & decreasing UHI effect in the city.

Utilization of all existing open spaces: There are various available open spaces in the Dehradun city which if properly utilized for the plantation and landscaping can increase the green cover of the city for eg plantation can be done in the periphery of cremation grounds, grave yards, school boundaries, public and semi public offices, Bus terminals, truck terminals, transport Nagar, Parade ground, factories, stone crushers, batching plants, low lying areas etc we have to identify & earmark all those open space.

Conclusion

GIS, GPS, and other devices should be used scientifically to analyze and figure out the various problems and potentials of any city. Scientists, Geographers, Urban planners and researchers can use the various available techniques to understand the issue and can in turn provide the best suitable scientific solutions, In this case study simple and low cost scientific devices were used to record the

temperature in various part of the Dehradun city, to validate the temperature variation within the city, Most of the times the research work is not initiated because of the cost and time factor, but if the research is properly planned then it can be executed and completed with low cost measures. With the help these studies very effective solutions can be proposed which can definitely help in reshaping the city and achievement of goals like balanced urban mass arrangement, heath benefits, environment improvement, environment sensitive development, urban sustainability & maintaining ecological balance.

References

Akbari, H. 2002. Shade trees reduce building energy use and CO2 emissions from power plants. *Environmental Pollution,* 116, pp.119-126.

Benefits of green infrastructure - Forestry Commission. 2010. Prepared by Land Regeneration and Urban Green space, Centre for Forestry and Climate Change, Forest Research, Farnham, Surrey, Benefits of green infrastructure, urban regeneration and green space partnership, report by forest research, Defra research contract number WC0807.

Chaudhry, P. 2006. Valuing recreational benefits of urban forestry- A case study of Chandigarh city. Doctorate Thesis. FRI Deemed University, Dehradun, India.

China to get vertical gardens in 2018 to help tackle pollution. 2018. Available from: http://www.iflscience.com/environment/china-to-get-vertical-gardens-in-2018-to-help-tackle-smog/.

City Development Plan: Dehradun Revised. 2007. Jawaharlal Nehru National Urban Renewal Mission (JNNURM), Urban Development Department, Government of Uttarakhand.

DeFries, R. and Pandey, D. 2010. Urbanization, the energy ladder and forest transitions in India's emerging economy. *Land Use Policy,* 27(2), pp.130-138.

Draft Urban and regional development plan formulation and implementation Guidelines (URDPFI), Ministry of Urban Development, Government of India, 2014.

Grahn, P and Stigsdotter, U.A. 2003. Landscape planning and stress. *Urban Forestry and Urban Greening,* 2, pp.01-18.

Grimm, N.B., Faeth, S.H., Golubiewski, N.E., Redman, C.L., Wu, J., Bai, X. and Briggs, J.M. 2008. Global change and the ecology of cities. *Science,* 319(5864), pp.756-760.

India State of Forest Report. 2009. Forest Survey of India, Ministry of Environment and Forests, Dehradun, Uttarakhand.

Satyawan, Manjit Singh and Sushma Gairola. 2015. Land Use /Land Cover Change Detection Using Geospatial Technique: A Case Study of Sahaspur Block in Dehradun District (Uttarakhand). *International Journal of Science, Engineering and Technology Research*, 4(1).

Jain, S., Laphawan, S. and Singh, P.K. 2013. Tracing the changes in the pattern of urban landscape of Dehradun over last two decades using RS and GIS. *International Journal of Advanced Remote Sensing and GIS,* 2(1), pp.351-362.

Jain, S., Siddiqui, A., Tiwari, P.S. and Shashi, M. 2015. Urban Growth assessment using CA Markov Model: A case study of Dehradun city. *9th International Geographic Union,* Delhi, India.

Jim, C.Y. and Liu, H.H.T. 2000. Statutory measures for the protection and enhancement of the urban forest in Guangzhou City, China. *Forestry,* 73, pp.311-329.

Kavitha B.D, Gayathri, N.K. 2017. Urbanization in India. *International Journal of Scientific Research and Education*, 5(1), pp.6166-6168.

Kershaw, T.J., Sanderson, M., Coley, D. and Eames, M. 2010. Estimation of the urban heat island for UK climate change projections. *Building Services Engineering Research and Technology*, 31(3), pp.251-263.

Mahfooz, N.Z. 2011. Legal framework for environment impact assessment in India: a contemporary appraisal in corporate perspective. *Chartered Accountant Journal,* 59(12), pp.18721879.

Master plan of Dehradun for 2005-2025. Town and country planning Organization, Government of Uttarakhand.

Myrup, L.O. 1998. A numerical model of the urban heat island. *Journal of Applied Meteorology,* 8, pp.908-918.

Nowak, D.J., Crane, D.E. and Stevens, J.C. 2006. Air pollution removal by urban trees and shrubs in the United States. *Urban Forestry and Urban Greening,* 4(3-4), pp.115-123.

Nowak, D.J., Rowntree, R.A., McPherson, E.G., Sisinni, S.M., Kerkmann, E.R. and Stevens, J.C. 1996. Measuring and analyzing urban tree cover. *Landscape and Urban Planning,* 36, pp.49-57.

Omvir Singh, Poonam Arya, Bhagwan Singh Chaudhary. 2013. On rising temperature trends at Dehradun in Doon valley of Uttarakhand, India. *Journal of Earth System Science*, 122(3), pp.613-622.

Singh, J. 2013. Core area demarcation specifically planned to decongest the city traffic - a case study Dehradun city. *ITPI Journal,* 10(2).

Singh, J. 2014. The role of methodological and specifically planned spatial traffic law enforcement an appropriate approach to decongest, manage and regulate the traffic in planned and unplanned cities. Case Study - Dehradun City. Institute of Town Planners, India.

Singh, O., Arya, P., Chaudhary, B.S. 2013. Rising temperature trends at Dehradun in Doon valley of Uttarakhand. *Journal of Earth Science,* 122(3), pp.613-622.

United States. Environmental Protection Agency. Reducing Urban Heat Islands: Compendium of Strategies. Available from: https://www.epa.gov/heat-islands/reducing-urban-heat-islands-compendium-strategies.

Urban heat island. Available from: https://en.wikipedia.org/wiki/Urban_heat_island.

List of most polluted cities by particulate matter concentration. Available from: https://en.wikipedia.org/wiki/List_of_most_polluted_cities_by_particulate_matter_concentration

Cloud Publications
International Journal of Advanced Remote Sensing and GIS
2017, Volume 6, Issue 1, pp. 2297-2305
ISSN 2320 – 0243, Crossref: 10.23953/cloud.ijarsg.295

Research Article

Study of Cropping Pattern, Crop Ranking and Crop Combination in Somb River Basin at Lower Shiwalik Hills

Vipin Kumar

Department of Geography, Banasthali University, Banasthali, Rajasthan – 304022, India

Publication Date: 11 August 2017

DOI: https://doi.org/10.23953/cloud.ijarsg.295

Abstract The studies related to agriculture become more pertinent for those areas, where agriculture contributes more than 80 percent of net income, either through its direct cultivation or through its allied occupations. The aim of present study is to assess the cropping pattern, crop combination, and crop ranking in the Somb river basin using geospatial techniques and secondary data. Here, agriculture is single primary occupation and the basic source of economy. As well as more than 50 percent of total workers are engaged in agriculture and smallholders farmers, who grow crops using low intensity practices of land. Hence, a scientific and systematic study is highly required to assessing and mapping the cropping pattern in the watershed.
Keywords: *Crop combination; Crop pattern; Crop ranking; Irrigation*

1. Introduction

Agriculture is one of the leading occupation in India and it plays a vital role in shaping the economic condition of the farmers as well as the whole country. It contributes about 16 per cent of total GDP and 10 per cent of total export. Over 60 per cent of total land of the country is arable making it the second largest country in term of total arable land. Agriculture provides food to the masses, green fodder for livestock and supplies raw material to various agro-based industries. Hence, systematic, scientific, and proper cropping pattern and crop combinations are the most important aspect for better out-put in agriculture. Cropping pattern indicates the proportion of area under various crops at a point of time where as the crop combination indicates to grow different types of crops under the same agriculture field. Both Cropping pattern and combinations area dynamic concept as it changes over space and time. Terrain, topography, slope, temperature, amount and reliability of rainfall, soil and availability of water for irrigation are some factors responsible for the cropping pattern and combination in any area (Husain, 2010). Cropping pattern and combination are also the part of behavioral approach in geography, because it reflects the performance of the farmer for various crops sown in an agricultural field. Hence, by considering the facts related to better cropping pattern, the present research has been attempted to analyzing the irrigation facilities, cropping pattern, crop ranking and crop combination in the Somb river basin.

1.1. Study Area

The Somb river is a tributary of Yamuna river, arise from the outer slope of the lower part of Shiwaliks range in the district Sirmaur (Himachal Pradesh, India) and takes a southerly course, which drains in

the plain land of district Yamunanagar (Haryana, India). The extension of Somb drainage basin lies between $77^0$18/E to $77^0$34/E longitude and $30^0$9/N to $30^0$29/N latitude and total calculated area is 492 kms^2 (Figure 1). The northern part or the area falls in Himachal Pradesh is a dissected hilly track and not more useful for agriculture, whereas the southern part is plane and favorable for agriculture.

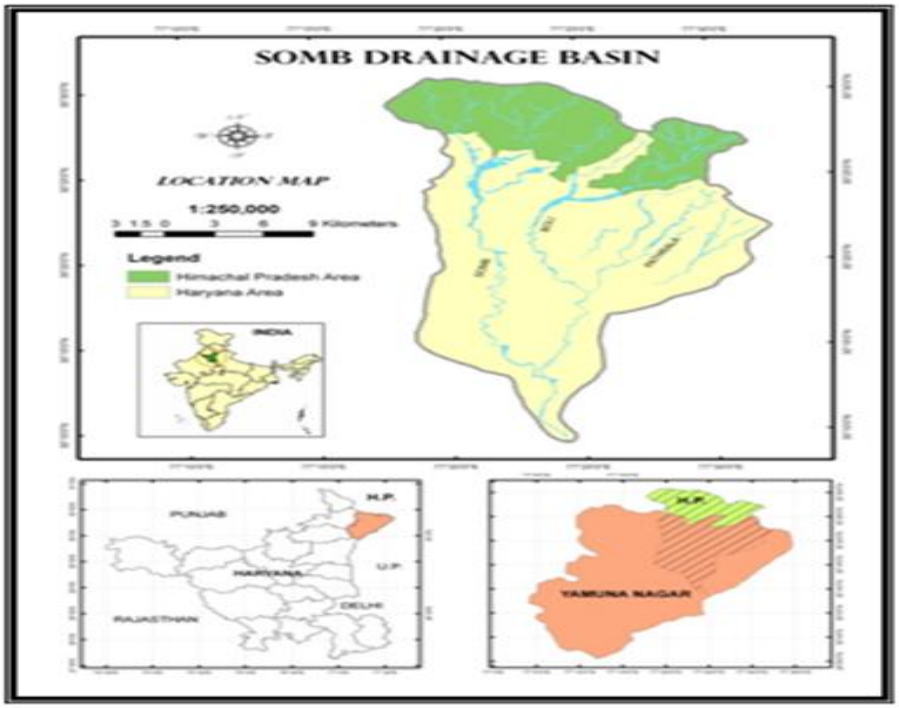

Figure 1: *Somb Drainage Basin*

1.2. Climate

The watershed has a sub-tropical continental monsoon climate, where we find great variation in climatic elements. Normally, the period from November to February is cold, this is followed by the summer season from March to the end of June. The south-west monsoon mostly breaks in the last week of June or first week of July and continues up to about the middle of September. The period from mid September to the mid of November is the post monsoon or transition season. In winters, frost sometimes occurs during December and January. The watershed also gets occasional winter rains from cyclones or western disturbances. The rainfall is mostly restricted to rainy season. The study area is characterised by the high velocity hot winds and dust storms during the summer months of May and June. The temperature for the last ten years varies from 3^0C in January to 36^0C in June.

1.3. Soil

The study area has occupied the outer most range of Shiwaliks lying west of Yamuna River. The soils, due to the variation in topography, intensity of erosion, parent material, and other factors, exhibit variations in many characteristics like texture, depth, colour, drainage, moisture status etc. The soil analysis of the soil samples taken by various agencies suggest that P_H value varies from 6.7 to 8.1. On the steep slopes, the soil is dry and tends to support xerophytic vegetation. The plain area is formed by alluvial deposits of the Somb River and its tributaries and the main river Yamuna and its other tributaries.

1.4. Objectives

The major objectives of the study are:

a. To assess and mapping of the cropping pattern
b. To assess the crop ranking
c. To study the crop combination

2. Data Source and Methodology

The present study is carried out basically with the help of Geo-coded IRS- P6 FCC merged LISS-III with 23.5 m spatial resolution, data of March, 2005. The area of watershed has been delineated on the bases of topographical sheets no. 53 F/6, F/7, F/8 and F/11 on 1:50,000 scales, obtained from Survey of India. Some secondary data has been collected from the following departments of Haryana and Himachal Pradesh government:

- Department of Agriculture, Sirmaur (Himachal Pradesh) and Yamunanagar (Haryana)
- Department of Irrigation, Sirmaur (Himachal Pradesh) and Yamunanagar (Haryana)
- Krishi Vigan Kainder (KVK), Yamunanagar (Haryana)
- Division Soil Conservation Officer (DSCO), Department of Agriculture, Yamunanagar (Haryana)
- Haryana Remote Sensing Application Centre (HARSAC), HAU-Campus, Hissar

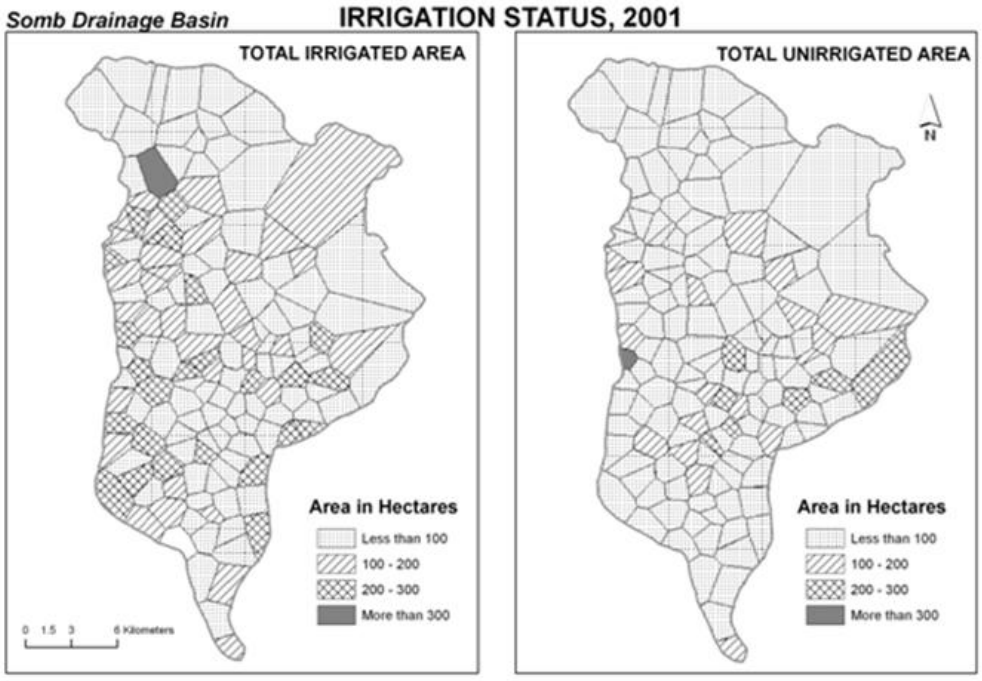

Figure 2: *Somb Drainage Basin: Irrigation Status 2001*

On the basis of data collected from irrigation department, agriculture department and primary survey, the irrigated and non irrigated areas has been identified. The study is based on the proportion of cropland under ten major crops, which are divided into two categories- Kharif crops and Rabi crops. To study the cropping pattern, a comparison of the relative strength of various crops is made by ranking them according to the percentage of net shown area occupied by each.

Crop combination analysis has been done by using the Weavers method modified by Doi after substituting $\sum d^2/ n$ with $\sum d^2$ i.e. the sum of squared differences. In this method, the minimum value of deviation decides the number of crops to be included in crop combination. The Weaver formula is as:

$$\Gamma^2 = \sum d^2/n \text{ or } \Gamma = \sqrt{\sum d^2/n}$$

Where Γ = value of crop combination, d is the difference of the actual crop percentage from the theoretical norm and 'n' is the number of crops in the given combination.

Finally, ArcGIS (version 9.2) software has been used to prepare the maps.

3. Results and Discussion

3.1. Area under Irrigation Facilities

Irrigation facilities play a vital role for the development of agriculture as well as vegetation cover. According to irrigation department of Yamunanagar, Haryana, tube-well (with electricity and without electricity) are the main sources of irrigation, beside this government canal and river water is used for this purpose at some agriculture lands. Approximately 160 square kilo meters (16000 ha.) agriculture land is irrigated by tube-wells. Irrigation facilities are poor in hilly areas (Figure 2). Water harvesting earthen dams are also constructed in Kathgarh, Rampur Gainda, Bhagwanpur, Darpur, Bagpat, Khillanwala, Ibrahimpur, Dhanoura and Salempur villages.

Table 1: *Somb Drainage Basin - major crops and there characteristics*

Crop	Time	Time harvesting	Climate	popular verities	Soil required	More suitable areas
Paddy	Nursery sown in June and transplanted in July -August	Sep. to Nov.	Hot-Wet	IR-8, IR-106, Pusa-2.21,Jaya, jhona-349 & 351, Basmati-217 & 370	Clay to Clay loam	Cultivated at all agricultural land but more yield in flood areas of streams
Maize	June-July	Oct. Nov.	Hot-Wet	Ganga 5, Ganga I, Vijay, Sona	Loam (well drained)	Pedimount Areas
Bajra	July-Aug	15th Sep. to 15thOct	Hot	Hybrid Bajra No.1, No. 4 and B.J. 104	Sandy or Sandy loam (Well drained)	Southern plain areas of low land
Wheat	Oct. to Dec.	March to April	Cold	Kalyana, Sona (K-227), Sonalika (S-308), H.D. 2004, P.N.18, HDM-1553 and C-306	Well drained loam soil	All over the agricultural land
Gram	Oct. to Dec.	March to April	Cold	PB-7, G 104, C-164	All types but Sandy loam, clay loam with well drained are more favorable	Southern plain areas of low land
Sugarcane	Mid. Feb. to Mid. April	Nov to Dec.	Hot-Wet	Co. 1148, Co. 975, Co. 453, Co. 212 Co. 124, Co. 158.	Loam and Clay	Pedimount and plain areas

Ground nut	March	Aug-Sep	Hot-Wet	…….	Well drained sandy soil	Selected villages
Barley	Oct.- Nov.	March to April	Cold	…….	Sandy loam and loam with well drained texture	Areas situated near streams
Pules	July- Aug	Oct. Nov.	Hot	Mash48, Mash I-1, T-9, Moong No.54, shining Moog No. 1, Massar No. 9-12	Sandy or Sandy loam(Well drained)	Selected Areas (Subsidiary Crop)
Vegetable	Oct.-Nov.	March to April	Cold	…….	All area with high organic Carbon in soil	Selected Areas (Subsidiary Crop)
Oil seed	Early September	Early December	Average	……..	Sandy or Sandy loam(Well drained)	Pedimount and Plain areas.
Vegetable and green fodder	Early March	Early June	Average	……..	Well drained sandy soil	Mostly all areas for green fodder and Stream banks have Melon

Department of Agriculture, Yamunanagar, Haryana, India.

Table 2: *Somb Drainage Basin - area under various crops*

Crop	Area under crop ($km^{2)}$	Percentage of total agricultural land	Percentage of total area
Kharif	1.478	0.6	0.30
Rabi	0.487	0.2	0.10
Kharif + Rabi (Double Cropped)	253.964	99.1	51.60
Current Fallow	0.239	0.1	0.05
Total	**256.168**	**100.0**	**52.05**

Satellite image interpretation, March, 2005.

3.2. Copping Patterns

The crops of the watershed area are divided into two main categories viz. Kharif and Rabi locally known as *Sawani* and *Sadhi* respectively. The former one is the summer season harvest and the latter is the winter season harvest. Any crop, which does not strictly fall within these two categories, is known as zaid crop and its harvest is called the zaid-Rabi or zaid-Kharif, according to the harvest with which it is assessed. *Toria* (an oilseed) is cultivated as zaid Kharif and vegetables, melon and green fodder as zaid Rabi. A brief account of various crops sown in watershed is given in Table 1.

According to the field study and the data collected from Agriculture Departments of district Yamunanagar, Haryana and district Sirmaur, Himachal Pradesh, total agriculture land in watershed is approximately more than 50% of the whole area. The result is a low yield per hectare, but the increase in the adaptation of new technology and use of inputs has substantially increased the agriculture production.

In the present watershed, more than 99 percent of total agriculture land is double cropped area, which is cultivated in both Kharif and Rabi season. Only one percent of agriculture land is single cropped and

follow land area. Some crops have also harvested in hilly areas of watershed, but its area is negligible (Table 2).

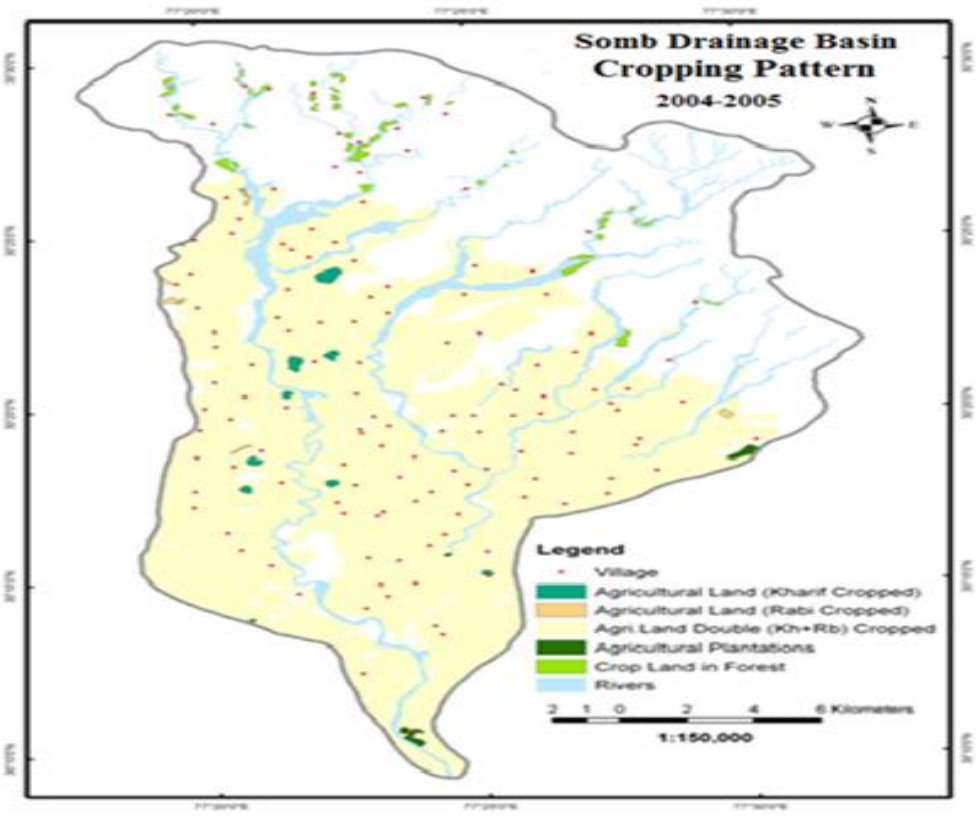

Figure 3: *Somb Drainage Basin: Cropping Pattern (2004-2005)*

The present cropping pattern has pre-dominance of cereals, where wheat, sugarcane, and paddy occupy more than one third area. There has been a big spurt in area under these croups (especially wheat and paddy) after green revolution of 1960-61 due to increasing growth in irrigation facilities.

3.3. Crop of Kharif Season

Kharif is a very important cropping season during June to October. It occupies more than Rabi cropped area in the watershed. Paddy and Sugarcane are very common crops of this season and both occupy more than 88 percent of total sown area (Table 3).

3.4. Crop of Rabi Season

The Rabi crops are cultivated with the advent of the winter season, generally from the end of October to beginning of November. The main Rabi crops are Wheat, Gram, Barley, Pulses and the commercial crops are Groundnut, Oilseeds, and Cotton. In the study area, only Wheat is predominated Rabi crop on whole agriculture land (Table 3).

3.5. Crop Ranking

The study of agriculture region is of great importance in geographical studies. The regional dominance of various crops can be determined by comparing the relatively a real strength of various crops. This can be obtained by ranking them, for each paragon, according to the percentage of the total harvested cropland occupied by each crop (Porwal, 1994).

Table 3: *Somb Drainage Basin - percentage of area, production, and average yield of Kharif and Rabi crops*

Kharif crops				Rabi crops			
Crop	**Areal distribution (% to net sown area)**	**Production (%)**	**Av. yield in kgs/hact.**	**Crop**	**Areal distribution (% to net sown area)**	**Production (%)**	**Av. yield in kgs/ hact.**
Maize	5.90	2.71	1685.00	Wheat	89.4	96.5	3674.9
Paddy	55.24	44.76	2957.00	Gram	3.0	0.7	934.5
Sugarcane	33.40	49.30	5380.90	Cotton	3.0	0.5	604.9
Sunflower	1.40	1.90	5000.00	Groundnut	0.6	0.3	1671.6
Pulse	1.55	0.32	753.03	Sirson	1.3	0.7	1914.7
Other	2.51	1.01	1470.00	Other	3.4	1.3	1257.3
Total	100.00	100.00	3650.93	**Total**	**100.0**	**100.0**	**3402.8**

Based on sample analysis in the watershed area (2004-2005).

Table 4: *Somb Drainage Basin - crop ranking*

Crop	% of net sown area	Rank	% of total production	Rank	Av. yield in kgs/hact.	Rank	Compound rank	Final rank
Maize	3.01	5.00	1.44	4.00	1685.00	6.00	5.00	5.00
Paddy	28.25	2.00	23.75	3.00	2957.00	4.00	3.00	3.00
Sugarcane	17.10	3.00	26.15	2.00	5380.90	1.00	2.00	2.00
Sunflower	10.70	4.00	1.00	5.00	5000.00	2.00	3.60	4.00
Pulse	0.79	8.00	0.17	9.00	753.03	11.00	9.30	10.00
Wheat	43.60	1.00	45.60	1.00	3674.86	3.00	1.60	1.00
Gram	1.28	7.00	0.34	7.00	934.48	10.00	8.00	7.00
Cotton	1.31	6.00	0.22	8.00	604.86	12.00	8.60	8.00
Groundnut	0.28	10.00	0.13	10.00	1671.56	7.00	9.00	9.00
Sirson	0.65	9.00	0.35	6.00	1914.70	5.00	6.66	6.00

Based on sample analysis in Somb Drainage Basin.

The simplest form of the agricultural regionalization of first order is based on either the dominating crop (first ranking crop) or a specific indicator used to define an area. On the basis of crop dominance and ranking device, regions like Corn Belt, Cotton Belt were defined for the United States by American geographers (Singh and Dhillon, 1994). The crop ranking has been done on the basis of dominance of area under specific crops. As far as crop ranking is concerned, Wheat is the first ranking crop, which covers an area of more than 43 percent of net sown area. The crop Paddy covers 28.25 percent and Sugarcane 17.10 percent, and comes at second and third place respectively. The crops Sunflower, Maize, Cotton, Gram and Pulses are placed on fourth to eighth ranks respectively. The crop Mustard and Groundnut are insignificant crops as they occupy less than one percent area of net sown area (Table 4).

The crop ranking is also measured on the basis of three elements i.e. percentage of net sown area, percentage of total production, and average yield per hectare. It is observed that the Wheat crop has first ranked where as the Sugarcane has second and due to high yield. The crop Paddy has got third position. The crops Sunflower, Maize, Mustard, Gram and Cotton have lied at fourth to eighth rank respectively. The yield of various crops affects the ranking of this section as compared to the previous. But, it is better rather than first.

Table 5: *Somb Drainage Basin - crop combination*

Category	Crop combination	Percentage of crop land (a)	Percent theoretical base (b)	Difference squared $(b-a)^2$	Crop Combination Index
Monoculture	Wheat	43.60	100.00	3180.96	3180.96
Bi-Combination	Wheat	43.60	50.00	40.96	251.60
	Paddy	28.50	50.00	462.25	
Tri-Combination	Wheat	43.60	33.33	106.10	130.10
	Paddy	28.50	33.33	23.32	
	Sugarcane	17.10	33.33	263.41	
Tetra-Combination	Wheat	43.60	25.00	345.10	226.04
	Paddy	28.50	25.00	12.25	
	Sugarcane	17.10	25.00	62.41	
	Maize	3.01	25.00	483.56	
Penta-Combinaion	Wheat	43.60	20.00	556.96	255.11
	Paddy	28.50	20.00	72.25	
	Sugarcane	17.10	20.00	8.41	
	Maize	3.01	20.00	288.66	
	Cotton	1.31	20.00	349.31	
Hexa-Combination	Wheat	43.60	16.66	729.00	254.00
	Paddy	28.50	16.66	141.60	
	Sugarcane	17.10	16.66	0.25	
	Maize	3.01	16.66	184.68	
	Cotton	1.31	16.66	233.78	
	Gram	1.28	16.66	234.70	

Based on sample analysis in Somb drainage Basin.

3.6. Crop Combination

The crop combination reflects the variable position of the individual crops within themselves. It can also be helpful in interpreting some aspects of economic and social geography (Mohammad, 1978). A number of statistical methods have been applied by the geographers to study the crop combination.

For the analysis of crop combination, first the percentage of different crops, during the Kharif and Rabi season, to the total cropped area has been calculated. The crops having a real coverage of less than one percent are not included in the analysis of crop combination as they are insignificant as compared to dominated crops. The table 5 shows that minimum combination index i.e. 130.1 for a combination of Wheat, Sugarcane and Paddy indicate that the watershed area is a tri-crop combination region.

4. Conclusion

The indices of cropping pattern, crop ranking and crop combination indicate the complexities of crop distribution in quantitative manner. About 52 percent of total area of the basin is under cultivation with a wide variety of Kharif and Rubi crops like Maize, Paddy, Sugarcane, Sunflower, Pulse (Kharif crops) and Wheat, Gram, Cotton, Groundnut, Sirson (Rabi crops) and more than 99 percent of the total agriculture land is double cropped area. The crop Wheat is the first ranking crop, which covers an area of more than 43 percent of net sown area and Paddy covers 28.25 percent and Sugarcane 17.10 percent, and comes at second and third place respectively. The pattern of crops and crop combination are mostly controlled by topography, soil and irrigation facilities. The spatial variations of cropping pattern identified in the basin area are highly useful not only for watershed development planning but also for the economic development of the farmers lives in basin area.

References

Agricultures reports, *Department of Agriculture,* Government of Haryana, Haryana, India.

Agricultures reports, *Department of Agriculture,* Government of Himachal Pradesh, Himachal Pradesh, India.

Husain, M. 2010. Systematic Agricultural Geography. New Delhi, India: Rawat Publication.

Irrigation reports, *Department of Irrigation,* Government of Haryana, Haryana, India.

Mohammad, N. 1978. Agriculture Land-use in India. Delhi, India: Inter India Publication.

Porwal, M. C. 1997. Remote sensing analysis of environmental resources for planning and development. Delhi, India: APH Publishing Corporation, p.302.

Singh, J. and Dillon, S. S. 1994. Agriculture Geography. 2nd ed., New Delhi, India: Tata McGraw-Hill publishing Company Limited.

Cloud Publications
International Journal of Advanced Remote Sensing and GIS
2017, Volume 6, Issue 1, pp. 2360-2366
ISSN 2320 – 0243, Crossref: 10.23953/cloud.ijarsg.300

Research Article

A Geographical Study of Agricultural Loss due to Natural Hazard in the Villages of Raver Tehsil in Jalgaon District, Maharashtra, India

Mahendra Shaligram Mahajan

Department of Applied Geography, School of Environmental and Earth Sciences, North Maharashtra, Jalgaon, Maharashtra, India

Publication Date: 19 August 2017

DOI: https://doi.org/10.23953/cloud.ijarsg.300

Abstract Tsunami, Cyclones, floods, landslides, earthquake, volcanos etc natural disaster are experiences unexpected human life loss & economic loss. During the study period it is observed that 2507 farmers are intensively affected by different types of Natural hazards. In the list of farmers affected by different calamities, large numbers of farmers are affected by hail storms and cyclones (1382). During the study period about 12 villages in Raver Tehsil are affected by the flood of Hatnur Dam back water out of them 10 villages are identified by the govt. those are affected by flood hazards during 2011-15. These affected villages are located near the bank of Tapi, Suki, Mor. During the study it is observed that accumulated soil deposits in the Hatnur dam is not excavated. To protect economy of villagers, deposits should be excavated periodically. Northern part of the region is covered by Satpuda mountainous region and more or less all rivers source are originated from the mountain. All tributaries are flowing from mountainous region across steep slope of the land surface is a one of the reason of flood because all tributaries are flowing speedily and spread on outer area of the course.
Keywords *Agriculture; Backwater; Cyclone; Flood; Natural hazards; Raver*

1. Introduction

Tsunami, Cyclones, floods, landslides, earthquake, volcanos etc natural disasters are experiences unexpected human life loss and economic loss. Northern part of the region is covered by Satpuda mountainous region and more or less all rivers source are originated from the mountain. Raver is a north eastern tehsil of Jalgaon district, famous for banana plantation not only in the state but also in the India (Gupta et al., 2015). This tehsil is characterized by piedmont plain. Satpura mountain ranges and ravines and bad lands along the banks of river Tapi.

In the present research work, researcher has classified the effect of natural hazard into floods, effect of Back water of Hatnur Dam, heavy rainfall and other types of natural hazard such as climatic depression, high velocity winds and heavy rain.

Flood not only causes huge economic loss in the form of damage to houses, industries, public utilities, and property but also many human lives and of cattle heads are lost (Sharma, 2012).

2. Research Methodology and Data Collection

For the present study base map of the study region is compiled with the help of tehsil map. Primary maps are obtained from survey of India Topographical Maps. Data regarding economic reviews of farmers collected through questionnaires and personal interview of farmers in affected villages. An attempt has been made to analyze such voluminous data with the help of computer and interpreted by applying suitable statistical and cartographic techniques. Required data for the research work is collected from Government office of the study region (Tehisl and Agricultural office Raver).

3. Discussion

Heavy rainfall is the main cause of inland flooding. Flood in rivers valley region is a disaster which can destroy the total environmental set up of the area. It causes river bank erosion, depression of land, shifting of river course, river channel widening etc. The economy also gets affected due to damage of crops direct or indirect affecting the agriculture sector (Ismail and Mustaquim, 2013). Loss of agricultural production due to the reason of heavy rain, back water and Cyclone.

3.1. Agricultural Loss due to Back Water, Heavy Rain and other Natural Hazard during 2011-2015

Following table (Table 1) is showing loss of agricultural production due to the reason of heavy rain, back water and Cyclone or wind during 2011 to 2015.

Table 1: *Agricultural loss due to back water, heavy Rain and other Natural Hazard during 2011-2015*

Sr. No.	Hazard Type	Total area (ha)	Affected area (ha)	No. of farmers
1.	Back water	753.29(23%)	497.79(66.08%)	778
2.	Heavy rain	571.16 (19%)	296.27(51.87%)	347
3.	Natural Hazard	1823.09(58%)	887.24(48.66%)	1382
	Total	**3147.54**	**1681.3**	**2507**

Collected by the Researcher from Tehsil and agricultural office, Raver.

This table is clearly showing total affected area due to different natural hazards claimed by villagers, actual area sanctioned by state government and number of farmers affected by natural hazards. This table clears that out of total geographical area of the Raver tehsil about 1.84 % area is claimed as affected area.

Considering the above categories researcher has collected the data from the government offices. Analysis of such data reveals that during the period 2011 to 2015 area affected by hail storms, high wind velocity and cyclone are ranking hazards.

Raver is pioneer for the banana cultivation (Misrilal & Shri Kailas, 2012). Cotton is second ranking crop in the study region, affected by natural hazards. Farmers of the study region have cultivated 9 crops; out of them 7 crops have occupied significant proportion of culturable land. Yellow gram, wheat, Jawar, Corn vegetable, Soyabin and other minor crops are cultivated.

3.2. Village wise Agricultural Loss Due to Natural Hazard (Heavy rain, Cyclone, back water etc.)

During the study period in Raver tehsil about 36 villages (31.03%) are affected by the natural hazard like rain, cyclone, wind, various diseases on crops and other disaster types. Loss of agricultural crops are affected in area of 922.85 hector with loss of Rs.21.76 crores and 1426 families were affected. Due to the natural hazard highest affected village is Nimbol. The estimated loss of agricultural crops is about Rs.6.32 crore followed by Ainpur village Rs. 5.65 crore crops are loss.

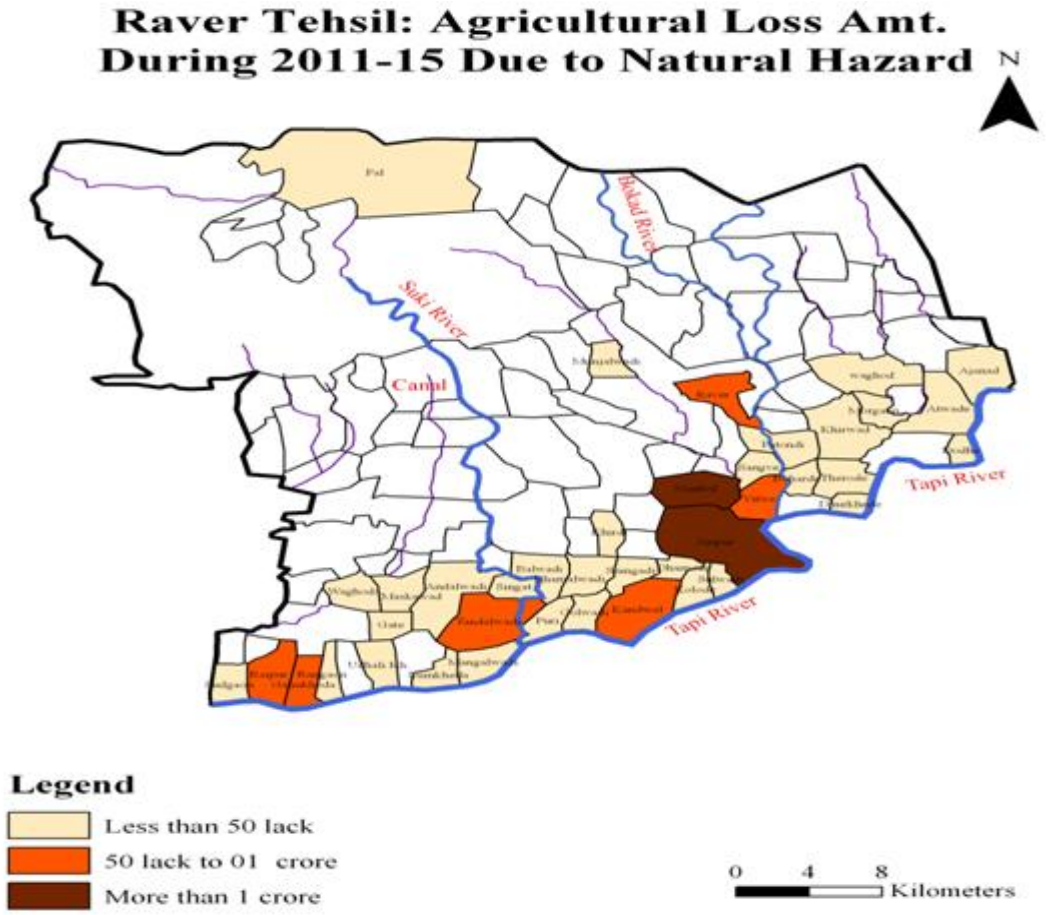

Computed by the Researcher.

Figure 1: *Raver Tehsil: Agricultural loss amount during 2011-15 due to natural hazard*

This map is showing location of affected villages and their loss in term of rupees (Figure 1). This map is clearly showing that more or less all villages those are located along Tapi River are affected by Hail storms, High velocity winds & Cyclones. This is the area of intensive Banana cultivation. Therefore huge loss of cash crop is discernible. This map clearly showing categories of cash crops in rupees ranging between 50 lakh and more than 1 crore rupees. Highest loss of banana crop with more than 1 crore rupees is found in two villages namely Ainpur and Nimbol. Ainpur and Nimbol are the big villages located near the bank of Tapi River. There are six villages having loss between 1 crore to fifty lacks namely Raipur, Gahukheda, Rangaon, Tandalwadi, Vitve Kandwel & Raver. Out of them four villages are located near the bank of Tapi. Villages having loss of 50 lack rupees are found in the southern belt of Rver tehsil. It is clear that southern part of Raver tehsil is victimized either by hail storms or strong wind destroying rich banana crop. Farmers should overcome these natural problems by changing crop rotation.

3.3. Village wise Agricultural Loss due to Back Water of Hatnur Dam

In the study region about 12 villages are affected by the floods of Hatnur Dam back water during 2011-15. It is observed that about 590 farmers are affected having estimated loss of Rs.9.27 crore of banana production.

Ainpur is mostly affected village by the back water of Hatnur Dam. During 2013-15 loss of crops of about Rs.4.25 crore rupees is found due to backwater (45% loss) Flood affected farmers have been identified by government of Maharashtra. According to state government about 149 farmers are affected in Ainpur village. Vitve village is also mostly affected village in Raver tehsil of Hatnur dam back water. In this village about 61.8 hector of land is affected, estimated loss of Rs.1.51 crore rupees during 2013.

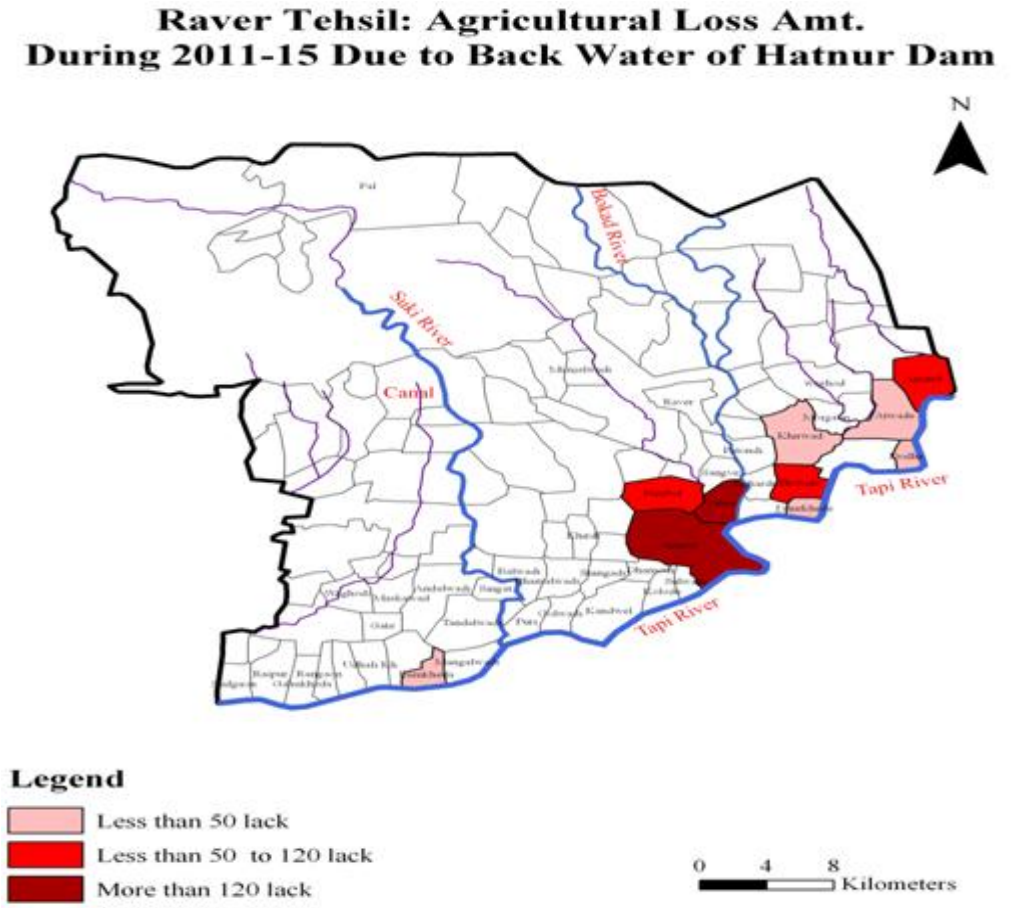

Computed by the Researcher.

Figure 2: *Raver Tehsil: Agricultural loss amount during 2011-15 due to back water of Hatnur Dam*

Nimbol village is ranked 3rd ranking village, its loss of agriculture during the survey of 2011-2015 is about Rs. 1.18 crore. Back water is affected to Nimbol village during 2013. In this village number of affected farmers are 96.

Therole and Ajnad village is highly affected village and loss of estimated agricultural production is Rs.98 lakh and 55 lakh respectively. The role village 50 hector area is affected and 115 farmers are affected in 2015.

It is concluded that Ainpur is frequently affected village by the back water of Hatnur Dam. The geographical and physical location of the Ainpur is responsible to this loss.

It is also concluded that Ainpur, Vitve and Nimbol village is affected due to the back water of Hatnur Dam having about 7 crores rupees agricultural crops loss. Figure 2 is displaying location of affected villages due to back water of Hatnur dam.

Hatnur dam is constructed on Tapi River (Chavan and Nile, 2012). It is in south west corner of the tehsil in village Mangalwadi. Near the bank of Tapi 15 villages are located towards the upper coarse of river tapi these villages affected by back water of Hatnur dam. Large area of these villages is occupied by influence of Hatnur Dam. When excess rainfall is burst near the source of river Tapi in Madhya Pradesh, areas of back water is increase and enter in the Banana fields.

Figure 2 is showing villages affected by increasing level of back water of Hatnur dam. There are 10 villages those are extensively affected by increasing back water of hatnur dam. Out of them Ainpur & Vitve displaying intensive loss of agricultural land and banana fields in these two villages there is a loss of more than 120 lack rupees.

Nimbol, Therole and Ajanad displaying loss of agricultural production about 50 to 120 lack rupees while five villages have loss less than 50 lack rupees. Map 2 is displaying location of affected villages due to back water of hatnur dam.

3.4. Village wise Agricultural Loss due to Flood/Heavy Rain

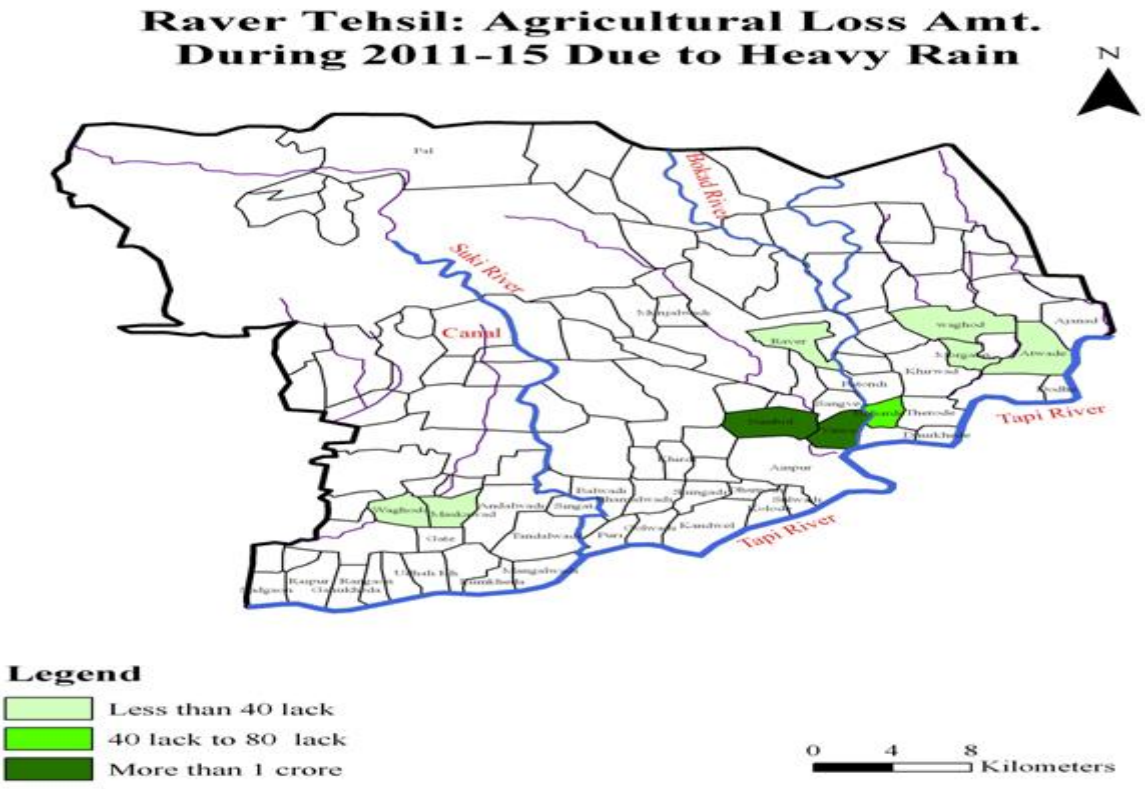

Computed by the Researcher.

Figure 3: *Raver Tehsil: Agricultural loss amount during 2011-15 due to back water of heavy rain*

Excess rainfall in short period is also harmful to the regional economy in the study region about northern 40% area is occupied by Satpuda upland rivers originated from this region are flowing across the study region and fed to river Tapi. Upper coarse of the rivers is elevated when these rivers reach on the piedmont plain, flowing velocity is more. Excess rainfall in a short duration accelerates the rate of flowing water and hence spread in outer area of the river creates flood hazards.

During the 2011-15 there are 10 villages identified by the govt. These are affected by flood hazards.

During study period agricultural loss is estimated as Rs.3,41,63,755 due to floods. State government has surveyed 10 villages those have 718.06 ha of land affected by floods of river Suki, Mor, Bokad & Tapi.

This table is showing area affected by floods, relief sanctioned by State government and number of farmers. This table clears that largest area affected by flood is found in Vitve, Nimbol, Beharde & Sangve villages. Considering agricultural loss of 491 farmers, govt. has sanctioned Rs.3,41,63,755. Location of villages affected by flood hazards clears the fact that influence zone of back water of Hatnur Dam is found up to 10 to 12 km. distance from river Tapi. To control the agricultural loss of the villages' govt. should take the action to control the back water (Figure 3). Considering the above scenario of flood affected villages highest flood affected village is Nimbol. Heavy rain in 2012 & 2014 about Rs. 1.5 crore agricultural expected crops are loss on 148 hector land. Total area of cultivated land is 252 hector of 239 farmers of Nimbol village. Vitve village is flood affected village during the study period this village is affected in 2011, 2012 & 2014. Last three year 87 farmers are affected in 240.35 hector cultivated land. Actually affected area is 164.2 hector i.e. 68% cultivated area is affected. In 2015 Beharde village is also idenfied as flood affected village. This year 65 farmers are beneficier of crops due to flood by GOM. In Beharde 59.15 hector land is cultivated out of them 30.51 hector (about 50%) land is flood affected about 73.66% lacs expected agricultural production is loss in this village.

4. Conclusion

From this study, we have concluded that:

- It is observed that the loss of agricultural crops is due to the back water of Hatnur dam. Moreover the relief, slope & soil in the study area are responsible to the flood severity.
- The outcome of the work suggest that Govt. should frame work the sustainable plan for channelizing the random flow of backwater, so it will be useful for the irrigation practices in neighborhood villages or tehsils.
- Need to organize the awareness programme in the villages to dig out the soil from the Dam and also the importance of soil benefits to the farmers.
- Government should construct channel along the foot of Satpuda, east west direction for the control of water flowing from the mountainous region.
- Govt. should constitute the committee for this purpose with the members from geographers, geologist, civil engineers or architect, social worker, environment experts etc. to look after the environmental and climatic situation of the study region.
- Specifically government should prepare the plan for natural disaster affected villages because these villages are affected every year.
- It is urging to agricultural officers to suggest crops those can subsist in flood areas.

References

Chavan, M.B. and Nile, K.S. 2012. Comparative study of quantitative and cartographic techniques of banana crop concentration in Raver Tehsil of Jalgaon District (M.S., India). *Journal of Geography and Geology,* 4(2), pp. 108-114.

Gupta, G., Patil, S.N., Padmane, S.T., Erram, V.C. and Mahajan, S.H. 2015. Geoelectric investigation to delineate groundwater potential and recharge zones in Suki river basin, North Maharashtra. *Journal of Earth System Science,* 124(7), pp.1487-1501.

Ismail, M.D. and Mustaquim, M.D. 2013. Socio-economic status of population in flood prone areas of Chanchal sub-division in Malda district, West Bengal. *International Journal of Research in Applied, Natural and Social Sciences,* 1(3), pp.141-152.

Sharma, D.D. 2012. Floods and flash floods in Himachal Pradesh: a geographical analysis. Available from: http://nidm.gov.in/ idmc/ Proceedings/Flood/B2-%206.pdf.

Cloud Publications
International Journal of Advanced Remote Sensing and GIS
2017, Volume 6, Issue 1, pp. 2449-2457
ISSN 2320 – 0243, Crossref: 10.23953/cloud.ijarsg.323

Research Article

Groundwater Prospect Evaluation in the Interfluves of the Rivers Brahmaputra and Kolong, Assam Using Remote Sensing and GIS Techniques

Satyajit Kataki[1], Santanu Sarma[1], Uttam Goswami[2]

[1]Department of Geology, Cotton University, Guwahati, Assam, India
[2]Department of Applied Geology, Dibrugarh University, Dibrugarh, Assam, India

Publication Date: 11 November 2017

DOI: https://doi.org/10.23953/cloud.ijarsg.323

Abstract Groundwater prospect evaluation in the interfluves of the Rivers Brahmaputra and Kolong, Assam has been studied by considering the geomorphology, lithology, drainage pattern and drainage density, slope and land use/land cover (LU/LC) of the area. The major geomorphic, lithologic and land use/land cover units of the area have been identified and delineated from satellite imageries. Slope map and drainage map of the study area were generated from the SOI toposheets as well as from the satellite imageries. The drainage density map was generated from drainage network of the interfluves using GIS. To demarcate the different groundwater-prospect zones of the study area, all the thematic layers are integrated by raster index overlay technique in GIS. Weights are assigned to different thematic layers and ranks are assigned to different categories/classes of the thematic layers for the overlay analysis in GIS. The resultant map was classified into groundwater prospect zones as very good, good, moderate and poor. The groundwater prospect zone map indicates that the most part of the area is having well to very good groundwater prospect zones.
Keywords *Drainage density; Hydrogeomorphology; Index overlay; Prospect zone*

1. Introduction

Groundwater is an essential component of the environment and economy. It sustains the flow in our rivers and plays an important role in maintaining the fragile ecosystems (Sedhuraman et al., 2014). Occurrence and movement of groundwater in an area is governed by several factors such as geomorphology, lithology, drainage pattern and drainage density, slope, land use/land cover (LU/LC) and the interrelationship among these factors. Geomorphic settings of an area plays an increasingly important role in hydrogeological studies as it can provide valuable supplementary information regarding groundwater recharge and their occurrence and distribution, thus initiating a recent trend in hydrogeomorphological studies (Goswami et al., 2002). The advent of remote sensing has opened up new vistas in groundwater prospect evaluation, exploration and management (Mondal, 2008). Remotely sensed data and GIS techniques are vital tools for delineation and evaluation of groundwater potential zones of an area (Krishnamurthy and Srinivas, 1995; Khan and Moharan, 2002; Sankar, 2002). Different geomorphic units that characterize the landform of the drainage basin contribute significantly to the recharge capability and groundwater prospect of specific areas of drainage basins. Groundwater prospect zone maps form a good database and help the hydrogeologists as well as the concerned departments in identifying potential around the problem

areas. These groundwater prospect zone maps may serve as helpful tools to the field geologists to quickly identify the prospective groundwater zones for conducting site specific investigations as well as to select the sites for planning recharge structures to improve sustainability of drinking water sources, wherever required. As a result, groundwater development and management in the study area becomes more efficient and easier.

In this study an attempt has been made to demarcate the groundwater prospect zones in the study area by considering the important geomorphic as well as hydrogeologic features of the area.

1.1. Study Area

The study area represents a part of Nagaon and Morigaon districts of Assam falling between longitudes 91º57'6"E and 93º4'46"E and latitudes 26º9'21"N and 26º37'17"N. It lies in the Survey of India Toposheets No. 78N/15, 78N/16, 83B/3, 83B/4, 83B/6, 83B/7, 83B/8, 83B/10, 83B/11, 83B/12, 83B/14, 83B/15, 83F/2 on scale 1:50,000 covering an area of around 2,100 sq. km. The study area, bounded by the Rivers Brahmaputra and Kolong, is situated on the southern bank of the River Brahmaputra and is endowed with fertile land and abundant rainfall during monsoon. Precipitation is the main source of groundwater recharge in the area. Physiographically the area represents almost a flat terrain but to some extent it is undulatory at western, south-western and eastern part of the area. The area is drained by a number of tributaries of the river Brahmaputra flowing from east to west. River Kolong, which is an anabranch of the River Brahmaputra, is the main distributary channel of Brahmaputra. Total length of the Kolong River is approximately 250 km. Other major rivers in the area are the Sonai, Kopili, Diju, Misa, Haria and Jamuna.

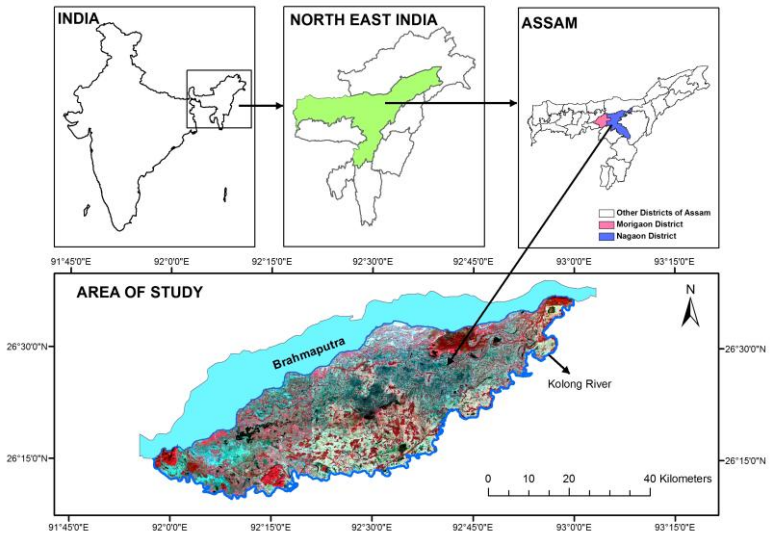

Figure 1: *Location map of the study area*

2. Database and Methodology

Since satellite data provides an opportunity for better observation and more systematic analysis of various resource parameters and other related features due to the synoptic and multi-spectral coverage of a terrain, IRS-IC, LISS III (December, 2005) and PAN image (13th March, 2007) data have been used to map the spatial distribution of various resource parameters which are relevant for finding groundwater prospect zones in the interfluves.

The methodology is divided into two parts. The first part deals with the delineation of hydrogeomorphic units considering parameters influencing the hydrogeological properties. It consists of generation of individual thematic layers (Figure 2) and integration of various thematic layers in GIS by raster index overlay technique to generate the groundwater prospect zones map. The second part deals with the evaluation of hydrogeomorphic and geologic units based on hydrogeological characteristics of the controlling parameters.

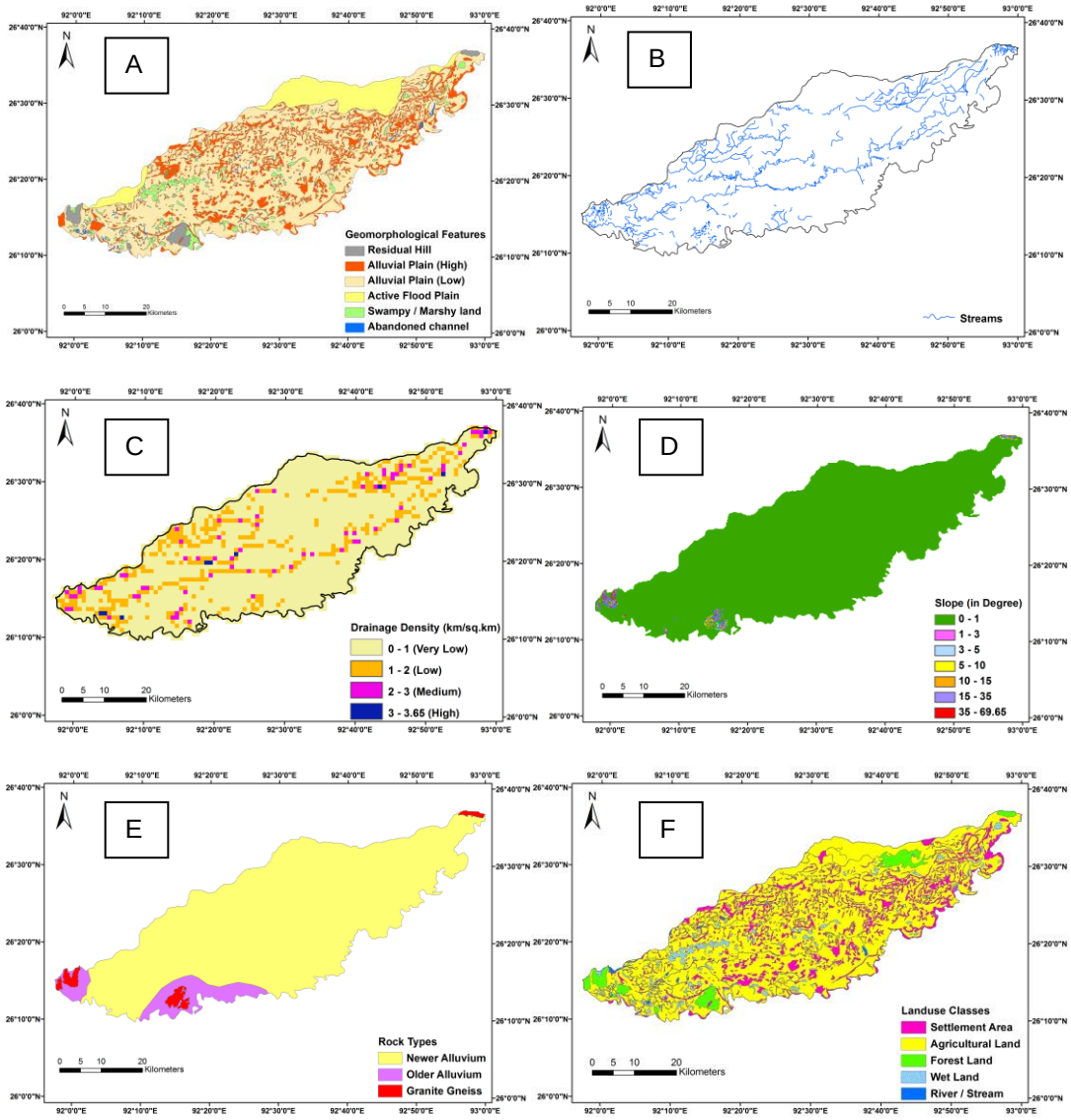

Figure 2: *(A) Geomorphological Map; (B) Drainage Map; (C) Drainage Density Map; (D) Slope Map; (E) Lithology Map; (F) Land use/Land cover Map*

The digitized vector maps pertaining to chosen parameters, viz. geomorphology, lithology, slope, drainage density and land use/land cover were converted to raster data of 10 x 10 m grid cell size. A simple mathematical model called Weighted Index overlay analysis is used for a combined analysis of multiparameter in raster format to generate the groundwater prospect map. Each raster map of these parameters was assigned respective theme weight and their class ranks.

Each thematic map was assigned a weight depending on its influence on the movement and storage of groundwater (Kumar et al. 2007; Avatar et al. 2010; Preeja et al. 2011; Narendra et al. 2013). Relative ranking of each thematic unit in a theme were assigned as knowledge based hierarchy using Spatial Analyst tool of ArcGIS. The Weights and Ranks were assigned to thematic maps and thematic units on a 10 point scale based on their influence on the groundwater recharge process (Table 1).

Table 1: *Assigned rank and weight for different features of various thematic layers*

Theme Unit	Feature/category	Rank	Weight
Geomorphology	Residual Hill	1	10
	Alluvial Plain (High)	3	
	Alluvial Plain (Low)	4	
	Active Flood Plain	4	
	Swampy/Marshy Land	1	
	Abandoned Channel	4	
Lithology	Younger Alluvium	3	8
	Older Alluvium	2	
	Granite	1	
Drainage Density	Very Low	5	7
	Low	4	
	Moderate	3	
	High	2	
	Very High	1	
Slope	Nearly Level (0 – 1)	7	10
	Very Gentle (1 – 3)	6	
	Gentle (3 – 5)	5	
	Moderate (5 – 10)	4	
	Strong (10 – 15)	3	
	Steep (15 – 35)	2	
	Very Steep (>35)	1	
Land use/ Land Cover	Settlement area	1	5
	Agricultural Land area	3	
	Forest Land	2	
	Wet Lands	3	
	Streams/ Rivers	3	

These five thematic raster layers were integrated by Raster Index Overlay technique in GIS to create a groundwater prospect zone map for drinking purpose. In the index overlay technique, the values were calculated using the following formula:

$$S = \sum Sij\ Wi / \sum Wi \ldots (1)$$

Where, S = Weighted score of a pixel
Wi = Weight for the ith output map
Sij = Rank of the jth class of the ith map

Values of j depend on the class occurring at the current location.

In the groundwater prospect zone map (Figure 4), four zones viz. poor, moderate, good and very good, within the study area were delineated.

3. Results and Discussion

The various terrain parameters considered in the present study, i.e., geomorphology, lithology, slope, drainage density, land use/land cover etc. are believed to be the controlling factor of the precipitation, flow and storage of water in the area and, hence, influence the groundwater storage potential of the area. A drainage map of the area gives an idea about the permeability of rocks and also gives an indication of the yield of the basin (Wisler and Brater, 1959). Therefore, a drainage map of the study area was generated from the digitized base map as well as satellite imagery (Figure 2b). In the study area it has been observed that no systematic drainage pattern has been developed on sand surface. Most of rivers/streams present in the area are meandering in nature that develops in flood plains due to sluggish river flow. A network of streams up to the 4^{th} order has been identified; the 2^{nd} to 3^{rd} order being the dominant. The hydrogeological significance of these influencing parameters is discussed on the basis of their response to the groundwater occurrence and contribution to the recharge phenomena.

3.1. Geomorphology vs. Groundwater Prospects

The study area, comprised of the interfluves between the Rivers Brahmaputra and Kolong, can broadly be represented by a number of distinct geomorphic units' viz., residual hills, alluvial plains, active flood plains, swamps/marshy lands and abandoned channels etc (Figure 2a). Each of these units, being characterised by distinctive hydrogeologic features, also forms distinct hydrogeological unit.

Residual Hills: The residual hills of the area are highly fractured and jointed and their elevations vary from 100 to 435m above the plains. This unit is of minor hydrogeologic significance due to its unfavourable topography, lithology and structure. However, owing to the favourable factors like high amount of rainfall, low overall permeability of the formation and rugged topography, this unit represents a high runoff zone that contributes significantly to groundwater recharge in the plains.

Alluvial plains: Alluvial plain deposits occupy a major part of the study area with a huge thickness of unconsolidated alluvial sediment deposited mainly by the Brahmaputra and its tributaries and sub tributaries flowing through the area. Lithologically this zone consists mainly of gravel, sands, silts and clays mixed in varying proportions. Fluvial geomorphic features like palaeochannels, old meanders, channel-fill deposits etc. are common and as such, this unit form recharge as well as discharge areas with water table resting within 1 m to 5 m from ground surface. Because of their high porosity and permeability attributed by favourable lithologic composition, groundwater prospect in the alluvial plains is considered as very good.

Active Flood Plains: As this unit consists of unconsolidated materials, the groundwater potential in this area is considered to be very good. Natural levees are formed in these areas during flood recession which are good sites for shallow depth groundwater within around 30m from ground surface. Swampy/Marshy land: Because of low lying submerged conditions, groundwater prospect in this zone is considered as poor.

Abandoned channel: These are old abandoned courses of streams which were subsequently filled up with alluvial sediments and thus could act as highly productive shallow aquifer zones. Due to the high permeability of the deposited material such as gravel and coarse to medium sand, this geomorphologic unit is considered as very good prospect zone for groundwater.

3.2. Drainage Density vs. Groundwater Prospects

Drainage density is considered as one of the important parameters in the evaluation of groundwater potential, as it has direct impact on recharge volume. According to Strahler (1957) drainage density is an expression of the closeness of spacing of channels, thus providing quantitative measure of length of stream within a square grid of the area in terms of km/km^2. Areas having high drainage density are not suitable for groundwater development because of the greater surface run off. Thus, in the preparation of groundwater prospect zone map using GIS, the highest ranking was assigned for very low drainage density as it indicates good groundwater prospect zone and the lowest ranking was assigned for high drainage density as it implies low groundwater potential (Table 1).

To visualize the areas of sheet flow/channel flow four zones of different drainage density, viz. very low (0-1 km), low (1-2 km), moderate (2-3 km) and high (3-3.63 km) are derived based on spatial density analysis of drainage network in the study area (Figure 2c). As per the drainage density classification in the present study area more than 80% of the area falls under very low to low drainage density category which indicates good groundwater prospects.

3.3. Slope vs. Groundwater Prospects

Slope is one of the factors controlling infiltration of water, hence an indicator for groundwater prospect. Slope plays a key role in groundwater occurrence as infiltration is inversely related to slope. A break in the slope i.e., steep slope followed by gentler slope generally promotes an appreciable groundwater infiltration (Saraf and Choudhury, 1998). Topography relates to the local and regional relief and gives an idea about the general direction of groundwater flow and its influence on groundwater recharge (Gupta and Srivastava, 2010).

A slope map of the area generated from the digitized base map of the study area is shown in Figure 2d. The slope angle (in degree) in the area varies from 0° to >35°. On the basis of the slope, the study area has been divided into seven slope classes. The areas having 0° to 1° slope fall into the 'very good' category because of the nearly flat level terrain and having relatively high infiltration rate. Most of the study area falls under this category. The areas with 1° to 3° slope and 3° to 5°slope categories are considered as 'good' for groundwater storage due to slightly undulating topography with some runoff. The areas having a slope of 5° to 10° may cause relatively high runoff and low infiltration, and hence are categorized as 'moderate.' Slopes above 10° categories are considered as 'poor' due to higher slope and runoff.

In the preparation of groundwater prospect map low ranking is given to steep dip whereas high ranking is attributed to gentle slope as slope plays a significant role in infiltration verses runoff. From the slope map of the study area (Figure 2d) it has been observed that northeastern, western and southwestern parts of the area have high slope gradient of more than 15 degrees indicating poor groundwater prospects as water runs rapidly off the surface. On the contrary the rest of the area which forms the ¾th of the study area has good groundwater prospects due to nearly level to gentle slope of less than 5 degrees.

3.4. Lithology vs. Groundwater Prospects

Lithologically the area is occupied by consolidated formations belonging to Precambrian group of rocks, consisting of granites overlain by unconsolidated alluvial sediments of Quaternary age (Figure 2e). The Quaternary deposits, formed by the deposition of alluvial sediments viz., sands, silts, clays,

gravels and boulders comprising around 90 percent of the deposit, are highly favorable zone for groundwater. The other important lithological formation exposed in the area, mainly granite, has relatively no groundwater potential because of their massive nature and insignificant primary porosity.

3.5. Land Use/Land Cover vs. Groundwater Prospects

The land use/land cover (LU/LC) of an area plays a significant role in the development of groundwater resource. Infiltration and runoff are controlled by nature of surface material and the land use pattern. The rate of infiltration is directly proportional to the crown density of forest cover, i.e. if the surface is covered by dense forest, the infiltration will be more and the runoff will be less. With urbanization, the rate of infiltration decreases. From the point of view of land use, agricultural land with vegetation is an excellent site for groundwater exploration (Todd and Mays, 2005). The area with water bodies is good for groundwater recharge.

The major land use/land cover categories that were identified in the study area are Settlement area, Agricultural land, Forest land, River/Stream and Wet land (Figure 2f). The area under settlement category is 345.92 sq. km (16.47%), under agricultural land category is 1584.92 sq. km (75.47%) and Forest covers is 66.04 sq. km (3.14%) of the total geographical study area. There are several beels and wetlands in the area and the total area under this category is around 77.01 sq. km. The area under the river and stream category comprises only 26.11 sq. km. Thus the study area, covered by agricultural land, forest, wet land and water bodies has favourable groundwater potential. The weights and ranks are given to each category based on their groundwater prospects (Table 1).

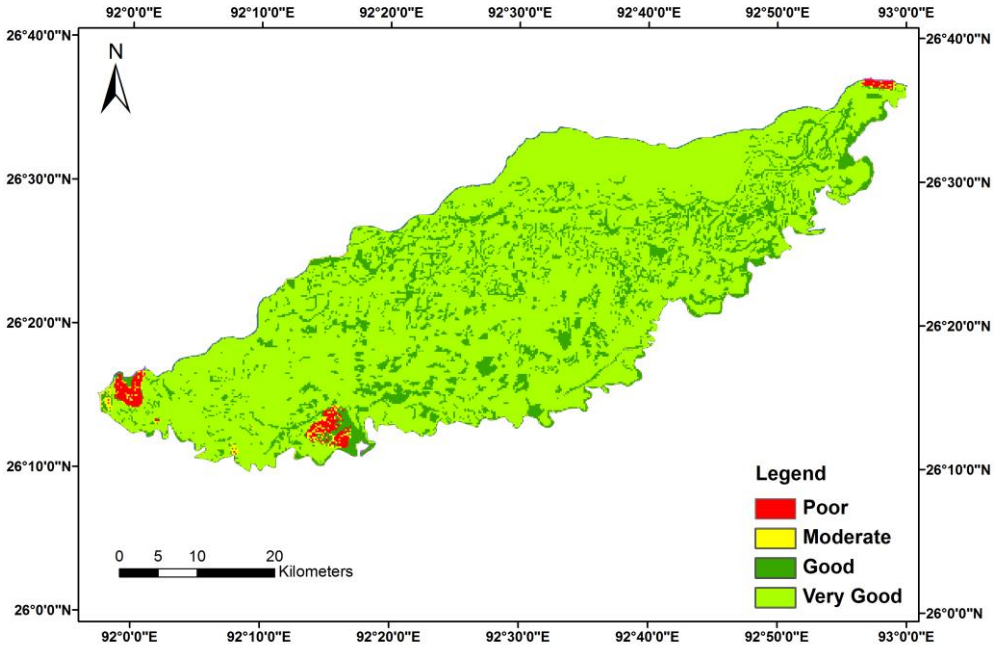

Figure 3: *Groundwater prospect zones of the study area*

3.6. Classification of Groundwater Prospect Zones

To demarcate the different groundwater-prospect zones of the study area, all the thematic layers such as geomorphology, lithology, drainage density, slope and land use/land cover are integrated applying the Eq.1 by raster overlay analysis technique through Spatial Analyst in ArcGIS. To get the groundwater prospect zones the values are classified into four classes by using the Equal Interval method of classification. Accordingly, the resultant groundwater prospect zone map of the study area was classified into very good, good, moderate and poor groundwater prospect zones (Figure 3).

It has been found that out of the total study area, 80.75% of the area belongs to very good groundwater prospect zones whereas 17.65% of the area belongs to good category, 0.48% of the area categorized as moderate and only 1.12% of the area belongs to poor category. Thus the groundwater prospect zone map indicates that the most part of the area is having well to very good groundwater prospect zones.

4. Conclusion

The study area is interfluves between the Rivers Brahmaputra and Kolong. Precipitation is the main source of groundwater recharge in the area. Different hydrogeomorphic and geologic units have been delineated based on hydrogeological characteristics of controlling parameters. About 84% of the study area is covered by agricultural land, forest, wet land and water bodies which indicate very good groundwater potential in the study area. Lithologically the area is highly favorable for groundwater development. 3/4th of the total study area has good groundwater prospects due to nearly level to gentle slope of less than 5 degrees. Most part of the study area belongs to very low to low drainage density category indicating more infiltration and recharge to the aquifer. For demarcation of different groundwater prospect zones, the capabilities of using Remote Sensing and Geographical Information System have been used. Thus the groundwater prospects zonation of the study area based on geoinformatics approach clearly indicates that with the favorable combination of alluvial plains, flood plains, low drainage density, nearly flat terrain, good forest cover, favorable lithology and the land use/land cover pattern, the study area is having a very good groundwater potential. The resultant groundwater prospect zones map of the study area could be useful for sustainable development and management of groundwater resource in the area.

References

Avtar, R., Singh, C.K., Shashtri, S., Singh, A. and Mukharjee, S. 2010. Identification and analysis of groundwater potential zones in Ken-Betwa river linking area using remote sensing and geographic information system. *Geocarto Int.*, 25, pp.379-396.

Goswami, U., Patgiri, A.D. and Sarma, J.N. 2002. Hydrogeologic and geomorphic settings of the lower Subansiri Basin, Assam, India. *Journal of Nepal Geological Society*, 27, pp.53-63.

Gupta, M. and Srivastava, P.K. 2010. Integrating GIS and remote sensing for identification of groundwater potential zones in the hilly terrain of Pavagarh, Gujrat, India. *Water Int.*, 35, pp.233-245.

Khan, M.A. and Moharana, P.C. 2002. Use of remote sensing and geographical system in the delineation and characterization of groundwater prospect zones. *J. Indian Soc. Remote Sensing*, 31(3), pp.131-141.

Krishnamurthy, J. and Srinivas, G. 1995. Role of Geological and geomorphological features in groundwater exploration: a study using IRS LISS data. *Int. J. Remote Sensing*, 16(14), pp.2595-2618.

Kumar, S., Rai, D., Rai, P. K., Shukla, A. B., & Saxena, A. 2007. To study the causes of fluoridated water problem in Unnao district and its feasible measure to solve the problem. In: Tiwari, V.K. and Pande, R.N. (Eds.), *Uttar Pradesh sodic land reclamation research, achievements*, pp.90-93.

Mondal, S. Md., Pandey, A.C. and Garg, R.D. 2008. Groundwater prospects evaluation based on hydrogeomorphological mapping using high resolution satellite images: a case study in Uttarakhand. *J. Indian Soc. Remote Sens.*, 36, pp.69-76.

Narendra, K., Rao, K.N. and Swarna Latha, P. 2013. Integrating remote sensing and GIS for identification of groundwater prospective zones in the Narava Basin, Visakhapatnam region, Andhra Pradesh. *Journal Geological Society of India*, 81, pp.248-260.

Preeja, K.R., Joseph, S., Thomas, J. and Vijith, H. 2011. Identification of groundwater potential zones of a tropical river basin (Kerala, India) using remote sensing and GIS techniques. *J. Indian Soc. Remote Sensing*, 39, pp.83-94.

Sankar, K. 2002. Evaluation of groundwater potential zones using remote sensing data in Upper Vaigai River Basin, Tamil Nadu, India. *J. Indian Soc. Rem. Sens.*, 30(3), pp.119-129.

Saraf, A.K. and Choudhury, P.R. 1998. Integrated remote sensing and GIS for groundwater exploration and identification of artificial recharge sites. *Int J Remote Sens.*, 19(10), pp.1825-1841.

Sedhuraman, M., Revathy, S.S. and Babu, S.S. 2014. Integration of geology and geomorphology for groundwater assessment using remote sensing and GIS techniques. *International Journal of Innovative Research in Science, Engineering and Technology*, 3(3), pp.10203-10211.

Strahler, A.N. 1957. Quantitative analysis of watershed geomorphology. *Am. Geophy. Union. Trans.*, 38, pp.913-920.

Todd, D.K. and Mays, L.W. 2005. *Ground water hydrology*. 3rd Ed., Hoboken: John Wiley & Sons.

Wisler, C.O. and Brater, B.F. 1959. *Hydrology*. New York: Willey.

Cloud Publications
International Journal of Advanced Remote Sensing and GIS
2017, Volume 6, Issue 1, pp. 2424-2435
ISSN 2320 – 0243, Crossref: 10.23953/cloud.ijarsg.313

Research Article

Studies on Assessment of Ground Water Pollution Vulnerability Index for CUTM Campus Paralakhemundi, Odisha through Application of "DRASTIC" Model

Madusmita Ghadai, Prafulla Kumar Panda, Narasimham M. L.

Department of Civil Engineering, Centurion University of Technology and Management, Odisha, India

Publication Date: 10 October 2017

DOI: https://doi.org/10.23953/cloud.ijarsg.313

Abstract Nowadays, the prediction of pollution risk and the protection of groundwater is very important. The sub-surface hydro-geological environment influences the pollutant to migrate from surface to sub-surface water. So groundwater contamination can be minimized by delineating and monitoring vulnerable areas. The main objective of this paper is to find out the groundwater vulnerability index in CUTM campus, Paralakhemundi, Odisha using DRASTIC model. This model has seven hydro-geological parameters Depth of Groundwater (D), net Recharge (R), Aquifer media (A) Soil media (S) Topography (T) Impact of vadose zone (I) hydraulic Conductivity (C). Estimation of DRASTIC Index has done by multiplying each parameter weight by its rating corresponding to a particular location in the study area and summing the products of all seven parameters listed above. In order to assign the ratings, field and laboratory tests have been conducted. Based on DRASTIC index values it was observed that the vulnerability class in the study area falls between high vulnerability to very high vulnerability. The results provide important information for the local authorities and decision making personals for effective management of ground water resource. GIS software has been used for analysis and mapping the groundwater vulnerability index in the study area.
Keywords *DRASTIC index, Groundwater vulnerability, GIS*

1. Introduction

The quality of groundwater is as important as that of quantity. The water quality gets deteriorated due to the high growth of population, unplanned growth of cities, mixed land use patterns, improper sewage system, and poor disposal of the wastewater both from household as well as industrial activities. In contrast to surface water pollution, sub-surface pollution is difficult to detect and of more difficult to control. Groundwater vulnerability is a function of different hydro-geologic settings of an area. In any given area, the groundwater within an aquifer, or the groundwater produced by a well, has some vulnerability to contamination from human activities. Water pollution is a serious problem in India as almost 70% of its surface water resources and a great number of its GW reserves are already contaminated by biological, organic, and inorganic pollutants (Rao and Mamatha, 2004). Even today more than 90% of our rural population is primarily dependent on GW (Chandrashekhar, Adiga, Lakshminarayana, Jagdeesha and Nataraju, 1999). The DRASTIC model was developed in US Environment protection Agency (USEPA) to evaluate groundwater pollution potential for the entire United States by (Aller et al., 1987). "DRASTIC" aquifer vulnerability mapping technique or numerical rating scheme has been developed for evaluating the potential for groundwater pollution in a given

area based on a set of hydro geological settings. This rating scheme is based on 7 factors chosen by over 35 groundwater scientists from throughout the United States by assigning relative importance weights and a point rating scale for each factor (Table 1). Lobo-Ferreira and Oliveira (2004) following "DRASTIC" model mapped the groundwater vulnerability of Portugal as a part of an investigation by a European commission's sponsored groundwater project. This was the first application in a European Union member state. The seven "DRASTIC" parameters and the final index were developed in GIS. Aller et al. (1987) developed a standardized system to evaluate groundwater pollution potential using hydro-geologic settings. Kimura (1997) worked on evaluating migration potential of contaminants through unsaturated subsurface in Texas Vulnerability Map. In this work the various vulnerability assessment methods were reviewed. Usha Madhuri and Srinivas (2004) worked on studies on assessment of Groundwater vulnerability index for the city of Visakhapatnam, Andhra Pradesh, India through application of "DRASTIC" model. GW vulnerability is a function of the geologic setting of an area, as this largely controls the amount of time, i.e. the residence time of the GW that has passed since the water fell as rain, infiltrated through the soil, reached the water table, and began flowing to its present location (Prior, Boekhoff, Howes, Libra, and VanDorpe, 2003). Rundquist et al. (1991) have produced state wide GW vulnerability assessment in Nabraska using DRASTIC/GIS model and identified the areas vulnerable to GW pollution and concluded that DRASTIC methodology can be executed successfully with minimal training and experience. Various parameters for GW quality like pH, EC, TDS, Cl, Na ,K, total hardness(TH),etc. were tested and thereafter ILWIS GIS software was used for mapping the spatial variations of these parameters and also salt affected areas were demarcated (Durbude, Naradrajan and Purandara, 2003). A GW vulnerability mapping methodology that requires less extensive site-specific data, and at the same time, is robust when data are uncertain and incomplete will be a useful screening tool (A. Rahman / Applied Geography 28 (2008)).

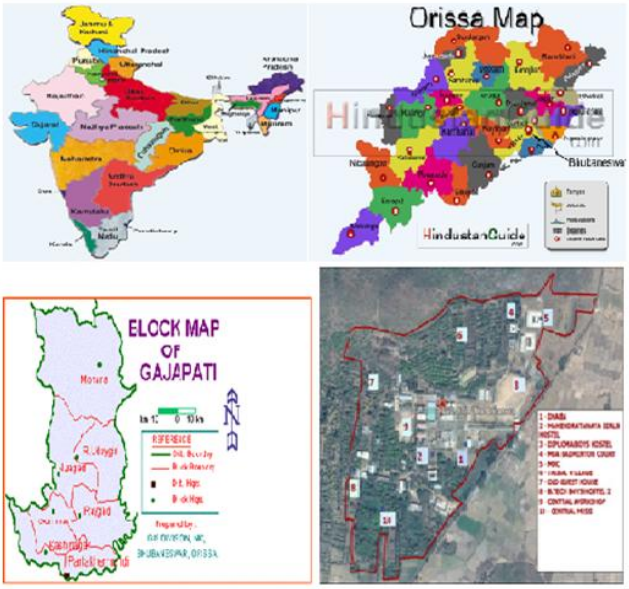

Figure 1: *Study area location*

1.1. Study Area

The study area JITM campus of Centurion University for Technology and Management (Figure 1) is located at Parakhemundi, Gajapati district, Odisha covering an area of about 70 acres of land (Latitude - 18°48'32.5", Longitude - 84°8' 11.9"). The current population of the campus is 2500. The main source of water is ground water. For the study area the principal sources of contamination are a) Kitchen

waste from the hostels and quarters, b) Waste water from toilets and bathrooms, c) Waste material from workshop and laboratories.

Fig.2 Flow diagram of "DRASTIC APPROACH"

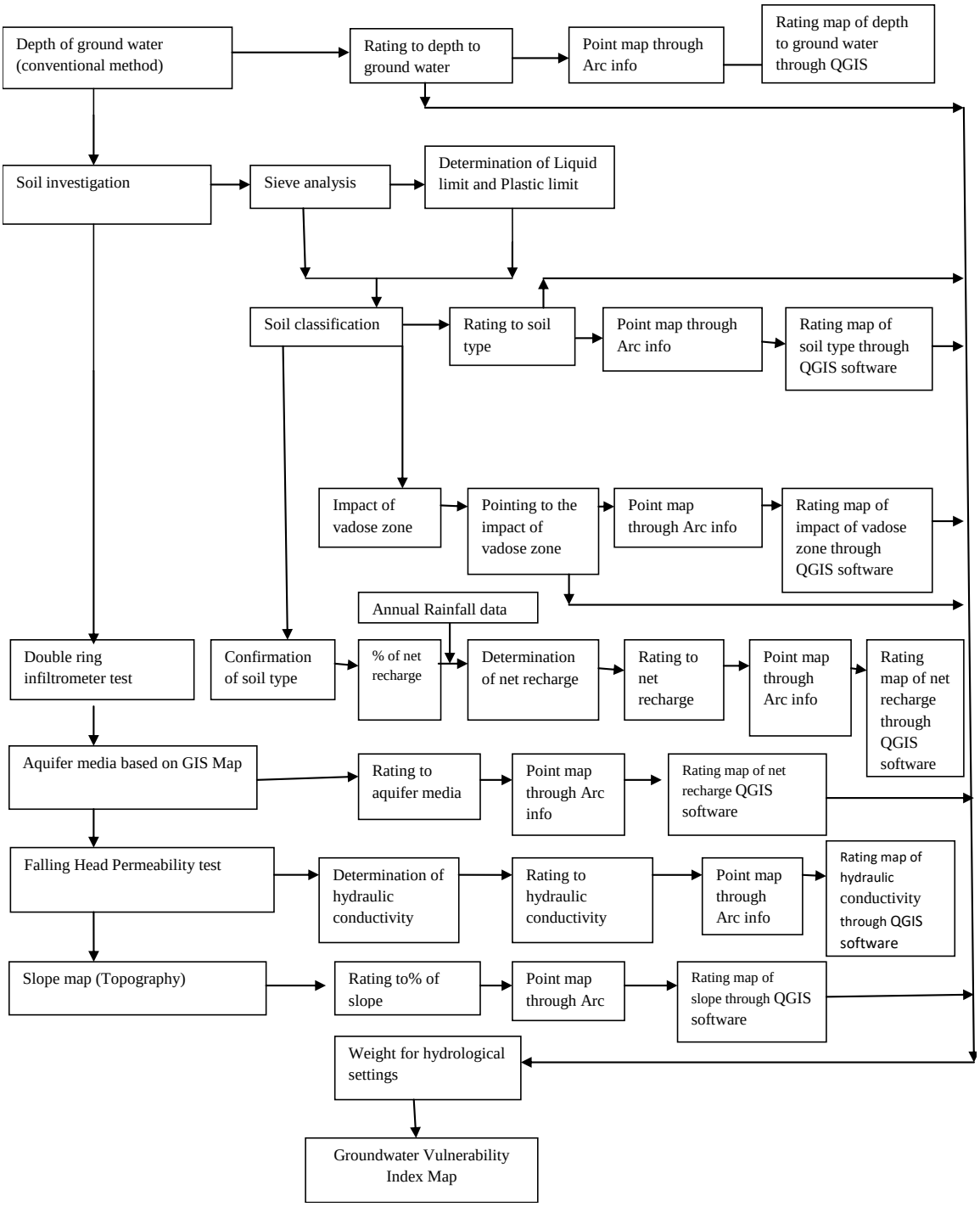

Figure 2: *Flow diagram of DRASTIC approach*

Table 1: *Weights assigned to various hydro geological parameters of "DRASTIC" model*

Factors	Importance weight
Depth to Ground water (D)	5
Net recharge (R)	4
Aquifer Media (A)	3
Soil Media (S)	2
Topography (T)	1
Impact of Vadose zone media (I)	5
Hydraulic Conductivity of the aquifer (c)	3

Source: *EPA document # 600/2-85/018-1985, Linda Aller et al., 1987*

2. Methodology

Determination of the "DRASTIC" index for a given area involves multiplying each factor weight indicated in Table 1 by its rating and summing the total. The total higher sum values represent greater potential for groundwater pollution, or greater aquifer vulnerability. For a given area each factor is rated from 1 to 10, indicating the relative pollution potential for that area. After assigned rating to each factor, each rating is multiplied by assigned weight, and the resultant numbers are summed as follows:

$D_rD_w + R_rR_w + A_rA_w + S_rS_w + T_rT_w + I_rI_w + C_rC_w$ = Groundwater Vulnerability Index (GWVI) … (1)

Where, r = rating for area being evaluated; W = importance weight for factor.

Table 2: *Groundwater vulnerability index*

S. No	Drastic Index	Degree of vulnerability
1	V<80	Low vulnerability
2	80≤V<120	Medium vulnerability
3	120≤V<160	High vulnerability
4	160≤V<185	Very High vulnerability
5	≥185	Extremely vulnerability

Source: *Added A and Hamza M. H, 1999*

The weight of each factors assigned according to its pollution potential and it varies from 1 to 5. The ratings assigned each parameter (1 to 10) depends on the magnitude of the parametric property influencing the contaminates transport. 35 groundwater scientists from throughout the United States have identified the degrees or vulnerability based on the magnitude of ground water vulnerability index as given in Table 2. Higher value of groundwater vulnerability index indicates the high pollution potential.

3. Results and Discussion

3.1. Depth to Groundwater (D)

The depth to groundwater has been measured from the open wells distributed within the study area. The depth to ground water ranges from 2 feet to 5 feet. According to this data the rating has been assigned and the rating map is shown in Figure 3.

Table 3: *Rating scale for the depth to groundwater*

Ranges (feet)	Ratings
0-5	10
5-15	9
15-30	7
30-50	5
50-75	3
75-100	2
>100	1
Weight	5

Source: *EPA document # 600/2-85/018-1985, Linda Aller et al., 1987*

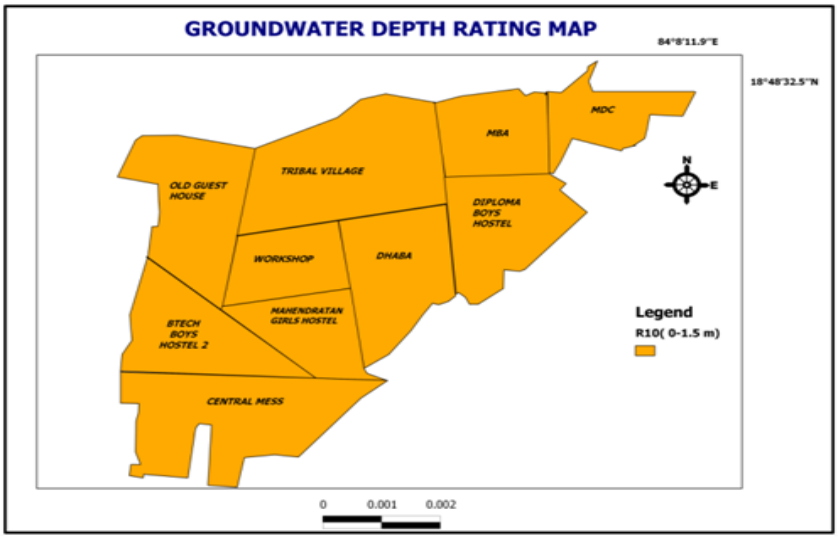

Figure 3: *GW depth rating map of CUTM campus*

Table 4: *Rating scale for the net recharge*

Annual recharge range (mm)	Ratings
0 – 50.8	1
50.8 – 101.6	3
101.6 – 177.8	6
177.8 – 254.0	8
>254.0	9
Weight	4

Source: *EPA document # 600/2-85/018-1985, Linda Aller et al., 1987*

3.2. Net Recharge (R)

The rainfall data for 10 years are considered and average rainfall is considered 1449.45mm for determining the net recharge based on soil type. The net recharge values as a % of annual rainfall for different soil type has been taken from the thesis by T. Usha Madhuri (2004) .The rainfall data is obtained from the records of, Irrigation Department, Paralakhemundi. Soil type is obtained from the various laboratory tests. The net recharge for the study area ranges 173.934mm to 246.4065mm from Figure 4 shows the net recharge rating map of CUTM Campus, Paralakhemundi.

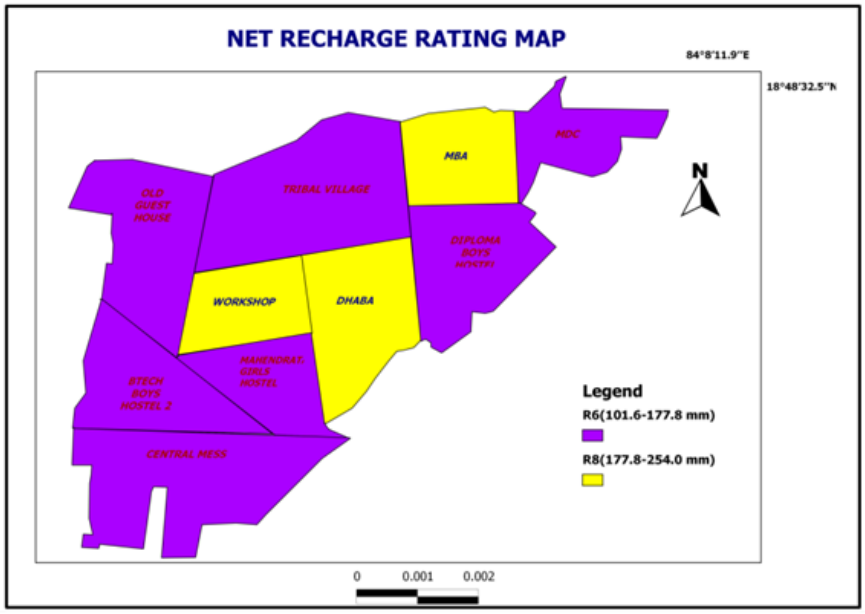

Figure 4: *Net recharge rating map of CUTM campus*

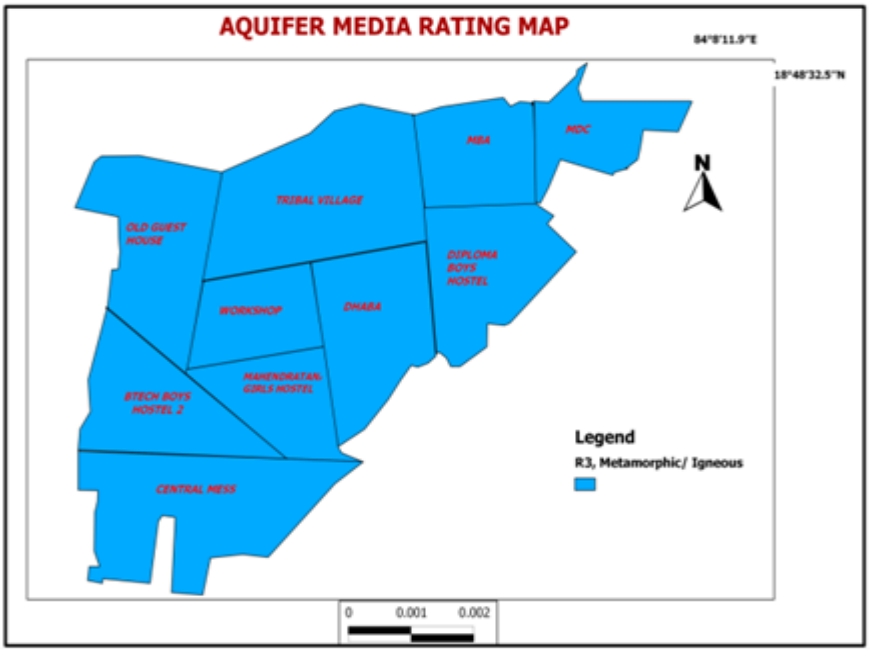

Figure 5: *Aquifer media rating map of CUTM campus*

Table 5: *Rating scale for the aquifer media*

Types of Aquifer media	Rating
Massive shale	2
Metamorphic/Igneous	3
Weathered Metamorphic Igneous	4
Thin bedded sandstone, Limestone, Shale sequences	6
Massive sandstone	6

Massive limestone	6
Sand and Gravel	8
Basalt	9
Karst Limestone	10
Weight	3

Source: *EPA document # 600/2-85/018-1985, Linda Aller et al., 1987*

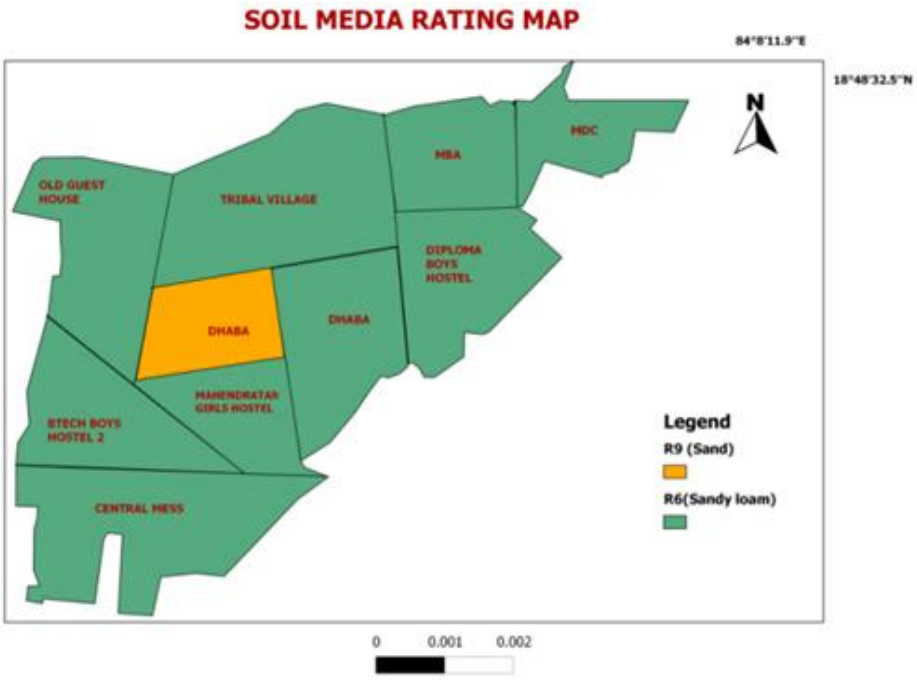

Figure 6*: Soil media rating map of CUTM campus*

3.3. Aquifer Media (A)

The aquifer for the study area is obtained from geology map from early study. The type aquifers in the study area are mainly Metamorphic/Igneous type. Based on this information the rating map with respect aquifer media is generated as a part of “DRASTIC” index calculations followings the standard rating scale specified earlier in Table 5 and the same is shown here as Figure 5.

Table 6: *Rating scale for the soil media*

Range	Rating
Thin or absent	10
Gravel	10
Sand	9
Shrinkage and or aggregate clay	7
Sandy loam	6
Loam	5
Silty loam	4
Clay loam	3
Non shrinkage and non-aggregated clay	1
Weight	2

Source: *EPA document # 600/2-85/018-1985, Linda Aller et al., 1987*

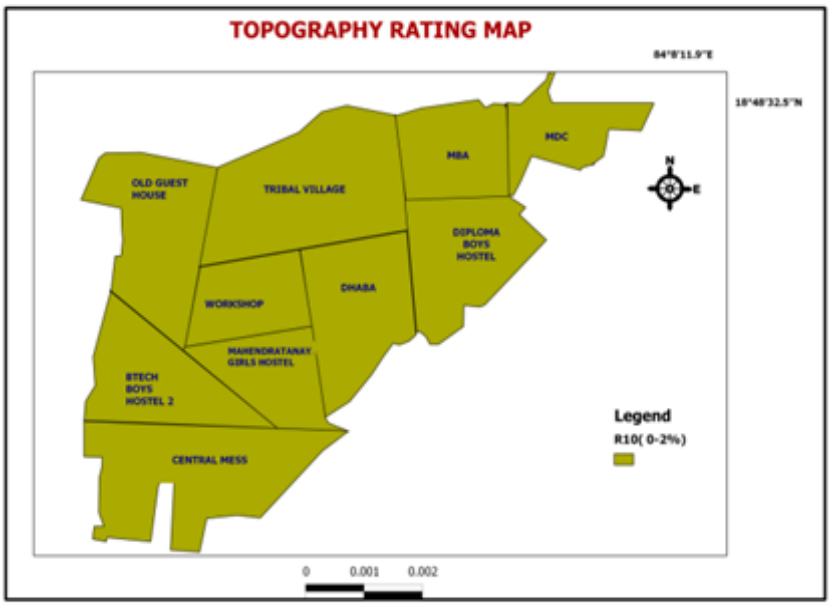

Figure 7: *Topography rating map of CUTM campus*

3.4. Soil Media (S)

Soil media in the study area defined from sieve analysis, liquid limit test and plastic limit test according to IS classification system. The study area is covered with SM, SC, and SP type of soil. Figure 6 shows the rating maps of soil media of the study area.

Table 7: *Rating scale for the topography*

Range % slope	Rating
0-2	10
6-Feb	9
12-Jun	5
18-Dec	3
>18	1
Weight	1

Source: *EPA document # 600/2-85/018-1985, Linda Aller et al., 1987*

3.5. Topography (T)

Topography refers to slope of an area. Areas with steep slopes, having large amounts of runoff and smaller amounts of infiltration are less vulnerable to GW contamination. Flat areas were assigned high rates because in flat areas the runoff rate is less, so more percolation of contaminants to the GW. The study area is nearly slope. So the rating is very high. The result and Figure 7 shows the topography rating map of CUTM Campus, Paralakhemundi.

3.6. Impact of Vadose Zone

The vadose zone's influence on aquifer pollution potential is essentially similar to that of soil cover, depending on its permeability, and on the attenuation characteristics of the media. The vadose zone is

evaluated on the basis of soil type. Impact of vadose rating map of CUTM Campus, Paralakhemundi is shown in Figure 8.

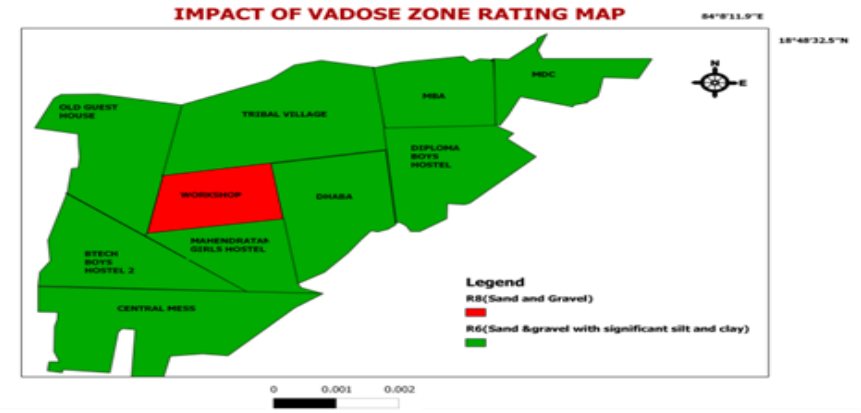

Figure 8: *Impact of vadose zone rating map of CUTM campus*

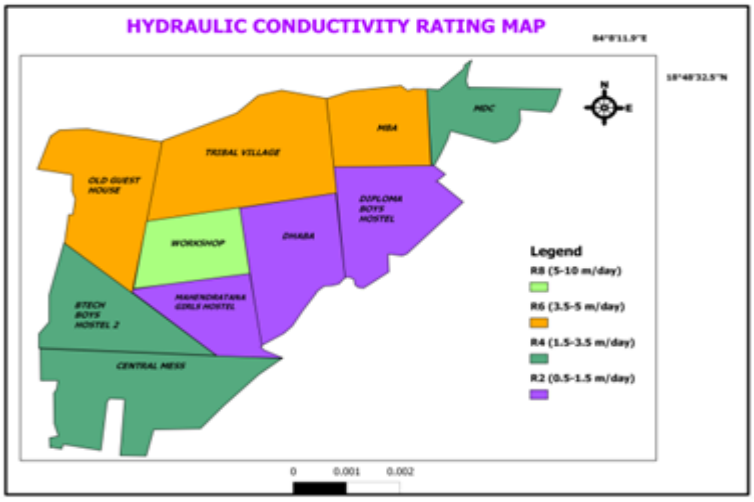

Figure 9: *Hydraulic conductivity map of CUTM campus, Paralakhemundi*

Table 8: *Rating scale for the vadose zone*

Range	Rating
Silt / Clay	1
Shale	3
Limestone	6
Sandstone	6
Bedded limestone, sand stone, shale	6
Sand and Gravel with significant silt and clay	6
Metamorphic / Igneous	4
Sand and Gravel	8
Basalt	9
Karst lime stone	10
Weight	5

Source: *EPA document # 600/2-85/018-1985, Linda Aller et al., 1987*

Table 9: *Rating scale for the hydraulic conductivity*

Hydraulic conductivity (m/day)	Rating
0.005-0.5	1
0.5-1.5	2
1.5-3.5	4
3.5-5	6
10-May	8
>10	10
Weight	3

Source: *EPA document # 600/2-85/018-1985, Linda Aller et al., 1987*

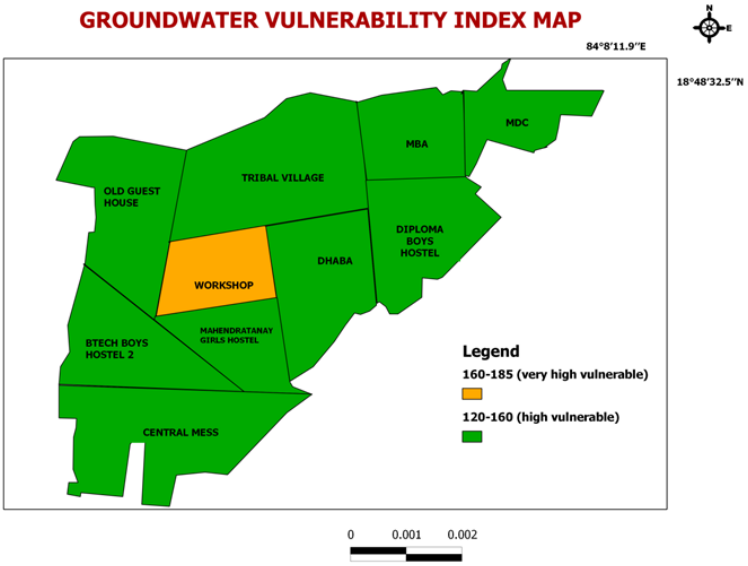

Figure 10: *GWVI map of CUTM campus, Paralakhemundi*

Table 10: *Ground water vulnerability index*

Area / Location	Depth	Net recharge (mm)	Aquifer media	Soil media	Topography (% of slope)	Impact of vadose zone	Hydraulic conductivity (m/day)	DRASTIC index
Weights	5	4	3	2	1	5	3	
Dhaba	4'4", R=10	188.4285, R=8	Metamorphic/ Igneous, R=3	SM, R=6	NL, R=10	SM, R=6	1.0499, R=2	149
Mahendra tanaya girls hostel	3', R=10	173.934, R=6	Metamorphic/ Igneous, R=3	SC, R=6	NL, R=10	SC, R=6	1.430, R=2	141
Diploma boys hostel	3'7", R=10	173.934, R=6	Metamorphic/ Igneous, R=3	SC, R=6	NL, R=10	SC, R=6	1.30, R=2	141
MDC	4', R=10	173.934, R=6	Metamorphic/ Igneous, R=3	SC, R=6	NL, R=10	SC, R=6	1.885, R=4	147
MBA badminton court	4', R=10	188.4285, R=8	Metamorphic/ Igneous, R=3	SM, R=6	NL, R=10	SM, R=6	3.866, R=6	151
Tribal village	3', R=10	173.934, R=6	Metamorphic/ Igneous, R=3	SC, R=6	NL, R=10	SC, R=6	3.973, R=6	153
Old guest house	3'4" , R=10	173.934, R=6	Metamorphic/ Igneous, R=3	SM-SC, R=6	NL, R=10	SM-SC, R=6	4.943, R=6	153
B. Tech Boys hostel 2	2'7", R=10	173.934, R=6	Metamorphic/ Igneous, R=3	SC,R=6	NL, R=10	SC, R=6	2.334, R=4	147

Work Shop	3'7", R=10	246.4065, R=8	Metamorphic/ Igneous, R=3	SP, R=9	NL, R=10	SP, R=8	7.129, R=8	183
Central Mess	2', R=10	173.934, R=6	Metamorphic/ Igneous, R=3	SC, R=6	NL, R=10	SC, R=6	3.086, R=4	147

3.7. Hydraulic Conductivity (C)

Hydraulic conductivity of the study area is obtained by falling head permeability test. Hydraulic conductivity of the study area ranges from 1.0499 m/day to 7.129m/day. Considering the data obtained the rating assigned to each area. Figure 9 indicates the hydraulic conductivity rating map.

The final steps are the calculation of the GWVI using equation 1. Considering the ratings along with weightages listed in Table 1 the values or GWVI have been obtained and the final results are shown in Table 10 and Figure 10 shows the GWVI map for the study area which is obtained by superimposing the layer shown in Figure 2 to 8 after incorporating the weightages of the DRASTIC parameters.

4. Conclusion

Groundwater plays an important role in drinking and other house hold work in CUTM campus, Paralakhemundi, Odisha. In this study DRASTIC model is used to assess the groundwater vulnerability in the study area. Seven parameters included, which represents the hydro-geological setting of the study area, are Depth to water, Net recharge, Aquifer media, Soil media, Topography, Impact of vadose zone, and hydraulic Conductivity. The results of groundwater vulnerability to pollution assessment shows index value which varies from 141 to 183. According to the results, the study area divided into two zones i.e. high vulnerable and very high vulnerable zone. The maximum area has been fallen under high vulnerable zone (Figure 10).

References

Aller, L., Bennett, T., Lehr, J.H., Petty, R.J. and Hackett, G. 1987. DRASTIC: A standardized system for evaluating ground water pollution potential using hydrogeologic settings: NWWA/EPA Series, EPA-600/2-87-035.

Chandrashekhar, H., Adiga, S., Lakshminarayana, V., Jagdeesha, C.J., Nataraju, C. 1999. A case study using the model 'DRASTIC' for assessment of groundwater pollution potential. *In Proceedings of the ISRS national symposium on remote sensing applications for natural resources*. June 19-21, Bangalore.

Durbude, D. G., Naradrajan, N. and Purandara, B. K. 2003. Mapping of ground water quality parameters in GIS environment. In B. Rao, R. Venkateshwar, M. K. Ram, C. S. Sarala and C. Raju (Eds.), Hydrology and watershed management. Proceedings of the international conference, 18-20, 2002, Hyderabad: B.S. Publishers, pp.568–577.

Kimura, Y. 1997. Evaluating migration potential of contaminants through unsaturated subsurface in Texas Vulnerability Map. *CE 397 GIS in Water Resources, The University of Texas, Austin, USA*.

Lobo-Ferreira, J.C. and Oliveira, M.M. 2004. Groundwater vulnerability assessment in Portugal. *Geofísica Internacional*, 43(4), pp.541-550.

Prior, J. C., Boekhoff, J. L., Howes, M. R., Libra, R. D. and VanDorpe, P. E. 2003. Iowa's groundwater basics: A geological guide to the occurrence, use, and vulnerability of Iowa's aquifers. In Iowa Geological Survey Educational Series: Vol. 6, Iowa: Iowa Department of Natural Resource Press. *http://www.igsb.uiowa.edu/Pubs/GWBASICS/default.htm*

Rahman, A. 2008. A GIS based DRASTIC model for assessing groundwater vulnerability in shallow aquifer in Aligarh, India. *Applied Geography*, 28, pp.32-53.

Rao, S. M. and Mamatha, P. 2004. Water quality in sustainable water management. *Current Science*, 87(7), 942-947.

Rundquist, D. C., Rodekohr, Donn A., Peters, Albert J., Ehrman, Richard L., Di, Liping and Murray, Gene. 1991. State wide groundwater-vulnerability assessment in Nebraska using the DRASTIC/GIS model. *Geocarto International*, 6(2), 51-58.

Usha Madhuri, T. and Srinivas, T. 2004. A study on ground water quality in commercial areas of Visakhapatnam. *Pollution Research*, 23(3), pp.565-568.

Cloud Publications
International Journal of Advanced Remote Sensing and GIS
2017, Volume 6, Issue 1, pp. 2416-2423
ISSN 2320 – 0243, Crossref: 10.23953/cloud.ijarsg.312

Research Article

Determination of Spectral Characteristics on Archaean Komatiites in Ghattihosahalli Schist Belt (Gsb) of Kumminagatta, Chitradurga District, Karnataka, India

Basavarajappa H.T.[1], Manjunatha M.C.[1], Rajendran S.[2], Jeevan L.[1]

[1]Department of Studies in Earth Science, Centre for Advanced Studies in Precambrian Geology, University of Mysore, Manasagangothri, Mysore-570006, Karnataka, India
[2]Department of Earth Science, Sultan Qaboos University, Muscat, Oman

Publication Date: 10 October 2017

DOI: https://doi.org/10.23953/cloud.ijarsg.312

Abstract Komatiites contain economic important nickel, chromium, titanium and copper deposits and their spectral absorption characters are highly important in the remote sensing technique to map and explore such deposits bearing rocks. This study integrates hyperspectral signatures; petrological and geochemical characters of serpentinite bearing ultramafic komatiite rock noticed at the Ghattihosahalli Schist Belt (GSB), near Kumminagatta village, in the Chitradurga district of Karnataka, India and demonstrate specific spectral absorptions of the rock. The measurement of spectral signatures of the rock using spectroradiometer produced significant absorptions near 700, 900 to1100, 1400, 2300, 2380 and 2470 nm in the 350-2500 nm wavelength. The spectral absorptions depend mainly on the optical and physico-chemical characters of the rock and are studied with the spectra of mineral library of USGS and JPL and characterized. This study can be used in the remote sensing technique to map similar rocks and bearing mineralization of the remote areas.
Keywords *Geochemical data; GSB, Komatiite; Kumminagatta; Spectral signatures*

1. Introduction

Komatiite is an economic minerals bearing rock and study of this rock is also significant to understand the evolution of the Earth's crust and mantle. The rock contains valuable deposits of nickel, chromium, titanium and copper which are of economic interests (Arndt et al., 2008). Komatiite magma erupted on the Earth's surface through partial melting in the mantle at depths far greater than those that yield the modern basaltic magmas (Arndt et al., 2008). Similar studies provide important evidences to thermal and chemical evolution of the planet, and nature of the Precambrian mantle (Arndt et al., 2008). The spinifex texture of Komatiite (STK) is characterized by presence of parallel and radiate arrangements (spiky, randomly oriented leaves or needles) of elongate olivines and pyroxenes implying the rapid crystallization from an ultramafic liquid (Nesbitt, 1971; Arndt et al., 2008). In India, the Komatiites occurrence of Ghattihosahalli Schist Bet (GSB) is spinifex textured and contains high Mg content (ultramafic composition, Vishwanatha et al., 1977). It is volcanic/ sub-volcanic origin (Jayananda et al., 2008) formed around 3384 M.Y (Prabhakar and Namratha, 2014). Detailed field studies have been carried out by Ramakrishnan et al., (2012), Jayananda et al., (2013), and Prabhakar and Namratha (2014). The trace element analyses of the Komatiite rock shows 2625 ppm, 1588 ppm, 2360 ppm of nickel, chromium, and titanium respectively (Arndt et al., 2008; Jayananda et al., 2008). This study

characterizes the hyperspectral signatures of such economic important Komatiite rock and correlates petrographic and major elements chemistry in interest of mapping the rock.

1.1. Study Area

Ghattihosahalli Schist Belt (GSB) of Karnataka, India consists of volcano-sedimentary sequence includes the ultramafic Komatiites, steatite, amphibolites with interlayered fuchsite quartzite and barite beds (Vishwanatha et al., 1977; Radhakrishna and Sreenivasaiah, 1974). It is correlated with the Sargur Group, which is older than the greenstone sequences of the Dharwar Supergroup in Karnataka (Vishwanatha and Ramakrishnan, 1975; Chadwick et al., 1981; Paranthaman, 2005). The GSB is about 15 km long and 300 m wide, represents a linear en echelon array of enclaves of the high-grade supracrustal rocks occurred very close to western margin of the Chitradurga Schist Belt (CSB) in the Western Dharwar Craton (Narayana and Naqvi, 1980; Jayananda et al., 2008; Ramakrishnan et al., 2012). The study area, Kumminagatta village in the Chitradurga district of Karnataka lies in between 13°56' to 14º00’ the north latitude and 76°14' to 76°19’ the east longitude at elevation ranges from 813 to 848m above Mean Sea Level (Figure 1). Here, the occurrences of serpentinite bearing Komatiites in the GSB are mapped by Vishwanatha et al. (1977). In the field, the rocks occurred as circular exposure and showed undoubted spinifex texture, deformed nodular structure stacked randomly and accentuated by thin stringers of magnetite in hand specimen (Vishwanatha et al., 1977).

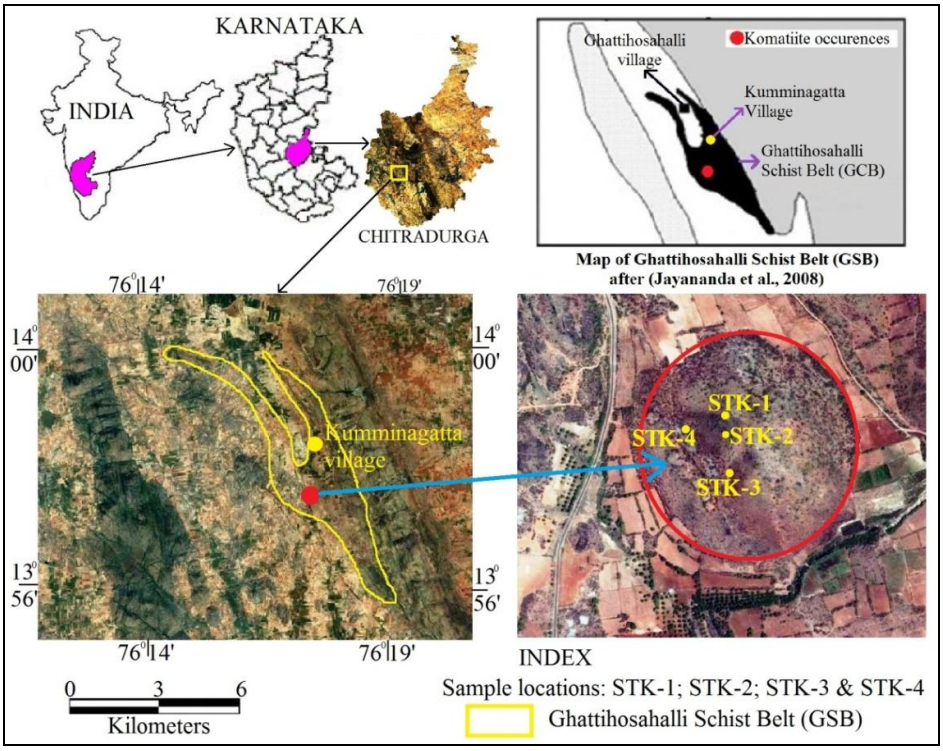

Figure 1: *Google Earth image shows the sample locations (STK-1; STK-2; STK-3 & STK-4) of the Archaean Komatiite in the Ghattihosahalli Schist Belt*

2. Methodology

In this study, four representative rock samples of spinifex textured Komatiites (STK-1; STK-2; STK-3 & STK-4) have been collected during field visits for laboratory study. Hyperspectral measurements of field samples are carried out using a spectroradiometer instrument, FieldSpec-3 (Laboratory Analytical

Spectral Device), in the wavelength of 350-2500nm at the Geological Survey of India (GSI), Bengaluru. The instrument has the spectral resolution of 3 nm (at 700 nm) and 10 nm (at 1400/2100 nm). The obtained spectral curves are further interpreted and compared with the spectra of the standard spectral libraries (USGS and JLP) using ENVI v4.2 (Basavarajappa et al., 2015; Rajendran et al., 2014). The samples are studied for petrographic characters using a microscope by preparation of microscopic thin sections and were analyzed for major chemical elements. Survey of India (SoI) topomap (57C/5 [grid: B-1]) of 1:50,000 scale is used during the field work to study the Komatiite rocks and the samples are collected using a handheld GPS (Garmin-12) instrument.

2.1. Field Study

At southern part of Kumminagatta village, a prominent circular hill (Figure 1) shows exposure of komatiite rocks associated with talc-actinolite-tremolite schist and hard meta-peridotite. In the field, the rocks showed a well developed coarse spinifex textures consist of randomly oriented plates and bundles of altered olivines in fine grained matrix ranging from 1 to 8 cm in length and 0.5 to 5 mm in width (Figure 2a, b, c). Here, the Komatiites are interlayered and well exposed on the top of the hill; while the massive exposures are found at the lower levels of the hill (Jayananda et al., 2008). During the field work, four rock samples of massive, dark reddish brown and showed spinifex grass texture are collected. Lensoidal and bladed crystals of olivine and randomly stacked and accentuated by thin stringers of magnetite are observed in fresh samples (Ramakrishnan et al., 2012). The olivines of the rocks are showed alteration of serpentine by weathering process (Ramakrishnan and Swami Nath, 1981). At few places, the Komatiite is associated with quartzite signify that its occurrence is ultramafic subaqueous volcanism and chemical precipitation of eruption (Jayananda et al., 2008).

Figure 2: *Field photographs (a, b, & c) show the spinifex textures in the outcrop of Komatiites at south of Kumminagatta village of Ghattihosahalli Schist Belt*

2.2. Petrography and Geochemistry

The Komatiites are mainly made up of olivine and altered serpentine minerals with streaks of magnetites which are observed under petrological microscope (Ramakrishnan et al., 2012). The Komatiite exhibited bundles of long & short olivine's, sub-parallel and cross cutting serpentines (olivine altered product) with small isolated patches of fibrous asbestos (Figure 3a & b). The major element analysis of the rock samples showed high concentrations of SiO_2 (40.37 %), MgO (32.42 %) and Fe_2O_3+FeO (10.17 %) and low amounts of K_2O (0.10 %), CaO (2.37 %) and Na_2O (0.25 %) (Table 1: Narayana and Naqvi, 1980).

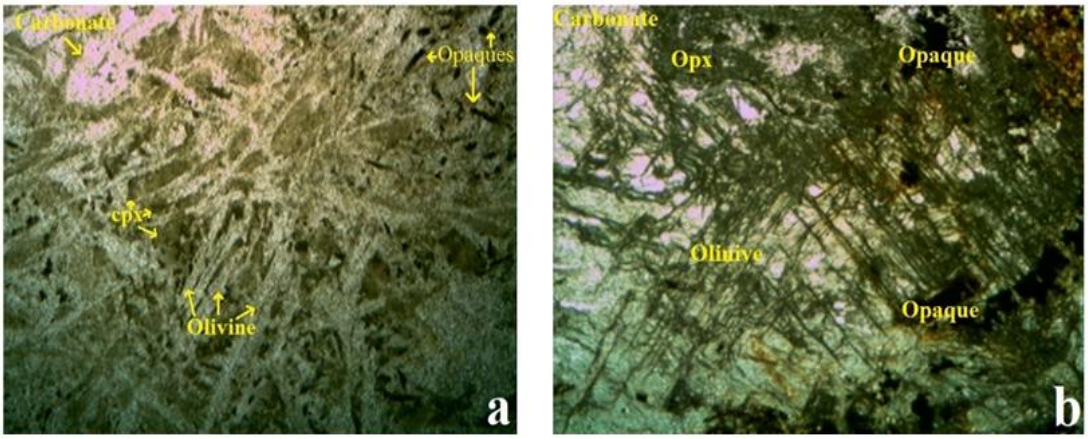

Figure 3: *Microphotographs show a. spinifex texture of the Komatiite and b. the parallel and randomly oriented olivine blades of serpentine with minor carbonate and fine grained opaque minerals (PPL, 4x)*

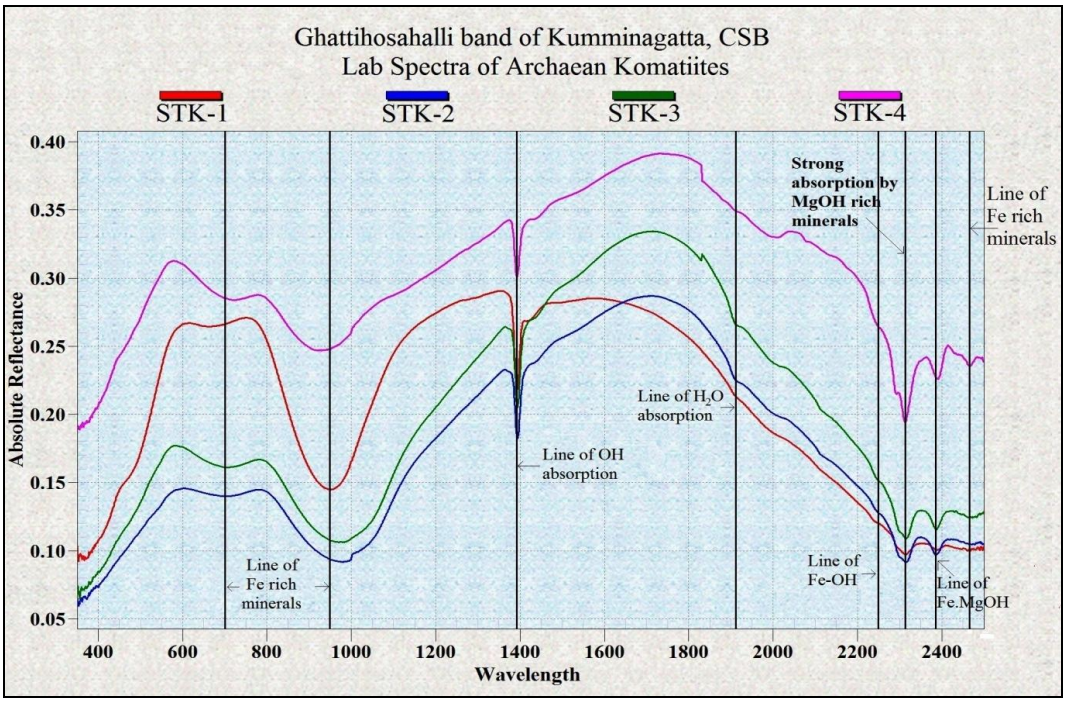

Figure 4: *Laboratory spectral plots of Archaean Komatiites of the Kumminagatta village, Karnataka*

2.3. Interpretation of Hyperspectral Signatures

Study of hyperspectral signature of minerals using “laboratory grade” spectroscopic principles (Clark et al., 1990) is more significant for identification and mapping of surface mineralogy and rock types. Mapping of rock types based on absorption signatures in the spectral wavelength and spectral bands of satellite data are carried by several geologists. In remote sensing technique, an extensive range of minerals are mapped, including the MgO-rich serpentines (Rajendran et al., 2012, 2013, 2014), based on their absorption characters in the spectral wavelength (Rowan et al., 2006; Ali Mohammad, et al., 2009). Laboratory spectroradiometer instrument has their own light source for illumination of the specimen and has very high spectral resolution and measuring reflectance percentages of samples

from 400 to 2500 nm (Lipton, 1997). The troughs in the obtained spectra are the absorption features representing the diagnostic characters of a unique mineral can be interpreted by studying the width and depth of the spectra (Lipton, 1997). The study of minerals of phyllosilicates showed narrow spectral absorption features near 2.2 µm wavelength region due to mainly presence of A1-OH contents in the minerals. The octahedral sites in the phyllosilicates are occupied by magnesium instead of aluminum, the combination OH stretch produces (Mg-OH bending) strong absorption features in the vicinity of 2.30 to 2.35 µm (Hunt, 1977, 1979; Abrams et al., 1988; Mars and Rowan, 2010; Rajendran et al., 2012, 2014; Rajendran and Nasir, 2014).

In this study, the Mg-rich altered serpentine minerals are a key element to recognize Komatiite (King and Clark, 1989). As well as, spectral absorptions of the OH and H2O contents of the rocks and bearing minerals that are representing the metamorphic reaction (by water within Archaean Komatiites, Shrivastava et al., 2009) can be interpreted in the near 1.39 to 1.90 µm respectively (Ali Ali Mohammad et al., 2009). The spectra of the Komatiite samples are given in Figure 4. It shows well identified absorption features near 700, 900 to1100, 1400, 2300, 2380 and 2470 nm. In the spectra, the shallow absorptions near 700 nm and the broad deep absorptions from 900 to 1100 are due to presence of ferrous iron content present on the surface of the samples. The sharp and deep absorption at 1400 nm is due to presence of OH and H2O contents present in the altered minerals of the samples. The significant absorption at 2300 is due to presence of the Mg-OH and the shallow absorptions near 2380 and 2470 are influenced by the FeMg-OH contents in the samples.

Table 1: *Integration of hyperspectral & geochemical signatures on Archaean Komatiites*

S. No.	Elements	STK-1	STK-2	STK-3	STK-4	Average	Lab spectra (µm)	Best matches
1.	SiO^2	39.43	42.18	40.08	39.81	40.37		
2.	TiO_2	0.23	0.19	0.19	0.27	0.22		
3.	Al_2O_3	2.09	3.21	3.54	4.13	3.24		
4.	Total FeO	8.73	9.22	11.61	11.13	10.17	0.7, 0.94 & 2.47 µm	Fe rich minerals
5.	MnO	0.14	0.11	0.15	0.16	0.14		
6.	MgO	32.87	31.12	31.31	34.39	32.42	2.311 to 2.319 µm	Serpentinite & Mg(OH) rich type of minerals
7.	CaO	3.01	2.56	2.69	1.24	2.37		
8.	Na_2O	0.21	0.27	0.23	0.30	0.25		
9.	K_2O	0.15	0.08	0.09	0.10	0.10		
10.	P_2O_5	0.09	0.15	0.12	0.16	0.13		
11.	H_20^+	7.61	9.60	9.81	7.89	8.72	1.39 & 1.90 µm	OH & H_2O type of minerals
	Total	94.56	98.69	99.82	99.58			

3. Results and Discussion

Understanding of spectral absorptions features of the Komatiite rocks based on their optical and physico-chemical characters is significant in remote sensing technique to map the rock and explore the economic important minerals of the rock. Here, the study of petrological characters and chemical analyses of the four rock samples showed that these are composed of olivine and altered serpentine minerals and have high SiO_2 (40.37%), MgO (32.42%), FeO (10.17%) and H_2O (8.72%) contents in average of analyses. The measurement of hyperspectral signatures of the rock in the 350-2500 nm

wavelength showed absorption features near 700, 900 to1100, 1400, 2300, 2380 and 2470 nm. Table 2 shows the specific absorption values in the wavelengths. The features of absorptions are mainly depends the surface minerals of the rock samples. The weathered olivine minerals of the rock developed the ferrous iron rich rock surface which produced broad Fe-OH absorption at the wavelength of 900-1100 nm evidently in the spectral plot. As well as, the occurrence of serpentines in the rock, due to hydrothermal alteration of olivine, produced Mg-OH and FeMg-OH absorptions at 2300, 2380 and 2470 nm significantly. The chemical analyses of the samples showed presence of the 8.72% of H2O contents in the samples which may be due to presence of water during metamorphic reaction. The H2O contents and the OH contents present in the altered minerals developed together the absorption at 1400 nm clearly. The comparative study of minerals spectra of mainly the olivine and serpentine minerals from the spectral libraries namely USGS and JPL correlated well and more confirmed such interpretations of the spectral absorption features to the specific wavelengths. Thus, the petrological study showed the minerals of the rock and chemical analyses produced the concentration of chemical elements of the rock which are characterized the spectral absorption features. This study clearly demonstrated and documented the spectral absorption features of the Komatiite rock which depend the optical and physico-chemical characters of the rock.

Table 2: *Spectral absorption values of the Archaean Komatiite rocks*

Wavelengths in nm	Sample No.			
	STK-1	STK-2	STK-3	STK-4
700	665	704.4	707	725.4
900-1100	948.5	977.4	972.2	924.9
1400	1392.2	1392.6	1392.2	1392.6
2300	2314.6	2314.6	2314.6	2312.8
2380	2384.5	2384.5	2386.3	2389.8
2470	2461.5	2473.8	2466.8	2465

4. Conclusion

Characterizing of Archaean Komatiite's by hyperspectral signature using a portable field instrument can save time and great expense to map the rock and bearing economic mineral for exploration. In this study, the hyperspectral signatures of the Komatiite rock samples of Kumminagatta village in the Chitradurga district of Karnataka state, India are measured and the specific absorptions features of the rock are recorded and interpreted with their field, petrological and chemical analyses results. Spectral curves of the Komatiite samples showed the absorption features which are depends mainly the major mineral constituents and elements concentrations. The features are unique and recommended to use to map Komatiite. The study clearly demonstrated the spectral absorption features are characterized by the optical and physicochemical characters of the rock. The study on the spectral absorption characters of the Komatiites allows the user to choose the specific spectral bands in the hyperspectral bands to map Komatiite and explore economic minerals of the rock elsewhere.

Acknowledgment

The authors are indepthly thank Prof. K.G. Asha Manjari, Chairman, Department of Studies in Earth Science, University of Mysore, and Dr. Dinesh Gupta and Sri. N.S. Gadagkar, Remote Sensing division for their encouragement concern to this study. We are also thankful to Ms. Nisha Rani, Mr. Sumit Kumar Ahirwar and Mr. Chethan Kashyap, for their valuable suggestions and assistance to this study. Geological Survey of India, Bangalore is thanked for permission and measuring spectral data.

This study is supported by the UGC grant (MRP No.42.73 (SR)/2012- 13, dt:12.03.2012) and UGC-CAS (phase-I).

References

Abrams, M.J., Rothery, D.A. and Pontwal, A. 1988. Mapping in the Oman ophiolite using enhanced landsat thematic mapper images. *Tectonophysics*, 151, pp.387-401.

Ali Mohammad, Q., Basavarajappa, H.T. and Rajendran, S. 2009. Integration of VNIR and SWIR Spectral Reflectance for Mapping Mineral Resources; A Case study, North East of Hajjah, Yemen. *Journal of Indian Society of Remote Sensing*, 37, pp.305-315.

Arndt, N.T., Lesher, C.M. and Barnes, S.J. 2008. *A Text Book of Komatiite*. Cambridge University Press, *UK,* pp.10-15.

Basavarajappa, H.T., Manjunatha, M.C. and Rajendran, S. 2015. Integration of Hyperspectral Signatures and Major elements of Iron ore deposits around Holalkere range of Megalahalli, Chitradurga Schist Belt, Karnataka, India. *The Indian Mineralogist*, 49(1), pp.85-93.

Chadwick, B., Ramakrishnan, M. and Viswanatha, M.N. 1981. Structural and metamorphic relations between Sargur and Dharwar supracrustal rocks and peninsular gneiss in Central Karnataka. *Journal of the Geological Society of India*, 22, pp.557-569.

Clark, R.N., King, T.V.V., Klejwa, M., Swayze, G.A. and Vergo, N. 1990. High spectral resolution reflectance spectroscopy of minerals. *J. Geophys. Res.*, 95, pp.12653-12680.

Ramakrishnan, M. and Swami Nath, J. 1981. Early Precambrian Supracrustals of Southern Karnataka. *Geological Society of India,* Govt. of India, 112, pp.41-60

Hunt, G.R. 1977. Spectral signatures of particulate minerals in the visible and near infrared. *Geophysics*, 42, pp.501-503.

Hunt, G.R. 1979. Near-infrared (1.3-2.4) spectra of alteration minerals-potential for use in Remote Sensing. *Geophysics*, 44(12), pp.1974-1986.

Jayananda, M., Kano, T., Peucat, J.J. and Channabasappa, S. 2008. 3.35Ga Komatiite volcanism in the Western Dharwar Craton, Southern India: Constraints from Nd isotopes and whole-rock geochemistry. *Precambrian Research*, 162, pp.160-179.

Jayananda, M., Tsutsumi, Y., Miyazaki, T., Gireesh, R.V., Kowe-u, K., Tushipokla, T., Hiroshi, H. and Kano, T. 2013. Geochemical constraints on Meso- and Neoarchaean regional metamorphism and magmatism in the Dharwar Craton, Southern India. *Journal of Asian Earth Sciences*, 78, pp.18-38.

King, T.V.V. and Clark, R.N. 1989. Spectral characteristics of serpentines and chlorites using high resolution reflectance spectroscopy. *Journal of Geophysical Research*, 94, pp.13997-14008.

Lipton, G. 1997. Spectral and microwave remote sensing: an evolution from small scale regional studies to mineral mapping and ore deposit targeting. International Conference on Mineral Exploration, *Geomatics International Inc.,* Burlington, Canada, pp.43-58.

Mars, J.C. and Rowan, L.C. 2010. Spectral assessment of new ASTER SWIR surface reflectance data products for spectroscopic mapping of rocks and minerals. *Remote Sens. Environ.*, 114, pp.2011-2025.

Narayana, B.L. and Naqvi, S.M. 1980. Geochemistry of Spinifex-textured peridotitic Komatiites from Ghattihosahalli, Karnataka, India. *Journal of Geological Society of India,* 21(4), pp.194-198.

Nesbitt, R.W. 1971. Skeletal crystal forms in the Ultramafic rocks of the Yilgarn block, Western Australia: Evidence for an Archaean Ultramafic liquid. *Geol. Soc. Austr. Spec. Publ.*, 3, pp.331-347.

Paranthaman, S. 2005. Geology and Geochemistry of Archaean Ghattihosahalli mafic-ultramafic complex, Chitradurga, Karnataka. *J. Geol. Soc. India*, 66, pp.653-657.

Prabhakar, B.C. and Namratha, R. 2014. Morphology and textures of Komatiite flows of J.C Pura Schist Belt, Dharwar Craton, *Journal of Geological Society of India*, 83, pp.13-20.

Radhakrishna, B.P. and Sreenivasaiah, G. 1974. Bedded baryte from the Precambrian of Karnataka. *J. Geol. Soc. India*, 15, pp.314-315.

Rajendran, S., Al-Khirbash, S., Pracejus, B., Nasir, S., Al-Abri, Amani Humaid, Kusky, T.M. and Ghulam, A. 2012. ASTER detection of chromite bearing mineralized zones in Semail ophiolite massifs of the northern Oman mountain: exploration strategy. *Ore Geol. Rev.*, 44, pp.121-135.

Rajendran, S., Nasir, S., Kusky, T.M., Ghulam, A., Gabr, S. and Elghali, M. 2013. Detection of hydrothermal mineralized zones associated with Listwaenites rocks in the Central Oman using ASTER data. *Ore Geol. Rev.*, 53, pp.470-488.

Rajendran, S., Nasir, S., Kusky, T.M. and Al-Khirbash, S. 2014. Remote sensing based approach for mapping of CO2 sequestered regions in Semail ophiolite massifs of the Sultanate of Oman. *Earth Sci. Rev.*, 135, pp.122-140.

Rajendran, S. and Nasir, S. 2014. Hydrothermal altered serpentinized zone and a study of Ni-magnesioferrite - magnetite - awaruite occurrences in Wadi Hibi, Northern Oman Mountain: Discrimination through ASTER mapping. *Elsevier-Ore Geology Reviews,* 62, pp.211-226.

Ramakrishnan, M., Mahabaleshwar, B. and Viswanathan, S. 2012. The abundances of some Trace-elements in the First-ever reported sample of Spinifex-Textured Komatiite from Ghattihosahalli, Karnataka. *Journal of Geological Society of India,* 79, pp.361-366.

Rowan, L.C., Schmidt, R.G. and Mars, J.C. 2006. Distribution of hydrothermally altered rocks in the Reko Diq., Pakistan. *Remote Sensing of Environment,* 104(11), pp.74-87.

Shrivastava, K.L., Mathur, A. and Chauhan, M. 2009. Recent Advances in the Understanding of Komatiites with special reference to Ore Genesis. Earth System Sciences*,* Felicitation Volumes in Honour of Prof. V.K. Verma, *Concept Publishing Company*, New Delhi, India, 1, pp.295-323.

Vishwanatha, M.N. and Ramakrishnan, M. 1975. The Pre-Dharwar supracrustal rocks of Sargur schist complex and their tectono-metamorphic significance, *Journal of the Indian Mineralogist*, 16, pp.48-65.

Viswanatha, M.N., Ramakrishnan, M. and Narayana Kutty, T.R. 1977. Possible spinifex texture in a serpentinite from Karnataka*. J. Geol. Soc. India*, 18, pp.194-197.

Cloud Publications
International Journal of Advanced Remote Sensing and GIS
2017, Volume 6, Issue 1, pp. 2442-2448
ISSN 2320 – 0243, Crossref: 10.23953/cloud.ijarsg.321

Research Article

Identification of Optimum Shortest Path using Multipath Dijkstra's Algorithm Approach

Kumari Pritee[1], Garg R.D.[2]

[1]Research Scholar, Centre for Transportation Systems (CTRANS), IIT Roorkee, Uttarakhand, India
[2]Associate Professor, Geomatics Engineering, IIT Roorkee, Uttarakhand, India

Publication Date: 30 October 2017

DOI: https://doi.org/10.23953/cloud.ijarsg.321

Abstract Many route mappings were done with the help of API of Google maps but do not provide geospatial Routing functionality like overlay, interpolation etc. This project aims to find the shortest path between two or more points by using multipath Dijkstra's algorithm via PgRouting. Dijkstra's algorithm provides advantages on time required for selecting the network and building graph over the algorithm speed. In that case, A-star is always preferred over Dijkstra's algorithm. Dijkstra's algorithm has a computational complexity of O (n2) with a network consisting of n nodes. This Project explains the steps to prepare the data by converting shape files into SQL files and import it into PostgreSQL/PostGIS, make routing topology, indexes, and queries, dynamically assign costs by PgRouting, and write a custom function 'plpgsql' using PL/pgSQL (Procedural programming structured query language) supported by PostgreSQL. This report provides all geospatial functions with dynamic support via PgRouting which allows many clients, like Quantum GIS and Udig, represents client visualization for modification of data and attributes for instantly reflecting changes via PgRouting. PgRouting Provides a framework by which cost parameters are calculated dynamically. This paper specifies the routing of Varanasi city roads using Dijkstra's algorithm and PgRouting. This article focuses on dynamic routing on the complex network like Varanasi City over the web mapping application so that Client can easily find their shortest route along with Cost parameters.
Keywords *Dijkstra's algorithm; Geographic information system; PostgreSQL/PostGIS; PgRouting; GeoServer; Web services*

1. Introduction

With the excessive needs of applications of Geoinformatics, GIS and their web based applications have been increasing day by day. Traveling is a necessity of daily life. Network Analysis provides a function for many fields i.e. Traffic tourism, Telecommunications and so on. Network Analysis faces lots of problem in a complex network. Most of the peoples (especially in developing countries like India) facing lots of problem on public transportation like railway, bus, minibus, ferry even after they had their own vehicle. The reason is unawareness of complicated road network. People always want to easily gather all the information for unvisited destination and reach as soon as possible. They actually prefer easily reachable and most economical route compared to another route for their destination. Route selection provides a time saving and easily accessible shortest route between origin and destination. Sometimes a longer route can be more convenient than a shorter route, in order to avoid various difficulties like traffic, restrictions. A good knowledge provides a sophisticated routing of

road network along with relative cost. As the user makes queries for shortest route from one node to another, System generates route accordingly on the basis of input factors e.g. cost, time and so on. We have seen many applications including Google maps which show the shortest path between two points. But in our application, it is not only the shortest path distance in general geographic sense but it also provides cost parameter dynamically including time and the capacity of the line. We propose a road-routing web based geographic information system which helps to find the shortest path between source and destination in order to optimize it by implementing new technologies through which cost parameters are calculated dynamically with the help of PgRouting.

Earlier PgRouting enables only Dijkstra's algorithm for shortest path searching. So at that time, PgRouting was named as PgDijkstra. After that, it was extended to provide routing functionality via various algorithms i.e. A-star and enabling the low-level interface to algorithms. It makes possible of use of diverse data, algorithms etc. with the help of WebGIS that helps in spreading it over the web. WebGIS communicates through interfaces for finding the shortest path. Shortest path algorithm provides a minimum weight route between source and destination and building graph. In this article, the shortest path is found by using Dijkstra's algorithm Proposed by Edsger Dijkstra in 1959. This algorithm provides precise results compare to the previous algorithm. It follows many steps for searching minimum cost path among ordered path. The first step is to explore search region and expand it. The second step is to obtain network topology information i.e. the connection between arcs and provide more optimal analysis result for huge data. It is beneficial for saving a lot of memory and proves easily gathering information from huge nodes. The architecture is shown in Figure 1:

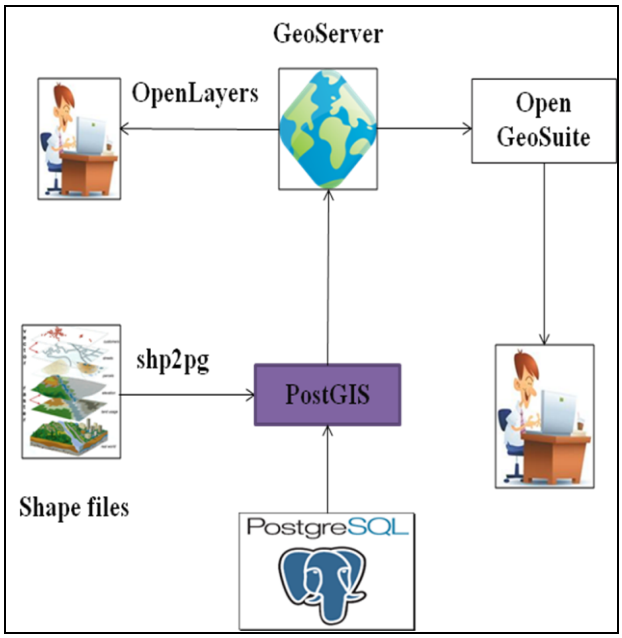

Figure 1: *Architecture of project*

Dijkstra's algorithm calculates the length of shortest route among all routes between two vertices included in a graph. The working of this algorithm has been explained using seven steps.

i. Choose search region providing set S of vertices and select source and destination vertices.
ii. Initialize source node to zero which is solved and identify rest unsolved node connected to source node which is assumed as the origin.

iii. Calculate candidate distance by adding distance to the solved node and length of the arc connecting between solved and unsolved nodes.
iv. After that algorithm chooses smallest candidate distance.
v. Then unsolved is changed into solved node.
vi. If there will be a tie in candidate distance, then choose arbitrarily.
vii. Repeat these steps with all unsolved node until the destination is reached.

This WEBGIS based system provides the information of specific areas between two points, source, and destination, including sequence, node, edge, cost information.

Lots of work and research paper have been earlier done for optimizing and planning a route but there are fewer works has been done on the route finding problem. Route finding process can be designed using new methodologies. So, here this research paper discussed and solved one of the problems of route finding. This paper has been focussed on the dynamically representing route on the basis of cost parameters using Dijkstra's algorithm. With the help of this routing, modification for various heuristics is made easily accessible. It also enhances and solved the problem described in earlier methodologies. This article also helps in creating a creating conceptual model for route finding and easy modification of various heuristics. In the next section, implementation of some previous has been explained.

2. Literature Review

To enhance the performance of earlier route finding system and provide a cost effective route, multi modal transport network and multi agent information system provide the solution to the problem of human transport needs. A conceptual model has been designed to enhance the performance and accuracy of earlier implemented route finding system (Chiu et al., 2005). A new dynamic restricted algorithm based on direction and area has been developed for a large network containing many nodes and arcs and provides benefits of using it by combining with another algorithm e.g. Dijkstra's algorithm (Xi et al., 2006). Introducing practical example of PgRouting on OpenStreetMap road network data provides an explanation of all steps including routing queries, cost assigning and modifying results (Kastl et al., 2009). An improved algorithm by extending PgRouting has been implemented to obtain the road conditions at the destination and provide emergency route decision planning by calculating travel time consumption of route on the basis of location and situations of accidents (Chosumrong et al., 2012). The complexity of road network and heavy traffic always tends to a big challenge for finding the shortest path. Instead of these problems, a system has been designed for Colombo city to provide the shortest route for a future date according to present road condition, traffic conditions, road closures etc. by using Geographic Information system (GIS), ASP.net and GPRS technology (Firdhous et al., 2012). PgRouting application in road and highway level provides a quick speed, fast execution and convenient operation for the shortest path finding the application and extensive application in path optimization. On the basis of this absorption, it provides a benefit of traveling salesman problem solution and highway grade analysis (Zhang and He, 2012). Web based 3D indoor routing system on the OpenStreetMap datasets has been developed using new HTML (Hypertext Multiple Language) extension and XML3D (Extensible Markup Language) (Goetz, 2012). Comparing of different open source tools in the world of WebGIS provides different technical support, documentation and unique weighted professional services (Akbari and Peikar, 2014). PgRouting always provides good results with Dijkstra's algorithm. A comparison of the performance of Dijkstra's shortest path calculation and Neo4j graph database for OpenStreetMap (OSM) dataset provides large transportation network based shortest path algorithm where memory is not an issue (Miler et al., 2014). To avoid obstacles in the road network and provide alternative route a web based GIS platform has been developed using modified Dijkstra's algorithm with PgRouting on the OpenStreetMap road network (Yusoff et al., 2014).

3. Implementation

Table 1 indicates all software used and their application for this implementation. This implementation used both PgRouting and Dijkstra's algorithm to find the shortest path with dynamically changing cost (weight). Better emergency routing systems have been provided by PgRouting with Dijkstra's algorithm. In this implementation, two main modules and two user modules have been used. The main module consists of the core module and Web module while user module consists of application user and admin user. Shortest path computation by connecting GeoServer with a database created by PostgreSQL/PostGIS is carried out by core module. Web module makes it available over the web by providing a user interface via Open Layers. Application and admin user are carried out on the client side and accessed through the web simultaneously.

Table 1: *Software applications*

Technology used	Version	Function
PostgreSQL	9.2.5	Database
PostGIS	2.1.1	Spatial Database
ArcGIS	10.0	Coordinate Transformation
PgRouting	2.0.0	Routing
Open JUMP	1.2.1	Client, desktop GIS
GeoServer	2.3.4	Visualization/Web based client mapping application
Firefox	5.0	Web browser
PL/PgSQL		Procedural language
OpenGeo Suite (GeoExplorer)/OpenLayers	2.4.5	For user interface

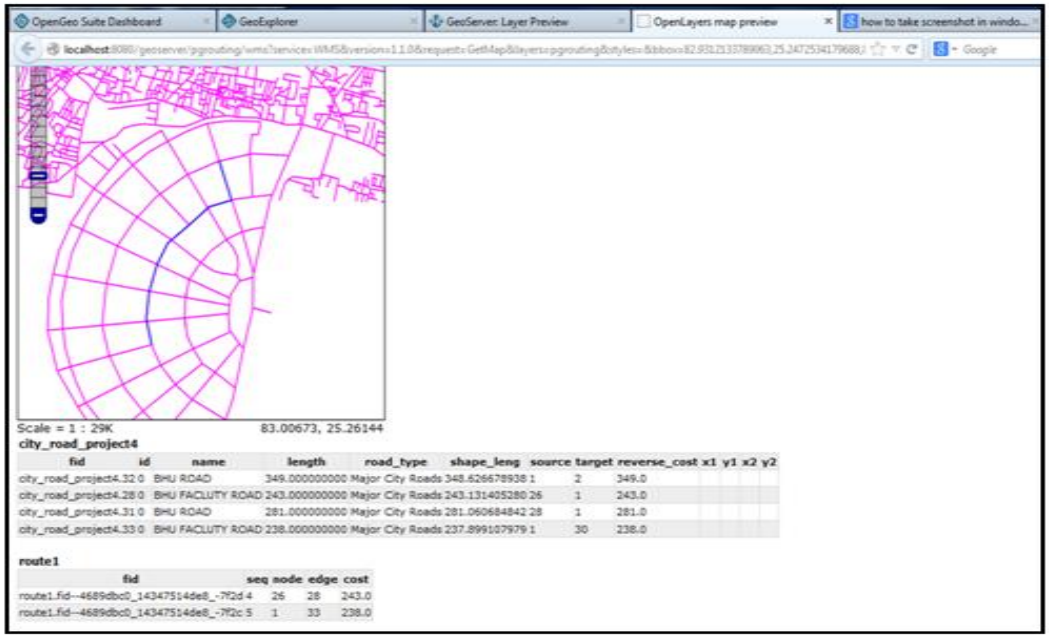

Figure 2: *Shortest path result and their details*

The following query retrieves information from city_road_project4,

```
"gid" IN (SELECT id2 AS gid from pgr_dijkstra ('SELECT gid AS id,
                source::integer,
                target::integer,
                length::double precision AS cost,
                FROM city_road_project4',
        30, 60, false, false) a LEFT JOIN city_road_project4 b ON (a.id2 = b.gid)
```

The implementation of the shortest path with dynamically updating cost depends on the transport network consisting of nodes, links, and routes. Here, the prerequirements are windows 7, an editor like Gedit or Mouse pad, GeoServer for the routing application and Internet connection. Here we have used latest PostgreSQL9.2.5 with PostGIS 2.0.0. The cost has been dynamically calculated with the help of latest PgRouting 2.0.

Cost may be a factor of time, distance and lots of attributes.

PL/pgSQL is a procedural language used for performing complex computations, functions and triggers procedures.

Dijkstra's algorithm with aided PgRouting functionality provides shortest path finder system with dynamically changing cost. With this aided functionality four parameters are added automatically which is source_id, target_id, directed and has_reverse_cost. Source_id indicates starting point while target_id indicates destination point. There are two Boolean variables i.e. directed and has_reverse_cost. If first is true, then the graph tends to be directed. If latterly is true, then reverse_cost used in opposite direction. The reverse_cost stores all the cost of traversal edge in reverse direction.

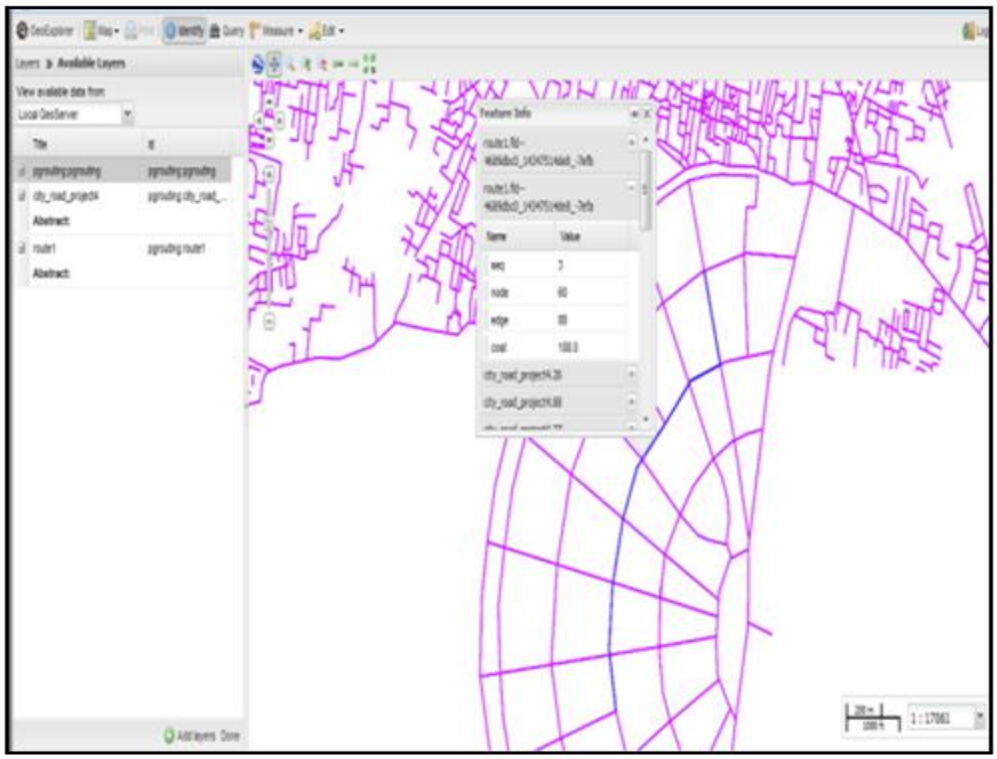

Figure 3: *Shortest path description using OpenGeo Suite (Geoexplorer)*

First of all, a database has been loaded from the project data directory. This directory contains Shapefile of Varanasi (city_road_project4) for small sized network data which is basically known as database dumps. After that Shapefile has been copied into the bin folder of PostgreSQL.The Shapefile city_road_project4 has been converted into SQL file with the help of shp2pgsql in command prompt. After importing the database dump, PostGIS and PgRouting functions have been added to a database. Small sized sample network data with a minimum number of attributes has been also loaded, which is being downloaded from sample data website. The pgr_create Topology has been used to create a network topology through which source and target or destination Id has been assigned for the linkage of the road with vertices within a certain tolerance. Before creating network topology, source and target column has been added and wait for a minute to an hour depending upon network size.There are two columns which are automatically added after creating network topology. One column is geography_columns containing table records providing “geometry” attribute with its SRID information and other is vertices_tmp containing a list of all vertices or nodes of the network. Here wrapper functions are used to improve core functions and performance of the system. After that, the result has been transformed into a readable format. The shortest path and their description of their attributes are shown in Figure 2 using GeoServer.

Figure 3 shows the description of sequence, node, edge and cost of shortest path.

The result in QGIS can be visualized via DB Manager Plug-in using the following query:-

```
CREATE TABLE route AS SELECT seq, id1 AS node, id2 AS edge, cost, geom. FROM pgr_dijkstra
('SELECT gid AS id,
                source::integer,
                target::integer,
                length::double precision AS cost,
                FROM city_road_project4',
        30, 60, false, false) a LEFT JOIN city_road_project4 b ON (a.id2 = b.gid)
```

Function output provides the description of vertex_id, edge_id and cost. The vertex_id enables the identifier of the source and a target vertex. The edge_id and cost contain an identifier of crossed edge and cost of a current edge.

4. Conclusion

With the increasing demand of routing application, this paper implements the used of PgRouting with Dijkstra’s algorithm in Varanasi road network and proves a very efficient and convenient operation with dynamically updating cost. It is useful for traffic conditions, analyzing road conditions, journey planner etc. It also expands and explores many routing functions used in PostgreSQL on the basis of three factors i.e. shortest, fastest, traffic free, alternative route in obstacles and natural route. The application has been implemented on web platforms like GeoServer and Geoexplorer due to the high penetration of both technologies. It will create an added benefit at Varanasi city where traffic congestion is very high. On the technology based, we can develop one server named PyWPS and on that server, we can implement PgRouting to find the shortest path. The Future work will be the development of a web based system with an enhanced algorithm with comparatively low investment cost with increased processing and execution sped. High accuracy with good data quality in case of emergency response should be increased. Additional features e.g. future date, SMS, email alerts, hospitals, schools etc should be included.

References

Akbari, M. and Peikar, S.R.H. 2014. Evaluation of free/open source software using OSMM model case study: WebGIS and spatial database. *ACSIJ Advances in Computer Science International Journal*, 3(11), pp.34-43.

Chiu, D.K.W., Lee, O.K.F., Leung, H.F., Au, E.W.K. and Wong, M.C.W. 2005. *A multi-modal agent based mobile route advisory system for public transport network*. Annual Hawaii International Conference on System Sciences, USA, p.92b.

Chosumrong, S., Bozon, N. and Raghavan, V. 2012. Multi-criteria emergency route planning based on analytical hierarchy process and PgRouting. *Geoinformatics*, pp.159-167.

Firdhous, M.F.M., Basnayake, D.L., Kodithuwakku, K.H.L., Hatthalla, N.K., Charlin, N.W. and Bandara, P.M.R.I.K. 2012. Route planning made easy - an automated system for Sri Lanka. *CoRR*, pp.1211-2495.

Goetz, M. 2012. Using Crowd sourced indoor Geodata for the creation of a three-dimensional indoor routing web application. *Future Internet*, pp.575-591.

Kastl, D., Philipona, C., Junod, F. and Patrushev, A. 2009. FOSS4G routing with PgRouting tools and open street map road data. *FOSS4G2009 Tokyo/Osaka PgRouting workshop*, pp.1-20.

Miler, M., Medak, D. and Odobasic, D. 2014. The shortest path algorithm performance comparison in graph and relational database on a transportation network. *Information and Communication Technology, Traffic Transportation,* 26(1), pp.75-82.

Xi, C., Qi, F. and Wei, L. 2006. *A new shortest path algorithm based on heuristic strategy*. Intelligent Control and Automation, the Sixth World, Congress, Dalian, China, pp.2531-2536.

Yusoff, N.M.R.N., Shafri, H.Z.M., Muniandy, R. and Wali, I.M. 2014. Development of obstacle avoidance technique in web-based geographic information system for traffic management using open source software. *Journal of computer science*, pp.1259-1268.

Zhang, L. and He, X. 2012. Route search base on PgRouting. *Software Engineering and Knowledge Engineering,* 2, pp.1003-1007.

Cloud Publications
International Journal of Advanced Remote Sensing and GIS
2017, Volume 6, Issue 1, pp. 2436-2441
ISSN 2320 – 0243, Crossref: 10.23953/cloud.ijarsg.320

Research Article

Using Geographic Information Systems to Develop a Robust Electricity Utility Network

Junaid Qadir, Faizan Jalal

University of Kashmir, Hazratbal, Srinagar – 190006, Jammu and Kashmir, India

Publication Date: 26 October 2017

DOI: https://doi.org/10.23953/cloud.ijarsg.320

Abstract Electricity distribution reform is widely viewed today as fundamental to improving domestic and commercial performance and financial viability in different countries all over the world. Several steps have been taken in this regard to improve the performance by undertaking several measures such as reduction of technical and commercial losses, improvement in load management, strengthening of metering, billing and collection avenues, enhancement of attention towards the quality of electric supply and customer care. The role of Geographic information system (GIS) in electric utility has gained much attention worldwide. Using GIS an electric distribution utility uses a network of physical facilities to provide electric power and energy to customers connected to those facilities throughout a geographical area. Each component of the distribution system (i.e., asset) has a physical location and associated data. So does each customer. In order to design, maintain, operate and manage the electric distribution network it is necessary to utilize the geospatial data. A geographic information system (GIS) is a convenient and powerful way to collect, organizes, maintain and manage this geospatial data and display it on a geographic map. The present study focuses on the use of Geographic information system to develop a robust electricity utility network that helps in distribution system planning, analysis and asset management.
Keywords *Asset; Electric utility; Geographic information system; Geospatial data*

1. Introduction

Utilities all over the world are facing immense pressure and unprecedented change and now the focus has been on to develop new strategies to overcome any deficiencies pertaining to power supply transmission, load management, and other commercial services. The need of hour is efficient management and optimum utilization of installed capacity to meet the supply demand. Advancement in hardware, software, and networking technology has created opportunities for the utility industry to build and benefit from more comprehensive and sophisticated Geographic information system (GIS). Better use of geospatial data is one of the key areas of focus for many electrical utility companies. A Geographic information system (GIS) is a system of hardware, software, and procedures designed to support the capture, management, manipulation, analysis, modelling and display of spatially referenced data for solving complex planning and management problems (Rhind, 1989). GIS is playing a vital role in the field of planning and analysis with respect to the geographically organized demographic information to improve decision making (Prasad, 2006, Maps and Census). A common approach is to generate maps using existing GIS data sets, then send out crews to collect and verify field data for utility features and this is only accurate way to ensure the integrity of the data (James L.

Sipes, 2004). With the radical change electrical utility industry is facing, the consumer choice has become the top most priority in every country. The goal of incorporation new tools & techniques is to satisfy the growing and changing system load demand during the planning period within operational constraints and with minimal costs. The planning process comprises several phases; one of the most important is the optimization of the electric distribution networks. The network optimization is considered a hard-combinatorial optimization problem due to number of limitations network voltage level, network structure, quantum and location of loads, routes and types of feeders and voltage drop (Mathankumar et al., 2015). In this process it is important to have on time accurate relevant data and information on the electric distribution systems and its assets, and possibly to have data from other utilities. Computerization and development of various Geographic information systems have opened new horizons for all decision making processes as well as manipulation and dissemination of information (Mathankumar et al., 2015). The present study focuses on the use of Geographic Information system (GIS) to facilitate easily updatable and accessible database to cater the needs of design, monitoring and maintaining reliable quality electric supply.

2. Methodology

Satellite data was acquired and Thematic layers such as buildings and road network were extracted and represented in form of polygons and lines, also service lines and customer connection point were digitized and integrated in GIS environment. A personal geodatabase was involved with dataset projected using coordinate system WGS84 zone 43N. The personal geodatabase contain features named as building, roads, consumer points and service lines. The area of Interest was delineated from the satellite image and subsequently used to subset other thematic layer. The coordinate points of the transformer and low tension poles acquired with the handheld GPS and customer records were linked together and captured into the geodatabase using add XY coordinate in Arc Map 10.1. Electricity distribution network Map and data was created which shows the spatial location of the transformer, Low Tension poles as well as relationship between all asset and customer connectivity to the transformer.

The methodology for the study has been divided into different categories:

1. **Consumer & Asset indexing:** Each customer is uniquely indexed based on the electrical system codification, from the source of supply to the end customer end. Enable feeder wise energy accounting (33 KV feeders & 11 KV) also Distribution transformer wise energy accounting. Creation of database for each asset and individual customer indicating the exact geographical location.

2. **GIS based Mapping for Electrical Network:** Mapping of complete electrical network up to low voltage system and customer supply points with latitude and longitude overlaid on satellite image. Incorporation of present details of localities, landmarks and existing network details upto consumer level.

3. **GIS Based Consumer Indexing:** Activities involved are preparation of Base Map, Fixing Topographical details, GPS survey, Single Line Diagrams, Mapping and documentation of Network, Mapping and indexing of consumers, Database of electric network, consumer Database development, Segregation of consumers, 11 KV feeder wise and Distribution Transformer wise.

4. **GIS based Mapping:** Network creation (SLD/equipments/geographic representations/SS design), System Analysis (cost benefit analysis/reconductoring/network configuration/load flow studies/ load balancing/ short circuit studies). System optimization, Reports, Trend analysis.

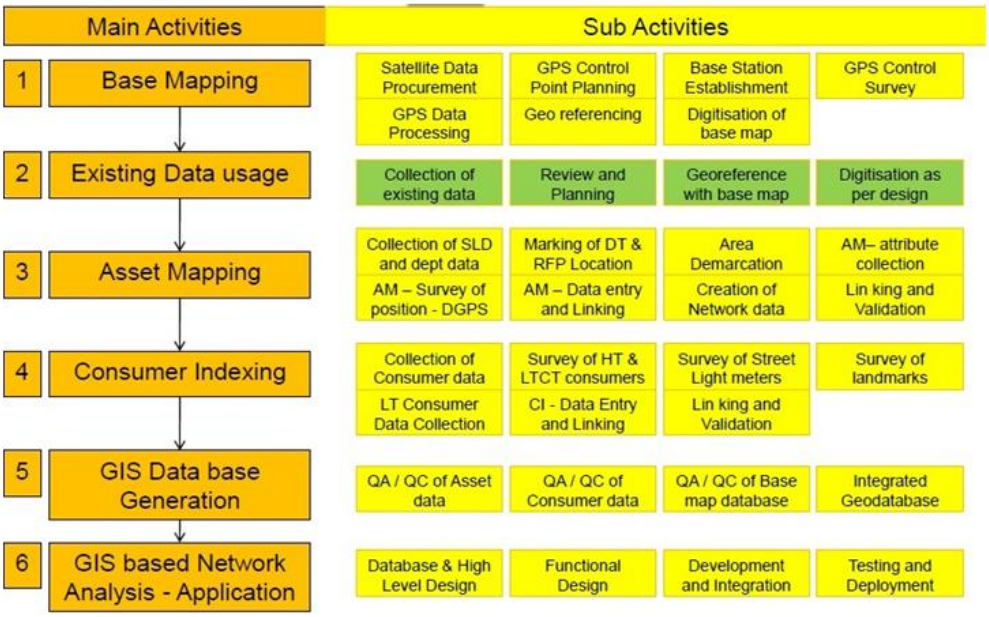

Figure 1: *Flowchart showing the methodology adopted for the study*

3. Results and Discussions

3.1. Indexing and Mapping of Consumers

The purpose is to identify and locate the consumer in geographic space (Figure 2), which is being fed from main lines. There are many instances when the connection on the ground exists but the records are not properly maintained. It may be the case of unauthorized connection. On the other hand connection exists in the electric record, but it may not exist on the ground. With the help of GIS the main LT lines coming from the Distribution transformer (DT) and all services connections coming out from main LT can be can be checked & verified with reference to the consumers connected (Figure 3).

3.2. Mapping of Electric Network

The electric network and route is digitized and mapped on the base map at suitable scale using Arc Map (Figure 4), so that changes in the network can be timely made and updated on periodic basis. With the use of GIS software queries regarding the length of feeder, specifications of the network, number of consumers, HT/LT conductor, Transformer details can be easily obtained and even a proposal for new feeder design and feeder bifurcation can be suggested correlating and examining with the existing and proposed load of the feeder. It is important to note here GIS software helps in identifying the areas of high losses, and proven to be an important asset in electric utility mapping, segregating the energy input and consumption Distribution Transformer-wise and 11/33 KV feeder-wise. The losses are assessed by subtracting the total energy utilization of the consumers from the energy supplied to the respective Distribution Transformer and 11/33 KV Feeder.

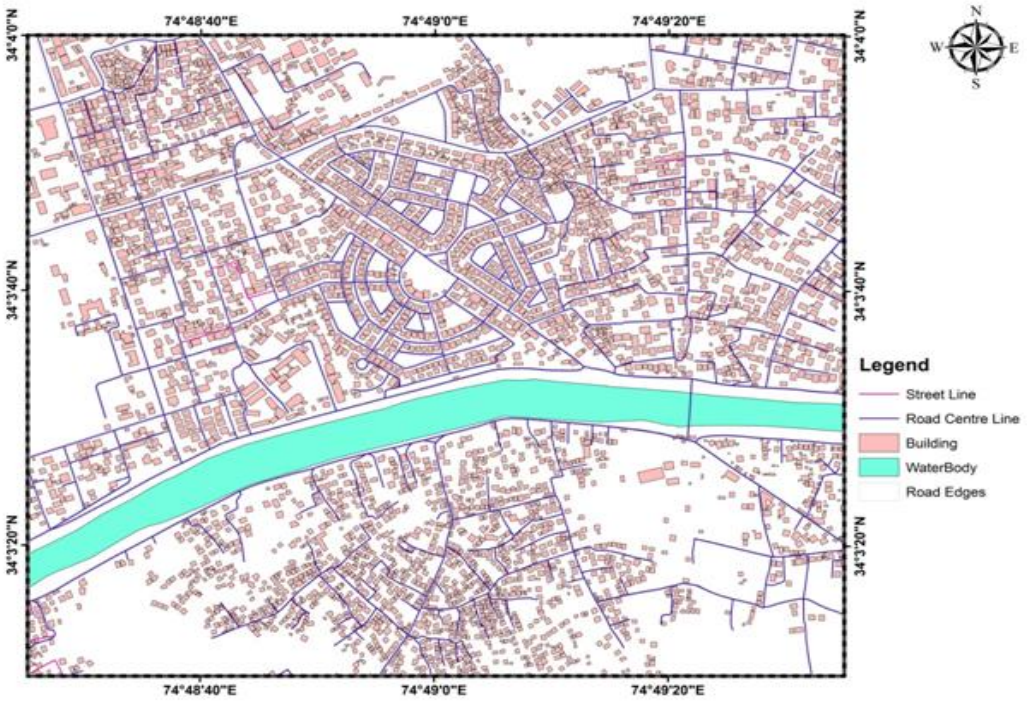

Figure 2: *Map showing Aerial view of distribution network*

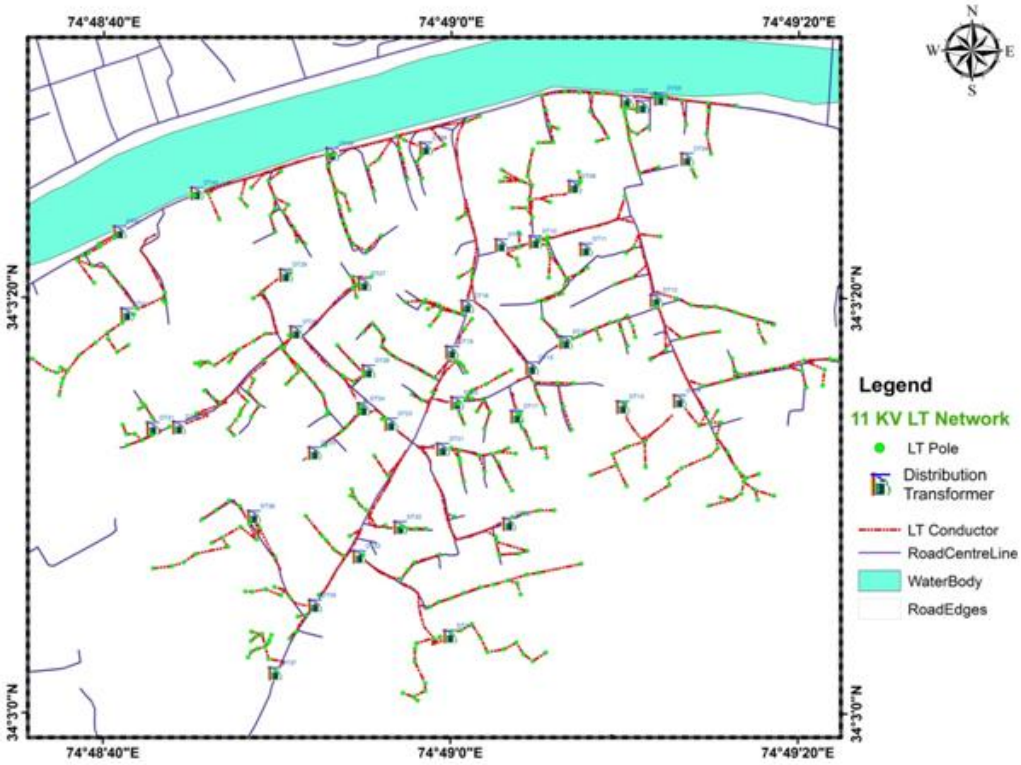

Figure 3: *Map showing 11 KV LT Network of Jawahar Nagar, Substation Rajbagh, Srinagar Jammu & Kashmir, India*

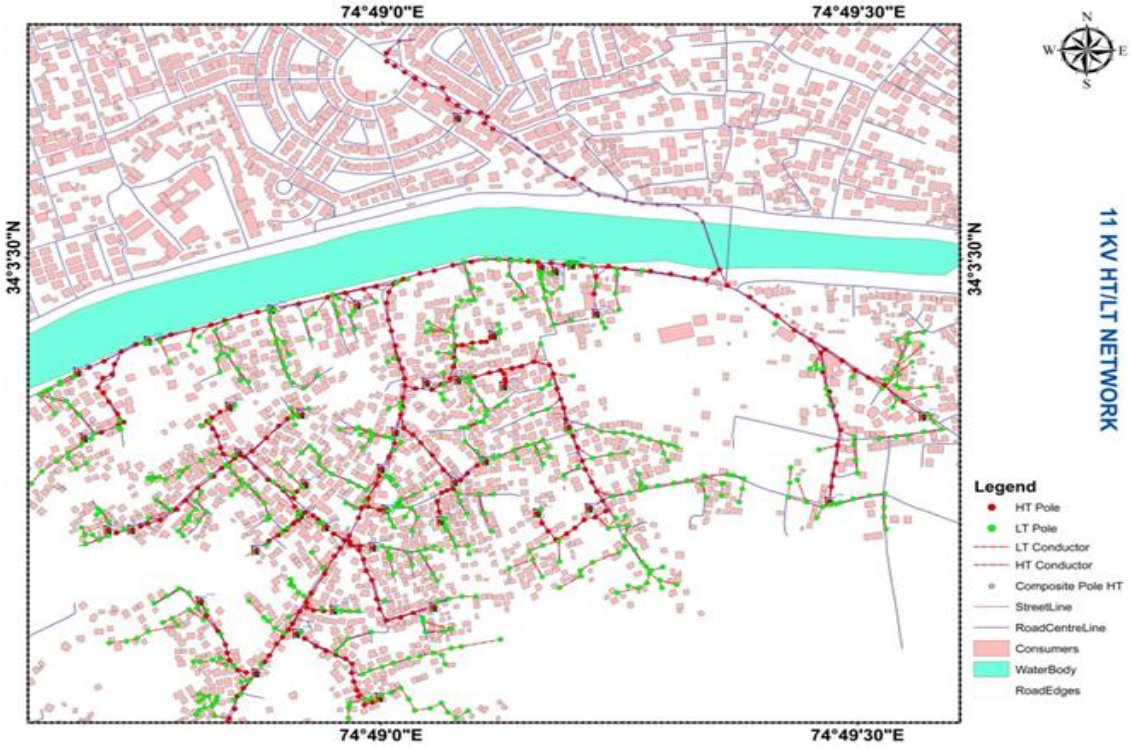

Figure 4: *Map showing Final HT/LT Network of Jawahar Nagar, Substation Rajbagh, Srinagar - Jammu & Kashmir, India*

3.3. Energy Audit, Load flow and Network Analysis

In electric utility sector, GIS is being used for a number of applications like distribution network mapping, network analysis, load flow studies, asset management, energy audit and customer care. Spatial data analysis is helping the users to analyze patterns in spatial data for MIS and Business Intelligence, with the intent to improve network efficiency and customer services (Jayant Sinha, 2013). Energy audit has to be directly integrated with metering, billing and collection with minimal manual intervention. It has to capture electrical distribution network and energy parameters for feeder-wise and DT-wise loss analysis and identification of sections of revenue leakages. Therefore, 100% metering of consumers, substation feeders and distribution transformers is an essential requirement for total energy accounting. The foremost technical challenge is to affect a seamless integration of the entire business processes both the new systems and current legacy systems, unless the utility chooses to discard the latter altogether. The network analysis tool uses advance algorithms for calculating phase imbalances, identifying low-voltage or overloaded sections, calculating section-wise loss level sand taking decisions on system optimization through network reconfiguration. Geographic Information Systems (GIS) is being used in electric utilities for energy audit and network analysis, and emerging as a powerful tool for load planning and management with the focus to improve the quality of electricity supply and other related services. The electrical network overlaid on geographic area base map is handy for the utility in not only managing assets and their maintenance, but also for mapping the consumers for energy audit applications. By integrating GIS with electrical and network analysis application, various analytical studies are possible for load flow analysis, short circuit analysis, efficiency calculations and optimization.

Table 1: *Comparison before and After GIS implementation*

Before GIS Implementation	After GIS Implementation
The HT line Regulation has not been calculated easily and not maintained within the norms.	The HT Regulation has been calculated easily and maintained within the norms.
Difficult to identify the HT LT pole location, DT and not to control overload Distribution Transformer. Fuse of call to be attended slowly.	Easy to identify the HT LT pole location. Avoid overload Distribution Transformer and locate the new DT at load centre point. Fuse of call to be attend slowly.
The damaged pole and snapped conductor are difficult to identify there more chance to happen Fatal and Non-fatal accident. The fault trips are frequently happened.	The damaged pole and snapped conductor are easily identifying there less chance to happen Fatal and Non-fatal accident. The fault trips are happened rarely.
The maintenance and operation cost is high due to it requires high man power. This result having less efficiency.	Due to Computer technique it requires less man power and operational cost. This result having High efficiency.

4. Conclusion

Geographic Information System helps users to integrate in simplest form and has tendency to manage the information and represent it in numerous interactive maps. The Web based Geographical Information System (GIS) is not limited to a certain Science or unique technology, but it has very extended branches of usage in a lot of the daily activities. GIS provides us to show all accumulated data which are stored in any format for long time as visible layers linked between location data and attributes. Our future perspective is to integrate this Electric Network Utility of GIS with SCADA to really simulate the real time flow of the energy across the networks, and which is aimed to be kept in server environment for any time any where identification and demarcation of any effect in the system / energy flow at any junctions across the networks. On integration with SCADA we could also provide diversified solutions in this electrical utility network sector.

References

James L. Snipes. 2004. Spatial Technologies: GIS for Utilities. Available From: *http://www.cadalyst.com/gis/spatial-technologies-gis-utilities-8616.*

Jayant Sinha. 2013. Integrating issues and challenges of IT reforms in Power Distribution. Available From: *https://jayantsinha.wordpress.com/tag/distribution-network-analysis/.*

Mathankumar, S. and Loganathan, P. 2015. GIS Based Electrical System Planning and Network Analysis. *World Engineering & Applied Sciences Journal*, 6(4), pp.215-225.

Mathankumar, S. and Loganathan, P. 2015. Detection of Power Theft in HT Consumer Using SCADA Interfacing with GIS System. *International Journal of Research in Engineering and Applied Sciences*, 5(7).

Rhind, D. 1989. Why GIS? *ARC News*, Vol. 11, No. 3, Summer 1989, Redlands, CA: Environmental Systems Research Institute, Inc.

Prasad, M. 2006. Maps and Census. *GIS Development: Asia Pacific*. The Monthly Magazine on GIS, Vol. 10, No. 12, pp.7-48, December 2006.

Cloud Publications
International Journal of Advanced Remote Sensing and GIS
2017, Volume 6, Issue 1, pp. 2458-2465
ISSN 2320 – 0243, Crossref: 10.23953/cloud.ijarsg.325

Case Study

Mining Activity Monitoring Through Remote Sensing and GIS- A Case Study from Wani Area of Yavatmal District, Maharashtra

Sanjeev Verma[1], Deepak B. Malpe[2]

[1]Maharashtra Remote Sensing Application Center (MRSAC), Nagpur, Maharashtra, India
[2]Department of Geology, R.T.M. Nagpur University, Nagpur, Maharashtra, India

Publication Date: 25 November 2017

DOI: https://doi.org/10.23953/cloud.ijarsg.325

Abstract Remote sensing (RS) and Geographic Information System (GIS) is a powerful tool for managing and planning the mining activities and has an advantage of synoptic view, temporal capability and can observe the inaccessible areas. Open cast mining activities has direct impact on earth surface which can be studied and quantified using remote sensing technology. In the present paper, we examined the areal expansion of the coal mines and their impact on the surrounding area of Wani using RS and GIS technique. The LANDSAT, IRS and High resolution satellite data of Google, having resolution of 30m, 23m, and 50cm respectively have been used. Changes in the crop land due to mining activities were calculated using heads-up interpretation of satellite data using ArcGIS software. Present study has shown that in Wani area crop land has decreased by 6.46% in the span of 26 years following the expansion of mining activities in the area.
Keywords *Crop land; GIS; Mining effect; Remote sensing*

1. Introduction

Nagpur, Chandrapur, Yavatmal and Wardha districts of Maharashtra hosts large deposits of coal. So far 5576 million tons of coal reserves have been proved in the State. In Yavatmal district, coal is mostly confined to Wani taluka. Due to Coal mining activities in Wani taluka, three important natural resources are affected viz. fertile top soil, crop land and ground water resources. Mining activities cause generation of coal dust which has potential health hazard. Inhalation of coal dust causes black lung disease, cardiopulmonary disease, hypertension and other related ailment in the population living near the coal mine (Finkelman et al., 2002). Open cast mining involves removal of overburden including valuable top soil as well as the natural vegetation cover. These activities are associated with harmful effects on the local environment and also biodiversity (Mahalik and Satapathy, 2016). Regular monitoring and management of such mining area is essential from natural resources and socio-economic point of view through modern technologies like Remote Sensing (RS), Geographic Information System (GIS) and Global Positioning System (GPS) for sustainable development.

2. Study Area

The present investigation covers Wani taluka of Yavatmal district and is bounded by longitudes 78°46'18"E to 79°8'59"E and latitudes 19°45'48"N to 20°11'26"N (Figure 1). The area is bordered by Chandrapur district along eastern and southern side and by Zari-Zamni and Maregaon talukas of

Yavatmal district on the western side. The Wani taluka geographically covers 910.47 km^2 area and includes 162 villages.

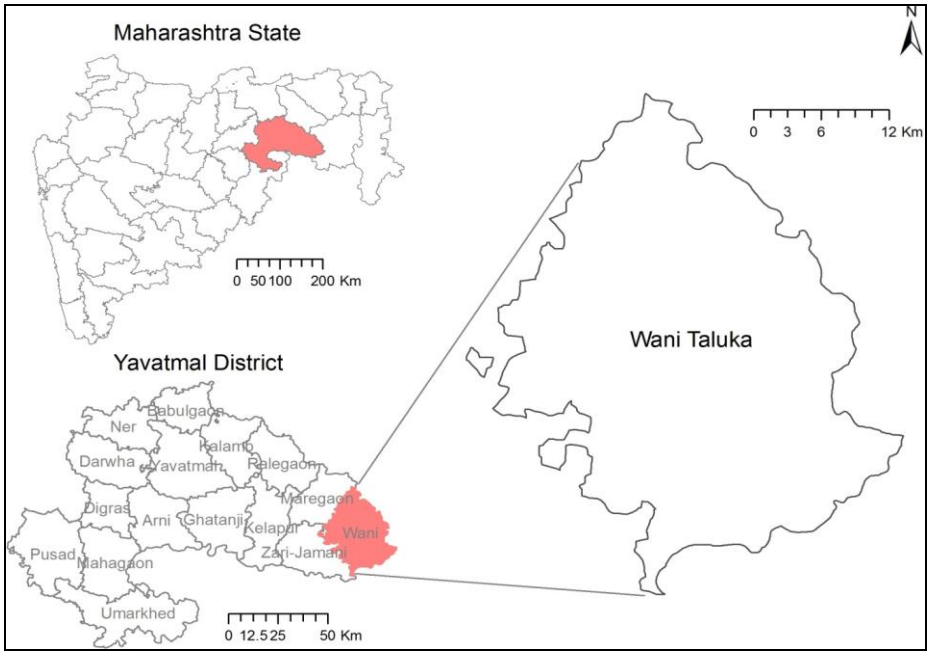

Figure 1: *Location map of study area*

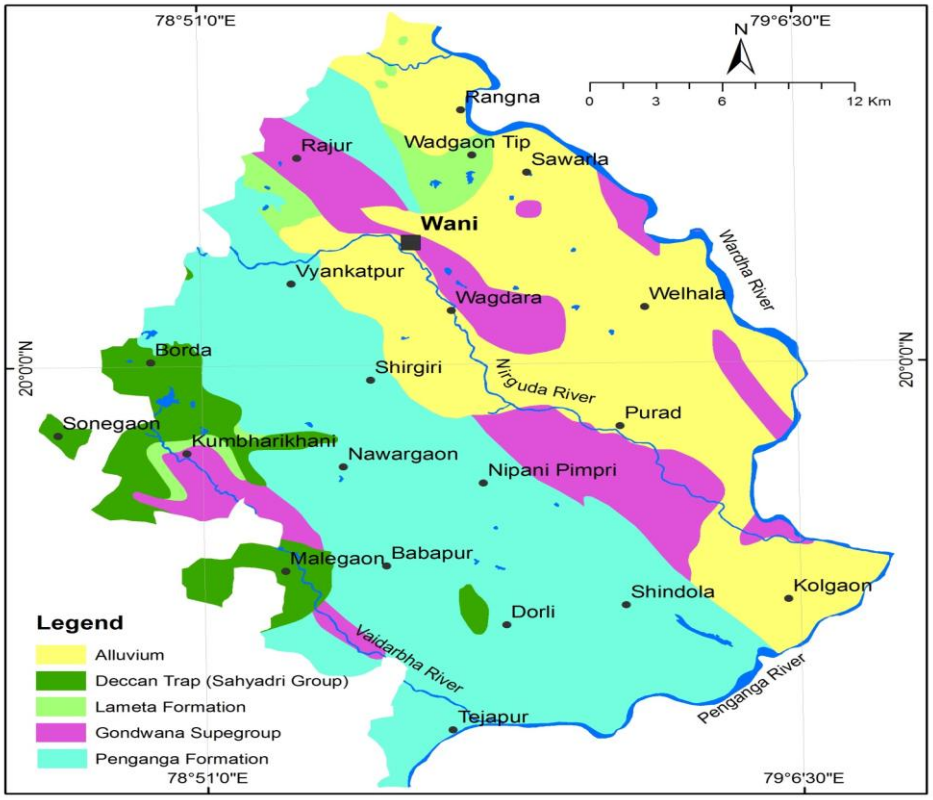

Figure 2: *Geological map of Wani taluka*

Geologically Wani taluka is covered by Neoproterozoic Penganga Group rocks represented by limestone and shales, which are overlain by Carboniferous to Permian Lower Gondwana rocks. Gondwanas are represented by sandstone, shale and coal beds of Barakar Formation and sandstone of Kamthi Formation. They are overlain by buff, pink and violet coloured clays and cherty limestones of Lameta Formation of uppermost Cretaceous age. All the older formations are overlain by Deccan Traps of Deccan Volcanic Province of uppermost Cretaceous to Eocene age. Alluvium is present mostly along eastern side of the area along Wardha and Penganga Rivers (Figure 2). The economic mineral present in the Wani taluka are coal, limestone, dolomite and clay.

3. Materials and Methods

In the present work, multi temporal LANDSAT TM and IRS P6 LISS-III data (Table 1) covering kharif (Aug-Nov), rabi (Jan-Mar), zaid (April-May) seasons for the year 1989, 2005-06, 2011-12 and single season high resolution data (Google) for the year 2009 and 2016 have been used to address spatial and temporal variability in land cover classes like crop land, coal depot, active mining area and mining plantation. The land cover polygons as seen on the satellite data are delineated on screen, using ArcGIS software and a land use land cover map is prepared. Geo-referenced cadastral village boundary maps available with Maharashtra Remote Sensing Application Centre (MRSAC), is used as vector layer for analysis purpose. This cadastral map is combined with land use land cover map and village wise statistics is generated. Village wise area for land use land cover is calculated for the year 1989, 2005, 2009, 2012 and 2016 for Wani taluka.

Table 1: *Details of satellites data used in mapping mining activities*

Year	Path Row - 100-58/ satellite/sensor	Date
1989	Landsat - sensor - TM	5 November 1989
2006	IRS P6 - sensor - LISS III	4 November 2005, 15 January 2006, 21 April 2006
2009	IRS P6 - sensor - LISS III	29 April 2009
2011	IRS P6 - sensor - LISS III	November 2011
2012	IRS P6 - sensor - LISS III	January 2012, April 2012
2016	High Resolution Satellite data - Google	April 2016

4. Results and Discussion

The results of the study area are given below:

Coal Depot

The coal depots are the places where coal is stored and transported to other places in the country. In the study area, coal depots are mainly situated in 12 villages along Major State Highway No. 14 (MSH-14) and State Highway No. 314 (SH-314). The list of 12 villages and their area is listed in the Table 2.

The large collection of past and present satellite images makes it possible to analyze spatiotemporal pattern of environmental elements and impact of human activities in past decades (Gong et al., 2008). Ghose and Majee (2001) studied the air pollution caused due to coal mining and suggested that the volume and variety of air borne dust particles in the ambient air is increasing due to coal mining and causing air pollution problems in the surrounding areas.

Table 2: *Villages affected by coal depot in Wani taluka of Yavatmal district*

S. No.	Village Name	Village Area (km^2)	Year Wise Area of Coal Depot (km^2)			
			2006	2009	2012	2016
1	Bramhani	6.03	0.12	0.12	0.15	.07
2	Kasbe Wani	16.16	0.37	0.37	0.11	0.10
3	Lalguda	3.25	0.12	0.12	-	-
4	Nilapur	6.70	0.20	0.20	.026	-
5	Nimbala	5.04	0.11	0.11	.026	.08
6	Parsoda	3.99	0.16	0.16	0.081	.11
7	Zarpat	2.74	0.05	0.05	.060	.02
8	Wanjari	12.22	0.08	0.08	0.01	-
9	Rajur	6.64	0.49	0.64	.099	.03
10	Chikhalgaon	7.18	0.35	0.56	0.47	0.46
11	Kalmana Kh	5.28	0.42	0.67	0.28	0.27
12	Bhandewada	2.24	-	-	0.03	0.014
	Total	77.47	2.47	3.08	1.34	1.20
	Taluka area	910.47 km^2	0.27%	0.34%	0.14%	0.13%

In the present area, the coal dust and particulate matter created during coal storage and transportation is causing air pollution which resulted in respiratory problems in the rural population in the affected area. It is also affecting agricultural areas, vegetation health and land productivity. Our studies showed that the total area affected due to coal dust in the ambient atmosphere while transportation from mine to coal depot is about 13.75 km^2 along the route especially in the North and North West side of Wani town. Another observation is that, the area under coal depot is decreasing from 3.08 km^2 (0.34 % of taluka) in the year 2009 to 1.20 km^2 (0.13 % of taluka) in 2016. Despite this decreasing trend, its impact in the form of coal dust in atmosphere is remarkable in the adjacent areas with blanket of coal dust (Figure 3 and 4). New permanent fallow land mainly falls in this impact zone. Similarly, fertile land is converted into fallow land and new layouts are also coming up in the impact zone.

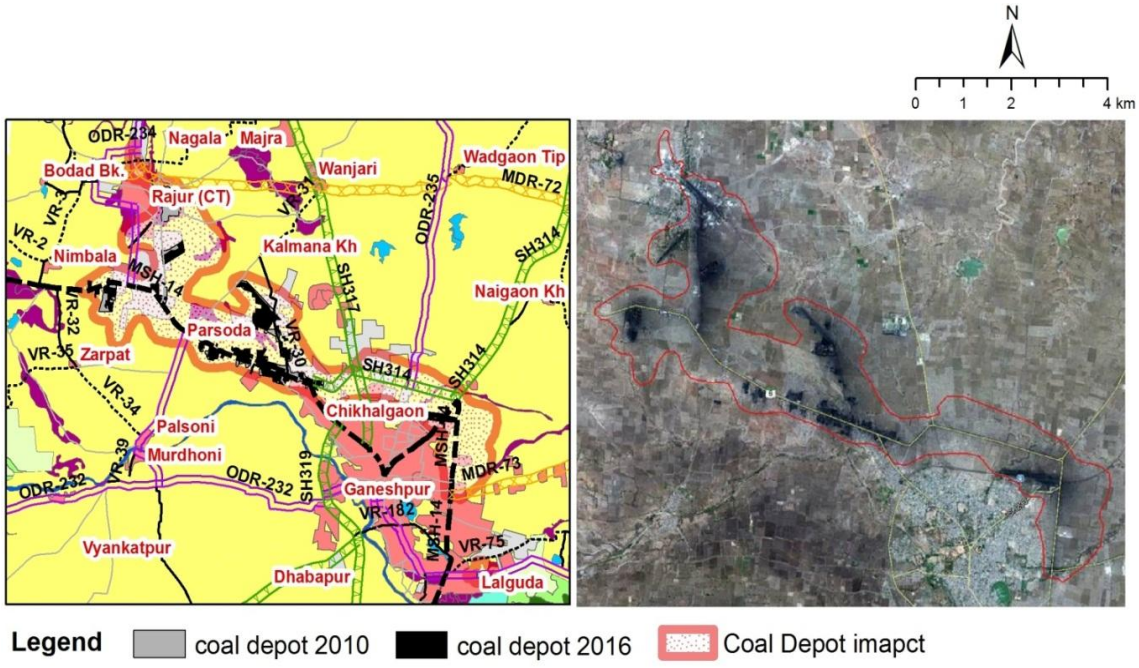

Figure 3: *Impact of coal depot near Wani town, Yavatmal district, Maharashtra*

Figure 4: *Feld photos showing impact of coal dust on vegetation in study area*

Mining and Crop Land

In the study area it is observed that, the mining activity (including mine plantation) acquired only 7 villages in the year 1989 with an area of 2.72 km^2 (0.29% of taluka) under mining. The area of mining increased to 38.82 km^2 during the year 2006 and total villages under mining were 26 (4.26 % of taluka). In the year 2012, mining area in Wani taluka has been increased to 47.98 km^2 (5.26% of taluka), while in the year 2016, mining area in the taluka has increased to 56.66 km^2 (6.22% of taluka) and total 37 villages (partially or fully) comes under mining activities (Table 3, Figure 5). The average rate of mining in this region is 2.1 km^2 per annum.

Table 3: *Villages affected by coal mining activity (including mine plantation) in Wani taluka of Yavatmal district*

Year	No. of villages under Mining	Area under Mining activity (km^2)	% With respect to Taluka area (910.47 km^2)
1989	7	2.72	0.29
2006	26	38.82	4.26
2012	34	47.98	5.26
2016	37	56.66	6.22

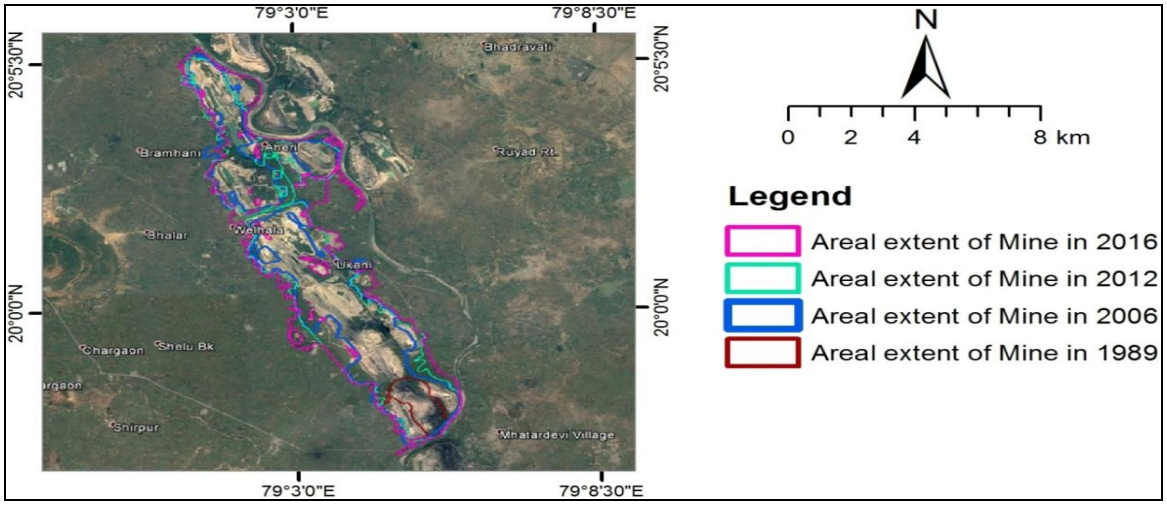

Figure 5: *Areal extent of coal mining near Wani town, Yavatmal district, Maharashtra during 1989-2016*

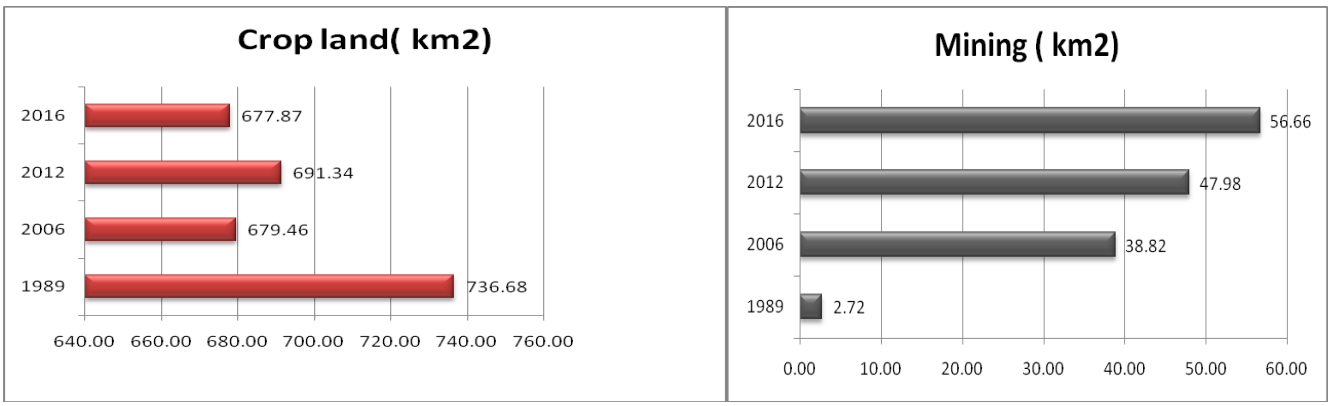

Figure 6: *Comparison of crop land, mining activity during 1989 to 2016*

Table 4: *Comparison of Land Use Land Cover in Wani taluka, Yavatmal district, Maharashtra*

	1989		2006		2012		2016	
Level 1	**Area (km^2)**	**Area (%)**	**Area (km^2)**	**Area (%)**	**Area (km^2)**	**Area (%)**	**Area (km^2)**	**Area (%)**
Built up	10.28	1.13	13.04	1.43	17.78	1.95	19.94	2.19
Crop land	736.68	80.91	679.46	74.63	691.34	75.93	677.87	74.45
Fallow land	3.80	0.42	18.12	1.99	1.86	0.20	4.77	0.52
Wasteland	24.38	2.68	25.98	2.85	19.58	2.15	19.19	2.11
Dense Forest	31.15	3.42	30.58	3.36	23.08	2.54	23.08	2.54
Open Forest	39.48	4.34	39.52	4.34	45.20	4.96	45.17	4.96
Scrub Forest	47.83	5.25	48.11	5.28	47.54	5.22	47.27	5.19
Tree clad	0.19	0.02	0.33	0.04	2.84	0.31	2.83	0.31
Coal depot	0.19	0.02	2.64	0.29	1.34	0.15	1.21	0.13
Mining area	2.73	0.30	30.10	3.31	30.19	3.32	31.63	3.47
Mining Plantation	---	---	8.40	0.92	16.68	1.83	24.96	2.74
River	12.08	1.33	12.08	1.33	10.58	1.16	10.55	1.16
Water body	1.69	0.19	2.12	0.23	1.91	0.21	2.01	0.22
Total	910.48	100.00	910.48	100.00	910.48	100.00	910.48	100.00

Land Use and Land Cover

The comparison of land use and land cover of Wani taluka between1989 to 2016 showed that the fertile agricultural land and good soil cover is coming under mining activities (Table 4, Figure 6). The main crop land situated adjacent to river and Wani town have been decreased from 736.68 km^2 in 1989 to 677.87 km^2 in the year 2016 (Figure 6). There is an increase in built-up area from 10.28 km^2 to 19.94 km^2. We observed decrease in wasteland, increase in open forest and increase in mining area. Remarkable increase in Mining plantation from 8.40 km^2 to 24.96 km^2 in and around mining area has been observed (Figure 6). This plantation is mainly observed around coal mining areas for waste dump stabilization.

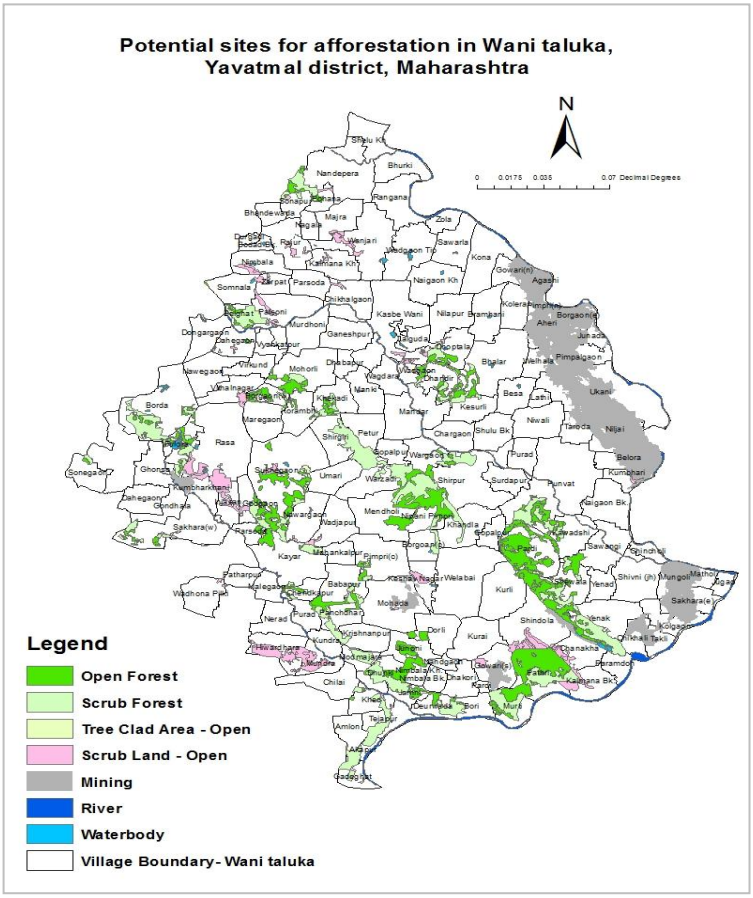

Figure 7: *Potential sites for plantation in Wani taluka, Yavatmal district, Maharashtra*

5. Conclusion and Recommendations

The land use-land cover map of Wani taluka of the year 2016, indicate that the open scrub is 19.19 km^2 (2.11% of the taluka). The open forest and scrub forest in the taluka is 45.16 km^2 and 47.27 km^2 respectively, while the mining area in the taluka is 56.66 km^2 (6.22 % of taluka) out of the geographical area (910.47 km^2). In the study area, there is a scope for development of 111.62 km^2 (12.26 % of area), which comes under open forest, scrubs forest, tree clad open and wasteland.

It is recommended that, various afforestation programmes can be undertake in such identified location in taluka to compensate the loss of cropland, fertile soil and environmental degradation caused due to mining activities. Recommended potential sites for afforestation are given in Figure 7. During afforestation programmes native faunal species should be planted and for better results, ecological variables must be considered while selecting species for plantation. This can help in stabilization of soil and enrichment of soil organic matter and soil nutrients. In the initial stages of afforestation quick growing grasses with short life cycle, legumes and forage crops shall be planted, which will improve soil nutrients and organic matter. Plantation of mixed species of economic importance should be carried out after 2-3 years of grass plantation (Kolhe and Khot, 2015).

Special monitoring and management techniques are required for village or parcel around coal depot. It is recommended to restrict the location of new coal depot along roadside. They should be located within identified zone near Wani town with good infrastructure facilities and may be declared as industrial zone. Such identified areas play a key role in restricting the land, air and water pollution. Constant research and development efforts are required to find out newer and latest technologies and methodology for the sustainable development.

Acknowledgements

We are thankful to Head, Department of Geology, R.T.M. Nagpur University, Nagpur and Director, MRSAC, Nagpur for the facilities. DBM is thankful to UGC-SAP-DRS-II for the financial assistance.

References

Gong, J., Sui, H., Ma, G. and Zhou, Q. 2008. A review of multi-temporal remote sensing data change detection algorithms. *The International Archives of the Photogrammetry, Remote Sensing and Spatial Information Sciences*, Part B7, pp.757-762.

Ghose, M.K. and Majee, S.R. 2001. Air pollution due to coal mining and its control in Indian context. *Journal of Scientific and Industrial Research*, 60, pp.786-797.

Finkelman Robert, B., Orem, W., Castranova, V., Tatu Calin, A., Belkin Harvey, E., Zneng, B., Lerch Harry, E., Maharaj Susan, V. and Bates Anne, L. 2002. Health impacts of coal and coal use: possible solutions. *International Journal of Coal Geology*, 50, pp.425-443.

Mahalik, G. and Satapathy, K.B. 2016. Environmental impacts of mining on biodiversity of Angul - Talcher Open Mining Site, Odisha, India. *Scholars Academic Journal of Biosciences*, 4(3a), pp.224-227.

Kolhe, M.R. and Khot, P.G. 2015. Emerging issues regarding environmental management in mining sector. *International Journal of Advance Research in Computer Science and Management Studies*, 3(6), pp.109-118.